The role of CD200 in kidney cancer immune evasion

Gemma Elizabeth Davies

Thesis submitted for the award of PhD

2023

Summary

Kidney cancer is the 7th most common cancer type in the UK, with around 13,300 new cases diagnosed every year, accounting for 4% of new cancer cases and 3% of all cancer deaths. Renal cell carcinoma (RCC) is the most common form of kidney cancer, of which clear cell renal cell carcinoma (ccRCC) is the most common and aggressive subtype, making up around 75% of cases. All RCC is resistant to chemotherapy and radiotherapy, so surgery is the gold standard treatment for early-stage disease. Late-stage disease however has limited treatment options, with poor response rates and high risk of relapse observed with immunotherapy. Therefore, new immune checkpoint therapeutic targets are urgently required.

Engagement of CD200 with its receptor is an immunosuppressive immune checkpoint which is overexpressed in several cancer types, enabling immune evasion and disease progression. CD200 is subject to ectodomain shedding, creating a functionally active soluble form known as sCD200. In this thesis, we characterise CD200 expression in normal kidney and RCC tissue, then examine its relationship firstly with proteases to establish their role in CD200 ectodomain shedding, and secondly with tumour-infiltrating immune cells to determine its effect on the anti-tumour immune response. We examined expression of ADAM9, ADAM17 and ADAM28 in combination with CD200, with high numbers of double positive cells present throughout ccRCC tumour tissue. ADAM9 was found to have a novel role in CD200 ectodomain shedding, resulting in a dose-dependent increase in sCD200 presence in our cell line experiments. CD200 expression was found to significantly alter RCC immune infiltrate compared to normal kidney, and we characterised a ccRCC-specific ‘high effector T cell’ immune signature which was associated with poor prognosis. Finally, we showed that both CD200 and sCD200 are able to protect tumour cells against NK cell-mediated cytotoxic activity. Taken together, this data shows that blockade of CD200 may be a potential therapeutic option for RCC patients.

Word count: 70,719

Acknowledgements

For my dad.
“How’re your bugs?”

I would firstly like to thank Professor Girish Patel for this opportunity, and his continuous guidance and support both in and out of the lab throughout the past few years. I would also like to thank Professor Matt Smalley for all of his help, encouragement and ideas to better this work.

This research would not have been possible without the input of my fellow GKP lab members, and I am so grateful for their help and friendship during my PhD. Dr Huw Morgan, thank you for your kind guidance, patience and troubleshooting support when things regularly went wrong. Dr Charley Lovatt, my pandemic lab buddy who taught me so many lab techniques whilst working incredibly hard herself, thank you for everything. Alex Gibbs, my fellow PhD student: equal parts barista and bioinformatician extraordinaire, thank you for all of your help and patience with my stupid questions. I wish you all the best with finishing your PhD.

I would also like to thank everyone at ECSCRI for all of their help over the years. I feel so lucky to have completed my PhD in this special place surrounded by so many incredible, inspiring scientists, and most of all, friendly faces.

The period over which this thesis has been made includes some of the most difficult years of my life. Beginning a PhD is daunting enough, but encountering a global pandemic within the first few months, and later losing my dad to cancer, whilst writing a thesis about cancer, has not been an easy ride. However, it was incredibly important to my dad that I didn’t give up and that this thesis was written, so here it is. I will never be able to find the words to thank my family and friends enough for getting me through this time. I so appreciate their love, support and enthusiasm for completing my PhD, let alone getting me through the loss of my dad. My mum and Craig have been the most incredible support system and I can truly never repay them. My little Leo and his unconditional love and cwtches on demand have also been invaluable. I am

also so grateful for my incredible friends who have been excited about this work even when I felt it was hopeless, and who have rallied round and supported me through this incredibly difficult time. I am so, so lucky to have you all.

Finally, I would like to thank the Wales Cancer Bank and the patients who kindly donated samples for use in this work, and my funders, KESS2 and Tenovus, for making this project possible.

Table of contents

List of Figures

List of Tables

Abbreviations

ADAM	A disintegrin and metalloproteinase
ADCC	Antibody-dependent cellular cytotoxicity
AJCC	American Joint Committee on Cancer
AKT	Protein kinase B
AML	Acute myeloid leukaemia
ANOVA	Analysis of variance
APC	Antigen presenting cell
AQP-1	Aquaporin-1
AU	Arbitrary unit
BAP1	BRCA associated protein-1
BCC	Basal cell carcinoma
BCL-XL	B cell lymphoma extra-large
BCR	B cell receptor
C-FLIP	Cellular FLICE (FADD-like IL-1β-converting enzyme)-inhibitory protein
CAIX	Carbonic Anhydrase IX
CCL	Chemokine (C-C motif) ligand
ccRCC	Clear cell renal cell carcinoma
CD200	Cluster of differentiation 200
CD200R	Cluster of differentiation 200 receptor
cDNA	Complementary DNA
chRCC	Chromophobe clear cell renal cell carcinoma
CI	Confidence intervals
CIBERSORTx	Cell type identification by estimating relative subsets of unknown RNA transcripts
CLL	Chronic lymphocytic leukaemia
CO2	Carbon dioxide
COPD	Chronic obstructive pulmonary disease
CrkL	Cellular homologue-like
CSC	Cancer stem cells
ctDNA	Circulating tumour DNA
CTG	Cell Titre-Glo
CTGF	Connective tissue growth factor
CTL	Cytotoxic T lymphocyte
CTLA-4	Cytotoxic T lymphocyte antigen-4
DAMP	Damage-associated molecular pattern
DC	Dendritic cell
DEG	Differentially expressed gene
DMSO	Dimethyl sulfoxide
DN	Double negative
DNA	Deoxyribonucleic acid
Dok	Downstream of tyrosine kinase

DP	Double positive
DR5	TRAIL death receptor 5
EAE	Experimental autoimmune encephalomyelitis
ECM	Extracellular matrix
EDTA	Ethylenediaminetetraacetic acid
EGFR	Epidermal growth factor receptor
ELISA	Enzyme-linked immunosorbent assay
EMT	Epithelial-mesenchymal transition
ERK	Extracellular signal-related kinase
FACS	Fluorescence-activated cell sorting
FasL	Fas ligand
FBS	Foetal bovine serum
FoxP3	Forkhead box P3
GFP	Green fluorescent protein
GM-CSF	Granulocyte/monocyte colony-stimulating factor
GP	General practitioner
GSEA	Gene set enrichment analysis
HER	Human epidermal growth factor receptor
HIF	Hypoxia-inducible factor
HLA	Human leukocyte antigen
HR	Hazard ratio
IF	Immunofluorescence
IFN	Interferon
Ig	Immunoglobulin
IHC	Immunohistochemistry
IL	Interleukin
ILC	Innate lymphoid cells
IPA	Ingenuity Pathway Analysis
IPEX	Immunodysregulation polyendocrinopathy enteropathy X linked syndrome
IRF-1	Interferon-regulatory factor-1
IS	Immunological synapse
ITIM	Immunoreceptor tyrosine-based inhibitory motif
kDa	Kilodalton
KICH	Chromophobe clear cell renal cell carcinoma
KIR	Killer cell immunoglobulin-like receptors
KIRC	Clear cell renal cell carcinoma
KIRP	Papillary renal cell carcinoma
LAG3	Lymphocyte-activation gene 3 protein
LN	Liquid nitrogen

mAb	Monoclonal antibody
MAPK	Mitogen-activated protein kinase
MDSC	Myeloid derived depressor cell
MET	Mesenchymal epithelial transition factor
MHC	Major histocompatibility complex
MM	Multiple myeloma
MMP	Matrix metalloproteinase
MT-MMP	Membrane-type matrix metalloproteinase
MTOC	Microtubule organising centre
mTOR	Mammalian target of rapamycin
MZ	Marginal zone
nAb	Natural antibody
NCAM	Neural cell adhesion molecule
NCR	Natural cytotoxicity receptor
NF-kB	Nuclear factor kappa-light-chain-enhancer of activated B cells
NICE	National Institute for Health and Care Excellence
NK	Natural killer
NSCLC	Non-small cell lung cancer
nTreg	Natural Treg
OS	Overall survival
PAMP	Pathogen associated molecular pattern
PBMC	Peripheral blood mononuclear cells
PBRM1	Polybromo-1
PBS	Phosphate-buffered saline
PCA	Principal component analysis
PCR	Polymerase chain reaction
PD-1	Programmed cell death protein-1
PD-L1	Programmed cell death protein ligand-1
PDGF	Platelet-derived growth factor
PDR	Positive regulatory domain
PFS	Progression free survival
PI3K	Phosphoinositide 3-kinase
PLIN2	Perilipin-2
pRCC	Papillary renal cell carcinoma
PTB	Phosphotyrosine-binding domain
pVHL	VHL protein
qRT-PCR	Real time quantitative reverse transcription PCR
RasGTP	Ras p21 protein activator-1
RCC	Renal cell carcinoma
RIN	RNA integrity number

RIPA	Radioimmunoprecipitation assay buffer
RNA	Ribonucleic acid
RSEM	RNAseq by expectation-maximisation
RT	Room temperature
SCC	Squamous cell carcinoma
sCD200	Soluble CD200
SCLC	Small cell lung cancer
SETD2	SET domain containing-2
SFM	Serum free media
SHP	Src homology region 2 domain-containing phosphatase
SOS-1-vav1-grb2	Son of sevenless homolog 1–vav guanine nucleotide exchange factor 1- growth factor receptor bound protein 2
STAT3	Signal Transducer and Activator of Transcription 3
TBST	Tris-buffered saline with 0.1% Tween
TCGA	The Cancer Genome Atlas
TCR	T cell receptor
Tfh	T follicular helper cell
TGF	Transforming growth factor
Th	T helper cell
TIGIT	T cell immunoreceptor with Ig and ITIM domains
TIM3	T cell immunoglobulin mucin receptor 3
TIMP	Tissue inhibitor of matrix metalloproteinases
TMA	Tissue microarray
TME	Tumour microenvironment
TNF	Tumour necrosis factor
TNM	Tumour/Node/Metastasis staging system
TRAIL	TNF-related apoptosis-inducing ligand
Treg	Regulatory T cell
VEGF	Vascular endothelial growth factor
VEGFR	Vascular endothelial growth factor receptor
VHL	von Hippel-Lindau
WT	Wild type
ZAP-70	Zeta-chain-associated protein kinase 70

Chapter 1: Introduction

1. Introduction

1.1 Cancer and the immune system

The observation that tumours often arise at sites of chronic inflammation, and that a relationship exists between the immune system and cancer development, was first made by Virchow in the 19th century (Gonzalez et al. 2018). This idea was however overlooked until a century later, when Dvorak showed that that immune cells infiltrate cancer tissue, and that carcinogenesis and inflammatory conditions share many common developmental pathways, later defining cancer as a “wound that does not heal” (Korniluk et al. 2017). Today, it is accepted that chronic inflammation is one of the critical hallmarks of cancer (Hanahan and Weinberg 2011). Research during the past two decades has demonstrated that inflammatory immune cells play essential roles in cancer-related inflammation at all disease stages, with infiltrating immune cells possessing both pro- and anti-tumour properties. Furthermore, we now know that the immune system plays a key role in cancer development from early neoplastic transformation to metastatic dissemination, with significant impact on clinical outcomes.

Normal anti-infection or wound healing immune responses are temporary, as demonstrated by the transient appearance and disappearance of immune cells throughout the immune response. However, during cancer development, the immune response is long term and low-grade, similar to that observed in chronic inflammation (Singh et al. 2019). This inflammatory environment leads to development of an immunosuppressive tumour microenvironment (TME), alongside production of growth factors and angiogenic factors which encourage tumour cell survival, disease progression, metastasis and immune evasion (Labani-Motlagh et al. 2020). The chronic inflammation demonstrated in cancer development is associated with many lifestyle and environmental risk factors, the most common of which include tobacco smoking (linked with development of at least 15 cancer types), dietary factors such as consumption of processed food and red meat (3 cancer types), alcohol consumption (7 cancer types), obesity (13 cancer types) and persistent bacterial infections, such as *Helicobacter Pylori* and *Human papilloma virus* which are linked with stomach and cervical cancer respectively (Bosch et al. 2002; Walser et al. 2008; Singh et al. 2019).

Inflammation can also contribute to the progression of cancer hallmark capabilities through the tumour-promoting effects of tumour-infiltrating immune cells. These cells supply active molecules such as growth factors and pro-angiogenic factors into the TME, resulting in the occurrence of significant cancer hallmark events such as epithelial-to-mesenchymal transition (EMT) and activation of extracellular matrix (ECM) modifying enzymes, enabling tumour growth, invasion and metastasis (Newton and Dixit 2012; Fedele and Melisi 2020). Inflammatory immune cells can also release reactive oxygen species into the TME, providing mutagenic signals to increase the genetic instability within the tumour cell genome, conferring a selective advantage to tumour cell subclones resulting in population growth and domination of the local tissue environment (Yao and Dai 2014). Together, this combination of inflammation and increased genetic alterations, alongside other hallmark capabilities, drive tumour progression by enabling tumour cell survival, proliferation and metastasis.

In contrast, the acute inflammatory responses observed during key immune events such as pathogen clearance and allograft rejection, are seemingly able to induce tumour cell death (Aguirre et al. 2019). Modulation of these responses are associated with tumour development, making cancer, alongside infection and cardiovascular disease, one of the three main causes of death following organ transplantation (Chapman et al. 2013). The clinically induced immunosuppression required to prevent allograft and transplant rejection leads to a significantly increased risk of cancer development, especially in the lung, liver and kidney. This tumour development is thought to be associated with the loss of immune surveillance, the concept of active detection and eradication of malignant cells by the immune system (Aguirre et al. 2019). Therefore, seemingly contradictorily, tumour growth may be initiated by stimulation of a robust and chronic immune response, however the process of tumour development itself induces an active anti-tumour response which must be evaded to enable disease establishment and progression. A number of strategies are employed by tumour cells to avoid immune cell recognition and elimination, allowing them to evade immune attack and become established as clinically detectable disease, a concept which has now been recognised as a further hallmark of cancer (Hanahan and Weinberg 2011). Therefore, to understand the pro- and anti-tumour roles of immune cells and the underlying basis of cancer cell

immune evasion, it is essential to understand how tumour cells and immune cells interact with each other.

1.1.1 The immune system

The immune system is a highly complex interactive network of lymphoid organs, cells, proteins and cytokines which protects the host from a wide range of foreign antigens including bacteria, microbes, viruses, toxins, as well as the body's own mutated cells (Nicholson 2016). Cells of the immune system are derived from common myeloid and lymphoid progenitors and can be broadly split into two "lines of defence": innate and adaptive immunity. Differentiation of immune cells from haematopoietic stem cells is illustrated in Figure 1.1.

Innate immunity is the first line of defence against intruding pathogens and is a non-specific, antigen-independent mechanism which can be induced quickly upon encountering an antigen (Marshall et al. 2018). Cells of the innate immune system are largely of myeloid origin and include granulocytes (basophils, eosinophils, neutrophils and mast cells), dendritic cells (DCs) and macrophages, while natural killer (NK) and innate lymphoid cells (ILCs) form the lymphoid arm of innate immunity. The innate immune response is able to recognise mutated or defective cells through recognition of the loss of "self" antigens, meaning the inhibitory signal provided by healthy cells to immune cells is lost, allowing the innate immune system to attack the mutated cell (Kubelkova and Macela 2019). Innate immunity has no immunologic memory and is therefore unable to recognise the same pathogen should the body be exposed to it again in future. Conversely, adaptive immunity is specific, antigen-dependant and has capacity for immunologic memory, enabling the host to mount a rapid and efficient immune response upon subsequent re-exposure to an antigen.

The adaptive immune system is comprised of subsets of T and B lymphocytes, which following antigen presentation from cells of the innate immune system, can generate differentiated populations of antigen-specific effector cells (Chaplin 2010). The adaptive immune system has "memory", where following a successful immune response, a population of memory cells remain in the tissue, providing a quick and effective antigen-targeted response upon future re-exposure to the same antigen.

Innate and adaptive immunity are complementary to each other and are not mutually exclusive mechanisms of host defence, therefore defects in either system can result in host vulnerability to infection.

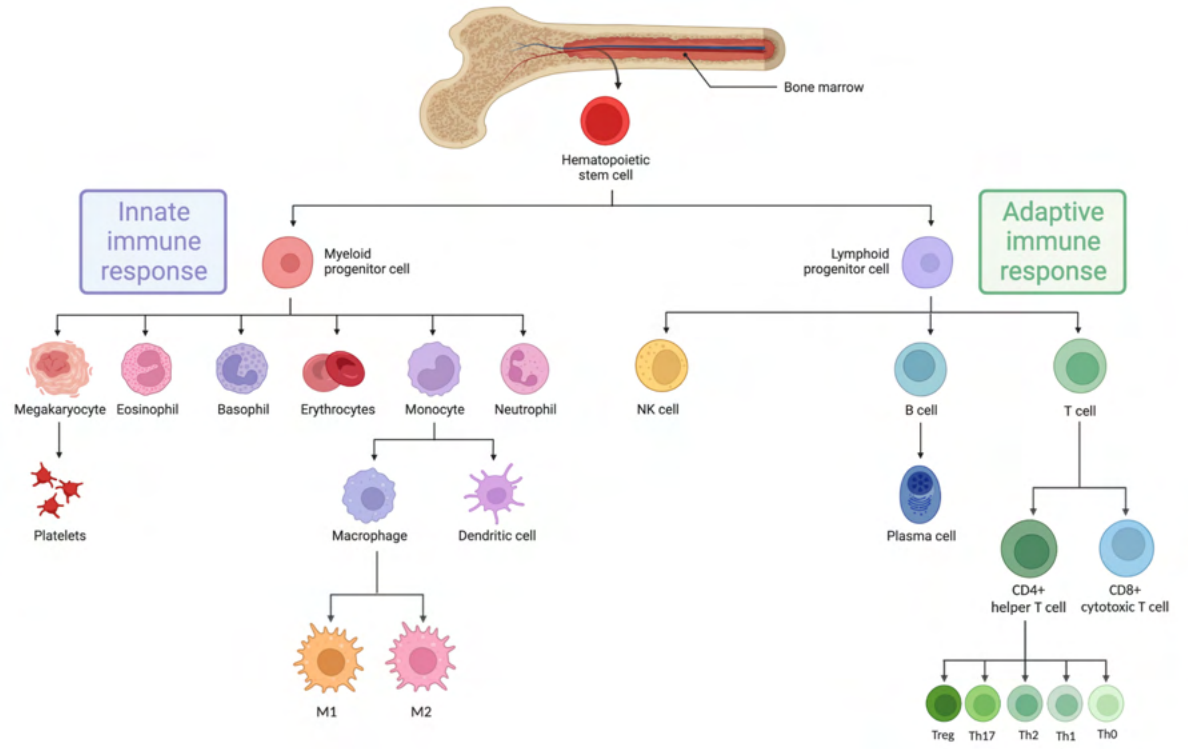

Figure 1.1 Haematopoietic stem cell differentiation into innate and adaptive immune cells Classical model of differentiation from bone marrow-derived haematopoietic stem cells which differentiate firstly into either myeloid or lymphoid progenitor cells. After production by the myeloid progenitor cells, megakaryocyte-erythrocyte progenitors produce platelets, while granulocyte-macrophage progenitors produce granulocytes (mast cells, basophils, neutrophils and eosinophils), macrophages and dendritic cells (DCs). Macrophages further differentiate into M1 and M2 macrophages. Lymphoid progenitor cells differentiate into natural killer (NK) cells, B cells, which differentiate further into plasma cells, and subsets of T cells: CD8+ cytotoxic T cells and CD4+ helper T cells, which further differentiate into regulatory T cells (Tregs), Th17, Th2 and Th1 cells. The innate immune system is primarily comprised of cells from myeloid origin, NK cells and DCs, while the adaptive immune system is primarily comprised of T and B cells. Created in Biorender.com.

The innate and adaptive immune responses can be further divided in to type 1 and type 2 categories, creating a specific and highly protective response to a wide variety of antigens. Type 1 immune responses are pro-inflammatory and are induced against intracellular microbes such as bacteria, protozoa and viruses. This response is characterised by the presence of the pro-inflammatory cytokines interferon-γ (IFN-γ) and tumour necrosis factor (TNF), and the immune response is comprised of type 1 cluster of differentiation-4 (CD4)+ helper T cells (Th1), NK cells and CD8+

cytotoxic T cells (CTLs) (Spellberg and Edwards 2001). Type 2 immune responses protect against large extracellular parasites, while regulating type 1-associated inflammation to prevent overactivation and maintain metabolic homeostasis. Type 2 immune responses are comprised of type 2 CD4+ helper T cells (Th2), mast cells, basophils, eosinophils and macrophages, while the overall response is characterised by the expression of the cytokines interleukin-4 (IL-4), IL-9 and IL-13 (Koyasu and Moro 2011). Chronic inflammation is associated with an imbalance of type 1 and type 2 immune responses and the release of various pro-inflammatory and oncogenic mediators including IL-2, IL-6, TNF, growth factors and cytokines, resulting in an inflammatory environment which can promote tumorigenesis (Qu et al. 2018; Basu et al. 2021). Th17 cells also play a key role in chronic inflammation, and their over expression accompanied by IL-17 results in tissue inflammation, also associated with tissue destruction, autoimmunity and vascular activation (Miossec and Kolls 2012).

1.1.2 Innate immune cells

1.1.2.1 Granulocytes

Granulocytes have a dense granule content within their cytoplasm, and the four main cell types: basophils, eosinophils, neutrophils and mast cells, are derived from a common granulocyte-macrophage progenitor. These cells are produced in large numbers at initiation of the innate immune response, however they are generally short lived (Alberts et al. 2002).

Basophils account for less than 1% of peripheral blood leukocytes and play a role in allergy response and host response to parasites after pathogen associated molecular pattern (PAMP) activation (Nakanishi 2010). Basophils contain basophilic granules and express the allergen- and parasite-responsive high-affinity immunoglobulin (IgE) receptor FcεR. Basophils are also the only circulating lymphocytes which contain histamine upon activation (Borriello et al. 2017). Basophils can also be induced to secrete cytokines to promote and regulate the adaptive immune response, and so could act as a link between the innate and adaptive immune systems (Min et al. 2006).

Eosinophils represent ~1% of circulating leukocytes and provide host responses to parasitic infections and allergens. These cells are characterised by large secretory granules containing growth factors, proteases, cytokines and enzymes and which are released by degranulation during active infection. Eosinophils express a large number of surface markers and can release cytokines including IL-10 and IL-4 to allow regulation of both the innate and adaptive responses (Long et al. 2016).

Neutrophils account for 50-70% of all circulating leukocytes and are microbicidal first responder cells during acute immune responses that phagocytose pathogens in response to PAMPs or damage-associated molecular patterns (DAMPs) (Kraus and Gruber 2021). Neutrophils can also modulate the immune response by production of cytokines to recruit other immune cells to the site of inflammation (Li et al. 2019).

Tissue-resident mast cells have a number of features unlike other granulocytes, in that they are present in tissues throughout the body, are long-lived and regulate a number of normal functions including vasodilation and vascular homeostasis. Alongside this they also have key roles in innate and adaptive immune responses, allergic and anaphylactic responses and immunity against parasites and toxins such as venoms (Krystel-Whittemore et al. 2016). Upon activation, mast cells employ a wide spectrum of methods to include a protective immune response against microbial and viral pathogens including phagocytosis, production of reactive oxygen species and antimicrobial peptides and release of granular and secreted mediators (Urb and Sheppard 2012).

1.1.2.2 Monocytes

Monocytes are mononuclear phagocytic cells which make up 5-10% of the peripheral immune cell population, with substantial pools in the lung and spleen that can be mobilised on demand (Ginhoux and Jung 2014). Monocytes are crucial for an effective immune response against pathogens and have a number of adhesion and chemokine cell surface receptors to recognise pathogens and enable migration from the blood to sites of infection or injury. Once recruited to tissues, monocytes mediate direct antimicrobial activity and can also enter lymph nodes while promoting adaptive immune responses alongside modulation of the inflammatory response by secretion of cytokines including Il-6, IL-1β and TNF (Agarwal et al. 1995). Monocytes further

differentiate into macrophages or dendritic cells (DCs), following stimulation by cytokines and/or microbial molecules (Chiu and Bharat 2016).

1.1.2.3 Macrophages

Macrophages are a heterogenous family of myeloid cells which have a number of roles in homeostasis and physiological processes, alongside vital duties in pathogen destruction, tissue repair and remodelling, clearance of cellular debris and regulation of the adaptive immune response (Zhang et al. 2021). Macrophages are generally split into two distinct differentiation states: the classically activated type 1 macrophage (M1) and the alternatively activated type 2 macrophage (M2). Cells in the naïve, undifferentiated (M0) state have been historically thought to be precursors for M1 or M2 differentiation with no specific function, however have since been found to have prognostic relevance, with high levels associated with poor outcome in various cancer types and so M0 macrophages may have a currently unexplored role in tumorigenesis (Zhang et al. 2022). M1 macrophages are polarised by Th1 cytokines including TNF and INF-γ, and express pro-inflammatory cytokines such as IL-1β, IL-6, IL-12 and TNF, alongside their role in antigen presentation to T lymphocytes to initiate an adaptive immune response. M2 macrophages are polarised by Th2 cytokines such as IL-4 and IL-13, and produce anti-inflammatory cytokines such as IL-10 and transforming growth factor beta (TGF-β), which suppress Th1-mediated inflammation and promote tissue remodelling and wound healing through production of matrix metalloproteinases (MMPs) and pro-angiogenic factors (Mills 2012; Martinez and Gordon 2014).

1.1.2.4 Dendritic cells

DCs are a heterogenous group of highly plastic cells arising from both myeloid and lymphoid progenitors, which exist in the blood and both lymphoid and non-lymphoid tissues. Myeloid dendritic cells are the most potent inducers of CD4 T cell activation and are central to the regulation of immune responses, while lymphoid dendritic cells have roles in maintaining tolerance. DCs have traditionally been divided into two discrete subtypes: conventional and non-conventional DCs including plasmacytoid DCs (Kushwah and Hu 2011). Conventional DCs be further divided into migratory

and lymphoid DCs. Migratory DCs migrate from peripheral tissues to lymphoid organs, while lymphoid DCs reside in the lymphoid organs and lack migratory function. Migratory DCs are found in the skin, lung, intestinal tract, liver and kidneys, while lymphoid DCs remain in lymphoid organs including the nodes, spleen and thymus. Non-conventional DCs are distinguished from conventional DCs by their unique ability to secrete high amounts of IFN in response to viral infections. These DCs have key roles in maintenance of peripheral tolerance as well as in induction of the autoimmune response.

DCs are responsible for initiating antigen-specific immune responses and have key roles in regulation of the immune response by forming a link between the microbial-sensing features of the innate immune system to the highly specific adaptive immune response (Mellman 2013). In response to danger signals such as microbes, inflammatory cytokines and tissue damage, immature DCs migrate towards the site of infection where they engulf antigens by phagocytosis, following which maturation occurs transforming them into professional antigen presenting cells (APCs). Mature DCs then migrate to the lymph nodes where they present their antigens to T cells to induce naïve T cell activation and effector differentiation, thereby initiating the adaptive antigen-specific immune response (Patente et al. 2019).

1.1.2.5 Natural killer cells

NK cells make up around 5-15% of circulating lymphocytes in healthy individuals, however these levels are significantly altered in the development of many diseases (Liu et al. 2021b). NK cells arise from a common lymphoid progenitor and mature in the bone marrow and secondary lymphoid organs including the lymph nodes and tonsils (Abel et al. 2018). In contrast to CD8+ cytotoxic T cells which require prior antigen exposure to initiate an immune response, NK cells invoke a cytotoxic response without the requirement for prior sensitisation, and are able to recognise and rapidly eliminate infected and mutated cells. NK cells are the first line of immune defence in the innate immune system, during which they also release immunoregulatory cytokines to promote an inflammatory response and the recruitment and activation of other immune cells (Schleinitz et al. 2010).

NK cells can be divided into subpopulations based on their expression of CD56, an isoform of neural cell adhesion molecule (NCAM) which mediates homotypic adhesion, and CD16 (FcγIII). The five NK subsets commonly observed in healthy individuals are: (1) $CD56^{bright}$ $CD16^{-}$, (2) $CD56^{bright}$ $CD16^{dim}$, (3) $CD56^{dim}$ $CD16^{-}$ (rare), (4) $CD56^{dim}$ $CD16^{bright}$, and (5) $CD56^{-}$ $CD16^{bright}$ (rare) (Poli et al. 2009). $CD56^{dim}$ cells are the most common subtype of NK cells in peripheral blood and secrete low amounts of cytokines, however they have significantly higher cytolytic capacity compared to $CD56^{bright}$ cells due to their greater expression of cytolytic granules, perforin and granzymes (De Maria et al. 2011). Conversely, $CD56^{bright}$ cells, which make up the majority of the NK population found in secondary lymphoid organs, secrete large amounts of cytokines upon activation, including IL-10, IL-13, IFN-γ and TNF, 13 (Moretta 2010; Wagner et al. 2017).

1.1.2.5i NK cell regulation

Due to the ability of NK cells to implement an immediate cytotoxic response upon detection of virus-infected or neoplastic cells without prior sensitisation, NK cell activity is tightly regulated by numerous highly specific inhibitory and activating receptors to protect healthy cells from attack (Zwirner and Ziblat 2017).

NK cells carry out their effector response through two mechanisms dependant on the presence or absence of infected cell surface ligands for their specific receptors; degranulation of cytolytic granules containing granzymes and perforin, or induction of death-receptor mediated apoptosis by secretion of cytokines such as tumour-necrosis factor related apoptosis-inducing ligand (TRAIL) and proteins such as Fas ligand (FasL) (Piersma and Brizić 2022). NK cells can express a wide range of activating and inhibitory receptors in various combinations, allowing response to a large range of stimuli and multiple layers of regulation (Sivori et al. 2019).

1.1.2.5ia Inhibitory receptors

The interaction of inhibitory receptors with their specific ligands of either major histocompatibility complex (MHC) class I molecules, otherwise known as the human leukocyte antigen (HLA) system, or non-MHC molecules, is essential for the regulation of NK cell effector functions and protection of normal cells from

inappropriate cytotoxic attack. The two major classes of inhibitory receptors are killer cell immunoglobulin-like receptors (KIR) and CD94- natural killer group 2 member A (NKG2A) heterodimers. KIRs are type I transmembrane glycoproteins which recognise HLA-A/B/C expression, while NKG2A are type II transmembrane receptors with a C-type lectin-like scaffold, recognising only HLA-E (Campbell and Purdy 2011). Mature NK cells express at least one type of inhibitory receptor for self HLA antigens, with only very few peripheral blood NK cells lacking these receptors in an anergic state (Sivori et al. 2019). Inhibitory receptor ligands are expressed by most healthy cells to prevent NK cell activation and protect them from destruction, as shown in Figure 1.2a. A list of inhibitory NK cell receptors and their ligands can be found in Table 1.1

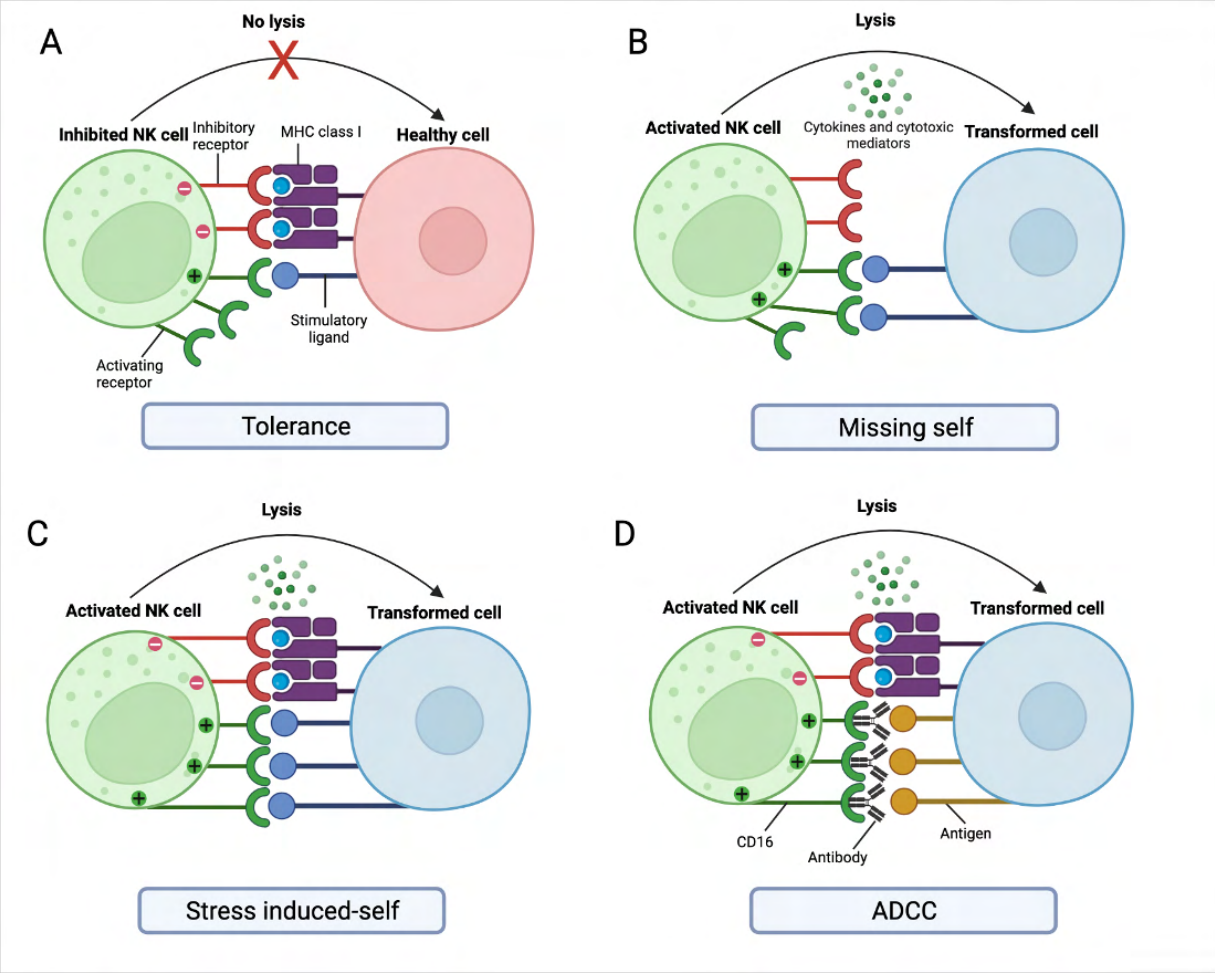

Figure 1.2 Engagement of NK inhibitory and activating receptors
NK cell regulation by inhibitory and activating receptors. (A) Expression of MHC class I ligands by healthy cells induces immune tolerance by engaging with NK cell inhibitory receptors, while dampening activating signals. (B) Cells which have lost MHC class I expression ("missing self") no longer provide inhibitory signals to NK cells and so are susceptible to NK cell attack. (C) Stress-induced overexpression of activating ligands override inhibitory signals leading to "induced-self" NK activation. (D) Antigen-specific antibodies bind to CD16 to initiate antibody-dependant cytotoxicity (ADCC). Adapted from Vivier et al 2012 and Morvan and Lanier 2016. Created in Biorender.com. *Abbreviations: MHC, major histocompatibility complex, NK, Natural killer cell.*

Both KIRs and NKG2A inhibitory receptors contain an immunoreceptor tyrosine-based inhibitory motif (ITIM) (I/VxYxxL/V) in the cytoplasmic domain. Upon interaction with their ligand, the ITIM is phosphorylated by a Src family kinase resulting in the recruitment and activation of tyrosine phosphatase Src homology region 2 domain-containing phosphatase-1 (SHP-1) and SHP-2 (Campbell and Purdy 2011). Recruitment of SHP-1 and SHP-2 leads to NK cell inhibition by dephosphorylation of critical tyrosine phosphoproteins that initiate activation receptor signalling, resulting in inhibition of cytokine production, degranulation and NK cell proliferation (Kumar 2018). This inhibition is temporary, and the NK cell can

be activated upon subsequent interaction with a target cell lacking the specific inhibitory receptor ligands.

Table 1.1 Inhibitory NK cell receptors and their ligands

Inhibitory receptor	Ligand
AIRM1	Unkown
CD244 (2B4)	CD48
CD85j	S100A9
CD94 (NKG2A)	HLA-E (MHC class I)
IRp60	Unknown
KIR2DL1	HLA-C2 (MHC class I)
KIR2DL2	HLA-C1 (MHC-class I)
KIR2DL3	HLA-C1 (MHC class I)
KIR2DL5	Unknown
KIR3DL1	HLA-Bw4 (MHC class I)
KIR3DL2	HLA-A3/-A11 (MHC class I)
KLRG1	Cadherins
LAIR1	Collagen
LILR	UL18 (MHC class I)
NKR-P1A	LLT-1
TIGIT	CD155 (PVR), CD112 (PVRL2, nectin-2)

Abbreviations: AIRM1, adhesion inhibitory receptor 1, CD, cluster of differentiation, HLA, human leukocyte antigen, KLRG1, killer cell lectin-like receptor G1, LAIR1, leukocyte-associated immunoglobulin-like receptor 1, LILR, leukocyte immunoglobulin-like receptor, LLT-1, lectin-like transcript 1, NKR-P1A, NK receptor P1A, TIGIT, T cell immunoreceptor with immunoglobulin and ITIM domains.

1.1.2.5ib Activating receptors

NK cells can be classed as resting or activated, based on their activity and expression of inhibitory and activating receptors. Activated NK cells are able to carry out lysis of target cells, however even prior to their activation, resting NK cells are not completely unresponsive, but their functions are more tightly regulated than NK cells which have been fully activated by IL-2 (North et al. 2007). Resting NK cells are less active and are generally less able to carry out their lytic functions compared to IL-2-activated NK cells (Bryceson et al. 2006).

NK cell activation requires two conditions to be met: firstly, target cells must not express MHC class I molecules, utilising the “missing self” hypothesis, that NK cells

preferentially kill cells with reduced or aberrant expression of MHC class I antigens, as shown in Figure 1.2b (Zamora et al. 2015). Secondly, the same cells must express ligands for NK cell activating receptors, which are upregulated on transformed or virally infected cells (Tremblay-Mclean et al. 2019). NK cells express a wide range of activating receptors, which, like the inhibiting receptors, are expressed in combination and have a range of ligands enabling widespread initiation of NK effector functions. Activating receptors include CD16, CD314, NKG2D, CD226 (DNAM-1), CD244 (2B4), members of the CD158 (KIR) family that carry a short cytoplasmic tail (KIR2DS and KIR3DS) and CD94 (NKG2C), among others (Zwirner and Ziblat 2017). A further group of activating receptors are the natural cytotoxicity receptors (NCRs) CD335 (NKp46), CD336 (NKp44) and CD337 (NKp30), which are potent inducers of NK cytotoxicity and have key roles in NK-mediated tumour cell immunosurveillance (Kumar 2018). A list of activating receptors and their ligands can be found in Table 1.2.

The majority of activating receptors including CD16, NCRs and activating KIRs, signal through immune-receptor tyrosine-based activation motifs (ITAMs) within their cytoplasmic domains (Medjouel Khlifi et al. 2022). Within the ITAM, tyrosine residues interact with gamma chains of the high affinity IgE receptor FcεRI (FcεRI-γ), zeta chains of CD3 (CD3-ζ) and DNAX activation protein of 120kDa (DAP12) transmembrane proteins to form homo- and hetero-dimer signalling subunits. Engagement of these receptors results in the subsequent phosphorylation of the ITAM tyrosine by Src family members, followed by binding of the tyrosine kinases SYK and zeta-chain-associated protein kinase 70 (ZAP-70) (Medjouel Khlifi et al. 2022). Signalling through a number of pathways is then initiated, including via the mitogen-activated protein kinase/extracellular signal-related kinase (MAPK/ERK) and phosphoinositide 3-kinase/protein kinase B (PI3K/Akt) pathways to regulate gene transcription (Lanier 2008).

Other groups of activating receptors lacking ITAMs signal through alternative mechanisms upon interaction with their ligands. NKG2D is a type II transmembrane receptor which has no ITAM, and instead forms a hexamer receptor complex with two DAP10 homodimer signalling units. Upon interaction with its ligand, the p85 subunit of PI3K and the son of sevenless homolog 1–vav guanine nucleotide exchange factor 1-growth factor receptor bound protein 2 (Sos-1-Vav1-Grb2)

complex are recruited to the phosphorylate motif in the DAP10 domain (Medjouel Khlifi et al. 2022). NKG2D is an important immunosurveillance receptor which responds to stress-induced ligand overexpression on virally infected and transformed cells (Figure 1.2c). Activation of this receptor leads to the downstream activation of Guanosine-5'- triphosphate (GTP)ases, ERK, Akt and signal transducer and activator of transcription 5 (STAT5), promoting NK cell target adhesion and immunological synapse (IS) formation (Upshaw et al. 2006).

A further alternative method of activation receptor induction is that employed by CD16 (FcγRIIIA), which initiates antibody-dependant cell-mediated cytotoxicity (ADCC) through recognition of the constant Fc portion of IgG antibodies bound to specific antigens displayed on infected or transformed cells (Figure 1.2d). Following this engagement, the release of cytotoxic granules results in tumour cell death, alongside release of proinflammatory cytokines such as IFN-γ and chemokines which leads to the recruitment and activation of further tumour-infiltrating immune cells to increase the cytotoxic response (Yeap et al. 2016). NK cell expression levels of CD16A have been positively correlated with the cytotoxic potency of NK cells, and levels are downregulated in the tumour microenvironment (TME) of many cancer types, contributing to NK cell dysfunction (Medjouel Khlifi et al. 2022).

Table 1.2 Activating NK cell receptors and their ligands

Activating receptor	Ligand
CD314 (NKG2D)	MIC-A/-B, ULBP-1/-2/-3/-4
CD335 (NKp46)	Viral HA, HSPG
CD16 (FcRγIII)	Fc portion of IgG
CD226 (DNAM-1)	PVR, CD122
CD244 (2B4)	CD48
CD336 (NKp44)	Viral HA
CD337 (NKp30)	BAT-3, HSPG, B7-H6
CD94 (NKG2C/NKG2E)	HLA-E (MHC class I)
KIR2DL4	HLA-G (MHC class I)
KIR2DS1	HLA-C2 (MHC class I)
KIR2DS2	HLA-C1 (MHC class I)
KIR2DS3	Unknown
KIR2DS4	Unknown
KIR2DS5	Unknown
NKp80	AICL

Abbreviations: AICL, activation-induced C-type lectin, BAT-3, HLA-B-associated transcript 3, HA, hemagglutinin, HLA, human leukocyte antigen, HSPG, heparan sulphate proteoglycan, MIC, MHC class I polypeptide-related sequence, PVR, polo virus receptor, ULBP, UL16 binding protein.

1.1.2.5ii NK cell activity

An activating NK cell IS is formed following the interaction of an NK cell with a target cell which both express activating stress-response ligands but lack inhibitory MHC class I ligands. Formation of an IS induces target cell death either through direct lysis caused by degranulation of lytic molecules, or target cell death receptor ligation (Orange 2008). NK cell degranulation and is used as an indirect measure of NK cell cytotoxic activity and the process can be divided into four major stages: (1) Formation of the IS between NK cell and target cell, followed by reorganisation of the actin cytoskeleton, (2) Polarisation of the microtubule organising centre (MTOC) and secretory lysosome towards the IS, (3) Docking of the secretory lysosome with the NK plasma membrane and (4) Fusion of the secretory lysosome with the plasma

membrane and release of lytic granules containing perforin, granzymes, TRAIL, granulysin and anti-microbial peptides into the target cell (Paul and Lal 2017). Perforin polymerises and forms pores in the cell membrane, facilitating the entry of granzymes into the target cell where they activate caspase molecules leading to the induction of apoptosis. NK cells can also induce apoptosis via the extrinsic pathway through the expression of FasL and TRAIL on their cell membrane, which interact with the death receptors Fas and TRAIL-R respectively on target cells. This interaction leads to ligation and formation of the death-inducing signalling complex with subsequent activation of death signalling via the caspase cascade (Sordo-Bahamonde et al. 2020).

NK cells are also effective producers of chemokines and pro-inflammatory cytokines which recruit other innate cells to the site of inflammation, such as neutrophils, macrophages and DCs, alongside other myeloid and lymphoid cells (Abel et al. 2018). These cytokines include TNF, IFN-γ, IL-5, IL-10, and granulocyte/monocyte colony-stimulating factor (GM-CSF). Production of chemokines such as IL-8, chemokine (C-C motif) ligand 3 (CCL3), CCL4 and CCL5 are essential to mediate antiviral, antibacterial and antitumour activity. Additionally, the activity of NK cells is also susceptible to influence from cytokines produced by other immune cells (Paul and Lal 2017).

1.1.3 Adaptive immune cells

Cells of the adaptive arm of the immune system arise from a common lymphoid progenitor in the bone marrow and differentiate into subsets of either T or B cells, depending on where the maturation occurs.

1.1.3.1 B lymphocytes

B cells develop in the bone marrow within niches which provide the appropriate stimuli to allow B cell survival and differentiation into plasma cells, which subsequently produce antibodies, and have a key role in humoral immunity. B cells are continuously produced in the bone marrow (Chaplin 2010; Marshall et al. 2018). B cells are the major component of the humoral response in adaptive immunity. B

cells produce highly specific Ig antibodies which are capable of directly neutralising pathogens, but also have further roles in activation of the complement cascade and cytokine production (Hoffman et al. 2016). B cells can recognise antigens directly with no need for priming from APCs. B cells can however act as APCs for T cell activation and secrete cytokines to strengthen the innate and adaptive immune responses (Marshall et al. 2018). B cells develop from a common lymphoid progenitor in the foetal liver and bone marrow, following which, rearrangement of the IG heavy and light chain genes creates a complete surface IgM class Ig molecule (Shahaf et al. 2016). In association with Igα and Igβ, the IgM molecules form a unique B cell receptor (BCR). Immature IgM+ B cells then migrate to secondary lymphoid organs, where they differentiate into long-lived follicular (FO) B cells or marginal zone (MZ) B cells, based on the strength of their BCR signalling (Pillai and Cariappa 2009). Following specific antigen presentation by an APC and recognition by the BCR, B cells next undergo either a T cell-dependant or -independent activation process to differentiate into short-lived antibody-secreting plasma cells or long-lived memory B cells. Plasma cells produce large amounts of antibodies providing effective protection against pathogens, while long-term memory B cells “remember” antigens from past infections, enabling a rapid response upon re-exposure to the same antigen. A third subtype, B1 cells, produce low affinity natural antibodies (nAbs) for regulation of tissue homeostasis in the absence of exogenous antigenic stimulation (Rodriguez-Zhurbenko et al. 2019).

1.1.3.2 T lymphocytes

T cells are responsible for cellular immunity and are derived from cells which migrate to the thymus, where they mature and differentiate into early thymic progenitors, before finally differentiating into functional T cells. In healthy adults, T cell numbers are maintained through division of mature T cells outside of the lymphoid organs (Chaplin 2010). T cells are responsible for many aspects of adaptive immunity, including responses to pathogens, allergens, and tumours, alongside maintenance of immunological memory and self-tolerance. T cell differentiation proceeds in a series of steps beginning with the migration of committed lymphoid progenitors from the bone marrow to the thymus, where they lose the potential to become B or NK cells and express a pre-T cell receptor (TCR), comprised of CD3, a non-rearranging pre-

Tα chain and a rearranged TCR β-chain (Aifantis et al. 2001). Upregulation of CD4 and CD8 co-receptors occurs following pre-TCR expression, resulting in their proliferation and upregulation, allowing transition of immature thymocytes from $CD4^-$ $CD8^-$ double negative (DN) to the $CD4^+CD8^+$ double positive (DP) stage. At the DP stage, the pre-Tα chain is replaced with a rearranged TCR α-chain forming a complete αβ TCR, which induces cell cycle progression and differential gene expression in developing T cells. DP cells can subsequently interact with endogenous peptides presented on MHC class I and II molecules within the thymus to determine differentiation into single-positive, CD4+ or CD8+ mature T cells, which then migrate into secondary lymphoid organs to execute their effector responses (Winandy et al. 1999).

1.1.3.2i Antigen presentation

The activation and differentiation of T cells is directly influenced by APCs of the innate immune system, and is crucial for initiation of the adaptive immune response, creating a link between the two systems (Gaudino and Kumar 2019). Upon encountering a pathogen, mature APCs (DCs, macrophages and B cells) phagocytose and internalise peptide fragments of the antigen, subsequently displaying those peptides bound to an MHC molecule on their membrane (Mantegazza et al. 2013). APCs next migrate into lymph nodes where they provide naïve T cells with the signals to stimulate differentiation and proliferation into antigen-specific T cells with a range of functions appropriate to the immunological challenge. T cells require two stimulatory signals to become fully activated, firstly the antigen-specific signal sent via the TCR, and secondly an additional co-stimulatory signal produced by the APC leading to full activation of the T cell, which is critical to sustain cell proliferation, differentiation into effector or memory status and avoid apoptosis (Frauwirth and Thompson 2002). MHC class I and II molecules are able to stimulate CD8+ and CD4+ T cells respectively and secure binding is essential to elicit a full immune response, with incomplete binding leading to apoptosis (Roche and Furuta 2015). Polarizing cytokine release from the APC is a further determinant of lymphocyte differentiation, with a number of possible outcomes depending on the cytokines present within the microenvironment (Willerslev-Olsen et al. 2013). The successful activation and differentiation of antigen-specific T cells leads to clonal

expansion of these differentiated cell populations as they migrate to the site of infection. Upon successful elimination of the pathogen, most T cells die, leaving behind a small proportion of memory T cells which are able to instigate a rapid immune response upon re-exposure to the same pathogen (Omilusik and Goldrath 2017).

1.1.3.2ii CD4+ T cells

CD4+ T cells play a key role in the innate and adaptive immune responses. Due to their ability to assist B cells in antibody production, activation of innate immune cells, cytotoxic T cells and non-immune cells, enhancement of macrophage microbial activity and production of chemokines and cytokines to recruit innate immune cells to infection sites, Th cells enhance both the cellular and humoral immune responses (Luckheeram et al. 2012). Naïve CD4+ T cells are activated through antigen presentation by MHC class II molecules, following which differentiation into one of seven phenotypes depends on the complex network of specific cytokine signalling and transcription factors present in the microenvironment, followed by epigenetic modifications (Zhu et al. 2010). The seven lineages of CD4+ T cells are T helper (Th) 1, Th2, Th9, Th17, Th22, T follicular helper (Tfh) and regulatory T cells (Tregs), which are distinguishable by their individual functions and cytokine profiles (Golubovskaya and Wu 2016).

Th1 cells are differentiated from naïve CD4+ cells in the presence of IL-12, IL-18 and IFN-γ secreted by macrophages and activated DCs (Golubovskaya and Wu 2016). Th1 cells are key regulators of type 1 immunity through their production of pro-inflammatory cytokines including IFN-γ, IL-2 and TNF, which stimulates neighbouring macrophages and DCs to increase their phagocytic and antigen-presenting functions, therefore enhancing the immune response (Zhu et al. 2010). Th1 cells play a key role in the anti-cancer immune response as they directly kill tumour cells through release of cytokines which activate death receptors on the tumour cell surface (Knutson and Disis 2005).

Th2 cells are induced by IL-2, IL-4, IL-25 and IL-33 produced by eosinophils and mast cells, and following differentiation are key mediators of type 2 immunity (Kasatskaya et al. 2020). Th2 cells induce immunoglobulin class switching to IgE

which activates other innate immune cells including mast cells and basophils, alongside secretion of IL-4, IL-5 and IL-13, which enhances the survival of B cells (Golubovskaya and Wu 2016).The role of Th2 cells in cancer development is unclear, with both pro- and anti-tumour roles reported (Ellyard et al. 2007), however Th2 cells are generally associated with a pro-tumour immune environment, tumour growth and metastasis. Th2 cells have been associated with cytokine release and T cell anergy, leading to the polarisation of M2 tumour-associated macrophages (Tokumaru et al. 2020), however direct evidence for cancer development in relation to the presence of Th2 cells has not been reported (Schreiber et al. 2021)

Th9 cells, a relatively newly discovered subtype, are induced through the production of TGF-β and IL-4, and due to their secretion of IL-9 and pro-inflammatory cytokines, have roles in growth promotion of mast cells and robust anti-tumour responses. Th9 cells also have further important roles in mucus production and eosinophil infiltration during allergic reactions (Chen et al. 2019).

Th17 cells are induced by IL-6, IL-21, IL-23 and TGF-β and have key roles in mediating responses against extracellular bacteria and fungi through their production of inflammatory cytokines including IL-17, IL-22, IL-26, TNF and CCL20 (Tesmer et al. 2008). The role of Th17 in anti-tumour immunity is unclear and may depend on tumour type. It has been reported that IL-17 derived from Th17 cells was associated with increased angiogenesis and poor outcomes in colorectal carcinoma, however in melanoma, Th17 produced more effective anti-tumour responses than Th1 cells. Furthermore, Th17 cells were able to promote dendritic cell infiltration and antigen presentation, resulting in a strong CD8+ anti-tumour response in mouse melanoma models (Chen et al. 2020).

Th22 cells are induced by IL-6 and TNF secreted from plasmacytoid DCs and have roles in skin inflammation and wound healing following their expression of IL-22, and CCR4, CCR6 and CCR10, which allow infiltration into the epidermis (Pan et al. 2022). Th22 cells are generally associated with cancer progression and poor prognosis, and recent studies suggest that targeting the IL-22/IL-22R pathway could be a potential therapeutic target (Doulabi et al. 2022).

Tfh cells are important mediators of B cell activity, with key roles in the differentiation of B cells into plasma cells and memory B cells, alongside the formation of germinal

centres. Tfh cells were first identified in the human tonsil, but are found throughout the germinal centres of secondary lymphoid tissues including the spleen and lymph nodes. Tfh cells are induced by the presence of IL-6, IL-12 and IL-21 and express the greatest quantity of co-stimulatory molecules and possess the TCRs with the highest antigen affinity of all Th subsets (Crotty 2019). Tfh cells produce IL-21, alongside expression of the co-stimulatory molecule CD40 which interacts with CD40-L on the B cell surface, to drive B cell proliferation. In the absence of Tfh cells, germinal centres do not form, resulting in loss of B cell-mediated antibody production (Stebegg et al. 2018). Due to their roles in regulation of B cells in both normal states and during development of diseases including cancer, this focus will examine Tfh cells as part of the normal and cancer-associated immune responses. Tfh cells are associated with unfavourable outcome in B-cell associated malignancies, while increased levels of Tfh cells are associated with better outcome in some solid tumour types, however the role of Tfh cells in cancer development is not yet well understood. The participation of Tfh cells in the anti-tumour response appears to be context-dependant and relies on the presence of various cytokines and interactions with other cells (Gutiérrez-Melo and Baumjohann 2023). This topic remains an activate research area, with Tfh cells thought to be a promising target to regulate cancer development either through the blockade of Tfh-associated B cell development in B-cell malignancies, or through boosting of the anti-tumour functions via the interaction of Tfh cells with CD8+ cytotoxic T cells (Niogret et al. 2021).

1.1.3.2iii CD4+CD25+Foxp3+ regulatory T cells

Regulatory T cells (Tregs) are a highly important subset of CD4+ cells, characterised by the nuclear expression of Forkhead box P3 (FoxP3), which maintain immune homeostasis by the active suppression of macrophages, DCs, B and T cells to limit inappropriate or excessive immune responses (Magg et al. 2012). FoxP3 is a critical regulator of Treg development, function and homeostasis and is essential for the suppressive function and activity of Tregs (Schmitt and Williams 2013). Tregs are primarily generated in the thymus (natural Tregs; nTregs), but can also be generated extrathymically at peripheral sites or generated *in vitro* from CD4+ T cells in the presence of TGF-β and IL-2 (induced Tregs, iTregs) (Shevach and Thornton 2014). nTregs are predominantly found in the lymph nodes and blood stream, and

constitutively express Foxp3, with key roles in providing tolerance to self-antigens. iTregs are found in barrier tissues and recognise foreign antigens with high affinity in states of chronic inflammation to control the inflammatory response (Schmitt and Williams 2013). Lack of functional Tregs results in a range of primary immunodeficiencies including immunodysregulation polyendocrinopathy enteropathy X linked (IPEX) syndrome, Omenn syndrome and hyper IgE syndrome, and so protocols to induce or restore Treg function have gained interest in recent years (Schmetterer et al. 2012).

Due to their key role in regulation of immune responses, both in normal conditions and in the development of diseases including cancer, this thesis will examine the role of Tregs as part of the normal and cancer-associated immune responses. Tregs regulate the immune response and maintain immune homeostasis through a number of mechanisms depending on target cell type and activation status, as well as the location and cytokine and microorganism milieu of the immune reaction. Treg actions may occur either through the release of immunosuppressive cytokines such as IL-10, TGF-β and IL-35, metabolic disruption, induction of apoptosis and downregulation of co-stimulatory molecules on APCs such as DCs (Schmidt et al. 2012).

1.1.3.2iv CD8+ cytotoxic T cells

CD8+ T cells or are often referred to as cytotoxic T lymphocytes (CTLs) due to their main function of destroying infected or malignant cells in an antigen-dependant manner. Following recognition of MHC class I molecules presenting antigenic peptides, CD8+ T cells proliferate and differentiate into either CTLs or memory CD8+ T cells, and migrate to sites of infection (Cui and Kaech 2010).

CTLs are highly cytotoxic, IL-2 dependant, and rapidly express TFN, IFN-γ, granzymes and perforin upon antigen recognition and activation (Kelso et al. 2002). Following activation, CTLs use three major mechanisms to kill target cells: (i) via the interaction of FasL on CTLs with Fas on target cells, triggering the classical caspase cascade and subsequent apoptosis of the target cell, (ii) secretion of cytokines, primarily TNF and IFN-γ, to also trigger the caspase cascade resulting in Fas-mediated apoptosis and increased MHC class I antigen presentation, and (iii) production and release of cytotoxic granules including perforin, to form a pore in the

cell membrane, and granzymes to degrade the target cell membrane and induce apoptosis followed by phagocytosis (Barry and Bleackley 2002).

The other final product of CD8 cell differentiation is memory CD8+ T cells, which provide antigen-specific, long-term immunity against viral and bacterial agents. These cells are found in high numbers in peripheral tissues and are long-lived and maintained through IL-15 and IL-17-driven self-renewal, ready to rapidly respond to secondary infections (Turtle et al. 2009). Memory T cells exist in a “pro-growth” state, characterised by the mRNA expression of anti-viral cytokines, chemokines and cytotoxic proteins which allow them to expand and develop their effector functions faster than naïve CD8+ T cells to create a rapid and antigen-specific response (Samji and Khanna 2017).

1.1.4 The cancer-immunity cycle

The generation of immunity to cancer is a cyclic process known as the cancer-immunity cycle, which is self-propagating and leads to an accumulation of immune-stimulatory factors that increase and broaden T cell responses. This cycle is characterized by inhibitory factors which result in immune regulatory feedback mechanisms that limit or stop development of immunity. The cancer-immunity cycle can be divided into seven major steps which begins with the release of antigens from the cancer cell and ends with the killing of cancer cells, releasing antigens to restart the cycle (Chen and Mellman 2013), as described in Figure 1.3.

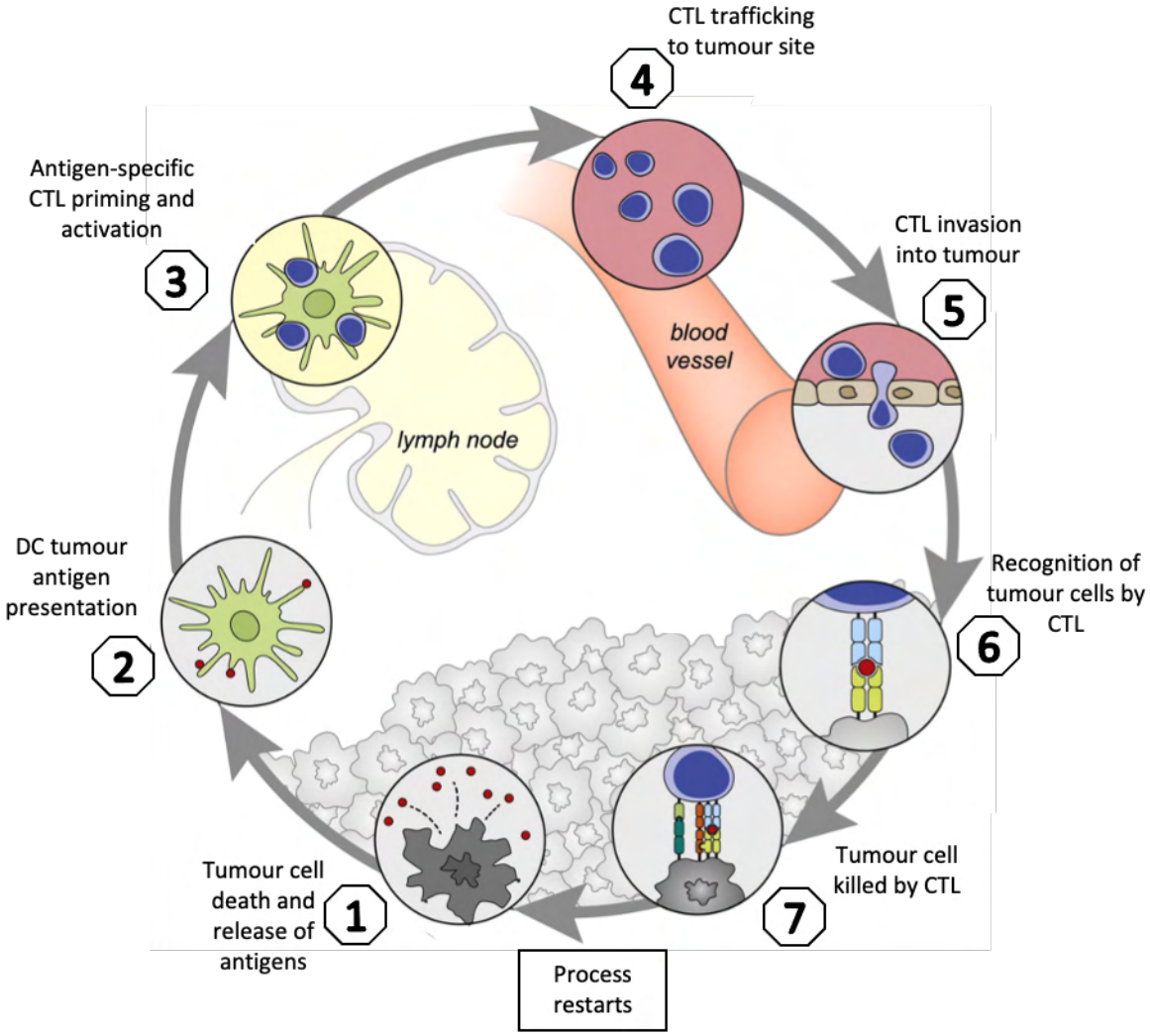

Figure 1.3 The cancer-immunity cycle
The cancer-immunity cycle is a cyclic process of anti-tumour immune responses, beginning with tumour cell death and associated release of antigens (step 1). Antigens are presented to CTLs resulting in their priming and activation, following which the CTLs are trafficked to the tumour site where invasion occurs (steps 2-5). Tumour cells are recognised by the CTLs (step 6), and the cycle ends with tumour cell killing by CTLs resulting in the release of cancer cell antigens (step 7), which restarts the process. Adapted from Chen and Mellman 2013. Created in BioRender.com.
Abbreviations: CTL, cytotoxic T lymphocyte, DC, Dendritic cell.

The first step in the cycle is the capture of cancer cell antigens by DCs, created through the loss of cellular regulatory processes and accumulation of genetic alterations. This step must be accompanied by immunogenic signals such as proinflammatory cytokines and factors released by dying cancer cells, otherwise peripheral tolerance to the tumour antigens may be induced and no T cell responses will be induced. In step 2, DCs present the tumour antigens to T cells on MHC class I and II molecules, resulting in the priming and activation of antigen-specific effector T cell responses (step 3). At this point, the nature of the immune response has been determined, with the critical balance between the ratio of effector T cells compared to Tregs being key to the outcome. The activated effector T cells next traffic to tumours through the blood vessels (step 4) and infiltrate the tumour bed (step 5), where they recognise and bind to cancer cells through their TCR and MHC class I-bound antigens (step 6), and the cancer cell is killed (step 7). Following cancer cell death, the release of additional tumour-associated antigens triggers step 1 of the process, restarting the cancer-immunity cycle (Chen and Mellman 2013). In cancer patients, a number of issues may cause the cycle to not complete correctly, including non-detection of tumour antigens, incorrect recognition of antigens as self rather than foreign resulting in Treg-induced immunosuppressive responses rather than effector responses, or incomplete tumour infiltration (Motz and Coukos 2013).

1.1.5 Cancer immunoediting

Cancer immunoediting is the theory that the immune system is able to both constrain and promote tumour development. The theory proceeds through three key stages: elimination, equilibrium and escape (Dunn et al. 2004), represented in Figure 1.4. Throughout these three phases, tumour immunogenicity is edited by the adaptive immune system and edited tumours are able to escape the immune system resulting in unrestrained growth.

1.1.5i Elimination

The elimination phase is the classical concept of cancer immunosurveillance, where innate and adaptive immune cells are able to detect transformed cells that have

escaped intrinsic tumour suppression mechanisms such as p53, and eliminate them before they become clinically apparent (McCoach and Bivona 2018). These tumours cells express stress-induced molecules, cancer cell antigens such as MHC class I molecules and NKG2D ligands recognised by CTLs and NK cells, Fas and TRAIL-R, tipping the balance to an effective anti-tumour response resulting in the elimination of the cancer cells and the end of the immunoediting process (Mittal et al. 2014).

1.1.5ii Equilibrium

In the equilibrium phase, tumour cells which were not destroyed in the elimination phase enter a dynamic equilibrium where the tumour mass is controlled by immunologic mechanisms, however the tumour cells have not been destroyed (Dunn et al. 2004). Unlike the elimination stage, where both adaptive and innate immunity is involved, the equilibrium stage only involves the adaptive immune system. This equilibrium process can occur over a period of many years or even throughout the life of the host, however tumour cells at this stage may be highly genetically unstable and have high mutational burden. This, coupled with the selective pressure from the adaptive immune system, can select for tumour subclones with reduced immunogenicity that can evade immune recognition and subsequent destruction, tipping the balance towards immune escape and development of clinically apparent disease (Rojas-Domínguez et al. 2022).

1.1.5iii Escape

The escape stage is the final stage of immunoediting. By this stage, cancer cells have acquired significant beneficial genetic and epigenetic changes, allowing them to evade detection and elimination by the immune system and grow to present as clinically apparent disease. Escape from immune control is now recognised as one of the hallmarks of cancer (Hanahan and Weinberg 2011). These tumours exhibit unrestrained growth and are likely to be able to evade further innate and adaptive immune responses (Dunn et al. 2004). Mechanisms to enable tumour escape can be classified into three main types: (i) Loss or downregulation of tumour antigens and/or antigen-presenting mechanisms, in combination with reduction of co-stimulatory molecules resulting in reduced immune recognition and activation, (ii) Upregulation

of anti-cytotoxic mechanisms and (iii) Induction of an immunosuppressive TME through upregulation of suppressive immune cells such as Tregs, alongside production of anti-inflammatory cytokines and overexpression of inhibitory immune checkpoint ligands (Mittal et al. 2014).

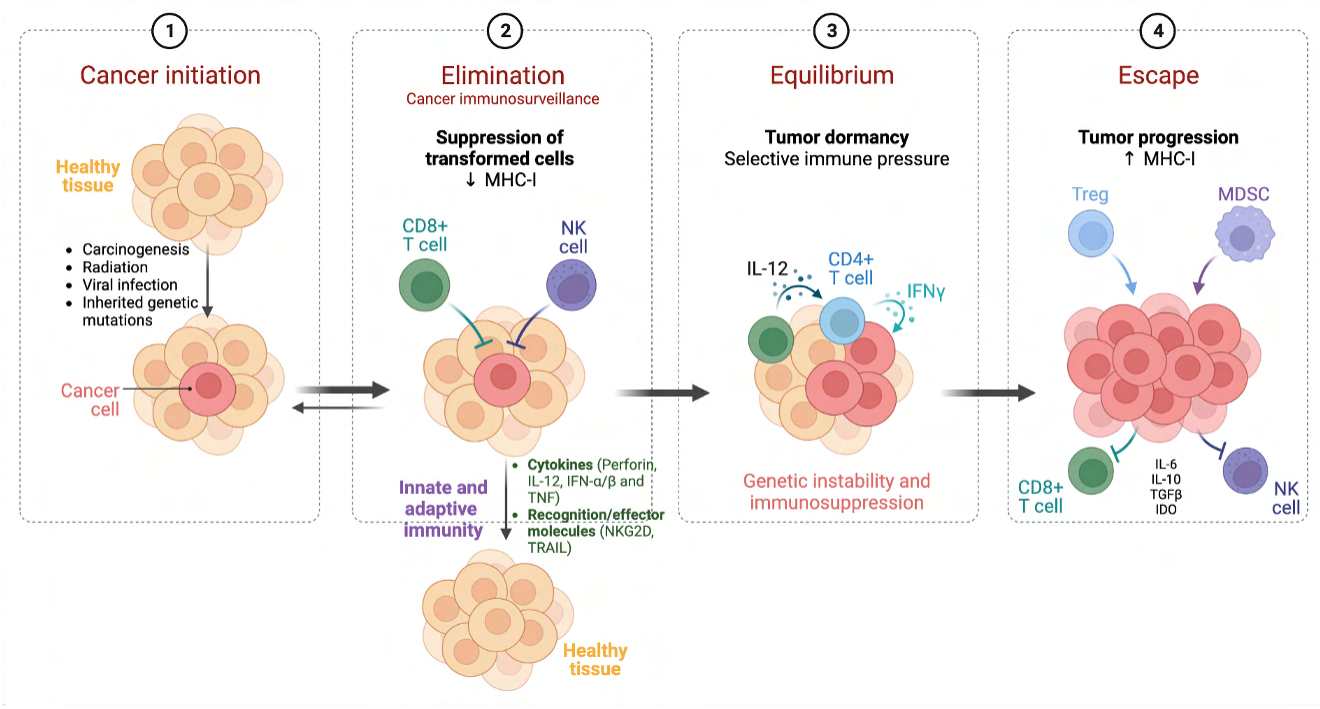

Figure 1.4 Cancer immunoediting
The three phases of cancer immunoediting. (1) Healthy cells gain mutations and begin cancer development, (2) The immune system acts as an intrinsic tumour suppression mechanism to identify and eliminate tumour cells. Transformed cells express high levels of cell stress ligands and tumour antigens which can be recognised by both the innate and adaptive immune systems, following which they can be destroyed. If the immune system is unable to eliminate the transformed cells, surviving tumour cells may enter the equilibrium phase. If the immune system is able to successfully clear the tumour cells, the healthy cells remain as healthy tissue. (3) In the equilibrium phase, tumour cells are either chronically maintained in an equilibrium state by the adaptive immune system which prevents further growth, or selection for cells with poor immunogenicity creates a subpopulation which may acquire further mutations and tip the balance into the escape phase. (4) Poorly immunogenic and immunosuppressive cell variants escape immune control and become clinically detectable. Tumour cells use several mechanisms to escape immune control including decreased immune recognition, increased resistance to immune effector responses and generation of an immunosuppressive TME through recruitment of immunosuppressive cytokines. Adapted from Schreiber et al 2011. Created in BioRender.com.
Abbreviations: MDSC, myeloid derived suppressor cell, MHC, major histocompatibility complex, NK, Natural killer cell, Treg, regulatory T cell.

1.1.6 Mechanisms of immune escape

Cancer cells are able to avoid immune destruction by a number of mechanisms including avoiding immune recognition and disabling effector cell function. These mechanisms allow escape from both the innate and adaptive immune responses,

enabling unrestricted tumour development and growth. Tumour cells are also able to induce and recruit immunosuppressive immune cells and cytokines within the TME to prevent an effective anti-tumour immune response. The identification of these various escape mechanisms have also formed the basis for the generation of immunotherapeutic strategies (Kim and Cho 2022).

1.1.6.1 Decreased immune recognition

The immune system is able to distinguish between malignant and normal cells based on the expression of MHC-antigen complexes displayed on their cell surface, which are recognised by antigen-specific T cells. One of the most common mechanisms to reduce tumour antigenicity and immune recognition is downregulation of MHC class I molecules, which can be done with no impairment to the cell's survival or ability to grow and metastasise (Cornel et al. 2020). This downregulation has been described in 40-90% of human cancers and is an independent prognostic factor in many cancer types including breast, prostate and lung cancers, where this mechanism may also contribute to immunotherapy resistance (Taylor and Balko 2022). The loss of MHC class I molecules should in principle result in NK cell-mediated killing of these cells through the "missing self" hypothesis, however MHC class I negative tumours have not been reported to have a higher NK cell infiltration than those with normal expression. This implies utilisation of further mechanisms of immune evasion and reduction of NK anti-tumour activity, such as expression of inhibitory cytokines including TGF-β, which enable tumour cells to avoid "missing-self" surveillance by NK cells (Taylor and Balko 2022).

1.1.6.2 Immune resistance

Downregulation of cell surface antigens is a mechanism used by tumour cells to avoid immune cell detection and killing. These cells may also develop further resistance mechanisms to avoid the cytotoxic effects of effector immune cells. Resistance can develop through expression of anti-apoptotic molecules such as cellular FLICE (FADD-like IL-1β-converting enzyme)-inhibitory protein (c-FLIP) and B cell lymphoma extra-large (BCL-XL), or through constitutive activation of pro-oncogenic transcription factors such as STAT3. A further mechanism is through

downregulation and mutation of death receptors such as the TRAIL death receptor 5 (DR5) and Fas, enabling cells to resist apoptosis induced by CTLs and NK cells (Vesely et al. 2011).

1.1.6.3 Immunosuppressive TME

Interactions between tumour cells and the surrounding TME are essential for tumour initiation, growth, invasion and metastasis. The TME is a complex heterogenous ecosystem comprised of the ECM, vasculature, endothelial cells, fibroblasts, the lymphatic system and infiltrating immune cells. Development of a locally immunosuppressive TME is a key mechanism for tumour cell evasion of innate and adaptive anti-tumour immune responses, with significant impact on patient survival and response to treatment (O'Donnell et al. 2018). The presence and activation status of immune cells infiltrating the TME, alongside their production of cytokines and chemokines, affect the balance between an anti- or pro-tumour TME (Labani-Motlagh et al. 2020).

Tumour secretion of regulatory cytokines, growth factors and proteases alter the phenotype of the immune infiltrate. This, alongside increased recruitment of immunosuppressive regulatory cells to the tumour site creates an immunosuppressive environment, reducing the effectiveness of the anti-tumour response (Baghban et al. 2020). TGF-β is a key mediator of this activity and is able to inhibit multiple stages of anti-tumour immunity simultaneously, including inhibition of DC activation and migration, direct inhibition of T cell and NK cell function and promotion of CD4+ cell differentiation in to Th2 and Tregs (Labani-Motlagh et al. 2020). Vascular endothelial growth factor (VEGF) has also been reported to have immunosuppressive effects through inhibition of the function and interactions of T cells and DCs, reducing cytotoxicity of NK cells and preventing sufficient antigen uptake and presentation (Ribatti 2022). VEGF is also a critical factor for development of tumour angiogenesis, one of the hallmarks of cancer. Alongside increasing the tumour's potential to survive and grow, establishment of new abnormal vasculature forms a physical barrier which prevents the trafficking of effector immune cells into the tumour (Geindreau et al. 2021). In addition to these agents, a number of inflammatory mediators present in the TME such as TNF-α, IL-6, IL-10, IL-12 and IL-23 are able to contribute to cancer development, metastasis and immune evasion

through suppression of key immune cells such as macrophages and T cells, and so have become attractive targets for cancer treatments (Morris et al. 2022).

1.1.6.4 Negative co-stimulatory pathways

Immune cell activation is tightly regulated by a balance between co-stimulatory and co-inhibitory signals to avoid overactivation of the immune response, chronic inflammation and autoimmunity. For an immune cell to become activated, the balance of stimulatory and inhibitory signals, referred to as immune checkpoints, must favour the stimulatory signal. However, in cancer, the signal is often weighted towards the inhibitory signal, resulting in downregulation and inhibition of the required anti-tumour response. Immune regulation is mediated by immune cells including macrophages and Tregs, regulatory cytokines such as TGF-β, and immune checkpoints including cytotoxic T-lymphocyte-associated protein 4 (CTLA-4), programmed death protein 1 (PD-1), T cell immunoglobulin and mucin domain-3 (TIM3), T cell immunoglobulin and ITIM domain (TIGIT) and lymphocyte activation gene-3 (LAG3) (He and Xu 2020). In normal conditions, these mechanisms are able to maintain homeostasis, however tumour cells are able to enhance these regulatory mechanisms to enable immune escape and subsequent tumour growth (Marin-Acevedo et al. 2018).

Immune checkpoints are negative co-stimulatory pathways which are activated by interaction with their specific ligand. This interaction regulates the activation and function of T cells at various points in the immune response. The most well studied immune checkpoints are CTLA-4 and PD-1, however several others with roles in cancer development have been identified. CTLA-4, LAG3, TIM3 and TIGIT interact with their ligands during the T cell priming stage resulting in limited T cell activation, while PD-1 interacts with its ligand during the effector phase to regulate the activity of activated T cells (Dyck and Mills 2017). Ligation of these receptors results in ITIM inhibitory signalling, which can be inhibited by blocking antibodies preventing ligand-receptor interactions. Several monoclonal antibody immune checkpoint inhibitors (ICIs) are now licenced to treat a number of solid and haematological malignancies, which aim restore the anti-tumour immune response by to reducing T cell suppression (He and Xu 2020).

1.1.6.4i CTLA-4

One of the most well studied immune checkpoints is CTLA-4, the main role which is thought to be minimisation of normal tissue damage due to inappropriate immune responses (Verhagen et al. 2008). This interaction has however also been reported to inhibit IL-2 production in CD4+ lymphocytes, block T cell proliferation, induce TGF-β production and induce cell cycle arrest, allowing cancer development and immune evasion (Verhagen et al. 2008; Hannani et al. 2015). CTLA-4 is expressed exclusively on activated effector T cells and Tregs, and plays a key role in regulation of T cell activation during priming.

In resting naïve T cells, CLTA-4 is an intracellular protein, which upon engagement of the TCR and the co-stimulatory signal CD28, is rapidly induced on the cell surface. Once expressed on the cell surface, CTLA-4 interacts with its ligands CD80 (B7-1) and CD86 (B7-2) on APCs, in competition with the CD28 receptor. CTLA-4 receptors bind with higher affinity and lower surface density to B7 ligands than CD28 and therefore outcompete for B7 ligand binding (Wu et al. 1997). The resulting ratio of CD28:B7 to CTLA-4:B7 binding is the determining factor of T cell activation, as CTLA-4:CD80/CD86 binding does not produce a stimulatory signal and prevents T cell activation, resulting in anergy (Sansom 2000). If, however sufficient co-stimulatory signalling can occur in the absence of CTLA-4, proliferation of T cells alongside increased cell survival and differentiation into effector or memory cells can take place. Conversely, Tregs constitutively express CTLA-4 and this is crucial for their immunosuppressive functions through sequestration of CD80 and CD86 expression by APCs, preventing binding of effector T cells to APCs (Ha et al. 2019).

1.1.6.4ii PD-1/PD-L1

PD-1 is a cell surface receptor commonly expressed on T cells, B cells, NK cells and some myeloid cells, however it is best characterised in T cells where its expression is induced on the cell surface following antigen presentation. The interaction of PD-1 with its ligands PD-L1 (B7-H1) and PD-L2 (B7-DC) has gained significance throughout recent years, with the approval of several checkpoint inhibitors in many cancer types. PD-1 ligands PD-L1/2 are expressed on a variety of cell types

including T cells, B cells, DCs and myeloid cells, however tumour cells can also express PD-L1 to inhibit anti-tumour T cell responses within the TME, and expression is associated with poor prognosis in many cancer types (Dyck and Mills 2017). PD-L2 expression is restricted to APCs and is primarily expressed on DCs and monocytes, however depending on the microenvironment can also be induced on other cell types including macrophages (Philips et al. 2020). PD-1 and PD-L1/2 are members of the B7 family, which bind to their associated receptors on T and B cells to initiate downstream co-stimulatory or co-inhibitory signalling.

The interaction of PD-1 with its ligands suppresses T cell proliferation and survival by reducing IFN-γ, TNF and IL-2 production and inhibiting anti-apoptotic gene production (Bardhan et al. 2016). If signalling through PD-1 and the TCR occurs in the same T cell, this leads to a further reduction in T cell activation as PD-1 signalling prevents phosphorylation of key TCR signalling components (Mizuno et al. 2019). Chronic antigen exposure such as that found in chronic infection or cancer development can result in persistent PD-1 expression on T cells, which upon ligation with PD-L1/2 results in anti-tumour T cell anergy and exhaustion and this is associated with poor prognosis in many cancer types (Leite et al. 2015).

1.1.6.4iii Immune checkpoint inhibitors

Immune checkpoint inhibitors (ICIs) targeting CTLA-4 and PD-1/PD-L1 have shown good success when used as first- or second- line therapies in several cancer types, including melanoma, renal cell carcinoma (RCC), non-small cell lung cancer (NSCLC), bladder cancer and head and neck carcinoma (Monteiro et al. 2023). A list of ICIs and their approved uses can be found in Table 1.3. ICIs are monoclonal antibodies which aim to restore T cell function, inhibit Treg activity and reverse T cell exhaustion to promote natural anti-tumour immunity (Dyck and Mills 2017). In cancer types with high levels of immune infiltration in their TME, evidence of re-invigoration of anti-tumour immunity upon treatment with ICIs has led to their approval with high levels of success (Maleki Vareki 2018).

1.1.6.4iiia Anti-CTLA-4 antibodies

Ipilimumab, a fully humanised IgG1α anti-CTLA-4 monoclonal antibody (mAb) was the first ICI to be approved by the FDA in 2011 for treatment of metastatic and/or unresectable melanoma. Significant improvements in overall survival were observed of up to 10 years in some patients during clinical trials and Ipilimumab is now also approved as an adjuvant therapy for melanoma patients following surgical resection to reduce the risk of disease relapse (Eggermont et al. 2016). It is unclear exactly how ipilimumab induces an anti-tumour response, however blocking CTLA-4 is thought to enhance the T cell priming phase, promoting activation and proliferation of effector T cells, and simultaneously reducing Treg-mediated suppression of T cell responses.

Despite the promising long-term responses observed in some patients, the broad and non-specific activation of the immune system created by CTLA-4 blockage is associated with a substantial risk of immune-related adverse reactions, reported in over 80% of patients during clinical trials, with grade 3 or higher reactions reported in 10-26% of treated patients (Fellner 2012). These reactions which range from rashes, and endocrinopathies to gastrointestinal problems are consistent with the induced disruption in immune homeostasis characterised by the clonal expansion and activation of new T cell clones, which are normally prevented by CTLA-4-mediated control of CD80 and CD86 signalling (Fecher et al. 2013). This high level of toxicity has reduced the use of Ipilimumab as a single agent treatment, favouring use in combination with anti-PD-1 ICIs to enhance the anti-tumour response.

1.1.6.4iiib Anti-PD-1/PD-L1 antibodies

Anti-PD-1 or anti-PD-L1 antibodies have shown great successes in reducing tumour growth, and a number of anti-PD-1 ICIs are now approved for treatment of many cancer types (Table 1.3). These treatments target the T cell effector phase to restore function to exhausted T cells, resulting in increases in CD8+ T cytotoxic T cell levels and tumour infiltration, ultimately creating an increase in the CD8:Treg ratio and restoring anti-tumour responses (Liu et al. 2021a). Pembrolizumab, a humanised highly specific IgG4 mAb approved for use in advanced or unresectable melanoma, was the first PD-1 ICI to be approved. Due to the successes found in melanoma

treatment, Pembrolizumab has since also been approved for use in in the treatment of PD-1+ metastatic NSCLC, chemotherapy-resistant head and neck squamous cell carcinoma (SCC) and relapsed classical Hodgkin lymphoma (Fessas et al. 2017). Nivolumab is a similar PD-1 IgG4 humanised mAb which has been approved for use in several cancer types including RCC, melanoma and NSCLC. PD-L1 inhibitors such as Atezolizumab, Durvalumab and Avelumab are also highly effective in the treatment of several cancer types. These treatments provide highly targeted inhibition of PD-L1, while still allowing interaction of PD-1 with PD-L2 to maintain self-tolerance and prevent overactivation of the immune system (Ai et al. 2020).

As PD-1/PD-L1 signalling is typically restricted to the TME, unlike the global effects and high incidence of side effects observed with CTLA-4 ICIs, PD-1 ICIs cause lower levels of side effects. Combination therapies of CTLA-4 and PD-1 ICIs have shown good success rates, however the combination of inhibitors working in both the priming and effector phases can lead to a significant increase in adverse effects including rash, gastrointestinal effects and thyroiditis (Somekawa et al. 2022). This combination therapy does however significantly increase treatment efficacy, with the two treatments working synergistically in different locations and at different phases, and so combination treatment of ipilimumab and nivolumab has been approved for several cancer types including RCC, NSCLC, melanoma and colorectal cancer (Vafaei et al. 2022).

1.1.6.4iv Alternative immune checkpoints

The success of CTLA-4 and PD-1 ICIs for the treatment of various cancer types has led to interest in identification of further alternative checkpoints in the hope of discovering future therapeutic single or combination ICI opportunities. Well characterised checkpoints being actively researched for clinical use include LAG3 (Huo et al. 2022), TIM3 (Acharya et al. 2020) and TIGIT (Harjunpää and Guillerey 2020), however these ICIs are yet to be approved for patient use. A further immune checkpoint that has been studied in relation to cancer immune evasion is CD200.

Table 1.3 Approved ICIs for the treatment of cancer.

Adapted from Robert 2020, Lao et al. 2022 and Shiravand et al. 2022.

Drug	Cancer type	Indication
CTLA-4 inhibitors		
Ipilimumab	Melanoma	• Monotherapy for metastatic and unresectable disease • Adjuvant therapy for surgically resectable high-risk disease
PD-1 inhibitors		
Nivolumab	Melanoma	• Monotherapy for metastatic and unresectable disease • Adjuvant therapy for surgically resectable high-risk disease
	NSCLC	• Metastatic disease that has progressed following chemotherapy
	SCLC	• Metastatic disease that has progressed following chemotherapy
	Head and neck SCC	• Recurrent/metastatic disease that has progressed following chemotherapy
	Bladder cancer	• Adjuvant therapy for high-risk patients after surgical resection
	RCC	• Metastatic disease
	Hepatocellular carcinoma	• Second line for patients who have previously received kinase inhibitors
	Hodgkin lymphoma	• Second line following relapse after autologous hematopoietic stem cell transplantation
	Colorectal cancer	• Second line following previous treatment and metastatic disease
Pembrolizumab	Melanoma	• Adjuvant therapy following complete resection when lymph node involvement is present
	NSCLC	• Metastatic disease irrespective of PD-L1 expression
	SCLC	• Metastatic disease
	Head and neck SCC	• Monotherapy for PD-L1 expressing tumours • Combination first-line therapy for unresectable metastatic disease
	Bladder cancer	• Monotherapy for high risk, non-muscle invasive tumours
	Hodgkin lymphoma	• Relapsed/refractory classical Hodgkin lymphoma
	Stomach and oesophageal cancer	• Recurrent locally advanced or metastatic disease • Adjuvant therapy for non-surgically resectable tumours

Atezolizumab	NSCLC	・Adjuvant therapy following resection and chemotherapy where >1% PD-L1 tumour expression ・First line for high PD-L1 expressing metastatic disease and with no EFGR or ALK mutations ・Metastatic disease that has progressed following chemotherapy
	SCLC	・First line combination therapy for advanced disease
	Hepatocellular carcinoma	・Combination therapy for unresectable metastatic disease
	Melanoma	・Combination therapy for *BRAF* V600-mutated unresectable or metastatic disease
	Urothelial bladder cancer	・Locally advanced or metastatic PD-L1 expressing disease or is not eligible for chemotherapy
Durvalumab	NSCLC	・Unresectable advanced disease which has not progressed on chemotherapy or radiotherapy
	SCLC	・First line combination therapy for advanced disease
Avelumab	Merkel cell carcinoma	・Metastatic disease
	Urothelial bladder cancer	・Advanced or metastatic disease which has not progressed on first line chemotherapy
	RCC	・First line treatment for advanced disease
Cemiplimab	SCC	・Locally advanced or metastatic disease where resection or radiotherapy are not possible
Combined CTLA-4 and PD-1 inhibitors		
Ipilimumab and Nivolumab	Melanoma	・Metastatic or unresectable disease
	RCC	・First line treatment for intermediate and poor-risk advanced and metastatic disease
	Colorectal cancer	・Metastatic disease that has progressed on other treatments
	NSCLC	・First line treatment for metastatic disease with >1% PD-L1 tumour expression and no EGFR or ALK mutations

Abbreviations: NSCLC, non-small cell lung cancer, RCC, renal cell carcinoma, SCC, squamous cell carcinoma, SCLC, small cell lung cancer.

1.2 The CD200 immune checkpoint

1.2.1 CD200

CD200, (also known as OX-2), is a type 1 transmembrane glycoprotein related to the B7 family of receptors. This protein is comprised of two Ig-like domains and has a single transmembrane domain with a short, 19 amino acid intracellular domain (Hatherley et al. 2013). Due to its short cytoplasmic domain, CD200 has no known signalling motif and so functions through interaction with a receptor, known as CD200R (Liu et al. 2016). CD200 expression was first characterised in rats as a 41- to 47-kDA cell surface glycoprotein (McCaughan et al. 1987). Expression patterns have since been found to be well conserved in humans and found on a variety of both haematopoietic and non-haematopoietic cells including B cells, some subsets of activated T cells, neurons, endothelial cells, epithelial cells, DCs and thymocytes (D'Arena et al. 2020).

Constitutive expression of CD200 is controlled by two positive regulatory domains (PDR1 and PDR2) within the core promotor region. PDR1 contains important transcriptional binding sites for CCAAT/Enhancer-binding Protein beta (C/EPBβ), which is a critical factor for both constitutive and inducible CD200 expression (Kotwica-Mojzych et al. 2021). Inducible CD200 expression is also regulated through IFN-γ and TNFα, mediated by the nuclear factor kappa-light-chain-enhancer of activated B cells (NF-κB) pathway, STAT1 and interferon-regulatory factor-1 (IRF-1) (Pontikoglou et al. 2016). CD200 expression is also induced by p53 and activated caspases as DCs undergo apoptosis, indicating an immunoregulatory signal that leads to apoptosis-associated immune tolerance (Rosenblum et al. 2004).

1.2.2 CD200 receptor

CD200 receptor (CD200R) has a similar structure to CD200, containing two Ig domains, however the cytoplasmic domain is longer inferring potential capacity for signalling through a cellular signalling domain (Ngwa and Liu 2019). CD200R expression is restricted to cells of myeloid lineages, some populations of activated T cells, B cells and NK cells (Kawasaki and Farrar 2008). CD200R is expressed on both CD4+ and CD8+T cells, with higher expression observed on CD4+ T cells. The broad distribution of CD200 but immunologically restricted expression of CD200R is

consistent with a specific and controlled immunoregulatory function for this interaction.

Like CD200, CD200R was firstly identified in rats and five isoforms of CD200R (1-5) are currently known. CD200R1 is however the only functional CD200 receptor identified in humans with a 52% and 53% amino acid homology with mouse and rat CD200R respectively (Kotwica-Mojzych et al. 2021). In rodents, the CD200R2-5 isoforms were found to have short, non-signalling cytoplasmic tails which may function through ligand binding, however their roles are not clearly characterised and these alternate forms are not thought to be present in humans (Wright et al. 2003; Hatherley et al. 2005).

1.2.3 CD200:CD200R signalling

The specificity of CD200:CD200R binding was initially determined using an anti-CD200R antibody, where binding affinity was found to be ~0.5μM (Wright et al. 2003). Unlike other inhibitory receptors, CD200R does not signal through an ITIM and instead contains an NxPY sequence in its cytoplasmic domain which acts as a binding site for proteins with a phosphotyrosine-binding (PTB) domain (Wright et al. 2003). Phosphorylation at Y286 and Y297 are critical for CD200R function, while phosphorylation at Y289 is non-essential. Following phosphorylation at Y286 and Y297, recruitment of inhibitory adapter proteins downstream of tyrosine kinase 1 (Dok1) and Dok2 occurs, which subsequently bind SHIP and Ras p21 protein activator (RasGAP), resulting in inhibition of Ras/MAPK pathway activation (Kotwica-Mojzych et al. 2021) (Figure 1.5). siRNA knockdown has shown that the Dok2:CD200R interaction is essential for initiation of CD200R signalling, while knockdown of SHIP or Dok1 has no effect (Mihrshahi et al. 2009). Instead, Dok1 is thought to form a complex with CT10 sarcoma oncogene cellular homologue-like (CrkL) to create a feedback loop around Dok2 and RasGAP, negatively regulating CD200R signalling (Mihrshahi and Brown 2010).

The CD200:CD200R interaction is critical for maintaining immune homeostasis through regulation of self-tolerance and avoiding inappropriate overactivation of the immune response. CD200 has been most well studied in the central nervous system (CNS), where it is mostly expressed on neurons, but also other cell types including

astrocytes and oligodendrocytes (Kojima et al. 2016). CD200 interacts with CD200R, sending inhibitory signals to prevent pro-inflammatory microglial activation. Loss of CD200 results in an accumulation of activated inflammatory microglia, promoting neuroinflammatory disease development. Conversely, in mice with spontaneous mutations resulting in neuronal CD200 overexpression, decreased microglial activation and increased protection against axonal injury are observed (Walker and Lue 2013).

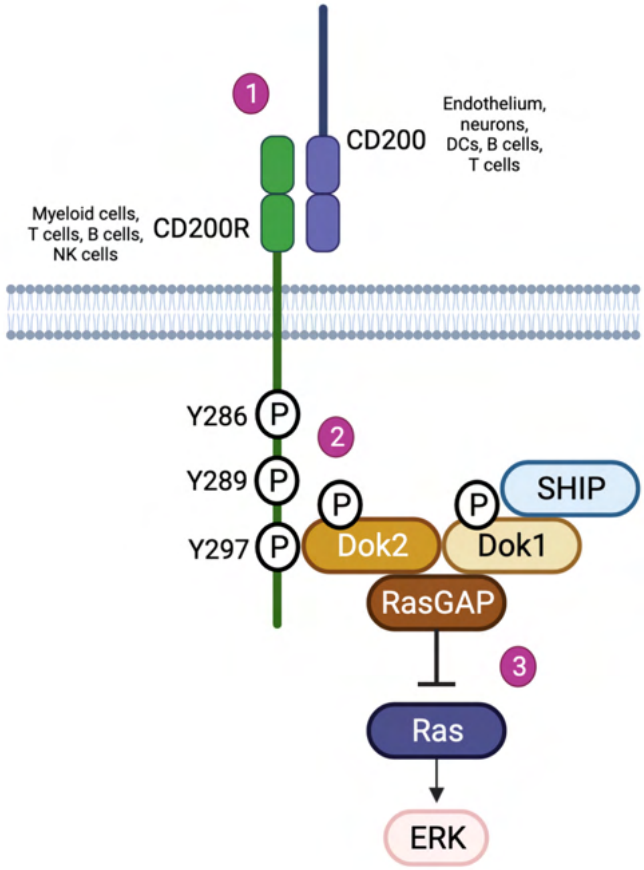

Figure 1.5 Downstream CD200R signalling following CD200 binding
Following ligand binding (1), phosphorylation of key CD200R tyrosine residues results in recruitment of Dok1 and Dok2 (2). Inhibitory effectors SHIP and RasGAP are subsequently recruited and work together to reduce downstream signalling via the Ras/MAPK pathway and suppress immune function (3). Created in BioRender.com.

1.2.4 Immunosuppressive activities of CD200

The first evidence of an immunosuppressive role for CD200 was generated from C57B/6 CD200$^{-/-}$ mice (Hoek et al. 2000). Whilst these mice were normal in appearance with normal lifespan and fertility, comparisons with WT mice revealed

significantly higher numbers of CD11b+ myeloid cells paired with significant increases in the granulocyte and activated macrophage populations. Enlarged lymph nodes with significantly increased levels of activated macrophage and microglia aggregates were also observed. As the absence of CD200 was found to result in an increase in myeloid cells, which express CD200R, it was hypothesized that $CD200^{-/-}$ mice exist in a state of persistent myeloid activation due to the loss of CD200-mediated control (Rijkers et al. 2008). Ligation of myeloid cell CD200R has been shown to inhibit degranulation and inflammatory cytokine release by myeloid cells including mast cells, monocytes and macrophages, alongside reduced histamine release from basophils (Gorczynski 2001; Jenmalm et al. 2006). The differential expression of CD200R on T and B cell subsets also suggests the CD200:CD200R interaction may also be a direct regulator of lymphoid cell function (Gorczynski 2012). CD200 has a range of roles in both normal processes including bone development and homeostasis, infection response, transplant acceptance and reproductive biology, and pathologies including neuroinflammation, autoimmune and allergic disorders and cancer growth (Gorczynski 2012; Zhao et al. 2019).

1.2.4i Autoimmunity

CD200-mediated myeloid cell control has been studied in $CD200^{-/-}$ mice, where increased susceptibility to the development of autoimmune diseases such as collagen-induced arthritis (CIA) and experimental autoimmune encephalomyelitis (EAE), a murine model of multiple sclerosis, was found (Valente et al. 2017). C57BL/6 mice are usually resistant to CIA development, however $CD200^{-/-}$ mice and CD200R-Ig-treated mice developed severe arthritis with high CD68+ macrophage infiltration of the synovial joints, which is characteristic of CIA development (Hoek et al. 2000). High inflammatory macrophage infiltration was also observed in advanced EAE disease models and blockade of the CD200:CD200R interaction resulted in an increased infiltration of T lymphocytes (Meuth et al. 2008). Both the CIA and EAE models are dependent upon the effects of antigen-specific T cells, however as no dysregulation of T cell activity was present in either model, these effects on myeloid cells and macrophage regulation appear to be a direct effect of CD200-mediated signalling in the prevention of autoimmunity (Hoek et al. 2000).

1.2.4.ii Transplant tolerance

Mouse models with systemic overexpression or infusion of CD200-Fc protein demonstrated tolerance of skin, renal and cardiac transplants (Gorczynski et al. 2013; Oweira et al. 2019). CD200-induced allograft tolerance was also associated with an increase in infiltrating Tregs and a shift from type 1 to type 2 CD4+ Th cell cytokine production. Combined, these immune changes resulted in inhibition of T cell proliferation and CTL induction, suggesting a role for CD200 signalling in the generation of tolerogenic T cell responses (Gorczynski 2001; Vaughan et al. 2020).

1.2.5 CD200 expression in cancer

The first indications of a role for CD200 in cancer development came from studies using transplanted EL4 thymoma cells in C57BL/6 mice. In these studies, mice generated a *graft vs leukaemia* response resulting in tumour cell rejection. Mice treated with a soluble form of CD200 were found to have increased tumour growth and inhibited immune responses, resulting in increased mortality rates compared to control mice (Gorczynski 2001). CD200 has since been implicated in a number of haematological malignancies including multiple myeloma (MM), lymphocytic leukaemia (CLL) and acute myeloid leukaemia (AML), and solid cancers such as melanoma, breast, prostate, lung, renal and ovarian (Holmannová et al. 2008; Moreaux et al. 2008; Twito et al. 2013a).

1.2.5.1 CD200 and cancer stem cells

Tumours are composed of a heterogenous population of differentiated cells and cancer stem cells (CSCs), which have long term self-renewal capacity and the ability to evade immune detection and elimination (Gay et al. 2016). CD200 has been identified on CSCs in combination with other CSC surface makers such as CD44 and CD133 in several cancer types including glioblastoma, breast and prostate (Kawasaki et al. 2007). CD200 expression was found to be expressed approximately three-fold higher in CSCs compared to non-CSCs, suggesting that CD200 may serve as a marker for CSC populations (Kawasaki and Farrar 2008). Comparison of

CD200 expression compared to the associated normal samples can be found in Figure 1.6.

Additionally, in basal cell carcinoma (BCC), a rare population of CD200 expressing cells was found to have significantly greater tumour initiating properties compared to CD200- CSCs. This rare population accounted for only 1.63 ± 1.11% of BCC cells but was able to initiate tumour growth from as few as 10,000 cells *in vivo,* while CD200- cells were unable to form tumours (Colmont et al. 2013). Furthermore, CD200 is a marker of human hair follicle bulge stem cells which reside in an "immune privileged" site where cells are protected from inflammation and immune attack (Ohyama et al. 2006). Due to the roles of CD200 in normal cell immune tolerance and tumour immunity combined with its CSC expression, it is hypothesised that CD200 plays a key role in cancer development and ability of tumour cells to evade immune detection (Jung et al. 2015).

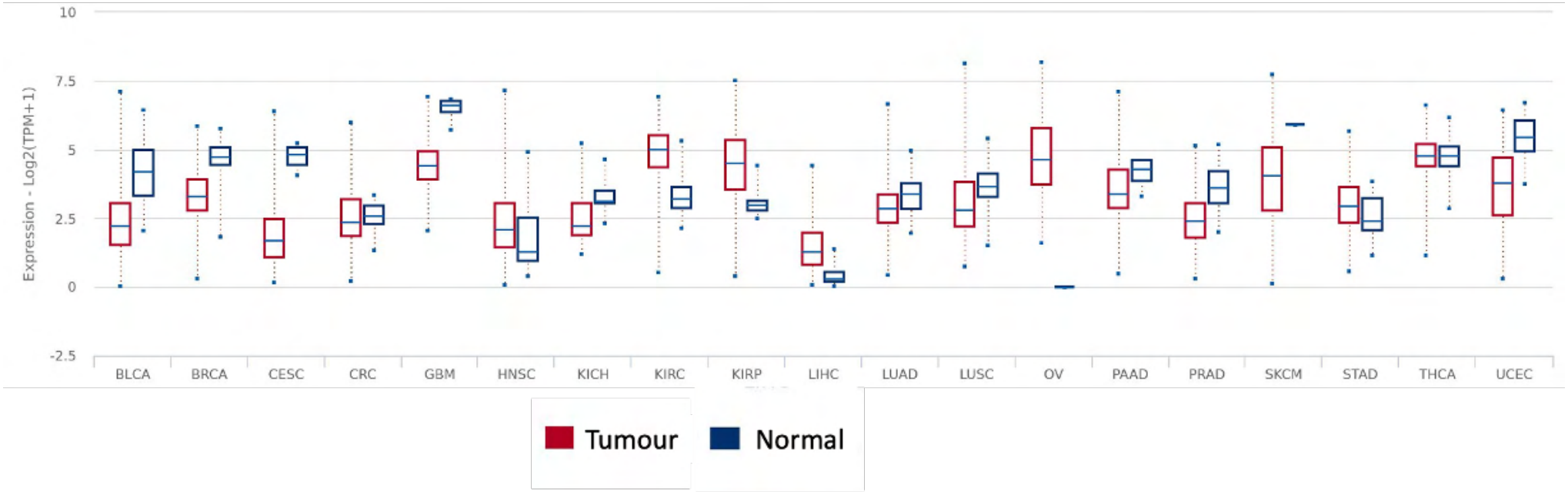

Figure 1.6 CD200 expression in solid cancers compared to associated normal tissue
Log2 transcript count per million (TPM) CD200 expression data taken from The Cancer Genome Atlas (TGCA) programme, compared to normal healthy samples. CD200 expression is increased in KIRC and KIRP compared to normal kidney tissue.
Adapted from https://tcia.at/expression#CD200.
Abbreviations: BLCA, bladder urothelial carcinoma, BRCA, breast invasive carcinoma, CESC, cervical squamous cell carcinoma and endocervical adenocarcinoma, CRC, colorectal carcinoma, GBM, glioblastoma multiforme, HNSC, head and neck squamous cell carcinoma, KICH, kidney chromophobe, KIRC, kidney renal clear cell carcinoma, KIRP, kidney renal papillary cell carcinoma, LIHC, liver hepatocellular carcinoma, LUAD, lung adenocarcinoma, LUSC, lung squamous cell carcinoma, OV, ovarian serous cystadenocarcinoma, PAAD, pancreatic adenocarcinoma, PRAD, prostate adenocarcinoma, SKCM, skin cutaneous melanoma, STAD, stomach adenocarcinoma, THCA, thyroid carcinoma, UCEC, uterine corpus endometrial carcinoma.

1.2.5.2 CD200 expression in haematological malignancies

1.2.5.2i Acute myeloid leukaemia

CD200 expression has been well studied in AML, where cells have been shown to overexpress CD200 which is associated with poor prognosis and increased risk of relapse (Khan et al. 2020). A number of immunosuppressive effects have been reported in relation to AML CD200 expression, including reduced cytotoxicity of effector immune cells and increased Treg frequency (Coles et al. 2012). High CD200 expressing patients were found to have alterations in both the adaptive and innate immune responses. Suppression of type 1 CD4+ memory T cells and CD8+ CTLs was observed in the high CD200 expressing group and was found to be due to the direct interaction between tumour CD200 and CD200R on patient T cells (Coles et al. 2012). Changes observed in the innate compartment included a significant reduction in NK cell frequency and a reduction in the frequency of CD56+CD16+ cytolytic NK cells, alongside a reduction in NCR expression (NKp30, NKp44 and NKp46) on all NK cell subpopulations. NK cell degranulation and IFN-γ responses to tumour cells were also significantly reduced in high CD200 expressing patients (Coles et al. 2011). Blockade of CD200:CD200R signalling was found to restore both memory T cell and NK cell function, demonstrating a direct role for CD200-mediated immunosuppression in AML and also indicating a potential therapeutic target (Coles et al. 2011).

1.2.5.2ii Chronic lymphocytic leukaemia

CD200 is expressed on the surface of CLL cells. However, unlike AML, expression does not correlate with any other clinical parameter and is found at all disease stages, suggesting that early upregulation of expression has a function in CLL development (D'Arena et al. 2020). *In vitro* studies have shown that in CLL, expression of CD200 is related to an increase Treg levels, suppression of T cell proliferation and response to tumour antigens, and polarisation of cytokines to Th2 (Mora et al. 2019; D'Arena et al. 2020). Further evidence for the role of CD200:CD200R signalling in CLL was reported following simultaneous injection of $CD200^{+}$/$CD200^{-}$ CLL cells and peripheral blood mononuclear cells (PBMCs) into

mice, where CD200 expressing tumours were not inhibited. Treatment with an anti-CD200 antibody resulted in inhibited tumour growth, alongside an increase in activated cytotoxic CD8+ T cells and IFN-γ production (Kretz-Rommel et al. 2007).

1.2.5.3 CD200 expression in solid cancers

1.2.5.3i Breast cancer

CD200 is well studied in breast cancer and is of interest as expression appears to have a bidirectional role in tumour development and metastasis. The pro-tumour role for CD200 was first established in mice transplanted with the EMT6, low CD200-expressing breast cancer cell line (Gorczynski et al. 2010). Following transplantation, tumour CD200 expression significantly increased upon immune challenge compared to immunocompromised mice, alongside increases in infiltrating CD8+ effector T cells (Curry et al. 2017). This immune pressure resulted in selection for CD200 expression and associated tumour growth and metastasis to the lymph nodes. Treatment with anti-CD200 mAbs resulted in reduction in tumour growth and improved anti-tumour effector responses (Gorczynski et al. 2010).

Conversely, during use of the highly aggressive 4THM cell line in a $CD200R^{-/-}$ mouse model, CD200 overexpression was found to be associated with reduced tumour growth and metastasis (Erin et al. 2015). In this study, primary tumour growth and metastasis to the lung and liver were significantly greater in the $CD200R^{-/-}$ mice compared to the $CD200^{tg}$ models. Decreased numbers of infiltrating CD8+ effector T cells were also observed, alongside heightened neutrophil infiltration, and increased inflammatory cytokine production. In this model, tumour associated chronic inflammation resulted in tumour progression and therefore, through suppression of the immune responses, a CD200-mediated anti-tumour effect was observed.

1.2.5.3ii Skin cancer

Melanoma cells express CD200 in melanocytic lesions and expression correlates with progression from nevi to melanoma, however much like in breast cancer, conflicting roles for CD200 signalling have been reported. CD200 expression on melanoma cells is associated with a reduction of type 1 cytokines and T cell proliferation which can be reversed by blockade of CD200 signalling (Siva et al.

2008). Conversely, CD200 expression on B16 melanoma cells was found to significantly inhibit tumour growth and metastasis and increase numbers of CD4+ and CD8+ T cells, resulting in prolonged survival (Talebian et al. 2012).

It is currently unclear why CD200 expression can have both pro- and anti-tumour roles in solid tumours but is only pro-tumorigenic in haematological cancers, where expression is generally associated with poor outcomes. Further study into the complexities of CD200 signalling may provide insights into the dual roles of CD200 in tumour development and allow clinical exploitation of the beneficial anti-tumour effects.

1.2.6 CD200 as a therapeutic target

Samalizumab is a humanised monoclonal antibody developed to bind CD200 and block its interaction with CD200R. This mAb has an Ig constant G2/G4 region which prevents ADCC of CD200+ immune cells (Mahadevan et al. 2019). Due to the strong evidence for the role of CD200 in the growth and immune evasion of several cancer types, this mAb is thought to be a promising immune checkpoint inhibitor for anti-cancer therapies. Phase I human clinical trials in CLL and MM patients (NCT00648739) used safety, identification of maximum tolerated dose and pharmacokinetics as primary end points. Secondary end points were salizumab binding to CD200, pharmacodynamic effects on circulating tumour cells and leukocyte subsets, and clinical responses. A dose-dependent decrease in CLL cell CD200 expression was observed, alongside reductions in CD200+CD4+ T cells. Decreased tumour burden was observed in 70% of CLL patients, where one patient achieved a durable partial response and 16 out of 23 patients had stable disease. Disease progression was however observed in all MM patients, with few changes observed in the immune infiltrate (Mahadevan et al. 2019). These results combined mild to moderate adverse effects and a good safety profile indicate potential successes for samalizumab as a clinically useful CD200 checkpoint inhibitor in CLL.

1.3 Ectodomain shedding

Ectodomain shedding is the mechanism of proteolytic cleavage of cell surface molecules resulting in the loss of extracellular domains, leading to the release of a

soluble form into the extracellular microenvironment. This mechanism is involved in a variety of normal processes including cell survival, growth factor signalling, cell adhesion and control of inflammation (Clark 2014). Ectodomain shedding also has further important roles in control of immune responses by regulating the release of cytokines, cytokine receptors, chemokines and many membrane anchored immunoregulatory molecules (Wong et al. 2016). Conversely, increased ectodomain shedding due to increased protease activity is a key pathological process seen in many diseases including cancer, Alzheimer's disease and multiple sclerosis. An imbalance of protease activity can lead to substantial tissue damage, so precise regulation by protease inhibitors is essential for homeostasis (Hadler-Olsen et al. 2011).

1.3.1 Families of proteases

Proteases were first grouped into 84 families in 1993 (Rawlings and Barrett 1993), which are now further subdivided into four main broad subgroups based on their catalytic mechanisms: serine, cysteine, aspartyl and metalloproteases. Serine and cysteine proteases pair a proton-withdrawing group with the amino acid residue at the active site to promote nucleophilic attack on the peptide bond. Aspartyl proteases and metalloproteases however activate a water molecule which serves as the nucleophile, rather than using a functional group of the enzyme itself (López-Otín and Bond 2008). Proteases link their catalytic domains to specialised functional molecules or domains to provide substrate specificity, modify their activation properties, set their cellular localisation, and edit their level of sensitivity to endogenous inhibitors. As proteases carry out irreversible hydrolytic reactions, their functions must be tightly regulated to avoid inappropriate activation. Protease activation is controlled by several mechanisms including regulation of gene expression, post-translational modifications such as glycosylation, proteolysis and activation of inactive zymogens (López-Otín and Bond 2008).

1.3.1.1 MMPs

Matrix metalloproteinases (MMPs), also known as matrixins, are found in the extracellular environment where they have roles in the degradation of matrix and

non-matrix proteins, morphogenesis, wound heading, tissue repair and response to injury. MMPs were first described in 1949 (Gersh and Catchpole 1949) as depolymerizing enzymes which facilitate tumour growth by making connective tissue stroma. The roles of MMPs in other biological processes were later discovered when in 1962, an MMP collagenase was found to be responsible for tadpole tail resorption (Gross and Lapiere 1962). Subsequent MMP research has developed significantly, with MMPs now known to be implicated in a wide range of normal and pathological processes in humans, viruses, bacteria, plants and animals (Laronha and Caldeira 2020).

Humans have 23 types of MMPs (MMP-1 to MMP-23), which are part of a family of multidomain zinc-dependant endopeptidases (Drahansky et al. 2016). Each MMP has a different substrate, however they can be subdivided according to their substrate specificity into collagenases, gelatinases, stromelysins, metrilysins, membrane-type MMPs (MT-MMPs) and other MMPs. The active sites of MMPs are zinc-dependant and highly conserved, with three histidine residues bound to catalytic zinc. MMPs are comprised of a variable length signal *N*-terminal peptide which targets the peptide for section, a pro-domain (around 80 amino acids) which keeps the protease inactive until removed, a catalytic domain (around 160 amino acids), with a zinc ion comprised of 5 β-sheets, three α-helices and three calcium ions, a linker of variable length (14-69 amino acids) which comprises the “hinge region”, a hemopexin-like domain (around 210 amino acids) characterised by four β-propellers and an additional transmembrane domain with a small cytoplasmic *C*-terminal domain (only present in MMP-14, -15, -16 and -24) (Laronha and Caldeira 2020) (Figure 1.7).

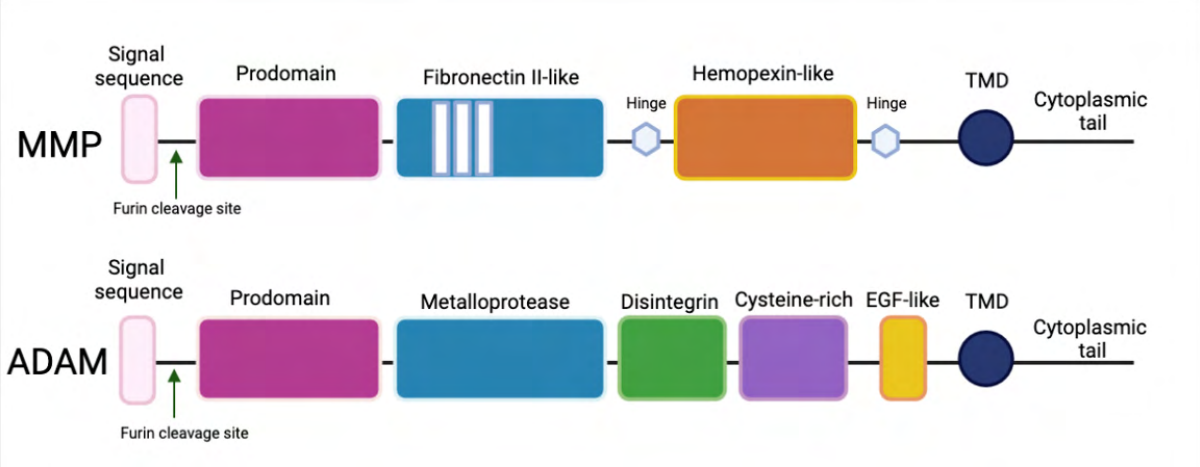

Figure 1.7 Matrix metalloproteinases and a disintegrin and matrix metalloproteinases structure The typical structure of an MMP is a prodomain with a furin cleavage site, a catalytic metalloproteinase domain with fibronectin type II repeats), a linker peptide and a hemopexin domain (except for MMP-7, -26 and -23), a linker peptide, a transmembrane domain and cytoplasmic tail or glycosylphosphatidylinositol (GPI) anchor. Common ADAM structure is a prodomain, a cleavage site for a furin or furin-like proprotein convertase, a metalloproteinase domain, a disintegrin domain, a cysteine-rich region, an EGF-like domain, a transmembrane domain (TMD) and a cytoplasmic tail. Adapted from Seals and Courtneidge, 2003 and Paulissen et al, 2009. Created in BioRender.com. *Abbreviations: ADAM, a disintegrin and metalloproteinase, MMP, matrix metalloproteinase, TMD, transmembrane domain.*

The primary biological function of MMPs is degradation of ECM proteins, glycoproteins, membrane receptors, cytokines and growth factors, however they are also involved in a number of biological processes including tissue repair and remodulation, cell proliferation and differentiation, embryogenesis, angiogenesis, apoptosis and wound healing (Löffek et al. 2011). The catalytic mechanism at the MMP active site during proteolysis has been well characterised in recent years. Hydrolysis of the peptide bond begins with a nucleophilic attack by the water and zinc molecules on the carbonyl carbon of the substrate. Proton transfer to the amine nitrogen occurs through the glutamic acid residue, promoting a gem-diol reaction intermediate with a tetrahedral geometry. The substrate is then broken down and the water molecule is released. The peptide is now stabilized at the active site due to the interaction between N-terminal residues and the S_1' pocket, and by new hydrogen bonds formed between the N-terminal, glutamate and water. The two key steps in this catalytic process are the structural rearrangement of the active site and the fate of the two obtained peptides (Laronha and Caldeira 2020).

The expression and activities of MMPs are mediated by cytokines, growth factors, hormones and cell-cell and cell-matrix interactions. Activity is further regulated by activation of precursor zymogens and inhibition by endogenous inhibitors, the tissue inhibitors of metalloproteinases (TIMPs) (Nagase et al. 2006). The balance between MMP and TIMP levels is therefore essential for homeostasis of ECM remodelling, with an imbalance leading to significant tissue damage and disease development.

Dysregulation of MMP activity leads to the progression of various pathologies resulting from tissue destruction, fibrosis and ECM weakening (Serra 2020). MMPs have also been implicated in the pathology of a number of diseases including arthritis, degenerative brain diseases, chronic inflammation and cancer invasion and metastasis (Nagase et al. 2006; Laronha and Caldeira 2020).

1.3.1.2 ADAMs

The A Disintegrin and Metalloproteinase (ADAM) family of multidomain transmembrane proteins belongs to the metzincins superfamily of metalloproteases. The ADAM structure consists of a prodomain, a metalloprotease domain, a disintegrin domain, a cysteine-rich domain, an EGF-like domain, a transmembrane domain and a cytoplasmic tail (Seals and Courtneidge 2003) (Figure 1.7). Unlike MMPs, whose main function is remodelling of the ECM, ADAMs are implicated in “sheddase” activities, proteolysis, and cell adhesion. Roles for ADAMs have also been widely described in development, fertility, inflammation, immunity and neurodegenerative diseases (Chou et al. 2020b). The main substrates of ADAMs are the ectodomains of other transmembrane proteins, including precursor forms of growth factors and cytokines, growth factor and cytokine receptors, and adhesion molecules (Duffy et al. 2011). The ADAM family is comprised of around 40 gene members, however only 21 of these are believed to be functional in humans. Several methods of regulation control ADAM activity including gene expression, redistribution of sheddases and substrates along the plasma membrane, enzymatic inhibition and allosteric control, all of which are key to prevent inappropriate inactivation (Mishra et al. 2017).

Altered ADAM expression has been implicated in various pathologies including rheumatoid arthritis and osteoarthritis, however their best documented roles are in

cancer formation and progression. A number of ADAMs including ADAM8, ADAM9, ADAM10, ADAM12, ADAM15, ADAM17 and ADAM28 have been described in cancer development, with expression generally associated with poor outcomes (Duffy et al. 2011; Mullooly et al. 2016)

1.3.1.2.1 ADAM9

ADAM9 is a membrane-anchored protein with a number of physiological functions including cell adhesion and the ectodomain shedding of a wide variety of cell surface proteins. ADAM9 has widespread tissue expression in various cell types and plays roles in a multitude of biological functions including wound healing, response to acute injury and myogenesis, as well as pathophysiological conditions including development of neurodegenerative diseases, inflammation, chronic obstructive pulmonary disease (COPD) and tumorigenesis (Chou et al. 2020b). The substrates of ADAM9 can be divided into three groups: (i) cytokines and their receptors, including CD40, TNF-α and IL-11 receptor, (ii) growth factors and their receptors, including pro-HB-EGF, GFG receptor 2 iiib and EphB4, and (iii) other molecules such as ADAM10, VEGFR2, Tie-2, angiotensin-1 converting enzyme, fibronectin and gelatin (Peduto 2009; Chou et al. 2020b). ADAM9 shares these substrates with a number of other ADAM family members including ADAM17 and ADAM10, however all ADAM family members have different biological functions, which could be due to unique amino acid combinations around the substrate cleavage site (Caescu et al. 2009). Ectodomain shedding by ADAM9 initiates signalling through a number of pathways including the MAPK, EGFR/AKT pathway and AKT/NF-κB pathways, with a range of outcomes including tumour development (Haoyuan and Yanshu 2020; Zhou et al. 2020). Increasing evidence has associated ADAM9 with tumour biology, with overexpression found in several cancer types and correlated with tumour aggressiveness and poor prognosis, alongside the development of chemoresistance, angiogenesis and metastasis. ADAM9 expression has been implicated in the development of several cancer types including melanoma, lung, prostate, liver, breast, pancreatic, renal and brain cancers (Mochizuki and Okada 2007; Chou et al. 2020b).

Due to the widespread tissue distribution and roles in normal functions of ADAM9, drug design specifically targeting only cancer related ADAM9 is a significant

challenge. Fisetin, (3,3‘,4',7-tetrahydroxyflavone), a natural flavonoid widely found in plants has been proposed for use as an anti-ADAM9 agent in cancer treatments due to its ability to phosphorylate ERK1/2, therefore reducing ADAM9 protein and mRNA levels via the ERK1/2 pathway (Chen et al. 2015). Fisetin has been shown to halt migration and invasion of cancer cells *in vitro*, however this is yet to be clinically approved for cancer treatment (Imran et al. 2021).

1.3.1.2.2 ADAM17

ADAM17 is the most widely studied family member due to its role in ectodomain shedding of the inflammatory cytokine TNF-α from its precursor product, and therefore ADAM17 is also known as TNF-α converting enzyme (TACE). ADAM17 is essential for normal development and loss of expression can lead to diminished immune responses and other complications including sepsis development. ADAM17 activity is regulated at multiple levels, however overactivation can occur through signalling through several pathways including ERK/MAPK, p38 MAPK and PKC, alongside activation through binding of iRhom2, which is essential for trafficking of ADAM17 to the cell membrane (Adrain et al. 2012). The sheddase activity of ADAM17 has been shown to significantly increase upon cell activation (Mishra et al. 2017). Aside from TNF-α, the other main substrates of ADAM17 include the precursor forms of the EGFR/HER ligands, amphiregulin and HB-EGF. Following activation from their inactive precursor forms, downstream signalling occurs resulting in increased cell proliferation, migration, invasion and metastasis. Therefore, via increased EGFR/HER signalling, ADAM17 is strongly implicated in cancer development and progression (Mullooly et al. 2016). ADAM17 overexpression has been reported in various cancer types including hepatocellular carcinoma, NSCLC, RCC and oesophageal squamous cell carcinoma and correlates with poor outcomes (Peng et al. 2018; Saad et al. 2019). ADAM17 has been widely studied as a therapeutic target in many cancer types using selective low molecular weight inhibitors and mAbs. The widespread distribution of ADAM17 and wide number of substrates has caused difficulties drug development with high numbers of side effects and poor clinical trial outcomes, meaning ongoing drug development is required to enhance specificity and efficacy (Calligaris et al. 2021). The newest non-

zinc-binding synthetic inhibitors which exploit iRhom2 to specifically target ADAM17 on immune cells are an exciting development which may allow selective targeting of inflammatory ADAM17 activities (Giese et al. 2021).

1.3.1.2.3 ADAM28

ADAM28 is widely expressed in normal lymphoid tissues including the lymph nodes, spleen and stomach. Expression in non-lymphoid tissues including the pituitary gland, trachea and lung has also been observed but not well characterised. ADAM28 has a wide range of biological functions, including tooth and muscle development, neurogenesis and cell-cell interactions. Substrates of ADAM28 include IGF-1, connective tissue growth factor (CTGF) and von Willebrand factor, cleavage of which leads to apoptosis of cancer cells within blood vessels (Miyamae et al. 2016).

ADAM28 overexpression has been associated with cancer cell proliferation, survival and migration as well as metastasis. Conversely, in some cancer types ADAM28 expression has been associated with strong protective effects against metastatic dissemination (Hubeau et al. 2020). ADAM28 is overexpressed in several cancer types including breast cancer, pancreatic cancer and NSCLC, with positive correlations with cancer cell proliferation, chemoresistance and tumour progression (Wei et al. 2019).

1.3.1.3 TIMPs

Tissue inhibitors of metalloproteinases (TIMPs) were originally characterised as inhibitors of MMPs, however their scope of inhibition has now been found to also include ADAMS and ADAMTSs (Di Carlo 2014). TIMPs are key regulators of ECM degradation and cell surface molecule shedding through control of ectodomain shedding. There are four homologous members of the TIMP family (TIMP1-4), all of which are capable of inhibiting all known MMPs, however the efficacy of their inhibition can vary, with some TIMPs having greater inhibitory strength than others. TIMP3 is primarily responsible for the inhibition of ADAMs and ADAMTSs, however all TIMPs can also inhibit all ADAM variants to some degree (Arpino et al. 2015). Reactivity for weaker inhibitory reactions can be increased by switching of amino acids, truncation of the C-terminal domain or mutations within the TIMP to increase

the affinity for specific MMPs (Nagase et al. 2006). TIMPs interact with MMPs and ADAMs at multiple active sites, allowing selective inhibition of different groups of proteases depending on their substrate specificity.

The balance between protease expression and TIMP regulation is vital for homeostasis. Proteases process many biologically active proteins such as cytokines and chemokines, alongside their roles in cell surface protein cleavage, as part of their regulatory roles in ECM turnover and maintenance of the local tissue environment. Dysregulation of TIMP inhibition can therefore result in development of a variety of diseases in combination with degradation of the ECM. TIMPs also have a number of their own biological functions independent of their interaction with proteases, including regulation of cell growth and differentiation, cell migration and roles in anti-angiogenic and anti- and pro-apoptotic processes (Brew and Nagase 2010).

1.3.2 Ectodomain shedding of CD200

Many cell surface molecules with inflammatory and immunoregulatory functions can also be found as a functionally active soluble form in serum. Soluble forms of cell surface proteins can be generated by alternative mRNA splicing, release from the cell surface in exosomes or through ectodomain shedding. CD200 is subject to ectodomain shedding, creating a soluble form (sCD200) which is believed to play a functional role in a number of pathologies including proliferative diabetic retinopathy, type 2 diabetes and several cancer types (Twito et al. 2013a; Xu et al. 2015; D'arena et al. 2021). CD200 ectodomain shedding can occur on cells of epithelial and lymphocyte origin, under both resting and activated conditions. The exact cleavage site(s) on CD200 remain to be elucidated, however in studies using Hek293 cells which were stably transfected with CD200R, it was demonstrated that sCD200 detected in CLL did not contain the cytoplasmic CD200 domain, however it did retain the functional extracellular domain which allows binding to, and phosphorylation of, CD200R (Wong et al. 2016). In diabetic retinopathy patients, sCD200 levels were found to be significantly higher than healthy individuals, whilst in haematological cancers such as CLL, patient serum sCD200 levels were found to correlate with disease aggressiveness and tumour burden (Twito et al. 2013a; Xu et al. 2015; D'arena et al. 2021). It is currently unknown which proteases are responsible for the

ectodomain shedding of CD200, however ADAM28 and ADAM17 have been shown to be involved in this process in CLL (Twito et al. 2013b; Wong et al. 2016). However, as a wide range of physiological stimuli can induce ectodomain shedding by different proteases, the full mechanism has not yet been elucidated and other proteases may also be involved in this process in both CLL and other cancer types.

sCD200 has been shown to be biologically active as it is still able to bind and phosphorylate CD200R. This interaction triggers downstream functions via CD200R and may play a role in normal functions and pathological conditions, however it is currently unknown if activation of the sCD200-CD200R pathway occurs with the same efficiency as when membrane CD200 interacts with CD200R (Wong et al. 2016). Our group has previously shown that the presence of sCD200 following ectodomain cleavage by MMP3 and MMP11 results in modulation of the immune response and apoptosis of NK cells in BCC (Morgan et al. 2022). Research to further characterise this process and determine the effect of sCD200 in other CD200 expressing cancer types is required.

One cancer type demonstrating overexpression of CD200 is renal cell carcinoma (RCC), the most common form of kidney cancer. CD200 expression in RCC has been identified through immunohistochemical staining and at the protein and mRNA levels in several studies (Moreaux et al. 2008; El Hanbuli et al. 2021), however the functional role of CD200 expression in RCC has not been fully explored.

1.4 Kidney anatomy

The human kidney is divided into two sections: the inner medulla and the outer cortex, each distinguished by the cell types and structures within them.

The inner medulla is composed of a tubular system, which can be subdivided by the epithelial cell structure of the tubules which form each part of the loops. The outer cortex is composed of a further complicated convoluted tubule system and the renal corpuscles, which form the functional filtration units of the kidney. The renal corpuscle is the main blood filtering component of the nephron, consisting of a knot of capillaries, known as the glomerulus, surrounded by the proximal end of the renal tubule comprised of a double walled glomerular capsule known as the Bowman’s capsule.

Urine formation has three main steps: glomerular filtration, reabsorption and secretion, which ensure that only waste and excess water are removed from the body while most water is reabsorbed. Each kidney contains over 1 million nephrons with a renal corpuscle containing a glomerulus, a network of capillaries surrounded by the Bowman's capsule. As blood flows through the glomerulus, blood pressure pushes water and solutes from the capillaries into the capsule through a filtration membrane which allows water and small solutes to pass through but blocks blood cells and large proteins. This filtrate moves into the proximal convoluted tubule where ions, water and nutrients are reabsorbed, toxins are removed, and filtrate pH is altered. The filtrate then moves through the descending and ascending loop of Henle where further water and ions are reabsorbed. The resulting filtrate contains waste as well as other substances including essential ions, amino acids and small proteins, and this flows into the distal convoluted tubule, where further water and vital nutrients are reabsorbed into capillaries, and waste and hydrogen ions are secreted out the renal tubule, finally forming urine. Urine flows into the collecting duct and passes out of the kidney into the bladder and ureter for excretion.

The renal tubules form around 90% of the renal cortex and are subdivided into the proximal convoluted tubule, thin descending limb of Henle, thick ascending limb of Henle, distal convoluted tubule, connecting tubule, and collecting duct which are histologically distinguishable. Kidney and nephron anatomy is shown in Figure 1.8.

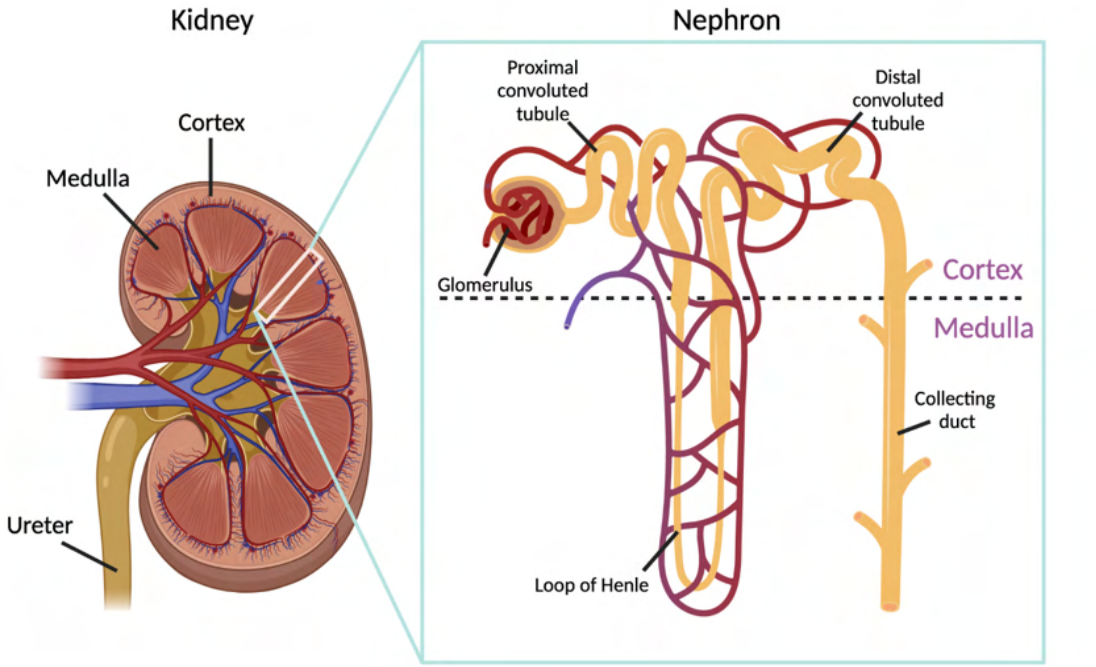

Figure 1.8 Kidney and nephron anatomy
The kidney is made up of two main parts, the outer cortex and the inner medulla. Blood enters through the renal artery and is subjected to filtration in the cortex through the capillaries of the glomerulus, following which the filtrate is subject to further filtration as it moves through the proximal convoluted tubule, out of the cortex into the medulla where it travels through the descending and ascending limbs of the loop of Henle, then back into the cortex to finally pass through the distal convoluted tubule. After water and essential ions have been reabsorbed by the tubules, the end product urine enters the collecting duct where it enters the urethra and is excreted by the body. Figure created with BioRender.com.

Cells of the proximal tubules stain more intensely eosinophilic than those the comprising distal tubules, with nuclei spaced further apart. The proximal convoluted tubule is lined by a simple cuboidal epithelium with each cell having a brush border of microvilli to increase the efficiency of reabsorption, which is often visible in histological staining. The distal convoluted tubule is also lined by a simple cuboidal epithelium but does not have a brush border. The lumens of distal tubules commonly appear smaller, but rounder and more open than those of the proximal tubules, which commonly have an irregular or star shaped lumen. As the proximal convoluted tubule is considerably longer than the distal convoluted tubule, a typical section of the renal cortex includes many more profiles of proximal tubules than of distal tubules.

The filtrate next moves into the loop of Henle which is composed of simple squamous epithelial cells and connects the proximal convoluted tubule to the distal convoluted tubule. The loop travels out of the cortex into the medulla where a concentration gradient of urea is formed as filtrate travels down the descending limb, allowing passive reabsorption of water. After travelling this length, the filtrate turns the ‘u’ shaped portion of the loop and travels up the thin ascending limb where sodium chloride diffuses out into the surrounding tissues along the concentration gradient. Finally in the thick ascending limb, further salts can be removed if required, before the filtrate moves on into the distal part of the convoluted tubule as a concentrated urine end product, which moves though the collecting ducts into the renal pelvis for excretion. The collecting ducts are formed of intercalated cells and principal cells, specialised epithelial cells associated with the regulation of acid-base homeostasis and sodium reabsorption.

1.5 Kidney cancer

Kidney cancer is the 7th most common cancer in the UK, with approximately 13,100 new cases diagnosed per annum (Kidney Cancer UK). Over the last decade, the UK incidence of kidney cancer has risen by 36%. While survival rates have increased in recent years, the 10-year survival rate remains at only around 52% (Cancer Research UK). The average 5-year survival rate for early stage kidney cancer is around 85%, however it is substantially lower in late stage disease where metastases are present, averaging at only around 12% (Office for National Statistics).

The risk of developing kidney cancer is associated with a number of clinical, environmental and genetic factors. Lifestyle factors such as cigarette smoking, alcohol consumption, hypertension and obesity are somewhat controllable, however environmental factors such as exposure to asbestos, petroleum products and ionizing radiation are less so (Petejova and Martinek 2016). Hereditary diseases such as Von Hippel-Lindau disease, autosomal dominant polycystic kidney disease, acquired cystic kidney disease and Birt-Hogg-Dubé syndrome also increase the risk of kidney cancer development by providing a genetic basis for the disease (Ayerbes et al. 2008; Pastore et al. 2015).

Kidney cancer symptoms are non-specific and therefore hinder diagnosis. A combination of flank pain, palpable abdominal mass, and gross haematuria was previously thought to be symptomatic of kidney cancer, however it is now accepted that this combination is rare (6–10% of presentations), and is only detectable at advanced stage (Pastore et al. 2015). Over 60% of patients are diagnosed during treatment or imaging for an unrelated condition, so due to this around 36% of patients are diagnosed at stage III or IV (Vasudev et al. 2020).

1.5.1 Kidney cancer subtypes

Kidney cancers can be subdivided into one of twelve subtypes now recognized by the World Health Organization classification of tumours of the urinary system (Lopez-Beltran et al. 2018). 90% of kidney cancers are renal cell carcinomas (RCC), of which 70% are the most aggressive clear cell (ccRCC) subtype. The remainder of cases comprise of papillary (pRCC, 10% of RCCs), chromophobe (chRCC, 5% of RCCs), benign tumours such as oncocytoma and other much rarer or unclassified subtypes (15% of all RCCs combined) (Farber et al. 2017), as shown in Figure 1.9.

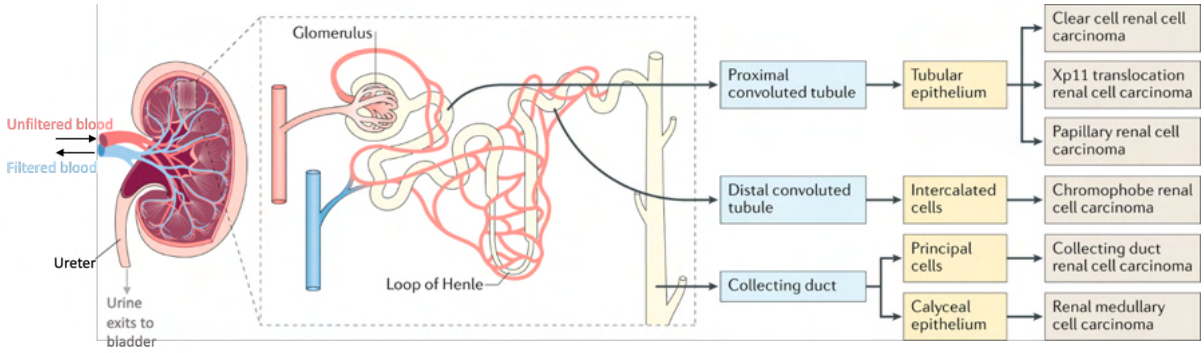

Figure 1.9 Cells of origin for RCC subtypes
The cells of origin for RCC are the proximal convoluted tubule, which gives rise to ccRCC and pRCC, the distal convoluted tubule, which gives rise to chRCC, and the collecting duct, which gives rise to rarer RCC subtypes such as renal medullary cell carcinoma. Created in BioRender.com.
Adapted from Dizman, 2020.

1.5.1i Clear cell renal cell carcinoma

Clear cell renal cell carcinoma (ccRCC or KIRC) is the most common RCC subtype. ccRCC has a distinctive histological structure, characterised by the presence of lipid-

rich clear cells with large cytoplasmic space, arranged in “nests” surrounded by delicate “chicken-wire” vasculature. Macroscopically, the tumour has variable degrees of necrosis, haemorrhage and cystic degeneration (Muglia and Prando 2015). The cell of origin for ccRCC is thought to be the epithelium of the proximal convoluted tubules of the renal cortex (Figure 1.9) (Ishihara et al. 2020). ccRCC is a highly metabolic cancer type, with higher levels of aerobic glycolysis found in ccRCC compared to other RCC subtypes. This is likely due to mutations in genes which control metabolism, including von Hippel-Lindau (VHL) in the hypoxia pathway, mammalian target of rapamycin (mTOR), and mesenchymal epithelial transition factor (MET) in the PI3K/AKT/mTOR pathway, resulting in high incidence of the Warburg Effect in ccRCC (Qi et al. 2021). Other common ccRCC mutations include SET domain containing-2 (SETD2), BRCA1-associated protein-1 (BAP1) and polybromo-1 (PBRM1), which are all key tumour suppressor genes located on chromosome 3p, in close proximity to VHL (Liu et al. 2020). These mutations are associated with late tumour stage, poor differentiation and prognosis and are currently being explored to determine how these mutations affect response to targeted therapy in ccRCC (D’Avella et al. 2018).

1.5.1ii Papillary renal cell carcinoma

Papillary renal cell carcinoma (pRCC or KIRP) is the second most common RCC subtype and generally has a slightly better prognosis than ccRCC (Farber et al. 2017). pRCC can occur sporadically or as a familial condition. pRCC presents as two subtypes: Type 1 (basophilic) and Type 2 (eosinophilic), which are histologically distinguishable and are associated with significantly different outcomes. Type 1 pRCC presents a single layer of basophilic cells on the basal membrane with small, clear cytoplasm and hyperchromatic nuclei. Type 2 pRCC presents with papillae covered with cells with highly granular eosinophilic cytoplasm, with prominent nucleoli in areas of necrosis. Type 2 pRCC usually presents as a high grade tumour, associated with metastasis and so is associated with worse prognosis than Type 1 pRCC (Muglia and Prando 2015). Like ccRCC, pRCC is thought to originate from the epithelium of the proximal convoluted tubule (Figure 1.9) (Ishihara et al. 2020). Similarly to ccRCC, mutations in MET, CDKN2A, SETD2, BAP1 and mTOR are all

characteristic features of pRCC development alongside chromosomal number changes (Angori et al. 2022).

1.5.1iii Chromophobe renal cell carcinoma

Chromophobe renal cell carcinoma (chRCC or KICH) is the third most common RCC subtype and is less aggressive than the other two common subtypes. Of the three subtypes, chRCC has best prognosis due to low rates of metastasis and is often curable by surgery alone (D'Avella et al. 2020). Histologically, chRCC is a homogenous tissue which presents as large pale cells with reticulated cytoplasm and a perinuclear halo (Muglia and Prando 2015). Unlike ccRCC and pRCC which arise from the proximal convoluted tubule, chRCC is thought to originate from the epithelium of the distal convoluted tubule (Figure 1.9) (Casuscelli et al. 2019). Common mutations found in chRCC development include PTEN, PT53 and mTOR (Garje et al. 2021).

1.5.2 Aetiology

RCC can develop due to lifestyle choices or genetic predisposition. Smoking is the most well studied lifestyle factor linked to RCC development, which is a dose-dependent and reversible risk factor, most commonly associated with white males (Reigle et al. 2021). Obesity, hypertension, chronic renal failure, and diabetes have also been defined as significant risk factors. Men are twice as likely to develop RCC compared to females and it is more common in patients ages 55-74, in developed regions such as Europe and North America and in areas with lower socioeconomic status (Kabaria et al. 2016).

Several genomic changes have been characterised in RCC development, including oncogenic mutations, metabolism pathway alterations and epigenetic reprogramming (Lopez-Beltran et al. 2018). The most common genetic alteration is a loss -of-function mutation in the tumour suppressor von Hippel-Lindau (VHL) gene, which regulates the hypoxia response pathway via hypoxia inducible factors (HIFs), promotes tumour cell survival in a hypoxic environment and is central to RCC development (Cowey and Rathmell 2009). Around 95% of ccRCC patients have a deletion in the short arm of chromosome 3p which contains VHL and other

commonly mutated genes in RCC development (Padala and Kallam 2022). Around 4% of RCCs are associated with hereditary conditions and these familiar forms of RCC develop at an earlier age (Petejova and Martinek 2016).

1.5.2.1 Von-Hippel Lindau gene

VHL is a tumour suppressor gene with a key role in ccRCC development which is altered in around 90% of cases, through either a sporadic or a familial manner (Nabi et al. 2018). VHL disease is the most common cause of inherited RCC, however it is rare and not well understood. Tumours associated with VHL disease develop in an autosomal-dominant fashion in patients who are born with one inactivated copy of VHL. For tumorigenesis, the “two-hit” hypothesis describes how a loss of function deletion or mutation in the remaining functional VHL allele results in loss of production of the functional protein product of the VHL gene, pVHL. Under normal conditions, pVHL forms complexes with other proteins including cellulin 2 and elongin B and C, forming the VBC complex. This complex is responsible for degradation of several intracellular proteins including hypoxia-inducible factor-1 alpha (HIF1α) and -2 (HIF2α), which bind DNA to serve as transcription factors for upregulation of several growth factors including VEGF, PDGFB and TGFα. These growth factors play key roles in vascularization of aggressive tumours with VHL gene alterations (Swiatek et al. 2020). In normal conditions, HIF1α and HIF2α are hydroxylated on proline residues and bind pVHL to polyubiquinate the HIF, targeting it for proteasomal degradation. In the absence of pVHL or in hypoxic conditions in both VHL disease related and somatic RCC development, HIF1α and HIF2α are not hydroxylated and subsequently accumulate in the cell where they form dimers with HIF1β. The dimers then migrate to the nucleus where they act as transcription factors for VEGF, PDGFB, TGFA and ECM proteins, resulting in increased angiogenesis, cell proliferation, glucose and lipid metabolism and cell cycle progression (Nabi et al. 2018; Kim et al. 2021). As VHL is inactivated in most sporadic RCCs, this partly explains the high vascularity seen in most RCC tumours (Baldewijns et al. 2010).

1.5.2.2 The mammalian target of rapamycin signalling pathway

The mTOR pathway is one of the most commonly deregulated pathways in human cancers, and is a key factor in RCC development (Faes et al. 2021). The mTOR pathway is responsible for regulation of the cell cycle, cell growth, differentiation and tumour progression and is a therapeutic target in several cancer types (Nabi et al. 2018). The mTOR-PI3K pathway is initiated by growth factor binding to the cell surface, resulting in activation of the phosphatidylinositol-3-kinase (PI3K) protein, which in turn activates mTOR. Activated mTOR creates mTOR complexes 1 and 2 (mTORC1 and mTORC2), which phosphorylate P70S6K and 4E-BP1/eukaryotic translation initiation factor 4E (4E-BP1/eIF4E). Phosphorylated P70SK migrates to the nucleus and initiates coding for the HIFA protein resulting in production of angiogenic proteins. Phosphorylated 4E-BP1 regulates the effects of oncogenic Akt signalling resulting in mRNA translation, cell growth and tumour progression (Clark 2009; Miricescu et al. 2021). Genetic mutations leading to constitutive activity of mTOR increase the risk of RCC metastasis and angiogenesis. Therefore, mTOR inhibitors have been widely trialled in RCC treatment, however they have failed to provide long-term benefits, indicating that RCC tumours do not depend solely on the mTOR pathway for survival (Faes et al. 2021).

1.5.2.3 Other pathways

The most commonly mutated genes in RCC are the tumour suppressors PBRM1, BAP1 and SETD2, all of which are found on the same chromosome as VHL, chromosome 3p, within a 50Mb distance (Hsieh et al. 2018). This chromosome is lost in approximately 90% of sporadic ccRCCs, so deletion of this region results in simultaneous one-copy loss of four key tumour suppressors, resulting in vulnerability to tumour development following loss of the second allele (Brugarolas 2013).

Loss of PBRM1 results in enrichment of pathways associated with cell motility and cytoskeleton development, however its role in tumorigenesis is unclear. In some reports, PBRM1 loss has been associated with a less immunogenic TME and upregulated angiogenesis, however conversely in some reports, PBRM1 loss has

been associated with extended progression free survival (PFS) (Carril-Ajuria et al. 2020; Liu et al. 2020).

BAP1 loss occurs in around 10-15% of ccRCC cases and is associated with upregulation of PI3K signalling and an increase in mTOR activation (Gulati et al. 2022). SETD2 loss is associated with ccRCC recurrence and poor prognosis, however the full effect of this loss remains to be explored (González-Rodríguez et al. 2020). These genes, alongside others within the mTOR, PI3K/ARK and VEGF pathways, have potential for use as both RCC biomarkers and drug targets, however research continues in these areas (Garje et al. 2018; Lopez-Beltran et al. 2018).

1.5.3 Disease staging

Cancer staging is used to determine the extent of disease development and make decisions on treatment course. RCC staging is completed using the American Joint Committee on Cancer (AJCC) TNM system, which classifies tumours based on the size of the tumour (T), lymph node involvement (N) and presence of metastasis (M) (Table 1.4) (Swami et al. 2019).

Table 1.4 RCC TNM staging according to AJCC 8th Edition
Adapted from Swami et al. 2019.

Primary Tumour (T)	
T0	**No evidence of primary tumour**
T1	**Tumour 7 cm or less in greatest dimension, limited to the kidney**
T1a	Tumour ≤ 4 cm, limited to the kidney
T1b	Tumour > 4 cm and ≤ 7 cm, limited to the kidney
T2	**Tumour more than 7 cm in greatest dimension, limited to the kidney**
T2a	Tumour > 7 cm and ≤ 10 cm, limited to the kidney
T2b	Tumour > 10 cm, limited to the kidney
T3	**Tumor extends into major veins or perinephric tissues but not into the ipsilateral adrenal gland and not beyond Gerota's fascia**
T3a	Tumour invades renal vein / branches, perirenal fat, renal sinus fat or pelvicaliceal system
T3b	Tumor extends into vena cava below the diaphragm
T3c	Tumor extends into vena cava above the diaphragm or invades vena cava wall
T4	**Tumor invades beyond Gerota's fascia (including contiguous extension into the ipsilateral adrenal gland)**
TX	**Primary tumour cannot be assessed**
Regional Lymph Nodes (N)	
N0	No regional lymph node metastasis
N1-3	**Increasing number or extent of regional lymph node involvement**
NX	**Regional lymph nodes cannot be assessed**
Distant Metastasis (M)	
M0	No distant metastases
M1	Distant metastases present

Combined, the TNM staging is used to calculate an overall disease stage of I-IV (Table 1.5). Diagnosis at early stage I and II, before the tumour grows outside of the kidney, is strongly associated with better outcomes, with 88.3% of patients surviving

five years following diagnosis when diagnosed at stage I, compared to 14% when diagnosed at stage IV (Cancer Research UK).

Table 1.5 RCC stages based on TNM classification.
Adapted from the American Cancer Society (2019).

Stage	Stage grouping	Stage description
I	T1	The tumor is 7cm across or smaller and is only in the kidney (T1), no spread to lymph nodes (N0) or distant organs (M0).
	N0	
	M0	
II	T2	The tumor is larger than 7cm across but is still only in the kidney (T2), no spread to lymph nodes (N0) or distant organs (M0).
	N0	
	M0	
III	T3	The tumor is growing into a major vein (renal vein or vena cava) or into tissue around the kidney, but not into the adrenal gland or beyond Gerota's fascia (T3). No spread to lymph nodes (N0) or distant organs (M0).
	N0	
	M0	
		OR
	T1 to T3	The main tumor can be any size and may be outside the kidney, but it has not spread beyond Gerota's fascia (T1-3). Cancer has spread to nearby lymph nodes (N1) but not to distant lymph nodes or other organs (M0).
	N1	
	M0	
IV	T4	The main tumor is growing beyond Gerota's fascia and may be growing into the adrenal gland on top of the kidney (T4). It may or may not have spread to nearby lymph nodes (any N). It has not spread to distant lymph nodes or other organs (M0).
	Any N	
	M0	
		OR
	Any T	The main tumor can be any size and may have grown outside the kidney (T1-4). It may or may not have spread to nearby lymph nodes (N0-1). Cancer has spread to distant lymph nodes and/or other organs (M1).
	Any N	
	M1	

1.5.4 Detection and diagnosis

Current National Institute for Health and Care Excellence (NICE) guidelines recommend that a patient aged over 45 presenting to the GP with blood in the urine (haematuria) without, or after treatment for, a urinary tract infection is to be sent to a suspected cancer pathway referral for urine cytology (NICE, 2019). However, many diseases other than RCC, including urinary tract or bladder infections, bladder cancer, and benign kidney conditions such as kidney stones can cause haematuria (Bagnall 2014). Conversely, not all kidney cancer cases present haematuria until the cancer is advanced and has metastasised, meaning that this symptom alone cannot be used as a definitive diagnostic test, particularly not for early stage diagnosis (Sugimura et al. 2001; Pastore et al. 2015). Upon GP referral, first line imaging for suspected RCC includes CT, PET and MRI scans, however each scan type has its own limitations and again cannot be relied on alone for complete diagnosis. If imaging reveals a renal mass or cyst, a kidney biopsy may then be taken for classification and grading, however controversy exists around the risky and intrusive nature of a kidney biopsy, as the mass may be benign and therefore not require removal (Sahni and Silverman 2009). Improvements in image-guided equipment and

percutaneous biopsies have made improvements surrounding these issues (Caoili and Davenport 2014), however development of biomarkers is necessary to identify patients who are at risk of RCC development at an early stage, without the need for unnecessary surgery.

1.5.4.1 Biomarkers

Biomarkers are useful tools for early disease detection, diagnosis, prognosis, measurement of treatment response and disease screening, however discovery of reliable biomarkers for RCC has proven to be a challenging area. Kidney cancers are genetically diverse with variable prognoses and response and recurrence rates, so biomarker research in these areas is vital to stratify patients to allow informed choices to be made regarding treatment decisions and improve patient outcomes (Marchioni et al. 2021).

RCC diagnoses are often unclear, with controversy around the current lack of standardised practices for pathology, particularly in how tumours are classified in to a particular subgroup (Warren and Harrison 2018). Immunohistochemistry (IHC) is the most commonly used technique in RCC pathology; however, this technique is semiquantitative and is dependent on a range of variables including choice of antibody, antibody concentration, fixation techniques, interpretation, and stratification criteria, alongside inconsistencies in specimen handling and other technical procedures. Therefore, identification of molecular markers in body fluids which can be standardised as biomarkers to aid diagnosis, prognosis and treatment choices are urgently required (Corrò and Moch 2018; Rossi et al. 2018).

Urine presents the ideal sample to develop diagnostic and prognostic tools for RCC and possesses many unique advantages over other sample types. It is readily accessible, easily obtained, non-intrusive to the patient, available in large amounts and may easily be stored and re-tested. With the use of appropriate biomarkers, urine testing could be used from early suspicion of disease and diagnosis, throughout treatment and during follow up to monitor the progress of the patient and determine the progression of the disease. Currently the only available urine test is for detection of haematuria, however this test has low sensitivity and specificity for RCC, and so is not used widely as a screening tool (Rossi et al. 2018). Various molecules

have been studies for use as RCC biomarkers, including the use of chemokines (Zeng et al. 2020), serum biomarkers (Silva et al. 2018) and circulating tumour DNA (ctDNA) (Farber et al. 2017), however no single biomarker has yet been found which can specifically and sensitively detect RCC. Use of the exosomal proteins Aquaporin-1 (AQP-1) and Perilipin-2 (PLIN2) as urinary biomarkers have had some success, levels of which have been shown to increase significantly in RCC and decrease by 80% after tumour removal (Morrissey and Kharasch 2013). Urinary AQP1 and PLIN2 concentrations have also been shown to discriminate between RCC subtypes, as they are elevated in patients with ccRCC and pRCC compared with other subtypes and control samples (Song et al. 2019). However, as testing has currently only been completed on small sample sizes, further trialling is required to see if this is an appropriately specific and sensitive biomarker. Other recent RCC biomarker studies have shown some promise in discrimination between RCC and healthy controls, with some even showing ability to distinguish between stages and grades, as listed in Table 1.6. Most published studies have however been based on retrospective data with small sample sizes and relatively short follow-up, hence there is limited data currently available on the sensitivity and specificity on these tests.

Table 1.6 Potential RCC biomarkers and their clinical applications
Adapted from Pastore et al, 2015 and Marchioni et al, 2021.

Sample	Marker	RCC vs HC	Stage	Grade
Serum	TRAF-1	✓		
	Hsp27	✓		
	SAA		✓	
	hsCRP		✓	✓
	GGT		✓	✓
	TRAIL	✓		
	M-65	✓		
	Anti-PHD3 Ab	✓		
	CAIX		✓	
	TuM2-PK	✓	✓	✓
	TKI	✓	✓	
	20S proteasome	✓		
	Survivin	✓		
	HIF2α	✓		
	PD-L1	✓		
	OPN		✓	
Urine	NMP-22	✓		
	NGAL	✓		
	KIM-1	✓		
	MMPs	✓		
	AQP-1	✓		
	PLIN2	✓		

Abbreviations: Anti-PHD3 Ab,: Anti-hypoxia-inducible factor prolyl hydroxylase-3 antibody, AQP-1, Aquaporin-1, CAIX, Carbonic anhydrase IX, GGT, Gamma-glutamyl transferase, HC, Healthy control, hsCRP, High sensitivity C-reactive protein, Hsp27, Heat shock protein β1, KIM-1, Kidney injury molecule-1, M-65, intact form of CK18, MMPs, Matrix metalloproteinases, NGAL, Neutrophil gelatinase-associated lipocalin, NMP-22, Nuclear matrix protein-22, OPN, Osteopontin, PLIN2, Perilipin 2, RCC, renal cell carcinoma, TRAF-1, Tumour necrosis factor receptor-associated factor-1, SAA, Serum amyloid, TK1, Thymidine kinase 1, TRAIL, tumour necrosis factor-related apoptosis inducing ligand, TuM2-PK, Pyruvate kinase type M2.

1.5.5 Immune evasion in RCC

RCC is a highly immunogenic cancer type, with high levels of tumour infiltrating T cells present throughout tumour development (Heidegger et al. 2019). While some level of anti-tumour response is successfully carried out by the immune system, as RCC is still able to develop and metastasize in many cases, this indicates the ability of RCC tumours to evade immune anti-tumour responses through the process of immune evasion. RCC tumours are highly heterogenous and the complex TME

provides favourable conditions for immune escape. RCC cells can evade the immune system using various mechanisms including abnormal expression of MHC class I molecules, overexpression of immunosuppressive cells including Tregs to dampen immune responses, induction of immunosuppressive cytokine expression including IL-10 and TGF-β, and overexpression of angiogenic factors including VEGF to promote tumorigenesis and growth (Jian et al. 2021). A further mechanism used by RCC cells is induction of apoptosis in immune cells through expression of FasL (Olive et al. 1999). A widely studied mechanism of immune evasion in RCC is overexpression of immune checkpoints, including the PD-L1-PD-1 axis, wherein PD-L1 inhibits PD-1 expressing CTLs and NK cells, and CTLA-4, which binds APCs, resulting in T cell inhibition (Wang et al. 2021a). These checkpoints have been exploited therapeutically by immune checkpoint inhibitors; however patient responses are generally poor. A less well studied immune checkpoint in RCC is CD200, which has been shown to be overexpressed in RCC (Moreaux et al. 2008), however the importance of this checkpoint in RCC development and its potential as a therapeutic target is currently unknown.

1.5.6 Treatment

The treatment course of kidney cancer is dependent on the disease stage, subtype and risk factors. Whilst surgery is still considered the gold standard treatment course in early-stage disease, the development of a wide range of therapeutic options has changed the landscape for RCC treatment for both early and advanced stage disease. The main challenge in RCC is chemotherapy resistance, found in all common subtypes, with only rare tumours such as transitional cell carcinoma and collecting duct carcinoma able to benefit from this treatment. Likewise, in most RCC patients, radiotherapy is only generally used for palliative symptom relief in unresectable or metastatic disease (Makhov et al. 2018). In recent years, the development of tyrosine kinase inhibitors (TKIs), angiogenesis inhibitors and ICIs has significantly increased the range of options for RCC treatment (Aldin et al. 2023). Targeted therapies against the VEGF and mTOR pathways have shown some success in RCC, however a high proportion of patients have been shown to relapse when single agent target therapies are used (Hsieh et al. 2017). Therefore, due to the large number of drugs now available, it is essential to use and combine the most

effective therapies while balancing improved outcomes against side effects and impact on quality of life.

1.5.6.1 Surgery

Radical or partial nephrectomy surgery is the gold standard treatment for localised, early stage RCC, which significantly increases long term overall survival rates to around 65% and can be curative in some cases. However, following nephrectomy for clinically localised disease, 20-40% of patients will still relapse, resulting in poor prognosis (Krabbe et al. 2014). In patients with advanced RCC, surgery is generally used only for palliative reduction of tumour burden and is rarely used to remove metastases, with 5 year survival rates of 5-25% (Krabbe et al. 2014). In these patients, other treatment options are generally considered, however in advanced disease, their use is aimed towards symptom control and palliative relief, rather than cure.

1.5.6.2 Targeted therapies

Due to the limited treatment opportunities presented when late-stage disease is diagnosed, selection of the correct treatment for the specific RCC subtype is important in selection of treatment for the greatest success rate. Many treatments and drug combinations have been trialled in late stage RCC, as is comprehensively described in (Sánchez-Gastaldo et al. 2017), however due to the wide genetic landscape of RCC, it is likely that different stages and subtypes will require different treatments. A number of comparative randomised controlled trials have been completed to review the outcomes of combinations of TKIs, angiogenesis inhibitors and ICIs, particularly in efforts to improve outcomes in patients with advanced disease. Due to the highly angiogenic nature of RCC development, several VEGFR TKIs including sunitinib, pazopanib, axitinib and cabozantinib have been developed to target and deactivate downstream pathways related to angiogenic processes (Hofmann et al. 2020). These drugs, alone or in combination with inhibitors of members of the mTOR pathway such as everolimus, are used for first- and second-line treatments in treatment of localised and metastatic RCC. A list of RCC targeted and immunotherapies currently recommended by NICE can be found in Table 1.7.

Table 1.7 NICE recommendations for RCC treatment
Adapted from NICE Renal Cancer Overview, 2019.

Treatment stage	Name	Target	Recommended Use
First line	Nivolumab + Ipilimumab	PD-1 Receptor, CTLA-4	Untreated advanced RCC that is immediate/poor risk
	Cabozantinib	VEGF, C-Met and AXL	Untreated advanced RCC that is immediate/poor risk
	Tivozanib	Multiple RTKs (Including VEGFR 1-3, c-KIT and PDGF)	Untreated RCC
	Pazopanib	Multiple RTKs (Including VEGFR 1-3 and PDGF)	Advanced RCC which has not received prior cytokine therapy, with ECOG status of 0 or 1
	Pembrolizumab	PD-1	Adjuvant treatment of RCC at increased risk of recurrance following nephrectomy, with or without metastatic lesion resection
	Sunitinib	Multiple RTKs (Including VEGF and PDGF)	Advanced and/or metastatic RCC patients who are suitable for immunotherapy with ECOG performance status of 0 or 1
Second line	Lenvatinib + Everolimus	Multiple RTKs (VEGFR 1-3, c-KIT and PDGF)	Patients who have received previous VEGF-targeted therapy with ECOG performance status of 0 or 1
	Cabozantinib	VEGFR, c-MET and AXL	Patients with advanced RCC after previous VEGF-targeted therapy
	Everolimus	mTOR	Patients who have progressed during or after previous VEGF-targeted therapy
	Nivolumab	PD-1 Receptor	Previously treated RCC
	Axitinib	Multiple RTKs (VEGFR 1-3, c-KIT and PDGF)	Advanced RCC who have failed on previous first-line Sunitinib or cytokine

Abbreviations: CTLA-4, Cytotoxic T-lymphocyte-associated protein 4, mTOR, Mammalian target of rapamycin, PD-1, Programmed cell death protein-1, PDGF, Platelet-derived growth factor, RTK, Receptor tyrosine kinase, VEGF, Vascular endothelial growth factor.

1.5.6.3 Immunotherapies

Prior to the development of targeted therapies, high-dose IL-2 was widely used in RCC treatment, however low complete response rates ranging from 20-33% and partial responses between 8-13% were generally observed (Amin and White 2014). Significant side effects are also associated with IL-2 treatment, which combined with low response rates, raised questions surrounding patient quality of life, leading to high interest in development of alternative treatment modalities.

The development of immunotherapies has changed the face of RCC treatment over the past 20 years. The use of ICIs alone, or in combination, for CTLA-4 and PD-1 showed promising results, as RCC is a highly immunogenic tumour with high levels of tumour-infiltrating lymphocytes, however resistance is commonly acquired to these treatments (Sánchez-Gastaldo et al. 2017). Combinations of ICIs with antiangiogenic drugs are currently being trialled to determine if this can overcome these resistance mechanisms.

1.5.6.3.1 PD-1 and CTLA-4 inhibitors

PD-1 is expressed in RCC tumour subtypes, with expression reported in 23% of ccRCC tumours, 10% of pRCC and 5.6% of chRCC tumours (Deleuze et al. 2020). CTLA-4 is also expressed on 1-7% of RCC cells, and expression increases with tumour stage (Kahlmeyer et al. 2019). Targeting of PD-1 and CTLA-4 separately was found to promote low response rates and high levels of adverse effects (Yang et al. 2007), however combination trials have found some durable responses in advanced patients which have not responded to other treatments. Nivolumab is a fully human IgG4 monoclonal antibody which is specific for PD-1 (Hanna 2019). RCC patients were used in the CheckMate 214 phase I study of nivolumab in combination with ipilimumab, an anti-CTLA4 antibody, where favourable responses and toxicity profiles were observed (Motzer et al. 2018). Treatment with these drugs in the subsequent CheckMate 219 phase III trial however found no improvement in disease free survival compared to placebo, and four deaths were attributed to the treatment (Motzer et al. 2023). Despite these poor trial results, nivolumab is approved for first-line treatment in combination with ipilimumab in intermediate/poor risk previously untreated advanced RCC, and as a second-line treatment alone in previously treated RCC (NICE, 2019).

The KEYNOTE-564 phase III trial however found significant improvements in disease free survival in RCC patients treated with pembrolizumab, another anti-PD-1 antibody, compared to placebo (Choueiri et al. 2021). Based on these outcomes, pembrolizumab has also recently been approved for use as an adjuvant monotherapy following nephrectomy, with or without metastatic lesion resection (NICE, 2022).

1.5.6.3.3 Combination therapies

The range of RCC treatments is wide and guidance for urologists is unclear. First- and second-line therapy decisions are based on a vast range of clinical and genetic factors; however, treatment directions are not clear cut. Poor results on monotherapy TKI and targeted therapies has led to interest in combination therapies to tackle both the angiogenic and immune response angles of RCC development. Whilst the results of recent immunotherapy trials such as KEYNOTE-564 have found some

success (Rassy et al. 2020), the poor successes of others such as CheckMate 219 indicate that further trials need to be completed to improve outcomes for RCC patients by combining immunotherapies with targeted therapies.

1.5.6.3.3i Immunotherapy and angiogenesis inhibitors

Angiogenesis via the VEGF pathway is a key factor for RCC growth and development. Whilst anti-angiogenic TKIs are already used in RCC management as monotherapies (Table 1.7), as RCC is a highly immunogenic cancer type, additional implementation of immunotherapies could further improve outcomes in patients with advanced disease. TKIs are currently only administered as monotherapies as an alternative strategy as a first-line treatment if the patient cannot tolerate or undergo immunotherapy. Second-line TKI therapy can then be considered following TKI monotherapy if combination therapies are unsuitable (Rini et al. 2008). Combination targeted therapy and immunotherapy trials have been ongoing for many years; however, success rates are generally low. The phase I CheckMate 016 study combined nivolumab with either the TKIs sunitinib or pazopanib, however both TKI combinations caused high-grade toxicities, limiting future development of either combination regimen (Amin et al. 2018). Combination therapy using bevacizumab, a monoclonal antibody targeting VEGF, and interferon, also showed a significant improvement in PFS compared to interferon monotherapy in the CALGB 90206 trial, however high levels of toxicity are also found in this combination of therapies (Rassy et al. 2020). Trials of immunotherapy and TKI combinations are ongoing, including the COSMIC-313 trial which showed superior efficacy when combining nivolumab, ipilimumab and cabozantinib, however again toxicity was a concern (Gebrael et al. 2023). Further combination treatments including pembrolizumab, lenvantinib and belzutifan in the MK-6482-016 trial (CT NCT04976634) are currently being investigated, with a 2026 study end date. Furthermore, Combinations of axitinib plus pembrolizumab (KEYNOTE-426) and axitinib plus avelumab (JAVELIN RENAL 101) have shown improved outcomes when used as first-line treatment in advanced disease (Rassy et al. 2020). This highlights the complexities of RCC treatment and difficulties facing health care providers of RCC patients, however further research is still required to define the appropriate treatment course for each individual patient.

1.6 Hypothesis and aims

RCC is a highly immunogenic cancer type, however only a subset of patients shows durable responses to treatments due to primary and acquired resistance mechanisms, such as the overexpression of immune checkpoint molecules. The identification of new immune checkpoints involved in RCC development and progression may provide opportunities for therapeutic intervention.
The immune checkpoint CD200 is overexpressed by cancer cells to evade immune attack and promote tumour growth. CD200 is overexpressed by several haematological and solid cancer types including RCC.

We hypothesise that CD200 expression will significantly alter the immune infiltrate of the tumour, including an upregulation of immunosuppressive Tregs and dysfunction of effector T and NK cells. As CD200 is subject to ectodomain shedding, we hypothesise that the overexpression of proteases observed in cancer and the subsequent increased abundance of the soluble form of CD200 may also have effects on immune activity and affect patient outcomes. Blockade of CD200 signalling and ectodomain shedding therefore has potential to reactivate anti-tumour T cell responses and reduce immunosuppression in RCC, reinvigorating the natural anti-tumour response.

Aims

1. Characterise CD200 expression in normal kidney and RCC tumours
   i. Bioinformatic analysis of publicly available data sets.
   ii. Immunofluorescent staining of patient-derived tissue samples.

2. Characterise immune infiltrate in RCC
   i. Determine the immune infiltrate of ccRCC, pRCC and chRCC compared to normal kidney.
   ii. Determine the effect of CD200 expression on immune cell infiltration.

3. Define the enzymatic mechanism for ectodomain shedding of CD200.
   i. Characterise proteases involved in RCC compared to normal kidney.
   ii. Determine the expression pattern of key proteases in RCC tissue.
   iii. Determine whether proteases have a role in CD200 ectodomain shedding.

4. Determine the biological activity of RCC CD200 and soluble CD200.

   i. Determine if CD200 and sCD200 can block NK cell killing of tumour cells.

Chapter 2: Materials and Methods

2. Materials and Methods

2.1 Human tissue samples

Normal human tonsil, stomach and kidney samples were obtained from US Biomax, Zyagen. Kidney cancer tissue microarrays (TMAs) were obtained from the Wales Cancer Bank (WCB project numbers 22/008 and 20/019). Normal human skin sections were obtained following a protocol approved by the local independent research ethics committee (09/WSE/02/01).

2.2 Immunofluorescence (IF)

Paraffin embedded tissue sections were heated at 60°C for 30 minutes to facilitate dewaxing, followed by submersion in Xylene (10 minutes x 2). Slides were then rehydrated by submersion in the following solutions: 100% ethanol (5 minutes x 2), 95% ethanol (5 minutes x 1), 70% ethanol (5 minutes x 1) followed by a wash in phosphate-buffered saline (PBS) (5 min x 1). Sections were then incubated in citrate buffer (8 mM sodium citrate, pH 6.0) or trisaminomethane ethylenediaminetetraacetic acid (TRIS EDTA) Buffer (10 mM Tris-HCl, 1 mM disodium EDTA, pH 8.0) for antigen retrieval, dependant on the antibody used as per manufacturer's instructions. Slides were then heated in a pressure cooker in a microwave at full power (750 W, 10 minutes), then allowed to cool to room temperature (RT). After drying, an ImmEdge PAP pen (Vector Laboratories) was used to draw a hydrophobic barrier around the sample. Non-specific binding was blocked by incubation with 10% donkey serum (Sigma-Aldrich) in PBS for 1 hour at RT. Specimens were then washed in PBS (5 min x 4) and primary antibodies diluted with 5% donkey serum in PBS were added and left for overnight incubation at 4°C. A summary of primary antibodies used can be found in Table 2.1.

Table 2.1 Primary antibodies used for immunofluorescence

Target	Species	Dilution	Company	Product Code
CD200	Goat	1:100	BD Biosciences	552023
ADAM17	Rabbit	1:100	Thermo Fisher Scientific	PA5-27395
ADAM28	Rabbit	1:100	Thermo Fisher Scientific	PA5-67323
ADAM9	Rabbit	1:100	Thermo Fisher Scientific	PA5-76732
CD45	Mouse	1:200	R&D	1430
CD3	Rabbit	1:100	Abcam	ab16669
CD4	Goat	1:100	R&D	AF-379-NA
CD25 (IL2RA)	Mouse	1:50	R&D	555534
FoxP3	Rabbit	1:100	Cell Signalling	98377s
CD45	Rabbit	1:200	Sigma-Aldrich	HPA000440
CD8	Mouse	1:100	Agilent Dako	M7103
CD56	Mouse	1:200	Cell Signalling	123C3

Sections were washed 4 times in PBS Tween-20 (0.05%) for 5 minutes and incubated at RT for 1 hour in the dark with the appropriate fluorescence-conjugated secondary antibodies, as listed in Table. 2.2, diluted at 1:500 in 1:1 volume PBS and BlockAid™ (Thermo Fisher Scientific), with 1µl of 20µg/ml DAPI for nuclear staining.

Table 2.2 Secondary antibodies used for immunofluorescence

Target	Fluorophore (nm)	Dilution	Company	Product Code
Donkey anti Goat	Alexa Fluor™ 488	1:500	Invitrogen	A11055
Donkey anti Goat	Alexa Fluor™ 568	1:200	Invitrogen	A11057
Donkey anti Rabbit	Alexa Fluor™ 488	1:500	Invitrogen	A21206
Donkey anti Rabbit	Alexa Fluor™ 568	1:200	Invitrogen	A10042
Donkey anti Mouse	Alexa Fluor™ 488	1:500	Invitrogen	A21202
Donkey anti Mouse	Alexa Fluor™ 647	1:500	Invitrogen	A31571

Specimens were washed 4 times in PBS Tween-20 (0.05%) for 5 minutes and a coverslip was mounted over the tissue using Vectashield® mounting medium (Vector Laboratories). Slides were then stored at 4°C. Fluorescent images were acquired using a DM6000B upright fluorescence microscope (Leica Microsystems), or Olympus SLIDEVIEW VS200 slide scanner at 40x magnification. Image analysis was performed using ImageJ (National Institutes of Health) or QuPath software

(Bankhead et al. 2017). Secondary antibody specificity was confirmed using positive and negative controls in the absence of primary antibody.

2.2.1 Staining quantification using QuPath

QuPath was used to determine the staining strength of CD200 and ADAM proteases. TMA cores firstly were defined using the TMA dearrayer tool and the cells in each core were detected using the cell detection feature based on DAPI expression, using all default conditions aside from the intensity threshold which was set to 15000.

To confirm the accuracy of the automated staining detection, cells were counted manually in small areas of different TMA cores (n=15) and compared to the result from the detection. Representative cell detection and manual counting vs automated detection correlation is shown in Figure 2.1.

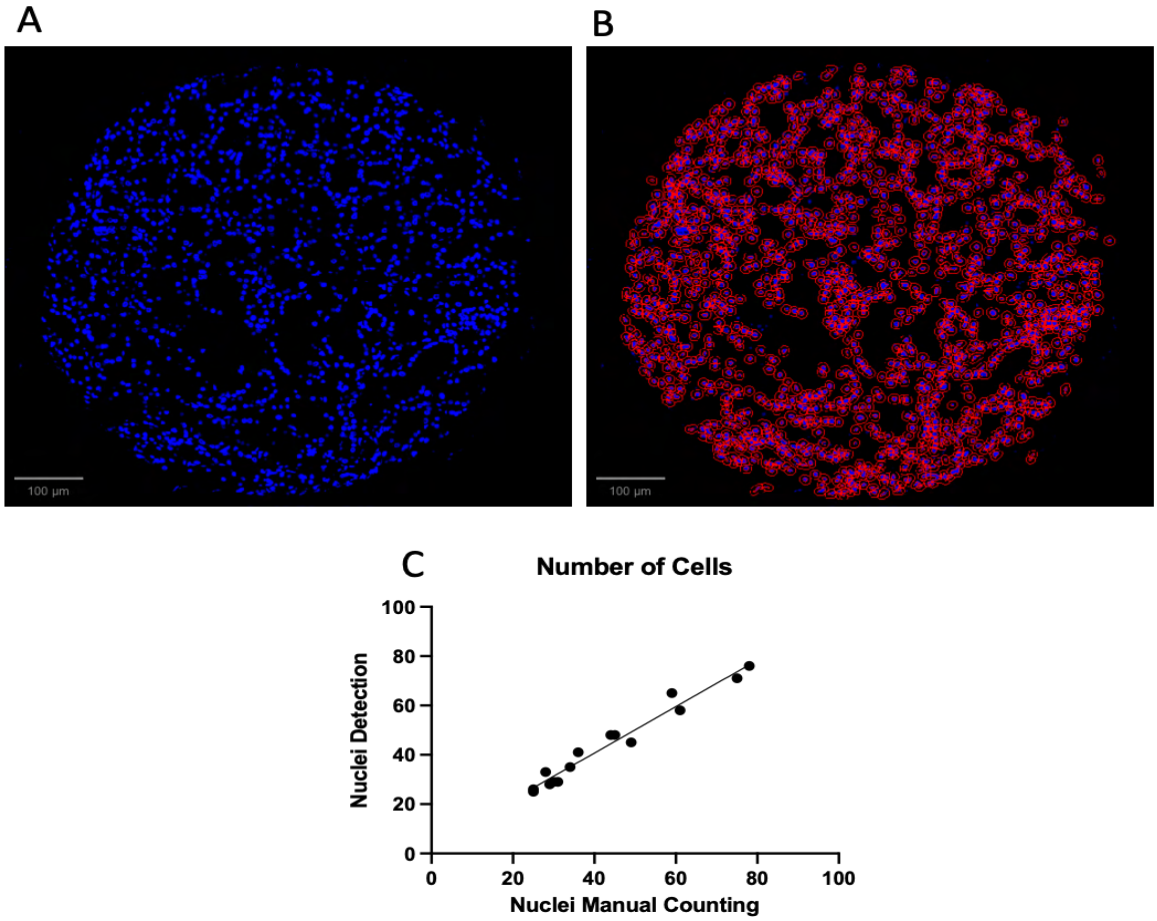

Figure 2.1 Cell detection based on nuclear DAPI expression and validation by manual counting
(A) Nuclear DAPI staining throughout the TMA core, (B) Automated cell detection based on nuclear DAPI expression, (C) Pearson correlation analysis found a very strong correlation between the manual and automated detection, with a r^2 value of 0.964, $p < 0.0001$ (n=15).

Areas of damaged tissue, artifacts or non-tumour tissue were next annotated and set to the *Ignore** classification to be removed from subsequent analysis. CD200, ADAM9, ADAM17 or ADAM28 cell intensity classifications were next defined using the cell intensity classification tool by firstly selecting the appropriate measurement according to the staining's location and channel, then three thresholds were defined to characterise weak (1+), moderate (2+) and strong (3+) staining for each channel, from which a H-score was automatically calculated by QuPath using the following calculation:

$$\text{H-score} = [1 \times (\%\text{ of 1+ cells}) + 2 \times (\%\text{ of 2+ cells}) + 3 \times (\%\text{ of 3+ cells})]$$

Any cells annotated as *Ignore** were removed from the final H-score number. To validate the automated detection and confirm correct thresholding, the number of cells in small tissue areas (n=15) were again manually counted and compared to those found by the automated detection. Representative CD200 staining intensity detection and comparison of manual vs automated scoring can be found in Figure 2.2.

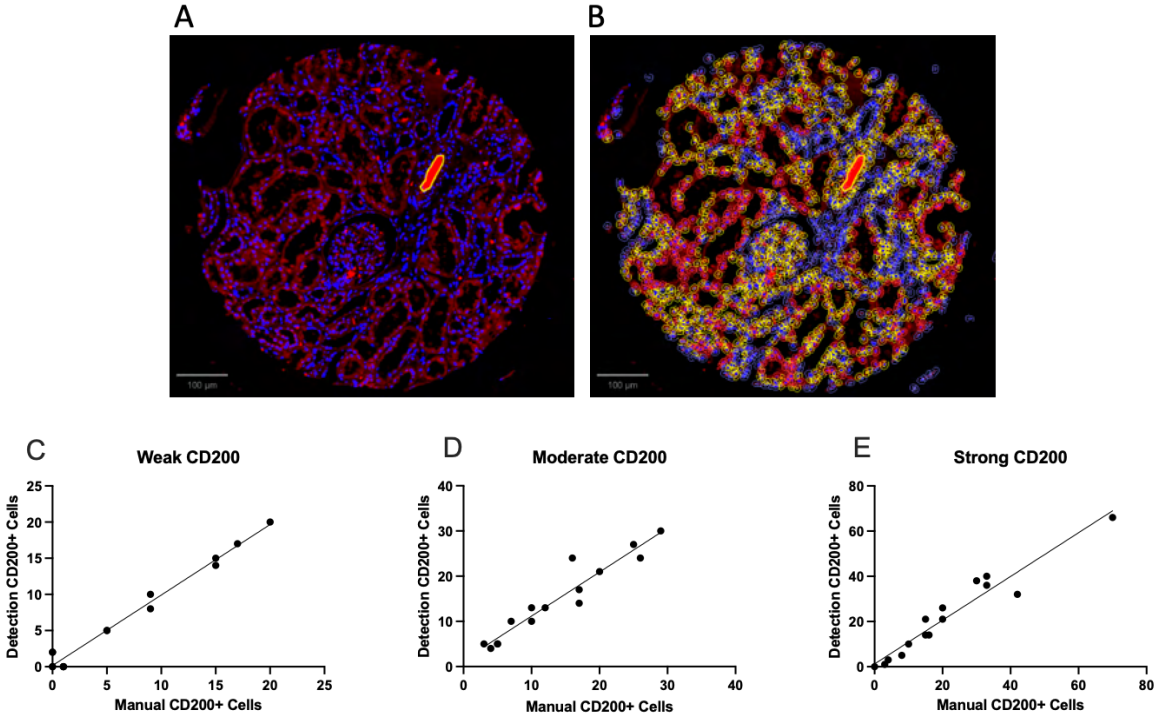

Figure 2.2 Detection of CD200 expression detection using automated cell detection and validation by manual counting
(A) CD200 staining throughout the TMA core. An artifact is highlighted in yellow and set to the *Ignore** classification to be excluded from analysis (B) Automated CD200+ cell detection based on three staining intensity thresholds. 1+ cells are highlighted in yellow, 2+ cells are highlighted in orange and 3+ cells are highlighted in red. Negative cells are highlighted in blue. Pearson correlation analysis found a very strong correlation between the manual and automated detection of (C) weak CD200+ cells, r^2 0.990, (D) moderate CD200+ cells r^2 0.957 and (E) strong CD200+ cells, r^2 0.965. All relationships were $p < 0.0001$ (all n=15).

Manual counting vs detection validation was also carried out in the same way for ADAM9, ADAM17 and ADAM28 for weak, moderate and strong staining, as shown in Figure 2.3.

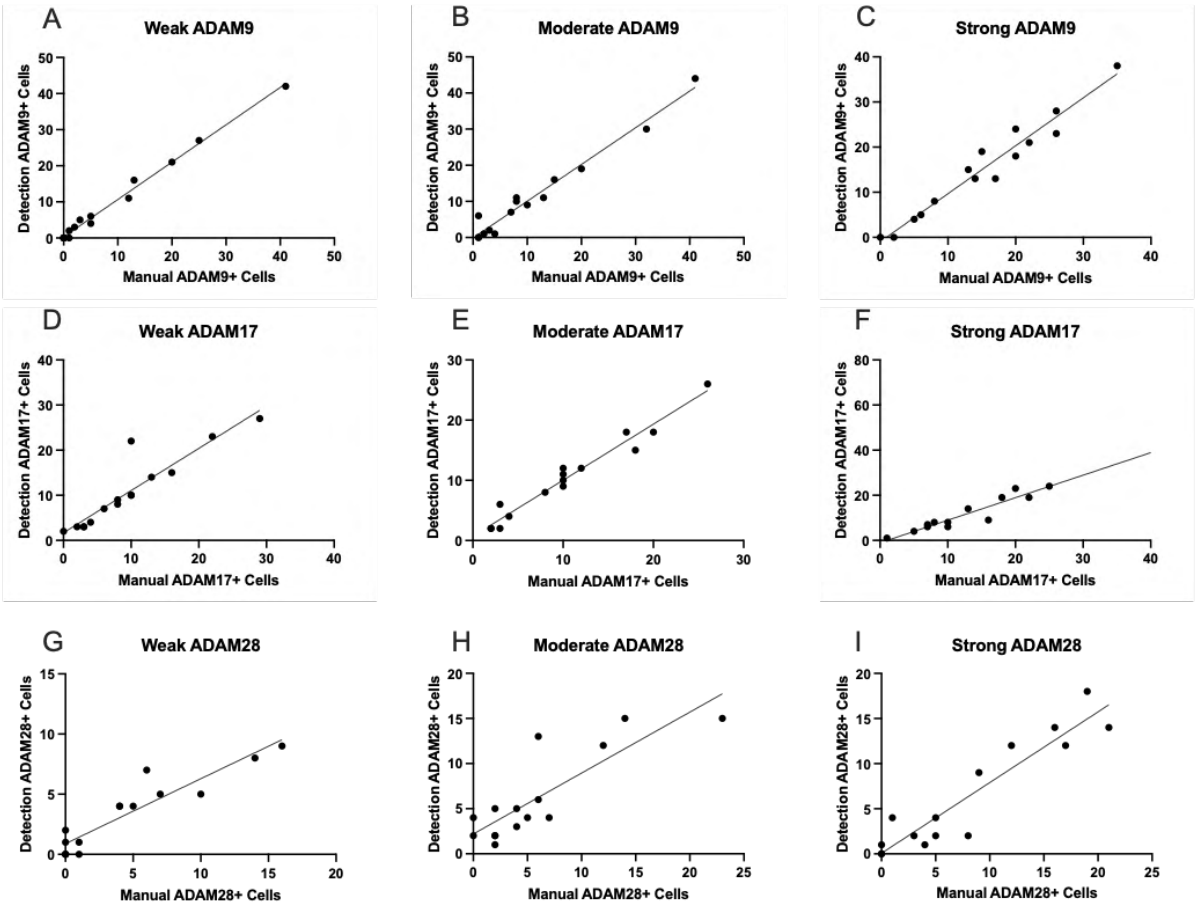

Figure 2.3 ADAM9, ADAM17 and ADAM28 expression validation using manual counting vs automated detection
ADAM proteases were detected using three thresholds to categorise weak, moderate and strong staining. Pearson correlation analysis was used to calculate the strength of the relationships. (A) Weak ADAM9 staining, r^2 0.992, (B) Moderate ADAM9 staining, r^2 0.966, (C) Strong ADAM9 staining, r^2 0.950, (D) Weak ADAM17 staining, r^2 0.947, (E) Moderate ADAM17 staining, r^2 0.940, (F) Strong ADAM17 staining, r^2 0.980, (G) Weak ADAM28 staining, r^2 0.920, (H) Moderate ADAM28 staining, r^2 0.892, (I) Strong ADAM28 staining, r^2 0.921, all $p < 0.0001$.

2.2.2 Immune cell quantification using QuPath

TMAs were dearrayed and cells were detected as previously described by nuclear DAPI expression using QuPath. As double or triple positive staining for cell surface markers was used to identify immune cells, single measurement classifiers were

firstly created with positive and negative thresholds for each channel using the appropriate area and channel filters. Composite classifiers were then created to combine the single measurement classifiers to determine positive immune cells with positive double- or triple staining. The combination of staining defining each immune cell type is shown in Table 2.3. Absolute immune cell positivity was determined as the number of positive cells per mm^2, while relative immune cell positivity was calculated as the immune cell percentage of CD45+ cells within the core.

Table 2.3 Antibody combinations for immune cell staining

Cell Type	Staining Combination
CD4+ T Helper (T_H)	CD45, CD4, CD3
CD8+ Cytotoxic T lymphocyte (CTL)	CD45, CD8
Treg	CD4, CD25, FoxP3
NK	CD45, CD56

To validate the automated detection classifiers, manual counting of each cell type was completed at various sections of tissue (n=15) and cell numbers were compared to the automated detections as previously described. Comparison of manual counting vs automated detection for each cell type can be found in Figure 2.4.

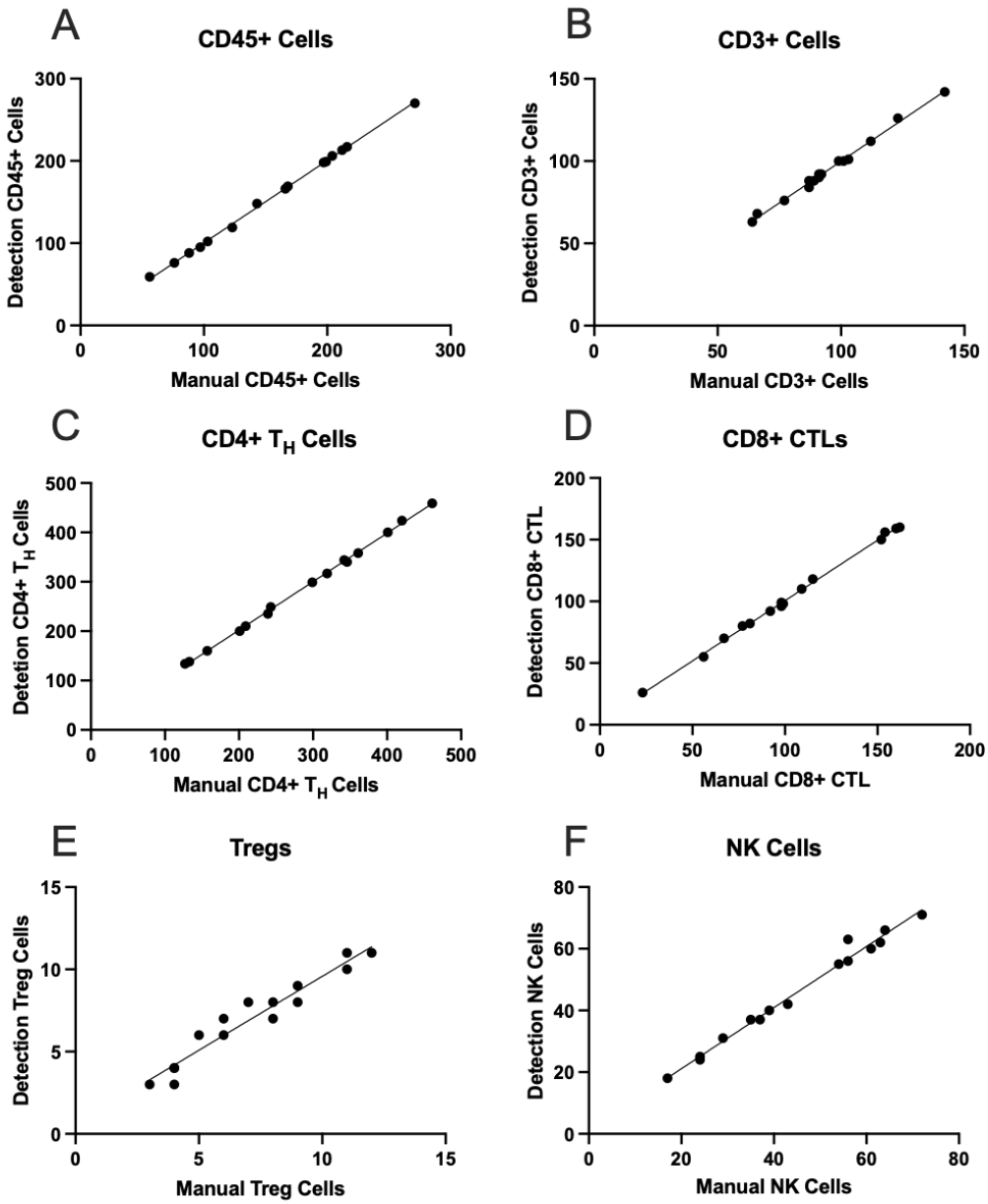

Figure 2.4 Immune cell staining validation using manual counting vs automated detection

Immune cells within small tissue areas were manually counted and cell numbers compared to the detected numbers. Pearson correlation analysis was used to compare the detections of (A) CD45+ cells, r^2 0.998, (B) CD3+ cells, r^2 0.994, (C) CD4+ T helper (Th) cells, r^2 0.999, (D) CD8+ cytotoxic T lymphocytes (CTLs), r^2 0.998, (E) Tregs, r^2 0.934 and (F) NK cells, r^2 0.986. All relationships were $p < 0.0001$.

2.3 Cell culture

The ccRCC cell lines A498, CAKI2, UMRC2, UMRC3, UOK121 and UOK143 were obtained from our group's previous PhD student Elise Rees. The HK2 cell line was a kind gift from Dr Chantal Colmont, Cardiff University. Cultures were regularly tested for the presence of mycoplasma. All cell culture products are from Gibco unless otherwise stated.

2.3.1 Characterisation of cell lines

For use in functional analysis and RNA sequencing, six ccRCC cell lines, A498, CAKI2, UMRC2, UMRC3, UOK121 and UOK143, and one normal kidney cell line, HK2 were used. All cells were cultured according to ATCC recommendations and RNA was assessed and all samples were found to be of high quality with ab RNA integrity number (RIN) of 10.

A498 is a widely used RCC cell line and is part of the NCI-60 cancer cell line panel, a group of 60 cell lines widely used by the National Cancer Institute for the screening of novel cancer therapies (Shoemaker 2006). A498 has mutated VHL (Trotta et al. 2018), however the p53 status has been reported to be both mutated (Brodaczewska et al. 2016) and wild type (WT) (Leroy et al. 2014). Adherent cell culture of A498 appears to be consistent with ccRCC tissue, with visible nests of epithelial cells with clear cytoplasm. The CAKI2 cell line is VHL WT (Pasha et al. 2019), p53 WT (Warburton et al. 2005), and does not express HIF-2α (Brodaczewska et al. 2016). CAKI2 was established from a primary kidney tumour and has an epithelial morphology in adherent culture. UMRC2 and UMRC3 are both part of the European Collection of Authenticated Cell Cultures (ECACC) and have mutated VHL (Wykoff et al. 2004). UMRC2 is thought to have mutated p53 (Cho et al. 2016), however the p53 status of UMRC3 is unknown. Both cell lines are established from metastatic primary renal adenocarcinoma and are able to produce clear cell tumours in athymic nude mice xenografts (Barton Grossman et al. 1985). UOK121 and UOK143 are both cell lines from sporadic ccRCC, and both have one hyper-methylated and one silent copy of VHL (Kuzmin et al. 1999; Alleman et al. 2004). UOK121 has high p53 expression (Brodaczewska et al. 2016), however the p53 status for UOK143 is unknown. UOK121 has no expression of HIF-1α, however UOK143 expresses normal levels of both HIF-1α and HIF-2α (Sourbier et al. 2012). HK2 is an

immortalised normal kidney cell line derived from the proximal convoluted tubule, which retains the functional characteristics of *in vivo* proximal tubules and primary proximal tubule cultures (Ryan et al. 1994). Cell line characteristics are summarised in Table 2.4.

Table 2.4 Cell line characteristics

Cell Line	RCC Subtype	Metastatic	VHL	HIF1a	Other Notable Mutations
A498	"Classical" ccRCC cell line, commonly used	No	Mut	WT	86 Common mutations including EGF, FGFR, MAPK and PIK3. High VEGF. Some reports state mutated p53 while others report WT
CAKI-2	ccRCC Also widely used to study pRCC	No	WT	WT	80 Common mutations including EGF, FGFR, MAPK, PDGFR, PBRM1 and VEGF. Low expression of HIF-2α. p53 WT.
UMRC-2	ccRCC	Yes	Mut	Mut	Mutated p53
UMRC-3	ccRCC	Yes	Mut	WT	
UOK-121	Sporadic ccRCC	Yes	Mut, some sources say WT. One hypermethylated and one silent copy.	Mut	Hyper methylated at VHL locus and expresses no detectable VHL transcript. Chromosome 3 loss, no HIF-1α expression.
UOK-143	ccRCC	Yes	Mut, One hypermethylated and one silent copy	WT	
HK2	Normal kidney	-	WT	WT	

2.3.2 Maintenance of cell lines

2.3.2.1 Adherent cells

A summary of the growth media and CO_2 conditions used for each cell line is summarised in Table 2.5.

Adherent cell lines were grown in T75 flasks containing 15ml of the appropriate media in a New Brunswick Galaxy 170s CO_2 incubator (Eppendorf) set to the correct atmosphere at 37°C. To sub-culture, once cells reached 80-90% confluency, media was aspirated and cells were washed using PBS at RT. Cells were detached from the flask using 5ml of either Versene™ 0.48mM EDTA solution or Trypsin (0.05%) then incubated at 37°c for 5 minutes, or until the cells became detached. 8ml of media containing foetal bovine serum (FBS) was added to the cells to inhibit enzymatic activity and the cell suspension was transferred to a 15ml Falcon tube™ (Corning). Cells were then pelleted by centrifugation at 120xg for 5 minutes at RT then supernatant was either discarded or stored at -80°C if required for later use. The cell pellet was then re-suspended in fresh media and reseeded into flasks at the desired densities.

Table 2.5 Summary of cell lines used and their growth media and CO_2 requirements

Cell line	Type	Metastatic	Growth Medium	CO_2
HK2	Normal Kidney	No	Dulbecco's Modified Eagle Medium (DMEM) 10% Heat inactivated foetal bovine serum (FBS) 1% L-Glutamine 1% Penicillin and Streptomycin	5%
UOK121	ccRCC	Yes		10%
UMRC2	ccRCC	Yes	DMEM 10% Heat inactivated FBS 1% L-Glutamine 1% Penicillin and Streptomycin 1% Non-essential Amino Acids (NEAA)	10%
UMRC3	ccRCC	Yes		
A498	ccRCC	No	Eagle's Minimum Essential Medium (EMEM) 10% Heat inactivated FBS 1% Penicillin and Streptomycin 1% NEAA 1% Pyruvate	5%
CAKI2	ccRCC	No	DMEM:RPMI 1640 (1:1) 10% Heat inactivated FBS 1% L-Glutamine 1% Penicillin and Streptomycin	10%
UOK143	ccRCC	Yes	Iscove's Modified Dulbecco's Medium (ISCOVES) 10% Heat inactivated FBS 1% Penicillin and Streptomycin	5%
HeLa	Cervical adenocarcinoma		RPMI 10% Heat inactivated FBS 1% L-Glutamine 1% Penicillin and Streptomycin	5%
NK92MI	Natural Killer		RPMI 1640 10% heat inactivated FBS 10% heat inactivated horse serum 1% L-glutamine 1% Penicillin and streptomycin	5%

2.3.2.2 Non-adherent cell culture

2.3.2.2a Non-adherent flask cultures

The NK92MI cell line was maintained in T175 flasks containing 25-35ml of media. Fresh media was added every 2-3 days to maintain cell confluency between $2x10^5$ – $1x10^6$ cells/ml. When required, cells were removed into a 50ml Falcon tube and centrifuged at 120xg for 5 minutes, resuspended in fresh media and plated as required.

2.3.2.2b 3D cell culture

Cells were seeded as single cell suspensions at 10 cells/µl into Nunclon Sphera™ petri dishes (Thermo Fisher Scientific) in 3mL cell line respective serum-free defined media supplemented with 1µg/ml fibroblast growth factor-2 (FGF-2), 1µg/ml epidermal growth factor (EGF) and 20µg/ml B27. Spheres were allowed to grow for 14 days before harvesting.

2.3.3 Cryopreservation of cell lines

Cell lines were prepared for cryopreservation in the same manner as sub-culturing; however, they were re-suspended in freezing medium following centrifugation. All cell lines were counted using a Via1-casette and NuceloCounter™ (Chemotec). For the ccRCC cell lines, 1-2×10^6 cells/ml were frozen in 90% growth medium with 10% dimethyl sulfoxide (DMSO) cryoprotectant, while the NK92MI cells were prepared using CryoStor CD10™ (StemCell Technologies). Cells were transferred to 2ml cryovials, placed in a RT CoolCell Biocision™ cryopreservation container (Dutscher Scientific) and stored at -80°C overnight, before being transferred to liquid nitrogen (LN) storage.

2.3.4 Thawing of cell lines

Cells were removed from LN and played on dry ice before rapid thawing in a bead bath set to 37°C. Thawed cells were placed into a 15ml Falcon tube with 9ml of media and centrifuged at 120xg for 5 minutes. Supernatant was then removed, cells were resuspended in 1ml fresh media and transferred into T75 flasks containing 14ml of media.

2.3.5 Mycoplasma testing and treatment

Monthly mycoplasma testing of all cell lines was carried out using the Promocell™ PCR Mycoplasma Test Kit. 1ml of cell culture supernatant was transferred to a microcentrifuge tube and spun at 500xg for 5 minutes to form a pellet. The

supernatant was then transferred to a fresh tube and centrifuged at 14,000xg for 15 minutes. The supernatant was then discarded, and the pellet resuspended in 100µl of DNA free water.

Lyophilised master mix was rehydrated by adding 23µl of rehydration buffer and 2µl of sample was added to each test reaction tube. For the positive control, 23µl of rehydration buffer and 2µl of DNA free water was used. For the negative control 23µl of rehydration buffer was used and 2µl of fresh cell culture media added to ensure all sample volumes were 25µl. Tube contents were mixed by flicking the tube and left to dissolve for 5 minutes at RT. The tubes were placed in a BioRad T100™ Thermocycler and set at the program described in Table 2.6.

Table 2.6 Thermocycler program for mycoplasma PCR testing

Temperature	Time	Number of Cycles
95°C	2 minutes	1
94°C	30 seconds	40
55°C	30 seconds	
72°C	40 seconds	
4-8°C	∞	

A 1.5% agarose gel containing 10µl Safeview™ nucleic acid stain (NBS Biologicals) was set with a 5mm comb. Reaction tubes were vortexed prior to electrophoresis. 8µl of each sample was loaded per lane with a 1kbp ladder and electrophoresis was run for 25 minutes at 100V, or until the samples had run to 2-3cm. The gel was imaged using the ChemiDoc MP Imaging System™ (BioRad) and bands were evaluated using the accompanying ImageLab™ software (BioRad). A mycoplasma positive sample is classed as a band between 265-278 bp, and the mycoplasma-positive control sample shows a distinct band at 270 bp. The negative control shows a band at 479 bp and as an internal control, should appear in every lane to show a successful PCR reaction has taken place.

Positive cultures were found during preliminary testing before use in any experiments. Cell lines were treated for 14 days with Plasmocin™ (Invivogen). Successful treatment was confirmed by repeating the PCR test after 1 passage post-

treatment. Batches of confirmed mycoplasma-negative cell lines were frozen for future use and infected cells were discarded.

2.3.6 Cell line transduction

2.3.6a GFP+ CD200+ and CD200- HeLa and ccRCC cells

Complementary DNA for CD200 was provided by IMAGE consortium (clone ID 5299899) and subsequently subcloned into the PINCO retroviral expression vector which co-expresses green fluorescent protein (GFP) from an internal cytomegalovirus (CMV) promoter (both kindly gifted from Alex Tonks, School of Medicine, Cardiff University). Phoenix packaging cells were transfected with either PINCO-CD200-GFP (CD200+) or PINCO-GFP (CD200-) using calcium phosphatase precipitation and cultured in DMEM +10% FBS +2% 200mM L-glutamine and 20U/ml Gentamicin. 8 ml of media was added onto sub-confluent cultures and the viral media was harvested by centrifugation at 450xg for 10 mins after incubation for 48 hours at 37℃. $1.8x10^6$ cells were plated in a 24 well plate and retrovirally transduced by incubation with 500µl of retroviral supernatant for 24 hours. Cells were then washed twice with PBS to remove any trace of the virus before being left to grow for 2 weeks in their respective media prior to flow cytometric sorting for GFP+ cells. GFP+ cells were then expanded and CD200 expression was confirmed in the cell lines by flow cytometry and western blot.

2.3.6b Fluorescence-activated cell sorting

Cells were dissociated from flasks using 5ml Versene™, centrifuged for 5 minutes at 120xg, resuspended in fresh media and counted. $10x10^6$ cells were placed into a fluorescence-activated cell sorting (FACS) tube, centrifuged and washed with 1ml FACS buffer comprising of PBS with 10% FBS and 0.1% sodium azide. Cells were then centrifuged to create a pellet and resuspended in 500µl of FACS buffer and passed through a 70µm cell strainer. A control sample of untreated GFP-negative cells was used for gating, and GFP+ cells were sorted directly into 96 well plates at $1x10^4$ cells/well. The populations were then expanded and transferred into T75 flasks.

2.4 Cell line co-culture experiments

2.4.1 Tumour cell line and NK cell co-culture

Cells were removed from flasks as described and plated in 96 well plates at a density of 5000 cells/well and left to adhere overnight. The following day, supernatant was removed, adherent cells were washed with PBS and NK cells were added at the desired effector:target (E:T) ratio in a total volume of 100μl of NK media or CD200+ cell line supernatant/well. Blank wells contained NK media only and control wells contained tumour cells only in NK media. Plates were incubated at 37°C for 4 hours following which the supernatant and NK cells were removed by vigorous washing with PBS. The impact of the NK cells on tumour cell viability was then assessed using the Cell-Titre Glo® assay.

2.4.2 Cell Titre-Glo

Cell viability was determined using the Cell Titre-Glo® (CTG) assay (Promega), a luminescence-based assay which quantifies the number of metabolically active cells in a sample through detection of ATP. Equal amounts of CTG and media were added to wells following co-culture and plates were covered with foil and mixed on an orbital shaker for 2 minutes at RT to induce cell lysis. Following incubation in the dark for 10 minutes, a CLARIOstar™ plate reader (BMG Labtech) was used to read luminescence at 560/590nm. Wells containing media and CTG only were used as blanks to which the sample readings were corrected, and cell viability of treated vs untreated cells was calculated.

2.4.3 ADAM9 overexpression assay

Cells were removed from flasks as described, counted and 750,000 cells were seeded into 6 well plates in 2mL total volume of serum-free media (SFM). Cells were left to adhere to the plate for 24 hours then Recombinant Human ADAM9 Protein (R&D Systems) was added to each well at a concentration of 0.5, 1 or 2μg/ml and left for 24 hours. Cells were then counted again, and supernatant was collected, centrifuged at 120xg for 5 minutes at 4°C then transferred to Pierce™ Protein Concentrator tubes (Thermo Fisher Scientific) and centrifuged at 4000 rpm for 1-2

hours at 4°C until around 1.5ml remained. Supernatant was either used straight away or stored at -80°C until required.

2.4.4 ADAM9 siRNA

Cell lines were removed from flasks as described, counted and 80,000 cells were seeded into 6 well plates in 2ml total volume of regular media and left for 24 hours to adhere to the plate. After 24 hours the media was removed, cells washed with PBS and 2ml of SFM supplemented with 10μl of lipofectamine and ADAM9 siRNA (L-004504-00-0005, Horizon, Dharmacon™) at a concentration of 800nM, diluted in Opti-MEM™ was added to each well. Control wells contained non targeting (NT) siRNA (D-001810-10-20, Horizon, Dharmacon™). Cells were left for 72 hours, following which protein and RNA were collected as described in section 2.7.1 and 2.6.1 respectively, and confirmation of knockdown was completed via western blot and qRT-PCR. Supernatant was collected for later use in ELISA.

2.5 ELISA

2.5.1 Collection of cell supernatant

Cells were grown to 70-80% confluency, after which the media was removed, cells were washed with PBS and replaced with 15ml fresh media or SFM for 48 hours. After 48 hours, the number of cells was counted and the media was collected into a Falcon™ tube and centrifuged for 5 minutes at 120xg, following which the supernatant was transferred into a Pierce™ 3K MWCO (Thermo Fisher) disposable ultrafiltration concentration tube and centrifuged for 1-2 hours at top speed (34,000xg), until around 1.5ml of media remained (10x concentration). Concentrated media was used straight away or stored at -80°C for future use.

2.5.2 sCD200 ELISA

Soluble CD200 in cell culture supernatant was quantified using a CD200 sandwich ELISA performed using a Human CD200 ELISA Kit™ (Abcam, ab267806).

Supernatant was collected and prepared as described. Seven standards were prepared starting at 2000 pg/mL, using serial dilutions of recombinant human CD200 in Sample Diluent NS. Using the 96 well plate pre-coated with monoclonal antibody included with the kit, 50µl of the CD200 standards or supernatant samples and 50µl of Antibody Cocktail were directly plated in triplicate and left to incubate at RT for 1 hour on a plate shaker set to 400 rpm. Each well was washed with 3 x 350µl Wash Buffer PT, and after the last wash the plate was inverted and tapped gently against clean paper towels to remove excess liquid. 100µl of TMB Development Solution was added to each well and the plate was incubated in the dark at RT for 10 min on a plate shaker set to 400 rpm. Colour development was stopped with 100µl of Stop Solution and the absorbances of each well were measured at 450nm using a CLARIOstar™ microplate reader (BMG Labtech). sCD200 concentration was determined using a standard curve derived from the CD200 standards, with each supernatant absorbance corrected against untreated samples of the cell line's respective culture media.

2.5.3 ADAM9 ELISA

Soluble ADAM9 (sADAM9) in cell culture supernatant was quantified using an ADAM9 sandwich ELISA performed using a Human CD200 ELISA Kit (Abcam, ab193690). Supernatant was prepared as previously described and reagents were prepared according to manufacturer's instructions. Seven standards were prepared starting at 4800 pg/mL, using serial dilutions of recombinant human ADAM9 in Assay Diluent B. Using the 96 well plate pre-coated with monoclonal antibody included with the kit, 100µl of the ADAM9 standards or supernatant samples were added to each well, plate was covered and left to incubate for 2.5 hour at 4°C with gentle shaking.

Each well was washed 4 times with 300µl 1x Wash Buffer, and after the last wash the plate was inverted and tapped gently against clean paper towels to remove excess liquid. 100µl of the prepared detection antibody was next added to each well and left to incubate for 1 hour at RT with gentle shaking. Wells were washed as previously described and 100µl of prepared 1x HRP-Streptavidin solution was added to each well and left to incubate for 45 minutes at RT with gentle shaking. Wells were washed as previously described then 100µl of TMB one-step substrate reagent was

added to each well and left to incubate for 30 minutes at RT in the dark with gentle shaking. 50µl of stop solution was added to each well and the plate was read immediately using a CLARIOstar™ microplate reader (BMG Labtech) at 450nm. sADAM9 concentration was determined using a standard curve derived from the ADAM9 standards, with each supernatant absorbance corrected against untreated samples of the cell line's respective culture media.

2.6 RNA analysis

2.6.1 RNA Extraction

Cells in culture were counted and 1-2 x 10^6 cells were collected for RNA extraction. Cells were detached using Versene™ or Trypsin, pelleted by centrifugation at 120xg for 5 minutes and RNA was isolated using the Qiagen RNeasy Plus Mini Kit™ (Qiagen, UK) as per the manufacturer's instructions. RNA concentration was then determined using a NanoDrop 2000™ spectrophotometer (Thermo Scientific).

2.6.2 RNA preparation for sequencing

The quality of the extracted RNA was assessed using the Agilent RNA 6000 Nano kit™, which can assess RNA quality quantitatively within the range of 25- 500 ng/µl of total RNA. The Nano chips were run on the Agilent 2100™ Bioanalyzer according to manufacturer's guidelines. RNA integrity was assessed on the 28S/18S rRNA ratio amongst several other characteristics of the RNA electropherogram trace, to generate an RNA Integrity Number (RIN). High quality RNA requires a minimum RIN of ≥ 6.8, concentration ≥ 20ng/µL and a 29S to 18S rRNA ratio of ≥ 2.

2.6.3 RNA Sequencing (RNAseq)

RNA sequencing was performed by Novogene (Cambridge, UK).

2.6.3.1 Library construction and sequencing

Library preparation and sequencing was completed by Novogene. Messenger RNA (mRNA) was purified from total RNA using poly-T oligo-attached magnetic beads.

After fragmentation, the first strand of complementary DNA (cDNA) was synthesized using random hexamer primers, and the second cDNA strand was created using either dTUP for directional libraries or dTTP for non-directional libraries. Both were then subjected to end repair, A-tailing, adapter ligation, size selection, amplification and purification, with an additional step of USER enzyme digestion for the directional library. The libraries were then checked with Qubit and real-time PCR for quantification and size distribution was checked using a bioanalyzer. Quantified libraries were then pooled, and clustering of the index-coded samples was performed, followed by sequencing on the Illumina PE150 platform with 20M reads, where paired-end reads were generated.

2.6.3.2 Quality control

Raw read data of fastq format was processed through in-house perl scripts, and clean reads were obtained by removing reads containing ploy-N, adapter and low-quality data.

2.6.3.3 Mapping to reference genome

An index of the reference genome was built, and paired-end clean reads were aligned using Hisat2 v2.0.5.

2.6.3.4 Quantification of gene expression level

Read numbers mapped to each gene were counted using featureCounts v1.5.0-p3. Fragments Per Kilobase of transcript sequence per Million base pairs sequenced (FPKM) was then calculated based on the length and read counts mapped for each gene. FPKM considers the effect of sequencing depth, gene length and read count at the same time, and is the most commonly used technique for estimation of gene expression level.

2.6.3.5 Differential expression analysis

Read counts were firstly adjusted using edgeR by one scaling normalised factor. Differential expression analysis of two conditions was performed using the edgeR R package (3.22.5). P values were adjusted using the Benjamini and Hochberg method and significance cut offs were set at 0.05. Absolute fold change values of -2 and +2 were also set as thresholds for significance to create lists of differentially expressed genes (DEGs).

2.6.3.6 Gene set enrichment analysis (GSEA)

GSEA is a powerful computational tool to determine if a predefined gene set shows significant differences between two biological states (Mootha et al. 2003; Subramanian et al. 2005). Gene lists were prepared by ranking from high to low fold change value between the two samples in question and loaded into GSEA. Gene sets were downloaded from the MSigDB molecular signatures database (http://www.gsea-msigdb.org/gsea/msigdb/index.jsp). Gene lists were then tested against the gene sets to determine if they were enriched at the top or bottom of the list and create an overall enrichment score (ES).

2.6.3.7 Ingenuity Pathway Analysis (IPA)

QIAGEN IPA is a powerful tool for network generation, pathway analysis, pathway activation prediction and comparison of RNAseq data sets (QIAGEN Inc., https://digitalinsights.qiagen.com/IPA) (Krämer et al. 2014). Raw gene lists were uploaded to IPA and expression core analysis was completed based on expression log ratio, using set cut offs of -2 and +2 log2 fold change and padj <0.05. Comparison analysis was then completed using the core analysis for each cell line to compare canonical pathways and diseases and functions in each data set.

2.6.4 Preparation of cDNA for Quantitative Analysis

cDNA synthesis was performed using the Quantitect Reverse Transcription Kit™ (Qiagen, UK) in 0.2ml PCR tubes as per manufacturer's guidelines. A BioRad T100™ Thermocycler was used following the conditions outlined in Table 2.7.

Table 2.7 cDNA synthesis thermocycler conditions

Stage	Temperature (ºc)	Time (Minutes)
Annealing	25	5
Synthesis	42	30
Reverse transcription inactivation	85	5

2.6.5 Quantitative real-time polymerase chain reaction (qRT-PCR)

Pre-designed TaqMan™ primer/probes were obtained from Applied Biosystems, as listed in Table 2.8.

Table 2.8 Taqman probes used in qRT-PCR

Gene Symbol	Assays on Demand Reference	Dye
CD200	Hs01033303_m1	FAM-MGB
ADAM17	Hs01041915_m1	FAM-MGB
ADAM28	Hs00248020_m1	FAM-MGB
ADAM9	Hs00177638_m1	FAM-MGB
ACTB	Hs00357333_g1	FAM-MGB
GAPDH	Hs02758991_g1	FAM-MGB

Reactions were run using the TaqMan Universal Master Mix™ (Applied Biosystems) according to the manufacturer's guidelines with a final volume of 15μl for 96-well plates or 10μl for 384-well plates. Housekeeping genes (GAPDH and β-actin) were used as a reference gene for each plate run. All reactions were run in three technical triplicates. All reactions were run on the QuantStudio 7 Flex Real-Time PCR system™ (Applied Biosystems), according to the cycling conditions listed in Table 2.9. QuantStudio software was used to run and analyse experiments, and gene expression analysis was completed using the 2ΔΔCt method to calculate fold change relative to housekeeping genes, and arbitrary units were calculated for analysis of expression levels.

Table 2.9 qRT-PCR cycling conditions on QuantStudio 7

Stage	Temperature (ºc)	Time	Cycles
Hold	50	2 minutes	1
Hold	95	10 minutes	
Melt	95	15 seconds	40
Annealing and extension	60	1 minute	

2.7 Protein analysis

2.7.1 Protein extraction

Cells were detached as previously described, counted and the required number of cells were pelleted by centrifugation at 200xg for 5 minutes, supernatant was removed, and the pellet was resuspended in 100µl radioimmunoprecipitation assay (RIPA) buffer per 1 x 10^6 cells. The composition of RIPA buffer can be found in Table 2.10. The suspension was then incubated on ice for 30 minutes, following which the pellet was mechanically disrupted by pipetting and left on ice for a further 30 minutes before centrifugation at 10,000xg for 10 minutes at 4°C.

Table 2.10 RIPA buffer composition

Reagent	Volume/Weight	Working Concentration
EDTA	0.4ml of 0.5M	2mM
NP-40	1ml	1%
Sodium Chloride	3ml of 5M	150mM
SDS	0.1g	0.1%
Sodium fluoride	0.21g	50mM
Sodium-deoxycholate	0.5g	0.5%
Tris hydrochloride	5ml of 1M	50mM
Distilled H_20	Made up to 100ml	

2.7.2 Protein quantification

Protein concentration was calculated using the Pierce™ bicinchoninic acid (BCA) assay (ThermoFisher). Samples were diluted 1:2 in RIPA buffer and 15µl was added

in duplicate alongside standards of bovine serum albumin (BSA) at known concentrations of 5, 25, 50, 125 and 250μg/ml to a clear, flat bottomed 96 well plate (Corning). BCA working reagent was made of 50 parts reagent A to 1 part reagent B, and 200μl was added to each well. The plate was covered and incubated at 37°C for 30 minutes, following which the absorbance of the plate was measured at 562nm using a CLARIOstar™ plate reader (BMG Labtech). Control wells containing RIPA buffer and working reagent were used as blanks, with all samples corrected against the values of these wells. A standard curve was generated from the BSA standards, and the concentration of the protein samples was calculated from the curve equation.

2.7.3 Western Blotting

A list of all solutions required for western blotting can be found in Table 2.11. Protein samples were diluted in RIPA buffer to equal concentrations (10-20ug of protein), following which 5μl Laemmli buffer (4x) was added and made up to 20μl total volume with RIPA buffer. Samples were then heated at 95°C for 4 minutes on a heating block and centrifuged to collect the sample at the bottom of the tube. TGXTM FastCast™ premixed acrylamide solutions (BioRad) were used to cast 1.5mm gels. 20μL of prepared samples were loaded into the wells in addition to a molecular weight marker (PageRuler Plus™, ThermoFisher) and empty wells were loaded with 20μl RIPA and Laemmli buffer (4x). The gels were run in a 10% sodium dodecyl sulphate (SDS) buffer at 200V until the desired marker separation was achieved. The Trans-Blot® TurboTM Transfer System (BioRad) was used to transfer to a polyvinylidene difluoride (PDVF) membrane. After washing in tris-buffered saline with 0.1% Tween (TBST), membranes were incubated with gentle agitation in blocking buffer of 10% BSA or skimmed milk in TBST for 1 hour at RT. Following incubation and washing in TBST, membranes were incubated in the desired primary antibody (see Table 2.12) diluted in 5% BSA or skimmed milk according to manufacturer's instructions in TBST and incubated overnight at 4°C on a roller. The following day, the membrane was washed for 4 x 5 minutes in TBST before incubating with horseradish peroxidase (HRP)-conjugated secondary antibody diluted in 5% BSA or skimmed milk in TBST for 1 hour at RT (see Table 2.13). Membranes are washed

again for 4 x 5 minutes in TBST before antibody binding was detected by incubating Lumina Forte™ chemiluminescence reagent (Millipore) on the membrane for 30-60 seconds (less for endogenous controls) and membrane transferred to the ChemiDoc MP Imaging System™ (BioRad) where chemiluminescence was detected and imaged. Membranes were then stripped using Restore™ Western Blot Stripping Buffer (Thermo Fisher), washed in TBST, blocked and re-probed to detect another protein of interest or endogenous control. Western blot data was quantified by densitometry, using ImageLab™ software (BioRad), where the pixel density in the selected lanes was quantified and compared.

Table 2.11 Solutions required for western blotting

Solution	Composition
4x Laemmli (Loading) Buffer	60mM Tris-Cl pH 6.8, 2% SDS, 10% glycerol, 5% β- mercaptoethanol, 0.01% bromophenol blue
TBST	1xPBS solution: 5 tablets 500mL dH2O with 0.5mL Tween (Sigma)
Resolving Gel	Made using TGXTM FastCastTM Acrylimide Kit, 7.5% #161-0171
Stacking Gel	Made using TGXTM FastCastTM Acrylimide Kit, 7.5% #161-0171
1x SDS-PAGE Running Buffer	3.62g Trizma (Sigma), 14.4g Glycine (Sigma) pH6.8 and add H2O up to 1 L
Trans-Blot Turbo Transfer Buffer	200mL 5x Trans-Blot Turbo Transfer Buffer and 200ml ethanol in 600mL of dH2O
Blocking Buffer	10% w/v non-fat dry milk powder (Marvel) or BSA powder (Sigma) in 3mL TBST
Antibody Dilution Buffer	5% w/v non-fat dry milk powder (Marvel) or BSA powder (Sigma) in 3mL TBST

Table 2.12 Primary antibodies used in western blotting

Target	Dilution	Source	Cat #	Species	Target Size (kDa)
CD200	1:500	R&D	AF2724	Goat	~47
ADAM9	1:1000	Thermo Fisher Scientific	PA5-76732	Rabbit	~75
ADAM17	1:500	Thermo Fisher Scientific	PA5-27395	Rabbit	~75
ADAM28	1:500	Thermo Fisher Scientific	PA5-67323	Rabbit	~53
GAPDH	1:5000	Millipore	MAB374	Mouse	~38
β-Actin	1:1000	Thermo Fisher Scientific	PA1-183	Rabbit	~42

Table 2.13 Secondary antibodies used in western blotting

Antibody	Dilution	Source	Cat #
Rb to Gt IgG (HRP)	1:3000	Abcam	ab97100
Gt to Rb IgG (HRP)	1:3000	Abcam	ab97051
Gt to Ms IgG (HRP)	1:3000	Abcam	ab98693

2.8 Bioinformatic analysis

2.8.1 Acquisition of publicly available RNAseq data sets

The Cancer Genome Atlas (TCGA) kidney renal clear cell carcinoma (KIRC), papillary (KIRP) and chromophobe (KICH) Firehose Legacy data sets were downloaded from https://gdac.broadinstitute.org/. The Illimminahiseq-rnaseqv2-RSEM_genes_normalised data files were used for analysis, consisting of RNAseq by expectation-maximisation (RSEM) gene-normalised RNAseq data for 537, 323 and 113 patients respectively. Corresponding patient clinical data was acquired from https://www.cbioportal.org/, including age, sex, race histological classification, TNM stage, OS time and status, PFS time and status and tumour laterality.

2.8.2 CIBERSORTx: Estimation of infiltrating immune cell fractions

CIBERSORTx (Cell type Identification By Estimating Relative Subset Of unknown RNA Transcripts), available at https://cibersortx.stanford.edu/, is a deconvolution algorithm that uses the LM22 gene set to analyse the relative expression of 547 genes to predict the proportion of 22 infiltrating immune cell types (Newman et al. 2019). The cell types analysed by LM22 include naïve and memory B cells, plasma cells, CD8+ T cells, naïve CD4+ T cells, memory resting CD4+ T cells, memory activated CD4+ T cells, Tregs, T follicular helper cells, gamma-delta T cells, resting and activated NK cells, M0, M1 and M2 macrophages, resting and activated dendritic cells, resting and activated mast cells, eosinophils, and neutrophils. The normalised Firehose Legacy RCC data sets were uploaded to CIBERSORTx with batch correction enabled to minimise cross-platform variation, as the LM22 gene set was generated from microarray and the Firehose sets were generated through RNAseq. Permutations for significance was set at 500 and significant results with $p<0.05$ were selected for further analysis.

2.9 Statistical analysis

Statistical analyses were performed using Graphpad Prism 9 software. Normality tests were run on each group of data and differences between 2 groups were analysed using unpaired t-tests on normally distributed data and Mann-Whitney U

tests on data that was not normally distributed. When comparing more than 2 groups, a one-way analysis of variance (ANOVA) was used to compare the group means with the Kruskal-Wallis multiple comparisons test used to compare the mean of each column with the mean of every other column. Post-tests were carried out as appropriate using the FDR method or Dunn's multiple comparisons test. Logrank analysis was used to compare differences between Kaplan-Meier survival curves. Correlation analysis was completed using the Pearson correlation coefficient for normally distributed data and Spearman correlation analysis for nonparametric data. Hazard ratios (HR) and their 95% confidence intervals were calculated using the Cox Proportional Hazards Regression main effects model. Principal Component Analysis (PCA) was completed using immune cell estimations generated by CIBERSORTx as variables and was based on parallel analysis. Statistically significant differences are marked on graphs as * = $p < 0.05$, ** = $p < 0.01$, *** = $p < 0.001$ and **** = $p < 0.0001$.

Chapter 3: Characterising RCC CD200 Expression and Ectodomain Shedding

3. Characterising RCC CD200 expression and ectodomain shedding

Ectodomain shedding is the mechanism of proteolytic cleavage of cell surface molecules, leading to the release of an active soluble form into the extracellular microenvironment. Ectodomain shedding has many functions involving the regulation of expression and function of cell surface molecules, and a wide variety of cellular and physiological processes including growth factor signalling, inflammation and cell survival (Clark 2014). After proteolytic cleavage, the released ectodomain can have a separate function of its own while the remaining transmembrane peptide may be internalised by endocytosis or be subject to further cleavage, commencing further internal signalling cascades (Mochizuki and Okada 2007; Clark 2014).

CD200 is susceptible to ectodomain shedding, creating a soluble form known as soluble CD200 (sCD200) (Wong et al. 2016). CD200 has gained interest in our group as the interaction of CD200 with its receptor, CD200R, acts as an immune checkpoint which is utilised by cancer cells to evade the immune system allowing cancer progression (Morgan et al. 2022). CD200 overexpression has been observed in many cancer types, and expression correlates with increased tumour burden, disease aggressiveness, disease stage and altered immune infiltrate in several cancer types. sCD200 has also been shown to be able to activate CD200R, however if the activation is as efficient as the full length membrane-bound form is currently unknown (Wong et al. 2016).

The proteases responsible for CD200 ectodomain shedding have not been fully established, however ADAM28 (Twito et al. 2013b; Wong et al. 2016) and ADAM17 (Wong et al. 2016) have been shown to be involved in this process in CLL, while our group has also shown that MMP3 and MMP11 are involved in this process in basal cell carcinoma (Morgan et al. 2022). Other proteases may however also be involved in this process.

Hypothesis

We hypothesise that multiple proteases are involved in CD200 ectodomain shedding, resulting in increased sCD200 levels in RCC. We also hypothesise that RCC CD200 in combination with protease expression will adversely affect prognosis.

Aims of this chapter

1. Determine which sheddases are overexpressed in RCC using literature search and RNA sequencing of RCC cell lines.

2. Establish CD200 and protease co-expression in RCC tissue samples using immunofluorescent staining.

3. Determine if proteases contribute to CD200 ectodomain shedding using sCD200 ELISA.

3.1 Characterising CD200 expression in kidney tissue

CD200 expression has been previously described on the endothelium of kidney glomeruli (Colmont et al. 2013), however expression has not been previously described in other parts of the kidney.

We studied CD200 expression using immunofluorescent (IF) staining on RCC tissue microarrays (TMAs), containing a total of 99 paraffin-embedded tissues of RCC patients. Of the 99 samples, 69 were ccRCC, 10 were chRCC, 12 were pRCC and 8 were normal kidney, with a range of different disease stages (I-IV) and tumour, node and metastasis (TNM) status (T1-3, M0-M1 and N0-N1) for each subtype. The CD200 staining intensity for each core was calculated using a threshold scoring system to divide positive cells into low, moderate or high intensity groups to provide an overall H-Score, as described in section 2.2.1 of the materials and methods chapter. We then analysed the CD200 expression strength in each core and the relationship between this expression and (i) RCC subtype, (ii) disease stage, (iii) age at operation and (iv) sex.

3.1.1 CD200 antibody optimisation

We firstly determined the specificity of the CD200 antibody by staining human skin, where CD200 has been shown to be a marker for the hair follicle bulge (Coles et al. 2011), as shown in Figure 3.1.

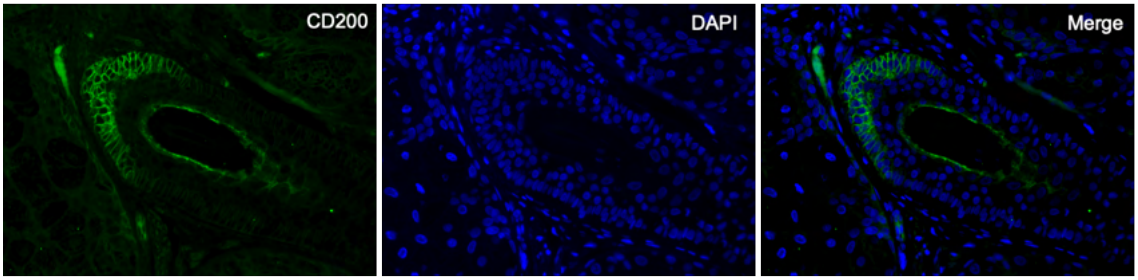

Figure 3.1 Optimisation of CD200 IF staining in human hair follicles
Representative images of CD200 staining in human skin hair follicles, an area known to be rich in CD200 expression, with positive staining found in the bulge cells to confirm the specificity of the antibody. Samples with no primary antibody were used as controls to confirm the staining (data not shown).

3.1.2 Characterising CD200 expression in normal kidney

Having confirmed the specificity of our antibody, we next examined CD200 expression on normal kidney within each kidney structure.

3.1.2.1 CD200 expression in the renal corpuscle

CD200 expression was firstly studied in the renal corpuscle and surrounding proximal tubules, as shown in Figure 3.2.

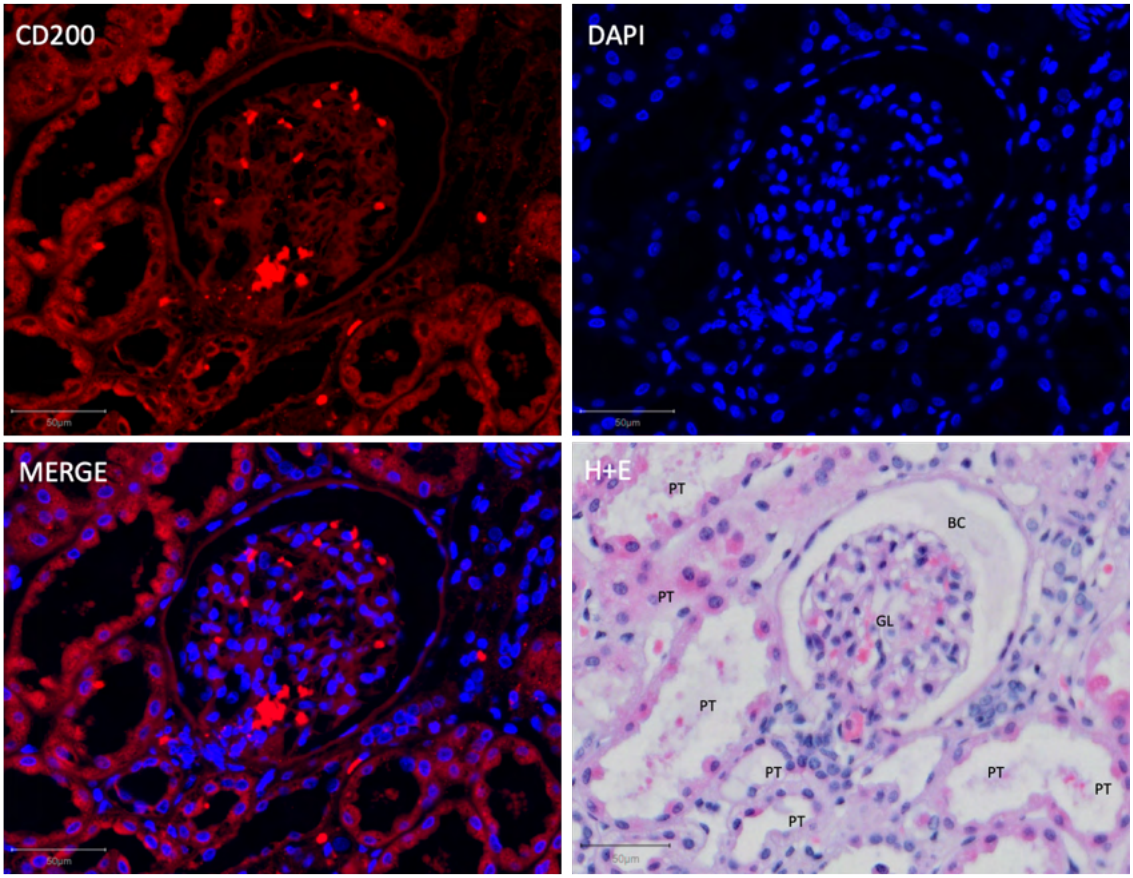

Figure 3.2 Representative CD200 staining within the renal corpuscle and surrounding tubules.
Staining for immunofluorescent CD200 and DAPI followed by H+E. Weak to moderate staining was found throughout the glomerular capillaries, with no staining observed on mesangial cells. Strong expression was observed on the surrounding proximal tubules. Scale bar represents 50 µm.
Abbreviations: ***BC*** *Bowman's capsule,* ***GL*** *Glomerulus,* ***PT*** *Proximal tubule*

Weak to moderate CD200 expression was observed on the endothelial capillary network within the glomerulus, with no staining overserved on the mesangial cells or podocytes. Weak staining was also observed on the simple squamous epithelial cells

of the Bowman's capsule. Strong CD200 expression was however observed on the attached and surrounding sections of proximal convoluted tubule.

3.1.2.2 CD200 expression in the distal and proximal convoluted tubules

To further study the CD200 expression within the proximal convoluted tubule compared to the other parts of the tubule system, we next looked at a different area of normal kidney tissue which comprised of sections of both proximal and distal convoluted tubule, as shown in Figure 3.3.

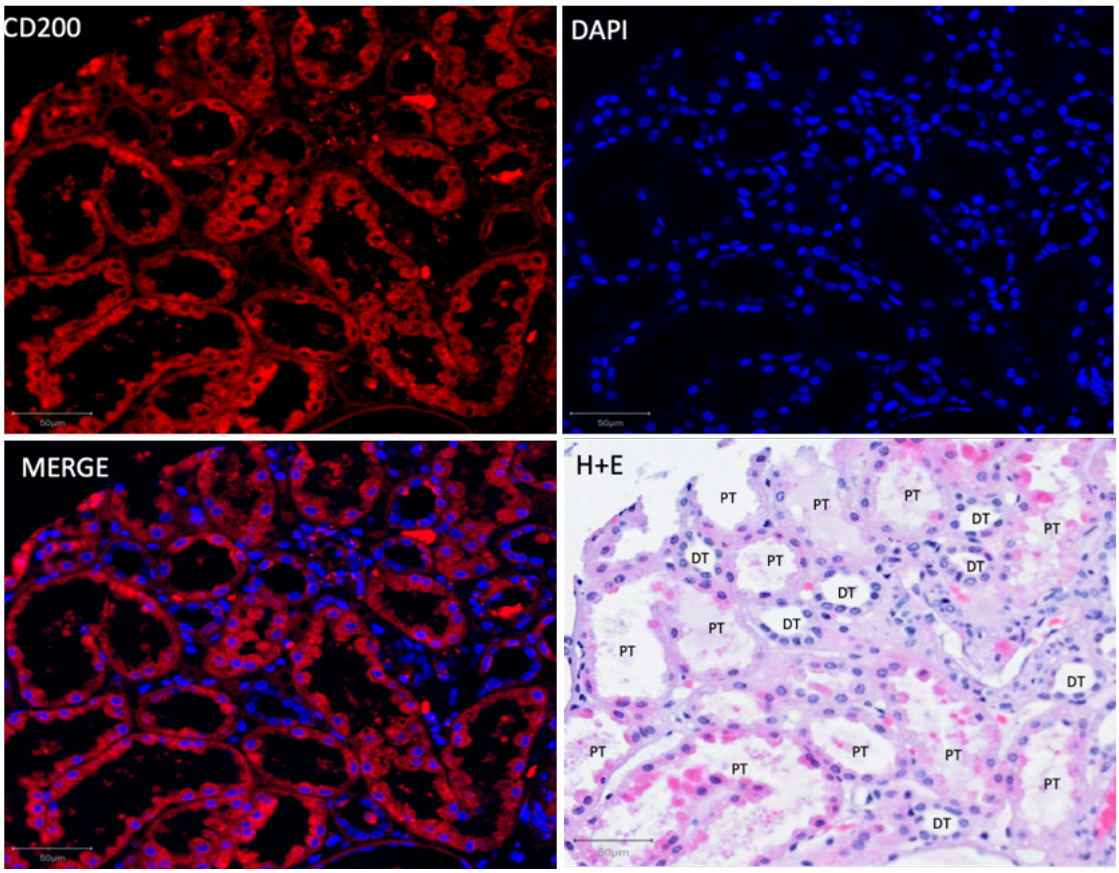

Figure 3.3 Representative CD200 staining within the proximal and distal convoluted tubules
Staining for immunofluorescent CD200 and DAPI followed by H+E. CD200 expression was present in both tubule types, however expression was stronger in the proximal tubules, discernible by their microvilli brush border, compared to the distal convoluted tubule which lacks a brush border and so has a more open, unobstructed lumen. Scale bar represents 50 μm.
Abbreviations: ***DT*** *Distal convoluted tubule,* ***PT*** *Proximal convoluted tubule.*

CD200 expression was noted on both the proximal and distal convoluted tubules, however expression was noticeably stronger in the proximal tubules. The proximal convoluted tubule is the site where around 65% of the filtrate's water and ions are

reabsorbed, and so the cells have an apical brush border to increase their reabsorption surface area which makes the lumen appear filled, which is a useful way to distinguish the proximal tubule from the other tubules. The cells of the proximal tubule also stain strongly eosinophilic and as the cells are large, when sectioned it can appear that there are less nuclei present than in other parts of the tubules, allowing for further distinction from the other tubule types. Conversely, the distal convoluted tubule appears smaller with an empty lumen as the cells have no brush border, with weaker eosinophilic staining and a higher number of nuclei apparent within a section. Generally, a lower number of distal convoluted tubules appear within a tissue section as the tubule is shorter than the proximal tubule and is less convoluted. Weak CD200 expression was noted in all distal convoluted tubules measured.

The strong CD200 expression observed in the proximal convoluted tubules is of interest to us, as the epithelium of the proximal convoluted tubule has been reported to be the cell of origin for clear cell (ccRCC) (Verma and Molitoris 2015) and papillary (pRCC) renal cell carcinomas (Muglia and Prando 2015), the two most common subtypes. The third most common RCC subtype, chromophobe (chRCC), is reported to originate from the distal convoluted tubule (Ozcan et al. 2014). Later in this chapter we will investigate whether the strong CD200 expression found on the proximal convoluted tubules in normal kidney is carried through into ccRCC and pRCC tissue, and if chRCC CD200 expression remains lower throughout disease development after originating from the distal convoluted tubule.

3.1.2.3 CD200 expression in the loop of Henle and collecting ducts

CD200 expression was next examined on the loop of Henle and collecting ducts, as shown in Figure 3.4.

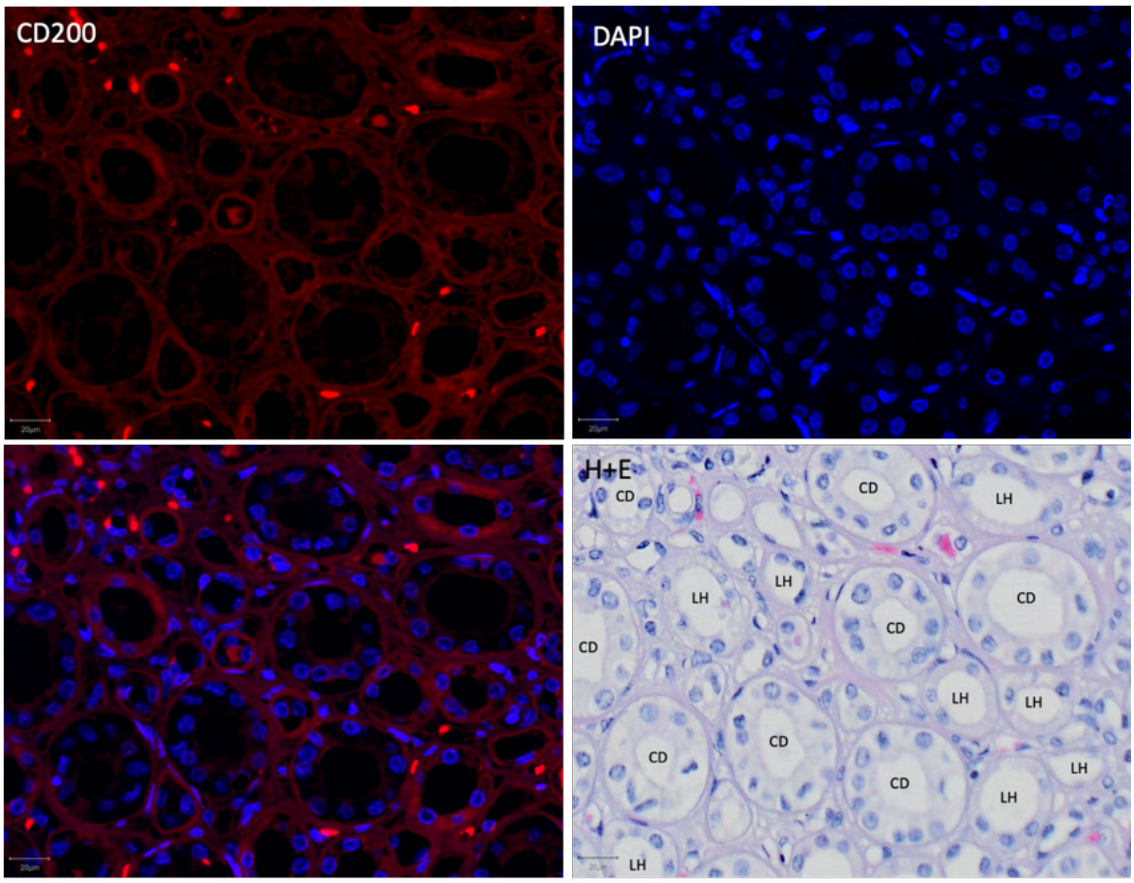

Figure 3.4 Representative CD200 staining within the collecting ducts and loop of Henle
IF staining for CD200 and DAPI followed by H+E. Weak CD200 expression was observed in the collecting ducts, with moderate expression noted in the loop of Henle. Collecting ducts are distinguishable by their pale cytoplasm and prominent lateral border, while the flat epithelial cells of the loop of Henle form a thin descending limb and thick and thin ascending limb. Scale bar represents 20µm.
Abbreviations: ***CD*** *Collecting duct,* ***LH*** *Loop of Henle.*

Weak CD200 expression was observed throughout the loop of Henle, however low to zero expression was found in the collecting ducts. This data shows that CD200 expression appears to gradually reduce with increased distance from the renal corpuscle, with strong expression observed in the proximal convoluted tubules, moderate expression found in the loop of Henle, moderate expression in the distal convoluted tubule and weak to no expression in the collecting ducts.

3.1.2.4 CD200 staining quantification

To quantify what we have observed, CD200 staining H-scores were next calculated for each kidney structure, as shown in Figure 3.5. H-scores of 0-99 were counted as weak expression, 100-199 were counted as moderate expression and 200-300 were counted as strong expression.

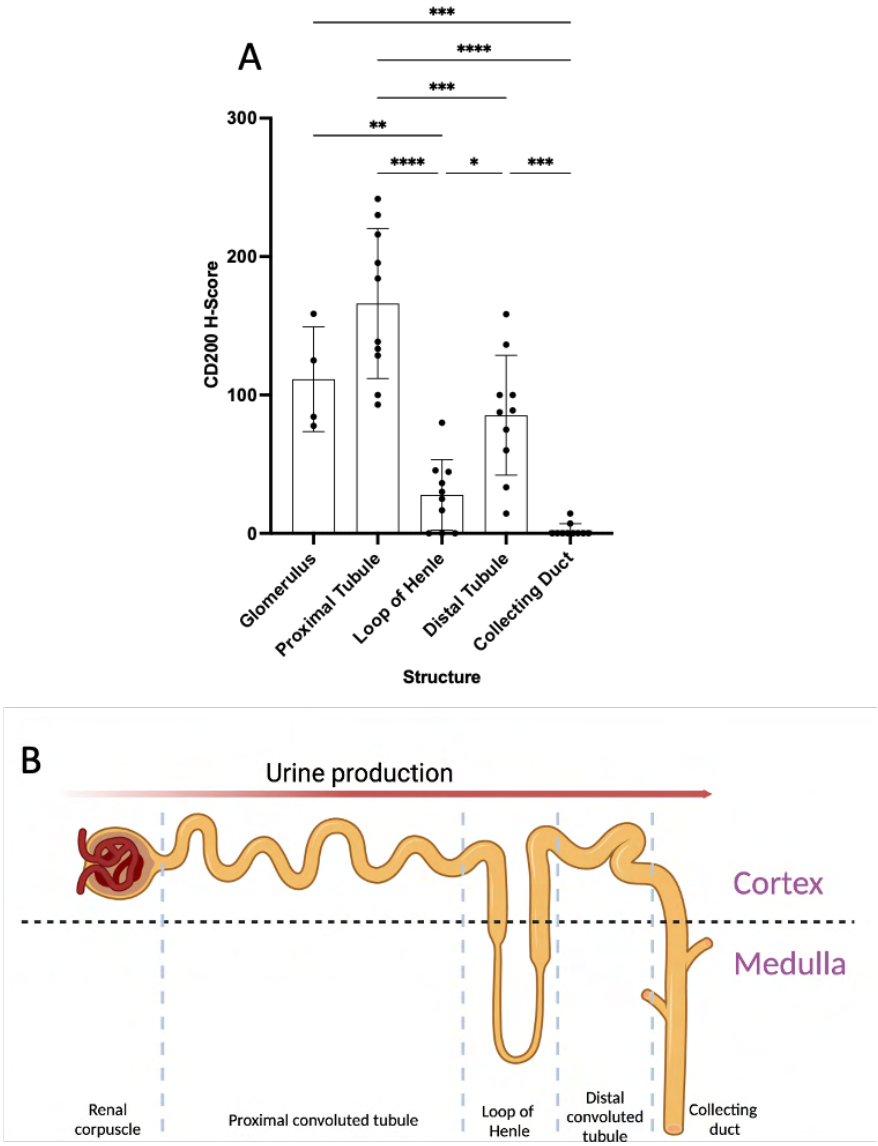

Figure 3.5 CD200 H-score comparison in normal kidney structures
(A) Comparison of CD200 H-score between normal kidney structures revealed reduced CD200 expression in cells furthest along the tubule system. All measurements were n=10 except glomeruli which were n=4 due to tissue availability. H-scores were compared using ANOVA, where *, **, *** and **** represent p<0.05, <0.01, <0.001 and <0.0001 respectively. (B) CD200 expression appears to reduce along the length of the nephron, with expression significantly lower in structures within the medulla compared to the cortex.
Created in Biorender.com.

CD200 H-scores were compared for each normal kidney structure, where the strongest scores were found in the proximal convoluted tubule and glomerulus (Figure 3.5a). Weak to moderate H-scores were also observed in the distal convoluted tubules, however the scores were found to be significantly lower than those in the proximal tubules (85.37 ± 44.31 vs 166.1 ± 54.19, p = <0.001). The lowest CD200 H-scores were found in the collecting ducts and loop of Henle, both of

which are found in the medulla, opposed to the other structures which are within the renal cortex. Interestingly, the collecting duct, which is at the end of the nephron system, was found to have significantly lower CD200 H-scores compared to the glomerulus (2.14 ± 4.82 vs 111.4 ± 37.82, p = <0.001) and proximal convoluted tubules (2.14 ± 4.82 vs 166.1 ± 54.19, p= <0.001) which are at the start of the nephron tubule system, as demonstrated in Figure 3.5b.

This data shows that in normal kidney, CD200 expression is strongest in the proximal convoluted tubules, the cell of origin for ccRCC and pRCC. CD200 is still present in the distal convoluted tubules, the cell of origin for chRCC, however levels were found to be significantly lower. We next aimed to establish CD200 expression in RCC tissue by determining if the expression we have observed in normal kidney is carried through into the tumour, and if so, whether the expression level is changed.

3.1.3 Characterising CD200 expression in RCC

3.1.3.1 CD200 expression in RCC subtypes

Using TMAs comprising of 62 ccRCC, 17 pRCC, 10 chRCC and 8 normal kidney samples, we next aimed to characterise CD200 expression in RCC subtypes using IF staining. Representative weak, moderate and strong CD200 staining in each subtype can be seen in Figure 3.6-3.8, however none of the chRCC samples were found to have strong staining.

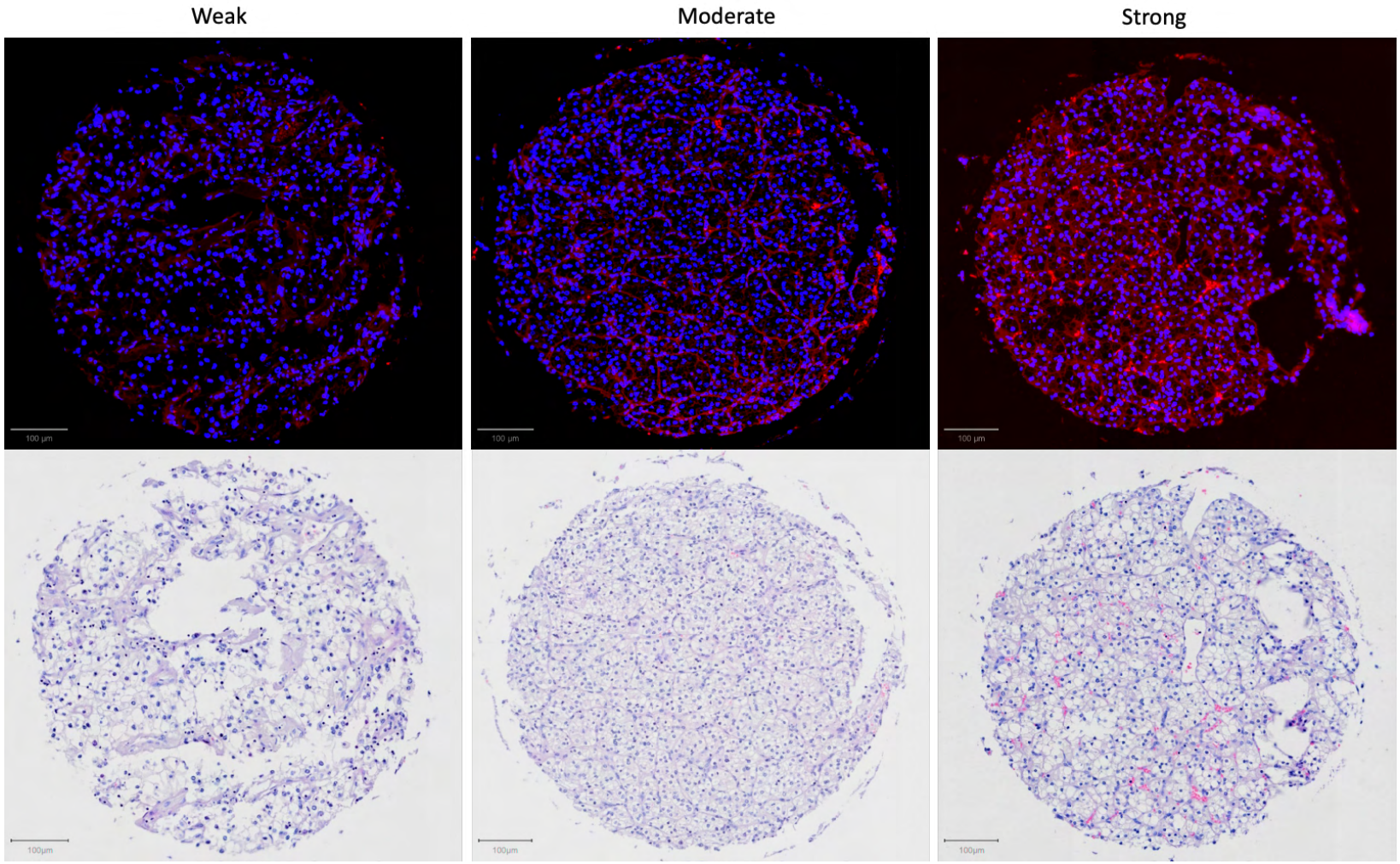

Figure 3.6 Representative weak, moderate and strong CD200 staining in ccRCC TMA cores with corresponding H+E staining
H-scores <100 were classed as weak staining, H-scores from 100-199 were classed as moderate staining and 200-300 were classed as strong.

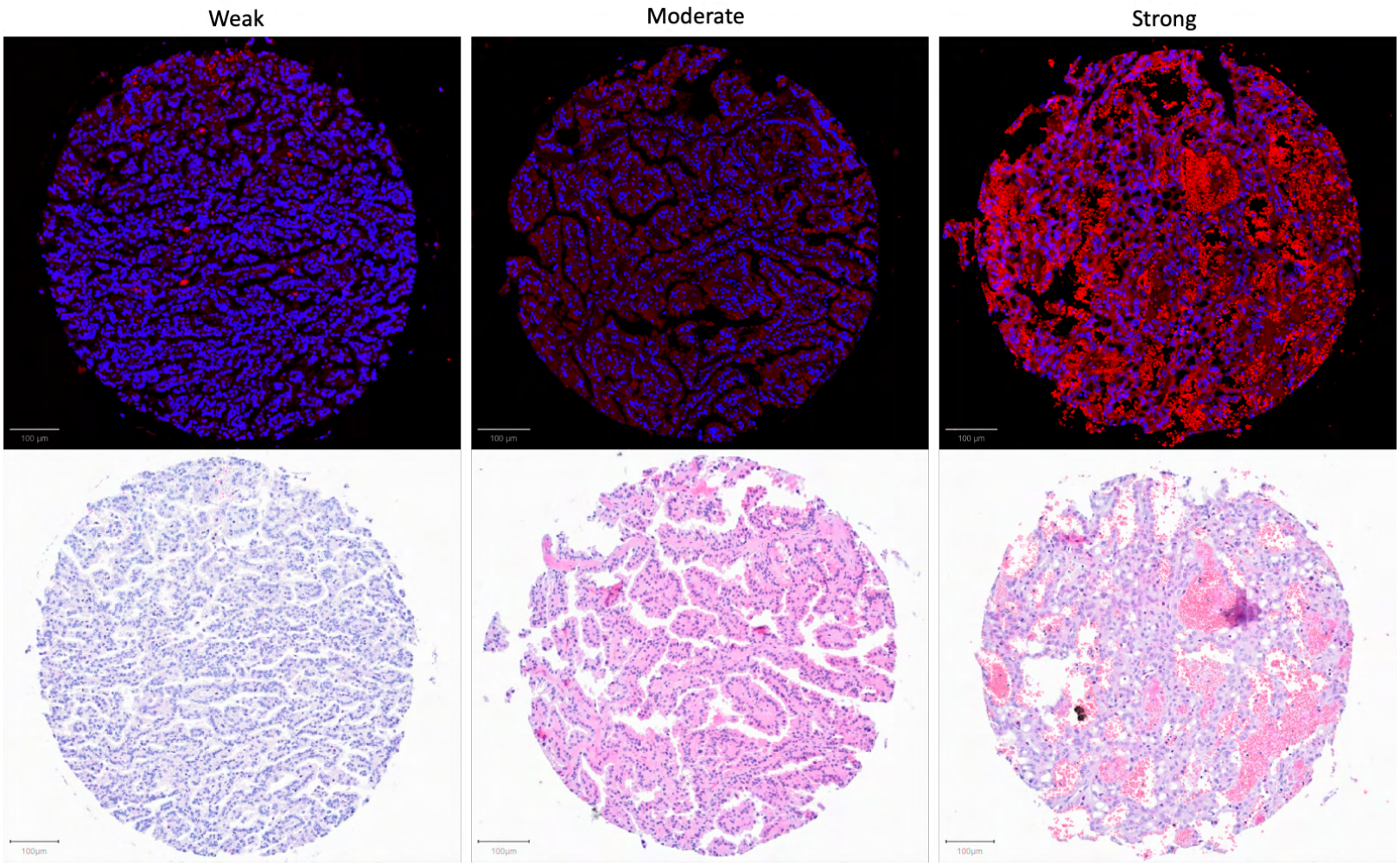

Figure 3.7 Representative weak, moderate and strong CD200 staining in pRCC TMA cores with corresponding H+E staining
H-scores <100 were classed as weak staining, H-scores from 100-199 were classed as moderate staining and 200-300 were classed as strong.

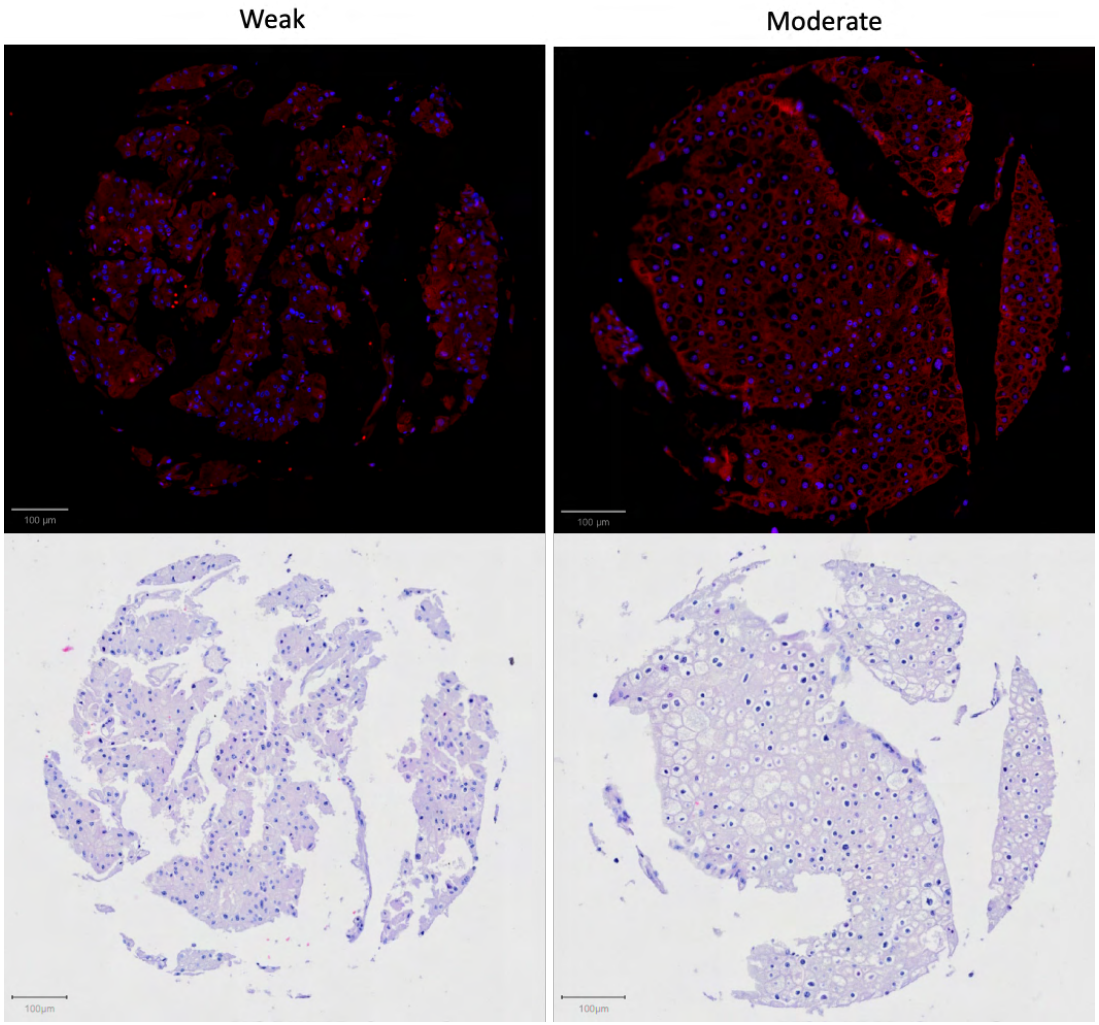

Figure 3.8 Representative weak and moderate CD200 staining in chRCC TMA cores with corresponding H+E staining
H-scores <100 were classed as weak staining and H-scores from 100-199 were classed as moderate staining. No chRCC samples exhibited strong staining with a H-score over 200.

CD200 H-scores were calculated as previously described between the RCC subtypes, as shown in Figure 3.9.

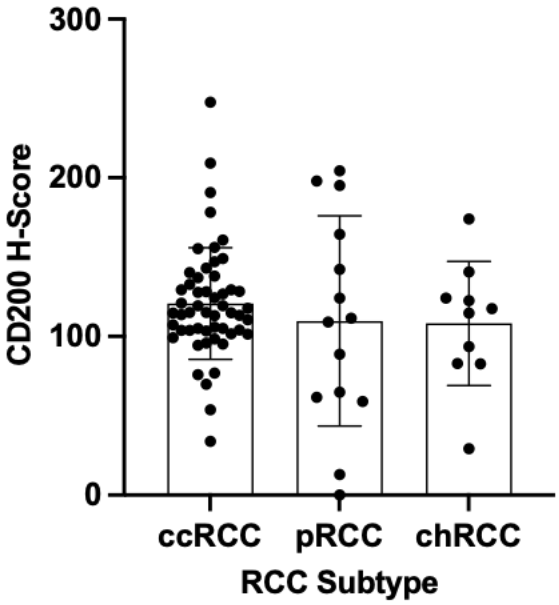

Figure 3.9 CD200 H-scores in RCC subtypes
H-scores for all samples were compared by RCC subtype. Mean CD200 H-score was highest in ccRCC, with the lowest mean H-score observed in chRCC. A Kruskal-Wallis test followed by Dunn's multiple comparisons test was used to compare the groups, however no significant differences were found between the subtypes.

CD200 H-score was found to be consistent between the subtypes, however the TMAs contained a much larger number of ccRCC samples (n=53) compared to pRCC (n=14) and chRCC (n=10). The strongest mean staining was observed in ccRCC, however the three subtypes had similar means and range of H-scores within the samples.

3.1.3.2 CD200 expression by TNM status

Having determined that CD200 expression is strongest in ccRCC, we next compared CD200 H-score by patient TNM status to determine if any changes in expression are observed. We next compared H-scores by tumour, node and metastasis status in RCC as a whole and within the subtypes as shown in Figure 3.10. T4 samples were only available in ccRCC.

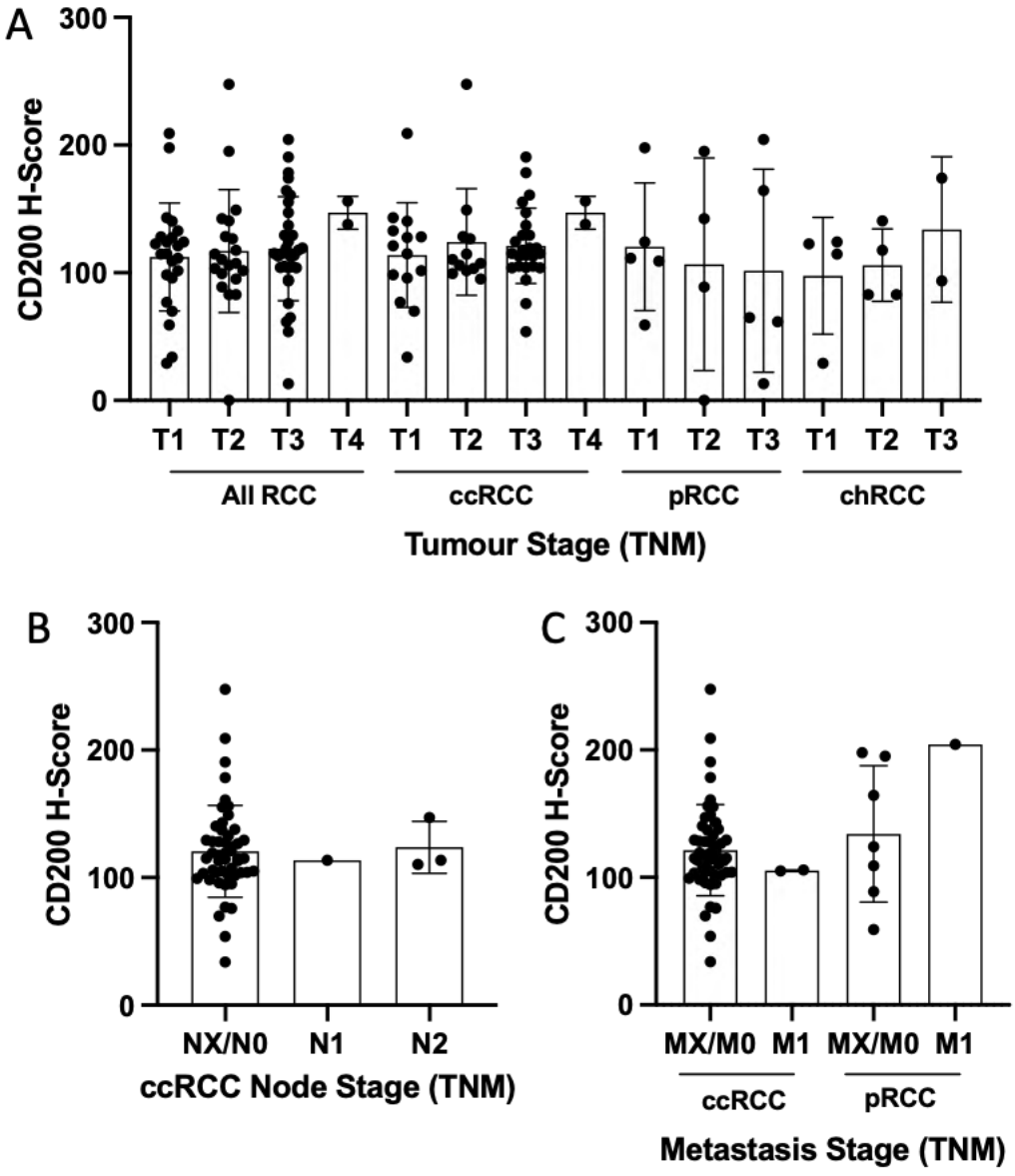

Figure 3.10 CD200 expression in RCC subtypes by TNM status
(A) CD200 H-score in all RCC, ccRCC, pRCC and chRCC were compared by tumour status. T4 samples were only available in ccRCC. (B) CD200 H-score in ccRCC samples compared by node status. All pRCC and chRCC samples were NX/N0 status, (C) CD200 H-score in ccRCC and pRCC compared by metastasis status. All chRCC samples were MX/M0 status. Analyses was completed using a Kruskal-Wallis test followed by Dunn's multiple comparisons test; however, no significant differences were found.

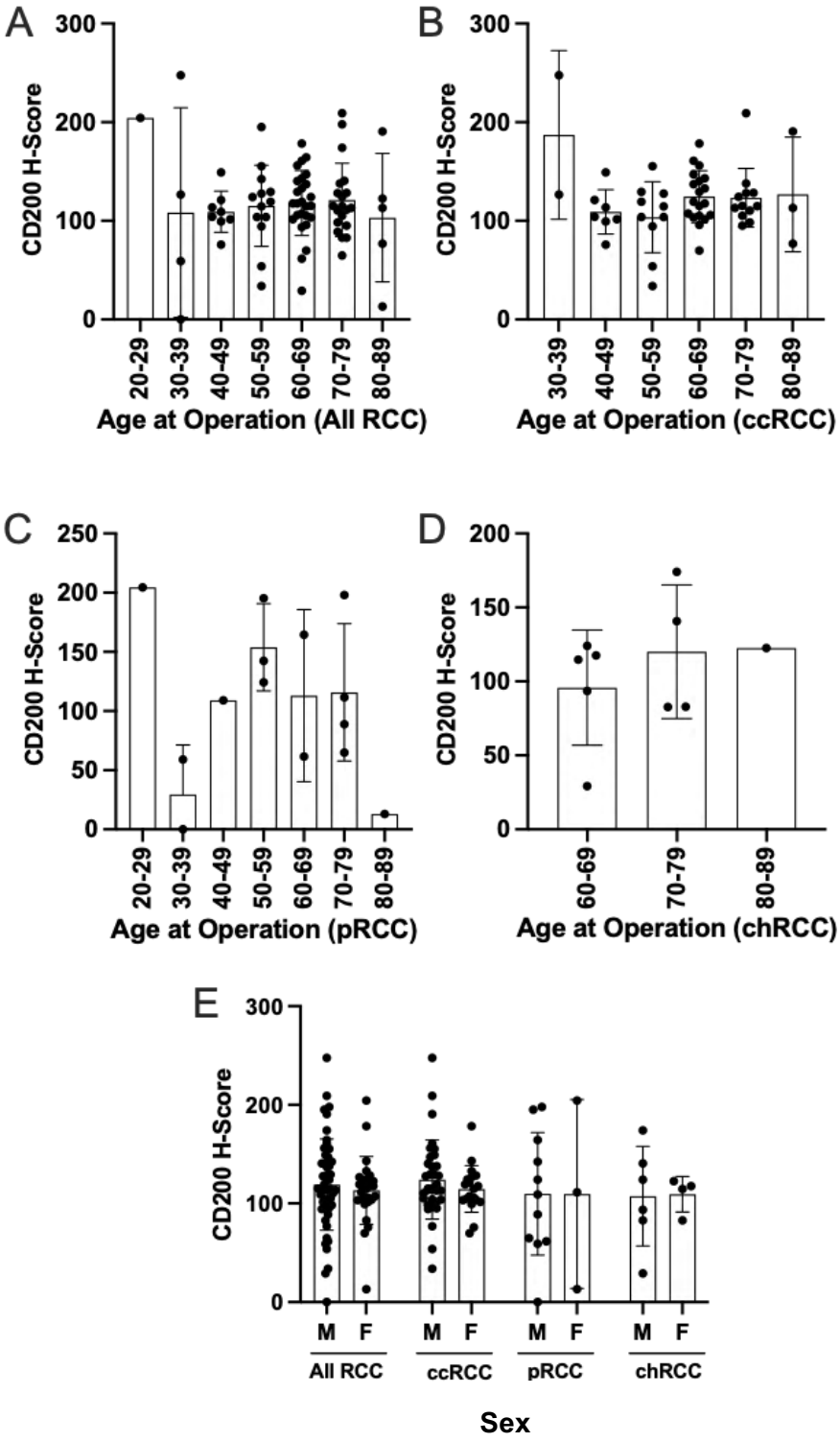

Figure 3.11 CD200 expression by age at operation and sex
CD200 H-score was compared against patient age and sex in: (A) All RCC, (B) ccRCC, (C) pRCC, (D) chRCC by age. (E) All RCC and subtypes by sex. A-D: Analysis was completed using a Kruskal-Wallis test followed by Dunn's multiple comparisons test; however, no significant differences were found between any group. E: Analysis was carried out using a Mann-Whitney test to compare male and female samples within each subtype, however no significant differences were found.

CD200 H-score was found to generally increase with T stage in all RCC, ccRCC and chRCC (Figure 3.10a), however expression was found to generally decrease with increased T stage in pRCC. No significant differences were observed between the stages in any of the subtypes, however this could be due to the small sample sizes within in each group. We next examined node involvement (Figure 3.10b), which was only present in our pRCC samples. Node status did not appear to have an effect on CD200 H-score, with no differences observed between the NX/N0, N1 or N2 groups, however again these are very small sample sizes and further research is required. No samples with N1 or N2 status were available for pRCC or chRCC. Metastasis status had no effect on CD200 H-score in ccRCC (Figure 3.10c), however in pRCC, an increase appears to be present in the M1 sample compared to the M0/MX group, however as this is only one sample further research on this would be required. No samples with M1 status in chRCC were available in our TMAs.

3.1.3.3 CD200 expression by age and sex

As TNM status did not appear to have a significant effect on CD200 H-score, we next examined the samples by patient characteristics to determine if any changes in CD200 expression could be associated with a certain characteristic. We firstly investigated CD200 H-score in our samples by patient age at operation and sex, as shown in Figure 3.11.

In RCC as a whole (Figure 3.11a), CD200 H-score was consistent across all age groups with no significant changes observed. H-score was also consistent across all groups in ccRCC (Figure 3.11b), where the highest score was found in the 30-39 group, however this was a very small sample size. All other groups had consistent expression with no significant differences observed between them. pRCC H-score was more variable between the groups (Figure 3.11c), with low expression observed in the 30-30 and 80-89 age groups, however again these were very small sample sizes. CD200 H-score in chRCC (Figure 3.11d) was found to be consistent amongst the small number of samples which fell into three age groups, however a slight, not significant increase in average

H-score was observed with increased age. This data could be improved by increasing sample number as many groups only contained one sample, however it appears that age does not have any meaningful effect on CD200 H-score in any RCC subtype. As age does not appear to have any effect on CD200 H-score in our data set, we next examined the samples by patient sex (Figure 3.11e). Analysis of CD200 H-score by patient sex revealed no significant differences in score between male and female patients in RCC as a whole or in any of the subtypes.

3.1.3.4 CD200 expression summary

We have shown that CD200 is expressed in all three RCC subtypes studied, with expression intensity found to be highest overall in ccRCC compared to pRCC and chRCC. From our studies on normal kidney, we found that CD200 expression is strongest on the cells of the proximal convoluted tubule, from which ccRCC and pRCC originate, and this expression appears to carry through into tumour expression with moderate levels observed in all samples from both subtypes. CD200 expression was also found on the distal convoluted tubule in the normal kidney, the cell of origin for chRCC, however the mean expression was found to be significantly lower than that of the proximal tubule. This CD200 expression again appears to carry through into the tumour, however interestingly the chRCC levels were found to be comparable to those observed in ccRCC and pRCC.

No significant differences in CD200 expression level were found between the subtype TNM stages, however expression was observed to increase with increased tumour (T) stage when we examined RCC as a whole, in ccRCC and chRCC, while interestingly expression appeared to decrease with increased T stage in pRCC, however these groups had small n numbers and so further research is required to understand this observation. No changes were observed when splitting the samples into groups based on node (N) or metastasis (M) status, however again small n number in these groups limit this study. CD200 expression was next examined by patient characteristics available from the clinical data associated with our TMAs, however no differences between groups were observed when examining the data by patient age at operation or sex,

implying that any differences observed in CD200 expression are likely to be associated with the tumour expression and not related to another characteristic. CD200 expression is summarised in Table 3.1.

Table 3.1 CD200 expression in overall RCC and RCC subtype TMA samples with mean expression and standard deviation.

	Mean ± SD			
TNM Stage	**All RCC**	**ccRCC**	**pRCC**	**chRCC**
All	-	120.80 ± 35.17	109.70 ± 66.24	108.20 ± 39.05
T1	112.40 ± 42.31	113.80 ± 41.02	120.30 ± 49.99	97.64 ± 45.79
T2	117.0 ± 48.09	124.20 ± 41.78	106.60 ± 83.29	106.0 ± 28.32
T3	118.80 ± 40.75	121.0 ± 29.50	101.60 ± 79.54	133.80 ± 56.96
T4	147.0 ± 12.78	147.0 ± 12.78	-	-
N0/NX	-	120.60 ± 35.99	-	-
N1	-	113.70 ± 0.00	-	-
N2	-	123.80 ± 20.30	-	-
M0/MX	-	121.40 ± 35.73	134.10 ± 53.43	-
M1	-	105.40 ± 0.51	204.40 ± 0.00	-

3.2 Determining CD200 Expression in ccRCC Cell Lines

Having demonstrated CD200 expression throughout both normal kidney and RCC tissue, we next examined CD200 expression in RCC cell lines for use in functional experiments and RNA sequencing.

3.2.1 CD200 expression in ccRCC cell lines

We firstly checked CD200 mRNA levels using qRT-PCR and protein expression using western blot in our cell lines, as shown in Figure 3.12. Transduced CD200+ and CD200- HeLa cell lines were used as positive and negative controls in the qRT-PCR and western blot analyses.

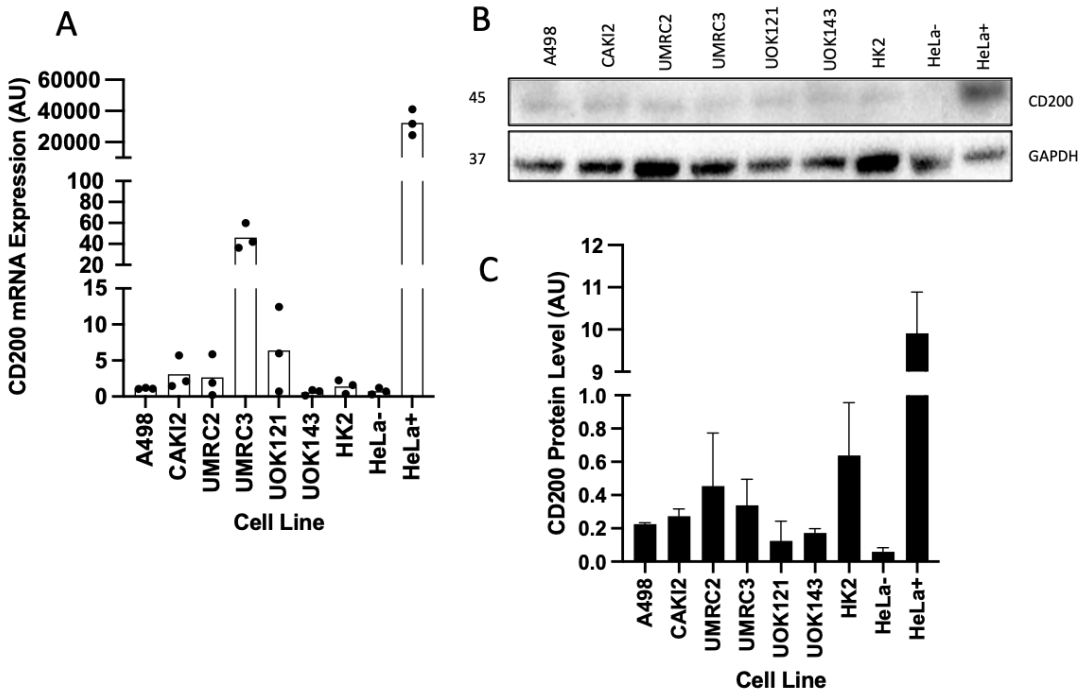

Figure 3.12 Analysis of ccRCC cell line CD200 expression
(A) RNA was extracted from six RCC cell lines, HK2 normal kidney cell line and CD200+ and CD200- transduced HeLa cell lines and CD200 gene expression was determined by qRT-PCR. Expression was normalised to β -Actin and CD200 expression was calculated according to the 2^-delta Ct method and is shown as arbitrary units (AU). Differences in gene expression were calculated using a Kruskal-Wallis test followed by Dunn's multiple comparison's test, where all cell lines were found to have significantly lower expression compared to HeLa+ (all $p < 0.0001$). (B) Whole cell lysate was extracted from the same cell lines and immunoblotted for CD200, representative image. (C) CD200 protein expression was normalised to GAPDH and CD200 level shown in arbitrary units (AU), all cell lines were found to have significantly lower expression than HeLa+ (all $p < 0.0001$). Values were obtained from an average of 3 independent experiments.

In our ccRCC cell lines, CD200 mRNA and protein levels were found to be unexpectedly low. In qRT-PCR analysis (Figure 3.12a), low levels of mRNA expression were observed in all ccRCC cell lines, however the UMRC3 cell line was again found to have the highest levels out of all ccRCC samples tested. CD200+ and CD200- transduced HeLa cell lines were used as positive and negative controls in these experiments, where the HeLa+ cell line was found to have around 100x higher CD200 expression compared to UMRC3 and was significantly higher than all other samples tested with a p value of <0.0001. CD200 protein expression was also examined using whole cell lysates probed for CD200 expression using western blot (Figure 3.12b), where again all ccRCC cell lines were found to have very low expression levels, and only the HeLa+

positive control showing a clear band. Quantification of this blot (Figure 3.13c) revealed that the HeLa+ cell line expression was over 20x stronger than that observed in UMRC2, the highest expressing ccRCC cell line, with all other samples again showing significantly lower expression than HeLa+, $p = <0.0001$.

3.2.2 2D vs 3D cell culture conditions

2D cell culturing conditions have been shown less closely mimic physiological conditions compared to 3D conditions, with limited spatial organisation of receptors and interactions with neighbouring cells, therefore influencing gene expression and cellular behaviour (Takahashi et al. 2015). 3D cultures are thought to more closely resemble *in vivo* conditions and are therefore more physiologically relevant, allowing more meaningful study of biological mechanisms such as cell number monitoring, viability, morphology, proliferation migration and response to stimuli (Anton et al. 2015). Importantly, 3D cultures have also been shown to display a significantly different and more relevant genotype to an *in vivo* model compared to 2D monolayers (Kappelmann-Fenzl et al. 2021). To determine if the traditional 2D cell culture methods used could be contributing to the lack of CD200 expression in our cell lines, we next grew the ccRCC cell lines in 3D culture in non-adherent petri dishes over at 14-day time period to determine if CD200 mRNA and protein expression could be restored through this technique. A growth time lapse is shown in Figure 3.13.

2D culture

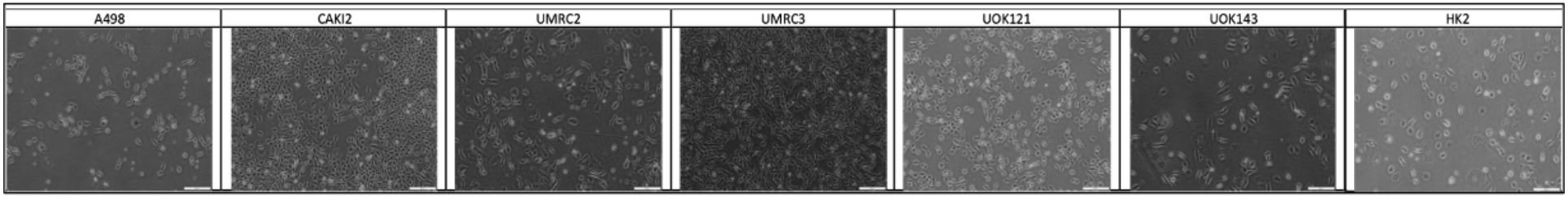

3D Culture in non-adherent petri dishes – 14 days at 10 cells/µl

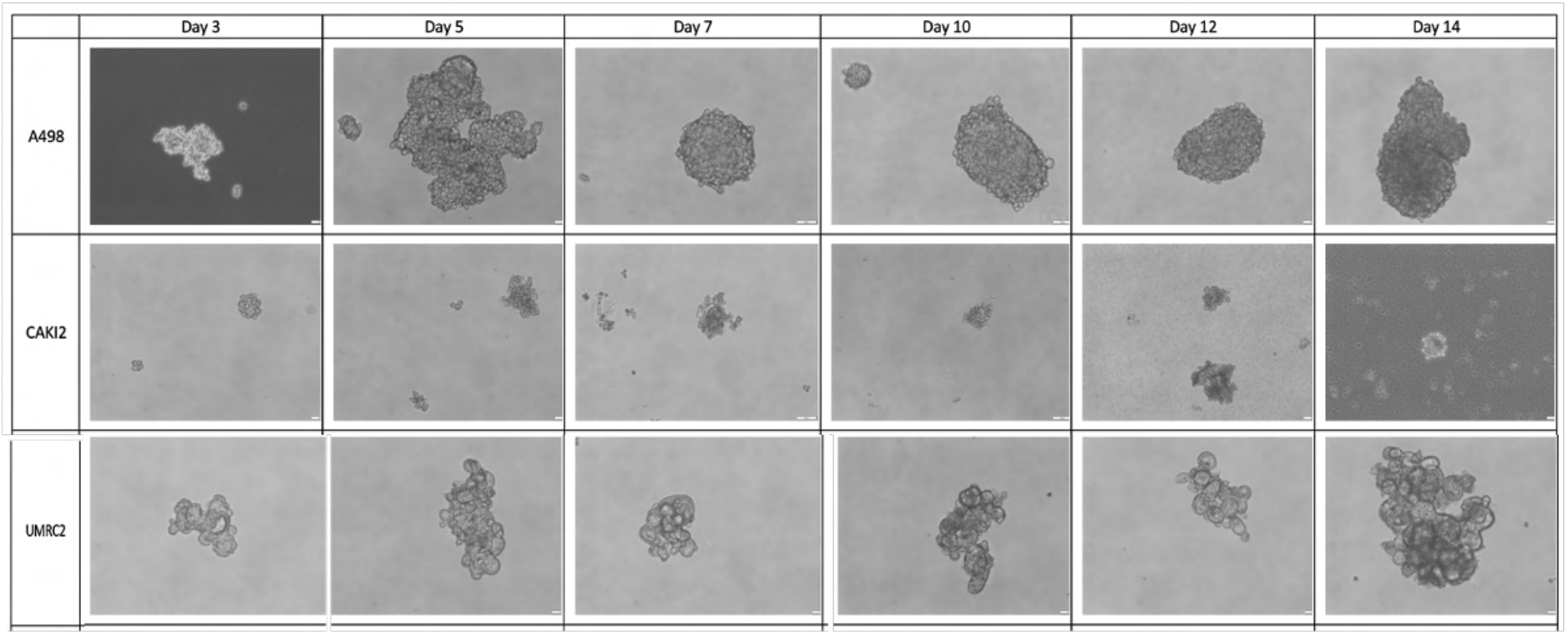

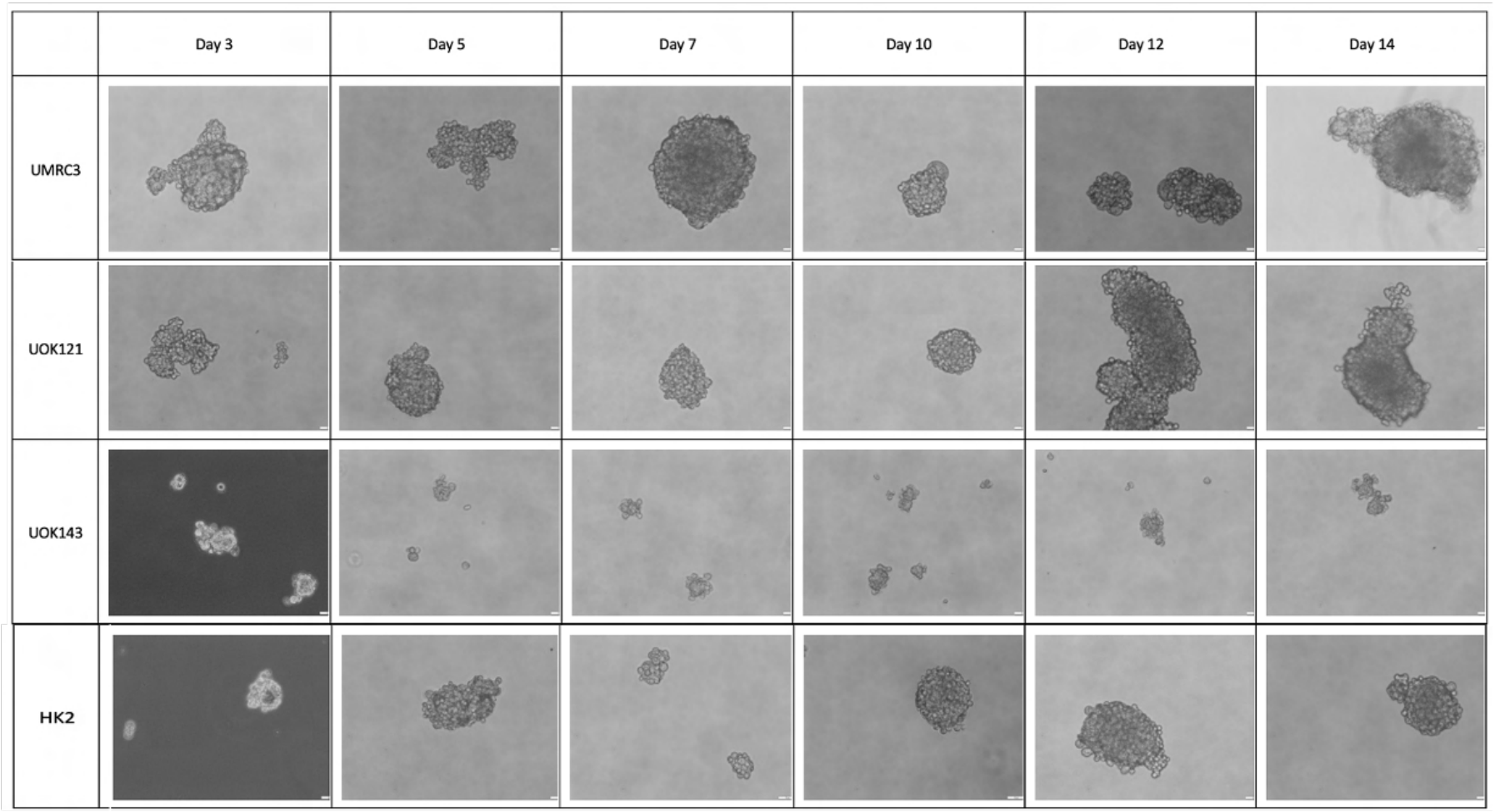

Figure 3.13 ccRCC cell lines grown in 2D and 3D culture
Top panel: Representative image of ccRCC cell lines grown in normal 2D adherent cell culture conditions. Bottom panels: Cell lines were plated in non-adherent 3D culture at 10 cells/μl and allowed to grow for 14 days. Representative images were taken at day 3, 5, 7, 10, 12 and 14, after which point, RNA was extracted to measure CD200 mRNA levels.

Most cell lines were found to grow well in non-adherent culture and were able to form discernible spheres by days 5 to 7, however the CAKI2 and UOK143 cell lines did not appear to survive as well in these culture conditions. Following 14 days in 3D culture, RNA was extracted from the spheres and was examined using qRT-PCR, as shown in Figure 3.14.

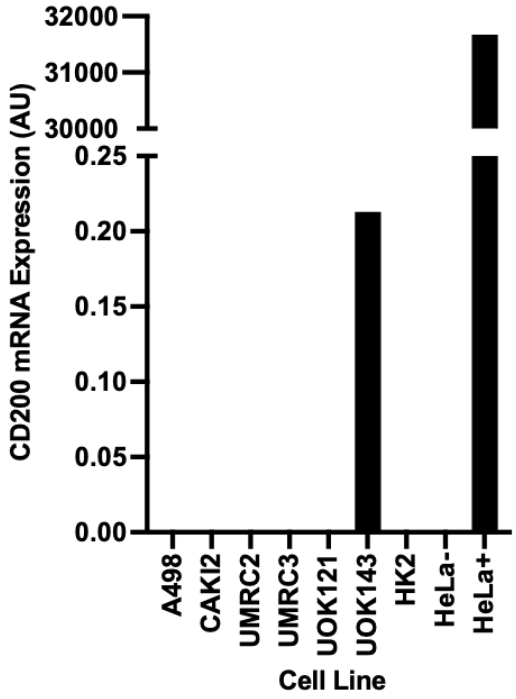

Figure 3.14 CD200 qRT-PCR using mRNA from cell lines in 3D ccRCC culture
RNA was extracted from six ccRCC cell lines grown in non-adherent 3D culture and HeLa CD200+ and CD200- HeLa cells grown in 2D culture for use as control, and CD200 gene expression was determined by qRT-PCR. Expression was normalised to β -Actin and CD200 expression was calculated according to the 2^-delta Ct method and is shown as arbitrary units (AU). n=1.

mRNA expression from the 3D cultured RCC cell lines revealed less expression than the 2D cell culture conditions, with all cell lines except UOK143 and HeLa CD200+ showing zero CD200 mRNA. Interestingly, the UOK143 cell line was found to have a low mRNA reading of 1.262 AU in 2D culture, but was found to have almost 6-fold lower mRNA levels in the 3D culture conditions with just 0.213 AU, implying that this cell line may be the most impacted by the change in culture conditions. It should be noted however that this experiment was only n=1 due to time constraints, and so further repeats and optimisation may show differing results.

3.2.3 CD200 transduction of ccRCC cell lines

As neither 2D nor 3D culture was able to induce CD200 expression in our ccRCC cell lines, we next attempted to transduce our A498 cell line to introduce CD200 expression, as described in the methods section (Tonks et al. 2005), which our group has previously successfully completed to generate a CD200+ HeLa cell line.

The A498 cell line was stably transduced either with a retrovirus co-expressing green fluorescent protein (GFP) under either an internal cytomegalovirus promoter as a CD200- control, or with the same retrovirus also containing CD200 DNA. After infection, cells were left to grow until they were 90% confluent in a T75 flask before sorting for GFP+ cells by fluorescence-activated cell sorting (FACS). Cells were gated on FSC and SSC to eliminate debris before FSC height and area gating was used to target single cells. Successfully transduced cells showed GFP positivity and dead cells were stained with DAPI and gated out, however unfortunately only a very low number of cells were found to be GFP+ and therefore successfully transduced. Due to these low numbers, a positive population could not be grown as the cells died in culture due to very low confluency. This transduction was attempted 3 times without success, so due to time constraints and virus availability we chose to only use our CD200+ HeLa cell lines for proof-of-concept experiments in the following experiments.

3.3 RNA Sequencing

RNA sequencing (RNAseq) data provides an unbiased data set showing the comparative level of RNA expression across cell lines, allowing examination of gene expression within signalling pathways to determine which genes are down- or upregulated compared to a control sample. We completed RNAseq on our six ccRCC cell lines using the normal kidney cell line (HK2) as control to determine which key genes are down- or upregulated in our ccRCC cell lines compared to normal kidney.

3.3.1 Comparison of ccRCC cell lines

To determine how similar our cell lines are to each other, we firstly used principal component analysis (PCA) to separate the samples based on their gene expression, as shown in Figure 3.15.

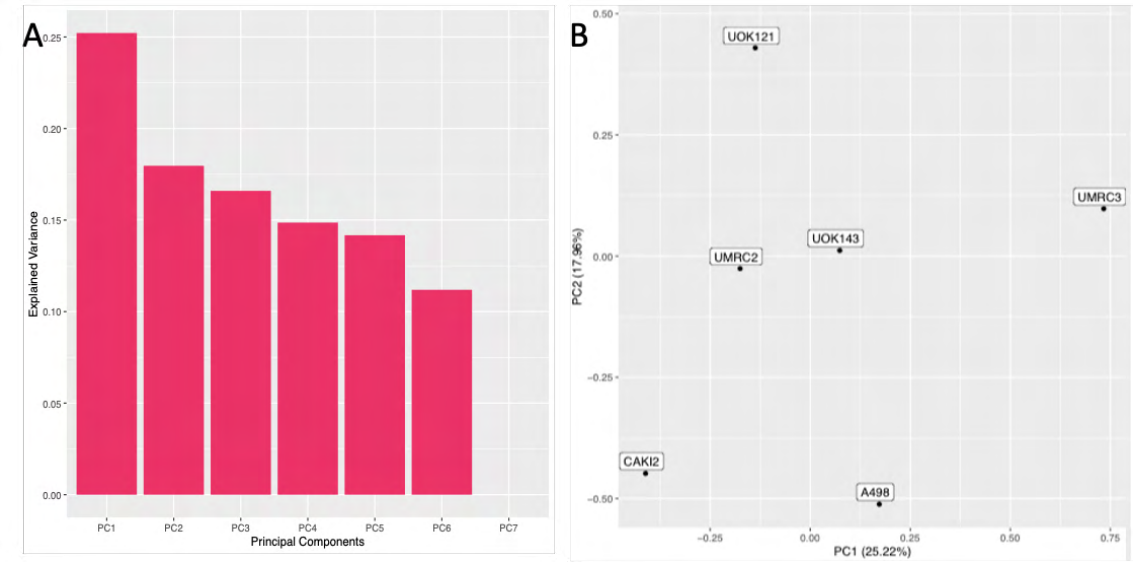

Figure 3.15 Principal component analysis of ccRCC cell lines
(A) Scree plot, PC1 explains 25% of variation between the samples. (B) UMRC2, UOK143 and UMRC3 are most similar along the PC2 axis. UMRC2 and UOK143 are most similar along the PC1 axis.

PCA reduces dimensionality in a data set and allows exploration of relationships between multiple variables, in this case gene expression. In this analysis we observed several similarities and differences between our cell lines. The scree plot (Figure 3.15a) shows that PC1 was able to account for around 25% of variance between the groups, while PC2 was able to account for around 18% of variance. Next, using PCA on PC1 and PC2 only (Figure 3.15b), we found that UMRC2, UOK143 and UMRC3 are most similar along the PC2 axis, while UMRC2, UOK121 and UOK143 appear to cluster together and are most similar along the PC1 axis. CAKI2, A498 and UMRC3 do not appear to cluster with the other cell lines and are separated along the PC1 axis, while UMRC3 is most different from all other cell lines and is separated along PC2 also.

To get a clearer picture of how different the cell lines are, we next created a heat map with our gene expression data and used hierarchical clustering to similarity, as shown in Figure 3.16.

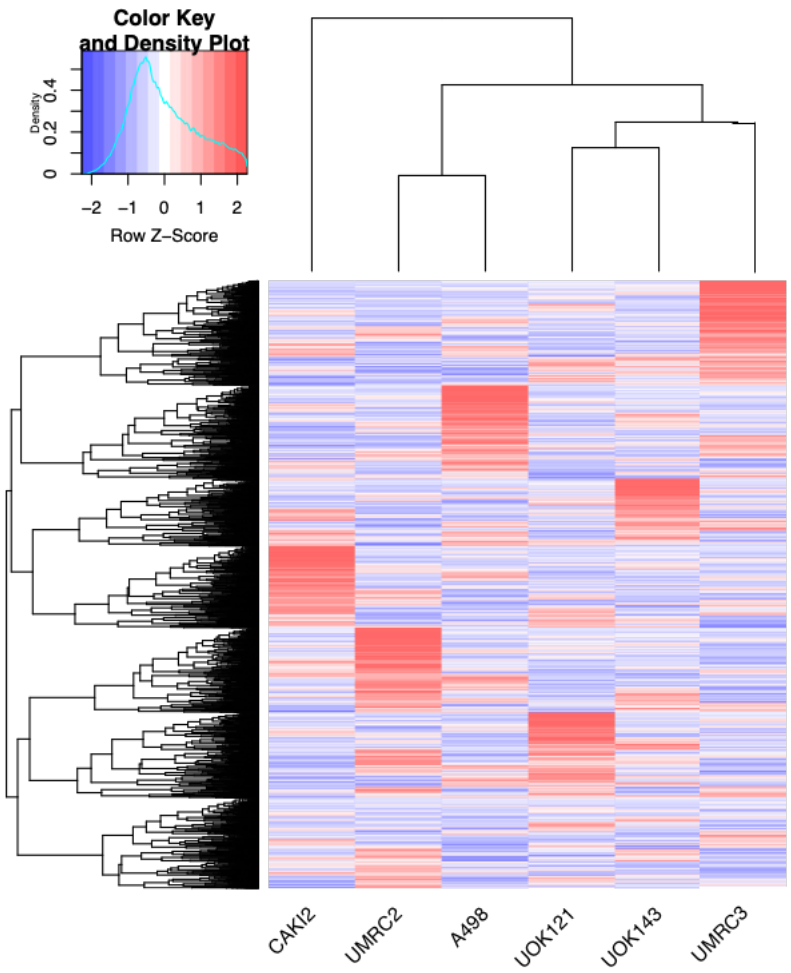

Figure 3.16 Heat map of ccRCC cell line gene expression with hierarchical clustering
UMRC2 was found to cluster most closely with A498, while UOK121 clustered most closely with UOK143. CAKI2 was found to be least similar to all other cell lines. Upregulated genes are shown in red and downregulated genes are shown in blue.

The hierarchical clustering shows variation in gene expression between all cell lines, however the clustering patterns show the most similarities between UMRC2 and A498 and between UOK121 and UOK143, with CAKI2 being the least closely clustered to any other cell line. The most strongly upregulated genes in each cell line, shown in red, appear to be different in each cell line, with more similarities between the groups seeming to come from the downregulated genes, represented in blue.

3.3.2 Comparison of ccRCC cell lines to normal kidney

We have shown that our ccRCC cell lines have a number of similarities and differences in gene expression, so we next calculated which genes are differentially expressed in our ccRCC cell lines compared to the normal kidney HK2 cell line, which was used as a control cell line. Creation of a list of normalised, differentially expressed genes (DEGs), allows us to determine which genes are up- or downregulated compared to the normal kidney, creating log2 fold change and significance values. To investigate the range of our DEG list, we firstly plotted the DEGs from each ccRCC cell line in volcano plots to represent how many significantly up- or downregulated genes are found compared to normal kidney. To reduce the number of significant genes included in this analysis, we used a stringent adjusted p value (padj) cut off of <0.01 and log2 fold change value of $\leq$-2 or $\geq$+2, as shown in Figure 3.17.

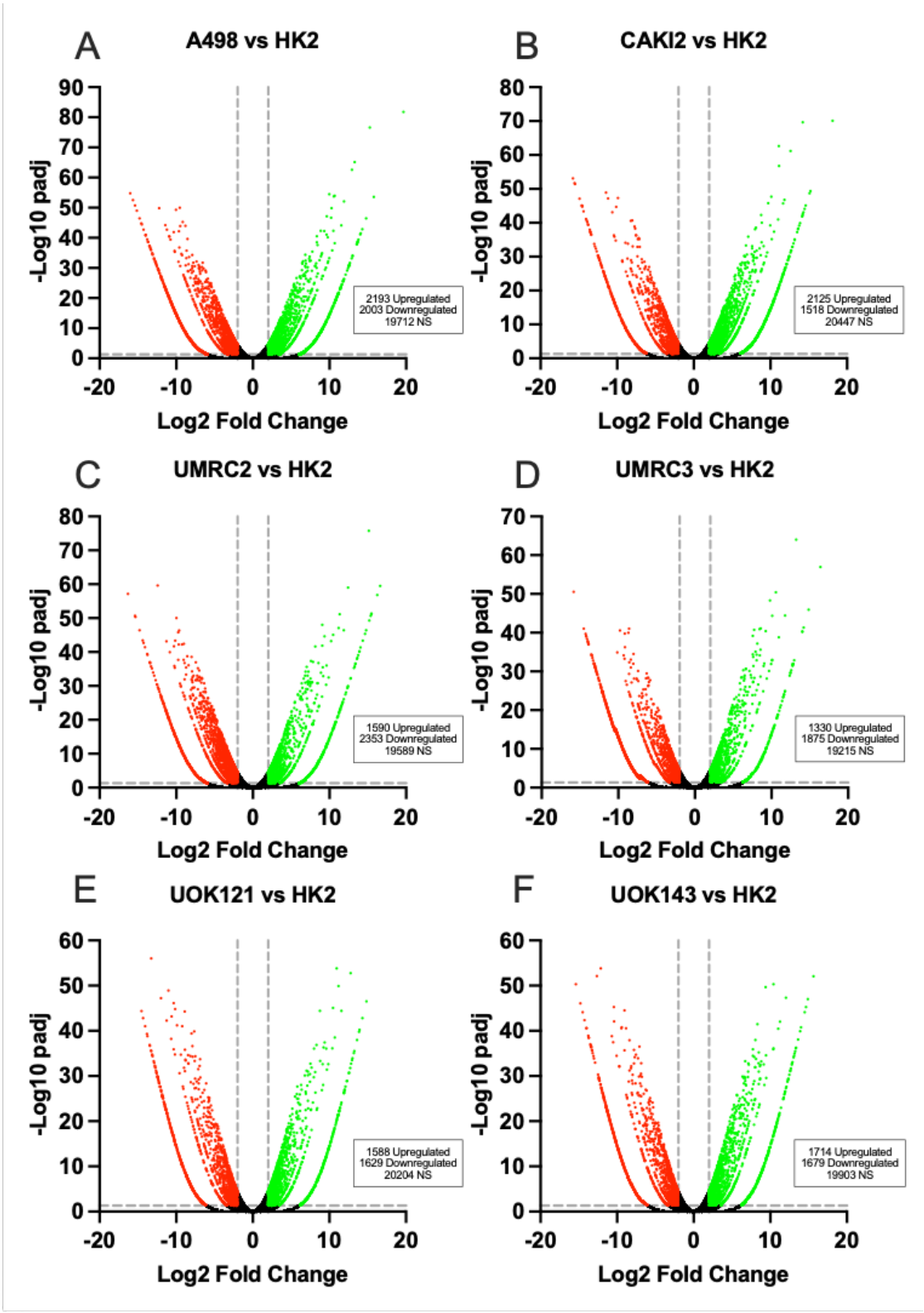

Figure 3.17 Volcano plots of significant ccRCC cell line vs HK2 DEGs
Visualisation of ccRCC cell line differentially expressed genes compared to HK2 normal kidney cells. Cut offs were padj <0.01 (-log10 >1.3) and log2 fold change of ≤-2 or ≥+2. (A) A498 vs HK2 (B) CAKI2 vs HK2 (C) UMRC2 vs HK2 (D) UMRC3 vs HK2 (E) UOK121 vs HK2 (F) UOK143 vs HK2. Red dots represent significantly downregulated genes and green dots represent significantly upregulated genes. Black dots represent non-significant genes.

These volcano plots reveal a high number of significant up- and downregulated genes in all ccRCC cell lines compared to the normal kidney samples, with the highest number of significant DEGs observed in A498 vs HK2. This data implies that the expression of a large number of genes are altered during ccRCC development compared to normal kidney, which may result in dysregulation of key pathways resulting in tumour progression.

To determine which cellular functions are most strongly up- or downregulated in ccRCC compared to normal kidney, using Qiagen Ingenuity Pathway Analysis (IPA), we next examined the top 10 cellular functions in our 6 ccRCC samples compared to HK2, as shown in Figure 3.18.

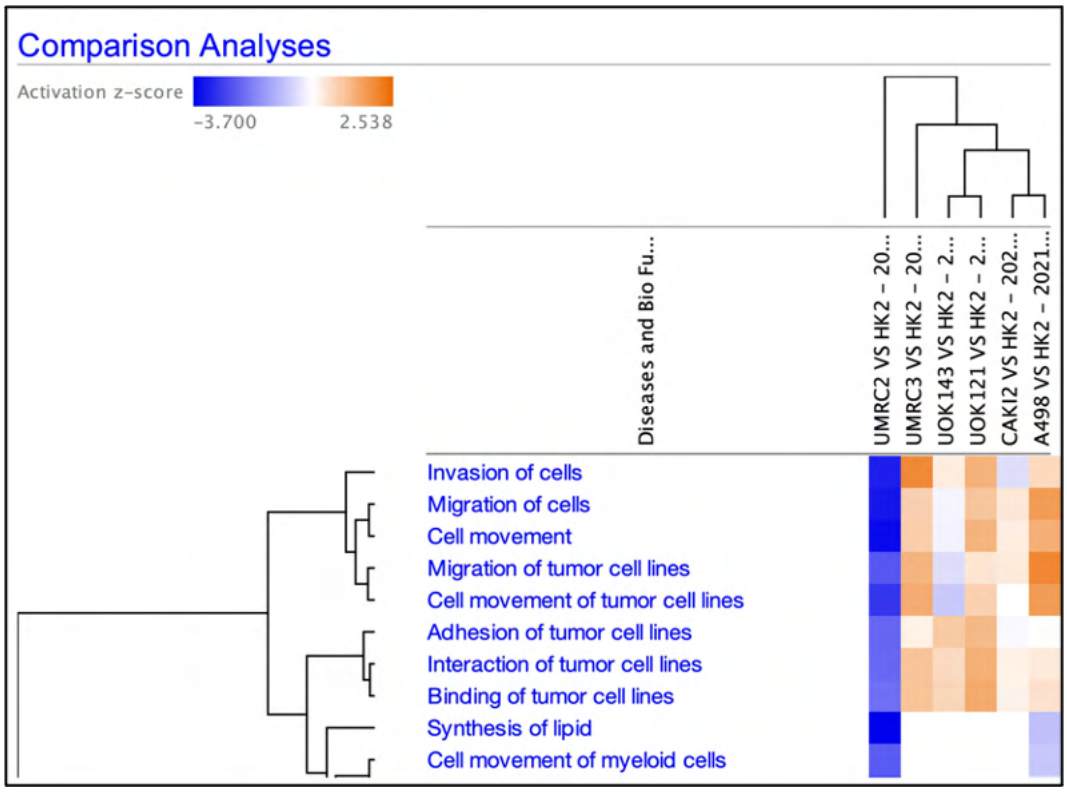

Figure 3.18 Heatmap of the top 10 cellular functions in ccRCC cell lines vs HK2
Cut offs of padj 0.05 and log2 fold change of -2 and +2 were used to filter the diseases and functions which were up- or downregulated in our ccRCC cell lines vs HK2. The most upregulated functions were involving invasion, migration and movement of cells, while the most downregulated functions were those involving genes involved in lipid synthesis and cell movement of myeloid cells. UMRC2 showed the strong downregulation of all functions whereas all other cell lines showed upregulation in almost all functions.

Comparison of the most up- or downregulated functions in the 6 RCC cell lines revealed the most upregulated functions are related to invasion, movement and migration of cells in 5 of the 6 cell lines, which would be expected in cancer cell lines compared to normal kidney cells. Interestingly however, in the UMRC2 samples, all of these functions were strongly downregulated. This result is unexpected as the UMRC2 cell line is reported to be developed from a patient with metastatic disease at the time of their nephrectomy, so it unclear why genes related to these functions are not upregulated as we have observed in the other cell lines.

Having established the differences in key functions in our cell lines, we next wanted to examine if the key genes in the RCC developmental pathway are under- or overexpressed in our samples. Using gene set enrichment analysis (GSEA), we used ranked DEG lists to explore the Kyoto Encyclopaedia of Genes and Genomes (KEGG) Renal Cell Carcinoma gene set, a curated gene set comprising of 70 key RCC genes including tumour suppressors, oncogenes, cytokines and growth factors which have key roles in RCC development via the HIF1α pathway. The KEGG RCC pathway is represented in Figure 3.19.

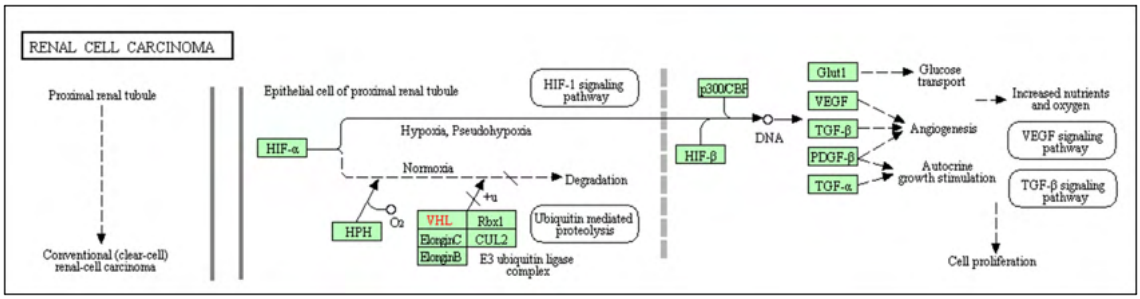

Figure 3.19 Pathway map of the KEGG renal cell carcinoma gene set.
Key genes from the KEGG renal cell carcinoma gene set responsible for RCC development via the HIF1α pathway are highlighted in green. Dashed lines represent the pathway in the presence of VHL, resulting in ubiquitin mediated proteolysis. Solid lines represent the pathway in the absence of VHL resulting in accumulation of HIF1α and subsequent production of growth factors including vascular endothelial growth factor (VEGF) and platelet derived growth factor (PDGF). Adapted from https://www.genome.jp/kegg-bin/show_pathway?hsa05211.

GSEA is a powerful tool for the interpretation of large data sets by comparing a ranked gene list to a gene set associated with a particular disease or biological process, creating an enrichment score (ES) which indicates the degree by which a gene set is overrepresented at the extremes of the ranked gene list.

Using the KEGG renal cell carcinoma gene set represented in Figure 3.19, GSEA was able to create an ES for each cell line, as shown in Figure 3.20.

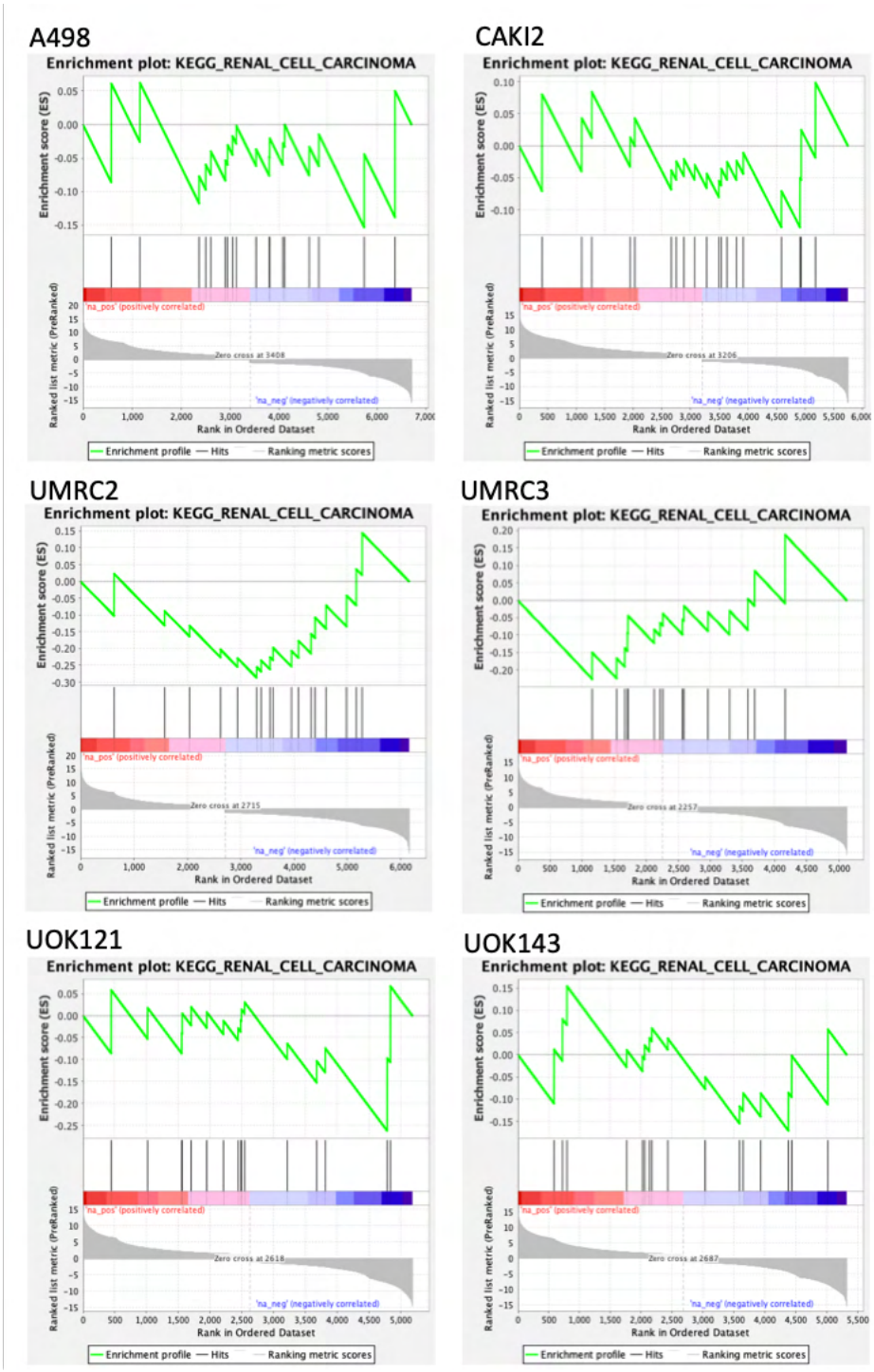

Figure 3.20 GSEA enrichment plots using KEGG renal cell carcinoma gene set
Ranked gene lists for each ccRCC cell line were run through GSEA to gain enrichment scores for key RCC genes which are overrepresented in the sample gene list.

Most genes which passed the threshold for core enrichment were negatively enriched in our ccRCC cell lines compared to the KEGG RCC gene set, resulting in a negative overall ES, as shown in Table 3.2. A high number of genes however also did not reach the cut off for core enrichment, resulting in a low overall number of genes which received an ES in all samples.

Table 3.2 Normalised enrichment scores for RCC cell lines vs HK2 using the KEGG RCC gene set

	Normalised Enrichment Score (NES)	p Value
A498 vs HK2	-0.471	0.990
CAKI2 vs HK2	-0.415	1.000
UMRC2 vs HK2	-0.867	0.644
UMRC3 vs HK2	-0.630	0.909
UOK121 vs HK2	-0.776	0.753
UOK143 vs HK2	-0.512	0.988

In A498, 16 genes reached the core enrichment threshold, however all were negatively enriched, including HIF1α. In CAKI2, 18 genes reached core enrichment. 5 genes were positively enriched including VEGFC, while HIF1α was negatively enriched, however this is to be expected as this cell line has WT VHL status (Pasha et al. 2019). 11 genes reached core enrichment in UMRC2, 9 of which were negative including members of the PI3K pathway and VEGFC. In this cell line, HIF1α and TGFβ were however found to be positively enriched, possibly indicating upregulation of the HIF1α pathway following VHL loss, while increased TGFβ has previously been associated with increased ccRCC aggressiveness and invasiveness (Sitaram et al. 2016). 14 genes reached core enrichment in UMRC3, with HIF1α, hypoxia inducible factor 3 (EGLN3) and PIK3R3 all positively enriched, indicating a hypoxic and pro-tumour environment. Only 4 genes reached core enrichment in UOK121, with VHL, TGFβ2 and TGFβ3 negatively enriched, and HIF1α positively enriched. This expression pattern indicates characteristic ccRCC upregulation of the HIF1α pathway resulting from inactive VHL, however via a different downstream pathway not including TGFβ, as we observed in UMRC2. Finally, in UOK143,

both VHL and HIF1α were found to be negatively enriched, while only 3 genes reached core enrichment: TGFβ2, ARNT2 and EGLN3.

This data shows significant differences between the gene expression in our 6 ccRCC cell lines, most notably the differences in VHL and HIF1α expression and their resulting downstream effector genes, implying that selection of cell lines for *in vitro* cell line studies should be made with these differences in mind as outcomes may be significantly different. To examine this further, we next investigated the expression of genes at the end of the HIF1α pathway from the KEGG RCC pathway, to see if the end point genes involved in angiogenesis and disease progression are altered compared to normal kidney, as shown in Figure 3.21.

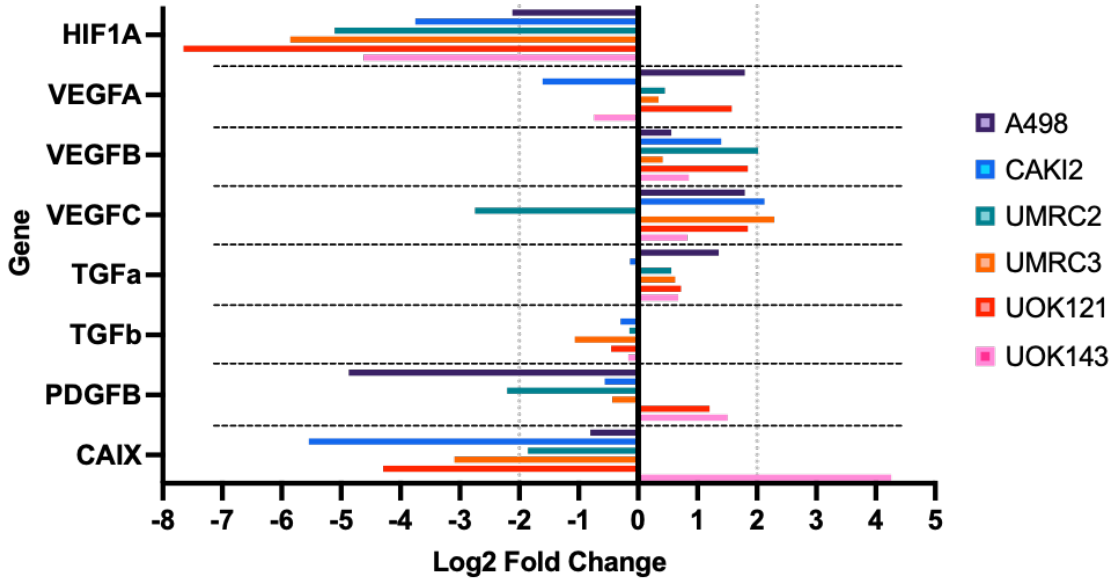

Figure 3.21 Log2 fold change expression levels of HIF1α pathway end point genes compared to HK2.
RCC differentially expressed genes in the HIF1α pathway. Significance cut offs of -2 and +2 log2 fold change were not reached for all genes, however HIF1α was found to be significantly downregulated in all cell lines compared to HK2. VEGFA, VEGFB and VEGFC were upregulated in all ccRCC cell lines compared to HK2, however few reached significance.

This data shows significant downregulation of HIF1A in all 6 ccRCC cell lines compared to HK2, which is an unexpected result as increase of HIF1α is one of the main parts of the HIF1α pathway in ccRCC, however it has been reported that overaccumulation of HIF1α protein leads to inhibition of HIF1A gene expression (Swiatek et al. 2020). The vascular endothelial growth factor (VEGF)

signalling pathway is the main angiogenic pathway associated with ccRCC development, with VEGFA associated with shorter overall survival and progression free survival (Wierzbicki et al. 2019), while VEGFB and VEFC are associated with metastasis (Yang et al. 2015; Ndiaye et al. 2019). In this data we observed overall upregulation of VEGFA, VEGFB and VEGFC, however only VEGFC reached the significance cut off levels in CAKI2 and UMRC3 (Log2 FC 2.126, padj = <0.001 and Log2 FC 2.291, padj <0.001 respectively). Overexpression of transforming growth factor-α (TGFα) and inactivation of TGFβ is a common signature of tumour development in hepatocellular carcinoma (Baek et al. 2010), while in ccRCC, attenuation of the TGFβ pathway results in cancer cell migration (Kubiczkova et al. 2012; Wang et al. 2022). Here we show general upregulation of TGFα in all cell lines except CAKI2 and downregulation of TGFβ in all cell lines, however none of the samples reached the significance cut off. Platelet derived growth factor B (PDGFB) is another transcription factor involved in the HIF1α signalling pathway which promotes proliferation of mural cells surrounding the blood vessels during angiogenesis. The role of PDGFB in ccRCC has not been well studied, however it has been linked to better prognosis and inhibition of tumour growth (Wang et al. 2015). Our data shows significant downregulation of PDGFB in A498 and UMRC2 (Log2 FC -4.870, padj = <0.001 and Log2 FC -2.205, padj = <0.001 respectively), non-significant downregulation in CAKI2 and UMRC3 and non-significant upregulation in UOK121 and UOK143. Carbonic anhydrase IX (CAIX) is a transmembrane metalloenzyme induced by the accumulation of HIF1α with several downstream effects including acidification of extracellular pH, increased tumour cell migration and loss of cellular adhesion. Overexpression of CAIX is an indictor or poor prognosis in many cancer types including breast, lung and bladder carcinomas, however conversely, low CAIX expression is an indicator of poor prognosis in ccRCC (Aldera and Govender 2021). In our data we see significant downregulation of CAIX in CAKI2, UMRC3 and UOK121 (Log2 FC -5.544, -3.089 and -4.289 respectively, all padj = <0.001) and non-significant downregulation in A498 and UMRC2. Interestingly however, we see significant upregulation of CAIX in UOK143 (Log2 FC 4.259, padj = <0.001).

This data begins to paint a picture of the general trends of HIF1α pathway endpoint gene upregulation in different ccRCC cell lines compared to the normal kidney. Upregulation of VEGF family members and TGFα resulting in angiogenesis and cell migration was observed, while downregulation of TGFβ, PDGFB and CAIX indicates poor prognosis and tumour progression. We have observed general trends across the cell lines, however as each cell line has different mutations and characteristics it is difficult to discern which upstream differences in gene expression are responsible for the subtle differences between the downstream gene expression of each cell line. As CAKI2 is the only one of our ccRCC cell lines to be confirmed VHL_{WT}, we next compared the gene expression between our 5 VHL_{mut} cell lines compared to that of the CAKI2 cell line by creating a new list of DEGs, with the same cut offs of -2/+2 Log2 fold change and padj value of <0.05.

3.3.3 Comparison of ccRCC cell lines to CAKI2

We firstly compared created a list of up- and downregulated DEGs in our VHL_{mut} ccRCC cell lines compared to the VHL_{WT} CAKI2 cell line, as shown in Figure 3.22.

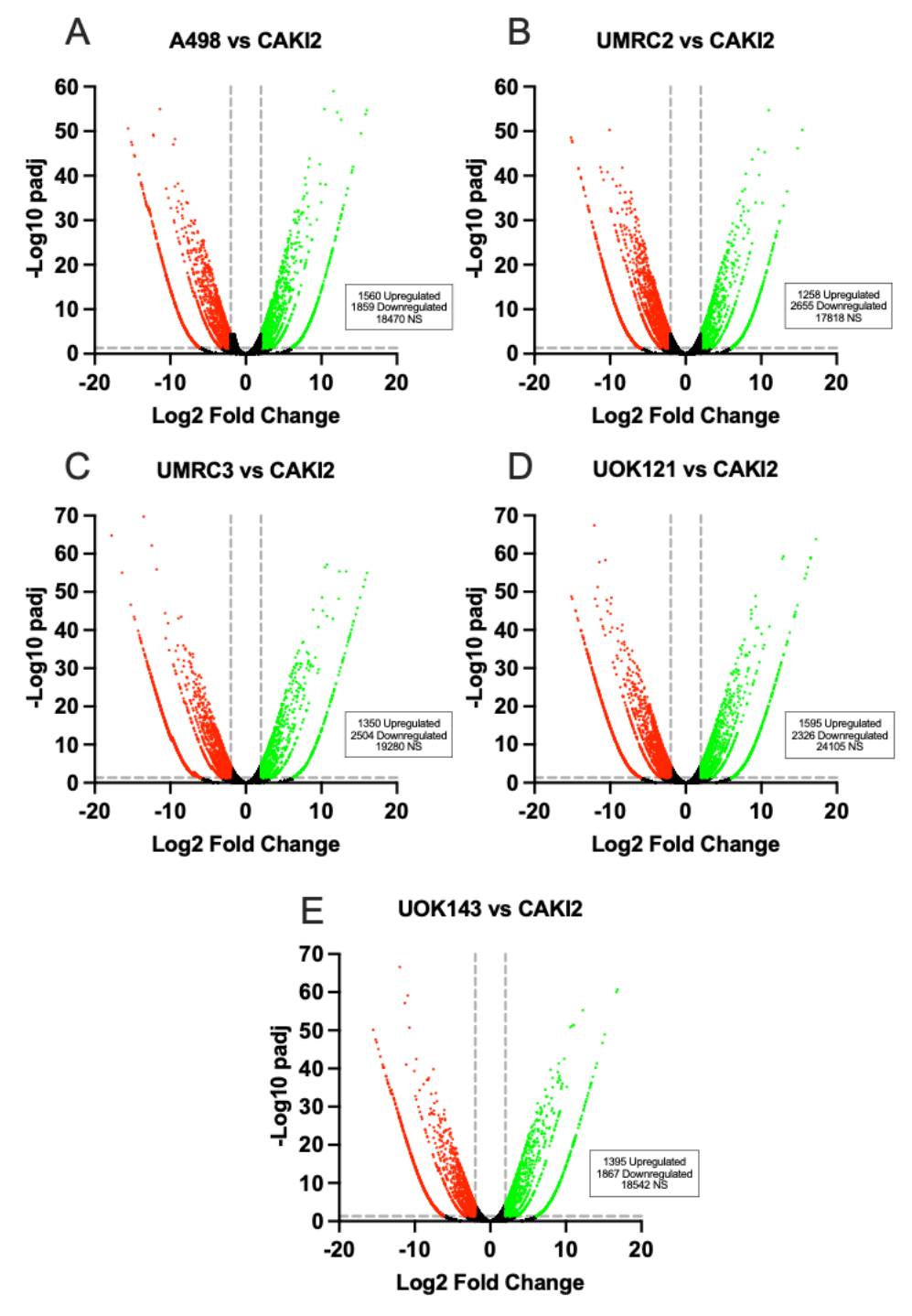

Figure 3.22 Volcano plots of ccRCC cell line DEGs compared to CAKI2
Visualisation of 5 VHL_{mut} ccRCC cell line differentially expressed genes compared to the VHL_{WT} CAKI2 cell line. Cut offs were padj <0.01 and log2 fold change of ≤-2 or ≥+2. (A) A498 vs CAKI2 (B) UMRC2 vs CAKI2 (C) UMRC3 vs HK2 (D) UOK121 vs HK2 (E) UOK143 vs HK2. Red dots represent significantly downregulated and green dots represent significantly upregulated genes. Black dots represent non-significant (NS) genes.

Each of the 5 VHL_{mut} ccRCC cell lines had a similar number of up- and downregulated DEGs when compared to CAKI2, however the majority of genes in each comparison did not reach the log2 fold change and/or padj value cut offs, indicating that only around 15-20% of all mapped genes are significantly differentially expressed in the presence or absence of a VHL mutation.

CAKI2 is a commonly used cell line to study ccRCC, however as it does not harbour the characteristic VHL mutation observed in around 90% of ccRCC cases, this cell line can be used to compare the downstream effects of a WT sample against a VHL mutated sample. Functional VHL been shown to alter the characteristics of CAKI2 cells compared to other ccRCC cell lines in a number of ways, including loss of HIF2α, downregulation of glycolysis and alteration of signalling pathways relating to cellular growth and proliferation (Da Nagaprashantha et al. 2013). Using our DEG lists generated by comparing gene expression of the 5 other ccRCC cell lines against CAKI2, we compared the gene expression of the HIF1α pathway endpoint genes to determine if VHL expression alters gene expression in these pathways, as shown in Figure 3.23.

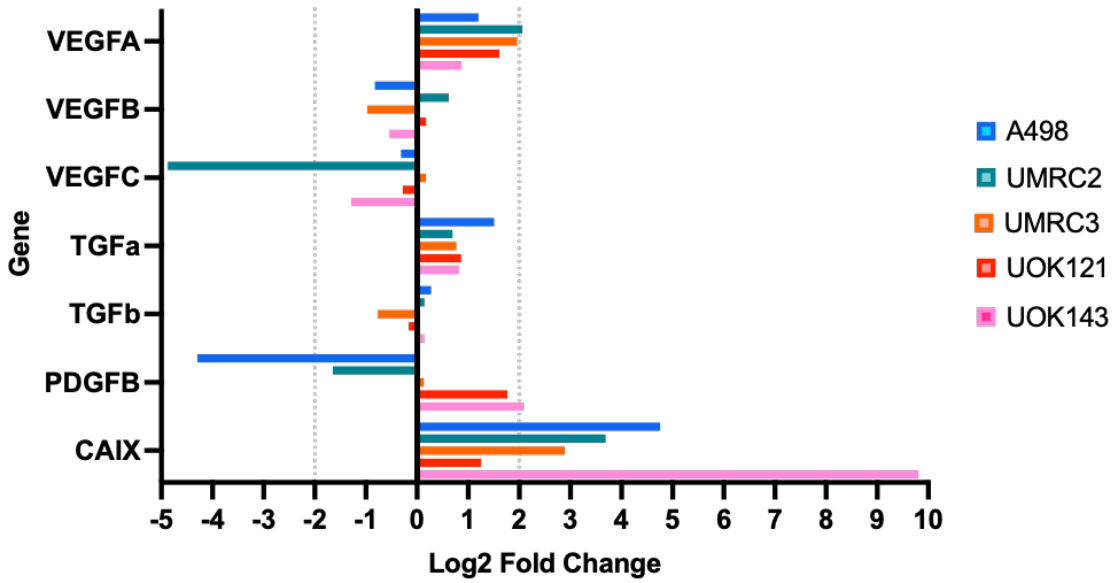

Figure 3.23 Log2 fold change expression levels of HIF1α pathway end point genes in VHL_{mut} ccRCC cell lines compared to VHL_{WT} CAKI2.
Significance cut offs of -2 and +2 log2 fold change were not reached for all genes, however VEGFA, TGFα and CAIX were found to be overexpressed compared to CAKI2 in all ccRCC cell lines. VEGFC and PDGFB were downregulated in most cell lines compared to CAKI2, however most samples did not reach the significance cut offs.

Analysis of key HIF1α pathway endpoint angiogenic genes in VHL_{mut} ccRCC cell lines compared to the VHL_{WT} CAKI2 cell line revealed significant changes in some genes. HIF1A was found to be significantly downregulated in UOK121 and UMRC3 compared to CAKI2 (Log2 FC -3.901, padj = <0.001 and Log2 FC -2.097, padj = <0.0001 respectively) and generally downregulated in UMRC2 and UOK143, however upregulation of HIF1A was observed in A498 compared to CAKI2. This general downregulation compared to CAKI2 may be due to the fact that as previously mentioned, overaccumulation of HIF1α protein can lead to reduced HIF1A gene expression, which would be expected when VHL is lost. In our cell lines vs HK2 analysis, CAKI2 was found to have the strongest downregulation of VEGFA out of the 6 ccRCC cell lines, and so it is unsurprising that all cell lines were found to have upregulation of VEGFA compared to CAKI2. High VEGFA mRNA and protein levels have been associated with shorter OS and PFS (Wierzbicki et al. 2019), and so while the VEGFA overexpression in our 5 ccRCC VHL_{mut} cell lines do not reach the log2 FC significance threshold, a clear general trend of upregulation of VEGFA is observed in VHL_{mut} cell lines compared to the VHL_{WT} CAKI2 cell line. No clear change is observed in VEGFB expression, however interestingly, VEGFC is strongly downregulated in UMRC2 compared to CAKI2 (Log2 FC -4.875, padj = <0.001), and weakly downregulated in the other cell lines, apart from UMRC3 which showed slight upregulation. The UMRC2 cell line was also found to have significant downregulation of BAP1, p53, VEGFC and PDGFB compared to HK2 implying an altered angiogenic signature in this cell line which varies from both normal kidney and from the VHL_{WT} cell line. TGFα was found to be weakly upregulated in all cell lines compared to CAKI2, however this is expected as CAKI2 was the only cell line showing downregulation of this gene compared to HK2. TGFβ was however found to be weakly upregulated in A498, UMRC2 and UOK143 compared to CAKI2, in line with reports that VHL is able to negatively regulate TGFβ in ccRCC (Mallikarjuna et al. 2018). PDGFB expression compared to CAKI2 was split across the cell lines, with A498 showing significant downregulation (Log2 FC -4.292, padj = <0.001) and UMRC2 also showing weak downregulation, while UMRC3, UOK121 and UOK143 were found to be weakly upregulated compared to CAKI2. Functional VHL has been

shown to repress PDGFB expression (Rafty and Khachigian 2002), so the reason for the downregulation we observe in A498 and UMRC2 compared to CAKI2 is unclear, however protein expression may differ from the mRNA output. Finally, we show a significant upregulation in CAIX expression compared to CAKI2 in 4 out of the 5 VHL_{mut} cell lines, with UOK121 showing only week upregulation. The strongest upregulation was however observed in UOK143 (Log2 FC 9.810, padj = <0.001). Low CAIX expression is associated with the absence of VHL mutation (Pantuck et al. 2007), while high CAIX expression has been suggested as a biomarker for ccRCC treatment response and prognosis (Brookman-May et al. 2013).

This data reveals a clear difference in angiogenic gene expression in VHL_{mut} cell lines compared to VHL_{WT} cells. VEGFA, TGFα and CAIX were found to be generally strongly upregulated in the VHL_{mut} cell lines compared to the VHL_{WT} cell line, while HIF1A, VEGFC and PDGFB were generally downregulated in the VHL_{mut} cell lines.

3.3.4 CD200 gene expression in ccRCC cell lines

CD200 gene expression was next examined by read count within the ccRCC cell lines, as shown in Figure 3.24.

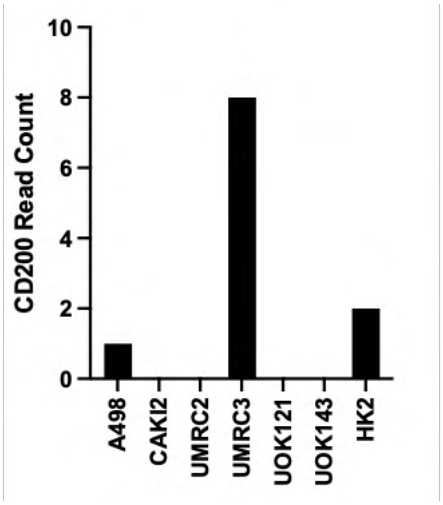

Figure 3.24 CD200 read count in ccRCC RNAseq data
CD200 read counts from the sequencing data were used as a read out of gene expression level. Zero read counts were found for four of the six ccRCC cell lines, while only two counts were found for the normal kidney HK2 sample.

RNAseq read counts were used as a read out of gene expression, and we found that four out of the six ccRCC cell lines had a read count of zero. Of the cell lines which did have some CD200 gene expression, UMRC3 had the highest read count value, while A498 and HK2 were found to have very low counts. This data is in line with what we have previously observed of very low CD200 expression by qRT-PCR and western blot, so as previously discussed, this could be due to cell culture conditions, and alternative CD200+ cell lines will need to be used for functional and proof-of-concept experiments.

3.4 Determining proteases involved in RCC development

To firstly understand which proteases are already known to play a role in RCC development, we conducted a literature search. Many proteases have been reported to be involved in a range of RCC processes including cell adhesion, growth, epithelial-to-mesenchymal transition (EMT), invasion, migration and metastasis, a full list of which is found in Table 3.3.

Table 3.3 Proteases known to be upregulated in RCC

Protease	Function in Cancer	Reference
ADAM8	Migration and invasion	(Mochizuki and Okada 2007)
ADAM9	Cell adhesion and invasion	(Fritzsche et al. 2008)
ADAM10	Cell growth and migration	(Twito et al. 2013)
ADAM12	Invasion and metastasis	(Gao et al. 2022)
ADAM17 (TACE)	Cell growth	(Erin et al. 2017)
ADAM19	Invasion and metastasis	(Mochizuki and Okada 2007)
ADAM28	Cell growth	(Twito et al. 2013)
MMP1	Invasion and metastasis	(Zakiyanov et al. 2019)
MMP2	Invasion and metastasis	(Di Carlo 2014)
MMP3	EMT and growth	(Zakiyanov et al. 2019)
MMP7	Invasion and metastasis	(Miyata et al. 2006)
MMP9	Invasion and metastasis	(Cho et al. 2003)
MMP10	Invasion and metastasis	(Zakiyanov et al. 2019)
MMP11	Migration and invasion	(Zakiyanov et al. 2019)
MMP14 (MT-MMP1)	Invasion and metastasis	(Narula et al. 2017)
MMP15 (MT-MMP2)	EMT and migration	(Narula et al. 2017)
MMP16 (MT-MMP3)	Invasion and metastasis	(Narula et al. 2017)
MMP26	Invasion and metastasis	(Zakiyanov et al. 2019)

As our literature search revealed a large number of proteases which are involved in RCC development, we next aimed to narrow down this list using RNA sequencing to find proteases which are overexpressed in ccRCC compared to normal kidney. This would allow us to pinpoint more specific targets to investigate further in regard to their role in CD200 ectodomain shedding.

3.4.1 Protease expression in RNAseq data

The differences in gene expression we have already observed between our cell lines show the large variation in the ccRCC genetic landscape, however all cell lines were found to retain a large number of similar genes which are likely to be

essential for disease development and progression. As we are interested in which proteases are involved in the development and progression of ccRCC, we next examined our ccRCC cell line vs HK2 DEGs to determine which proteases are up- or downregulated compared to normal kidney, as shown in Table 3.4.

Table 3.4 DEG list of all proteases in ccRCC vs HK2

		A498		CAKI2		UOK121		UOK143		UMRC2		UMRC3	
Gene ID	**Gene Name**	**Log2 FC**	**padj**	**Log2 FC**	**padj**	**Log2 FC**	**padj**	**Log2 FC**	**padj**	**Log2 FC**	**padj**	**Log2 FC**	**padj**
ENSG00000226469	ADAM1B	-2.327	0.308	-1.057	0.721	1.978	0.000	0.857	0.696	0.119	1.000	-5.272	0.207
ENSG00000069206	ADAM7	1.033	1.000					1.598	0.796	1.028	1.000		
ENSG00000151651	ADAM8	-0.872	0.172	-0.673	0.323	2.041	0.000	-1.414	0.020	-2.847	0.000	-0.637	0.428
ENSG00000168615	**ADAM9**	**5.309**	**0.000**	**4.259**	**0.000**	**3.910**	**0.000**	**4.033**	**0.000**	**5.477**	**0.000**	**4.913**	**0.000**
ENSG00000137845	ADAM10	0.667	0.242	0.183	0.814	1.178	0.025	0.071	0.969	-0.293	0.679	0.754	0.199
ENSG00000073670	ADAM11	2.915	0.000	1.600	0.011	-0.423	0.704	1.224	0.075	1.069	0.150	0.550	0.609
ENSG00000148848	ADAM12	5.433	0.000	4.928	0.000	3.327	0.000	5.655	0.000	0.757	0.226	-0.792	0.304
ENSG00000143537	ADAM15	0.316	0.655	-1.588	0.001	-1.021	0.060	-0.828	0.144	-0.697	0.225	-0.813	0.157
ENSG00000151694	**ADAM17**	**0.052**	**0.994**	**0.184**	**0.814**	**-0.229**	**0.769**	**-0.580**	**0.355**	**-0.025**	**1.000**	**-0.840**	**0.141**
ENSG00000168619	ADAM18					7.109	0.001	6.258	0.034	11.863	0.000		
ENSG00000135074	ADAM19	2.618	0.000	0.907	0.122	7.109	0.001	0.732	0.241	-2.781	0.000	-0.455	0.572
ENSG00000134007	ADAM20	-1.357	0.782	-4.687	0.473	1.227	0.400	-0.429	1.000	-1.362	0.789	-4.309	0.693
ENSG00000259158	ADAM20P1	-4.029	0.671	-0.084	1.000	-4.633	0.489	0.684	1.000	-4.032	0.679	1.333	0.657
ENSG00000139985	ADAM21	-3.051	0.072	0.392	0.790	0.021	1.000	1.050	0.320	0.120	1.000	1.386	0.208
ENSG00000008277	ADAM22	1.985	0.000	-0.181	0.854	-1.675	0.328	0.209	0.814	-1.651	0.007	0.667	0.339
ENSG00000114948	ADAM23	11.466	0.000	9.923	0.000	-0.989	0.134			11.057	0.000	7.793	0.000
ENSG00000042980	**ADAM28**	**3.842**	**0.000**	**3.319**	**0.000**	**0.021**	**1.000**	**-4.581**	**0.473**	**0.517**	**1.000**	**0.220**	**1.000**
ENSG00000197140	ADAM32	-0.172	1.000	-0.279	0.991	-0.514	0.730	-2.794	0.036	1.115	0.193	1.613	0.042
ENSG00000154734	ADAMTS1	-0.179	0.812	1.899	0.000	2.664	0.000	2.261	0.000	0.852	0.122	3.129	0.000
ENSG00000142303	ADAMTS10	3.601	0.000	1.064	0.073	-9.530	0.000	-3.386	0.000	-9.482	0.000	-9.191	0.000
ENSG00000151388	ADAMTS12	1.574	0.001	-12.488	0.000	-4.246	0.000	-12.378	0.000	-12.384	0.000	2.389	0.000
ENSG00000160323	ADAMTS13	1.871	0.000	1.961	0.000	0.059	1.000	0.667	0.345	-0.877	0.225	-0.573	0.526

		A498		CAKI2		UOK121		UOK143		UMRC2		UMRC3	
Gene ID	**Gene Name**	**Log2 FC**	**padj**	**Log2 FC**	**padj**	**Log2 FC**	**padj**	**Log2 FC**	**padj**	**Log2 FC**	**padj**	**Log2 FC**	**padj**
ENSG00000138316	ADAMTS14	-0.356	0.663	-0.673	0.323	-5.835	0.000	-0.014	1.000	-4.780	0.000	-3.522	0.000
ENSG00000166106	ADAMTS15	2.698	0.000	-0.742	0.239	-1.509	0.006	0.306	0.691	2.023	0.000	-6.193	0.000
ENSG00000145536	ADAMTS16	3.829	0.000	4.874	0.000	2.373	0.000	3.437	0.000	0.662	0.489	3.544	0.000
ENSG00000140470	ADAMTS17	-5.554	0.117	-2.528	0.329	-5.604	0.137	-0.841	0.721	-5.557	0.122	-1.682	0.693
ENSG00000140873	ADAMTS18	-0.802	1.000	-0.084	1.000	1.767	0.451	1.399	0.691	-0.807	1.000	-0.170	1.000
ENSG00000087116	ADAMTS2	7.768	0.000	0.190	0.991	-6.809	0.004	-3.524	0.026	3.135	0.000	-6.473	0.014
ENSG00000156140	ADAMTS3	-2.351	0.000	-1.234	0.018	-0.001	1.000	-1.584	0.002	-0.800	0.159	-0.617	0.325
ENSG00000154736	ADAMTS5	-1.149	0.671	2.807	0.001	5.005	0.000	-5.294	0.206	-5.300	0.192	5.497	0.207
ENSG00000049192	ADAMTS6	-4.253	0.000	-1.952	0.013	0.468	0.651	3.828	0.000	-3.701	0.000	5.716	0.000
ENSG00000136378	ADAMTS7	3.436	0.000	0.982	0.092	-5.044	0.000	0.813	0.202	-0.964	0.127	3.139	0.000
ENSG00000261143	ADAMTS7P3	1.591	0.782					1.999	0.628	4.703	0.458	-2.584	0.000
ENSG00000218052	ADAMTS7P4	5.107	0.292	8.660	0.000	6.930	0.002	4.152	0.691	7.529	0.000	5.093	0.320
ENSG00000163638	ADAMTS9	-1.669	0.001	-0.204	0.799	1.375	0.008	0.327	0.669	1.252	0.015	-3.629	0.000
ENSG00000241158	ADAMTS9-AS1	-5.297	0.185	-1.355	0.691	0.497	0.927	1.954	0.090	7.027	0.000	-5.016	0.320
ENSG00000241684	ADAMTS9-AS2	-2.089	0.001	-1.349	0.037	-0.697	0.361	-0.280	0.761	-0.489	0.519	0.230	0.812
ENSG00000178031	ADAMTSL1	6.404	0.018			9.671	0.000	4.152	0.691	6.401	0.019	9.300	0.000
ENSG00000156218	ADAMTSL3	0.817	0.584	4.020	0.000	7.103	0.000	5.985	0.000	3.055	0.000	7.299	0.000
ENSG00000143382	ADAMTSL4	-1.143	0.043	1.642	0.001	0.853	0.155	-4.062	0.000	-1.424	0.010	0.430	0.584
ENSG00000203804	ADAMTSL4-AS1	-0.802	1.000	-0.999	1.000	-0.897	1.000	-4.026	0.691	1.862	0.420	1.333	0.657
ENSG00000185761	ADAMTSL5	0.439	0.511	-4.696	0.000	-0.173	0.861	-0.687	0.306	-2.597	0.000	1.561	0.003
ENSG00000196611	MMP1	-8.941	0.000	-5.917	0.000	5.157	0.000	4.218	0.000	-0.452	0.628	-8.653	0.000
ENSG00000137673	MMP7	-1.048	0.047	1.552	0.002	-4.395	0.000	2.833	0.000	-5.722	0.000	-6.733	0.000
ENSG00000100985	MMP9	-6.148	0.000	-7.273	0.000	-3.325	0.000	-0.043	1.000	-5.596	0.000	-10.008	0.000

		A498		CAKI2		UOK121		UOK143		UMRC2		UMRC3	
Gene ID	**Gene Name**	**Log2 FC**	**padj**	**Log2 FC**	**padj**	**Log2 FC**	**padj**	**Log2 FC**	**padj**	**Log2 FC**	**padj**	**Log2 FC**	**padj**
ENSG00000166670	MMP10							6.853	0.000				
ENSG00000099953	MMP11	-2.938	0.000	0.890	0.130	-2.733	0.000	0.539	0.439	-3.676	0.000	-10.364	0.000
ENSG00000137745	MMP13	-0.665	0.746	-5.877	0.082	-1.724	0.451	-1.059	0.623	-5.775	0.077	-1.899	0.693
ENSG00000157227	MMP14	0.800	0.145	-7.490	0.000	1.749	0.000	0.486	0.471	-8.991	0.000	0.122	0.893
ENSG00000102996	MMP15	-1.590	0.001	-3.100	0.000	-2.365	0.000	-2.663	0.000	-4.832	0.000	-3.694	0.000
ENSG00000156103	MMP16	-5.051	0.000	1.207	0.029	0.537	0.467	-2.829	0.000	-4.268	0.000	-0.520	0.516
ENSG00000198598	MMP17	-7.196	0.001	0.829	0.397	0.526	0.704	-7.192	0.001	0.677	0.496	-6.909	0.002
ENSG00000123342	MMP19	1.242	0.463	-5.402	0.203	-5.347	0.215	-2.063	0.473	2.413	0.014	2.044	0.082
ENSG00000087245	MMP2	-2.837	0.000	-9.197	0.000	-2.119	0.002	-4.935	0.000	-9.093	0.000	-8.802	0.000
ENSG00000154485	MMP21	-4.029	0.671	-0.084	1.000	-4.077	0.704	-4.026	0.691	-4.032	0.679	-3.760	0.693
ENSG00000215914	MMP23A	2.563	0.308			3.041	0.123	3.432	0.056				
ENSG00000189409	MMP23B	1.033	1.000	0.836	1.000	0.938	1.000	1.040	1.000	1.028	1.000		
ENSG00000125966	MMP24	0.626	0.288	-2.458	0.000	-3.553	0.000	0.487	0.473	-0.038	1.000	1.629	0.001
ENSG00000126005	MMP24OS	2.942	0.000	2.897	0.000	2.216	0.000	2.991	0.000	2.670	0.000	4.388	0.000
ENSG00000008516	MMP25	2.631	0.005	2.147	0.033	-2.167	0.488	1.250	0.487	2.354	0.018	1.783	0.140
ENSG00000261971	MMP25-AS1	2.167	0.000	2.760	0.000	0.372	0.727	2.733	0.000	1.976	0.000	2.203	0.000
ENSG00000271447	MMP28	-0.579	0.716	-3.179	0.013	-7.169	0.001	-3.884	0.006	-7.121	0.001	-6.832	0.004

Many proteases were found to be significantly up- or downregulated compared to the HK2 normal kidney control sample (padj =<0.05), with a log2 fold change value of ≤-2 or ≥+2. Volcano plots showing protease expression in each cell line are shown in Figure 3.25. ADAM9 was the only protease found to be significantly overexpressed consistently when compared to normal kidney, with a log2 fold change of ≥+2 in every RCC sample, represented by a blue dot in each graph.

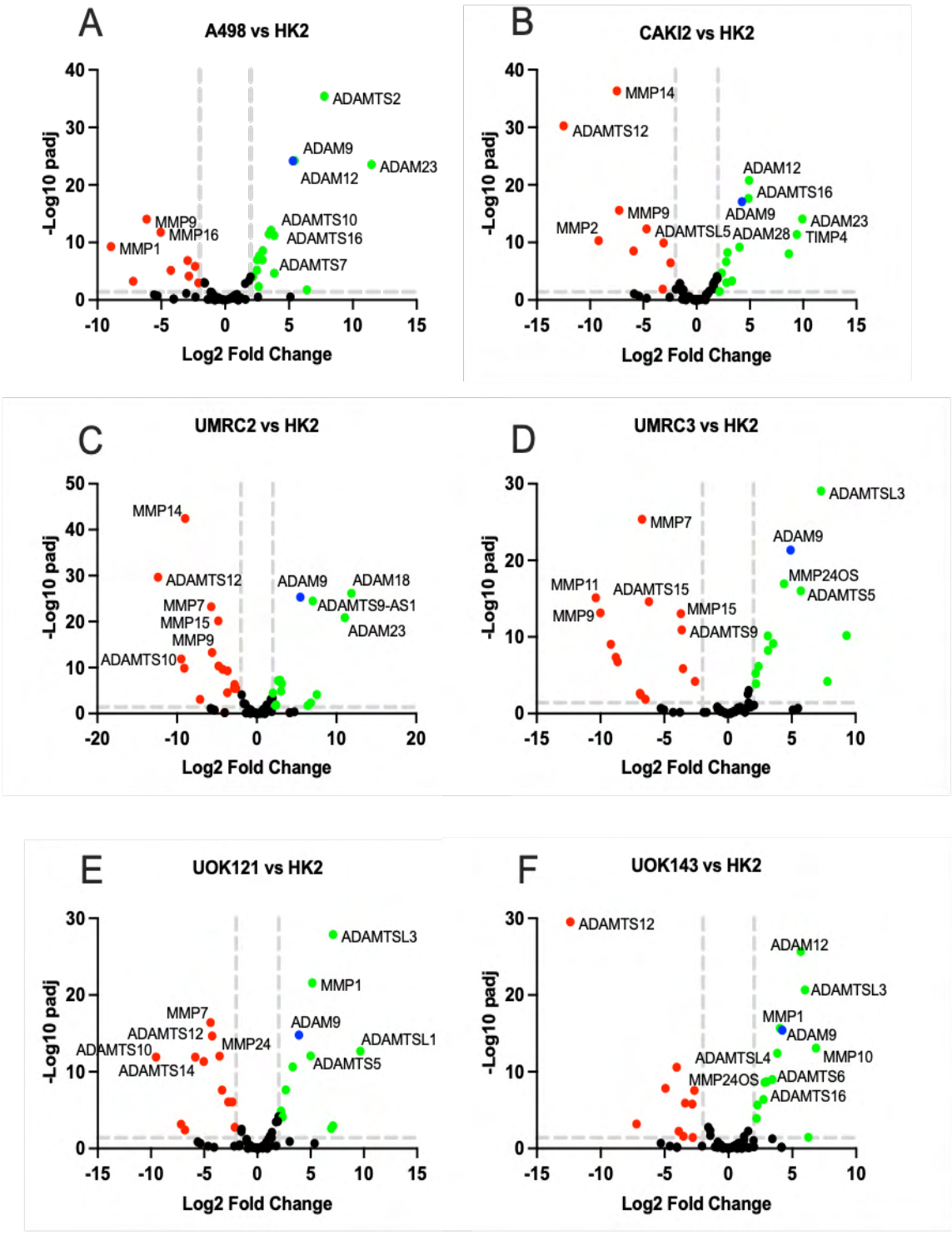

Figure 3.25 Volcano plots of proteases expressed in ccRCC cell lines vs HK2
Visual representation of protease padj value and log2 fold change value. Volcano plots feature each ccRCC cell line vs HK2, filtered for ADAMs, MMPs and TIMPs. (A) A498 vs HK2 (B) CAKI2 vs HK2, (C) UMRC2 vs HK2, (D) UMRC3 vs HK2, (E) UOK121 vs HK2 (F) UOK143 vs HK2. Significant genes (padj <0.05) with a log2 fold change value of <-2 are highlighted in red, >2 are highlighted in green and ADAM9, which is significantly upregulated in every sample, is highlighted in blue.

Interestingly, ADAM17 was not found to be significantly up- or downregulated compared to the normal kidney HK2 sample in any of the cell lines, however ADAM28 was found to be significantly overexpressed in A498 and CAKI2 compared to HK2, (log2 fold change +3.842 and +3.319 respectively, padj=<0.05).

This data indicates that ADAM17 is not found at significantly different levels in our ccRCC cell lines compared to normal kidney, and ADAM28 was only overexpressed in 2 out of 6 cell lines, so these proteases alone may not play substantial roles in the development of ccRCC. As ADAM9 was the only sheddase found to be significantly overexpressed in all 6 ccRCC cell lines compared to normal kidney, we chose to investigate ADAM9 further and to determine if it is involved in ccRCC development, and if it could have a role in CD200 ectodomain shedding.

3.4.2 Validating protease expression in RCC cell lines

To validate the expression of ADAM9, ADAM17 and ADAM28 observed in our RNAseq data in our ccRCC cell lines, we determined mRNA transcript expression using qRT-PCR and western blot analysis.

3.4.2.1 Protease mRNA expression

ADAM9 mRNA expression has been associated with tumour progression and prognosis in various cancer types, including in RCC (Fritzsche et al. 2008), while ADAM17 has also been shown to be overexpressed in many cancer types including RCC, with expression levels linked to increased tumour aggressiveness (Doberstein et al. 2013). ADAM28 has roles in metastasis and tumour progression in various cancer types, however its specific role in RCC development is yet to be elucidated (Mochizuki et al. 2012).

3.4.2.1.1 ADAM9 mRNA expression

To determine ADAM9 expression in our ccRCC cell lines, we firstly examined mRNA transcript expression. ADAM9 mRNA expression has been associated with higher ccRCC tumour grade, positive nodal status and metastasis (Fritzsche et al. 2008). Our 6 ccRCC and HK2 normal kidney cell lines were evaluated for ADAM9

expression, which was then compared to the read count data from our RNAseq analysis to determine if the levels were comparable, as shown in Figure 3.26.

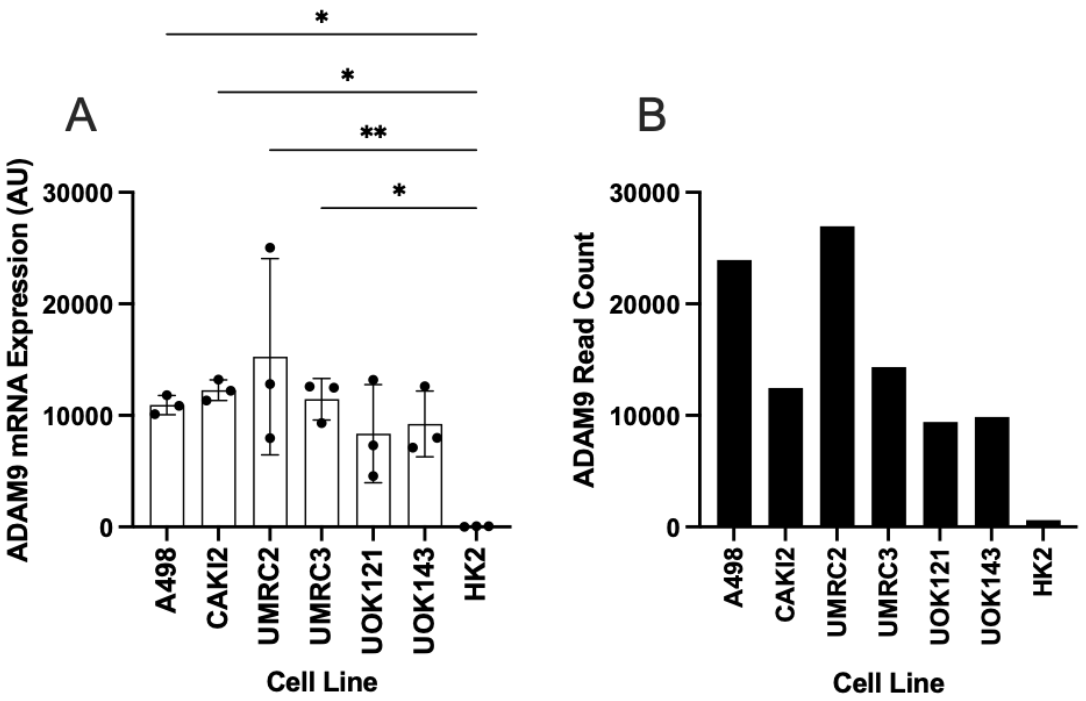

Figure 3.26 ADAM9 mRNA expression and read count level in RCC cell lines
(A) RNA was extracted from six RCC cell lines, one normal kidney cell line and ADAM9 gene expression was determined by qRT-PCR. Expression was normalised to β -Actin and ADAM9 expression was calculated according to the 2^-delta Ct method and is shown as arbitrary units (AU). Differences in gene expression were calculated using a Kruskal-Wallis test followed by Dunn's multiple comparisons test, where * represents $p < 0.05$ and ** represents $p < 0.01$. n=3. (B) ADAM9 read count data generated from RNA sequencing.

High ADAM9 mRNA levels were found across our RCC lines, with very little expression found in the HK2 normal kidney cell line (Figure 3.26a). The highest average ADAM9 mRNA expression was found in the UMRC2 cell line, which was significantly higher than that found in the HK2 cell line ($p=0.0018$). The A498, CAKI2 and UMRC3 cell lines were also found to have significantly higher mRNA levels compared to HK2 ($p=0.0218$, $p=0.0100$ and $p=0.0160$ respectively).

Comparison of our RNAseq read count values found the highest figure was again observed in the UMRC2 cell line, with the lowest value found in the HK2 sample (Figure 3.26b). This pattern followed what we saw in our mRNA expression data, confirming that ADAM9 expression is significantly increased in all ccRCC cell lines compared to normal kidney.

3.4.2.1.2 ADAM17 mRNA expression

ADAM17 is one of the most well studied sheddases in the ADAM family and expression is associated with poor outcome in ccRCC, where expression may have some use as a prognostic biomarker (Li et al. 2014a). We next examined ADAM17 mRNA expression in our cell lines compared to our RNAseq read count data, as shown in Figure 3.27.

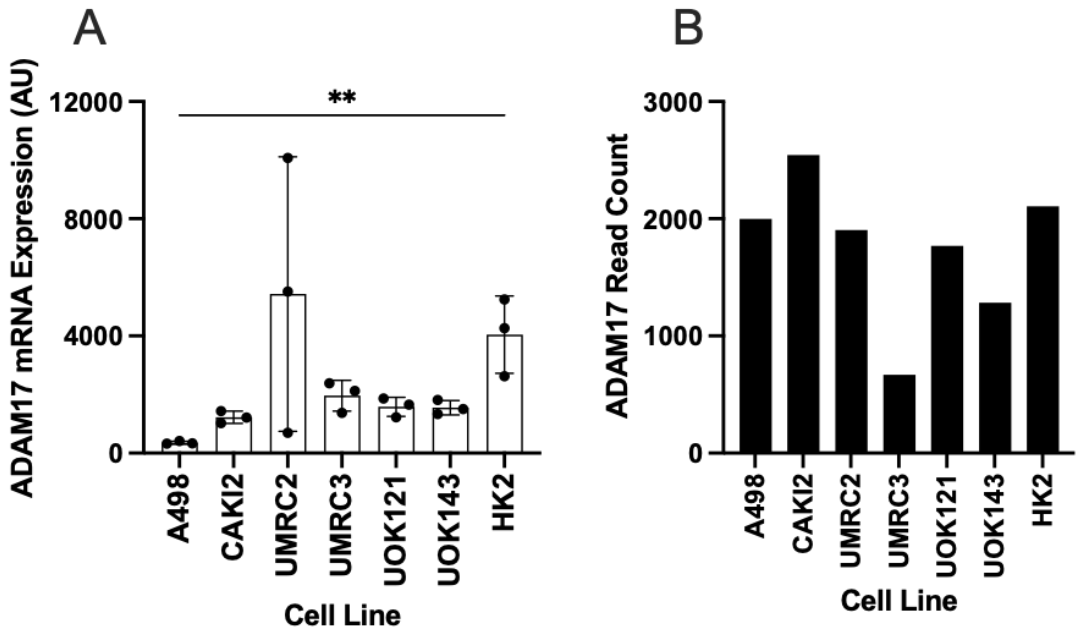

Figure 3.27 ADAM17 mRNA expression and read count level in RCC cell lines
(A) RNA was extracted from six RCC cell lines, one normal kidney cell line and ADAM17 gene expression was determined by qRT-PCR. Expression was normalised to β -Actin and ADAM17 expression was calculated according to the 2^-delta Ct method and is shown as arbitrary units (AU). Differences in gene expression were calculated using a Kruskal-Wallis test followed by Dunn's multiple comparisons test, where ** represents $p<0.01$. n=3. (B) ADAM17 read count data generated from RNA sequencing.

ADAM17 mRNA expression was found to be consistently lower in all cell lines than what was observed ADAM9 (Figure 3.27a). The highest average ADAM17 mRNA levels were seen in the UMRC2 cell line, while the lowest values were found in the A498 cell line, which had significantly lower levels than the HK2 normal kidney samples ($p=0.0095$).

Conversely, the highest read count figures were observed in the CAKI2 cell line (Figure 3.27b). We observed the lowest read count values in the UMRC3 cell line

and in this data the A498 read count figures are comparable to the other ccRCC cell line levels.

ADAM17 read count figures were also lower overall than those observed for ADAM9, with around a 10-fold expression decrease found in all ccRCC cell lines, however a similar figure was also seen for the HK2 cell line.

3.4.2.1.3 ADAM28 mRNA expression

ADAM28 mRNA expression and read count data was next explored in our samples, as shown in Figure 3.28. ADAM28 has not been strongly associated with ccRCC with very little literature available linking the two, however expression has been previously reported in the CAKI2 cell line in association with increased apoptosis in cell line studies (Mochizuki et al. 2012).

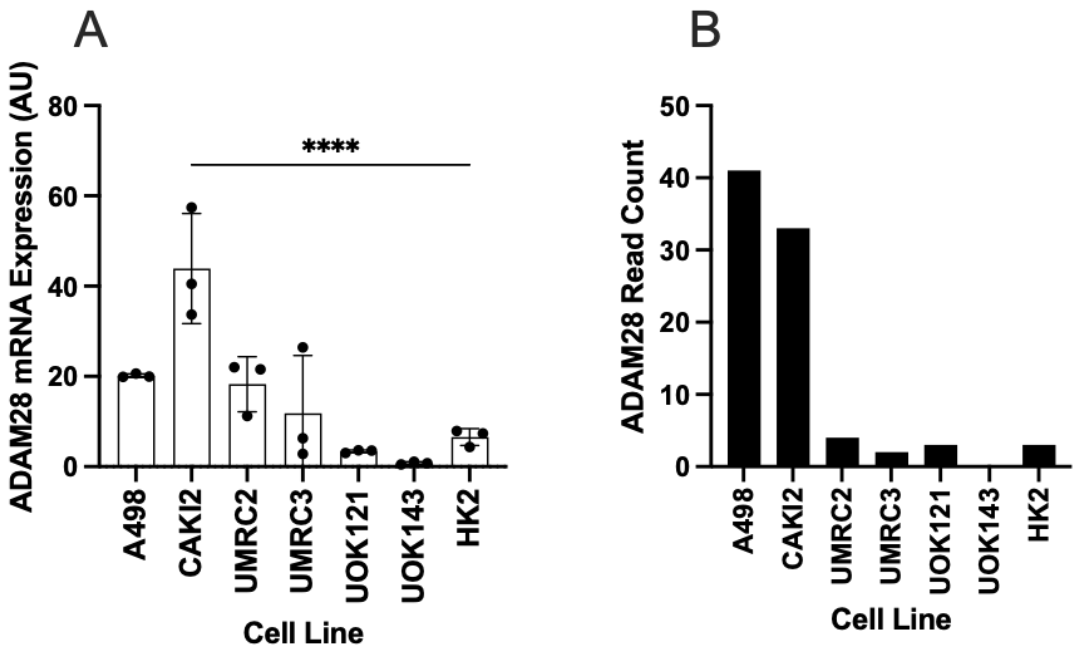

Figure 3.28 ADAM28 mRNA expression and read count level in RCC cell lines
(A) RNA was extracted from six RCC cell lines and one normal kidney cell line. ADAM9 gene expression was determined by qRT-PCR. Expression was normalised to β -Actin and ADAM9 expression was calculated according to the 2^-delta Ct method and is shown as arbitrary units (AU). Differences in gene expression were calculated using a Kruskal-Wallis test followed by Dunn's multiple comparisons test, where **** represents p <0.0001. n=3 (B) Read count data generated from RNA sequencing.

ADAM28 mRNA expression was found to be substantially lower in all cell lines compared to both ADAM9 and ADAM17 (Figure 3.28a), a pattern which is also mirrored in our RNAseq read count data (Figure 3.28b). Very low expression was seen across all cell lines; however, the highest mRNA values were seen in the CAKI2 cell line which was found to be significantly higher than the HK2 normal kidney cell line ($p<0.0001$). The lowest expressing ADAM28 mRNA ccRCC cell lines were UOK143 and UOK121, both of which had lower expression than the normal kidney samples.

Read count values followed similar patterns to the mRNA data with the A498 cell line showing the highest read count values while UOK143 again showed the lowest values. This data suggests that ADAM28 is present in very low levels in both RCC and normal kidney, however some cell lines have stronger expression than others. Therefore, due to its low levels, ADAM28 may play a less significant role than other proteases and may not be a major factor in ccRCC development.

This data has shown much higher expression levels of ADAM9 in our ccRCC cell lines compared to that of ADAM17 and ADAM28, with 4 out of 6 ccRCC cell lines also showing significantly higher expression than that found in the normal kidney HK2 cell line. Measurement of mRNA levels is an indication of gene expression, however this does not always translate into protein expression, so we next probed protein lysate from each cell line to determine expression of each protease by western blot analysis.

3.4.2.2 Protease protein expression

To determine whether the protease mRNA levels we have seen correlate with their expression at the protein level, whole protein lysate was extracted from each cell line and probed for ADAM9, ADAM17 or ADAM28 by western blot analysis.

3.4.2.2.1 ADAM9 protein expression

We firstly examined ADAM9 protein expression in our cell lines to determine whether cell line protein expression correlates with mRNA levels, as shown in Figure 3.29.

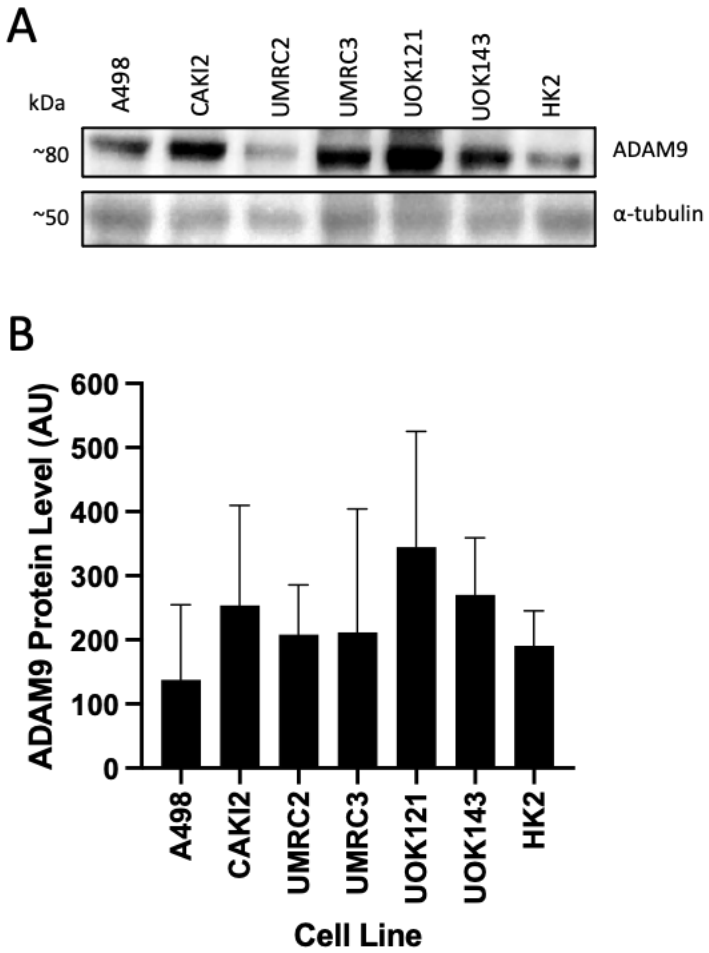

Figure 3.29 Western blot analysis of ADAM9 protein expression
Whole cell lysate was extracted from 6 ccRCC cell lines and the HK2 normal kidney cell line and immunoblotted for ADAM9. (A) Representative image. (B) Expression was normalised to α-tubulin and ADAM9 level shown in arbitrary units (AU). Values were obtained from an average of 3 independent experiments.

ADAM9 protein was found and high levels in all cell lines studied, including the HK2 normal kidney cell line (Figure 3.29a). This is an unexpected result as the HK2 cell line was found to have minimal ADAM9 mRNA expression, however all the ccRCC cell lines showed high protein levels following normalisation to the relevant housekeeping gene (Figure 3.29b) which correspond to the high mRNA levels observed in our earlier study.

3.4.2.2.2 ADAM17 protein expression

We next examined ADAM17 protein expression in our cell lines to determine whether cell line protein expression correlates with mRNA levels, as shown in Figure 3.30.

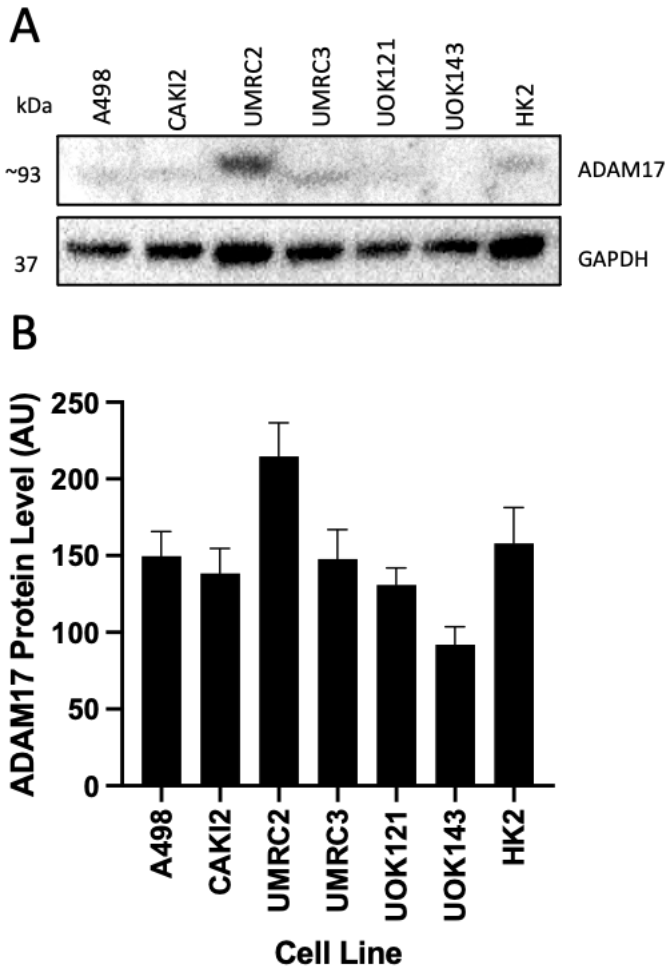

Figure 3.30 Western blot analysis of ADAM17 protein expression
Whole cell lysate was extracted from 6 ccRCC cell lines and the HK2 normal kidney cell line and immunoblotted for ADAM17. (A) Representative image. (B) Expression was normalised to GAPDH and ADAM17 level shown in arbitrary units (AU). Values were obtained from an average of 3 independent experiments.

Low levels of ADAM17 were found in all cell lines (Figure 3.30a), with similar protein expression observed across all ccRCC cell lines and the normal kidney cell line when normalised to the house keeping gene GAPDH (Figure 3.30b), mirroring what was found in our previous mRNA comparisons.

3.4.2.2.3 ADAM28 protein expression

Finally, we examined ADAM28 protein expression in our cell lines to determine whether cell line protein expression correlates with mRNA levels, as shown in Figure 3.31.

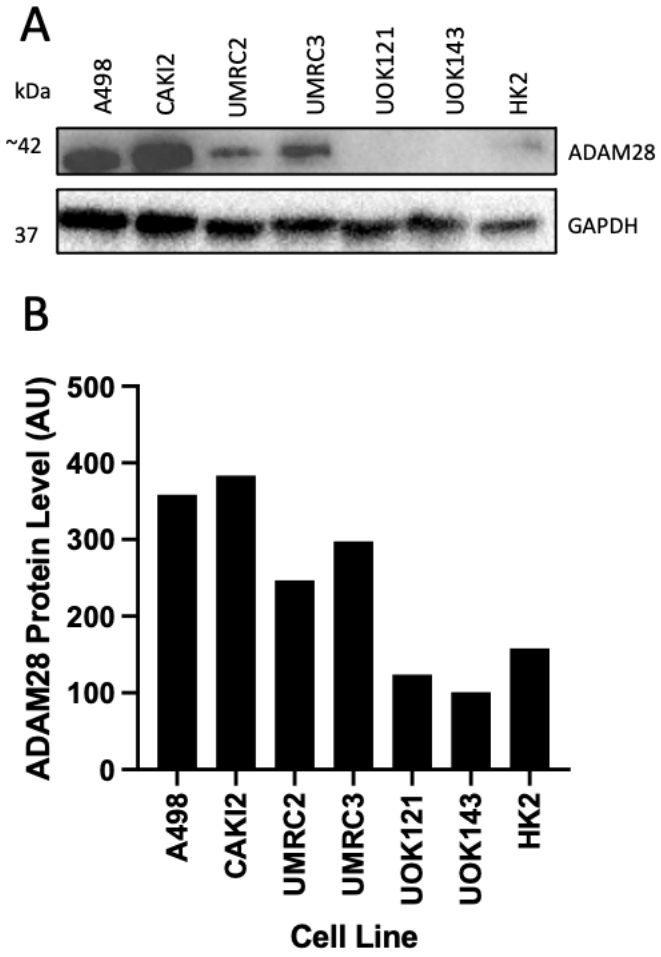

Figure 3.31 Western blot analysis of ADAM28 protein expression
Whole cell lysate was extracted from 6 ccRCC cell lines and the HK2 normal kidney cell line and immunoblotted for ADAM28. (A) Representative image. (B) Expression was normalised to GAPDH and ADAM28 level shown in arbitrary units (AU). Values were obtained from an average of 3 independent experiments.

Western blot analysis showed that as was found at the mRNA level, the CAKI2 and A498 cell lines had the greatest ADAM28 protein expression, with the UOK143 and UOK121 cell lines having the lowest protein expression (Figure 3.31a). Normalisation to the GAPDH housekeeping gene confirmed the highest expression in A498 and CAKI2 (Figure 3.31b).

3.5 Characterising protease expression in kidney tissue

Having now validated our RNAseq results for ADAM9, ADAM17 and ADAM28, we next wanted to determine their staining patterns and expression strength within the normal kidney and patient-derived tumour tissue.

3.5.1 Protease antibody optimisation

We next aimed to determine expression of our proteases of interest, ADAM9, ADAM17 and ADAM28 within patient-derived TMAs. Expression of these proteases is strong in normal human stomach (Love et al. 2017a), so we firstly optimised the antibodies on this tissue to ensure accurate staining, as shown in Figure 3.32.

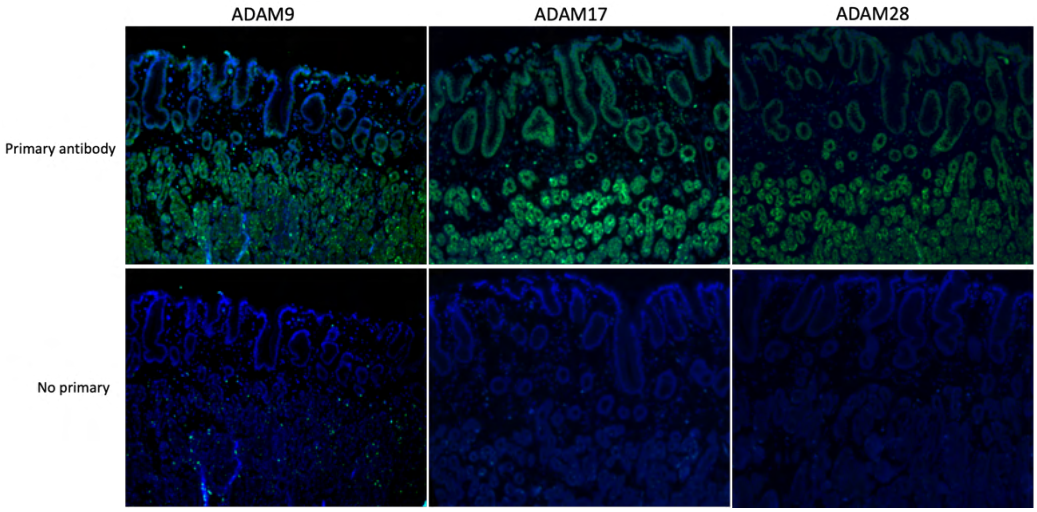

Figure 3.32 ADAM9, ADAM17 and ADAM28 staining optimisation on human stomach tissue
Representative image of ADAM9, ADAM17 and ADAM28 staining (green). Staining was completed on human stomach tissue as positive control to check antibody specificity and no primary antibody controls were carried out to check for background fluorescence.

As expected, strong membranous staining was found throughout the stomach tissue, with strong staining for all three proteases in the mucosa of the gastric pits and parietal cells. Control sections stained with no primary antibody were used to confirm the specificity of our antibodies.

3.5.2 Characterising protease expression in normal kidney

Having confirmed the specificity of our antibodies we next analysed the ADAM9, ADAM17 or ADAM28 expression strength by calculating H-scores for each core. We firstly examined the expression of the proteases in normal kidney structures, which have not been previously extensively studied in the literature. Strong ADAM9 expression has been previously reported in normal kidney, with stronger expression noted in the proximal convoluted tubule compared to the distal tubule (Uhlén et al. 2015). ADAM17 expression has been reported to be weak in normal kidney proximal tubule, glomerulus and podocytes (Fritzsche et al. 2008), while one study has shown weak ADAM28 expression in the collecting ducts of the normal kidney (Kato et al. 2018).

We firstly examined expression of ADAM9, ADAM17 and ADAM28 in the renal corpuscle, as shown in Figure 3.33.

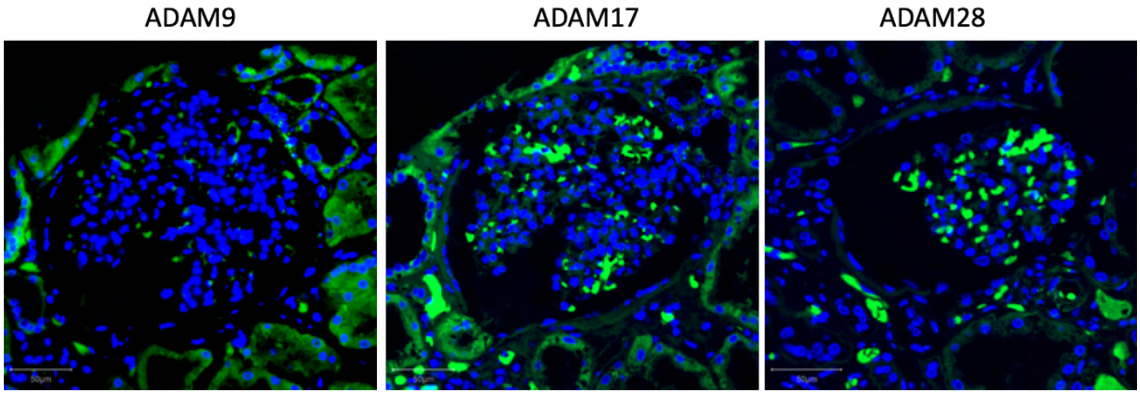

Figure 3.33 ADAM9, ADAM17 and ADAM28 expression within the renal corpuscle
Weak to negative ADAM9 and ADAM28 expression was observed throughout the glomerulus (green), with moderate to strong ADAM17 expression found throughout the glomerulus and Bowman's capsule. DAPI is represented in blue. Scale bar represents 50µm.

Weak ADAM9 expression was observed throughout the endothelial cells of the glomerulus capillary network, with no staining observed on the mesangial cells or Bowman's capsule. Moderate to strong ADAM17 staining was observed throughout the glomerulus, with moderate staining found on the simple squamous epithelial cells of the Bowman's capsule. Weak ADAM28 staining was observed throughout the renal corpuscle and surrounding tubules.

We next studied the expression of these protease in the proximal and distal convoluted tubules, as shown in Figure 3.34.

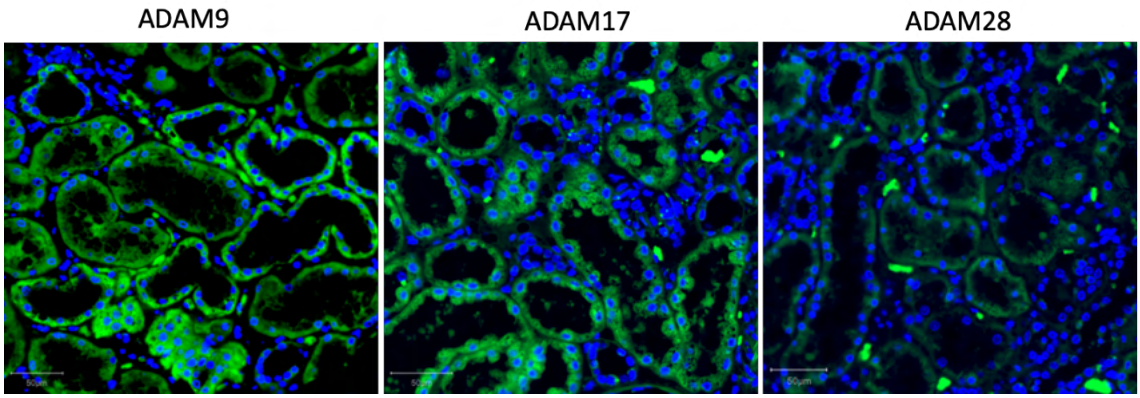

Figure 3.34 ADAM9, ADAM17 and ADAM28 expression within the proximal and distal convoluted tubules
Moderate to strong ADAM9 and ADAM17 expression (green) was observed in the proximal tubules, while ADAM28 expression was found to be weaker. In the distal tubules, ADAM9 and ADAM17 expression were again found to be strong, alongside weak ADAM28 expression. DAPI is represented in blue. Scale bar represents 50μm.

ADAM9 expression was found to be very strong in both the distal convoluted tubule and the proximal tubule. ADAM17 expression was found to be moderate in both the proximal and distal tubules, while ADAM28 expression was weak in both tubules. As ADAM9 and ADAM17 expression changed between the proximal and distal parts of the convoluted tubule, we next examined protease expression in the loop of Henle which connects the proximal and distal parts of the tubule, and the collecting duct, which is the last part of the tubule system, as shown in Figure 3.35.

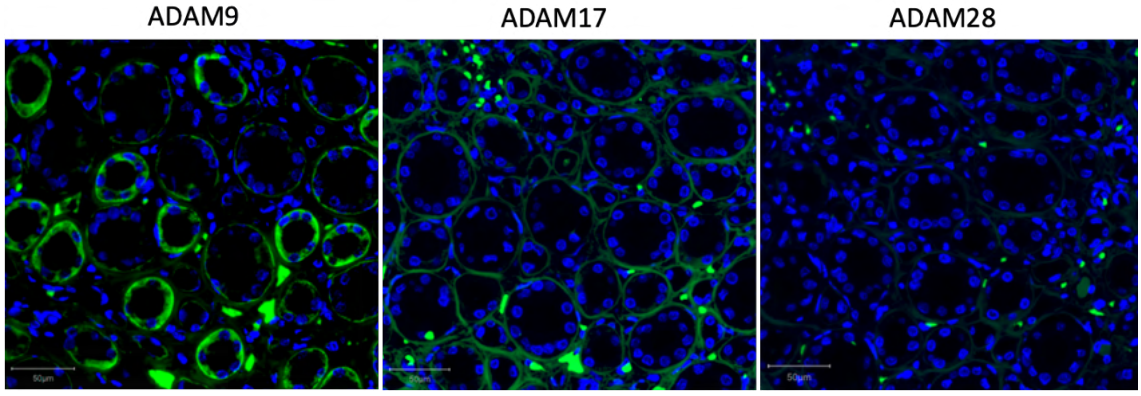

Figure 3.35 ADAM9, ADAM17 and ADAM28 expression in the loop of Henle and collecting ducts
ADAM9 expression (green) was found to be very strong within the loop of Henle but absent in the collecting ducts. ADAM17 was only found to be weakly present on the lateral borders of the collecting ducts, and ADAM28 was absent from these tissues. DAPI is represented in blue. Scale bar represents 50μm.

ADAM9 expression was found to be moderate in the loop of Henle, but absent from the collecting ducts. ADAM17 was only found to be weakly expressed on the lateral borders of the collecting ducts but negative within the loop of Henle and core of the collecting ducts. ADAM28 expression was negative in both the loop of Henle and the collecting ducts.

To quantify what we have observed, ADAM9, ADAM17 and ADAM28 staining H-scores were next calculated for each kidney structure, as shown in Figure 3.36. H-scores of 0-99 were counted as weak expression, 100-199 were counted as moderate expression and 200-300 were counted as strong expression.

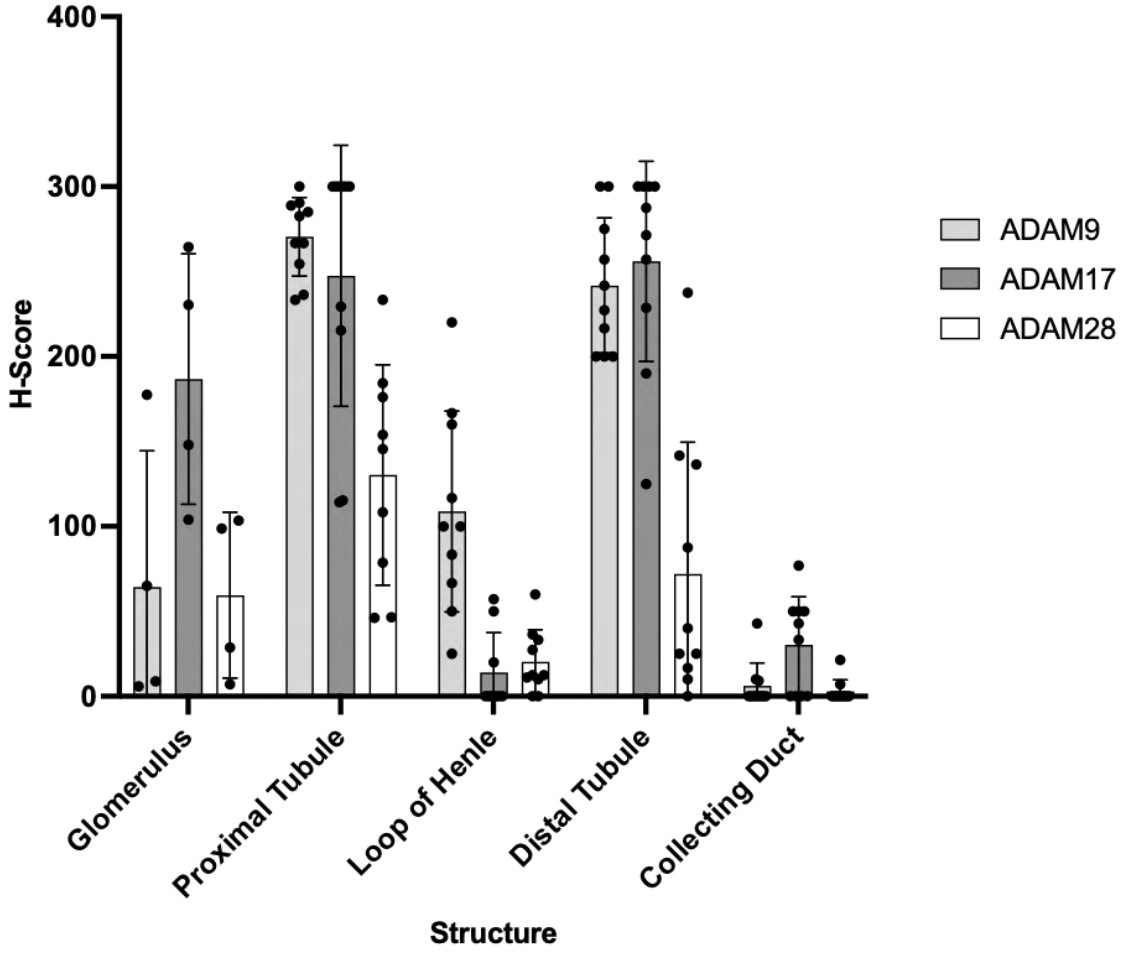

Figure 3.36 ADAM9, ADAM17 and ADAM28 H-score comparison in normal kidney structures.
ADAM9, ADAM17 and ADAM28 H-scores were compared across normal kidney structures. All measurements were n=10 except glomeruli which were n=4 due to tissue availability. H-scores were compared using a Kruskal-Wallis test with Dunn's multiple comparisons test. ADAM9 expression was found to be strongest in the proximal tubule, while ADAM17 was highly expressed in both the proximal and distal tubules. ADAM28 expression was weak throughout all structures, with weak to zero expression found in all structures.

Comparison of protease H-score revealed differences in protease expression within each structure. In the glomeruli, ADAM17 was found to have the highest expression levels, with ADAM9 and ADAM28 both showing weak expression throughout the renal corpuscle. The proximal tubule was found to have the highest expression levels of ADAM9, which were significantly higher than the levels of ADAM28 in these structures (270.50 ± 23.08 vs 137.20 ± 65.01, p = <0.001). In the loop of Henle, ADAM9 H-score was also found to be significantly higher than ADAM17 (108.80 ± 59.12 vs 14.13 ± 23.37, p = 0.001) and ADAM28 (108.80 ± 59.12 vs 20.31 ± 18.82, p = <0.001). In the distal tubule, both ADAM9 and ADAM17 were found to have high H-scores, with both found to be significantly higher than the expression of ADAM28 (241.8 ± 39.72 vs 55.44 ± 51.67, p = 0.001 and 254.3 ± 56.17 vs 55.44 ± 51.67, p = 0.008 respectively).

Having now characterised protease expression in the structures of the normal kidney, we next aimed to determine the expression of these proteases in RCC. As all three proteases exhibited the strongest expression in the proximal convoluted tubules, the cell of origin for ccRCC and pRCC, we next wanted to see if this strong expression is carried through and expressed on tumour cells, where they may have a role in disease development or progression. ADAM9 and ADAM17 were also found to show strong expression on the distal convoluted tubule, the cell of origin for chRCC, however ADAM28 expression was found to be weak in this structure.

3.5.3 Characterising protease expression in RCC tissue

Having established ADAM9, ADAM17 and ADAM28 expression in normal kidney, we next examined the expression of these proteases in RCC TMA samples. We also investigated the relationship between protease expression and RCC subtype, TNM stage, patient age at operation and sex.

3.5.3.1 ADAM9 expression

ADAM9 expression has been previously observed in both normal kidney and RCC subtypes, with expression associated with higher tumour grade, positive nodal status and metastasis (Miyamae et al. 2016). Cytoplasmic and membranous staining was seen in all tumour types, with all samples of all RCC subtypes showing some level of

positivity. Representative weak, moderate and strong ADAM9 staining in ccRCC, pRCC and chRCC is shown in Figure 3.37.

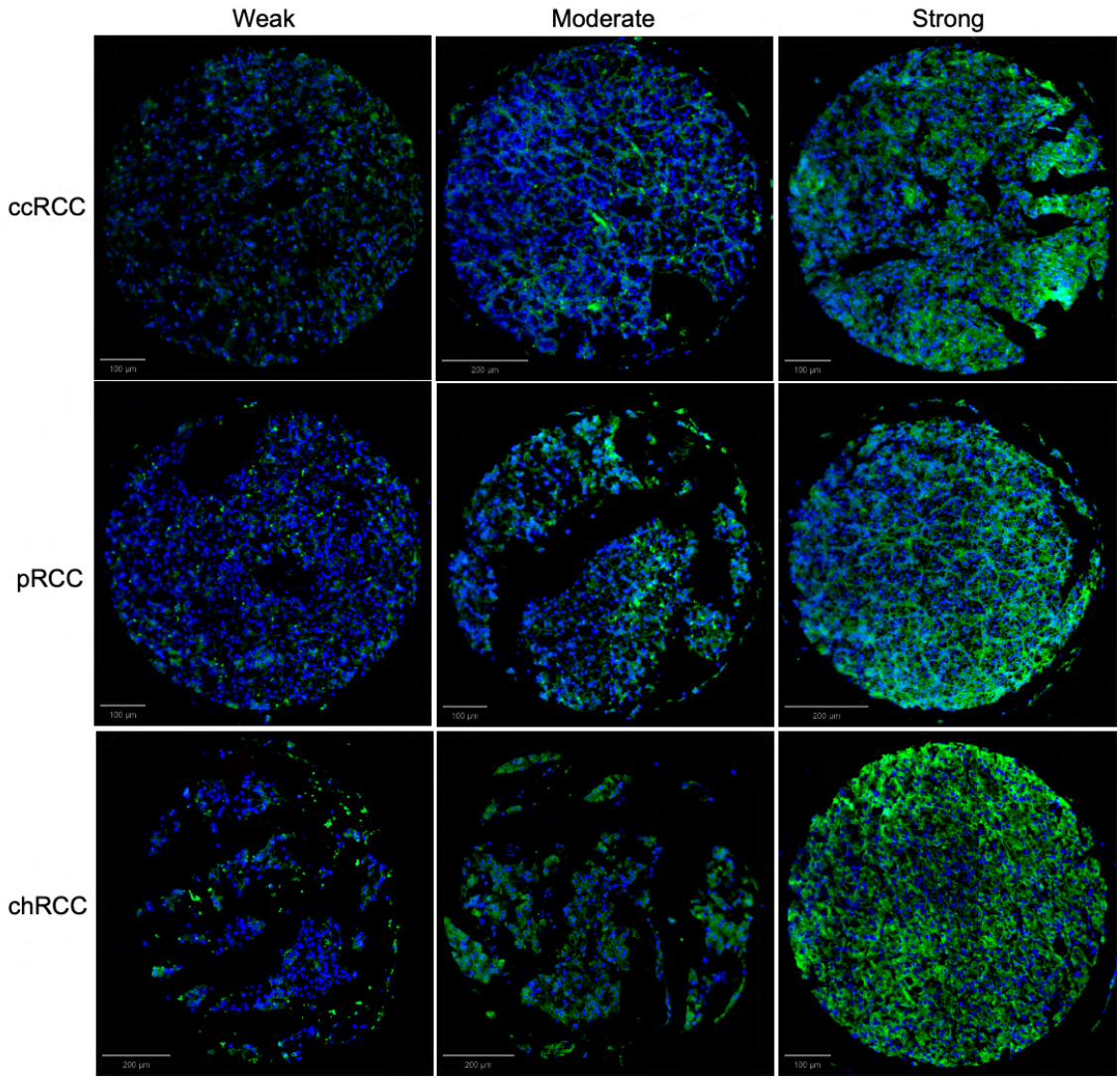

Figure 3.37 ADAM9 staining in RCC subtypes
Representative weak, moderate and strong ADAM9 (green) in ccRCC, pRCC and chRCC TMA cores. DAPI is represented in blue. Weak staining is classed as H-score <100, moderate staining is classed as H-score 101-200 and strong staining is classed as H-score 201-300. Scale bar represents 200µm.

3.5.3.1.1 ADAM9 expression in RCC subtypes

As before, ADAM9 H-score was calculated and was first examined by RCC subtype, as shown in Figure 3.38.

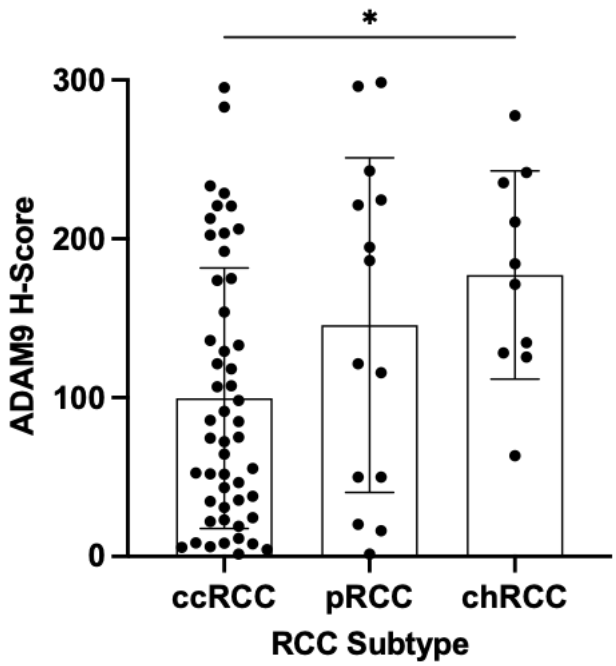

Figure 3.38 ADAM9 expression levels in RCC subtypes
ADAM9 H-score was compared across RCC subtypes. ADAM9 H-score was found to be significantly higher in chRCC compared to ccRCC. Analysis was completed using a Kruskal-Wallis test with Dunn's multiple comparisons test, where * represents $p < 0.05$.

Strong ADAM9 staining was seen in all RCC subtypes (Figure 3.38), however the average staining observed in chRCC and pRCC was higher than in ccRCC, with chRCC found to be significantly higher than ccRCC (177.3 ± 65.53 vs 99.67 ± 82.06, p=0.0301). This result is interesting as ADAM9 expression was strong in both the proximal convoluted tubule, the cell of origin for ccRCC and pRCC, and the distal convoluted tubule, the cell of origin for chRCC. This expression however appears to follow through into the chRCC tumour much more strongly than into the ccRCC and pRCC tumours.

3.5.3.1.2 ADAM9 expression by TNM status

We next aimed to determine if TNM status has any effect on ADAM9 expression, as shown in Figure 3.39.

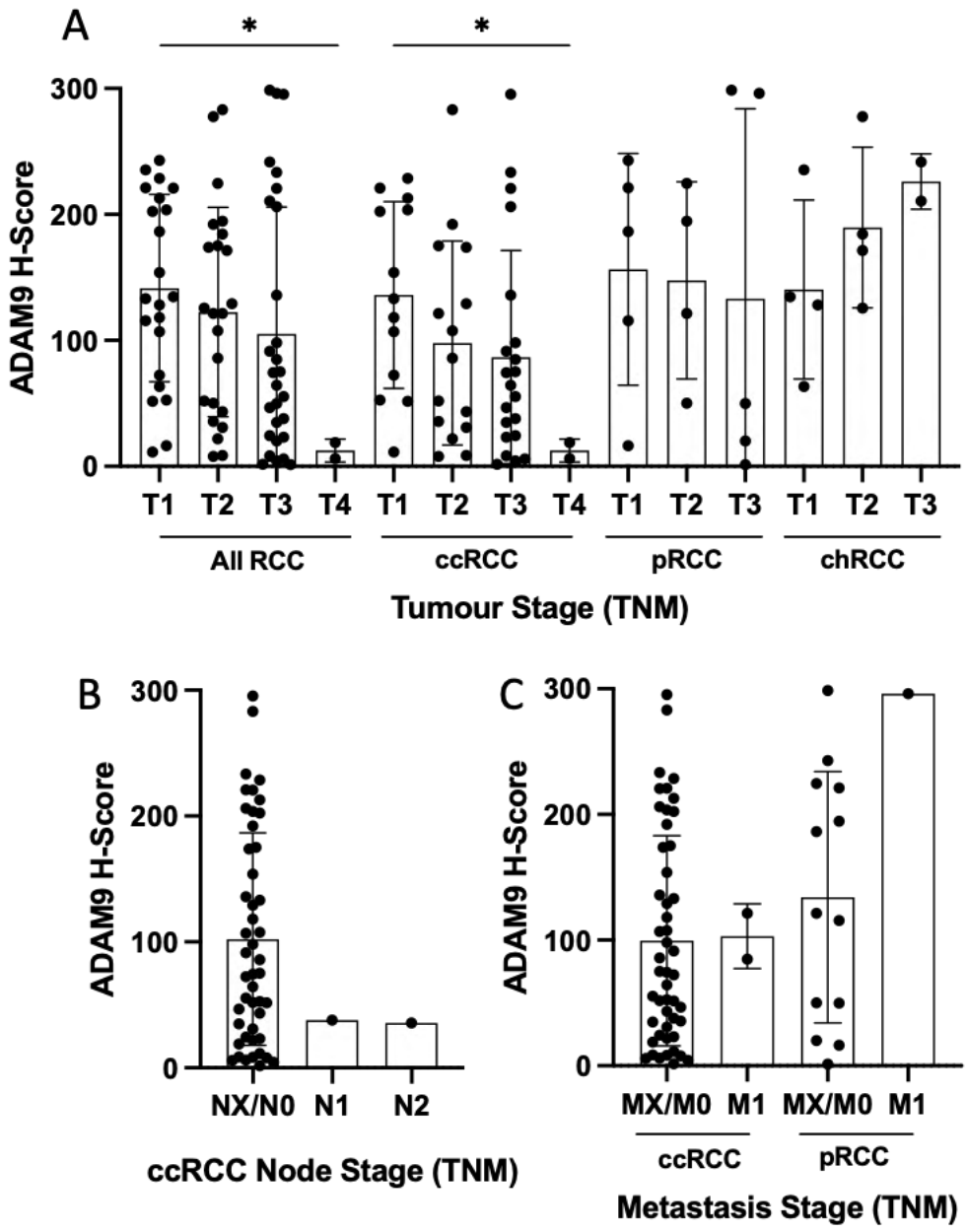

Figure 3.39 ADAM9 expression in RCC subtypes by TNM status
ADAM9 H-score was compared by TNM status. (A) ADAM9 H-score in all RCC, ccRCC, pRCC and chRCC by tumour status. T4 samples were only available in ccRCC. (B) ADAM9 H-score in ccRCC samples by node stage. All pRCC and chRCC samples were NX/N0 status, (C) ADAM9 H-score in ccRCC and pRCC by metastasis status. All chRCC samples were MX/M0 status. A-B: Analysis was completed using a Kruskal-Wallis test and Dunn's multiple comparison test, where * represents $p<0.05$. C: Analysis was completed using an unpaired t-test.

ADAM9 expression was found to be strongly influenced by tumour status in all RCC and in ccRCC (Figure 3.39a), where a gradual decrease in mean H-score was observed with increased T status. T1 was found to have significantly higher H-scores compared to T4 in all RCC (141.50 ± 74.41 vs 12.54 ± 9.05, p = 0.0290) and ccRCC (136.0 ± 74.05 vs 12.54 ± 9.05, p = 0.0381), however the most highly scoring individual samples were found in T2 and T3. A similar decrease in expression with increased T stage was observed in pRCC, however this was not found to be significant, possibly due to small sample size. Interestingly, an increase in ADAM9 expression was observed with increased chRCC T status, however again due to small sample sizes, no significance was found. The only samples with node involvement in our TMAs were in ccRCC, with low ADAM9 expression observed in the N1 and N2 samples compared to the NX/N0 group (Figure 3.39b), however as only one sample was available for each of these groups, this would be interesting to repeat with an increased number of samples. Metastasis stage appeared to have no effect on ADAM9 H-score in ccRCC (Figure 3.39c), however an increase was observed in the M1 sample compared to MX/M0 in pRCC. This group however contained only one sample and this work should be repeated with a greater number of samples.

3.5.3.1.3 ADAM9 expression by age and sex

We next analysed the ADAM9 expression levels in our samples by patient age at operation and sex, as shown in Figure 3.40.

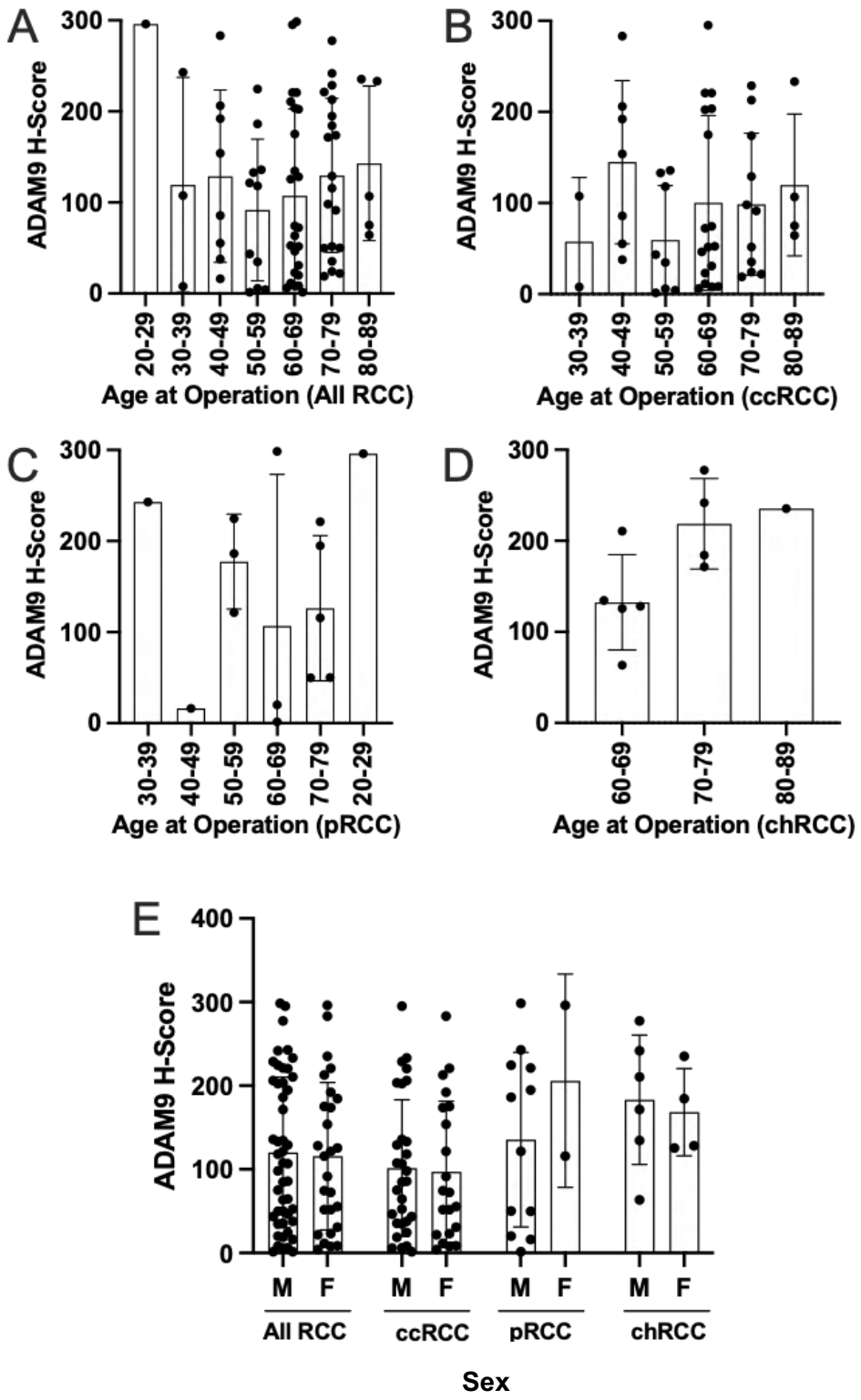

Figure 3.40 ADAM9 expression by age at operation and sex
ADAM9 H-score was compared by patient age and sex. (A) All RCC, (B) ccRCC, (C) chRCC, (D) pRCC by age, (E) All RCC and subtypes by sex. A-D: Statistical analysis was completed using a Kruskal-Wallis test and Dunn's multiple comparisons test. E: Analysis was completed using unpaired t-tests; however, no significance was found.

ADAM9 H-score generally increased with advanced age in all RCC (Figure 3.40a) and in each subtype (Figure 3.40b-d), however no significant differences were found in ADAM9 H-score between any of the age groups. No changes were observed between male and female patients within all RCC or in any subtype (Figure 3.40e), implying that any differences observed in ADAM9 H-score between samples are likely due to expression in the tumour itself, rather than patient characteristics such as age or sex.

3.5.3.1.4 ADAM9 expression summary

We have observed varied ADAM9 staining throughout our TMA samples, with the strongest average staining found in chRCC. A significant disease in H-score was observed with increased tumour status in ccRCC and pRCC, and an increase in H-score was associated with increased tumour status in chRCC. Neither node or metastasis status, nor patient characteristics such as age or sex were found to affect H-scores. ADAM9 H-scores are summarised in Table 3.5.

Table 3.5 ADAM9 H-Score summary for RCC subtypes and stages

	Mean ± SD			
TNM Stage	**All RCC**	**ccRCC**	**pRCC**	**chRCC**
T1	141.50 ± 74.41	136.0 ± 74.05	156.5 ± 91.98	140.04 ± 71.00
T2	122.5 ± 83.18	97.85 ± 81.05	147.7 ± 78.20	189.7 ± 63.74
T3	105.0 ± 100.9	86.75 ± 84.53	133.2 ± 15.07	226.2 ± 21.99
T4	12.54 ± 9.05	12.54 ± 9.05	-	-
N0/NX	-	102.2 ± 84.41	-	-
N1	-	37.90 ± 0.00	-	-
N2	-	35.50 ± 0.00	-	-
M0/MX	-	99.53 ± 83.66	134.1 ± 100.0	-
M1	-	103.1 ± 25.77	296.0 ± 0.00	-

3.5.3.2 ADAM17 expression

Having characterised ADAM9 expression in our TMA samples, we next aimed to establish ADAM17 expression in the same samples using serial TMA sections. ADAM17 has suggested as a biomarker for ccRCC, as expression correlates with poor prognosis (Fritzsche et al. 2008). We have already shown strong ADAM17 expression in the glomerulus and proximal and distal convoluted tubules of our normal kidney samples, so we next aimed to determine if this expression is carried through into RCC. Representative IF staining images can be seen in Figure 3.41.

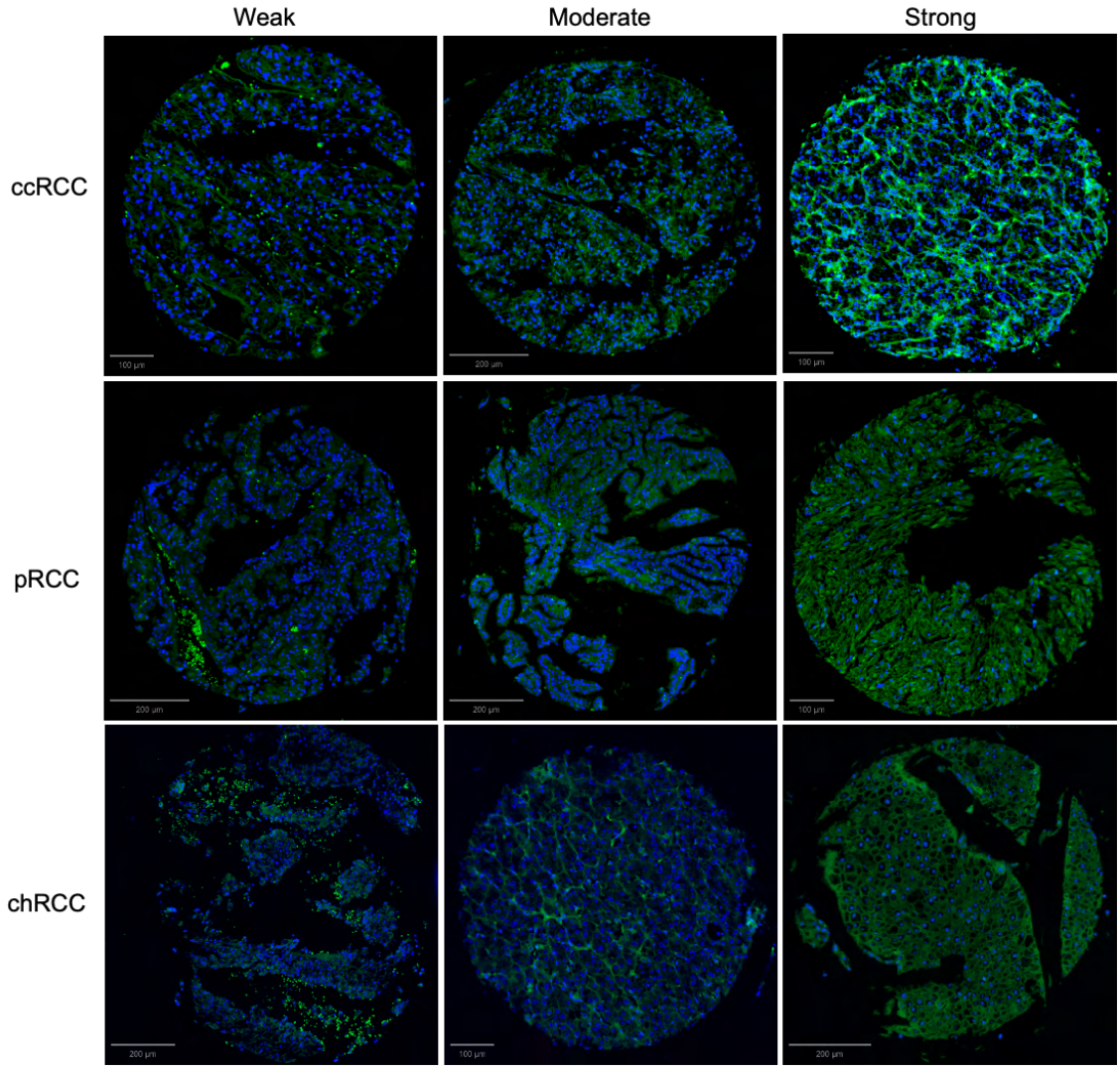

Figure 3.41 ADAM17 staining in RCC subtypes
Representative weak, moderate and strong ADAM17 staining (green) in ccRCC, pRCC and chRCC TMA cores. DAPI is represented in blue. Weak staining is classed as H-score <100, moderate staining is classed as H-score 101-200 and strong staining is classed as H-score 201-300. Scale bar represents 200µm.

3.5.3.2.1 ADAM17 expression in RCC subtypes

ADAM17 H-score was firstly compared between RCC subtypes, as shown in Figure 3.42.

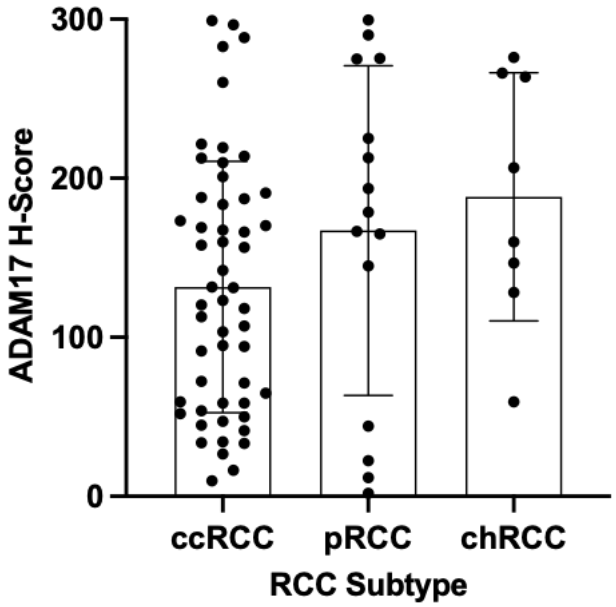

Figure 3.42 ADAM17 expression levels in RCC subtypes
ADAM17 H-score was compared between the 3 RCC subtypes. Analysis was completed using a Kruskal-Wallis test followed by Dunn's multiple comparison test; however, no significant differences were found between the three groups.

3.5.3.2.2 ADAM17 expression by TNM status

Mean ADAM17 expression was found to be highest in chRCC (Figure 3.42), which originates from the distal convoluted tubule, the structure which showed the highest ADAM17 expression in normal kidney. ADAM17 expression was also strong in the proximal convoluted tubule, the cell of origin for ccRCC and pRCC, however mean ADAM17 expression in these subtypes was found to be generally lower than chRCC. ccRCC samples were found to have varied ADAM17 expression strength, ranging from weak to very strong, so we next examined the samples by TNM status to determine if any clinical characteristic could be responsible for the differences in expression, as shown in Figure 3.43.

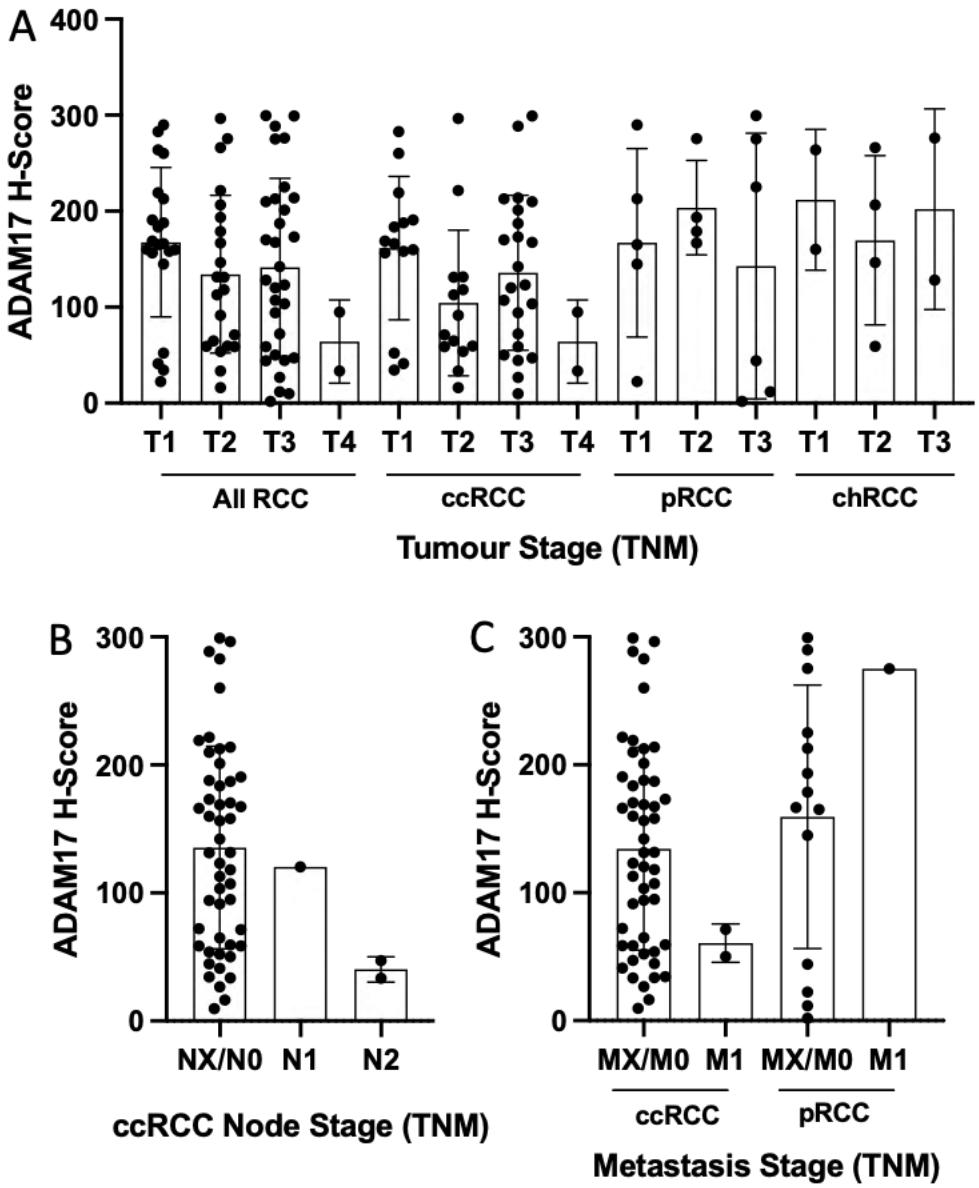

Figure 3.43 ADAM17 expression in RCC subtypes by TNM status
ADAM17 H-score was compared between the samples by TNM status. (A) All RCC. ccRCC, pRCC and chRCC by tumour status. T4 samples were only available in ccRCC. (B) ccRCC samples by node stage. All pRCC and chRCC samples were NX/N0 status, (C) ccRCC and pRCC by metastasis status. All chRCC samples were MX/M0 status. A-B:Analysis was completed using a Kruskal-Wallis test and Dunn's multiple comparisons test. C: Analysis was completed using unpaired t-tests. however, no significant differences were found between any of the groups.

As was found to be the case for ADAM9 expression, ADAM17 expression appears to be highly influenced by tumour status in ccRCC (Figure 3.43a). ADAM17 H-score was found to generally reduce with increased T stage in ccRCC, however the highest scoring individual samples were found in the T1-T3 groups. No clear link between T score and ADAM17 expression could be found in pRCC and chRCC, however these groups had a much smaller number of samples, and a correlation

may be found if this study was repeated with a larger number of samples. Node status in our ccRCC samples appeared to correlate with reduced ADAM17 expression (Figure 3.43b), with lower H-scores observed in the N1 and N2 samples compared to the NX/N0 group, however this would also need to be repeated with an increased number of samples. Metastasis status also appeared to relate to lower H-scores in ccRCC (Figure 3.43c), where lower H-scores were observed in the M1 group compared to the MX/M0 group, however this was not found to be the case in the pRCC M1 sample, which was higher than the mean of the pRCC MX/M0 group. Further repeats are required with a higher number of samples to characterise this expression pattern.

3.5.3.2.3 ADAM17 expression by age and sex

Having established the relationship between ADAM17 expression and sample clinical characteristics, we next examined our samples by patient characteristics of age at operation and sex, as shown in Figure 3.44.

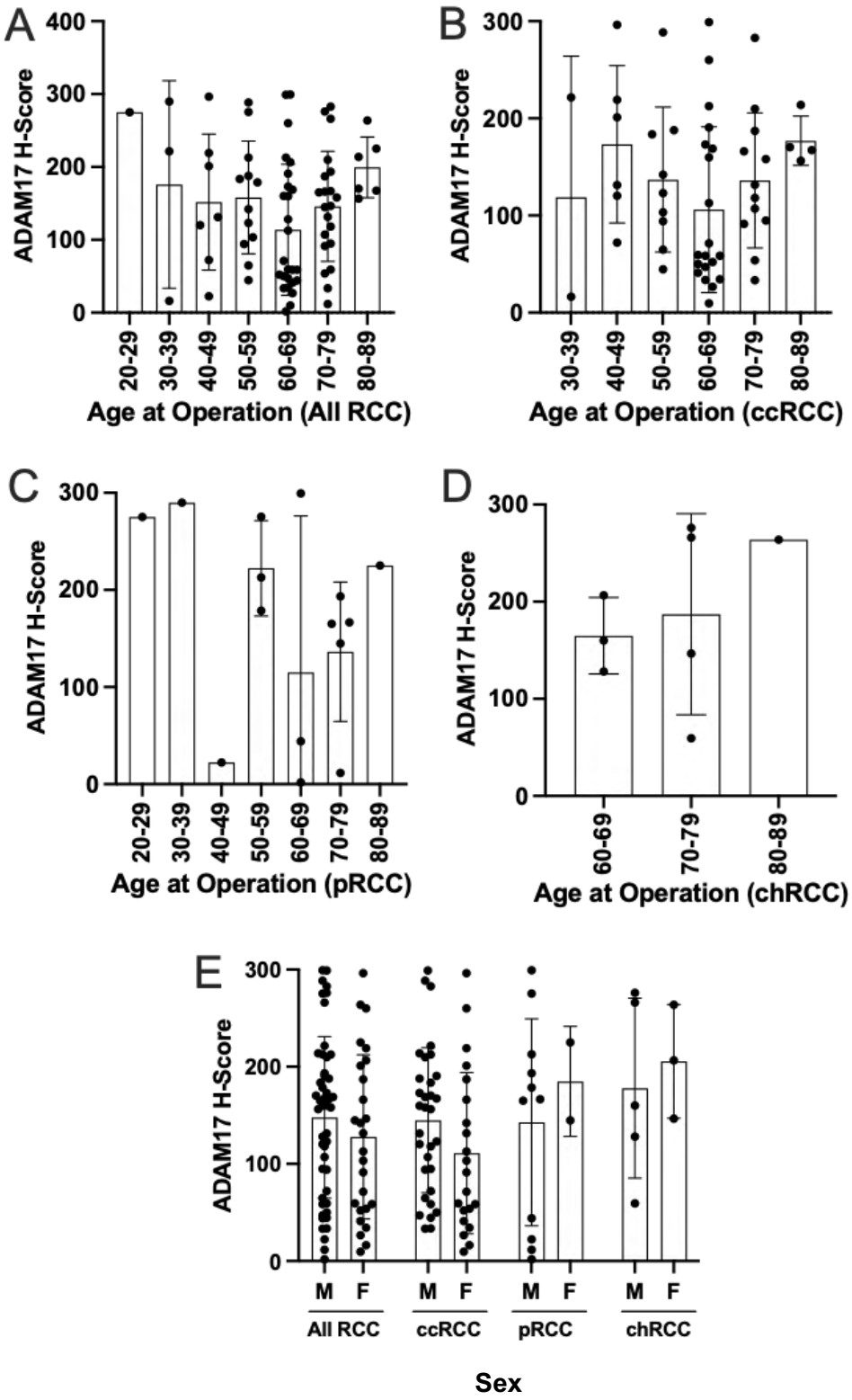

Figure 3.44 ADAM17 expression by age at operation and sex
ADAM17 H-score was compared by patient age and sex. (A) All RCC, (B) ccRCC, (C) pRCC, (D) chRCC by age, (E) All RCC and subtypes by sex. A-D: Statistical analysis was completed using a Kruskal-Wallis test and Dunn's multiple comparison test. E: Analysis was completed using unpaired t-tests; however, no significance was found.

ADAM17 expression was not found to be significantly influenced by patient age at operation in any of the RCC subtypes or all RCC (Figure 3.44a-d), however a general trend of increased H-score with increased age was observed. Patient sex was not found to significantly impact ADAM17 H-score (Figure 3.44e), however expression was generally found to be higher in females in ccRCC, but higher in males in pRCC and chRCC.

3.5.3.2.4 ADAM17 expression summary

We have shown a range of ADAM17 expression strength in our TMA samples, with the highest mean expression found in chRCC, but the strongest individual expression was found in ccRCC. No significant differences were found during analysis between RCC subtypes or TNM stages, however a general trend of decreasing ADAM17 expression was observed with increased tumour, node or metastasis status in ccRCC. Patient characteristics of age at operation and sex also showed no significant differences between groups, however a general trend of increased ADAM17 expression with increased age was observed in all subtypes, and females were found to have higher expression than males in pRCC and chRCC. ADAM17 expression is summarised in Table 3.6.

Table 3.6 ADAM17 H-Score summary for RCC subtypes and stages

	Mean ± SD			
TNM Stage	**All RCC**	**ccRCC**	**pRCC**	**chRCC**
T1	167.60 ± 77.79	161.50 ± 74.71	167.0 ± 98.28	211.90 ± 73.40
T2	134.30 ± 82.22	104.40 ± 75.76	203.60 ± 49.14	169.70 ± 88.29
T3	141.40 ± 92.71	135.80 ± 80.70	142.80 ± 138.20	202.10 ± 104.50
T4	64.25 ± 43.27	64.25 ± 43.27	-	-
N0/NX	-	135.50 ± 79.17	-	-
N1	-	120.30 ± 0.00	-	-
N2	-	40.30 ± 0.00	-	-
M0/MX	-	134.40 ± 79.25	159.40 ± 103.0	-
M1	-	60.64 ± 15.04	275.00 ± 0.00	-

3.5.3.3 ADAM28 expression

Having now characterised ADAM9 and ADAM17 expression in RCC, using a further serial TMA section we next aimed to establish ADAM28 expression in our samples. ADAM28 expression in RCC has not been well studied, however increased expression has been reported at the mRNA level in T1 status tumours (Li et al. 2014a). Representative staining is shown in Figure 3.45.

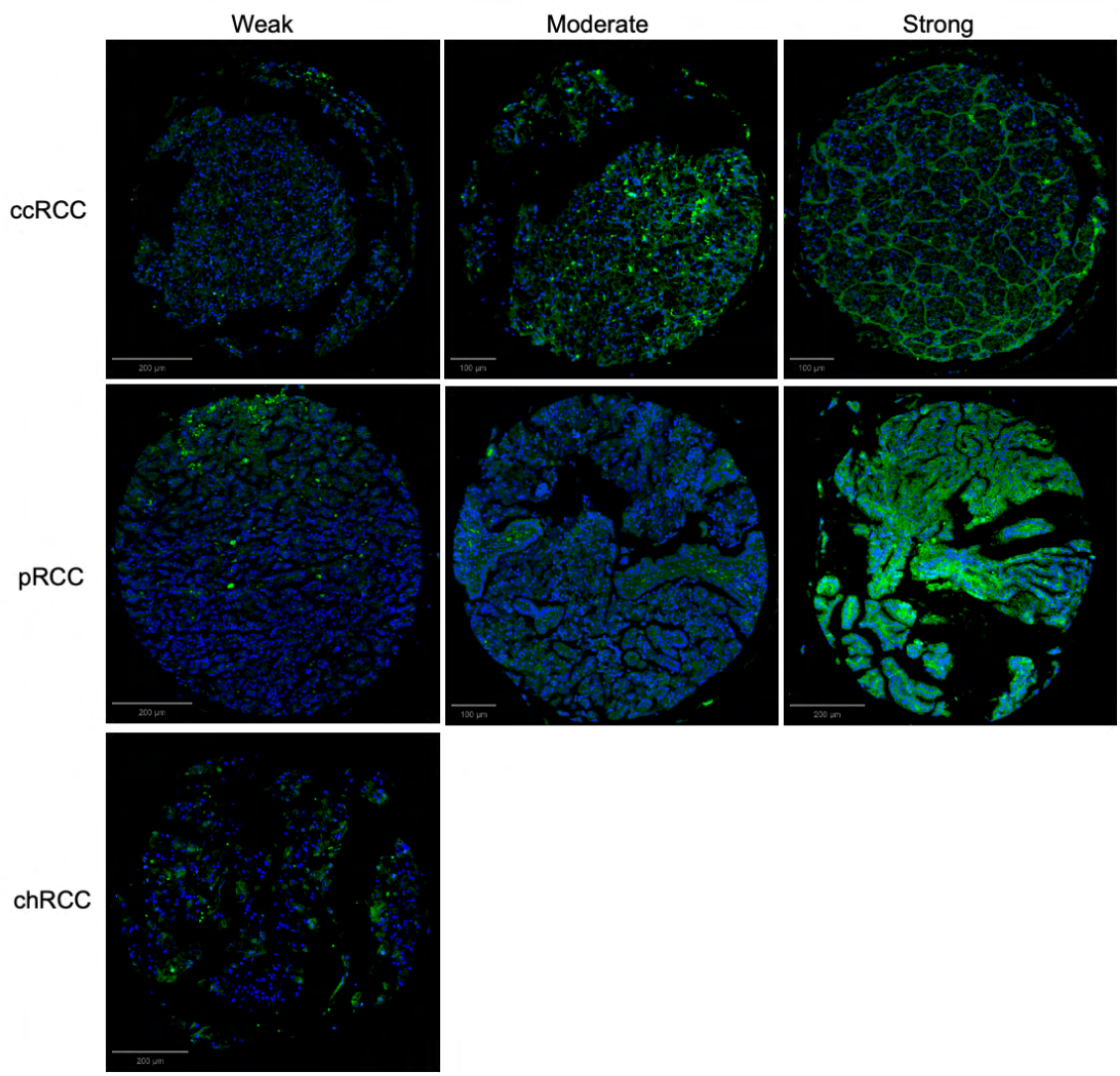

Figure 3.45 ADAM28 staining in RCC subtypes
Representative weak, moderate and strong ADAM28 staining (green) in ccRCC, pRCC and chRCC TMA cores. DAPI is represented in blue. Weak staining is classed as H-score <100, moderate staining is classed as H-score 101-200 and strong staining is classed as H-score 201-300. No moderate or strong staining was observed in chRCC. Scale bar represents 200μm.

3.5.3.3.1 ADAM28 expression in RCC subtypes

We firstly investigated the expression of ADAM28 in RCC subtypes, as shown in Figure 3.46.

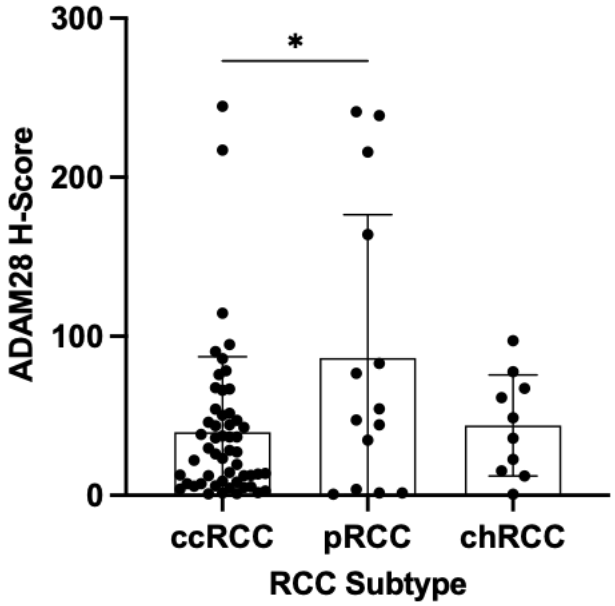

Figure 3.46 ADAM28 expression in RCC subtypes
ADAM28 H-score was compared across the 3 RCC subtypes. ADAM28 expression was found to be highest in pRCC compared to the other two subtypes. Analysis was completed using a Kruskal-Wallis test and Dunn's multiple comparison test, where * represents $p<0.05$.

Weak overall ADAM28 expression was observed throughout all TMA samples, however expression was found to be significantly higher in pRCC compared to ccRCC (86.27 ± 90.12 vs 39.72 ± 47.54, $p = 0.0213$). In the normal kidney, ADAM28 expression was found to be strongest in the proximal convoluted tubule, the cell of origin for pRCC and ccRCC, however it appears this expression does not carry through into the tumour state in both RCC subtypes.

3.5.3.3.2 ADAM28 expression by TNM status

We next examined if tumour TNM status has an effect on ADAM28 expression, as shown in Figure 3.47.

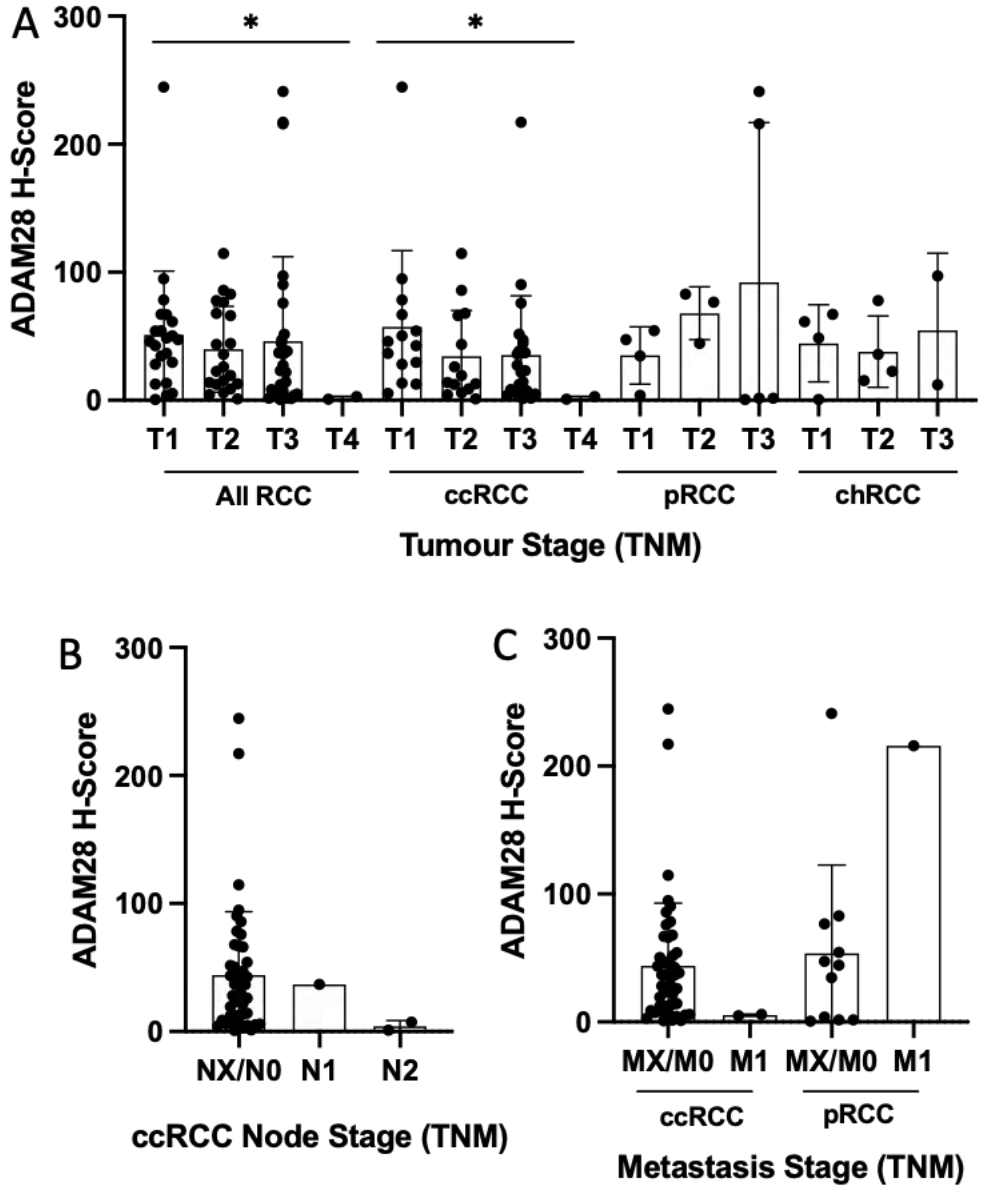

Figure 3.47 ADAM28 expression in RCC subtypes by TNM status
ADAM28 H-score was compared between samples by TNM status. (A) All RCC. ccRCC, pRCC and chRCC by tumour status. T4 samples were only available in ccRCC. (B) ccRCC samples by node stage. All pRCC and chRCC samples were NX/N0 status, (C) ccRCC and pRCC by metastasis status. All chRCC samples were MX/M0 status. A-B: Statistical analysis was completed using a Kruskal-Wallis test and Dunn's multiple comparisons test, where * represents $p<0.05$. C: Analysis was completed using unpaired t-tests.

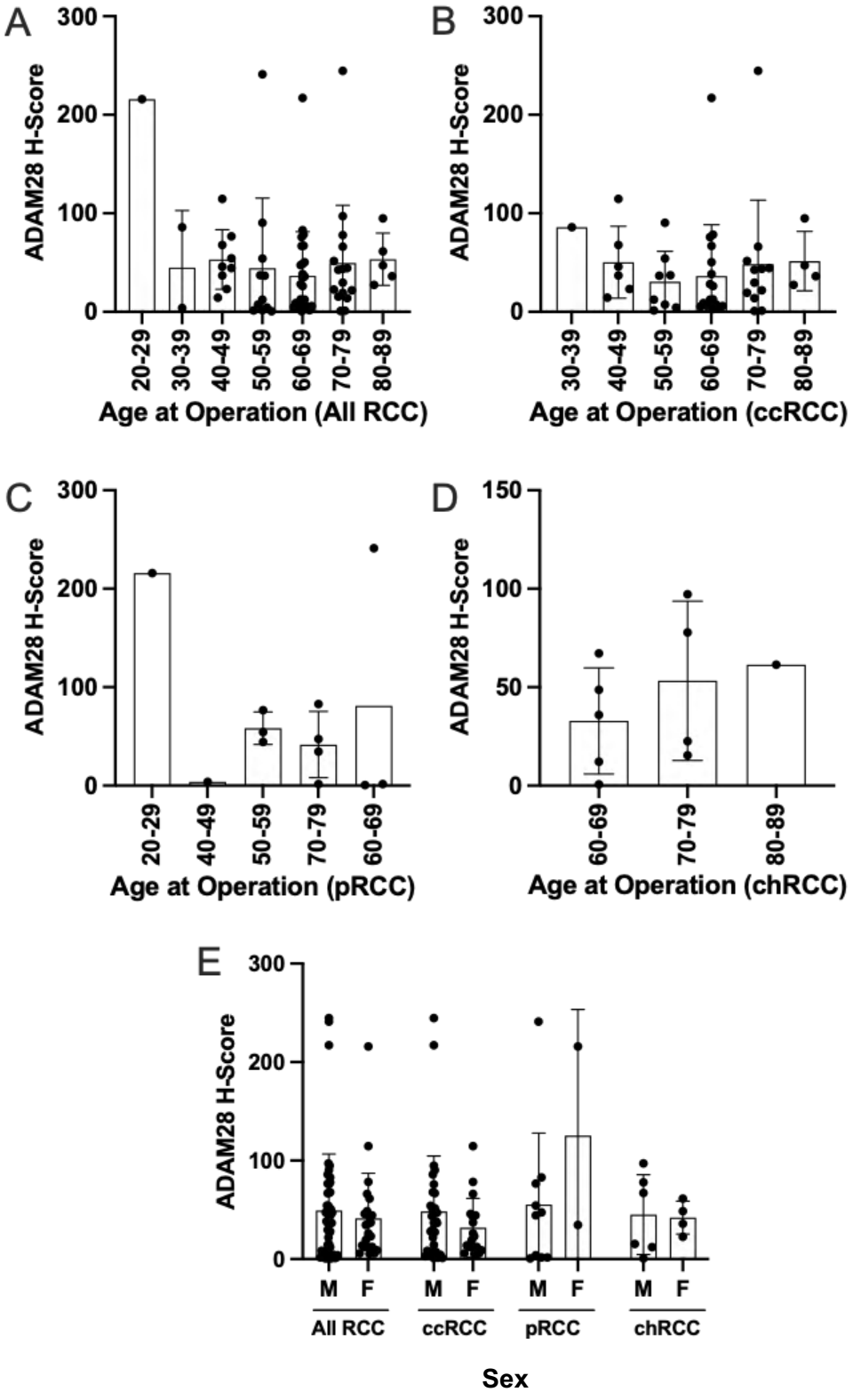

Figure 3.48 ADAM28 expression by age at operation and sex
ADAM28 H-score was compared by patient age and sex. (A) All RCC, (B) ccRCC, (C) pRCC, (D) chRCC by age, (E) All RCC and subtypes by sex. A-D: Statistical analysis was completed using a Kruskal-Wallis test and Dunn's multiple comparisons test. E: Analysis was completed using unpaired t-tests; however, no significance was found.

ADAM28 H-score appears to be negatively correlated with tumour status in ccRCC and RCC as a whole (Figure 3.47a), with T1 found to have significantly higher levels of ADAM28 compared to T4 (51.00 ± 49.82 vs 1.842 ± 1.311, p=0.0290). Interestingly, an increase in ADAM28 H-score was observed with increased T status in pRCC and no effect was observed in chRCC, however these are very small sample numbers and further repeats with increased n numbers would make this data more robust. A decrease in ADAM28 expression was observed with increased node status (Figure 3.47b) and metastasis status (Figure 3.47c) in ccRCC, however again these differences were not found to be significant due to the small sample sizes. The M1 pRCC sample was however found to have a higher H-score compared to the MX/M0 group, which would need to be repeated with further samples to increase n numbers and determine the true strength of this relationship.

3.5.3.3.3 ADAM28 expression by age and sex

Having determined ADAM28 expression in our samples based on clinical characteristics, we next examined expression based on the patients characteristics of age at operation and sex, as shown in Figure 3.48.

Weak ADAM28 expression was observed throughout all age groups, with no differences observed between any ages (Figure 3.48a-d). ADAM28 also did not appear to be influenced by patient sex (Figure 3.48e), with ccRCC and chRCC exhibiting similar mean expression in both sexes and only pRCC showing an increase in females compared to males, however only two samples were in this group and so further repeats with increased sample sizes would be required to confirm any relationship between sex and ADAM28 expression.

3.5.3.3.4 ADAM28 expression summary

ADAM28 expression was low throughout the TMA samples, but the highest overall expression was found in pRCC. As with ADAM9 and ADAM17, ADAM28 expression appears to be influenced by tumour status, with no effect observed with increased node or metastasis status, however increased sample sizes may show more

significant trends. Patient age at operation and sex also had no impact on ADAM28 expression, so it is likely that any differences observed in ADAM28 expression between individual samples is down to the tumour itself rather than patient characteristics. ADAM28 expression is summarised in Table 3.7.

Table 3.7 ADAM28 H-Score summary for RCC subtypes and stages

	Mean ± SD			
TNM Stage	**All RCC**	**ccRCC**	**pRCC**	**chRCC**
T1	51.00 ± 49.82	57.41 ± 59.56	35.07 ± 22.38	44.50 ± 30.24
T2	39.93 ± 33.47	34.50 ± 35.55	68.00 ± 20.69	37.93 ± 2.90
T3	46.16 ± 65.97	35.42 ± 46.18	92.16 ± 124.80	54.70 ± 60.14
T4	1.84 ± 1.31	1.84 ± 1.31	-	-
N0/NX	-	44.09 ± 49.43	-	-
N1	-	36.78 ± 0.00	-	-
N2	-	4.21 ± 4.41	-	-
M0/MX	-	43.88 ± 48.95	54.56 ± 69.09	-
M1	-	5.40 ± 0.71	215.9 ± 0.00	-

3.6 Protease Correlations with CD200

So far in this chapter we have established the staining intensity of CD200 and our proteases of interest, ADAM9, ADAM17 and ADAM28 in our TMA samples. As differences in expression were observed between samples, we next determined whether there was any correlation between CD200 staining intensity and protease staining intensity

3.6.1 ADAM9 and CD200 Correlations

We firstly examined the relationship between ADAM9 and CD200 expression in our samples, firstly in all RCC and then by subtype, as shown in Figure 3.49.

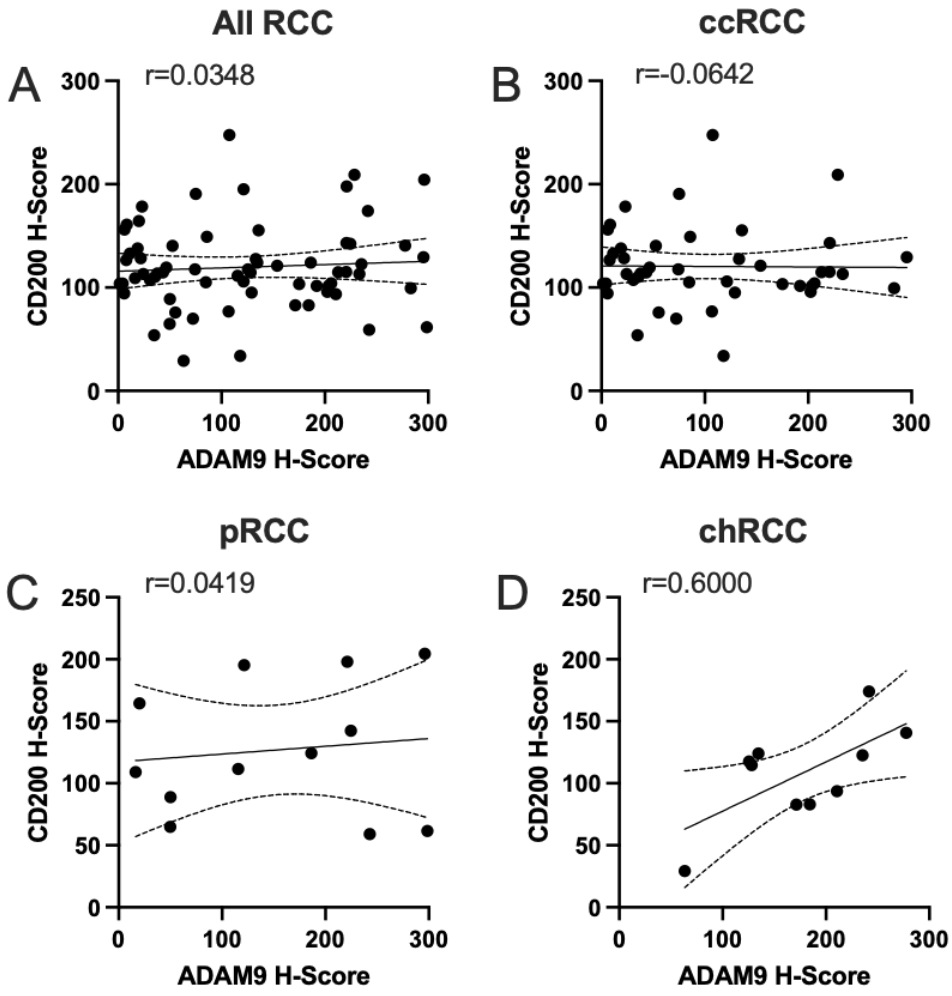

Figure 3.49 Correlation of ADAM9 vs CD200 H-Score
(A) All RCC, (B) ccRCC, (C) pRCC, (D) chRCC. Correlations were calculated using Spearman's rank correlation coefficient.

Weakly positive ADAM9 and CD200 correlations were observed in all RCC (Figure 3.50a) and pRCC (Figure 3.50c), while a weak negative correlation was observed in ccRCC (Figure 3.50b). Interestingly, a strong positive correlation (r=0.6000) was observed between ADAM9 and CD200 in chRCC (Figure 3.50d), however this relationship was not found to be significant.

3.6.2 ADAM17 and CD200 Correlations

We next investigated the relationship of ADAM17 with CD200 in our TMA samples, as shown in Figure 3.50.

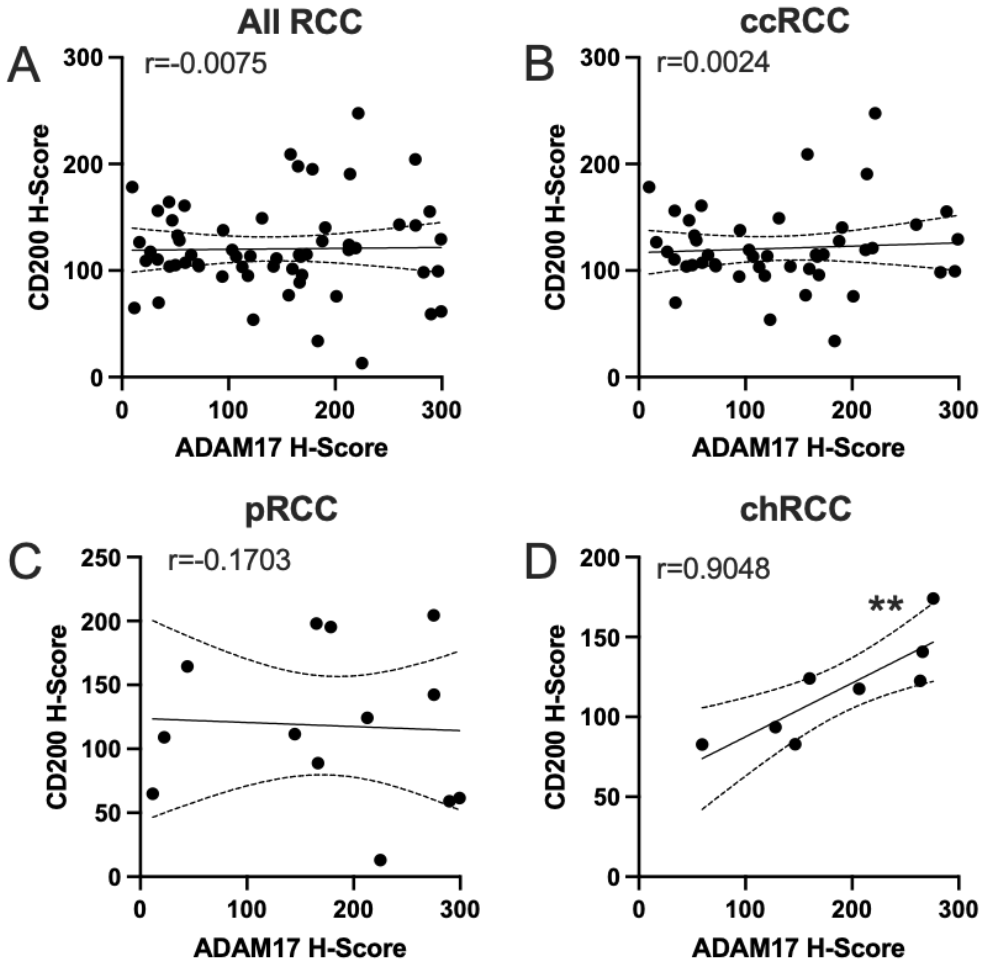

Figure 3.50 Correlation of ADAM17 vs CD200 H-Score
(A) All RCC, (B) ccRCC, (C) pRCC, (D) chRCC. Correlations were calculated using Spearman's rank correlation coefficient, where ** represents p <0.01.

Weak negative correlations between ADAM17 and CD200 were observed in all RCC (Figure 3.50a) and pRCC (Figure 3.50c), while a weak positive correlation was found in ccRCC (Figure 3.50b). As we found in our previous study of ADAM9 with CD200, ADAM17 was found to strongly correlate with CD200 expression in chRCC (Figure 3.50d), with a significant increase in ADAM17 expression associated with an increase in CD200 (r=0.9048, p=0.0046).

3.6.3 ADAM28 and CD200 Correlations

We finally investigated the relationship of ADAM28 with CD200 in our TMA samples, as shown in Figure 3.51.

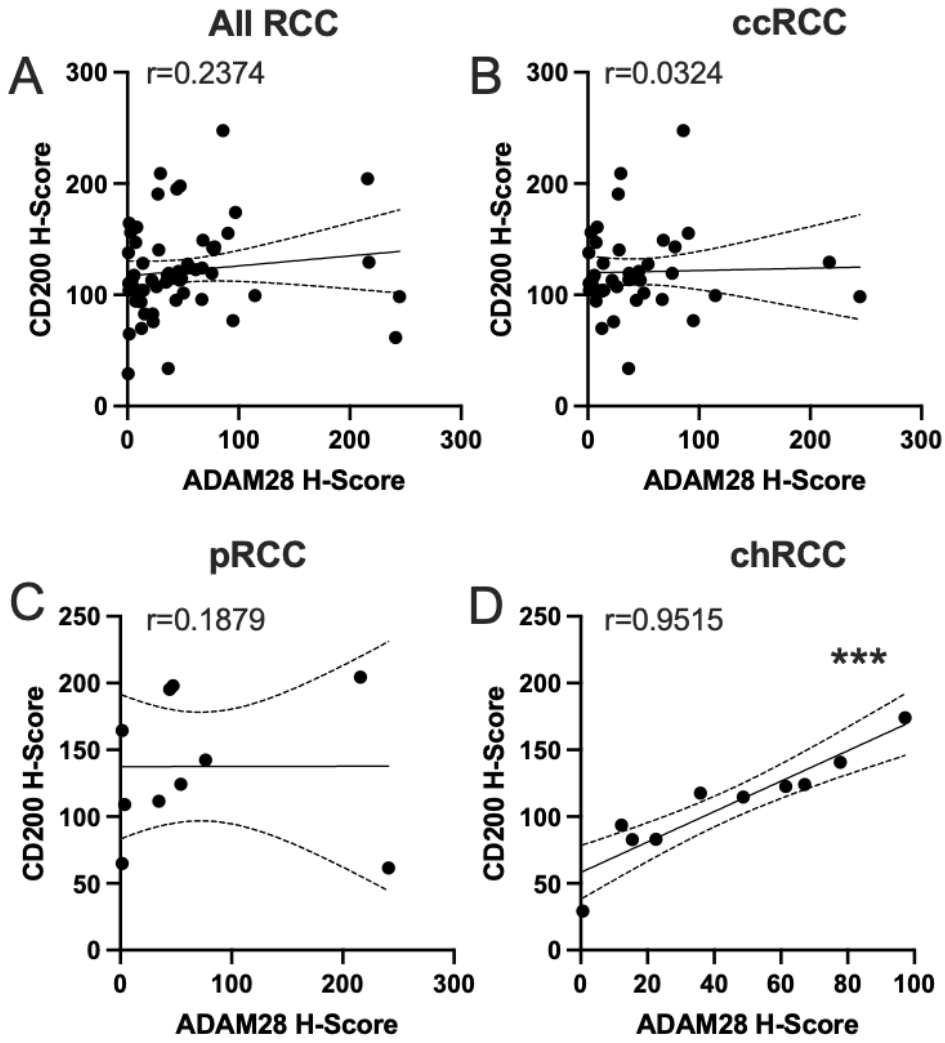

Figure 3.51 Correlation of ADAM28 vs CD200 H-Score
(A) All RCC, (B) ccRCC, (C) pRCC, (D) chRCC. Correlations were calculated using Spearman's rank correlation coefficient, where *** represents p <0.001.

Weak positive correlations were observed between ADAM28 and CD200 in all RCC (Figure 3.51a), ccRCC (Figure 3.51b) and pRCC (Figure 3.51c), however a strongly positive correlation was found in chRCC (Figure 3.51d) which was also highly significant (r=0.9515, p=0.001).

3.6.4 Protease and CD200 Correlation Summary

We observed mostly weakly positive correlations between CD200 and our proteases of interest. This could imply that processes involving both CD200 and ADAMs in RCC development may result in increased expression of both, however the process behind this and link between the two is currently unclear.

Weak correlations were observed between ADAM9 and CD200 in ccRCC and pRCC, possibly implying there is no strong link between their expression, however a strong relationship was observed in chRCC.

Positive correlations were also seen between ADAM17 and CD200 in all subtypes, which were weak in ccRCC and pRCC, and a strong and significant relationship was observed between ADAM17 and CD200 in chRCC.

A similar pattern of weak, positive correlations was observed between ADAM28 and CD200 expression in ccRCC and pRCC, and a very strong and significant relationship was observed in chRCC.

This data implies that CD200 and protease expression is strongly linked in chRCC and is less so in ccRCC, pRCC and RCC as a whole.

3.7 Protease and CD200 double positive cells

As we have now characterised CD200 and ADAM9, ADAM17 and ADAM28 expression and determined correlations between their expression strengths, we next determined the number of cells in each sample which were positive for both CD200 and our proteases of interest. The presence of both on the cell membrane in the same place may indicate that the two are able to interact, with the protease potentially placed where it could have a role in the ectodomain shedding of CD200.

3.7.1 ADAM9 and CD200 double positive cells

The number of cells which were positive for both CD200 and ADAM9 were identified within each core, representative staining can be seen in Figure 3.52.

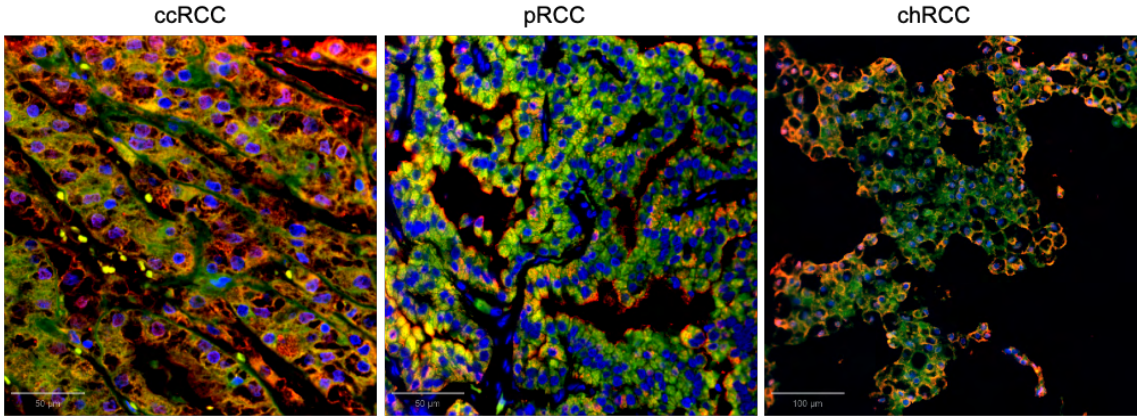

Figure 3.52 ADAM9 and CD200 double positive staining in RCC subtypes
Representative staining of ADAM9 (green), CD200 (red) and DAPI (blue) staining in RCC subtypes. Scale bar represents 50μm.

The number of double positive cells were firstly counted in each core for each RCC subtype and calculated as a percentage of the number of total cells in the sample, as shown in Figure 3.52.

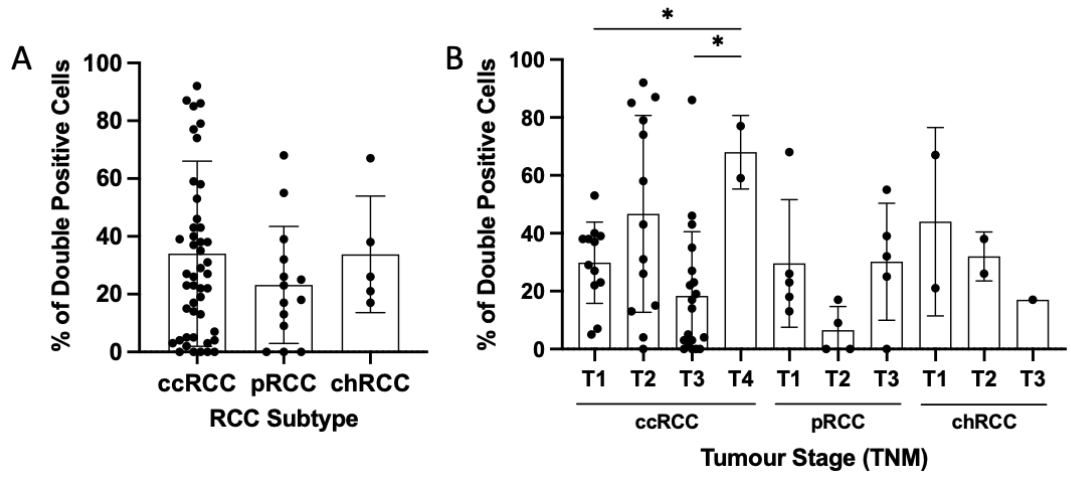

Figure 3.53 ADAM9 and CD200 double positive cell percentage of all cells
The percentage of cells which were positive for both ADAM9 and CD200 was calculated in (A) RCC subtypes. (B) By TNM tumour stage within subtypes. Analysis was carried out using a Kruskal-Wallis test and Dunn's multiple comparison test, where * represents p <0.05.

ccRCC was found to have the highest mean percentage of ADAM9 and CD200 double positive cells compared to normal kidney and the other RCC subtypes (Figure 3.53a). The lowest number of double positive cells was found in pRCC, and no relationship was found between ADAM9 and CD200 H-scores in this subtype, implying that a low number of cells express both and the level of their expression is not related to the other.

When we examined the percentage of double positive cells by TNM tumour stage, we found that the percentage significantly increased with increased T stage in ccRCC (Figure 3.53b), with T4 having a significantly higher number than T1 (68.00 ± 12.73 vs 29.83 ± 14.02, p = 0.0220) and T3 (68.00 ± 12.73 vs 18.37 ± 22.14, p = 0.0476). Interestingly, chRCC was found to have the opposite effect with T3 presenting a lower percentage of double positive cells than T1, however there was a small number of samples in this group. No trend was observed with T stage in pRCC, with T1 and T3 showing a similar percentage of double positive cells.

3.7.2 ADAM17 and CD200 double positive cells

The number of cells which were positive for both CD200 and ADAM17 was next examined. Representative double positive staining can be seen in Figure 3.54.

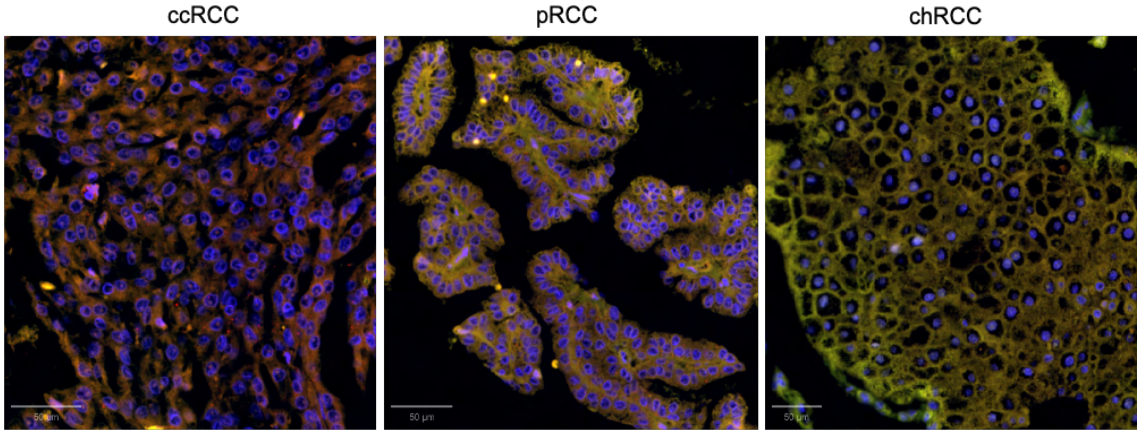

Figure 3.54 ADAM17 and CD200 double positive staining in RCC subtypes
Representative staining of ADAM17 (green), CD200 (red) and DAPI (blue) staining in RCC subtypes. Scale bar represents 50μm.

The number of cells which were positive for both ADAM17 and CD200 and ADAM17 were next counted in the RCC subtypes and split by tumour status, as shown in Figure 3.55.

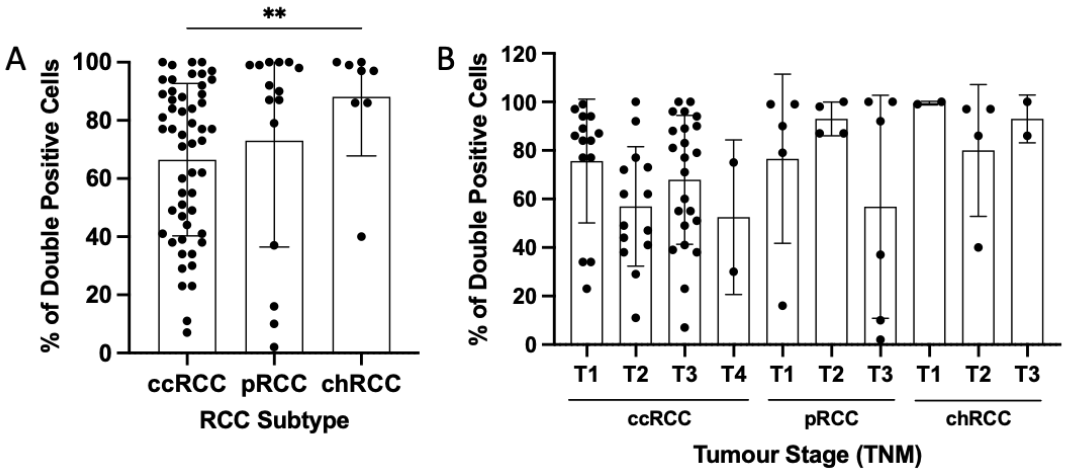

Figure 3.55 ADAM17 and CD200 double positive cell percentage of all cells
The percentage of cells which were positive for both ADAM17 and CD200 was calculated in (A) RCC subtypes. (B) By TNM tumour stage within each subtype. Analysis was carried out using a Kruskal-Wallis test and Dunn's multiple comparison test, where ** represents $p<0.01$.

The percentage of double positive ADAM17 and CD200 cells was found to be very high across all the subtypes (Figure 3.55a), however the percentage in chRCC was significantly higher than ccRCC (88.13 ± 20.29 vs 66.47 ± 26.21, $p = 0.0077$).

Examination of ADAM17 and CD200 cell double positivity by TNM tumour status (Figure 3.55b), found a decrease in percentage with increased T stage in ccRCC, which is the opposite for what we observed for ADAM9 and CD200 double positivity. No pattern was observed for pRCC or chRCC, so this data could show that in ccRCC only, as T status increases, CD200 positive cells switch expression from ADAM17 to ADAM9 and this may have a role in tumour progression.

3.7.3 ADAM28 and CD200 double positive cells

The number of cells which were positive for both CD200 and ADAM28 was next examined. Representative double positive staining can be seen in Figure 3.56.

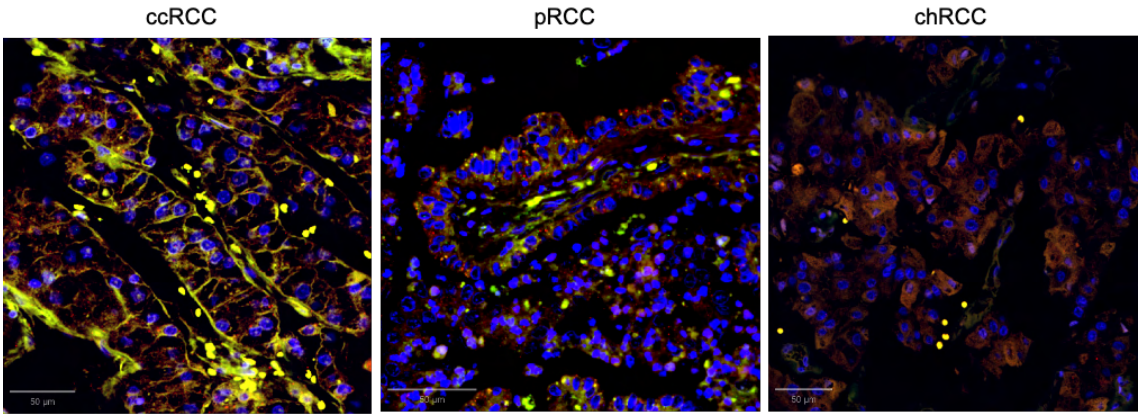

Figure 3.56 ADAM28 and CD200 double positive staining in RCC subtypes
Representative staining of ADAM28 (green), CD200 (red) and DAPI (blue) staining in RCC subtypes. Scale bar represents 50µm.

Having established the number of cells which are double positive for CD200 with ADAM9 or ADAM17, we next determined the number of cells which were positive for both CD200 and ADAM28, as shown in Figure 3.57.

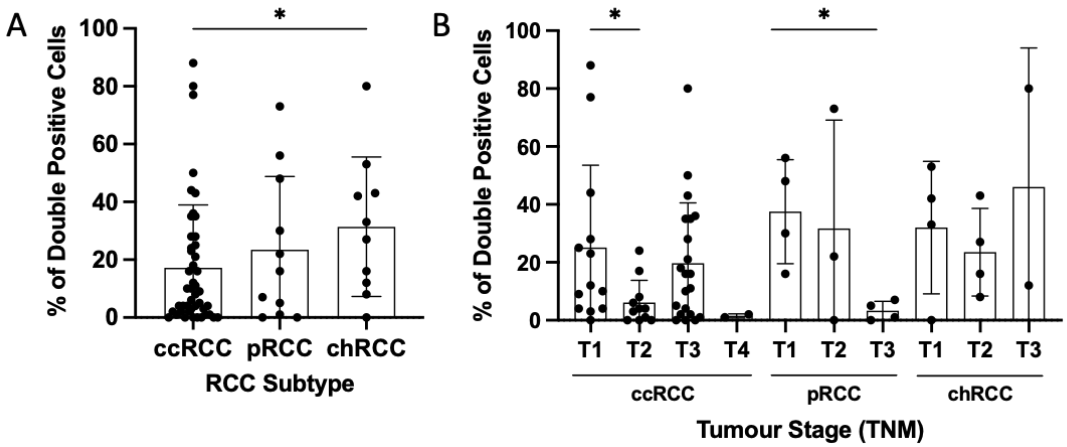

Figure 3.57 ADAM28 and CD200 double positive cell percentage of all cells
The percentage of cells which were positive for both ADAM28 and CD200 was calculated in (A) RCC subtypes. (B) By TNM tumour stage within the subtypes. Analysis was carried out using a Kruskal-Wallis test and Dunn's multiple comparisons test, where * represents $p<0.05$.

The percentages of ADAM28 and CD200 double positive cells were lower than those observed for ADAM9 and ADAM17 across the RCC subtypes (Figure 3.57a), however the percentage in chRCC was significantly higher than that found in ccRCC

(31.40 ± 24.14 vs 17.23 ± 21.77, p = 0.0489). As with ADAM9 and ADAM17 however, the correlation between ADAM28 and CD200 H-score was found to be strongest in chRCC, again implying that the highest number of ADAM28 and CD200 double positive cells were found in chRCC, and their expression is likely to be of similar strength. A lower number of double positive cells is observed in ccRCC and pRCC, however the weak correlations observed previously imply that the strength of the expression level of ADAM28 and CD200 on these cells is unrelated. As was the case for ADAM17, when examining double positive cells by TNM tumour stage (Figure 3.57b), the percentage of double positive ADAM28 and CD200 cells was found to reduce with increased T status in ccRCC, with T2 found to have a significantly lower percentage of double positive cells compared to T1 (6.09 ± 7.73 vs 25.15 ± 28.41, p = 0.0240). This effect was also observed in pRCC, with T1 found to have a significantly higher percentage of ADAM28 and CD200 double positive cells compared to T3 (32.00 ± 22.85 vs 48.00 ± 48.08, p = 0.0286).

3.7.4 Protease and CD200 double positivity summary

This data has shown that the percentage of double positive cells within a sample does not always correlate with the strength of the expression of either a protease or CD200. We have shown that the percentage of ADAM9 and CD200 double positive cells is highest in ccRCC, with a significant increase observed with increased TNM tumour status. As we have however already shown that there is no correlation between ADAM9 and CD200 H-scores in ccRCC, there appears to be no relationship between the number of cells which express both ADAM9 and CD200 and the strength of their expression. This pattern was the opposite to what was observed in both the ADAM17 and ADAM28 analyses, where the percentage of double positive cells was significantly higher in chRCC compared to ccRCC. This is interesting as we have already shown a strong correlation between ADAM17 and ADAM28 H-Score with CD200 H-score, so in chRCC, the double positive cells may have similar expression levels of both the protease and CD200. In both ADAM17 and ADAM28, percentage of double positive cells decreased with increased T stage in ccRCC, which again the opposite to what we observed in the ADAM9 analysis, implying that in ccRCC when T status increases, ADAM9 expression is expressed on

more CD200-expressing cells and ADAM28 and ADAM17 are expressed on less, however the strength of this expression may not be altered.

This data shows that these ADAM proteases and CD200 are expressed in a similar area on RCC cells, with a high percentage of double positive cells in all samples. This is interesting as these, and we hypothesise that these ADAMs may be able to interact with CD200 to play a role in ectodomain shedding from the cell membrane, creating the soluble form sCD200.

ADAM17 and ADAM28 have already been implicated in CD200 ectodomain shedding (Roemer et al. 2004b), however the ability of ADAM9 to cleave CD200 has not yet been investigated. As the number of ADAM9 and CD200 double positive cells significantly increases with ccRCC T stage, we next aim to investigate whether ADAM9 is able to cleave CD200 to create sCD200, and what effect this may have on ccRCC tumour progression.

3.8 Functional role of ADAM9 in CD200 ectodomain shedding

To determine if ADAM9 is able to cleave CD200 in the process of ectodomain shedding, we established an ELISA assay to determine the level of sCD200 in cell line supernatant. As we have already determined that our RCC cell lines do not express CD200 at either the mRNA or protein level, we used our transduced CD200+ and CD200- HeLa cell lines to determine the normal amount of sCD200 produced by 1 million cells in standard cell culture conditions. We then added ADAM9 peptide in incremental amounts and measured the resulting sCD200 levels in the CD200+ and CD200- HeLa supernatant by ELISA, as shown in Figure 3.58.

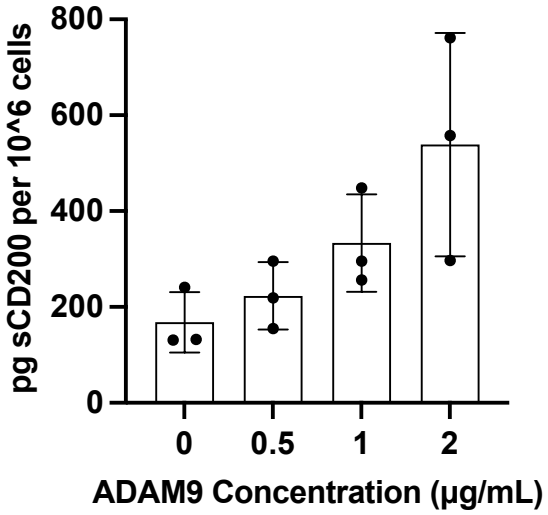

Figure 3.58 sCD200 ELISA on HeLa CD200+ supernatant to determine sCD200 concentration after addition of ADAM9 peptide.
sCD200 was found to incrementally increase with increased ADAM9 concentration. Statistical analysis was carried out using a Kruskal-Wallis test and Dunn's multiple comparisons test, however no significant differences were found. n=3.

sCD200 concentration was found to incrementally increase in line with ADAM9 peptide concentration in CD200+ HeLa cells.

As it appears that ADAM9 may have a role in the ectodomain shedding of CD200 creating additional sCD200, we next used siRNA to knock down ADAM9 in the HeLa+ cells to establish if sCD200 production was reduced. Knock down was confirmed using western blot and qRT-PCR, and the CD200 ELISA was repeated on the siRNA treated samples, as shown in Figure 3.59.

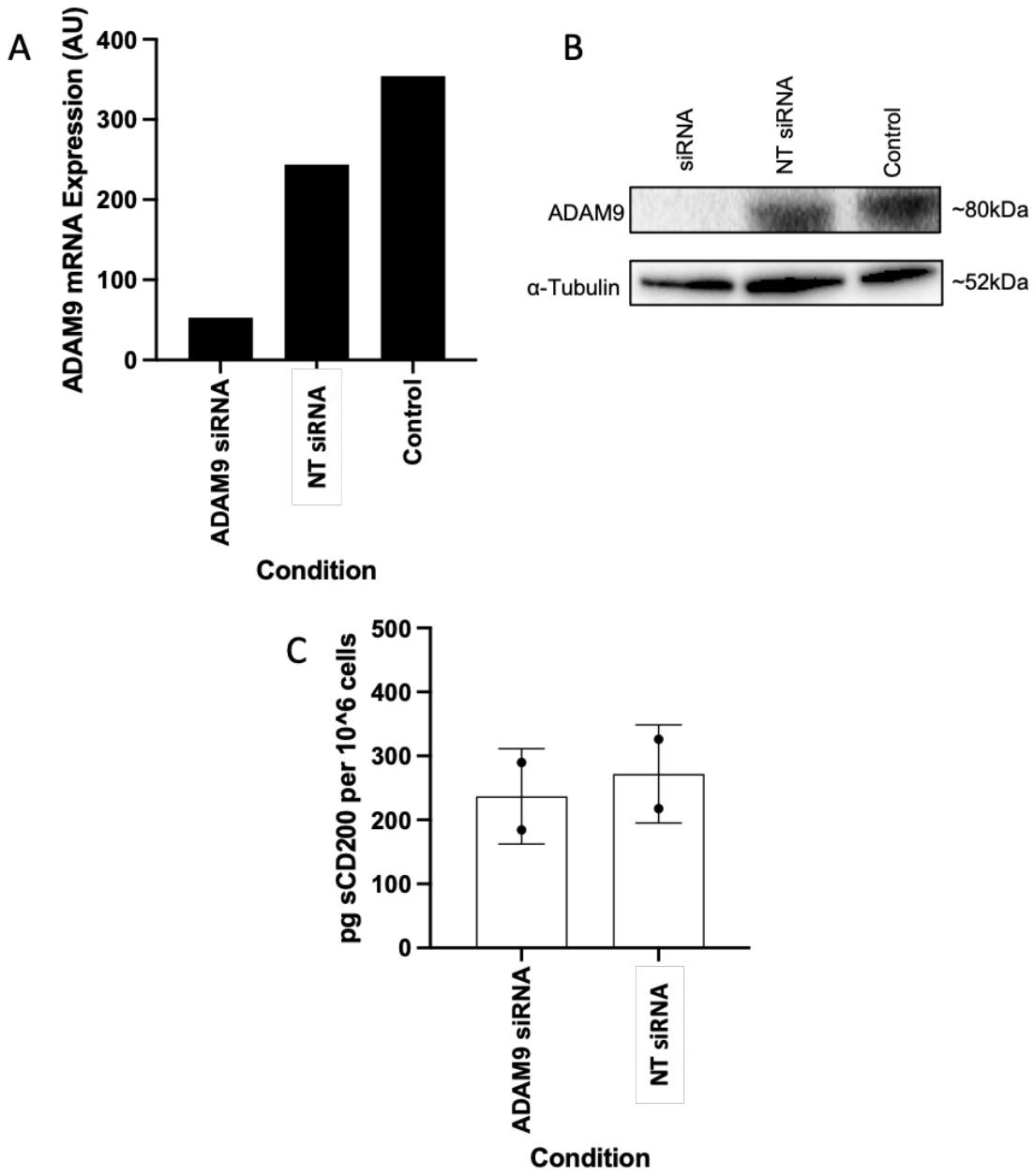

Figure 3.59 Confirmation of ADAM9 knockdown in HeLa CD200+ cells
(A) ADAM9 mRNA expression by qRT-PCR (n=3), (B) ADAM9 protein expression by western blot (n=2). (C) sCD200 ELISA shows lower sCD200 levels in siRNA samples compared to those subjected to ADAM9 non-targeting (NT) siRNA (n=2).

Analysis of ADAM9 mRNA following treatment with siRNA confirmed knockdown after 72 hours compared to the non-targeting (NT) siRNA-treated and control samples (Figure 3.60a), and western blot confirmed protein knockdown compared to the NT siRNA treatment (Figure 3.60b). CD200 ELISA found a reduction in sCD200 levels in the siRNA treated samples compared to the control, however possibly due to the small number of repeats, this change was not found to be significant.

3.9 Discussion

Ectodomain shedding is highly important in a wide variety of normal and pathological processes and is carried out on a diverse list of cell surface molecules including growth factors, cytokines and cell adhesion molecules. Ectodomain shedding can also be induced by a wide range of stimuli including phorbol esters, cytokines, growth factors and bacterial toxins resulting in liberation of biologically active ectodomains which can exhibit functions similar or distinct from their cell surface counterpart, with a wide range of potential downstream activation pathways. CD200 has been shown to be subject to ectodomain shedding to create a functional soluble form (Twito et al. 2013b; Wong et al. 2016), however the proteases responsible have not been fully established. ADAM17 and ADAM28 have been implicated in this process in CLL (Twito et al. 2013b; Wong et al. 2016; Morgan et al. 2022), however their involvement has not been established in RCC.

In this chapter we have identified three proteases of interest in RCC through a thorough literature search followed by investigation of RNAseq data. From the literature we identified 18 proteases which have roles in RCC development, including 7 ADAMs and 11 MMPs, from which we identified ADAM17 and ADAM28 due to their reported roles in CD200 ectodomain shedding (Twito et al. 2013; Li et al. 2014) and association with ccRCC progression and prognosis (Wong et al. 2016). Next, using our RNAseq data from 6 ccRCC cell lines and one normal kidney cell line, we calculated DEGs to identify which ADAMs, MMPs and TIMPs were significantly up- or downregulated in our cell lines, however the only protease which was significantly upregulated in all 6 samples was ADAM9. ADAM17 was not found to be significantly upregulated in any of the 6 ccRCC cell lines, and ADAM28 was only found to be significantly upregulated in 2 cell lines, A498 and CAKI2. As ADAM9 has been

associated with tumour progression, increased disease stage and metastasis in ccRCC (Mitsui et al. 2006), we chose to examine this protease further to determine if it could have a role in CD200 ectodomain shedding.

We validated our RNAseq data by using qRT-PCR and western blot, which mirrored our RNAseq read count data at the mRNA and protein level for ADAM9, ADAM17 and ADAM28, however we discovered during this analysis that our RCC cell lines did not express CD200, with low or zero read counts observed in all qRT-PCR and western blot analyses. This result was troublesome as CD200 expression has been previously reported in RCC through immunohistochemical analyses on patient-derived tumour tissue (Fritzsche et al. 2008), however this expression does not appear to translate into our cell lines. The use of 2D cell culturing techniques to replicate *in vivo* conditions is becoming increasingly controversial, with 3D cell culture thought to replicate the conditions of the body more closely. Differential gene and protein expression has been found between 2D and 3D culture in many cancer and non-cancer cell lines, resulting in behavioural changes in many cellular processes and drug responses, with up to 30% of genes found to be differently expressed between 2D and 3D cell lines (Love et al. 2017b; El Hanbuli et al. 2021). Cells grown in a traditional 2D monolayer receive an equal amount of nutrients and growth factors from the culture media, however this creates an unrealistic representation of healthy proliferating cells, as necrotic cells detach from the surface and are removed when media is changed. Cells in 2D culture are under constant stress and have been found to have a more flat and stretched morphology than they would appear *in vivo*, which can influence many cellular processes including proliferation, differentiation, protein and gene expression and apoptosis (Birgersdotter et al. 2005). 3D culture systems are however thought to mimic the *in vivo* environment more closely, allowing cell morphology to more closely resemble that naturally found in the body, in turn allowing more representative cell-cell interactions and cell-ECM interactions (Edmondson et al. 2014). 3D spheroids are comprised of cells in various stages of the life cycle, with healthy proliferating cells on the outer layers, the inner layers made of apoptotic and necrotic cells and the cells of the inner core in a quiescent or hypoxic state due to low oxygen and poor access to nutrients and growth factors and is thought to be more illustrative of a tumour or tissue setting. To determine if the lack of CD200 expression could have

therefore been due to the 2D cell culture conditions used with our ccRCC cell lines, we attempted to grow the cell lines in 3D suspension. All ccRCC cell lines did successfully form spheres and expanded well over a 14-day period, however subsequent qRT-PCR analysis found that CD200 expression was still not present in these cell lines. It is unclear why CD200 was not present in either 2D or 3D culture, however this could be a condition of cell culture in general or due to the lack of competition from other cells or immune cells. However, as CD200 expression has been demonstrated in RCC patient tissue (Gurski et al. 2017), we continued our investigations using patient-derived TMAs, which included normal kidney samples alongside ccRCC, pRCC and chRCC tissue samples.

We observed consistent CD200 expression throughout the tumour section, whereas in the normal kidney, individual structures expressed different levels of CD200 expression. In the normal kidney we observed a general CD200 expression gradient from the renal corpuscle down the convoluted tubules, with the lowest CD200 expression observed in the collecting duct at the end of the nephron, with structures within the renal cortex showing higher CD200 expression compared to structures in the medulla. As the proximal convoluted tubules are thought to be the cell of origin for ccRCC and pRCC, and the distal convoluted tubules are the cell of origin for chRCC, we aimed to explore if this expression was carried through into the tumour state. Similar expression levels were observed in all three RCC subtypes, with a slightly higher mean expression found in ccRCC, where increased tumour status also resulted in a slight increase in CD200 expression. This trend was also found in chRCC, however a decrease in CD200 expression with increased T stage was found in pRCC. Having shown CD200 expression throughout the RCC tumours, we next aimed to characterise expression of our proteases of interest in serial sections of the same tissue. ADAM9 and ADAM17 expression were found to have the highest overall expression levels in chRCC, but were found at varying levels in ccRCC and pRCC. Expression was found to decrease with increased T stage in ccRCC and pRCC. ADAM28 was present in low levels throughout the samples but expression was highest in pRCC. H-score correlation analysis of each protease with CD200 revealed a strong relationship between ADAM9, ADAM17 or ADAM28 with CD200 in chRCC, however weak relationships were observed between the two in other subtypes. These strong chRCC relationships could however be due to very small

sample size and should be made more robust with a further number of samples. Following this analysis, we studied the number of cells which were positive for both a protease of interest and CD200 within each sample, to determine if these proteases are positioned similarly on the cell membrane to be able to cleave CD200. We found the highest percentage of ADAM9 and CD200 double positive cells in ccRCC, which increased with T stage. Interestingly, the lowest number of ADAM17 or ADAM28 with CD200 double positive cells were found in ccRCC, and these number decreased with T stage. This may imply that as ccRCC disease progresses, the number of cells expressing both ADAM9 and CD200 increases, while the number of cells expressing ADAM17 or ADAM28 with CD200 decreases and so this balance may influence tumour progression. However, as the relationship between ADAM9 and CD200 H-score was found to be weak although the number of double positive cells increases with T stage, the strength of their expression is likely unrelated to each other. A further step for this analysis could be optimisation of the staining protocol to allow examination of all three proteases on the same sample, to determine if expression is observed in the same location, however this was not possible for us to complete due to time constraints.

Having established that ADAM17 or ADAM9 in combination with CD200 are often expressed on the same cells through RCC development, with high percentages of double positive cells observed within our samples, we aimed to determine if ADAM9 could have a functional role in the ectodomain shedding of CD200 to create the soluble form, sCD200, in the same way as ADAM17. Using our transduced CD200+ HeLa cell line, we added active ADAM9 peptide then measured sCD200 levels in the supernatant using ELISA, where we found an incremental increase in sCD200 with increased ADAM9 concentration. To validate this further, ADAM9 siRNA was used to knock down ADAM9 expression and a decrease in sCD200 was observed compared to the control. This data implies a role for ADAM9 in the ectodomain shedding of CD200 and is a novel finding which has not been demonstrated previously in the literature. As ADAM9 has been shown to be overexpressed in both RCC and other cancer types including breast cancer and NSCLC (El Hanbuli et al. 2021), both of which have also been shown to overexpress CD200 (Shintani et al. 2004a; Zhou et al. 2020), an interesting future direction would be to complete this work using

CD200+ cell lines from these cancer types to determine if a similar effect is observed.

3.10 Conclusions

In this chapter we have shown that a number of proteases are expressed in RCC including ADAM9, ADAM17 and ADAM28, which we have shown to be present in tissues of all three RCC subtypes. We have shown that CD200 is not present in ccRCC cell lines, however it is expressed in patient-derived tumour tissue and normal kidney. CD200 expression appears to follow from the normal kidney cell of origin into the associated RCC tumour subtype, however CD200 expression was similar between all three subtypes studied. The percentage of cells which were double positive for both CD200 and a protease is associated with advanced disease stage, particularly ADAM9 and ADAM17. We have shown that ADAM9 is the most strongly overexpressed protease in ccRCC compared to normal kidney at the RNA and protein level and is appropriately placed on the cell membrane to be able to interact with CD200. Finally, we have shown that the presence of ADAM9 results in increased sCD200 levels in cell line supernatant, and that ADAM9 knock down decreases these levels, and so ADAM9 may have a novel role in CD200 ectodomain shedding in RCC.

Chapter 4: Characterising RCC Immune Infiltrate

4. Characterising RCC immune infiltrate and relationship with CD200 expression

The immune landscape of RCC is highly variable, with T cells and macrophages forming the key components of the tumour microenvironment, however their phenotypes, relationships to each other within this ecosystem and the resulting effects on clinical outcomes are yet to be fully defined. The full picture of how immune cells interact and what can alter the number of these cell types during disease progression is currently unclear.

A further complication of the immune landscape is the presence of immune checkpoints which regulate and modulate the immune response. One such checkpoint, CD200, sends a unidirectional immunosuppressive signal to cells which express its receptor, CD200R. CD200:CD200R signalling has been shown to alter the TME and affect immune cell behaviour in various ways, including suppression of NK cell function and T-cell mediated responses, reduced infiltration of CD4+ and CD8+ T lymphocytes, induction of Tregs, M2 macrophages and tolerogenic dendritic cell phenotypes and switching of T cell phenotype from Th1 to Th2 (Minas and Liversidge 2006; Coles et al. 2011; Hayakawa et al. 2016; Aref et al. 2017; Xu et al. 2018; Katoh and Katoh 2019).

In the previous chapter, we have shown that CD200 expression is higher in RCC compared to normal kidney tissue, however it is not yet known how this change in CD200 expression affects the presence and activities of tumour infiltrating immune cells.

Hypothesis

We hypothesise that immune cell infiltrate will be significantly different between RCC tumour and normal kidney samples, revealing meaningful trends between key immune cells to create a characteristic immune signature which relates to poor prognosis. We also hypothesise that significant changes in immune infiltrate will be seen with increased CD200 expression, which will also have an effect on prognosis.

Aims of this chapter

1. Estimate the immune cell composition from bulk RNAseq data of normal kidney and ccRCC tumours to determine differences in immune infiltrate and establish a characteristic immune signature which relates to poor prognosis.

2. Use IF to determine the absolute and relative frequencies of CD45+, CD3+, CD4+, CD8+, FoxP3+ and CD56+ cells in TMA samples to confirm bioinformatic findings.

3. Estimate and compare the immune composition of the 3 most common RCC subtypes to determine differences in immune infiltrate and relationship with prognosis

4. Establish the effect of CD200 expression on ccRCC immune infiltrate to determine the relationship between tumour CD200 expression, immune cell infiltrate and patient prognosis.

4.1 Bioinformatic analysis of ccRCC RNAseq data sets

As ccRCC is the most common RCC subtype and has high numbers of infiltrating lymphocytes, we firstly examined the immune infiltrate in this subtype.

Publicly available ccRCC Firehose Legacy RNAseq data sets were downloaded from the Broad Institute website (https://gdac.broadinstitute.org/). Normal samples were separated from the RCC samples and checked for duplicates before uploading to CIBERSORTx as described in the methods section. Patient characteristics are displayed in Table 4.1.

Table 4.1 Patient characteristics in the ccRCC Firehose Legacy data set

Characteristic	Number
Number of samples	537
Age at Diagnosis	
Median	61
Range	26-90
Gender	
Male	346 (64%)
Female	191 (36%)
Stage	
I	272 (51%)
II	57 (11%)
III	125 (23%)
IV	83 (15%)
Tumour	
T1	22 (4.1%)
T1a	142 (26.4%)
T1b	111 (20.7%)
T2	55 (10.2%)
T2a	10 (1.9%)
T2b	4 (0.7%)
T3	5 (0.9%)
T3a	122 (22.7%)
T3b	53 (9.9%)
T3c	2 (0.4%)
T4	11 (2.0%)
Node	
N0	240 (45%)
N1	17 (3%)
N2	0
NX	280 (52%)
Metastasis	
M0	426 (79%)
M1	79 (15%)
MX	32 (6%)
Laterality	
Left	253 (47.1%)
Right	283 (52.7%)
Bilateral	1 (0.2%)
Race	
White	466 (87%)
Black/African American	56 (10%)
Asian	8 (1%)
Other	7 (1%)
Overall Survival (Months)	
Median	47.78
Range	0-149.05
Disease Free Survival (Months)	
Median	43.41
Range	0-133.84
Vital Status	
Alive	360 (67%)
Dead	177 (33%)

The ccRCC data set contained 537 samples with a median age of diagnosis of 61 with a range of 26-90. 64% of the samples were from male patients, with over half of

the samples (51%) being from stage I patients and the rest spread between stage II (11%), III (23%) and IV (15%). The most common tumour grade was T1a (26.4%), the most common node stage was N0 (45%) with 3% diagnosed as N1, and the most common metastasis stage was M0 (79%), with 15% defined as M1. 52.7% of tumours were right-sided, while 1 patient (0.2%) presented with bilateral tumours. 87% of patients were white, while 10% were black/African American and 1% were Asian. Median overall survival (OS) for the ccRCC group was 47.78 months with a range of 0-149.05 months, while median disease-free survival (DFS) was 43.41 months with a range of 0-1.33.84 months. At the end of the study, 67% of the patients were still alive. 92 normal patient samples were included; however, no characteristics were available.

We firstly investigated the ccRCC survival data and compared patient outcomes by sex, age, race and primary tumour laterality, to determine if any differences in OS were observed, as shown in Figure 4.1.

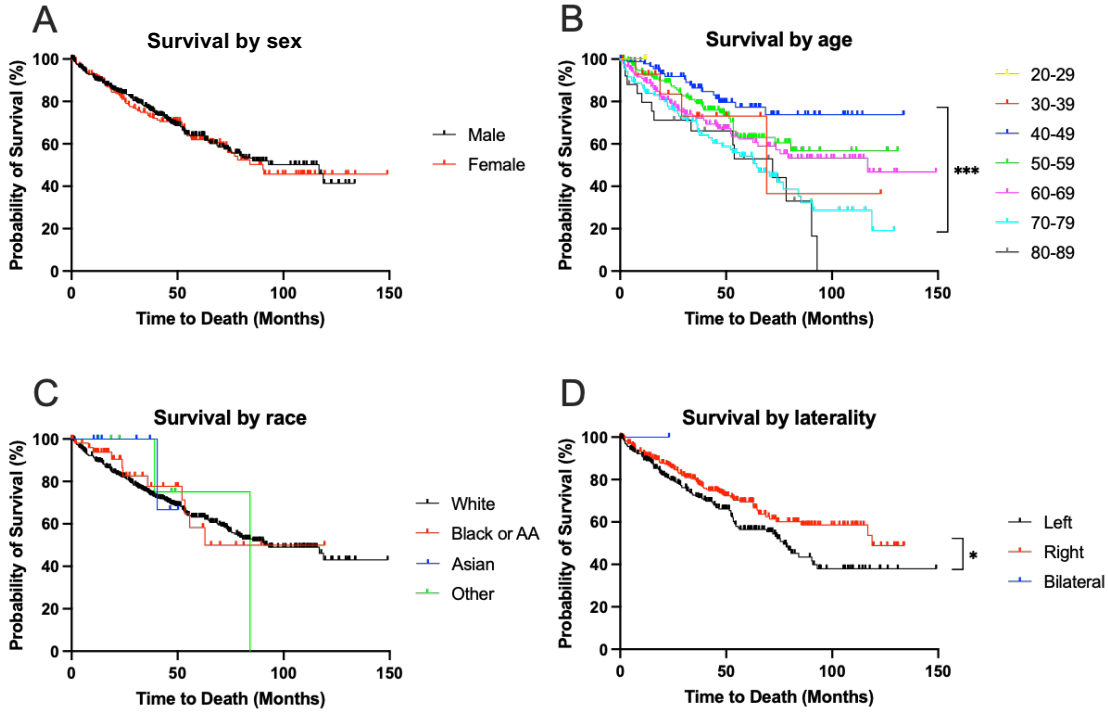

Figure 4.1 ccRCC overall survival curves by patient characteristics
(A) Survival by patient sex, (B) Survival by patient age at operation, (C) Survival by patient race, (D) Survival by primary tumour laterality. Kaplan-Meier curves were compared using a Logrank test, where * represents $p < 0.05$ and *** represents $p < 0.001$.

The survival curves for the male and female patients were similar (Figure 4.1a), with no significant differences found between the two, however male patients had a

longer median survival compared to female (116.75 months vs 90.41 months respectively). Patient age at operation made a large difference to survival outcome (Figure 4.1b) and the 40-49 age group curve was found to be significantly different to the 70-79 curve ($p<0.001$). No significant differences were found between the curves between race (Figure 4.1c), however the black or African American (AA) group was found to have the shortest median survival out of all of the groups (62.84 months). Interestingly, left-sided primary tumours were found to have a significantly worse overall survival compared to right-sided tumours (Figure 4.1d, median survival 76.97 months vs 118.76 months, $p=0.014$), however the reason for this is unclear.

ccRCC survival data was next compared by clinical characteristics of tumour, node and metastasis (TNM) status and overall disease stage, as shown in Figure 4.2.

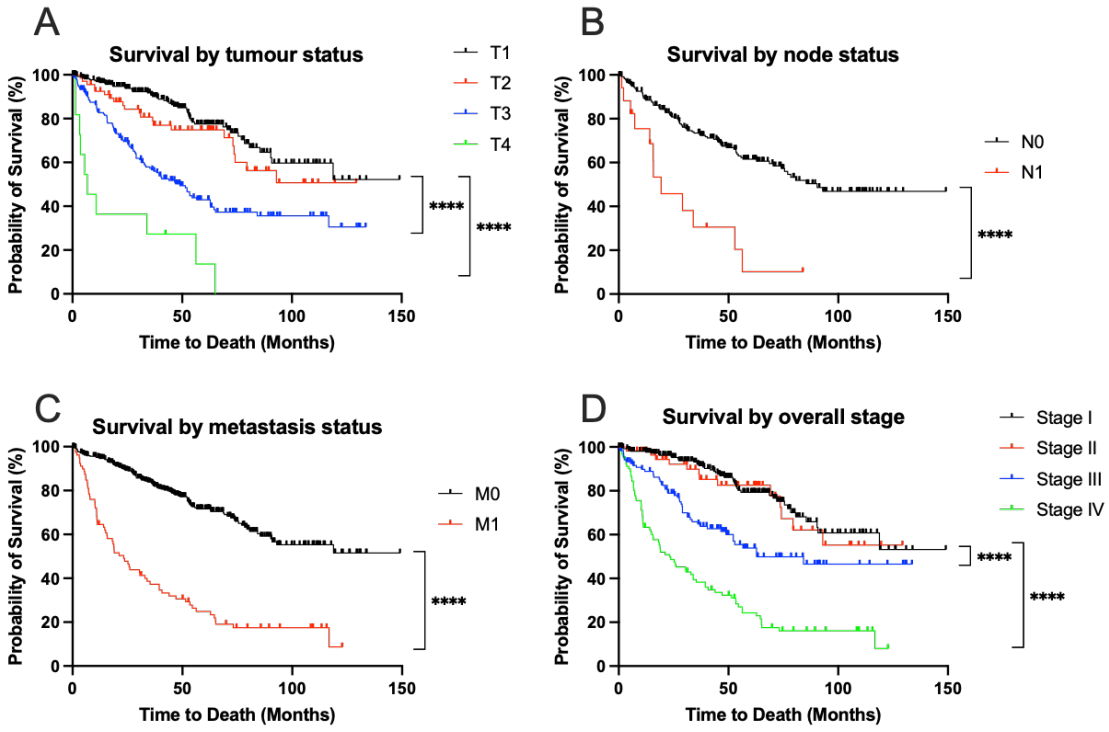

Figure 4.2 ccRCC overall survival curves by clinical characteristics
(A) Survival by tumour status, (B) Survival by node status, (C) Survival by metastasis, (D) Survival by overall stage. Kaplan-Meier curves were compared using a Logrank test, where **** represents $p < 0.0001$.

As expected, the survival curves for tumour status (Figure 4.2a) were significantly different between T1 and T3 and between T1 and T4 (both $p<0.0001$). The T4 group was found to have the lowest median survival of all groups of 6.77 months. The survival curve between node status N0 and N1 (Figure 4.2b) were also significantly

different from each other ($p<0.0001$), with N1 having a significantly lower median survival of 19.28 months compared to 90.41 months for the N0 group. The curves for metastasis status M0 and M1 (Figure 4.2c) were also significantly different from each other ($p<0.0001$), with a median survival of 23.29 months for the M1 group, however median survival could not be calculated for the M0 group as over 50% of patients were still alive at the end of the study. Overall stage curves (Figure 4.2d) were significantly different between stages I and III ($p<0.0001$) and between stage I and IV ($p<0.0001$). Stage IV was found to have the lowest median survival of all groups of 23.39 months.

This data shows that some patient characteristics such as age at operation and laterality of the primary tumour have a more significant effect on overall survival than others, such as patient sex or race. As expected, patients with a higher overall stage or TNM stage had a lower chance of survival, with stage III and IV showing the poorest overall survival outcomes and shortest median survival.

Patient survival data was next compared using Cox proportional regression analysis by patient characteristics and TNM status to determine the hazard ratio (HR) and therefore risk factor associated with each status, using either the lowest or most common type as a reference level. A HR >1 is considered to be at greater risk, while a HR <1 is considered to be protective or less at risk. A HR of exactly 1 implies an equal risk in both groups.

HRs were first calculated based on patient age, race, sex and tumour laterality, as shown in Figure 4.3.

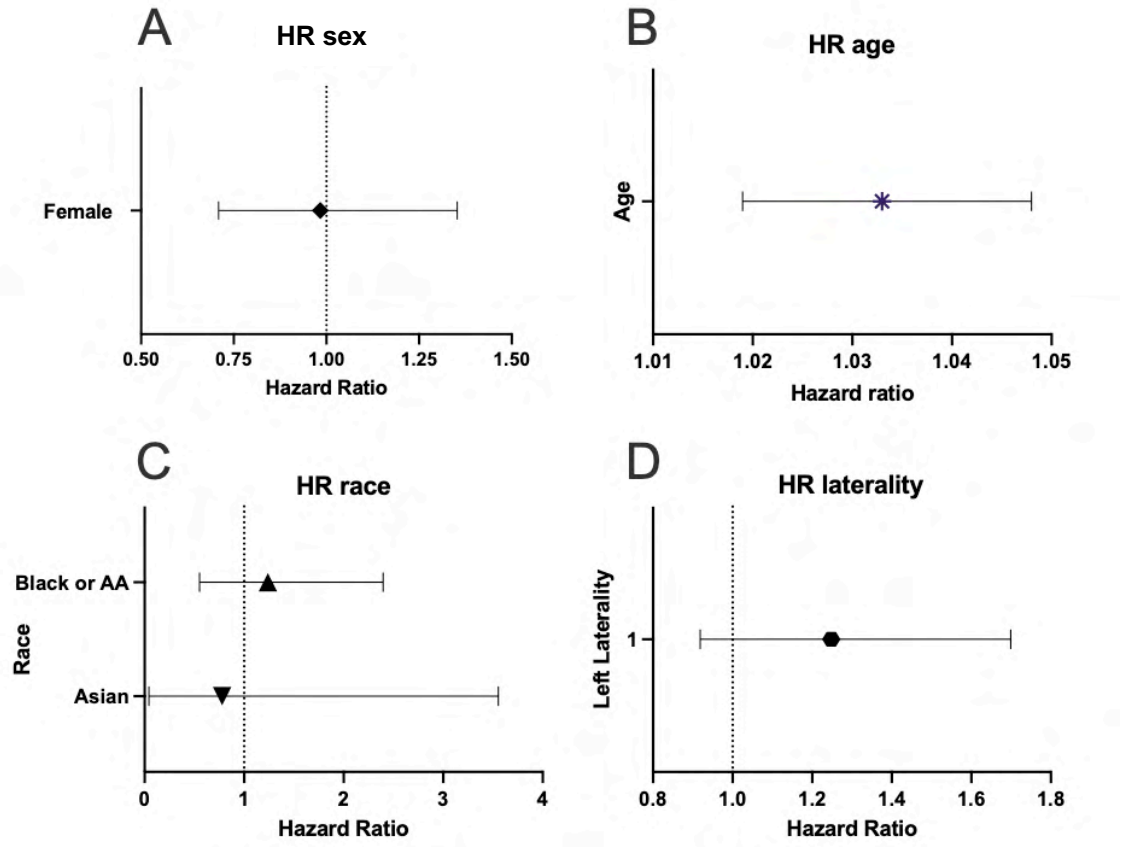

Figure 4.3 Hazard ratios based on patient characteristics
Hazard ratios (HR) were calculated using Cox proportional regression main effect analysis. (A) HR of female sex compared to male, (B) HR of increased age, (C) HR of black of African American or Asian compared to white, (D) HR of left primary tumour laterality compared to right.

Comparison of patient survival data by sex showed that females have a protective advantage compared to males (HR 0.983, 95% CI 0.709 to 1.353) however this was not found to be significant (Figure 4.3a). Increased age had a slightly increased risk compared to lower age (Figure 4.3b, HR 1.033, 95% CI 1.019 to 1.048). Comparison of race (Figure 4.3c) showed an increased risk for the Black/African American group compared to white (HR 1.239, 95% CI 0.5518 to 2.397), while interestingly the Asian group showed a slightly protective effect compared to white (HR 0.7795, 95% CI 0.0440 to 3.554). Figure 4.3d shows an increased risk for a left-sided primary tumour compared to a right-sided tumour (HR 1.248, 95% CI 0.9186 to 1.699) however again this increase was also not found to be significant.

HRs were next calculated based on clinical characteristics of tumour (T2-4), node (NX and N1) and metastasis (MX and M1) status compared to T1, N0 and M0 respectively, as shown in Figure 4.4.

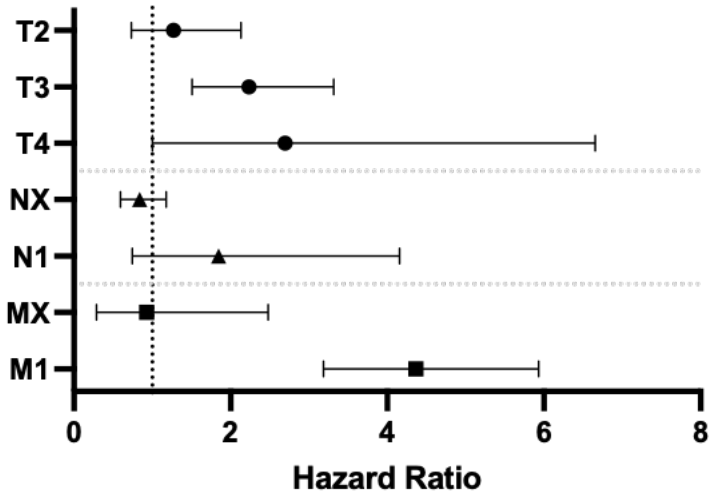

Figure 4.4 Hazard ratios based on clinical characteristics
Hazard ratios (HR) were calculated using Cox proportional regression main effect analysis using T1, N0 and M0 as reference levels for comparison to the respective groups.

Tumour status T2, T3 and T4 were compared to T1 and as expected, HR was found to increase with increased tumour stage, with T3 and T4 showing significantly increased risk compared to T1 (T3 HR 2.236, 95% CI 1.510 to 3.318, p=0.0400 and T4 HR 2.696, 95% CI 1.001 to 6.655, p<0.0001 respectively). N1 node status was also associated with a higher risk compared to N0 (HR 1.847, 95% CI 0.734 to 4.158), however this difference was not found to be significant. Metastasis status MX (undetermined) and M1 were compared to M0, with M1 found to have a significantly higher hazard ratio compared to M0 (HR 4.365, 95% CI 3.186 to 5.934, p<0.0001).

4.2 Estimation of ccRCC immune infiltrate compared to normal kidney

Having determined which patient characteristics influence patient survival, we next aimed to characterise the ccRCC immune infiltrate to study whether changes in immune cell levels or relationships could be responsible for any effects on patient survival. We firstly estimated the immune infiltrate in ccRCC samples compared to peritumoral normal kidney tissue in both the full ccRCC data set and the 92 pairs of matched ccRCC samples with their associated normal samples, to determine if

alternations in immune cell levels can influence disease progression and patient outcome.

ccRCC Firehose RNAseq patient data was run through the CIBERSORTx deconvolution algorithm to determine the immune cell fractions in each sample using the LM22 data set. LM22 comprises of 547 genes which can accurately distinguish between human hematopoietic cell populations, providing infiltration proportions for 22 cell types, namely naïve and memory B cells, plasma cells, CD8+ cytotoxic T lymphocytes (CTLs), naïve CD4+ T cells, resting and activated memory CD4+ T cells, CD4+ follicular helper T cells (Tfh), regulatory T cells (Tregs), gamma delta T cells, resting and activated natural killer (NK) cells, monocytes, M0, M1 and M2 macrophages, resting and activated dendritic cells, resting and activated mast cells, eosinophils and neutrophils. A list of genes used to characterise immune cells can be found in supplementary table S1.

Principal component analysis (PCA) was firstly used to determine the similarities between the CIBERSORTx 22 cell type immune fractions of the ccRCC and normal patient sample groups (Figure 4.5)

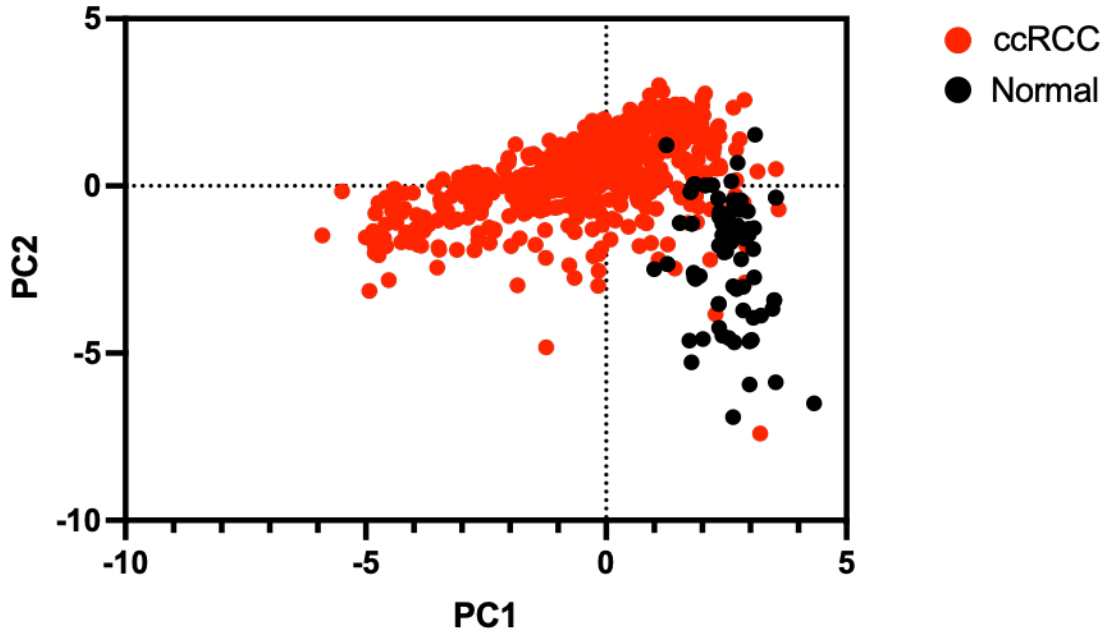

Figure 4.5 Principal component analysis of ccRCC immune cells compared to normal kidney
Most variation was observed along the PC2 axis, with normal kidney spreading along the range of the PC2 axis, while the ccRCC samples spread mostly along the PC1 axis.

PCA found that the ccRCC group has the most variation through the PC1 axis, while the normal group has more variation within the PC2 axis. This implies that the immune fractions are different between the two groups, and so the overall immune infiltrate in ccRCC is likely to be somewhat different to that found in the normal samples.

We next looked at each immune cell type from the LM22 set to determine which immune cell types are significantly altered in ccRCC compared to the normal kidney samples, as shown in Figure 4.6.

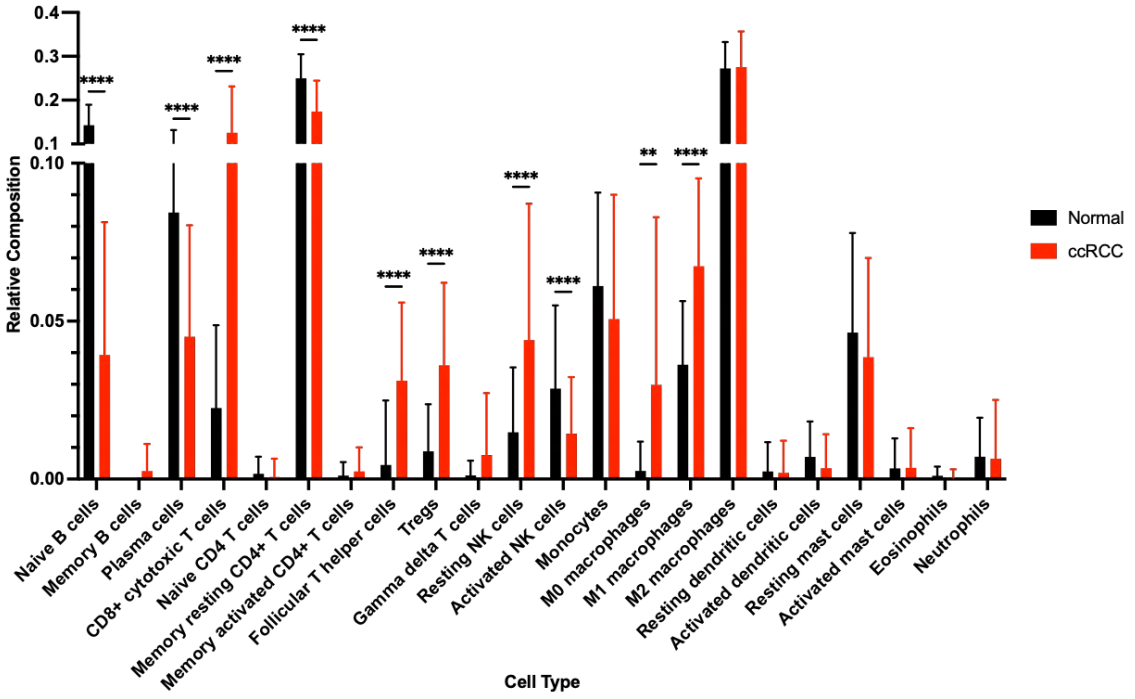

Figure 4.6 ccRCC vs normal kidney estimated immune cell fractions
Each cell type was compared to normal kidney in the full ccRCC data set using a Mann-Whitney tests with the Benjamini-Hocherg method for FDR correction, where ** represents p <0.01 and **** represents p <0.0001.

Significant differences were found between the ccRCC and normal samples for 10 of the 22 immune cell types studied, with naïve B cells, plasma cells, memory resting CD4 T cells and activated NK cells all found to be significantly higher in normal kidney than in ccRCC (all p<0.0001). CD8 cytotoxic T cells, T helper cells, Tregs, resting NK cells, and M1 macrophages all found to be significantly higher in ccRCC compared to normal (all p<0.0001), as were M0 macrophages (p=0.0010).

To investigate these changes further, we next plotted the average log2 fold change of the ccRCC samples compared to the average normal result against the p values found previously to determine which immune cell types are the most significantly altered in the ccRCC samples compared to the normal samples (Figure 4.7).

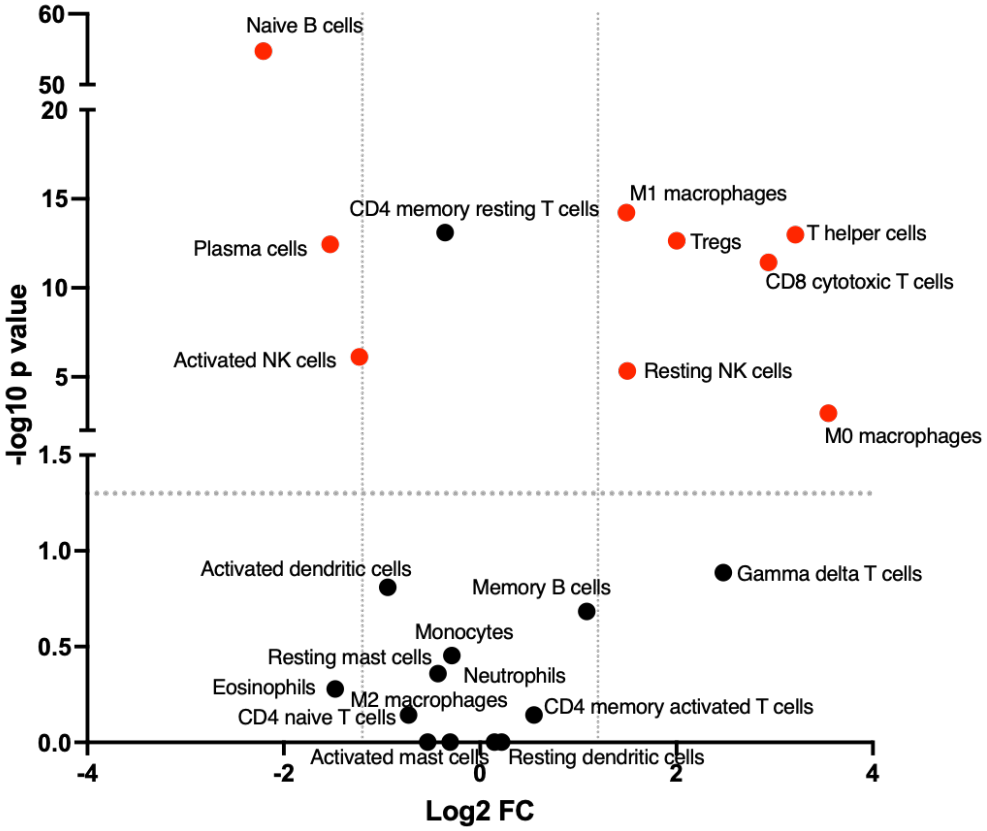

Figure 4.7 Comparison of ccRCC estimated immune infiltrate vs normal kidney
Cut offs of -1.2 and +1.2 log2 fold change and -log10 p >1.3 were used to determine significance. 9 out of the 22 immune cells were found to be significantly up or down in ccRCC compared to normal kidney. Significant cell types are highlighted in red.

The thresholds for a cell type to be considered significantly altered in ccRCC compared to the normal samples were log2 fold change values of +1.2 or -1.2, and p values of $p<0.05$ (log10 1.3). 9 out of the 22 immune cell types studied were found to be significant using these stringent cut offs, which were naïve B cells (log2 FC = -2.20 , log10 p = 54.73), plasma cells (log2 FC = -1.52, log10 p = 12.45), activated NK cells (log2 FC = -1.22, log10 p = 6.12), M1 macrophages (log2 FC = 1.49, log10 p = 14.23), Tregs (log2 FC = 2.00, log10 p = 12.65), Follicular T helper cells (log2 FC = 3.21, log10 p = 12.99), cytotoxic T cells (log2 FC = 2.93, log10 p = 11.43), resting NK cells (log2 FC = 1.49, log10 p = 5.33) and M0 macrophages (log2 FC = 3.54,

log10 p = 2.96). Although memory resting CD4 T cells were found to be significantly higher in normal kidney compared to ccRCC, this cell type did not meet the cut off for log2 fold change and so was not investigated further in this chapter.

Having determined that these 9 immune cell types are significantly increased or decreased in ccRCC compared to what is found in normal kidney, we next determined the amount of variability within the samples between the two groups, as shown in Figure 4.8.

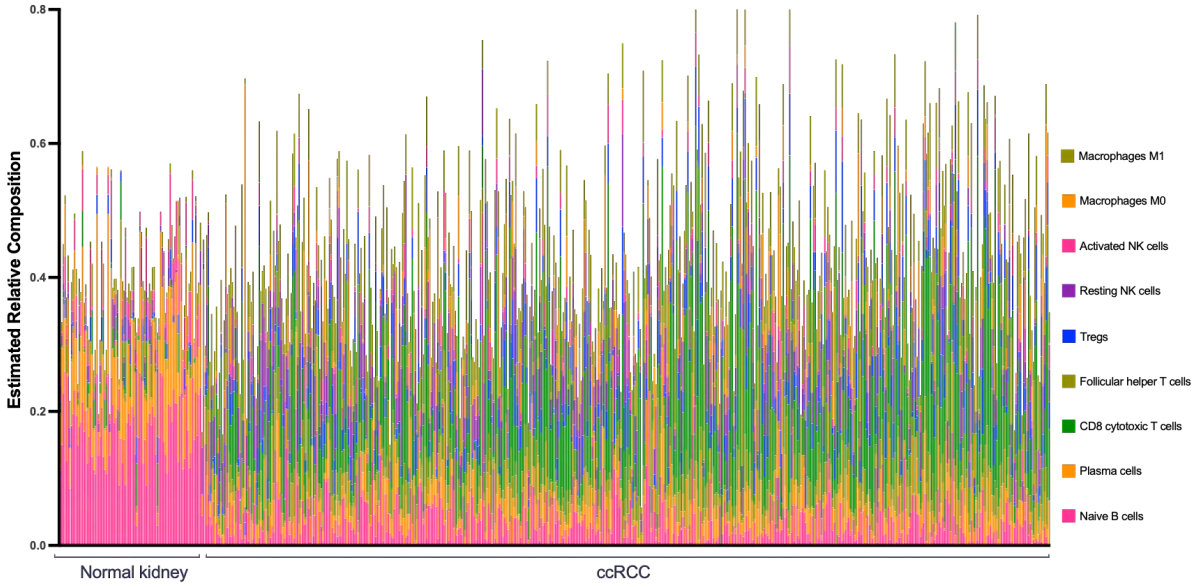

Figure 4.8 Visual representation of significant immune cell fraction between all ccRCC and normal kidney samples
Each line represents an individual sample. Missing values are the immune cell types which were not found to be significant in previous analyses. General trends of immune cell expression were seen throughout the ccRCC samples; however, levels of several cell types were altered compared to normal kidney, most notably Naïve B cells which were much lower in ccRCC compared to normal kidney.

Variability between the individual samples within both the ccRCC and normal groups was observed, however the clearest differences were seen between the ccRCC and normal groups, with the normal group showing notably higher amounts of naïve B cells compared to the ccRCC samples, which was expected as this cell type showed the strongest negative log2 fold change out of all the cell types in Figure 4.6. This shows that a degree of variability between samples is to be expected in both the ccRCC and normal groups which could be associated with individual patient characteristics.

Having determined the overall trends for each cell type in the ccRCC and normal kidney groups, we next looked at each of our 9 significant cell types individually to examine the data within each group, firstly as the whole data set compared to normal, then within the matched pairs. We then examined the overall survival data for high and low levels of each immune cell type to determine any effect on patient outcome associated with this cell type.

4.2.1 Cells of the innate immune system

Our analysis has shown significant differences in the estimated immune fractions of M0 and M1 macrophages and NK cells, so we will now investigate these cell types more in depth to understand their effect on patient outcome.

4.2.1.1 Macrophages

We firstly looked at the estimated immune fractions of undifferentiated M0 and differentiated M1 macrophages, levels of which were both found to be significantly altered compared to normal in the CIBERSORTx data set. Interestingly, M2 macrophages, which are generally considered to be cancer-associated macrophages, were not found to be significantly altered between the normal kidney and ccRCC groups as previously shown in Figure 4.6, so this cell type will not be studied in this section.

4.2.1.1.1 M0 macrophages

We firstly determined the estimated immune fraction of M0 macrophages in the normal kidney compared to the full ccRCC dataset, within the matched pairs and survival analysis of low vs high M0 macrophage level, as shown in Figure 4.9.

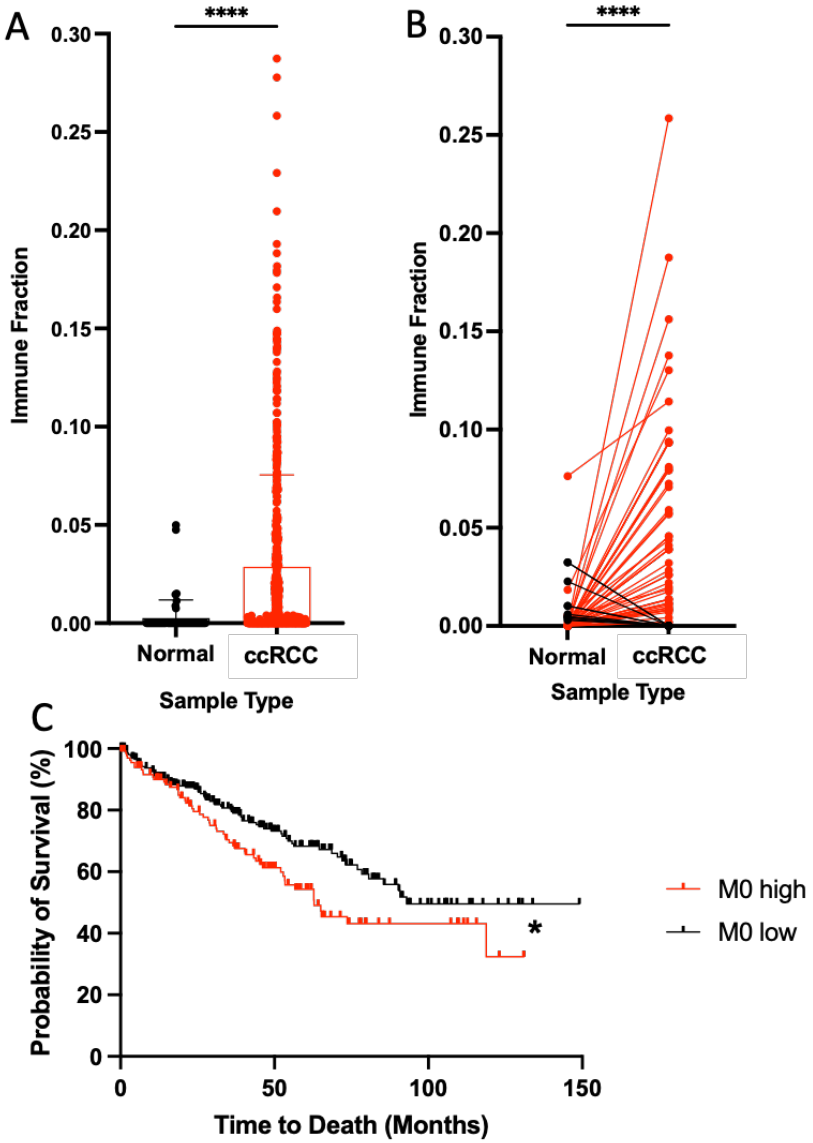

Figure 4.9 M0 macrophages in the ccRCC dataset, matched pairs and survival analysis
(A) Normal kidney vs ccRCC full data set, (B) Matched pair analysis, pairs higher in ccRCC are highlighted in red, those higher in normal kidney are in black, (C) Kaplan-Meier survival curves. Analysis was carried out using a Mann-Whitney test, Wilcoxon matched-pairs rank test and Logrank test respectively, where * represents p <0.05 and **** represents p <0.0001.

M0 macrophages were found to be significantly higher in ccRCC overall compared to normal kidney (Figure 4.9a, 0.030 ± 0.054 vs 0.002 ± 0.009, p<0.0001). Comparison

of the matched normal kidney and ccRCC pairs (Figure 4.9b) also showed that 52 out of the 93 pairs of samples had higher M0 macrophage levels in ccRCC compared to normal kidney (0.029 ± 0.047 vs 0.002 ± 0.009, $p<0.001$). A weak negative correlation between the two groups was found ($r=-0.137$), however this was not found to be significant. Both samples had zero M0 macrophages in 29 of the pairs, therefore 11 pairs were found to have higher levels of M0 macrophages in normal kidney compared to ccRCC. Comparison of patient survival data was next used to determine if high or low levels of M0 macrophages had any effect on overall survival (Figure 3.9c). Interestingly, the high M0 macrophage group had a significantly shorter survival compared to the low M0 group (62.84 vs 92.97 months, $p=0.0145$).

4.2.1.1.2 M1 macrophages

We next examined the levels of M1 macrophages in our datasets to determine the relationship of immune cell fraction and clinical outcome.

Levels of M1 macrophages in the normal kidney were compared to the full ccRCC dataset, within the matched pairs and survival analysis of low vs high M1 macrophage level, as shown in Figure 4.10.

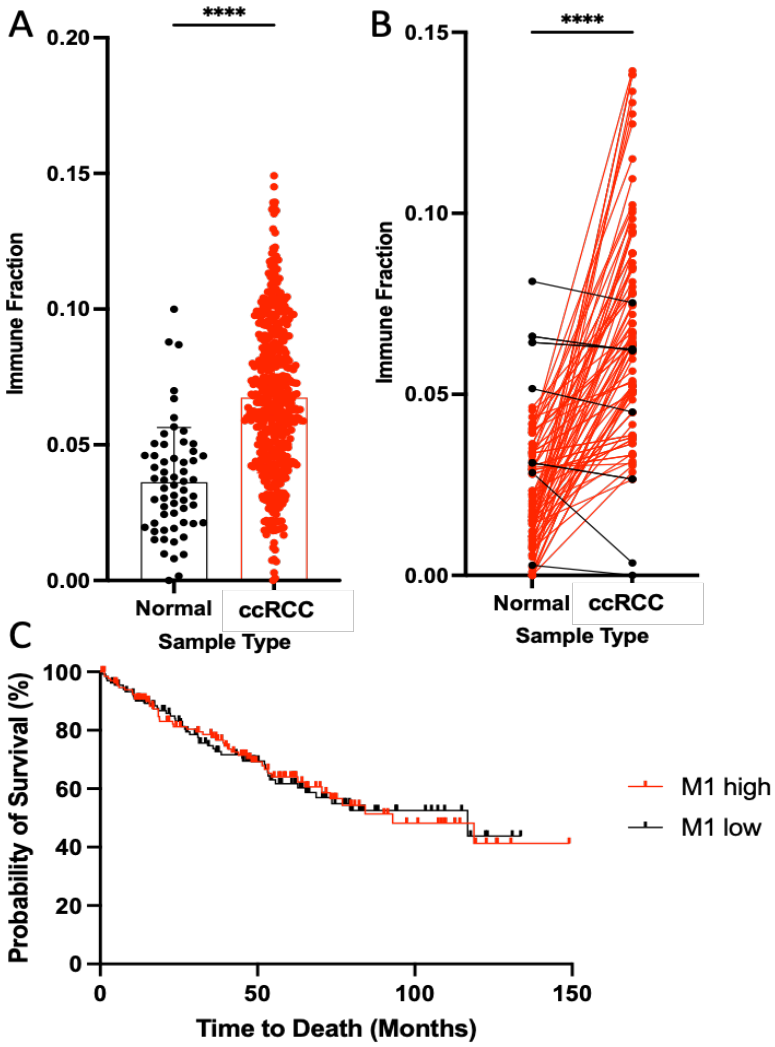

Figure 4.10 M1 macrophages in the ccRCC dataset, matched pairs and survival analysis
A) Normal kidney vs ccRCC full data set, (B) Matched pair analysis, pairs higher in ccRCC are highlighted in red, those higher in normal kidney are in black, (C) Kaplan-Meier survival curves. Analysis was carried out using a Mann-Whitney test, Wilcoxon matched-pairs rank test and Logrank test respectively, where **** represents p <0.0001.

As we observed in M0 macrophages, in the full ccRCC dataset, M1 macrophage levels were significantly higher in ccRCC compared to normal kidney (Figure 4.10a,

0.068 ± 0.028 vs 0.024 ± 0.017, $p<0.0001$). In the matched pair analysis, 81 out of the 93 pairs were found to be significantly higher in ccRCC compared to normal kidney (Figure 4.10b, 0.0673 ± 0.017 vs 0.024 ± 0.017, $p<0.0001$). A very weak positive correlation between the two groups was found ($r=0.0525$) which was not found to be significant. No significant effect on overall survival was found between the M1 macrophage high and low groups (Figure 4.10c), however the low M1 group was found to have a longer median survival compared to the high group (116.75 months vs 92.97 months).

4.2.1.2 Natural Killer (NK) cells

We next looked at the innate immune cells which have cytotoxic roles against tumour cells, NK cells.

We firstly compared the estimated immune fraction of NK cells in the ccRCC data set compared to those in the normal kidney set. CIBERSORTx classes NK cells as either naïve, 'resting' NK cells which are in a quiescent state in the absence of activating signals, or 'activated' NK cells, following exposure to cytokines such as interleukin (IL)-, IL-12, IL-15, IL-18, IL-21 and IL-27. Upon resolution of inflammation, active NK cells return to the resting state, however chronic exposure to activating stimuli during viral infection, cytokine treatment or tumorigenesis can lead to NK cell exhaustion. Therefore, reversal of NK cell exhaustion is now a key goal in immunotherapy to boost antitumour immunity.

The full ccRCC data set was firstly compared to the normal kidney data set to determine any significant differences in both resting and activated NK cells, as shown in Figure 4.11.

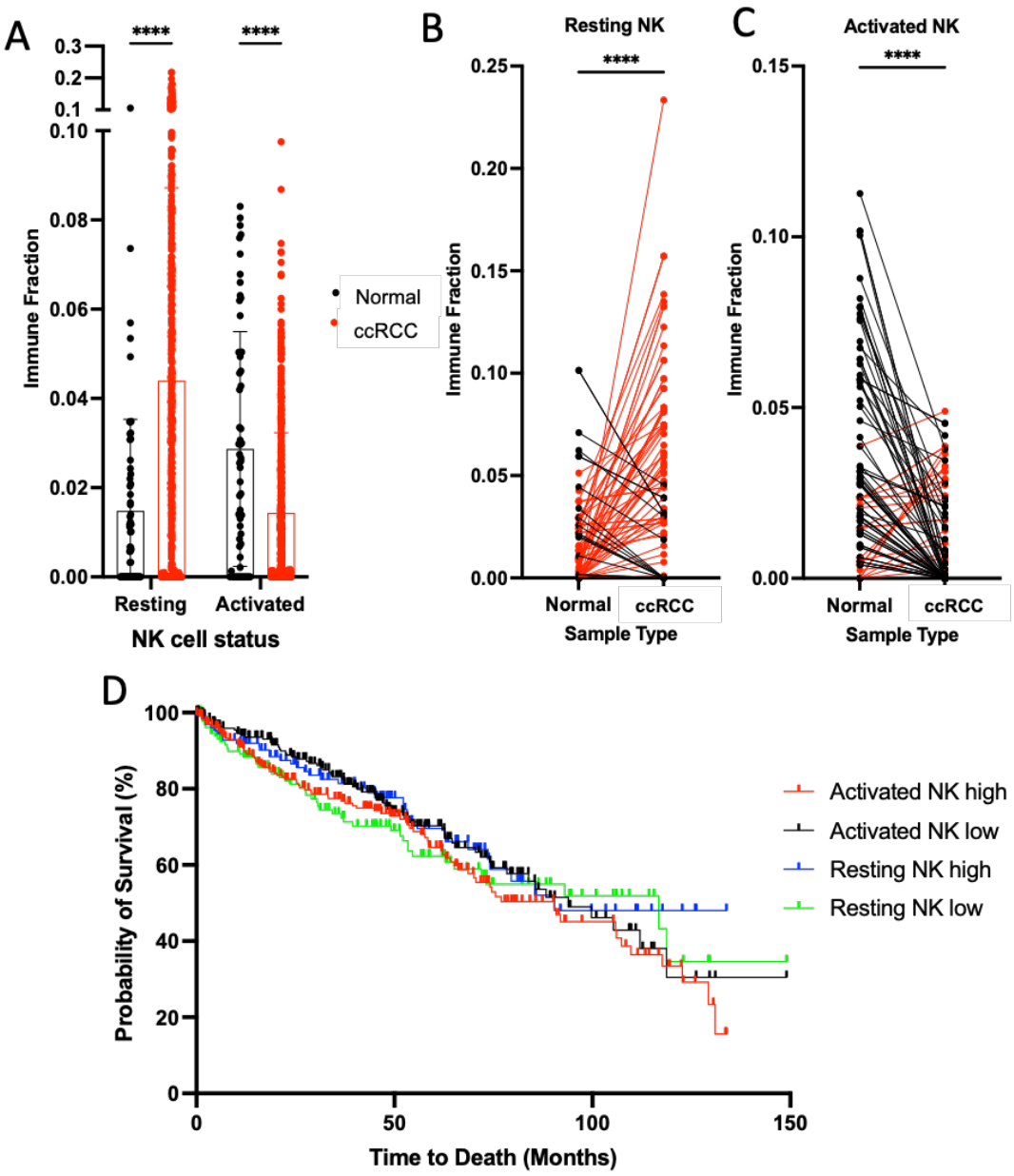

Figure 4.11 Resting and activated NK cells in the ccRCC dataset, matched pairs and survival analysis
(A) Normal kidney vs ccRCC full data set, (B) Matched pair analysis of resting NK cells, pairs higher in ccRCC are highlighted in red, those higher in normal kidney are in black, (C) Matched pair analysis of activated NK cells (D) Kaplan-Meier curves comparing high and low groups of activated and resting NK cells. Analysis was carried out using a Mann-Whitney test, Wilcoxon matched-pairs rank test and Logrank test respectively, where **** represents p <0.0001.

Comparison of the full ccRCC data set compared to normal kidney revealed that the estimated immune fraction of resting NK cells was significantly higher in the ccRCC group compared to the normal kidney group (Figure 4.11a, 0.044 ± 0.044 vs 0.015 ± 0.0211, p<0.0001). Conversely, activated NK cells were found to be significantly higher in the normal group compared to the ccRCC data set (0.031 ± 0.028 vs 0.013

± 0.017, p<0.0001). Matched pair analysis of the resting NK cells found that 60 out of the 93 pairs had higher levels in ccRCC compared to normal kidney (Figure 4.11b, 0.046 ± 0.046 vs 0.015 ± 0.021, p<0.0001), while 16 of the pairs were found to have zero values for both cell types. A significant weak positive correlation was also found between the two groups (r=0.2543, p=0.0072). Conversely, analysis of activated NK cells in the matched ccRCC and normal kidney samples found a higher estimated immune fraction in normal kidney compared to ccRCC, with 67 out of the 93 pairs reflecting this (Figure 4.11c, 0.031 ± 0.028 vs 0.010 ± 0.014, p<0.0001). 5 pairs were found to hold zero values for both cell types and a weakly positive correlation was also found between the two groups (r=0.1690), however this was not significant. These low levels of activated NK cells in the ccRCC samples are unexpected, as NK cells are the first line defence against tumour cells in the humoral immune response, so we would expect an increase in activated NK cells as the disease progresses. Kaplan-Meier analysis of overall survival data (Figure 4.11d) found no significant differences between the survival curves for resting NK cells, however median survival was higher in the low group compared to the high group (116.75 months vs 90.41 months). Activated NK cell level also did not have a significant effect on survival, however median survival was again slightly longer in the low group compared to the high group (93.92 months vs 90.41 months).

As we have observed unexpected results in the estimated immune fractions of activated and resting NK cells, we next explored the data further by splitting the full ccRCC dataset by stage to determine if there is a relationship between disease stage and levels of these cell types, as shown in Figure 4.12.

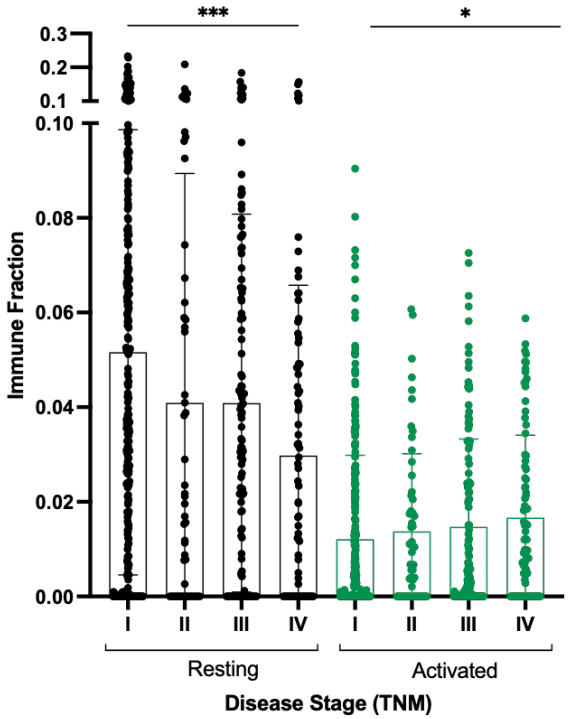

Figure 4.12 Estimated resting and activated NK immune fraction by ccRCC stage
The full ccRCC data set was split into stage and resting and activated NK cell fraction were compared using a Kruskal-Wallis test with Dunn's multiple comparisons test, where * represents $p < 0.05$ and *** represents $p < 0.001$.

By splitting the ccRCC samples by stage, we found that the estimated immune fraction of both resting and activated NK cells are inversely altered by disease stage. Resting NK cells were found to significantly decrease with increased stage, with stage I showing a significantly higher fraction compared to stage IV (0.051 ± 0.047 vs 0.029 ± 0.036, $p = 0.0002$). Conversely, activated NK cells were found to significantly increase with increased ccRCC stage, with stage IV showing significantly higher levels compared to stage I (0.016 ± 0.017 vs 0.012 ± 0.017, $p = 0.042$). This data implies that the ccRCC NK immune response is somewhat dysfunctional, as the cytotoxic active NK cell response which should be the body's first line defence against tumour cells appears to be delayed, and only begins to increase during late-stage disease. Interestingly however, the mean stage IV value for ccRCC was still found to be lower than the mean value for the normal kidney samples (0.0166 ± 0.0174 vs 0.0317 ± 0.0289).

To further understand the relationship of resting and activated NK cells within the same ccRCC sample, using Spearman's correlation analysis we next determined the correlation between resting and activated NK cells within each sample, as shown in Figure 4.13.

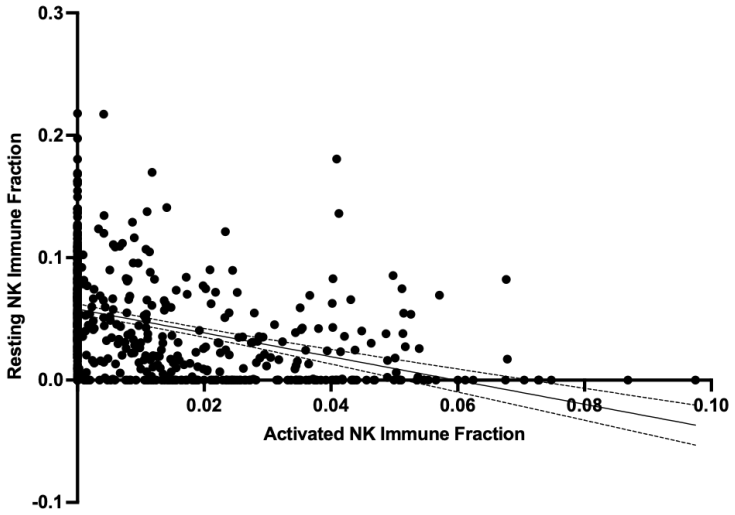

Figure 4.13 Correlation of resting vs activated NK cells in each ccRCC sample
Spearman correlation analysis found a moderately strong, significantly negative correlation between resting and activated NK cells (r=-0.523, p <0.0001).

A moderately strong, significant negative correlation was found between the resting and activated NK cell fractions within each ccRCC sample (r=-0.5230, p<0.0001), implying that as the levels of one cell type goes up, the other goes down, which may be in indicator of the strength of the cytotoxic immune response.

4.2.2 Cells of the adaptive immune system

The estimated immune fraction of naïve B cells and plasma cells which are part of the humoral immune system, and follicular T helper, cytotoxic T cells and regulatory T cells (Tregs) which are part of the cellular immune system were all found to be significantly altered in our ccRCC samples compared to normal kidney. We next investigated these cell types further to understand their effect on ccRCC patient survival.

4.2.2.1 B Cells

In this section we will study the levels of naïve B cells and plasma cells within the ccRCC data set, as we have already found a significant difference in the levels compared to normal kidney. No significant difference was found between the levels of memory B cells in ccRCC and normal kidney, so these will not be studied in this section.

4.2.2.1.1 Naïve B cells

We firstly looked at the expression of naïve B cells in the whole ccRCC group compared to the whole normal kidney group, in matched pairs and in survival analysis, as shown in Figure 4.14.

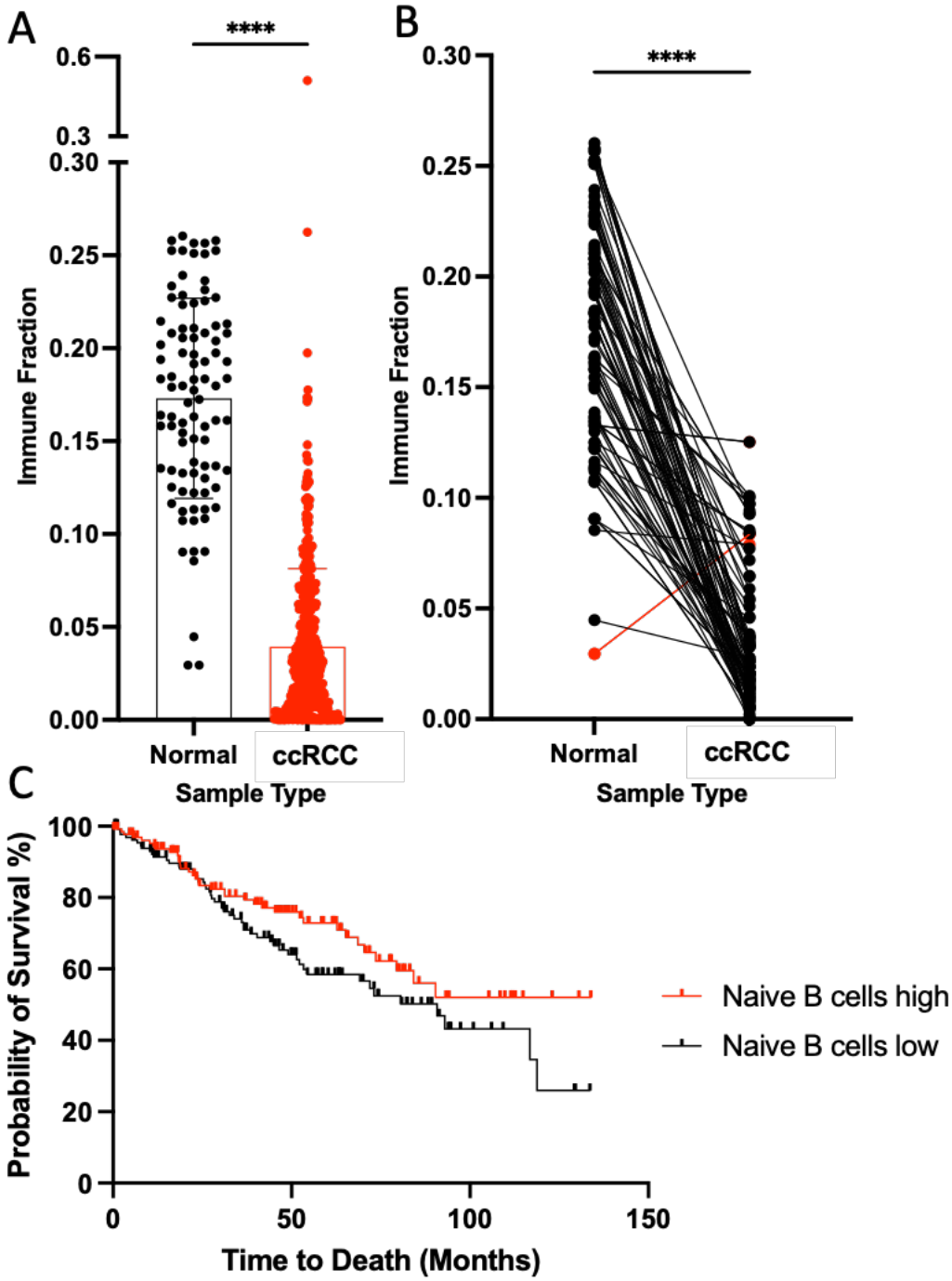

Figure 4.14 Naïve B cells in the ccRCC dataset, matched pairs and survival analysis
(A) Normal kidney vs ccRCC full data set, (B) Matched pair analysis, pairs higher in ccRCC are highlighted in red, those higher in normal kidney are in black, (C) Kaplan-Meier survival curves. Analysis was carried out using a Mann-Whitney test, Wilcoxon matched-pairs rank test and Logrank test respectively, where **** represents p <0.0001.

Comparison of the full ccRCC data set showed that the estimated immune fraction of naïve B cells was significantly higher in normal kidney compared to ccRCC (Figure 4.14a, 0.037 ± 0.040 vs 0.173 ± 0.053, p<0.0001). 90 out of the 92 matched pairs

were found to have higher levels of naïve B cells in normal kidney compared to ccRCC (Figure 4.14b, 0.173 ± 0.053 vs 0.034 ± 0.032, p = <0.0001), and a weak correlation was found between the two groups (r=-0.1377), however this was not significant. Kaplan-Meier analysis of overall survival data found no difference between the high and low groups of naïve B cells (Figure 4.14c). Median survival for the low group was 90.8 months, however median survival for the high group could not be calculated as more than 50% of patients were still alive by the end of the study. This may imply that high levels of naïve B cells could be beneficial to survival compared to low levels, and as the levels of naïve B cells were found to be significantly decreased compared to normal kidney, low levels of naïve B cells may contribute to ccRCC disease progression.

4.2.2.1.2 Plasma cells

We next looked at an example of differentiated B cells, plasma cells, in the ccRCC and normal samples to determine the differences in estimated immune fraction between the two groups.

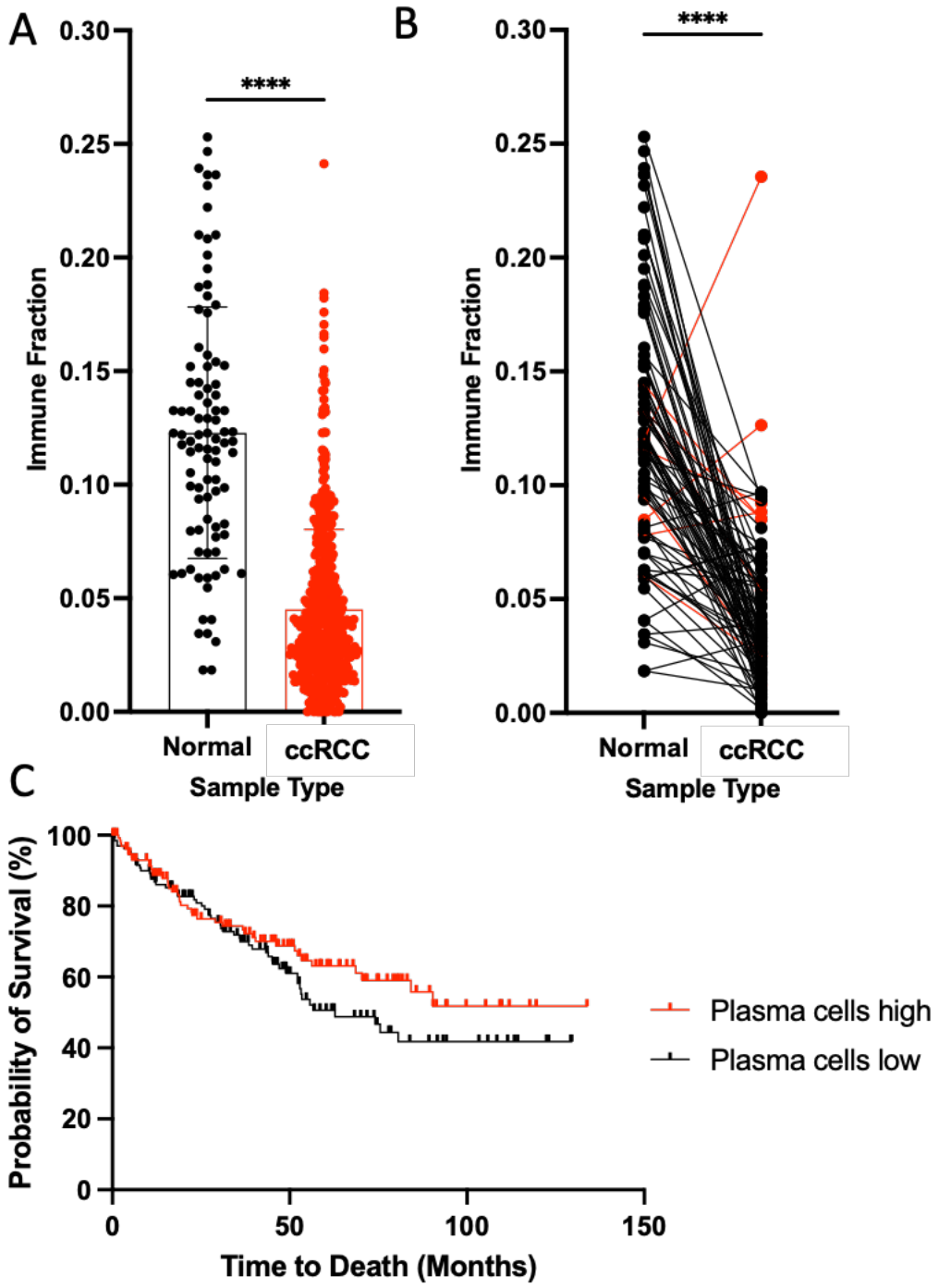

Figure 4.15 Plasma cells in the ccRCC dataset, matched pairs and survival analysis
(A) Normal kidney vs ccRCC full data set, (B) Matched pair analysis, pairs higher in ccRCC are highlighted in red, those higher in normal kidney are in black, (C) Kaplan-Meier survival curves. Analysis was carried out using a Mann-Whitney test, Wilcoxon matched-pairs rank test and Logrank test respectively, where **** represents p <0.0001.

As was the case for naïve B cells, the estimated immune fraction of plasma cells was found to be significantly higher in normal kidney compared to the whole ccRCC dataset (Figure 4.15a, 0.042 ± 0.033 vs 0.122 ± 0.055, p<0.0001). Within the

matched pair analysis (Figure 4.15b), 83 of the 92 pairs were also found to have higher levels of plasma cells in normal kidney compared to ccRCC (0.122 ± 0.055 vs 0.041 ± 0.033, p = <0.0001). A very weak negative correlation was found between the two groups (r=-0.063) which was not found to be significant. No significant differences between the survival curves for the high and low plasma cell groups were found (Figure 14.5c). The median survival for the low group was 62.81 months, however the median could not be defined for the high group as over 50% of patients were still alive at the end of the study.

4.2.2.2 T cells

The estimated immune fractions of the key T cell types Tfh cells, CTLs and Tregs, were found to be significantly altered in ccRCC compared to normal kidney, so we next investigated these cell types in further detail to determine their role in ccRCC development and patient survival. Other, less common subtypes of T cells such as memory CD4+ T cells and gamma delta T cells also make up a part of the adaptive immune response, however as these cell types were not found to have significant differences between ccRCC and normal kidney, we have not studied these cell types in this section.

4.2.2.2.1 Follicular T helper cells (Tfh)

We next aimed to study the effect of Tfh levels in our ccRCC samples to determine their role in development and overall survival.

We firstly looked at the estimated immune fraction of Tfh cells in our ccRCC and normal kidney data sets, matched pairs and survival analysis, as shown in Figure 4.16.

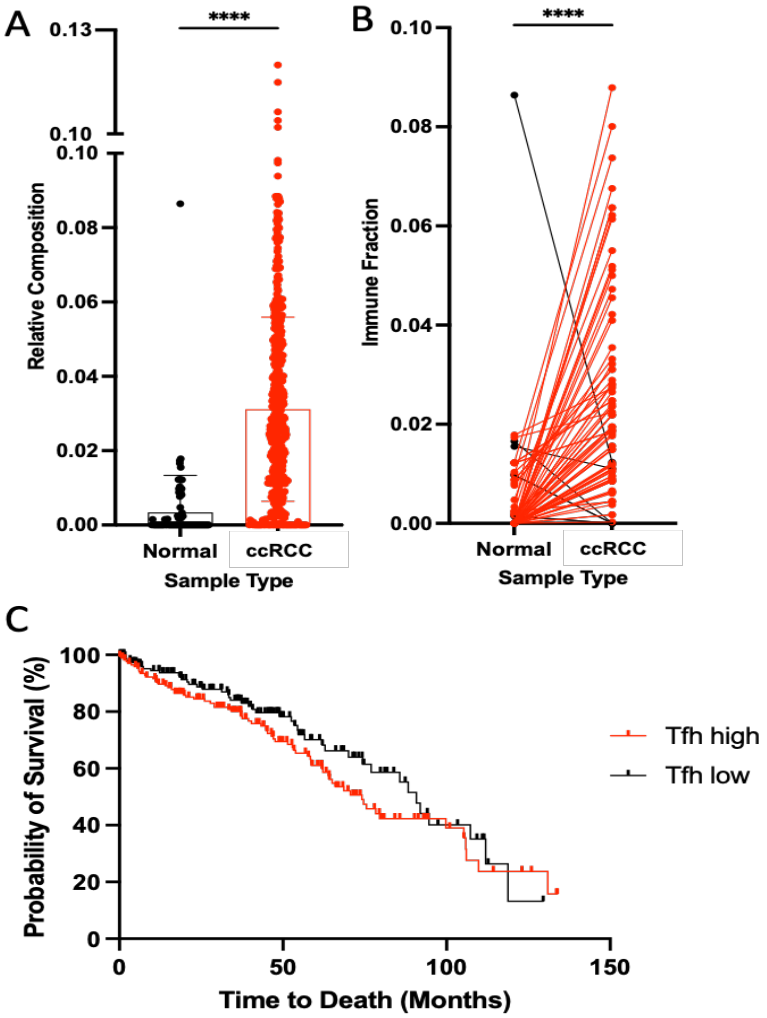

Figure 4.16 Tfh cells in the ccRCC dataset, matched pairs and survival analysis
(A) Normal kidney vs ccRCC full data set, (B) Matched pair analysis, pairs higher in ccRCC are highlighted in red, those higher in normal kidney are in black, (C) Kaplan-Meier survival curves. Analysis was carried out using a Mann-Whitney test, Wilcoxon matched-pairs rank test and Logrank test respectively, where **** represents p <0.0001.

Comparison of the full ccRCC data set compared to normal kidney revealed a significantly higher immune cell fraction of Tfh cells in ccRCC compared to normal kidney (Figure 4.16a, 0.0315 ± 0.0253 vs 0.0034 ± 0.0099, p<0.0001). Analysis of the matched ccRCC and normal kidney pairs also found this effect in 78 out of the 92 pairs (Figure 4.16b, 0.0214 ± 0.0203 vs 0.0034 ± 0.0099, p<0.0001), where a weakly positive correlation was also found between the two groups (r=0.1723) however this relationship was not found to be significant. No significant differences were found between the survival curves for high or low levels of Tfh cells (Figure 4.16c),

however median survival was found to be higher in the Tfh low group compared to the high group (90.8 months vs 74.15 months).

As Tfh levels have been shown to be associated with a good prognosis in some cancer types but with a poor prognosis in others, we next looked at Tfh cell level by ccRCC stage to determine if there was a relationship between immune cell fraction and disease stage, as shown in Figure 4.17.

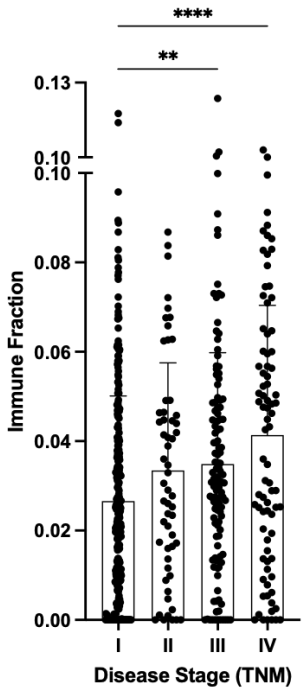

Figure 4.17 Estimated Tfh immune fraction by ccRCC stage
The full ccRCC data set of Tfh estimated immune fraction was split into stage and the groups were compared using a Kruskal-Wallis test with Dunn's multiple comparison test, where ** represents p <0.01 and **** represents p <0.001.

A significant increase in Tfh cell level was associated with increased Tfh cell stage, with both stage III showing significantly higher levels compared to stage I (0.0349 ± 0.0249 vs 0.0265 ± 0.0235, p=0.0046), and stage IV compared to stage I (0.0413 ± 0.029 vs 0.0265 ± 0.0235, p<0.0001). This data links to what we have observed in the survival analysis, where high Tfh levels were found to have a shorter median than the low group.

As Tfh cells also play a key role in the activation of CD8+ cytotoxic T cells (CTLs), we next studied these cells in our samples to determine the role of these cells in ccRCC development and overall survival compared to normal kidney.

4.2.2.2.2 Cytotoxic T cells (CTLs)

As we have already shown an overexpression of Tfh cells in ccRCC compared to normal kidney and a resulting negative association with prognosis, we next aimed to determine the differences in estimated immune infiltrate of CTLs in ccRCC compared to normal kidney, and their effect on overall survival.

We firstly looked at the levels of CTLs in the full ccRCC data set compared to the normal kidney, matched pairs and survival analysis, as shown in Figure 4.18.

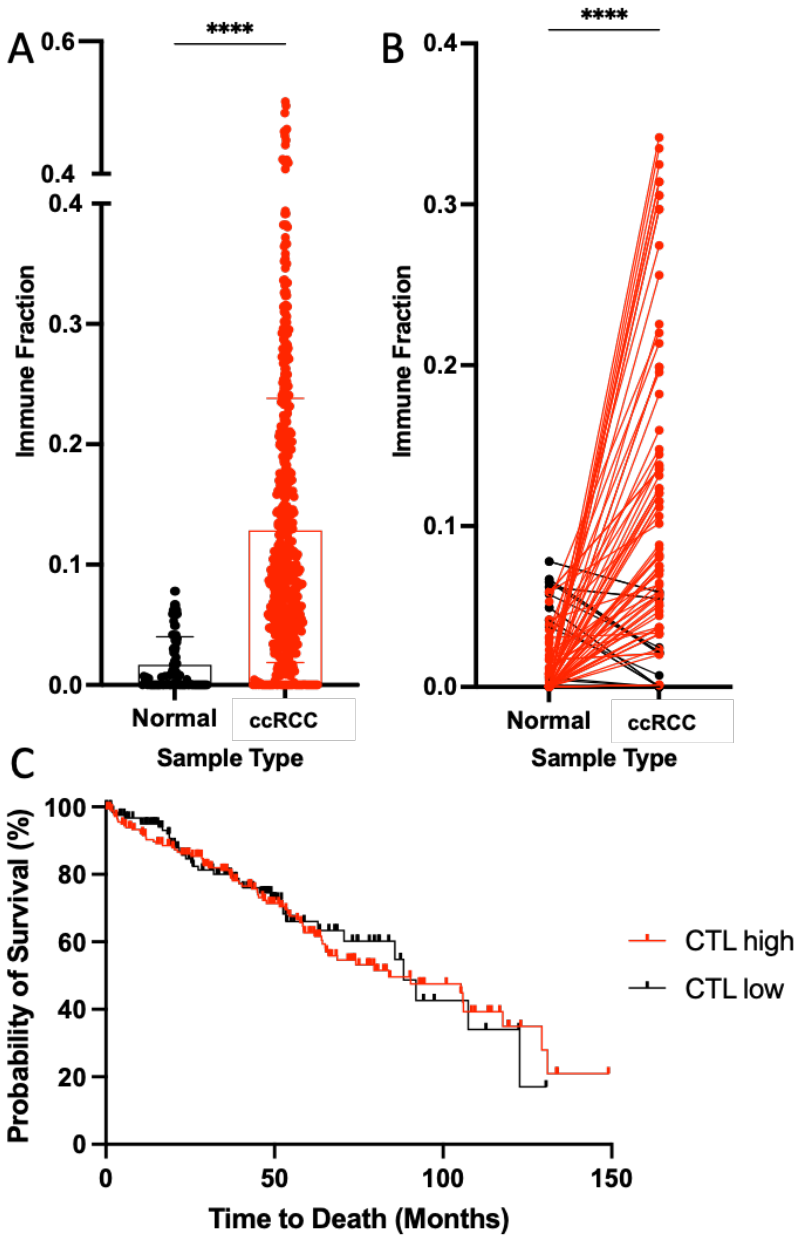

Figure 4.18 CTLs in the ccRCC dataset, matched pairs and survival analysis
(A) Normal kidney vs ccRCC full data set, (B) Matched pair analysis, pairs higher in ccRCC are highlighted in red, those higher in normal kidney are in black, (C) Kaplan-Meier survival curves. Analysis was carried out using a Mann-Whitney test, Wilcoxon matched-pairs rank test and Logrank test respectively, where **** represents p <0.0001.

The estimated CTL immune fraction was significantly higher in ccRCC compared to normal kidney (Figure 4.18a, 0.1284 ± 0.1099 vs 0.0167 ± 0.0233, p<0.0001), while 73 out of the 92 pairs of ccRCC and normal kidney samples were found to be higher in the ccRCC group compared to the normal kidney group (Figure 4.18b, 0.1005 ± 0.0948 vs 0.0167 ± 0.0233, p<0.0001). A weakly negative correlation was found

between the two groups (r=-0.1473); however, this was not found to be significant. No significant differences between the survival curves were found for the high and low groups of CTLs (Figure 4.18c), however median survival was slightly longer in the low group compared to the high group (88.3 months vs 83.9 months). While this result is unexpected, as the anti-tumour immune response provided by the CTLs would be expected to increase survival, this may indicate a dysfunctional and/or exhausted CTL state in later disease stages resulting in an ineffective cytotoxic response, in line with what has been reported in previous studies (Nakano et al. 2001).

To determine if this could be the case, we next examined CTLs by ccRCC disease stage, as shown in Figure 4.19.

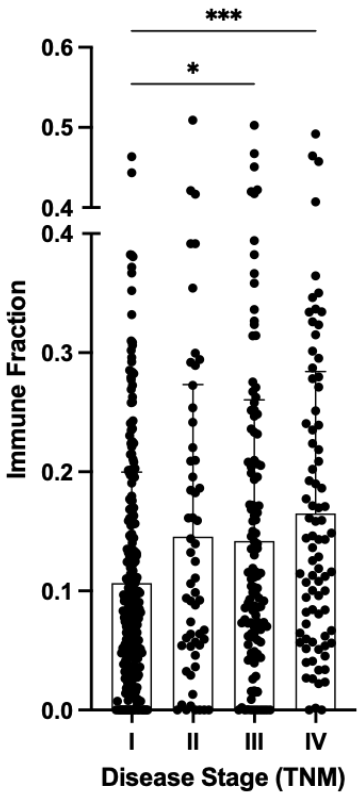

Figure 4.19 Estimated CTL immune fraction by ccRCC stage
The full ccRCC data set of CTL estimated immune fractions was split into stage and groups were compared using a Kruskal-Wallis test and Dunn's multiple comparison test, where * represents p <0.05 and *** represents p <0.001.

As we observed in the stage analysis for the Tfh cells, CTL levels were also found to increase with stage, with stage III showing significantly higher levels than stage I (0.1420 ± 0.1184 vs 0.1065 ± 0.0933, p=0.0343) as did stage IV (0.1650 ± 0.1191 vs

0.1065 ± 0.0933, p=0.0002). This may imply a dysfunctional and/or exhausted CTL state at a higher ccRCC disease stage.

4.2.2.2.3 CD4:CD8 Ratio

The CD4:CD8 ratio is used to determine the state of the immune system, with a ratio over 1 considered normal.

As CIBERSORTx provides only immune fractions rather than absolute cell numbers, we were not able to calculate the CD4:CD8 ratio for our samples, however Spearman correlation analysis, Kaplan-Meier survival analysis and Cox proportional hazards regression was used to calculate the relationship between the immune fractions of the two cell types in each of the ccRCC samples, as shown in Figure 4.20.

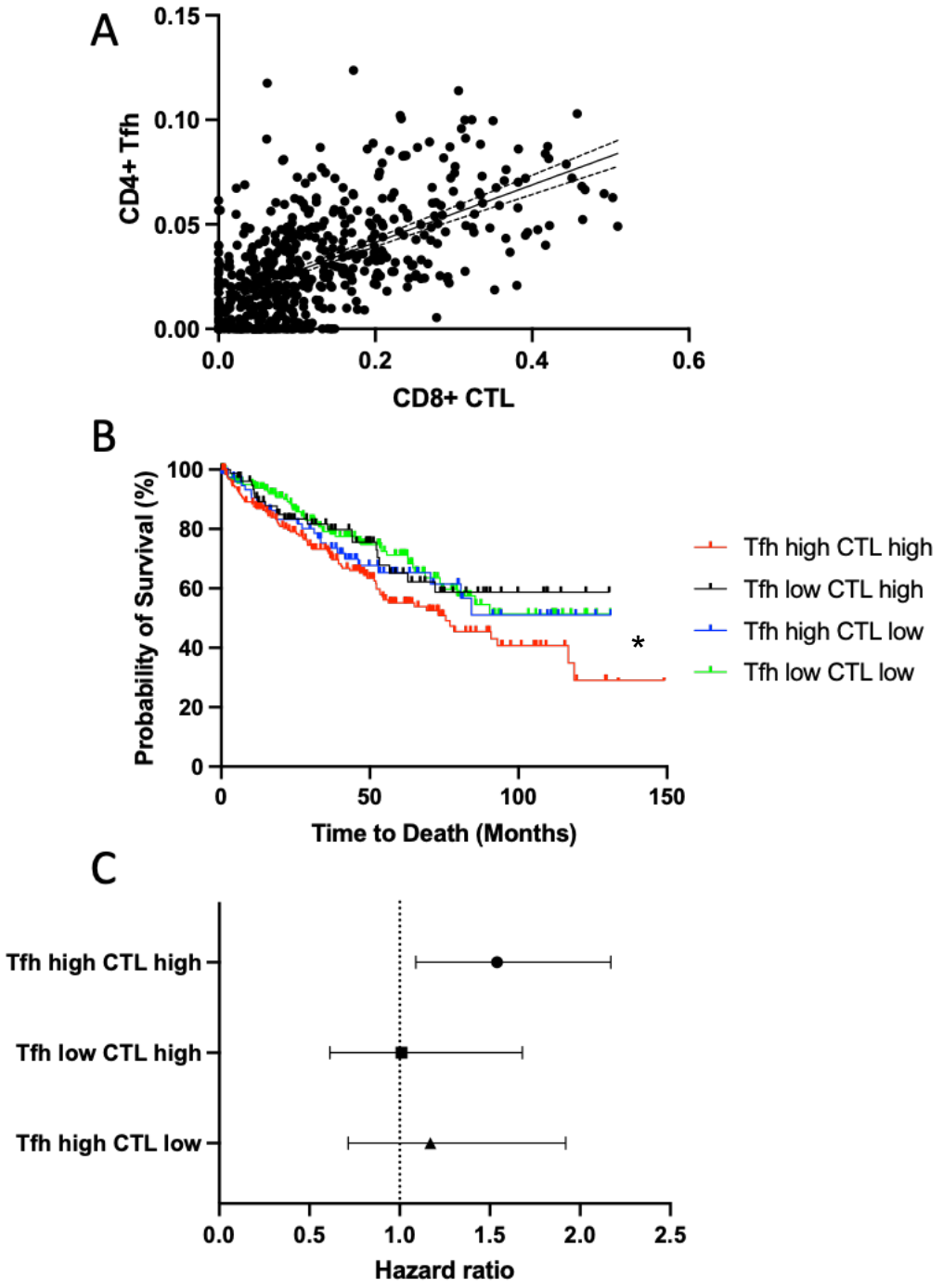

Figure 4.20 Analysis of the CD4:CD8 ratio in ccRCC samples
(A) Spearman correlation analysis found a strong, significant correlation between TfH CD4+ cells and CTL CD8+ cells within the same sample, r = 0.593, p <0.0001. (B) Logrank analysis of Kaplan-Meier curves found the Tfh_{high} CTL_{high} group had significantly shorter median survival compared to the Tfh_{low} CTL_{low} group, p = 0.014, * represents p <0.05. (C) Cox proportional hazards regression using the Tfh_{low} CTL_{low} group as baseline found the greatest increased risk in the Tfh_{high} CTL_{high} group.

A significant strong positive correlation was found between Tfh cells and CTL (Figure 4.20a, r=0.5937, p<0.0001), which implies that as Tfh levels increase, so do CTL levels. These increases would be expected to result in an overall increase of cytotoxic immune response and therefore implies a positive effect on prognosis. As

this has however not been the case when we have previously looked at both Tfh cells and CTLs separately, we next used survival analysis to compare overall survival statistics for combinations of high and low levels of these cell types (Figure 4.20b). Median survival could only be calculated for the Tfh_{high} CTL_{high} group (median survival 75.53 months), the combination which had the worst survival outcome, as in the other groups more than 50% of patients were still alive by the end of the study. Survival curve comparison revealed that the only significant difference between any of the groups was that the Tfh_{high} CTL_{high} group had a significantly lower chance of survival compared to the Tfh_{low} CTL_{low} group ($p=0.0145$), which implies that both Tfh and CTL cells must be found at high or low levels to have a significant positive or negative prognostic impact. HRs for each combination were next determined using the Tfh_{low} CTL_{low} group as a baseline (Figure 4.20c). HRs above 1 indicate that this factor poses a risk to survival, and as expected, he Tfh_{high} CTL_{high} group was found to have the highest risk compared to the Tfh_{low} CTL_{low} group (HR 1.54, 95% CI 1.09 to 2.17), closely followed by the Tfh_{high} CTL_{low} group (HR 1.17, 95% CI 0.714 to 1.92).

4.2.2.2.4 Regulatory T cells (Tregs)

We next investigated the effect of Treg levels on clinical outcome in our data set.

We firstly looked at the levels of Tregs in the full ccRCC data set compared to the normal kidney, matched pairs and survival analysis, as shown in Figure 4.21.

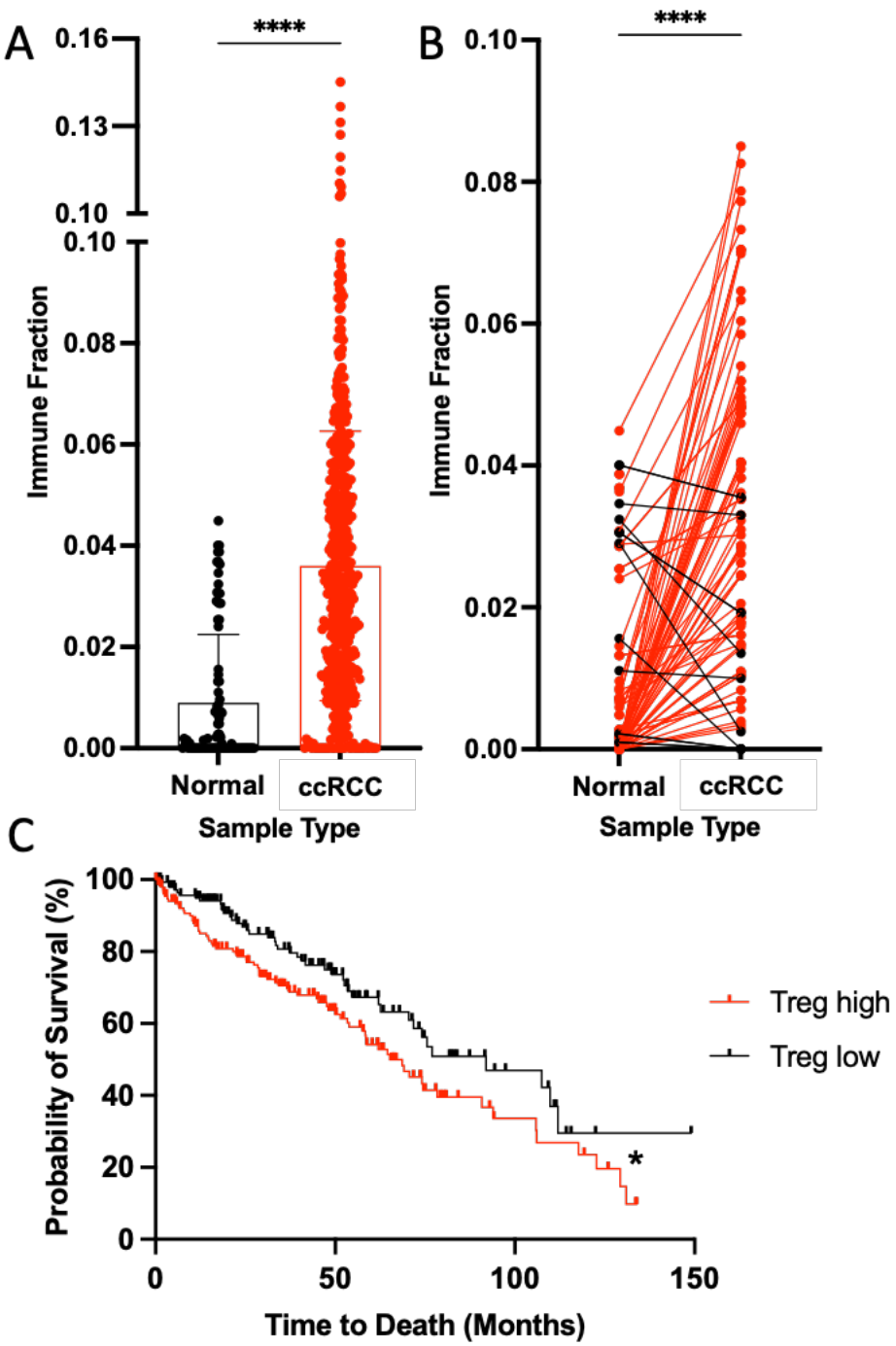

Figure 4.21 Tregs in the ccRCC dataset, matched pairs and survival analysis
((A) Normal kidney vs ccRCC full data set, (B) Matched pair analysis, pairs higher in ccRCC are highlighted in red, those higher in normal kidney are in black, (C) Kaplan-Meier survival curves. Analysis was carried out using a Mann-Whitney test, Wilcoxon matched-pairs rank test and Logrank test respectively, where **** represents p <0.0001.

The Treg estimated immune fraction was significantly higher in the full ccRCC data set compared to normal kidney (Figure 4.21a, 0.0360 ± 0.0265 vs 0.0089 ± 0.0135, p<0.0001), and 72 of the 92 matched pair samples were also found to have significantly higher levels of Tregs in ccRCC compared to normal (Figure 4.21b,

0.0367 ± 0.0276 vs 0.0089 ± 0.0135, p<0.0001). A weakly positive but not significant correlation was also found between the two groups (r=0.1223). Analysis of the survival curves (Figure 4.21c) revealed a significant difference in overall survival, where the high Treg group is associated with a significantly shorter survival time compared to the low group (median survival 65.24 months vs 91.95 months, p=0.0123).

As it has previously been reported that Treg infiltration increases with ccRCC stage, we also wanted to determine if this is the case for our samples, as shown in Figure 4.22.

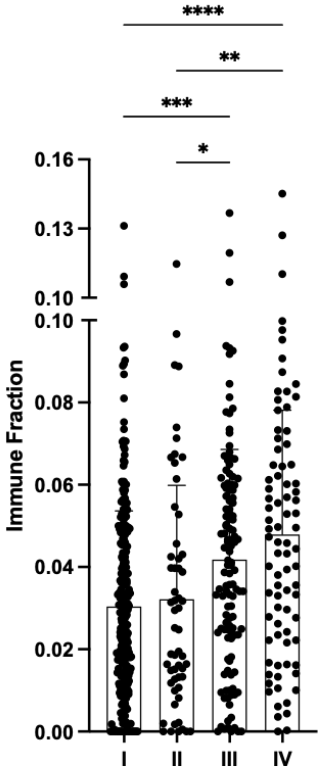

Figure 4.22 Estimated Treg immune fraction by ccRCC stage
The full ccRCC data set for Treg estimated immune fraction was split into stage and groups were compared using a Kruskal-Wallis test and Dunn's multiple comparisons test, where * represents p <0.05, ** represents p <0.01, *** represents p <0.001 and **** represents p <0.0001.

A significant increase in Treg estimated immune fraction was found with increased ccRCC stage, with stage III showing significantly higher levels of Tregs compared to both stage I (0.0418 ± 0.0268 vs 0.0304 ± 0.0232, p=0.0002), and stage II (0.0418 ± 0.0268 vs 0.0321 ± 0.0277, p=0.0486). Stage IV also had significantly higher Treg levels than both stage I (0.0479 ± 0.0301 vs 0.0304 ± 0.0232, p<0.0001) and stage II (0.0479 ± 0.0301 vs 0.0321 ± 0.0277, p=0.0032).

4.2.2.2.5 CD8:Treg Ratio

As we have already shown significant increases in estimated immune fraction of both CD8+ CTLs and Tregs in our ccRCC samples compared to normal kidney, we next aimed to determine if the CD8:Treg ratio has an effect on ccRCC outcome. As previously mentioned, CIBERSORTx is only able to calculate an estimated immune fraction rather than absolute cell number, so Spearman correlation analysis was used to determine a relationship between Tregs and CTLs, rather than calculating a ratio, as shown in Figure 4.23.

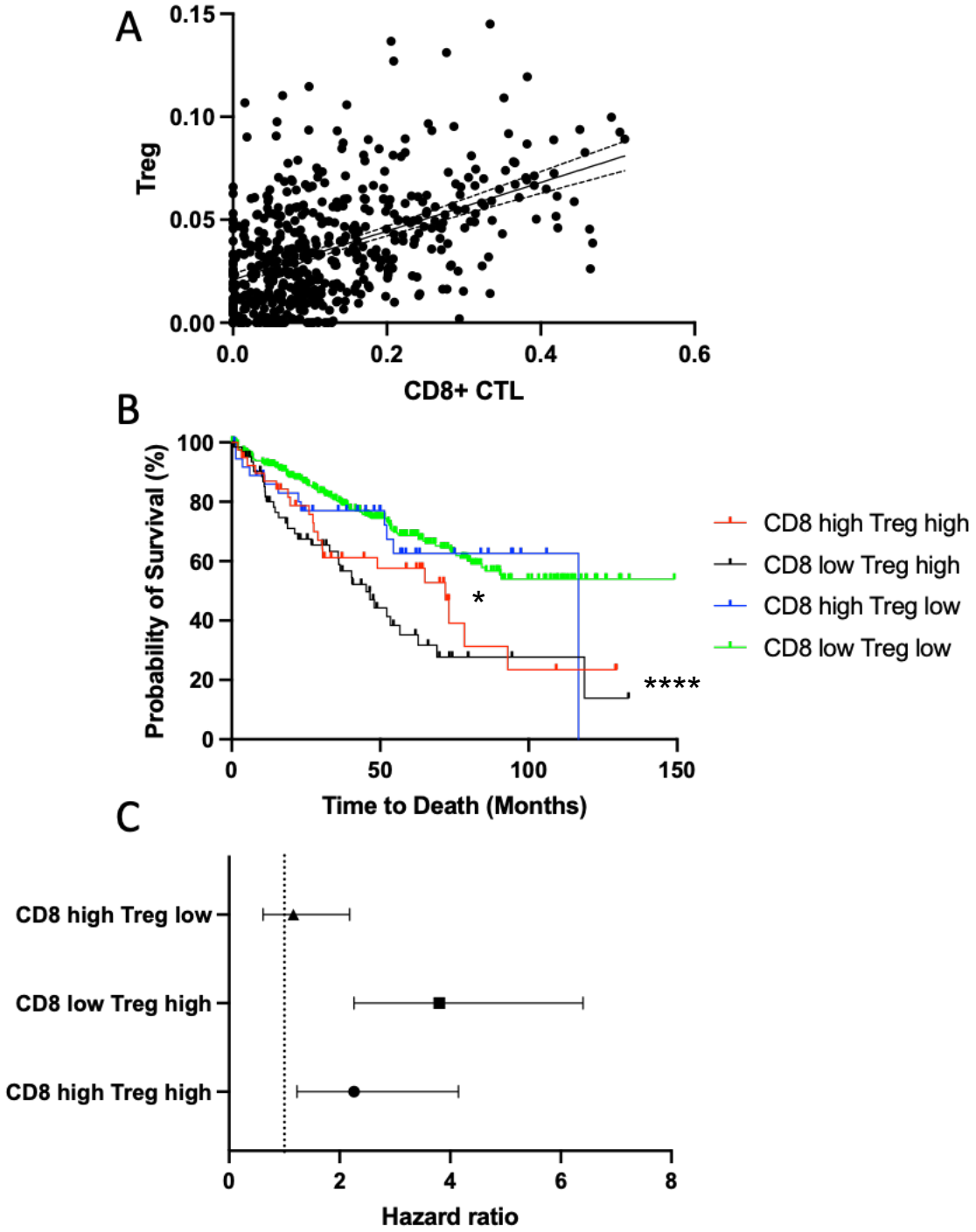

Figure 4.23 Analysis of the CD8:Treg ratio in ccRCC samples
(A) Spearman correlation analysis found a moderately strong, significant correlation between CTL CD8+ cells Tregs within each sample, r = 0.463, p < 0.0001. (B) Logrank comparison of Kaplan-Meier survival curves found the CTL_{low} $Treg_{low}$ group had significantly higher median survival compared to the CTL_{high} $Treg_{high}$ group (p = 0.022) and the CTL_{low} $Treg_{high}$ group (p <0.0001), * represents p < 0.05, **** represents p < 0.0001, (C) Cox proportional hazards regression using the CTL_{low} $Treg_{low}$ group as baseline found the greatest increased risk in the $CD8_{low}$ $Treg_{high}$ group.

Spearman correlation analysis found a significant, moderately strong positive correlation between the CTL and Treg groups (Figure 4.23a, r=0.4631, p<0.0001), implying that generally as levels of one cell type increases, so does the other. However, as this is not a perfect correlation, one cell type may increase more than the other which may have then an impact on the CD8:Treg ratio, resulting in an altered immune response. Based on this, we next examined if the CD8:Treg ratio has an impact on patient OS, and we compared the survival data for high and low groups of both cell types. The estimated immune fraction of CTLs compared to Tregs was found to have a significant impact on patient survival. The CTL_{low} $Treg_{high}$ group had a shorter median survival compared to the CTL_{high} $Treg_{high}$ and the CTL_{high} $Treg_{low}$ groups (45.27 months vs 71.94 months and 116.75 months respectively). Interestingly, although this group contained around half of the total number of samples, median survival was not able to be calculated for the CTL low Treg low group as over 50% of the patients were still alive by the end of the study. Comparison of the survival curves revealed that the CTL_{low}, $Treg_{low}$ group had a significantly better chance of survival compared to both the CTL_{high} $Treg_{high}$ group (p=0.0224) and the CTL_{low} $Treg_{high}$ group (p<0.0001). HRs were then determined for each combination using the CTL_{low} $Treg_{low}$ group as a baseline, with the CTL_{low} $Treg_{high}$ group showing the greatest HR (HR 3.8, 95% CI 2.26 to 6.4), followed by CTL_{high} $Treg_{high}$ (HR 2.26, 95% CI 1.23 to 4.14).

We have already shown that the relationship between Tfh and CTLs as an indicator of CD4:CD8 ratio, and the relationship between CTLs and Tregs as an indicator of CD8:Treg ratio are associated with significant effects on patient overall survival. We next examined the relationships between all of our key immune cell types which were found to be significantly altered in ccRCC compared to normal kidney with each other.

4.2.3 Immune cell hazard ratios and correlations

In this chapter we have so far shown that 9 out of the 22 immune cell types calculated by CIBERSORTx have significantly altered estimated immune fractions in ccRCC compared to normal kidney, and that each of these has an effect on the overall immune infiltrate, patient survival and prognosis.

HRs for high levels of each cell type compared to low levels were generated to determine which cell types pose the greatest risk to survival, as shown in Figure 4.24.

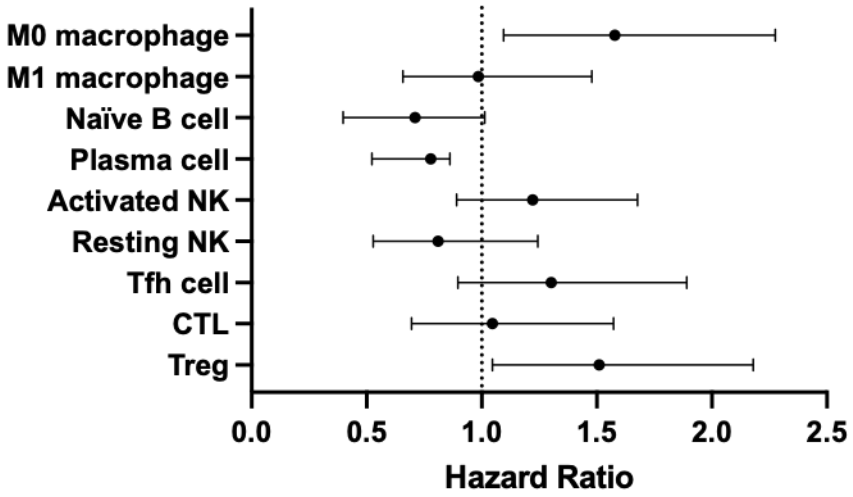

Figure 4.24 Hazard ratios for high levels of immune cells vs low levels
Cox proportional hazard regression was used to calculate HR score for high levels of each immune cell type compared to low levels which were used as the baseline for each cell type. High levels of M0 macrophages were found to have the highest HR, closely followed by Tregs.

High levels of M0 macrophages were found to incur the greatest risk to patient survival (Figure 4.24, HR 1.578, 95% CI 1.095 to 2.276), closely followed by Tregs (HR 1.510, 95% CI 1.047 to 2.180). As expected, the cell types with the lowest HRs were naïve B cells (HR 0.710, 95% CI 0.397 to 1.014) and plasma cells (HR 0.778, 95% CI 0.522 to 0.862) in line with what we have previously discussed, where high levels of these cell types are considered normal and so impose a low risk to survival. Interestingly, high activated NK cells were found to have an increased risk (HR 1.222, 95% CI .891 to 1.677) compared to resting NK cells which were found to be protective (HR 0.810, 95% CI 0.52*8* to 1.244), again showing the notable difference between the resting and activated state of NK cells.

The anti-tumour immune response is highly complex as each immune cell type may interact with many others to produce either a direct effector response or to activate other cells to create a response, so we next wanted to see how our key cell types

correlate together in both the normal kidney samples and in the ccRCC samples, as shown in Figure 4.25.

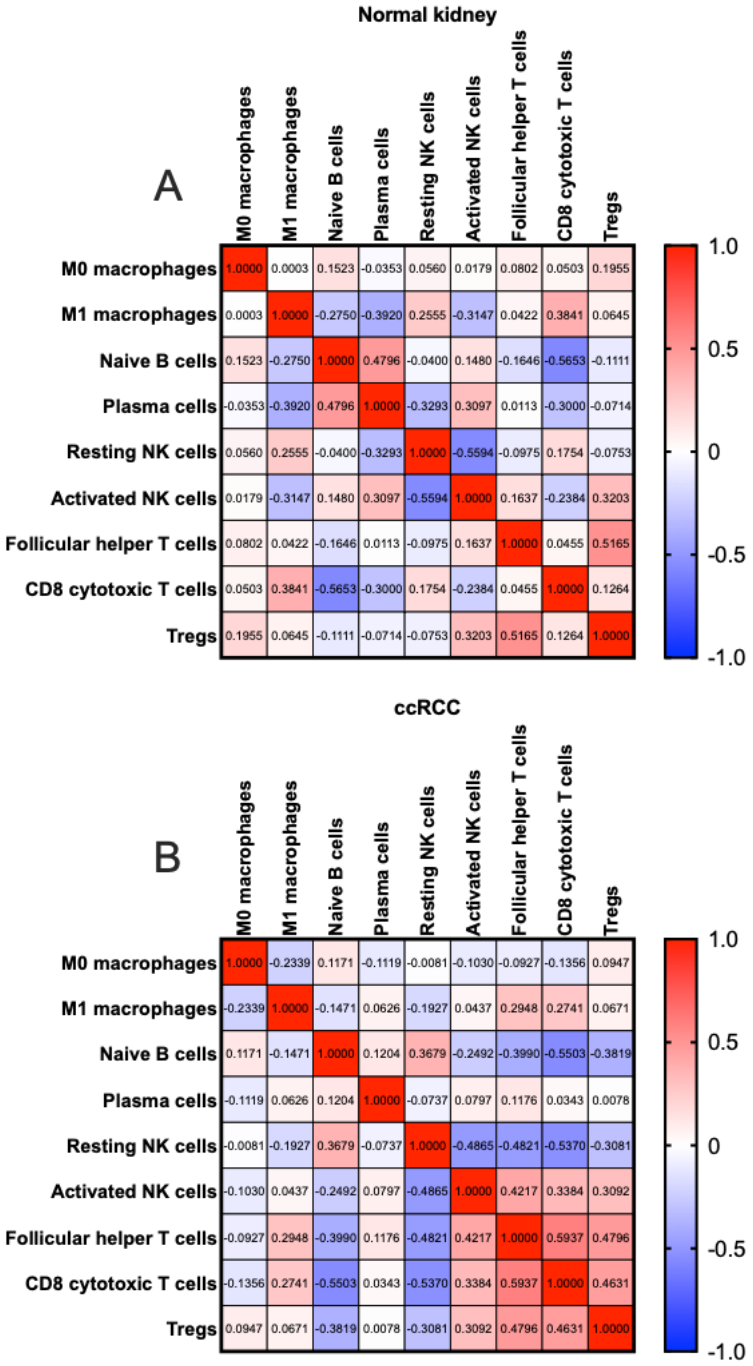

Figure 4.25 Spearman correlations of 9 key immune cells in normal kidney and ccRCC. The estimated immune fraction for the 9 key immune cells within the normal kidney or ccRCC group were compared using Spearman correlation analysis. Red represents a positive correlation and blue represents a negative correlation. (A) Normal kidney correlations, (B) ccRCC correlations. r values are represented within each box.

Spearman correlation analysis of the 9 significant immune cell types of interest within the normal kidney and ccRCC dataset sets revealed obvious differences between the two datasets. Within the normal dataset (Figure 4.25a), the strongest positive correlations were found between naïve B cells and plasma cells (r=0.4796, p<0.0001) and between Tfh cells and Tregs (r=0.5165, p<0.0001). This result is expected as these positive relationships are important to maintain normal immune function while preventing autoimmunity. The strongest negative associations were found between naïve B cells and CTLs (r=-0.5653, p<0.0001) and between resting and activated NK cells (r=-0.5594, p<0.0001). As we have already shown that in normal kidney, estimated immune fractions of naïve B cells were significantly higher than in ccRCC, while CTLs are significantly lower, this relationship suggests a possible link between the levels of these two cell types in normal kidney.

In the ccRCC samples (Figure 4.25b), the positive relationship between naïve B cells and plasma cells was found to be much weaker (r=0.1204, p=0.005), implying that the positive relationship is skewed, which was expected as we have already discussed a significant decrease in estimated immune fraction in both cell types in ccRCC compared to normal kidney. In the ccRCC samples, moderately strong positive relationships were found between our key T cell types with activated NK cells: Tfh cells (r=0.4217, p<0.0001), CTLs r=0.3384, p<0.0001), and Tregs r=0.3092, p<0.0001). Interestingly however, opposite but similar strength negative relationships found between these T cell types and resting NK cells: Tfh cells (r=-0.4821, p<0.0001), CTLs r=-0.5370, p<0.0001), and Tregs r=-0.3081, p<0.0001), implying an overall negative correlation between resting NK cells and effector T cells. As was found in the normal samples, a moderately strong negative relationship was also found between resting and activated NK cells in the ccRCC samples (=-0.4865, p<0.0001), however interestingly this relationship was not quite as strong, once again showing that the relationships between these key immune cell types is different in the ccRCC disease state compared to that of normal kidney.

As the strongest negative and positive correlations between the cell types appear to be between the effector T cells and resting and activated NK cells, we chose to focus on these cell types only going forward to determine what other patient characteristics may influence the estimated immune fraction of these cell types in ccRCC.

4.2.4 Immune cell fractions based on patient characteristics

We have already shown that patient characteristics such as age, sex and tumour laterality can affect overall survival generally in our data sets, however we have not yet determined if these characteristics have any effect on immune infiltrate, which may contribute to the patient survival. We firstly looked at the estimated immune fraction of resting and activated NK cells, Tfh, CTL and Tregs by sex, to determine if any differences could be found, as shown in Figure 4.26.

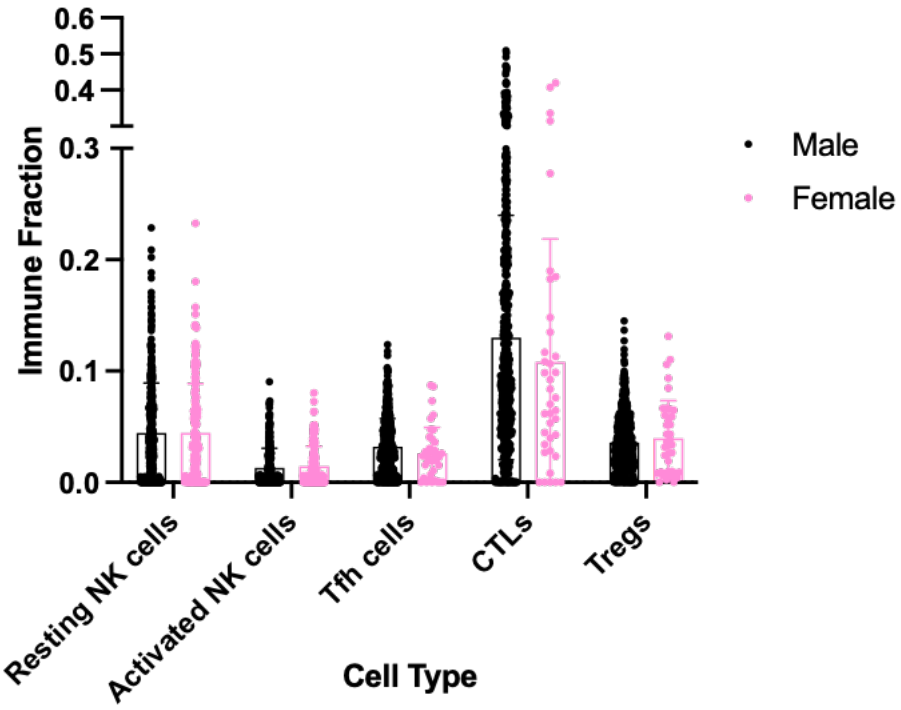

Figure 4.26 Immune cells by patient sex
The estimated immune fractions of the key 5 immune cells were compared by patient sex. Analysis was completed using a Mann-Whitney test; however, no significant differences were found between any of the groups.

The estimated immune fractions for all cell types were found to be similar between males and females in all immune cell types, with no significant differences observed between the groups. This could however be due in part to the smaller number of female samples compared to the males (118 female vs 345 male).

We next examined the immune cell fractions by patient age at operation to determine if any differences were apparent between the groups split by decade, as shown in Figure 4.27.

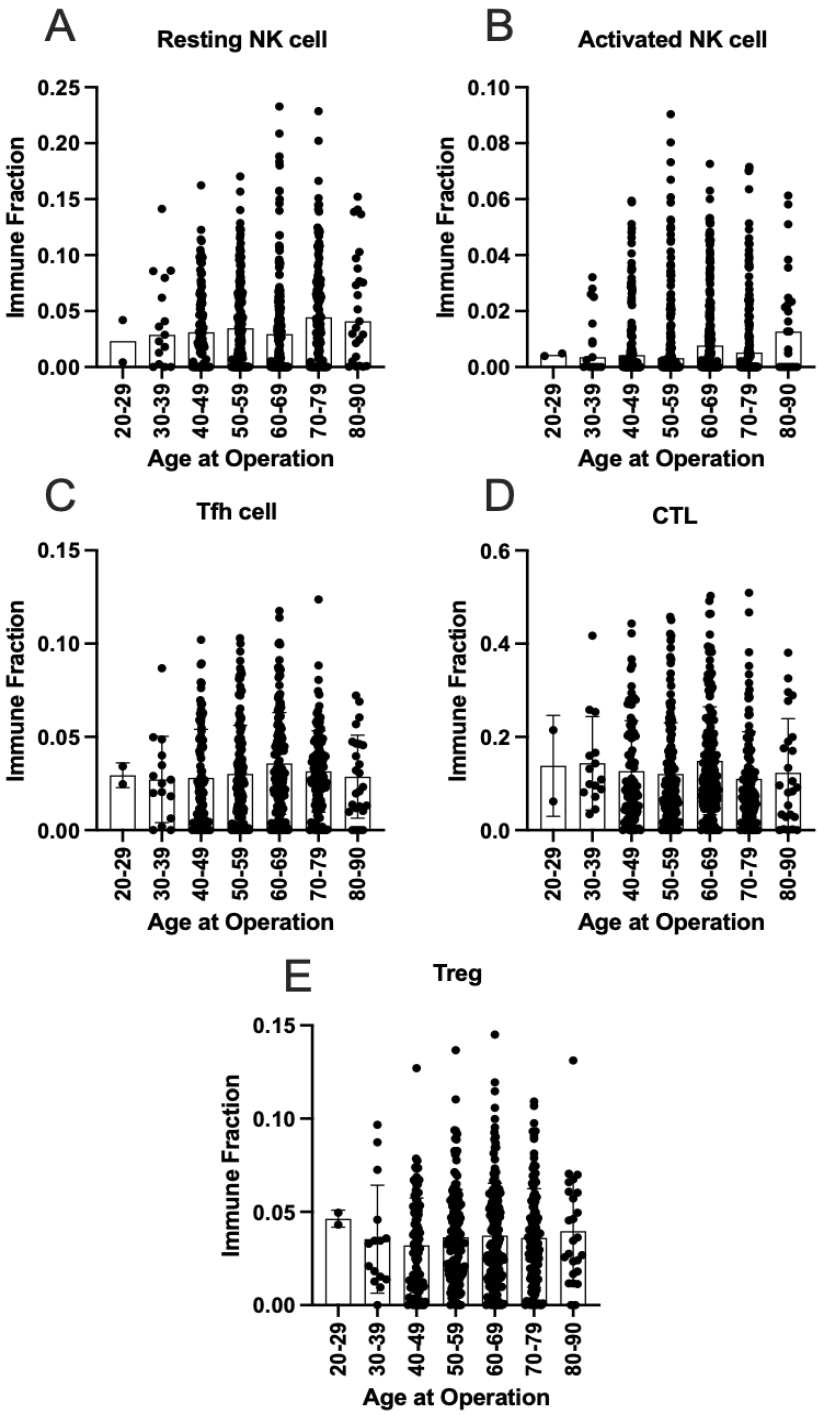

Figure 4.27 Immune cells by patient age at operation
(A) Resting NK cells by age at operation, (B) Activated NK cells, (C) Tfh cells, (D) CTLs, (E) Tregs. Analysis was completed using a Kruskal-Wallis test with Dunn's multiple comparisons test; however, no significant results were found.

No significant differences in estimated immune fraction were found between any of the age groups studied (Figure 4.27a-e). In our previous analysis, we found a significantly decreased chance of survival was associated with increased age, with

the 70-79 age group showing a significantly lower survival chance compared to the 40-49 age group (Figure 4.1b), however this difference does not seem to be associated with the levels of NK, Tfh, CTL or Treg cells.

As we have also shown that tumour laterality had a significant impact on patient survival, with left-sided tumours having significantly lower probability of survival compared to right-sided tumours (Figure 4.1d), we next looked at immune cells by tumour laterality to determine if any differences were present between these groups, as shown in Figure 4.28.

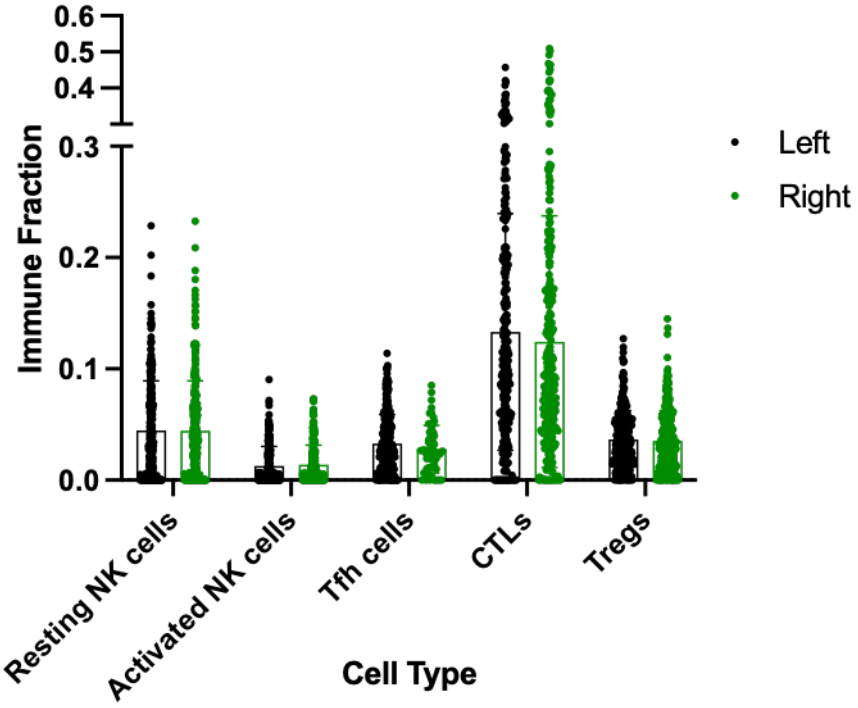

Figure 4.28 Immune cells by primary tumour laterality
Estimated immune fraction for the key 5 immune cell type was compared by primary tumour laterality. Analysis between groups was completed using a Mann-Whitney test, however no significant differences were found between any groups.

As was the case for sex and age, no significant differences in immune cell level were found when comparing the left- and right-sided tumour groups, with the two groups having a similar number of samples (251 left-sided vs 281 right-sided).

4.2.5 Characterising the ccRCC immune signature

Combining all of the data from this chapter so far, we have found that samples with high Tfh cell, CTL, Treg and resting NK cell estimated immune fractions combined

with low fractions of activated NK cells were generally higher ccRCC stage and had shorter overall survival. We define this as a 'high effector T cell' immune signature due to the high levels of effector T cells present in these samples, compared to the opposite group which can be defined as the 'low effector T cell' signature group. We next aimed to determine what effect this high effector signature has on patient overall survival compared to the opposite low signature, which is more suggestive of the conditions found in normal kidney tissue, as shown in Figure 4.29.

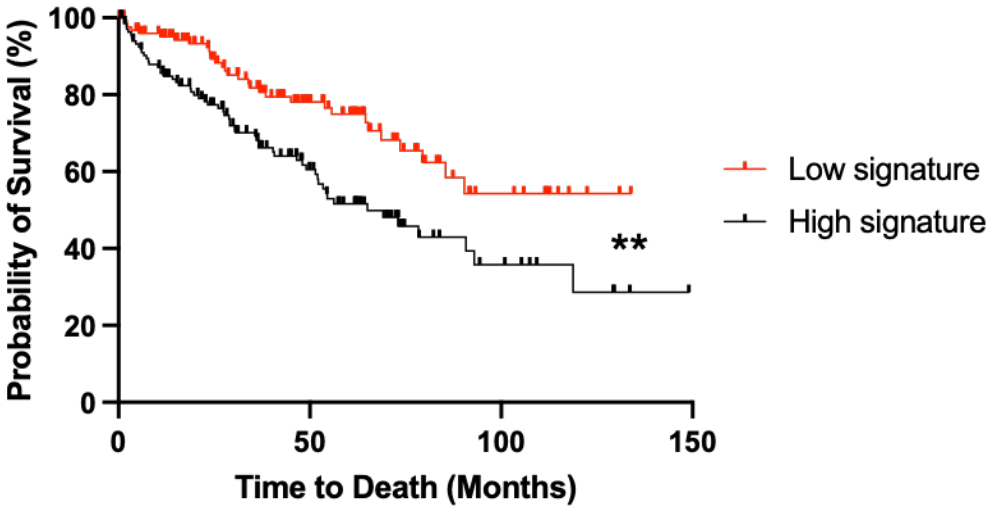

Figure 4.29 Survival analysis of the high effector immune signature compared to the low signature
Logrank analysis of Kaplan-Meier survival curves found a significant difference between the two curves, with the high signature found to have a significantly shorter median survival compared to the low signature, p = 0.001.

The high effector ccRCC immune signature was found to have a significantly lower survival chance compared to the low signature group (high group median survival 65.05 months, however median survival unable to be calculated for the low group as over 50% of patients were still alive, p=0.0014). As we have already shown that all these cell types increase with advanced ccRCC stage, we can assume that this immune cell signature will also increase with stage, and so may have some use as a prognostic measure.

As this analysis was completed using RNAseq data of whole ccRCC tumour samples, which may include non-tumour areas such as stroma and peritumoral normal tissue, our next aim was to investigate this immune signature using IF

staining of patient-derived ccRCC tumour tissue samples, to determine if a similar outcome is observed compared to what we have seen in this bioinformatic analysis.

4.3 Defining the immune response in ccRCC patient tissue samples

So far in this chapter we have used CIBERSORTx's 'digital cytometry' platform as a novel way to estimate the immune fraction of 22 immune cell types using RNAseq data. This platform allows analysis of a large number of samples with direct comparisons between them, however as the results are calculated as an estimated immune fraction rather than absolute numbers, we next aimed examine how closely this resembles the actual immune composition of patient-derived tumour tissue and normal kidney using TMA samples, in which we are able to count absolute cell numbers.

As we have already shown that the estimated immune fraction of NK cells, Tfh cells, CTLs and Tregs are significantly altered in ccRCC compared to normal kidney, and that levels of these cell types have been shown to be closely associated with clinical outcome, we next used double or triple IF staining for each cell type on ccRCC and normal kidney tissue, to determine the immune infiltrate of each of these cell types in each sample.

4.3.1 TMA patient characteristics

TMAs were acquired from the Wales Cancer Bank. The patient characteristics for the TMAs used can be found in Table 4.2.

Table 4.2 TMA patient characteristics

	ccRCC
	n=256
Age at Diagnosis	
Median	63
Range	28-84
Gender	
Male	156 (61%)
Female	100 (39%)
Tumour	
T1	55 (21.5%)
T1a	43 (16.8%)
T1b	55 (21.5%)
T2	32 (12.5%)
T2a	2 (0.8%)
T2b	2 (0.8%)
T3	9 (3.5%)
T3a	30 (11.7%)
T3b	25 (9.7%)
T3c	1 (0.4%)
T4	2 (0.8%)
Node	
N0	57 (22.3%)
N1	1 (0.4%)
N2	1 (0.4%)
NX	197 (77%)
Metastasis	
M0	11 (4%)
MX	245 (96%)

The TMAs used included 10 normal kidney samples and 256 ccRCC patient samples, of which 61% were from male patients and the median age at operation was 63, with a range of 28-84. The most common tumour grades were T1 and T1b (both 21.5%), while the most common node grade was N0 (22.3%) with only 1 sample found to be N1 or N2 (0.4%). None of the samples were found to be positive for metastasis, with 4% graded at M0 and all other samples graded as MX (unknown). Unfortunately, associated patient clinical outcome data was not available with our TMs, however ccRCC disease stage, TNM stage, age at operation and sex data was available and was used for comparison of immune cell levels between these groups.

4.3.2 Characterising the immune infiltrate in ccRCC samples

Using QuPath to analyse IF stained TMAs, tumour tissue was firstly stratified into tumour or non-tumour areas, then overall cell detection was run by counting the number of DAPI-positive cells within each core, as described in the methods section. Next, positive thresholds were set for each stain and detection was run on the DAPI-positive cells to determine the number of cells positive for each stain.

4.3.2.1 CD45+ tumour infiltrating lymphocytes

We firstly defined the number of tumour-infiltrating lymphocytes, characterised by the expression of the common leukocyte antigen, CD45. The number of CD45+ cells were counted (cells/mm^2) and the positive cell percentage of the total cells within the sample was determined, as shown in Figure 4.30.

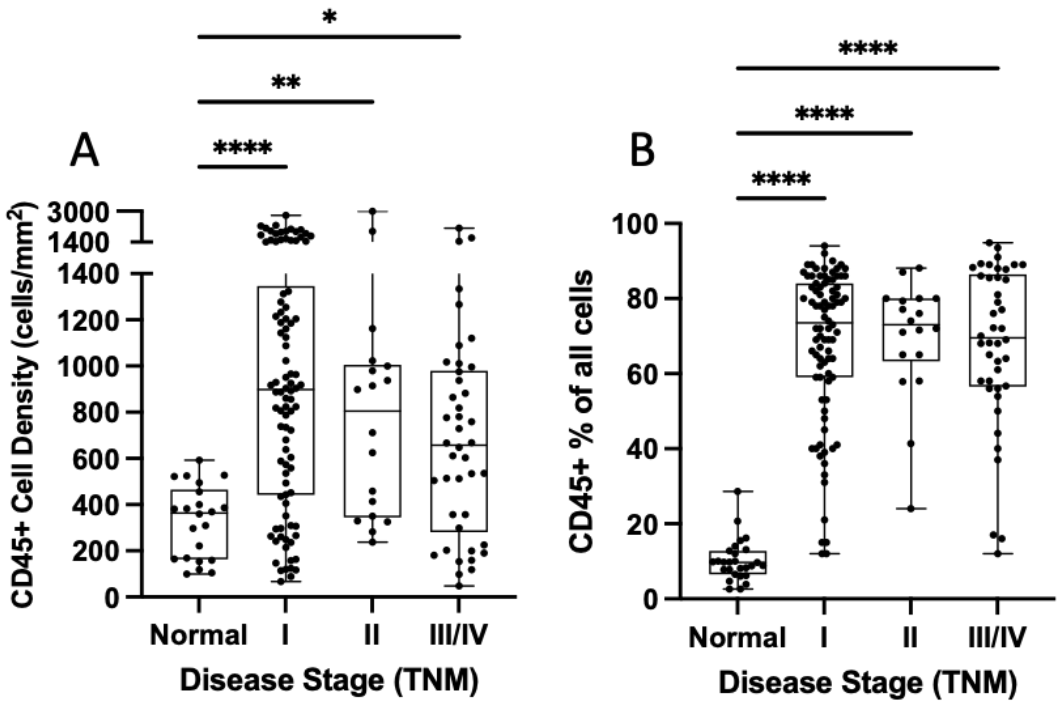

Figure 4.30 CD45+ cell density and percentage of all cells in TMA cores by stage
(A) CD45+ cells/mm^2 in normal kidney tissue and ccRCC samples by stage, (B) CD45+ cell percentage of total cells in normal kidney and ccRCC tissue samples. Analysis was completed using a Kruskal-Wallis test with Dunn's multiple comparisons test, where * represents $p < 0.05$, ** represents $p < 0.01$ and **** represents $p < 0.0001$.

CD45+ cell density was significantly higher in all ccRCC stages compared to normal kidney; however, no significant differences were found between the stages (Figure 4.30a). CD45+ cell density was the most significantly increased at stage I compared to normal (962.8 ± 615.1 vs 326.9 ± 156.8, $p<0.0001$), however stage II was also significantly higher than normal (866.6 ± 681.7 vs 326.9 ± 156.8, $p=0.0093$), as was stage III/IV (688.5 ± 455.7 vs 326.9 ± 156.8, $p=0.0244$).

The CD45+ percentage of DAPI+ cells was also significantly higher at all ccRCC stages compared to normal, however no significant differences were found between any stages (Figure 4.30b). Stage I again had the most significantly higher percentage of CD45+ cells compared to normal (67.76 ± 20.68 vs 10.1 ± 5.55, $p<0.0001$), followed by stage II (69.31 ± 16.06 vs 10.1 ± 5.55, $p<0.0001$), then stage III/IV (67.87 ± 21.29 vs 10.1 ± 5.55, $p<0.0001$).

Interestingly, the density of CD45+ cells/mm^2 was found to reduce as stage increased, however the positive percentage of all cells did not change. This may be due to the physical changes seen within the tissue structure as stage increases, as the cells become larger and large hollow “nests” characteristic of ccRCC tissue develop, meaning less cells are found within the sample overall, but a similar percentage of the cells are CD45 positive.

The level of variation in lymphocyte density seen between the ccRCC stages and normal tissue implies that CD45+ ccRCC tumour immune infiltrate is significantly different to that found in normal tissue. While no significant changes in CD45+ lymphocyte density or percentage of overall cell number were found between the disease stages, the immune infiltrate for specific cell types when other cell surface markers are considered may still show significant changes by tumour stage.

4.3.2.2 CD3+ T cell infiltrate

CD3 is a protein complex and T cell co-receptor which has roles in activating both Tfh and CTL cells, which is used as a T cell marker. The density of CD3+ cells (cells/mm^2) and relative frequency (percentage of CD45+ cells) was next measured to determine each TMA core's level of tumour infiltrating T cells, as shown in Figure 4.31.

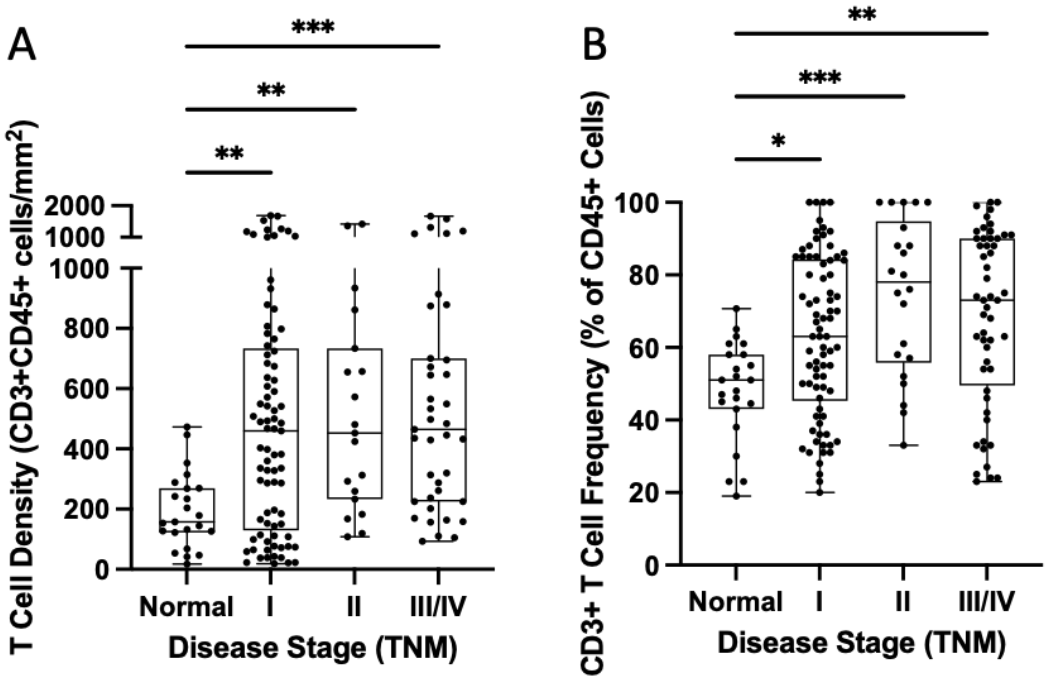

Figure 4.31 CD3+ cell density and percentage of CD45+ cells in TMA cores by stage
(A) CD3+ cells/mm^2 in normal kidney tissue and ccRCC samples by stage, (B) CD3+ cell percentage of CD45+ cells in normal kidney and ccRCC tissue samples. Analysis was completed using a Kruskal-Wallis test with Dunn's multiple comparisons test, where * represents p <0.05, ** represents p <0.01 and *** represents p <0.001.

All ccRCC samples had significantly higher densities of CD3+ cells/mm^2 compared to the normal samples (Figure 4.31a). Stage I has the most samples within the group, and while there was a large amount of variation within the group, stage I had a significantly higher number of CD3+ cells compared to normal (496.3 ± 409.1 vs 194.2 ± 124.4, p=0.003). Stage II showed no significant differences compared to stage I; however, it was again significantly higher compared to normal (538.4 ± 388.2 vs 194.2 ± 124.4, p=0.007). Stage III/IV was found to have similar average CD3+ cell

levels to stage I and II and the levels were also significantly higher than the normal samples (561.3 ± 408.6 vs 194.2 ± 124.4, $p<0.001$).

High CD3+ percentages of CD45+ cells were found for all ccRCC samples, with a significant increase in all stages seen compared to normal (Figure 4.31b). As with the density measurements, stage I showed a high amount of variation within the group, but overall was significantly higher than the normal samples (63.06 ± 22.20 vs 48.10 ± 13.90, $p=0.029$). Stage II was also found to be significantly higher than the normal samples (74.38 ± 21.54 vs 48.10 ± 13.90, $p<0.001$) as was stage III/IV (68.23 ± 24.20 vs 48.10 ± 13.90, $p=0.002$). As stages II and III/IV showed higher numbers of positive cells than stage I, this suggests that a higher number of T cells is associated with advanced stage disease, however these differences were not found to be significant.

As previously discussed in this chapter, T cells are divided into two main subtypes depending on their expression of the cell surface markers CD4 and CD8. Having demonstrated that CD3+ T cell density and CD45+ cell frequency is altered between ccRCC disease stages and is also significantly different from normal tissue, we next investigated whether our previously identified CD4+ and CD8+ T cell subpopulations of interest demonstrated a similar change.

4.3.2.3 CD4+ T Helper cells (Th)

In our previous bioinformatic analysis using CIBERSORTx, the only CD4+ T cell subset which could be calculated was the T follicular helper cell (Tfh), a specialised subset of CD4+ cells that are characterised by the expression of CXCR5 (Laurent et al. 2010), which we were not able to stain for in our analysis due to antibody availability. We therefore completed IF staining for a more generalised T helper (Th) cell population which we defined as CD45+ CD3+ CD4+ lymphocytes. Representative Th staining can be seen in Figure 4.32.

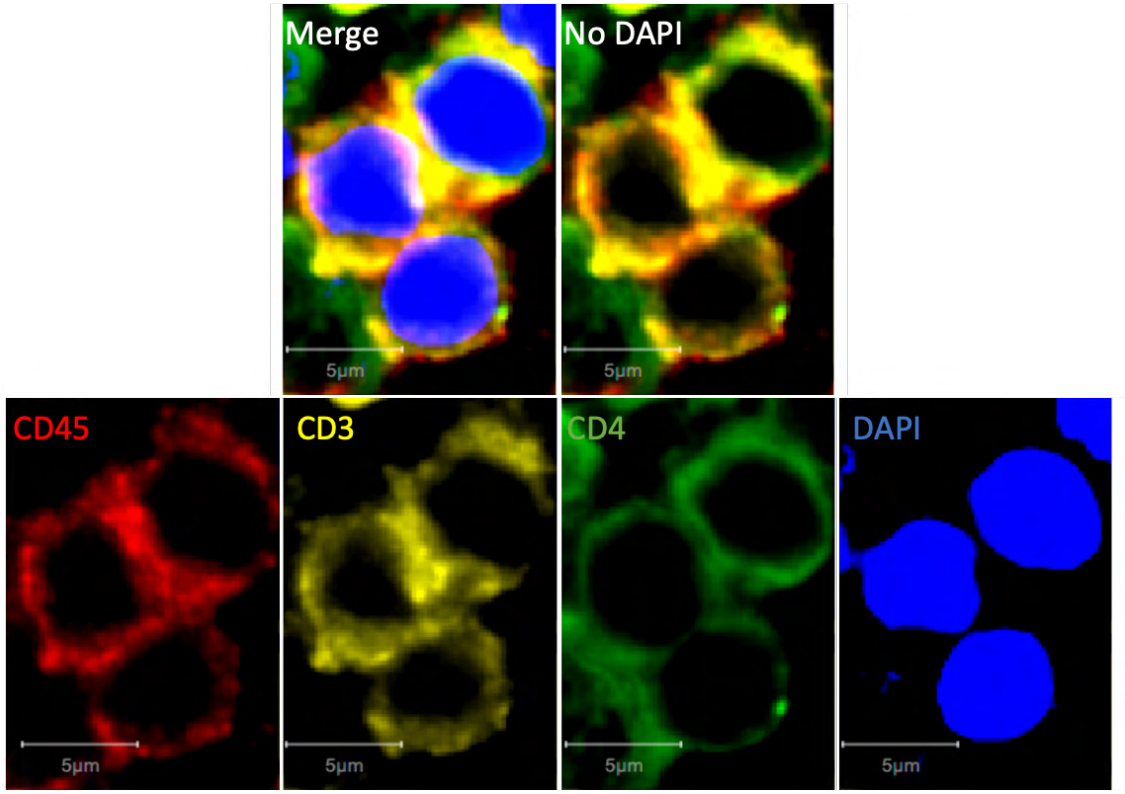

Figure 4.32 Positive IF staining for CD4+ Th cells
Positive immunofluorescent Th staining for CD45+CD3+CD4+DAPI+ immune cells in ccRCC tissue. Scale bar represents 5µm.

We firstly looked at the density/mm^2 and relative frequency of CD4+ Th cells within our ccRCC and normal tissue cores, where numbers of CD45+CD3+ CD4+DAPI+ cells were counted and quantified, as shown in Figure 4.33.

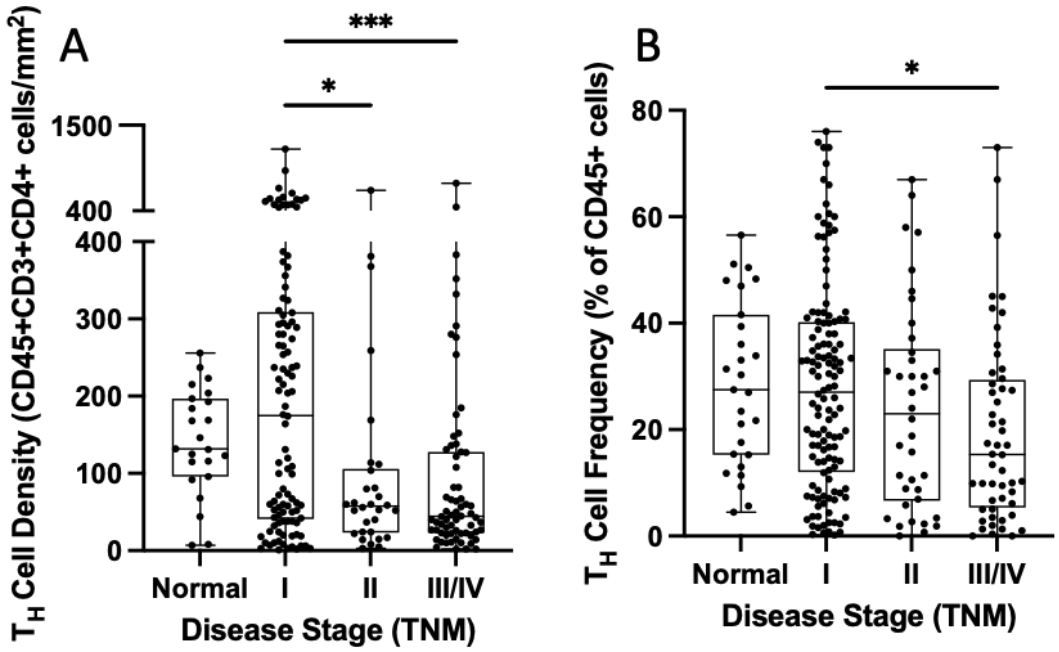

Figure 4.33 Th cell density and percentage of CD45+ cells in TMA cores by stage
(A) Th cells/mm^2 in normal kidney tissue and ccRCC samples by stage, (B) Th cell percentage of CD45+ cells in normal kidney and ccRCC tissue samples. Analysis was completed using a Kruskal-Wallis test with Dunn's multiple comparisons test, where * represents $p < 0.05$ and *** represents $p < 0.001$.

A significant decrease in Th cells/mm^2 was observed with increased ccRCC stage (Figure 4.33a), with stage I showing significantly higher numbers of CD4+ Th cells than stage II (213.6 ± 214.2 vs 102.2 ± 142.6, p=0.036) and stage III/IV (213.6 ± 214.2 vs 96.19 ± 129.5, p=0.0003). Almost all samples in stage II and II/IV had lower Th cell densities than normal kidney, however no significant differences were observed between the normal kidney samples and any ccRCC group. The Th cell frequency of CD45+ cells also showed a significant decrease with stage (Figure 4.33b), with stage I showing a significantly higher frequency of CD45+ Th cells than stage III/IV (28.09 ± 19.53 vs 19.58 ± 17.50, p=0.025). The normal samples group was also generally higher than most ccRCC samples, however no significant differences were found.

Th cell density and frequency was next assessed by patient sex and age at operation, to determine if these characteristics may have an impact on Th cell tumour infiltration, as shown in Figure 4.34.

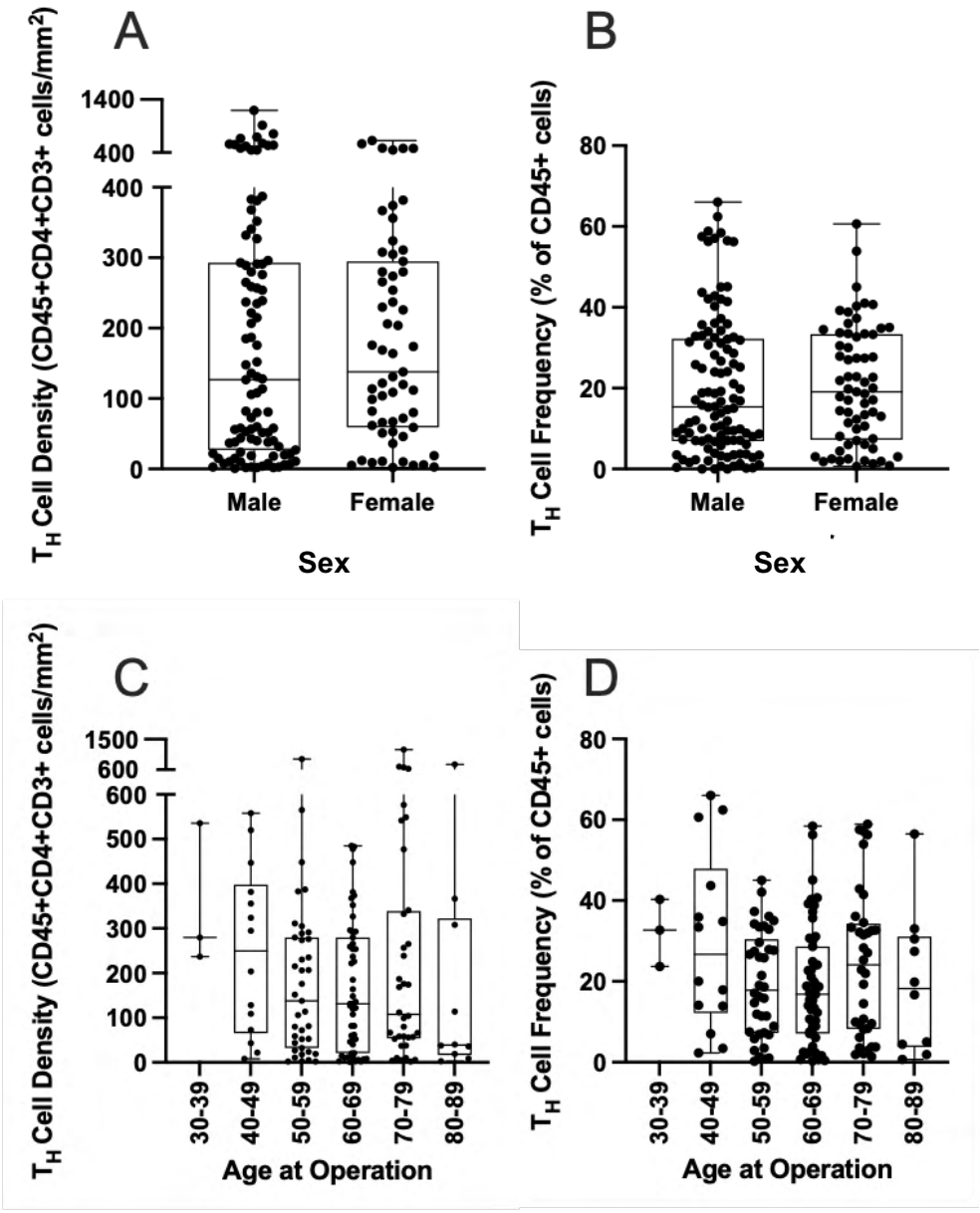

Figure 4.34 Th cell density and frequency of CD45+ cells by sex and age at operation
(A) Th cell density/mm^2 by sex, (B) Th cell frequency by sex, (C) Th cell density/mm^2 by age at operation, (D) Th cell frequency by age at operation. Analysis was completed using a (A-B) a Mann-Whitney test or (C-D) a Kruskal-Wallis test with Dunn's multiple comparisons test; however, no significant differences were found between any of the groups.

No significant differences in Th cell density or frequency were observed when the samples were split by patient sex (Figure 4.34a and b respectively) or by patient age at operation (Figure 4.34c and d respectively). A general decrease in Th cell density and frequency was observed with increased age at operation, however no significant differences were found between any of the groups, possibly due to the small n numbers in some of the groups.

4.3.2.4 CD8+ Cytotoxic T Cells (CTLs)

CTLs are defined as CD45+ CD3+ CD8+ lymphocytes, however unfortunately due to antibody availability, triple immunofluorescent staining was not possible, so CTLs were identified as CD45+ CD8+ DAPI+ cells. Representative CTL staining can be seen in Figure 4.35.

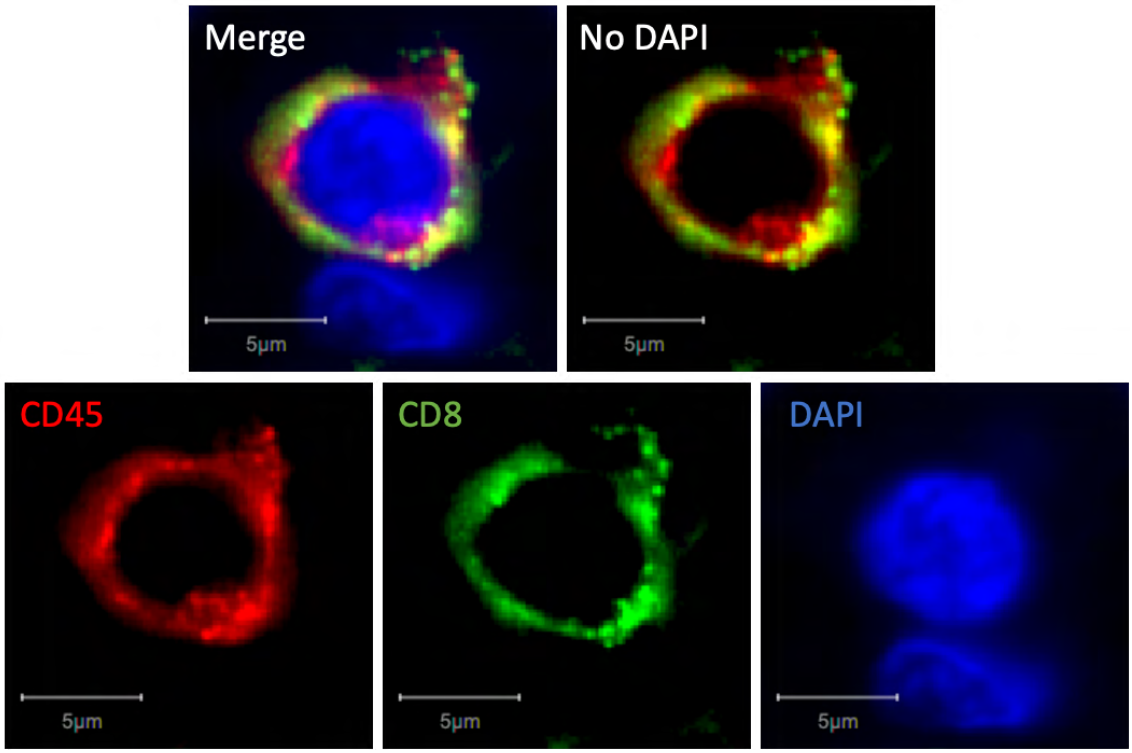

Figure 4.35 Positive IF staining for CD8+ CTL cells
Positive CTL immunofluorescent staining for CD45+CD8+DAPI+ immune cells in ccRCC tissue. Scale bar represents 5µm.

We firstly counted the cell density/mm^2 and frequency of CD45+ cells in our ccRCC samples, as shown in Figure 4.36.

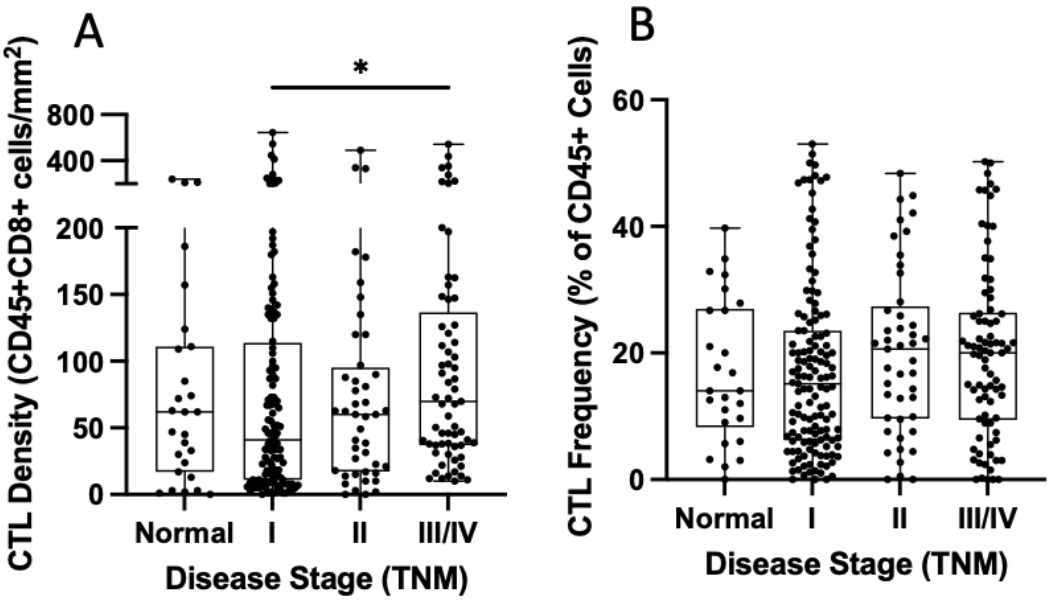

Figure 4.36 CTL cell density and percentage of CD45+ cells in TMA cores by stage
(A) CTL cells/mm^2 in normal kidney tissue and ccRCC samples by stage, (B) CTL cell percentage of CD45+ cells in normal kidney and ccRCC tissue samples. Analysis was completed using a Kruskal-Wallis test with Dunn's multiple comparisons test, where * represents $p < 0.05$.

Unlike what we have previously observed for the Th cells in our TMA samples, which showed a significant decrease in cell density, CD8+ CTLs showed a significant increase in cell density/mm^2 with increased ccRCC stage (Figure 4.36a). A large amount of variation was observed within the sample groups, however cell density/mm^2 was found to be significantly higher at all ccRCC stages compared to normal kidney (stage I 55.38 ± 76.90 vs 8.214 ± 6.887, stage II 56.18 ± 59.77 vs 8.214 ± 6.887, stage III/IV 64.78 ± 94.62 vs 8.214 ± 6.887, all $p<0.0001$), however no significant differences were found between the ccRCC stages.

Again, in contrast to what was seen for Th cell frequency, which decreased with increased ccRCC stage, CTL frequency of CD45+ cells showed a general increase with disease stage (Figure 4.36b), with all ccRCC stages again found to be significantly higher than normal kidney (stage I 23.39 ± 19.59 vs 4.24 ± 4.53, stage II 22.66 ± 16.51 vs 4.24 ± 4.53, stage III/IV 24.46 ± 18.31 vs 4.24 ± 4.53, all $p<0.0001$), however no significant differences were found between stages.

These results suggest that CD8+ CTL levels significantly increase in ccRCC compared to normal kidney, however there is not a significant change in CTL levels between ccRCC stages.

CTL density and frequency was next assessed by patient sex and age at operation, as shown in Figure 4.37.

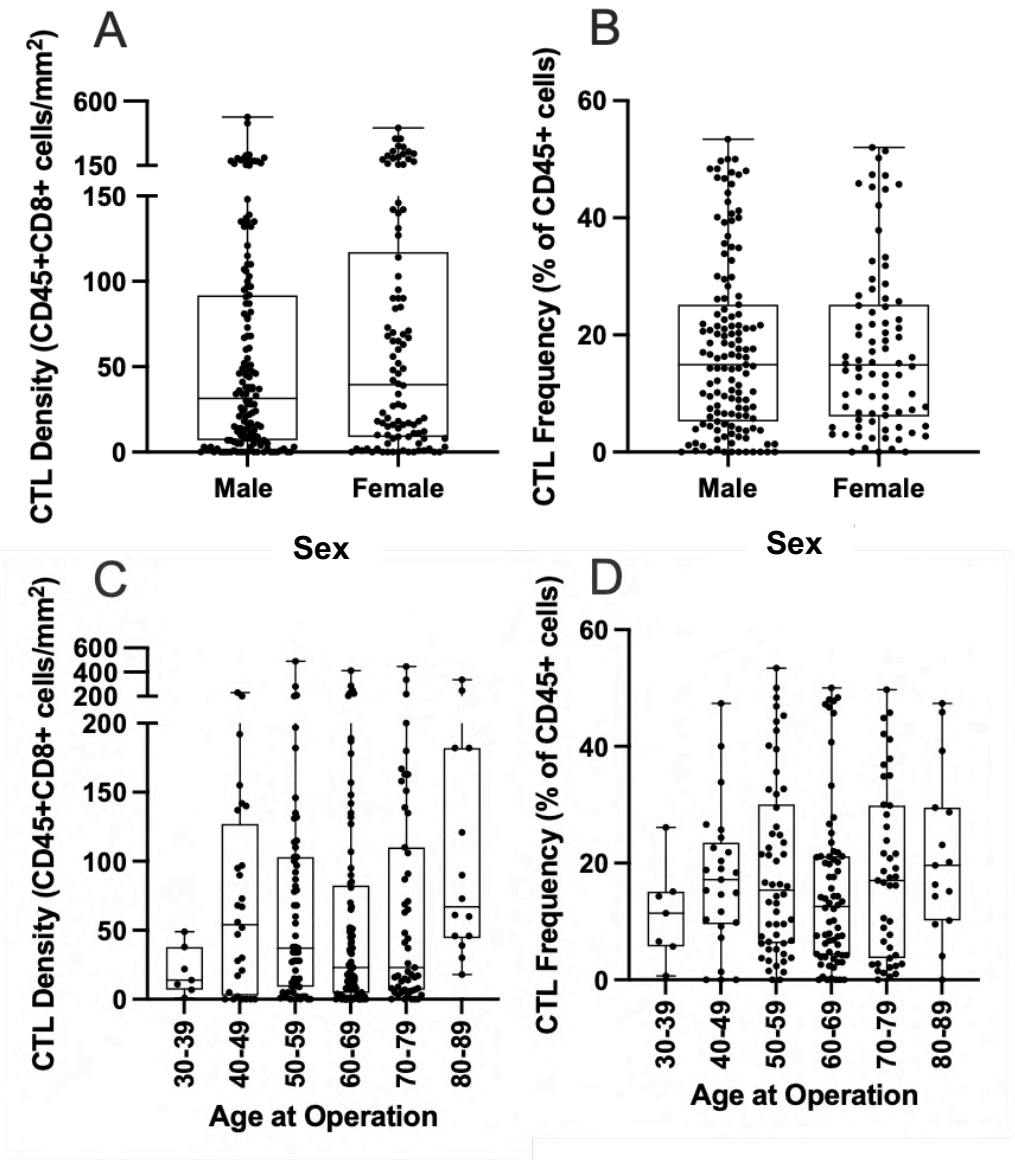

Figure 4.37 CTL cell density and frequency of CD45+ cells by sex and age at operation
(A) CTL cell density/mm^2 by sex, (B) CTL cell frequency by sex, (C) CTL cell density/mm^2 by age at operation, (D) CTL cell frequency by age at operation. Analysis was completed using (A-B) a Mann-Whitney or (C-D) a Kruskal-Wallis test with Dunn's multiple comparisons test; however, no significant differences were found between any of the groups.

No significant differences were observed in CTL density or frequency when the ccRCC samples were split by sex (Figure 4.37a and b respectively). No trend was observed in the density of CTL cells in samples when split by age at operation (Figure 4.37c), however a general increase in CTL frequency was observed with increased age at operation (Figure 4.37d). No significant differences were however found between any of the groups, possibly due to the small n numbers in some of the groups.

4.3.2.5 CD4:CD8 Ratio

The interactions between CD4+ and CD8+ T cells are crucial for normal immunity and this ratio is often used as a measure for overall immune system health. A CD4:CD8 ratio over 1 is considered normal, with the ratio often decreasing significantly in cancer, and so increasing this ratio back to normal levels is one of the main aims of immunotherapy. Having established the absolute numbers and percentage of CD45+ cells of both CD4+ Th and CD8+ CTLs, we next sought to determine the CD4:CD8 ratio within our samples, as shown in Figure 4.38.

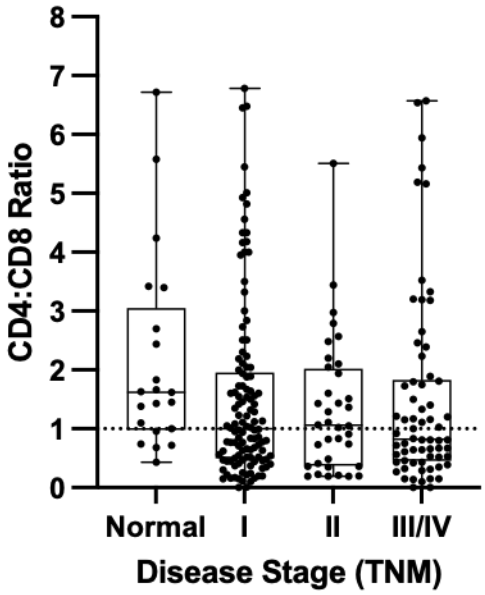

Figure 4.38 CD4:CD8 Ratio in normal kidney and ccRCC tissue samples
The CD4:CD8 ratio was compared within the normal and ccRCC samples at stages I, II and III/IV. Analysis was completed using a Kruskal-Wallis test with Dunn's multiple comparisons test; however, no significant differences were observed between any of the groups.

No significant differences in CD4:CD8 ratio were observed between any ccRCC stages or the normal samples, however all ccRCC stages generally had lower ratios than the normal samples (Figure 4.38). As expected, the normal samples were mostly within the normal range of over 1 (median 1.6, range 0.43 to 6.72). Stage I ccRCC had a large amount of variation within the group, but most samples were out of the normal range (median 1.0, range 0.01 to 6.78). Stage II also showed a range of variation within the group (median 1.1, range 0.19 to 5.51) as did stage III/IV (median 0.9, range 0.1 to 6.57).

As we have only observed general trends when analysing CD4:CD8 ratio in samples as a group, correlation analysis was used to reveal the relationships between the density of CD4+ Th cells and CD8+ CTLs within each ccRCC sample and to determine the strength of these relationships, as shown in Figure 4.39.

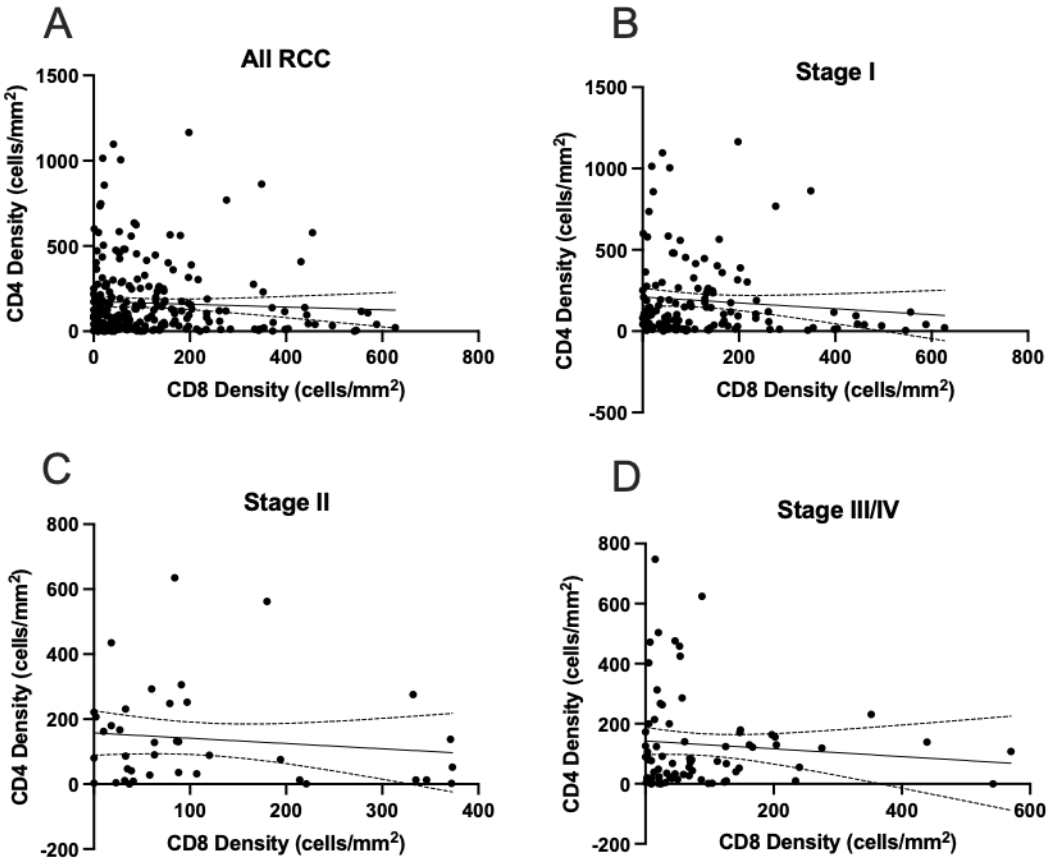

Figure 4.39 Correlation analysis of CD4 and CD8 cells in ccRCC samples
Spearman correlation analysis was used to determine the strength of the relationships of CD4 and CD8 cell density within each ccRCC sample. (A) All RCC, r = -0.019, (B) Stage I, r = 0.064, (C) Stage II, r = 0.110, (D) Stage III/IV, r = -0.001.

Weak and moderate correlations between CD4+ and CD8+ cells were observed in the ccRCC samples; however, the strength of the relationships may have been more significant with a larger sample size. A very weak negative correlation was found between CD4 and CD8 cells when all ccRCC samples were analysed together (r=-0.019, Figure 4.39a). Weak positive correlations were found between CD4 and CD8 cells in ccRCC stage I (r=0.064, Figure 4.39b) and II (r=0.110, Figure 4.39c), however neither were found to be significant, and a very weak negative correlation was found in stages III/IV (r=-0.001, Figure 4.39d).

As no strong relationships between CD4 and CD8 cells were observed at any ccRCC stage, this data may imply that these two T cell types do not directly influence the expression of the other. Instead, their expression may be influenced further by other cell types, such as Tregs, so we next examined the Treg density/mm^2 and frequency of CD45+ cells in our TMA samples.

4.3.2.6 Tregs

Tregs are defined as CD4+ CD25+ positive cells, however they are characterised by the expression of the nuclear transcription factor FoxP3, along with nuclear DAPI expression. Representative positive staining can be seen in Figure 4.40.

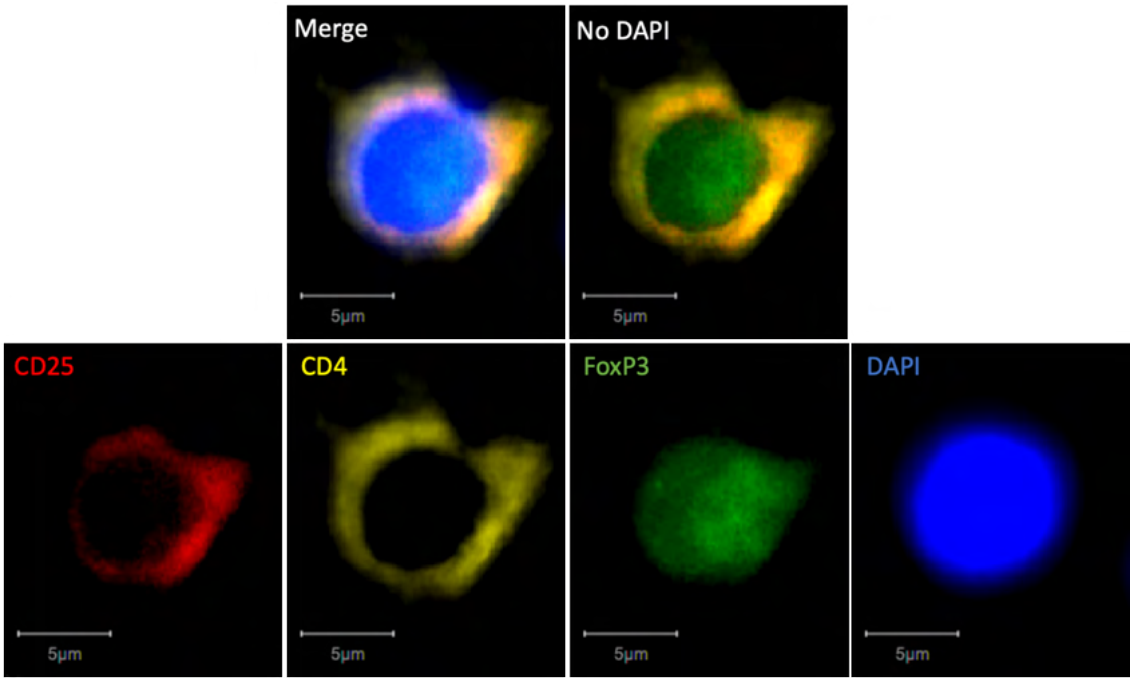

Figure 4.40 Positive IF staining for Tregs
Positive Treg immunofluorescent staining for CD25+CD4+FoxP3+DAPI+ immune cells in ccRCC tissue. Only cells with fully nuclear FoxP3 were counted as Tregs. Scale bar represents 5µm.

We firstly calculated the Treg density/mm^2 and frequency of CD45+ cells in our TMA samples, as shown in Figure 4.41.

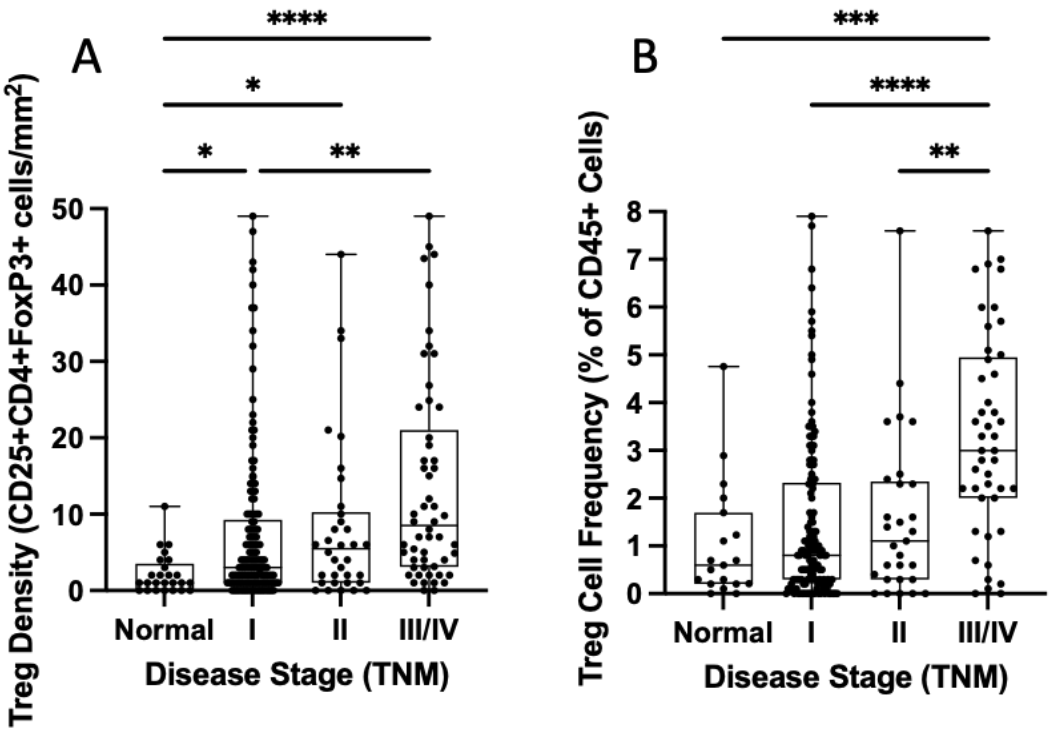

Figure 4.41 Treg cell density and percentage of CD45+ cells in TMA cores by stage
(A) Treg cells/mm^2 in normal kidney tissue and ccRCC samples by stage, (B) Treg cell percentage of CD45+ cells in normal kidney and ccRCC tissue samples. Analysis was completed using a Kruskal-Wallis test with Dunn's multiple comparisons test, where * represents p <0.05, ** represents p <0.01, *** represents p <0.001 and **** represents p <0.0001.

Significant increases in Treg cell density were found between ccRCC stages with increased stage (Figure 4.41a), with stage III/IV having significantly higher numbers of Tregs/mm^2 than stage I (13.66 ± 13.52 vs 7.49 ± 10.44, p=0.001). All ccRCC stages were also found to be significantly higher than normal, stage I (7.49 ± 10.4 vs 2.16 ± 2.62, p=0.0168), stage II (8.45 ± 10.70 vs 2.16 ± 2.62, p=0.019), stage III/IV (13.66 ± 13.52 vs 2.16 ± 2.62, p<0.0001).

Treg cell frequency of CD45+ cells also showed significant increases compared to normal kidney and with increased stage (Figure 4.41b). Stage III/IV was found to have a significantly higher percentage of CD45+ cells than normal tissue (3.30 ± 2.11 vs 1.04 ± 1.22, p=0.0003). Significant differences were also found between the ccRCC stages, with stage III/IV having significantly higher frequencies than stage I (3.30 ± 2.11 vs 1.46 ± 1.73, p<0.0001) and stage II (3.30 ± 2.11 vs 1.579 ± 1.715, p=0.0052).

These results strongly suggest that Treg density and frequency are significantly higher than those found in normal kidney tissue and that the increased density and frequency of Treg cells is associated with more advanced disease.

We next determined if patient characteristics of sex or age at operation have any impact on Treg density or frequency, as shown in Figure 4.42.

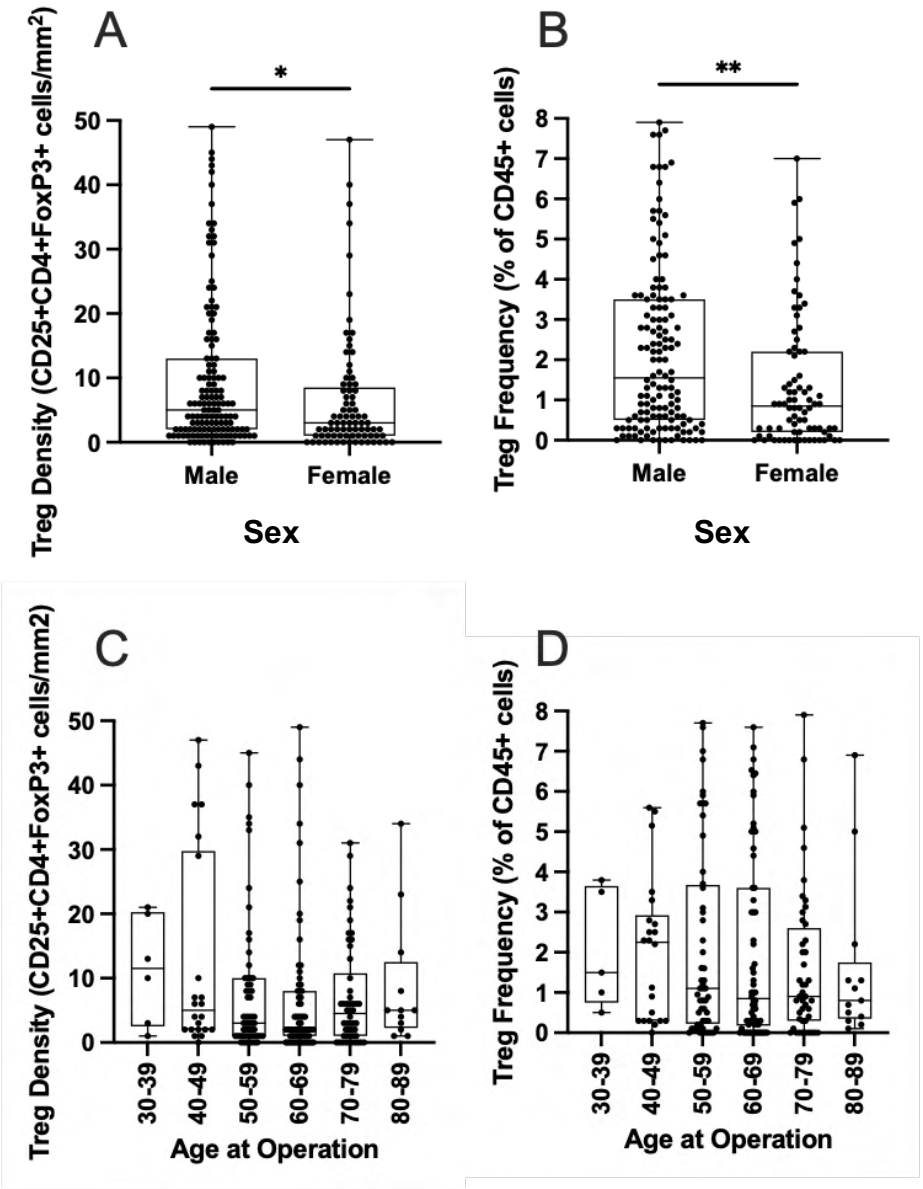

Figure 4.42 Treg cell density and frequency of CD45+ cells by sex and age at operation
(A) Treg cell density/mm^2 by sex, (B) Treg cell frequency by sex, (C) Treg cell density/mm^2 by age at operation, (D) Treg cell frequency by age at operation. Analysis was completed using (A-B) a Mann-Whitney or (C-D) a Kruskal-Wallis test with Dunn's multiple corrections test, where * represents $p < 0.05$ and ** represents $p < 0.01$.

Tregs were the only immune cell type which showed significant differences between the male and female patient groups (Figure 4.42a and b). Male patients had significantly higher levels of Tregs than females in both the cell density (9.70 ± 11.57 vs 6.61 ± 9.57, p=0.0115) and frequency of CD45+ cells (2.19 ± 2.07 vs 1.37 ± 1.62, p=0.0019). Comparison of Tregs by age at operation found a general decrease in cell density and frequency with increased age at operation, however no significant differences were found between any of the groups, possibly due to the small n numbers in some of the groups.

4.3.2.7 CD8:Treg ratio

The CD8:Treg ratio is a less commonly used but highly informative measure of the immune response within the tumour microenvironment. Low ratios (<1) have been associated with unfavourable outcome and poor response to chemotherapy, while high CD8:Treg ratios have been associated with positive chemotherapy response in breast cancer (Goda et al. 2022) and bladder cancer (Baras et al. 2016), however this ratio has not been characterised in ccRCC tissue. We next examined the CD8:Treg ratio in our samples, as shown in Figure 4.43.

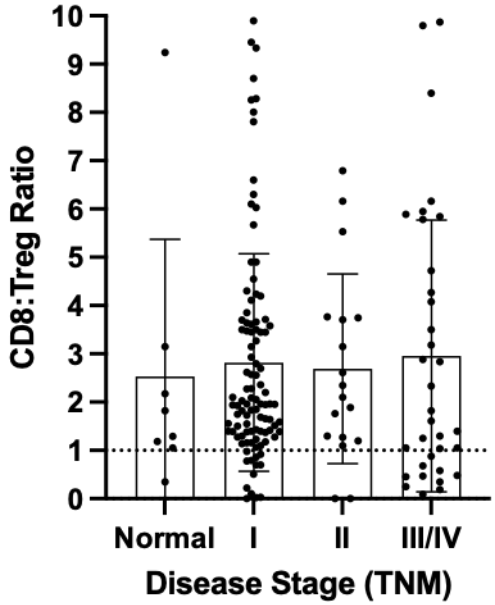

Figure 4.43 CD8:Treg ratio in normal kidney and ccRCC tissue samples
Comparison of the CD8:Treg ratio within normal and ccRCC samples. Analysis was completed using a Kruskal-Wallis test with Dunn's multiple corrections test; however, no significant differences were observed between any of the groups.

All sample groups were found to have a mean CD8:Treg of over 1 (Figure 4.43), with only a small number of all samples having a ratio below 1. The mean ratio was similar in the normal samples compared to the ccRCC samples (Normal ratio 2.532 ± 2.37 vs stage I ratio 2.818 ± 2.253, stage II 2.590 ± 1.964 and stage III/IV ratio 2.954 ± 2.813), with no significant differences found between any of the groups.

As most ccRCC samples were unexpectedly found to have a ratio over 1, we next used Spearman correlation analysis to further examine the relationships between the CD8 and Treg cells in each sample, as shown in Figure 4.44.

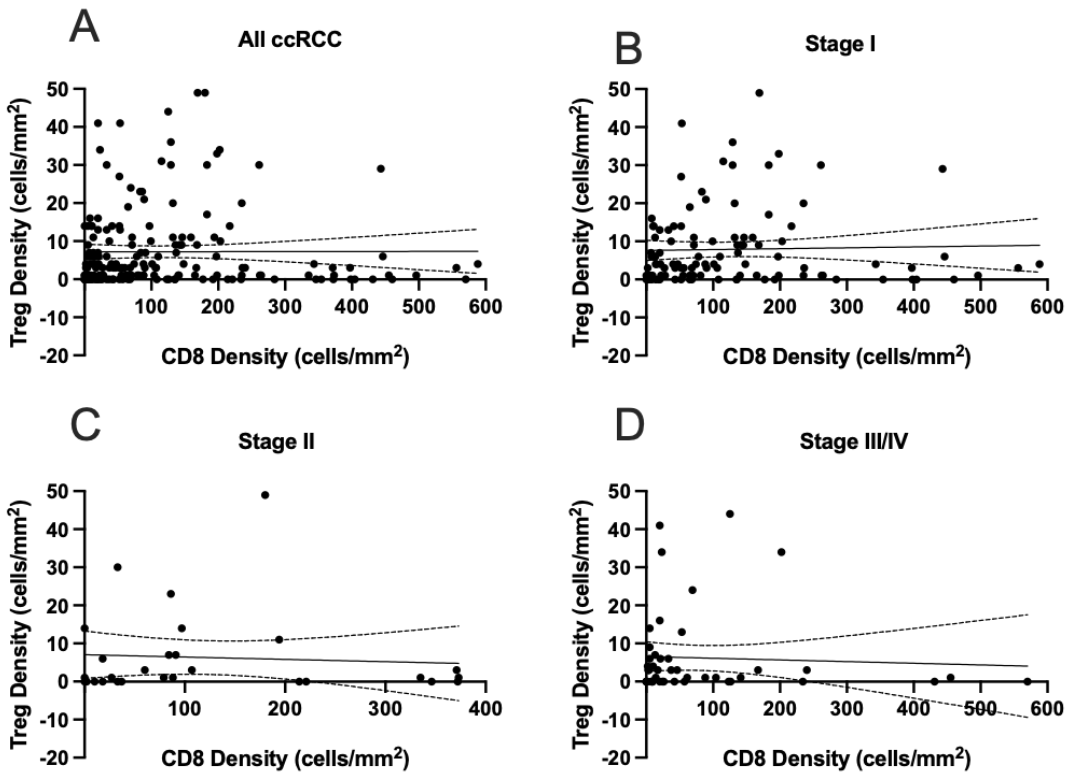

Figure 4.44 Correlation analysis of CD8 and Treg cells in ccRCC samples
Spearman correlation analysis was used to determine the strength of the relationships between Treg density and CD8 cell density within each ccRCC sample. (A) All RCC, r = 0.0930, (B) Stage I, r = 0.0906, (C) Stage II, r = 0.0088, (D) Stage III/IV, r = 0.0088.

A weak positive correlation was found in the ccRCC group as a whole (Figure 4.44a, r=0.0930). Similarly, weak positive relationships were also found in each ccRCC stage (Figure 4.44b-d, stage I r=0.0906, stage II, r=0.0485, stage III/IV, r=0.0088), however none of the relationships were found to be significant, implying that this

ratio is not affected by disease stage and therefore other factors may have a more significant impact.

4.3.2.8 NK cells

We finally quantified the number of NK cells in our TMA samples. NK cells are defined as CD45+ CD3- CD56+ lymphocytes, with CD56 considered the archetypal phenotypical marker of NK cells. In our previous CIBERSORTx analysis, NK cells were defined as either resting or activated NK cells, however due to the limitations of IF staining, where only a limited number of antibody combinations can be used, we were not able to stain for markers which may distinguish between the active and resting state of NK cells. Representative NK cell staining can be seen in Figure 4.45.

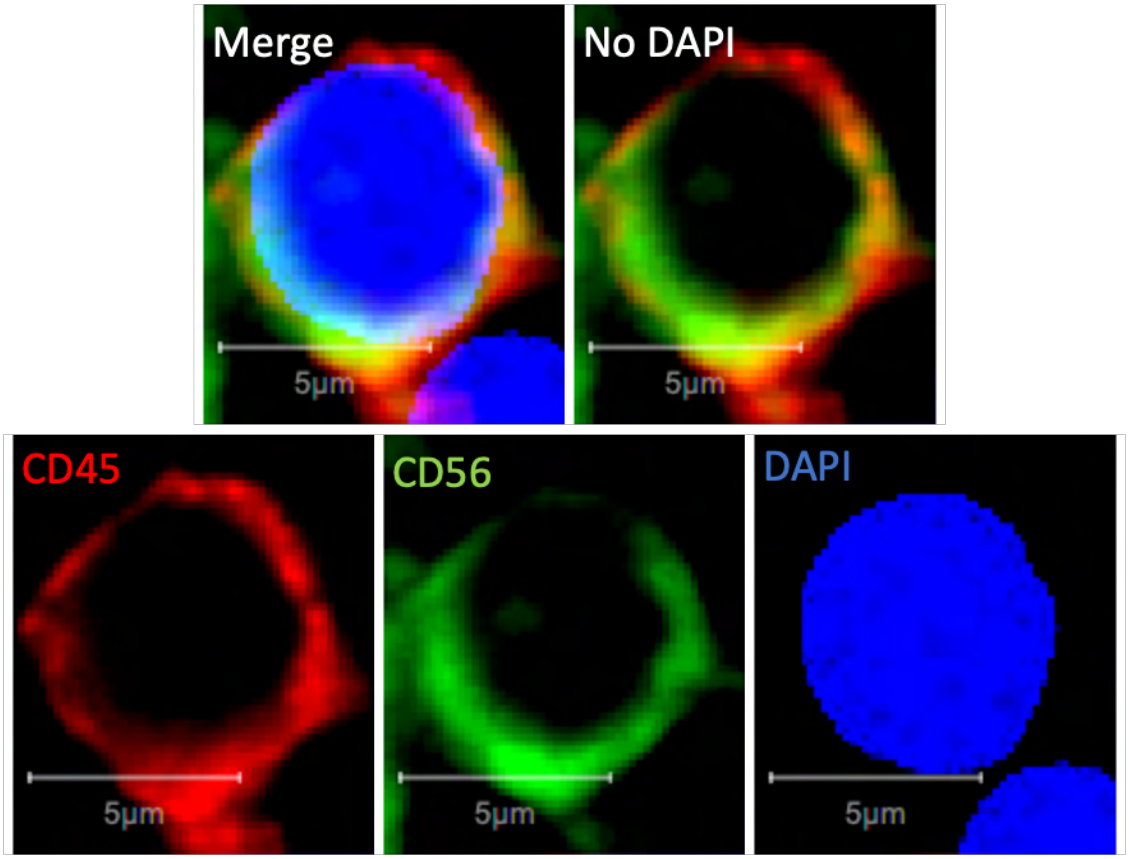

Figure 4.45 Positive IF staining for NK Cells
Representative positive NK immunofluorescent staining for CD45+CD56+DAPI+ immune cells in ccRCC tissue. Scale bar represents 5µm.

We firstly counted the NK cell density/mm^2 and frequency of CD45+ cells in each sample, as shown in Figure 4.46.

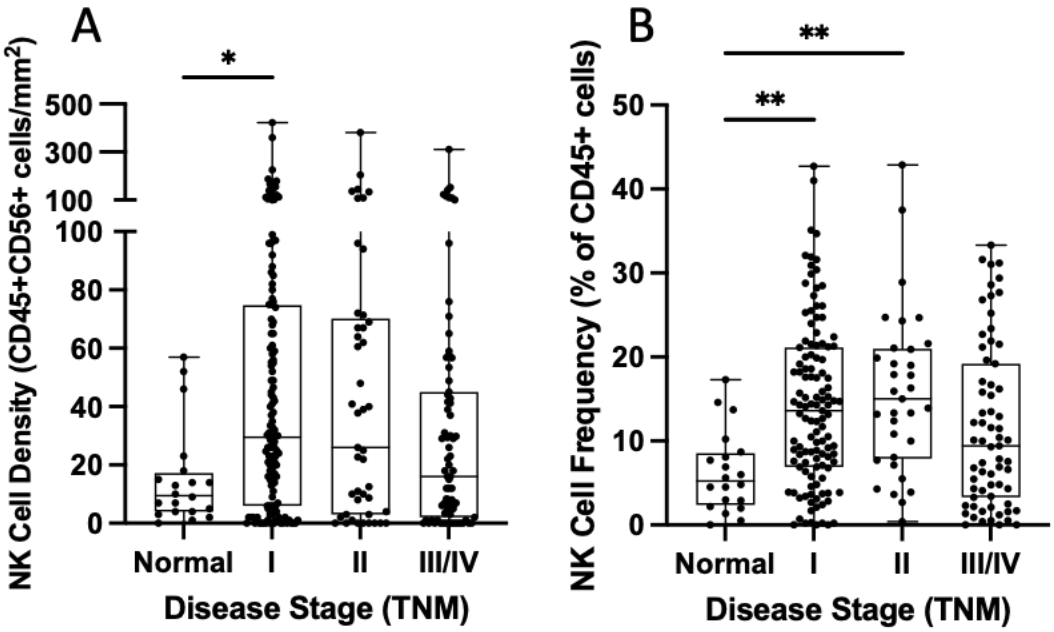

Figure 4.46 NK cell density and percentage of CD45+ cells in TMA cores by stage
(A) NK cells/mm^2 in normal kidney tissue and ccRCC samples by stage, (B) NK cell percentage of CD45+ cells in normal kidney and ccRCC tissue samples. Analysis was completed using a Kruskal-Wallis test with Dunn's multiple corrections test, where * represents $p < 0.05$ and ** represents $p < 0.01$.

A large amount of variability within the stage groups was found in the density of NK cells/mm^2 (Figure 4.46a). While a general trend of reduced cell density/mm^2 was observed as stage increased, no significant differences were found between the stages. Stage I ccRCC was however found to have significantly higher numbers of NK cells/mm^2 than the normal kidney samples (50.87 ± 63.32 vs 15.20 ± 16.92, p=0.0479).

A similar pattern was seen in the NK cell frequency of CD45+ cells (Figure 4.46b), with a decrease seen as stage increased, however no significant differences were found between ccRCC stages. Normal kidney again had the lowest frequency of CD45+ cells and was significantly lower than the stage I (6.23 ± 4.78 vs 14.30 ± 9.67 p=0.0019) and stage II (6.23 ± 4.78 vs 15.69 ± 9.63, p=0.0018) ccRCC sample groups.

NK cell density and frequency was next assessed by patient sex and age at operation, as shown in Figure 4.47.

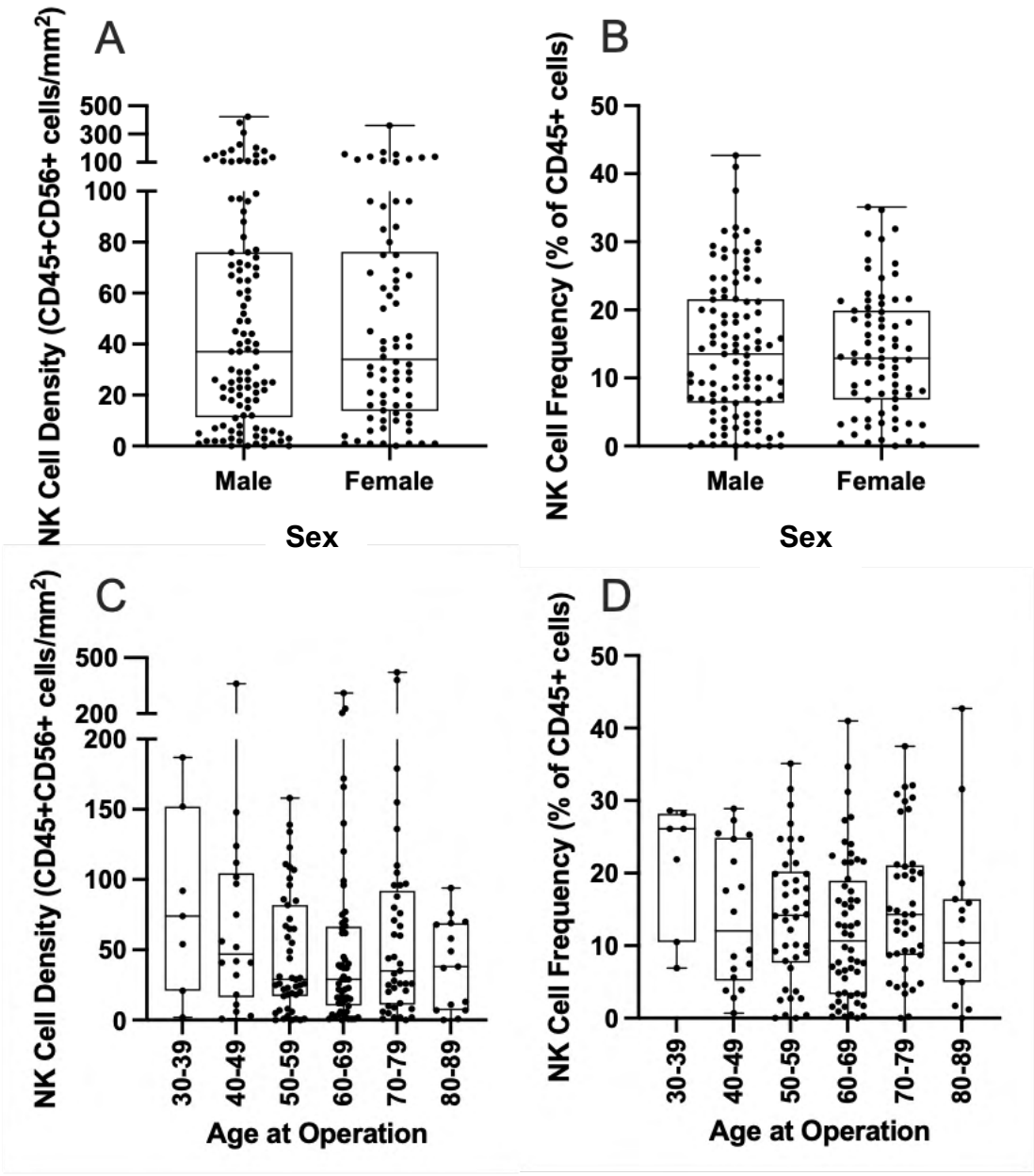

Figure 4.47 NK cell density and frequency of CD45+ cells by sex and age at operation
(A) NK cell density/mm^2 by sex, (B) NK cell frequency by sex, (C) NK cell density/mm^2 by age at operation, (D) NK cell frequency by age at operation. Analysis was completed using (A-B) a Mann-Whitney or (C-D) Kruskal-Wallis test with Dunn's multiple correction test; however, no significant differences were found between any of the groups.

No significant differences in NK cell density or frequency were found during comparison by sex (Figure 4.47 a and b respectively). A general decrease in NK cell density and frequency was observed with increased age at operation (Figure 4.47c

and d), however no significant differences were found between any of the groups, possibly due to the small n numbers in some of the groups.

4.3.3 TMA sample correlation analysis

Having now defined the Th, CTL, Treg and NK cell density/mm^2 and frequency of CD45+ cells in each of our TMA cores, we next used Spearman correlation analysis

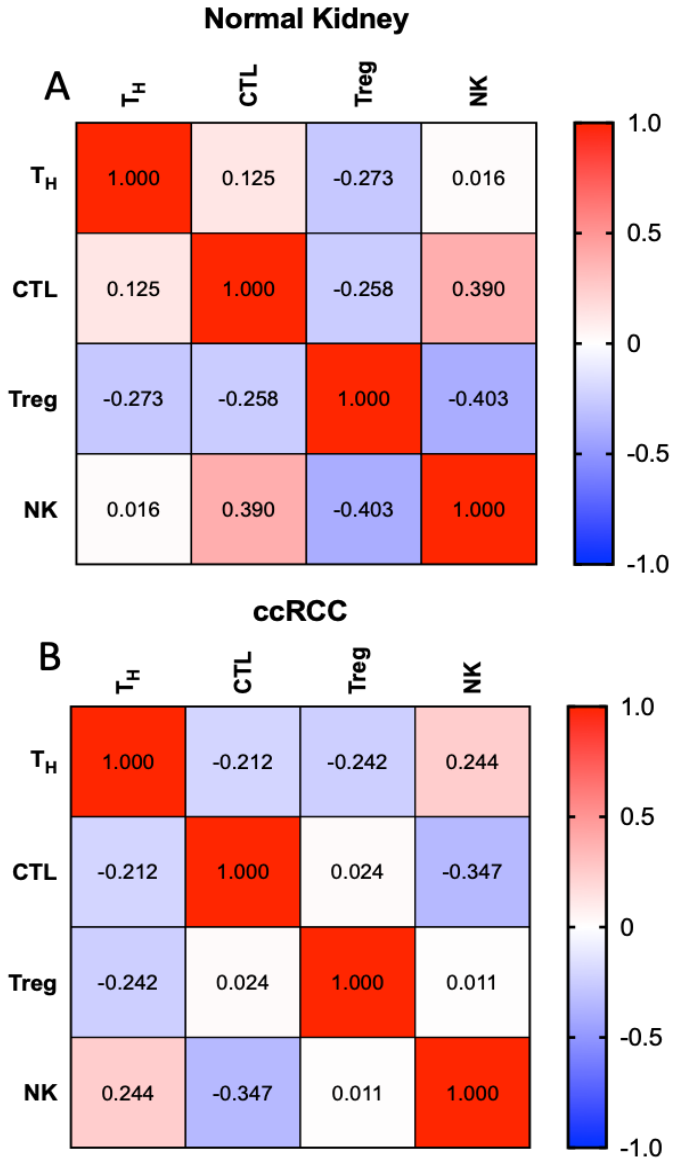

Figure 4.48 Spearman correlations of immune cells in normal kidney and ccRCC TMA samples Spearman correlation analysis was used to calculate the relationships between the estimated immune fraction of the key 4 cell types with each other in (A) Normal kidney correlations and (B) ccRCC. Red represents a positive correlation; blue represents a negative correlation. r values are represented within each box.

to determine the relationships between each immune cell type in our samples, as shown in Figure 4.48.

Within the normal kidney samples (Figure 4.48a), relationships between the T cell groups were found to be positive between NK cells and CTLs (r=0.390), between CTLs and Th cells (r=0.125) and very weakly between NK cells and Th cells (r=0.016), while Tregs had a negative relationship with NK cells (r=-0.403), Th cells (r=-0.273) and CTLs (r=-0.258). This implies that in normal kidney, Tregs are completing their required tasks of managing immune cell activation, as when Treg numbers increase, numbers of other T cell types reduce.

In the ccRCC samples however(Figure 4.48b), the relationships of CTLs with Th and NK cells were found to change from the positive relationships seen in the normal kidney to negative relationships, (r=-0.212, p=0.0088 and r=-0.347, p<0.0001 respectively), implying that these relationships may be an important characteristic of ccRCC compared to normal kidney. The negative relationships of Tregs with CTL and NK cells observed in normal kidney also change in the ccRCC samples, with both relationships becoming neutral and no effect observed (r=0.024 and r=0.011 respectively), however the negative relationship between Treg and Th cells remains negative in both normal kidney and ccRCC (r=-0.242, p=0.0027). Interestingly, NK cells are the cell type which seem to be most strongly affected in ccRCC compared to normal kidney and is the only cell type where the relationships with all other cell types are changed either from positive to negative or vice versa.

4.4 Comparison of estimated immune fraction in RCC subtypes

So far in this chapter, we have shown that the immune landscape of ccRCC is highly variable and differs significantly to that of normal kidney, with a significant impact on patient outcome. Using publicly available Firehose RNAseq datasets, we next chose to determine if there are any differences in immune composition between ccRCC and the other common renal cell carcinoma subtypes: pRCC and chRCC. Patient tissue was however not available for pRCC and chRCC, so in the same way we have previously completed the ccRCC bioinformatic analysis, we next analysed and ran pRCC and chRCC RNAseq data sets through CIBERSORTx to enable comparison of the estimated immune fractions and determine any differences between the subtypes.

4.4.1 Patient characteristics in RCC subtype datasets

Publicly available Firehose Legacy RNAseq data sets for ccRCC, pRCC and chRCC samples, with their associated patient clinical data, were examined in depth to estimate each subtype's survival outcomes and predicted immune infiltrate using CIBERSORTx as previously described, to find differences and similarities between the subtypes. Table 4.3 contains the characteristics for each data set.

Table 4.3 Patient characteristics in RCC subtype RNAseq datasets

	KIRC	KIRP	KICH
	n=537	n=286	n=66
Age at Diagnosis			
Median	61	61	50
Range	26-90	28-88	17-86
Gender			
Male	346 (64%)	212 (74%)	39 (59%)
Female	191 (36%)	74 (26%)	27 (41%)
Stage			
I	272 (51%)	177 (62%)	21 (32%)
II	57 (11%)	29 (10%)	25 (38%)
III	125 (23%)	59 (21%)	14 (21%)
IV	83 (15%)	21 (7%)	16 (24%)
Tumour			
T1	22 (4.1%)	23 (8%)	5 (7.6%)
T1a	142 (26.4%)	106 (37.1%)	5 (7.6%)
T1b	111 (20.7%)	62 (21.7%)	11 (16.7%)
T2	55 (10.2%)	20 (7%)	19 (28.8%)
T2a	10 (1.9%)	8 (2.8%)	0
T2b	4 (0.7%)	5 (1.7%)	6 (9.1%)
T3	5 (0.9%)	9 (3.1%)	1 (1.5%)
T3a	122 (22.7%)	39 (13.6%)	14 (21.2%)
T3b	53 (9.9%)	11 (3.8%)	3 (4.5%)
T3c	2 (0.4%)	1 (0.3%)	0
T4	11 (2.0%)	2 (0.7%)	2 (3%)
Node			
N0	240 (45%)	130 (45%)	40 (61%)
N1	17 (3%)	19 (7%)	3 (5%)
N2	0	2 (1%)	2 (3%)
NX	280 (52%)	135 (47%)	21 (32%)
Metastasis			
M0	426 (79%)	92 (32%)	34 (52%)
M1	79 (15%)	9 (3%)	2 (3%)
MX	32 (6%)	185 (65%)	30 (45%)
Tumour Type			
Type 1	-	75 (26%)	-
Type 2	-	84 (29%)	-
Unknown	-	127 (44%)	-
Laterality			
Left	253 (47.1%)	159 (55%)	30 (45%)
Right	283 (52.7%)	125 (44%	36 (55%)
Bilateral	1 (0.2%)	2 (1%)	0
Race			
White	466 (87%)	202 (71%)	58 (88%)
Black/African American	56 (10%)	62 (22%)	4 (6%)
Asian	8 (1%)	6 (2%)	2 (3%)
Other	7 (1%)	16 (6%)	2 (3%)
Overall Survival (Months)			
Median	47.78	25.26	73.85
Range	0-149.05	0-194.65	0.99-153.61
Disease Free Survival (Months)			
Median	43.41	22.04	73.85
Range	0-133.84	0-194.65	0.99-153.61
Vital Status			
Alive	360 (67%)	242 (85%)	56 (85%)
Dead	177 (33%)	44 (15%)	10 (15%)

The three data sets differ significantly in size, in line with how common the subtypes are, with ccRCC consisting of 537 samples, pRCC having 286 samples (of which 75 were Type 1 and 84 were Type 2) and the rarest subtype, chRCC, having only 66 samples. In all of the data sets over half of the samples were from males with a median age of diagnosis of 61 for both ccRCC and pRCC and 50 for chRCC. The majority of samples in all subtype data sets came from low stage I or II tumours, with most tumour staging falling between T1a and T2. Most samples had a node stage classification of N0 or NX, and most samples had a metastasis stage of M0 or MX, with only 3% classified as M1 in both pRCC and chRCC. Primary tumour laterality was found to be almost even, with 47.1% left sided and 52.7% right sided tumours in

ccRCC, with 1 sample from a bilateral patient (0.2%). In pRCC, 55% of tumours came from left sided and 44% came from right sided tumours, with 2 bilateral samples (1%). In chRCC, 45% came from left sided and 55% came from right sided tumours, with no bilateral samples included in the data set. Almost all samples in all subtypes came from white patients, with black or African American samples making up just 10% in ccRCC, 22% in pRCC and 6% in chRCC, and Asian patients making up just 1% in ccRCC, 2% in pRCC and 3% in chRCC. Most patients in the data sets were still alive at the time of data set publication, with 67% still alive in ccRCC and 85% still alive in both the pRCC and chRCC sets.

4.4.2 Survival statistics

Survival data for the three RCC subtype data sets was firstly compared to determine the percentage chance of overall survival and disease-free survival (DFS) for each and the differences between them, as shown in Figure 4.49.

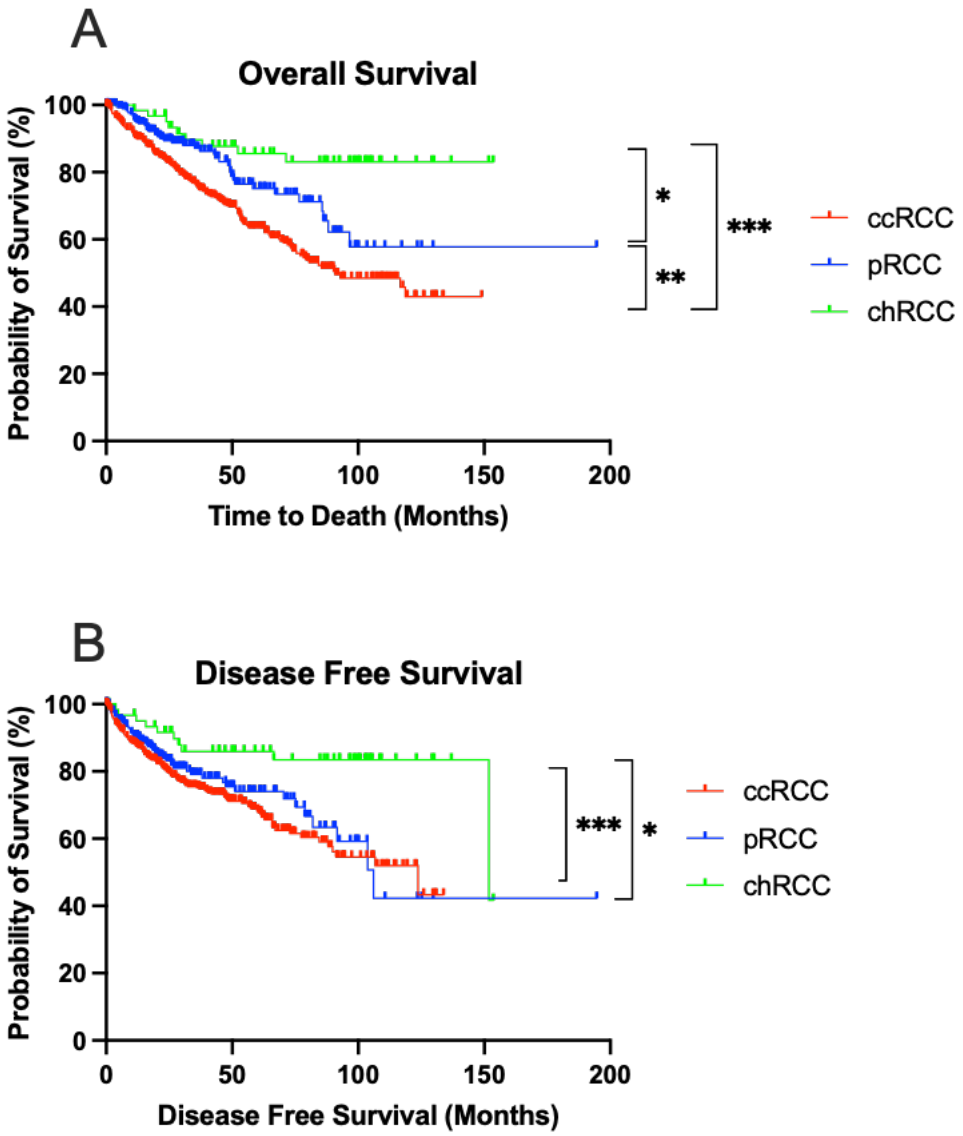

Figure 4.49 Overall survival and disease-free survival in the three RCC subtypes
(A) OS was compared between ccRCC, pRCC and chRCC, (B) DFS was compared between the three subtypes. Logrank analysis was used to compare Kaplan-Meier survival curves, where * represents $p < 0.05$, ** represents $p < 0.01$ and *** represents $p < 0.001$.

Comparison of the overall survival data available for the three RCC subtype datasets (Figure 4.49a) showed significant differences in the survival curves, with chRCC found to have the best overall survival chance compared to both pRCC ($p=0.0294$) and ccRCC ($p<0.0001$). pRCC also had a significantly better chance of survival than

ccRCC (p=0.0016). ccRCC median survival was 90.8 months, however median survival was not able to be calculated for pRCC or chRCC as over 50% of patients were still alive at the end of the study.

Comparison of the disease-free survival data for the three RCC subtypes (Figure 4.49b) also showed significant differences in the curves, again with chRCC having a significantly longer DFS than pRCC (p=0.0134) and ccRCC (p=0.0009). No significant difference was observed between the curves for pRCC and ccRCC.

pRCC was found to have the lowest median DFS of 106.04 months, followed by ccRCC at 123.72 months while chRCC had the longest DFS of 151.84 months.

Survival data was next compared between the three subtypes by the patient characteristics of sex, primary tumour laterality, age (data not shown) and race (data not shown) as shown in Figure 4.50.

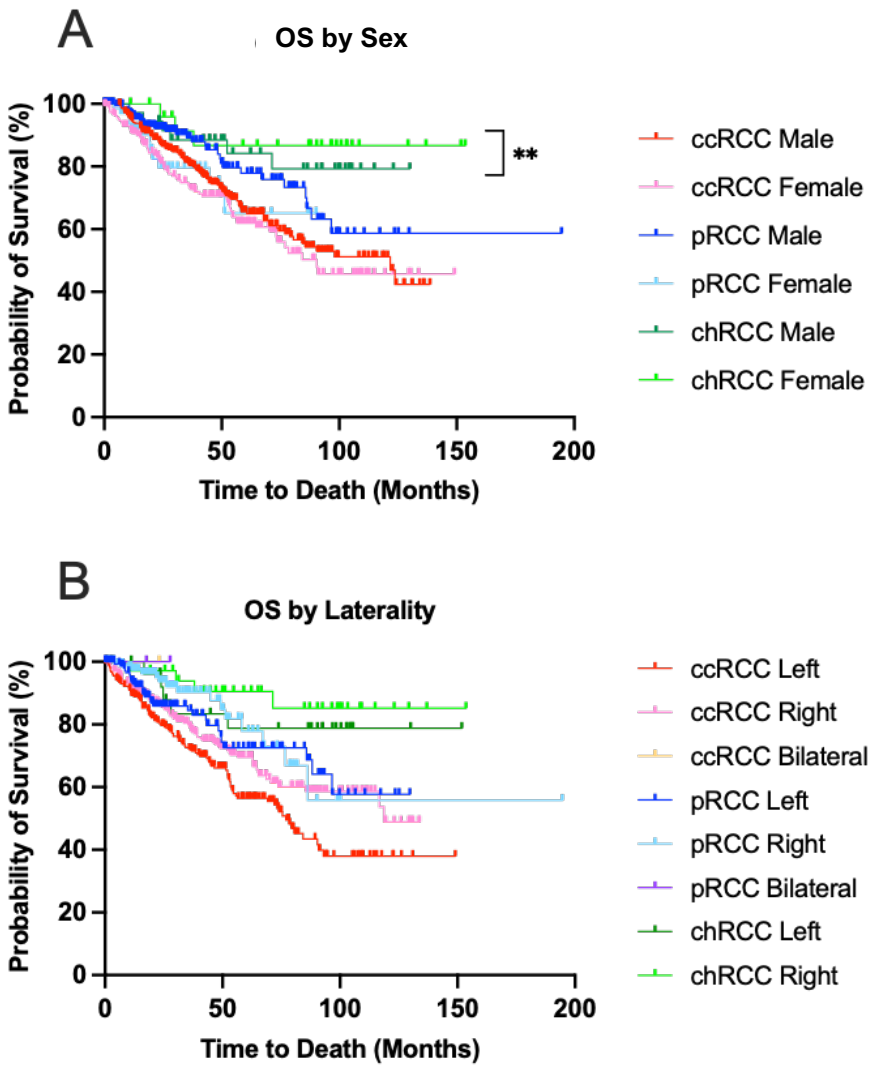

Figure 4.50 Overall survival by sex and laterality in RCC subtypes
(A) OS was compared by sex in ccRCC, pRCC and chRCC, (B) OS was compared by primary tumour laterality in the three subtypes. Logrank analysis was used to compare Kaplan-Meier survival curves, where ** represents p <0.01.

Survival curve comparison found no significant differences between male and female patients for any subtype (Figure 4.50a), and again ccRCC was found to have the lowest chance of survival out of the three subtypes. Female ccRCC patients were found to have the lowest median survival of 90.41 months, while male ccRCC patients were found to have a median survival of 116.75 months. Median survival

was not able to be calculated for male or female pRCC or chRCC patients as over 50% of patients were still alive by the end of the study.

As previously shown earlier in this chapter, left-sided ccRCC tumours have a lower chance of survival compared to right-sided tumours, however no significant differences in survival curves were found when comparing tumour laterality in pRCC or chRCC (Figure 4/50b). Median survival could not be calculated for the pRCC and chRCC groups as over 50% of patients were still alive at the end of the study, however left-sided ccRCC tumours were found to have the lowest median survival or 76.97 months, compared to right-sided tumours which had a median survival of 118.76 months.

Survival analysis was next completed for each subtype with age at operation split into decades (data not shown), and as expected, ccRCC was found to have the lowest median survival, with the 70-79 age group having the lowest median survival of all the groups studied of 64.52 months. This age group was also the most at risk in the other subtypes with a median survival of 71.35 months in chRCC and 76.58 months in pRCC. The 80-89 age group was found to be at the next highest risk, with a median survival of 71.94 months in ccRCC and 88.17 months in pRCC.

Survival analysis was lastly completed for OS by patient race (data not shown). ccRCC was found to have the lowest overall chance of survival, with the Black or African American group having the lowest median survival of 62.84 months, followed by the ‘other’ group of 84.23 months and the white group at 92.97 months. The Black or African American group was also found to have the lowest median survival in pRCC of 86.2 months, while no median survival statistics could be calculated for any of the chRCC groups as over 50% of patients were still alive at the end of the study.

Finally, pRCC can be split into Type 1 and Type 2 depending on the tumour histologic and cytogenetic features, so we performed comparison of the survival curves for these groups to determine if there is an effect on outcome, as shown in Figure 4.51.

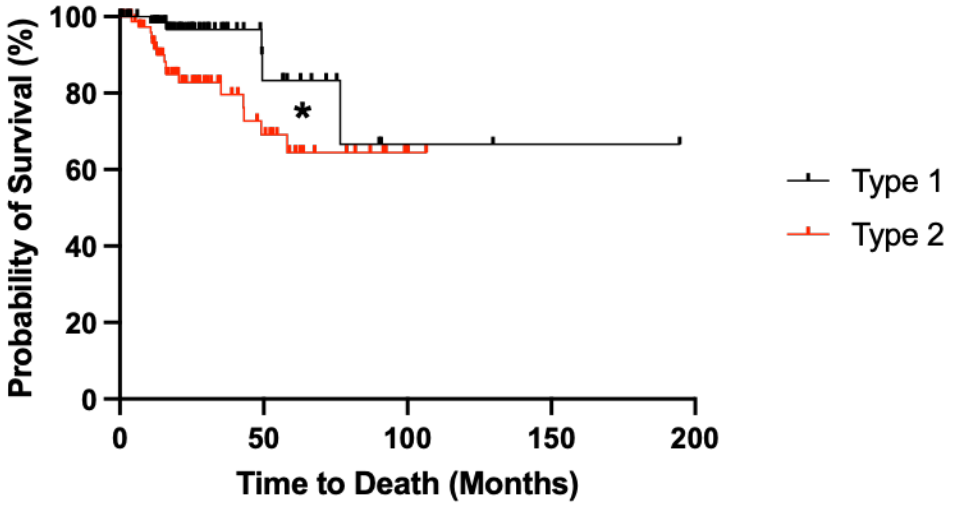

Figure 4.51 Overall survival by pRCC type
Logrank analysis was used to compare Kaplan-Meier survival curves between type 1 and 2 pRCC patients, where * represents p <0.05.

Type 2 pRCC was found to have a significantly lower chance of survival compared to Type 1 (p=0.0345), however median survival could not be calculated as over 50% of patients were still alive at the end of the study.

Out of the 3 RCC subtypes, ccRCC was found to have a significantly lower median survival than both pRCC and chRCC, and is also unfortunately the most common subtype. This pattern was still found to be the case when patients were split by characteristics such as sex, primary tumour laterality, age at operation and race. To determine if tumour immune infiltrate could be a factor which contributes to prognosis, we next ran the three RNAseq datasets through CIBERSORTx to determine differences in the estimated immune composition and their impact on patient survival.

4.4.3 Comparison of subtype estimated immune composition

CIBERSORTx is used to estimate the immune composition of 22 immune cell types based on the LM22 gene set which comprises of 547 genes which can accurately distinguish between human hematopoietic cell populations including 7 T cell types, NK cells, plasma cells, B cells and myeloid subsets based on their gene expression

profiles (GEPs). These GEPs are then transformed into the infiltrating immune cell proportions and the significant results ($p<0.05$) were selected for subsequent analysis. Following CIBERSORTx analysis, PCA was firstly run on the three sets of results to see how similar the CIBERSORTx results were, as shown in Figure 4.52.

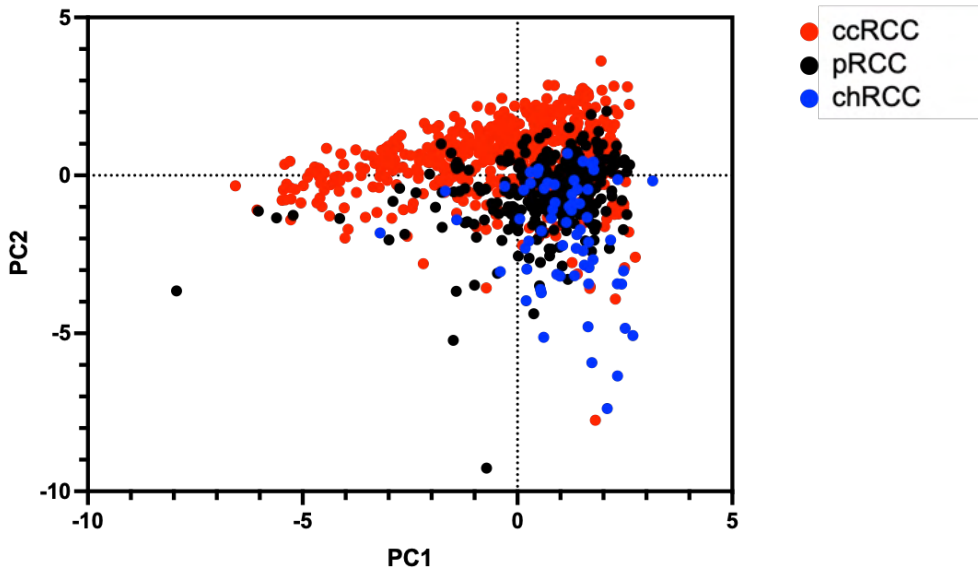

Figure 4.52 Principal component analysis of the estimated immune infiltrate of the three RCC subtypes
PCA was used to compare the estimated immune fraction data for the three RCC subtypes. ccRCC and pRCC were found to spread most widely along the PC1 axis, while chRCC spread along the PC2 axis.

PCA showed that ccRCC and pRCC are mostly spread over the same PC1 axis, while chRCC was spread more over the PC2 axis. This implies that ccRCC and pRCC will have a more similar immune composition to each other than to chRCC and so could result in differences in the immune landscape. To explore this further, we next compared the CIBERSORTx results for each cell type between the subtypes, as shown in Figure 4.53.

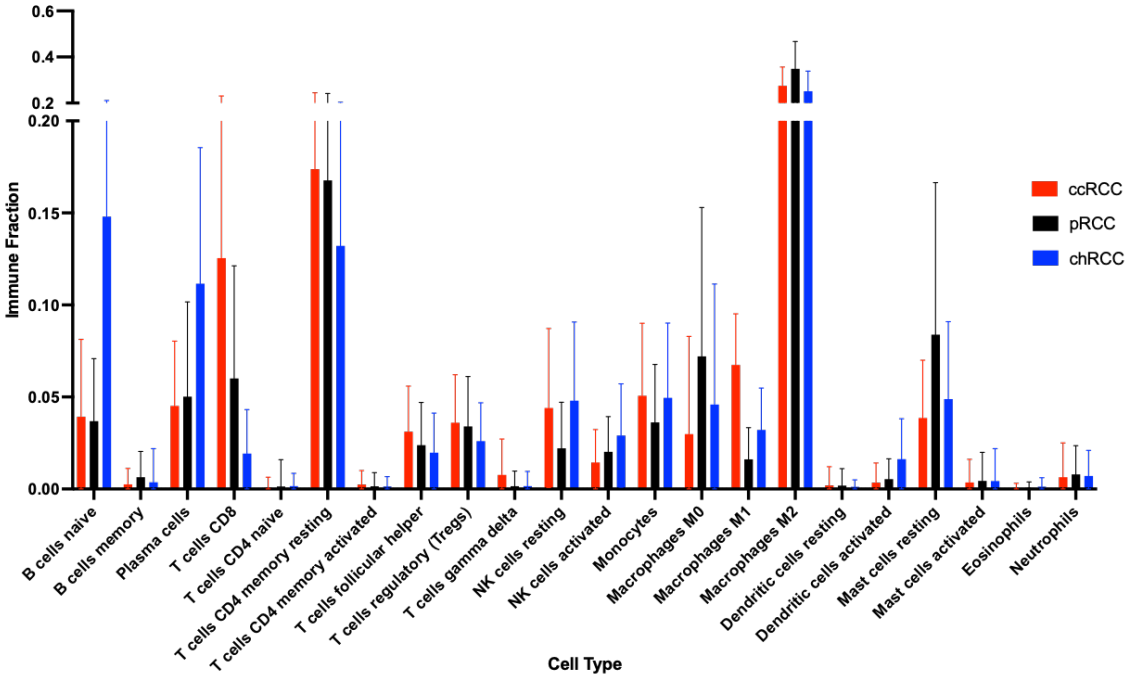

Figure 4.53 Comparison of RCC subtype estimated immune cell fractions
All 22 CIBERSORTx cell types were compared between the three RCC subtypes using a Mann-Whitney test with Dunn's multiple correction test. Significant differences were observed between many groups, as described in the text of section 4.4.3.

Comparison between the three RCC subtypes revealed significant differences between many immune cell types.

In ccRCC, levels of CTLs, Tfh cells, gamma delta T cells, resting NK cells, monocytes and M1 macrophages were all found to be significantly higher than those in pRCC (all $p<0.0001$). Conversely, levels of memory B cells, activated NK cells, M0 macrophages M2 macrophages and resting mast cells were all found to be significantly higher in pRCC compared to ccRCC (all $p<0.0001$). No significant differences were found between naïve B cells, plasma cells, naive CD4 T cells, memory activated or resting memory CD4 T cells, Tregs, resting or activated dendritic cells, activated mast cells, eosinophils or neutrophils.

Comparison of the ccRCC vs chRCC datasets also found significant differences between some immune cell types. In ccRCC, CTLs, memory resting CD4 T cells, Tfh cells and M1 macrophages were all found to be significantly higher than chRCC (all $p<0.0001$). Tregs ($p=0.0008$) and gamma delta T cells ($p=0.0052$) were also significantly higher in ccRCC compared to chRCC. Levels of naïve B cells, plasma cells, activated NK cells, activated dendritic cells were all significantly higher in chRCC compared to ccRCC (all $p<0.0001$), as were resting mast cells ($p=0.0072$).

No significant differences were found between memory B cells, naïve CD4 T cells, activated memory CD4 T cells, resting NK cells, monocytes, M0 and M2 macrophages, resting dendritic cells, activated mast cells, eosinophils and neutrophils.

Finally, comparison of the pRCC and chRCC datasets found that in pRCC, CTLs, resting memory CD4 T cells and M2 macrophages were all significantly higher than in chRCC (all $p<0.0001$). Tregs ($p=0.0099$), M0 macrophages ($p=0.0050$) and resting mast cells ($p=0.0002$) were all also significantly higher in pRCC compared to chRCC. In chRCC however, naïve B cells, plasma cells, resting NK cells, and activated dendritic cells were all significantly higher than in pRCC (all $p<0.0001$), as were activated NK cells ($p=0.0007$) and monocytes ($p=0.0012$). No significant differences were found between memory B cells, naïve CD4 T cells, activated memory CD4 T cells, Tfh cells, gamma delta T cells, resting dendritic cells, activated mast cells, eosinophils and neutrophils.

This data confirms what we have already shown in our previous ccRCC analysis, which is the subtype with the worst prognosis, that the levels of Tfh cells, CTLs, resting NK cells and Tregs are all higher than the other subtypes, while also having the lowest level of activated NK cells. This data suggests that our characteristic high effector T cell immune signature is unique to ccRCC and correlates with poor prognosis. Conversely, chRCC was found to have the best prognosis and showed the opposite immune signature to ccRCC, presenting the lowest levels of Th, CTL and Tregs with the highest level of activated NK cells, however the only outlier was the level of resting NK cells which was interestingly similar to the levels found in ccRCC.

4.5 Discussion

In this chapter we have investigated the immune infiltrate in ccRCC compared to normal kidney, between the three most common RCC subtypes and by ccRCC tumour CD200 expression by bioinformatic analysis, IF staining and functional co-culture assays. We have found significant differences in the levels of key immune cells and have found strong links to patient survival in relation to a characteristic high

effector T cell immune signature, which is altered further in relation to CD200 expression.

We firstly examined the survival data of a publicly available RNAseq dataset by patient and clinical characteristics to determine if any characteristics predispose a patient to shorter overall survival. Unsurprisingly, increased patient age and advanced TNM status were related to shorter survival times, however interestingly, primary tumour laterality was also shown to be an important characteristic, with left-sided tumours resulting in a significantly shorter overall survival compared to right-sided or bilateral tumours. This effect may be due to embryonic differences, anatomical differences, blood supply, lymphatic drainage or relationship to other organs, and has been observed in other studies (Guo et al. 2019). Metastasis status was found to be the greatest risk factor to patient survival, with an M1 status resulting in a 4-fold increased hazard ratio compared to an M0 status.

Next, estimated immune fraction for the 533 ccRCC samples and 93 normal kidney samples was calculated using CIBERSORTx, an online “digital cytometry” deconvolution algorithm which is able to compare large numbers of samples, providing an estimated immune fraction for 22 immune cell types. Significant differences were observed in the immune fraction of 10 of the 22 immune cell types between ccRCC and normal kidney. However, after further stringent analysis comparing log2 fold change and p value, only 9 immune cells were determined to be significantly over- or under expressed, and therefore classed as key immune cells, namely: naïve B cells, plasma cells, M0 and M1 macrophages, T follicular helper (Tfh) cells, cytotoxic T cells (CTLs), Tregs, activated NK cells and resting NK cells.

Tumour associated macrophages are a major cell type within the TME and play a critical role in both tumour development and the differentiation of T cells into their final effector states. M0 macrophages are naïve and are able to differentiate into M1 or M2 phenotypes depending on the cytokines and chemokines they are exposed to, while M1 macrophages are differentiated and have roles in antigen presentation and inflammation. M0 and M1 macrophages were both found to be significantly over expressed in ccRCC compared to normal kidney, with high levels of M0 macrophages significantly reducing overall survival compared to low levels, however the level of M1 macrophages had no effect on survival. The significant increases of both M0 and M1 macrophages in ccRCC compared to normal kidney may indicate

an important role for these cells in ccRCC disease progression and prognosis, as high M0 macrophage levels have been implicated in ccRCC metastasis development (Yaohai et al. 2020), however the presence of M1 macrophages is generally associated with positive outcome.

We next examined NK cells within our samples, where we found that the predominant NK phenotype is resting, whereas in the normal kidney, the active NK phenotype is significantly more prominent. This result was unexpected, as NK cells are the first line of defence against tumour cells in the humoral immune response, so an increased active, cytotoxic NK phenotype would be expected in a ccRCC disease state. This may be the case for a number of reasons, including lack of exposure to activating cytokines or tumour cell immune evasion, or a result of NK cell exhaustion, which results in decreased cytolytic activity leading to decreased levels of cytolytic molecules such as granzymes and perforin, IFN-γ and CD107a (Bi and Tian 2017; Sun et al. 2017). We have shown that the levels of activated NK cells increase with advanced disease stage, however interestingly, the levels remained lower than those found in the normal kidney samples. Survival was not significantly impacted by high or low levels of resting or activated NK cells, however the highest median survival was found in the low resting NK cell group, which we found was generally correlated with the high activated NK cell group. This indicates that the NK cell immune response is significantly altered in a ccRCC state compared to the normal kidney, leaning towards a resting, rather than an active phenotype. This dysfunctional NK-mediated humoral immune response may result in a reduction of overall cytotoxic ability, as resting NK cells do not produce the cytokines required to activate T cells and other parts of the anti-tumour response in the adaptive immune system, therefore resulting in disease progression.

Through our subsequent analyses we have shown high fractions of naïve B cells in normal kidney compared to ccRCC, implying that high levels of this cell type may be beneficial compared to low levels, however no significant change was observed between the two groups in our survival analysis. High estimated fractions of plasma cells were also present in normal kidney compared to ccRCC, which were also found to be protective compared to low levels, but not significant. The significant decrease in both naïve B cells and plasma cells found in ccRCC compared to normal kidney may imply that these cell types are highly affected during ccRCC development, and

that low levels of B cell-derived APCs could be a characteristic signature of ccRCC. These changes may have downstream effects including changes in activation of other immune cell types including T cells, leading to a highly altered immune cell landscape within the TME. However, as T Helper cells also secrete cytokines to trigger naïve B cell differentiation into plasma cells, ccRCC-related T cell dysfunction could also be a cause for the low plasma cell levels observed. IL-2 produced by T cells is an essential requirement for naïve B cell differentiation into plasma cells, so cancer-related dysfunction of T cells resulting in reduced production of IL-2 may be responsible for high numbers of naïve B cells, however a link between ccRCC and plasma cell myeloma has already been established (Syler et al. 2021) which may also explain the high numbers of plasma cells found in ccRCC.

ccRCC is a highly immunogenic cancer type, with the highest T cell infiltration score out of all TCGA cancer types studied (Wang et al. 2021b) and this is associated with prognosis and chemotherapy response rates. The ccRCC TME is highly immunosuppressive, resulting in T cell dysfunction and reduced cytotoxic ability, which has been shown to correlate with tumour grade (Kawashima et al. 2020).

We next examined each key cell type in our samples. Tfh cell levels, which have key roles in driving differentiation and proliferation of B cells resulting in potent antibody-driven immunity, however their role in the anti-tumour response is less clear. The estimated immune fraction of Tfh cells was significantly higher in both the full ccRCC data set and within the matched pair samples compared to normal kidney. We found a significant increase in Tfh level with increased ccRCC stage, however survival analysis found that median OS was around 19% longer in the low Tfh cell group compared to the high group. A significant decrease in plasma cell fraction was found in ccRCC compared to normal kidney, with low levels of plasma cells also correlating with lower median OS, so this may imply that although the levels of Tfh cells are increased in ccRCC, they may be dysfunctional as they do not appear to be driving B cells to proliferate and differentiate into plasma cells as would be expected. These high ccRCC Tfh cells levels could imply an activated immune response, as activated Tfh cells in turn activate other effector T cell types, and we found that these levels significantly increased with ccRCC overall stage, with stage IV showing significantly higher levels than stage I.

We next examined CTLs, responsible for key anti-tumour responses following activation, to invoke a specific and targeted cytotoxic immune response. As expected, we found a significantly higher estimated immune fraction in ccRCC compared to the normal kidney, with a significant increase found with increased disease stage and stage IV was significantly higher than stage I. Interestingly however, this increase in CTL level does not correlate with a better prognosis, with the low CTL group showing a 5% longer median survival time compared to the high CTL group. As we have previously found for Tfh cells, this increased CTL level but apparent inability to halt tumour progression may imply a dysfunctional and/or exhausted CTL state in higher disease stage, possibly resulting in impaired cytokine and cytotoxic granule production resulting in reduced tumour cell killing. The relationship between Tfh cells and CTLs was examined as a measure of the CD4:CD8 ratio. A CD4:CD8 ratio of less than 1 would be considered abnormal and is generally associated with a dysfunctional immune response in cancer, other diseases and during viral or bacterial infection. Ratios under 1 are commonly found in HIV (Castilho et al. 2022) and can be prognostic in some cancer types including triple-negative breast cancer (Wang et al. 2017), lung cancer (Clifford et al. 2017) and cervical cancer (Sanif and Nurwany 2019). This ratio has also been shown to be indicative of response to treatment in RCC, where increases in CD4:CD8 ratio have been found to follow IFN treatment (Hernberg et al. 1997).

While a ratio based on absolute cell numbers was not able to be calculated for our samples as CIBERSORTx is only able to compute the relative immune fraction not the absolute cell number, we did find a strong positive correlation between levels of Tfh cells and CTLs, showing that as one cell type increases so does the other, which would equate to a ratio close to 1. The increased levels of these two cell types should imply an activated and effective cytotoxic anti-tumour response, however comparison of survival curves for combinations of high and low Tfh and CTLs, we found that the high Tfh, high CTL group had the worst prognosis out of all possible combinations. This group also had an increased hazard ratio of 1.5 compared to the low group. This implies that although high levels of Tfh cells and CTLs are present in the ccRCC TME, they are dysfunctional and are not providing an effective anti-tumour response, and in fact seem to reduce probability of survival, so high levels of both cell types could have use as a prognostic measure.

We next investigated the estimated immune fraction of immunosuppressive Tregs, which control immune responses by CD4+ and CD8+ T cells to prevent autoimmunity and maintain homeostasis. In disease states including various cancer types, Treg levels increase and inhibit anti-tumour immune responses resulting in disease progression. We observed a significant increase in ccRCC Tregs compared to normal kidney, with a significant increase in relation to increased ccRCC stage. We observed a significant decrease in OS with high Tregs compared to low levels, implying that Treg levels are important in overall disease progression and therefore may also be able to be used as a prognostic factor. As we have however also shown a significant increase in both CD4+ Tfh cell and CD8+ CTL levels with increased ccRCC disease stage, this may imply that in ccRCC, Tregs do not necessarily stop differentiation of T cells into CD4+ and CD8+ effector cells and rather may contribute to their dysfunction, resulting in an ineffective overall cytotoxic immune response. We next analysed the relationship between CD8+ CTLs and Tregs as an indicator of the CD8:Treg ratio. The CD8:Treg ratio is less commonly used than the CD4:CD8 ratio, however it is still a highly informative way to study the state of the immune system and can be used as a measure of the cytotoxic to inhibitory immune cell ratio. Decreases in CD8:Treg ratio have been shown to correlate with poor prognosis in various cancer types, including ovarian (Curiel et al. 2004), lung (Clifford et al. 2017) and breast (Solis-Castillo et al. 2020), however this had previously not been established for ccRCC. We have shown a moderately strong positive correlation between the CTL and Treg immune fractions in our ccRCC dataset, however this was not a perfect correlation and so one cell type may increase disproportionally compared to the other, resulting in a change in the CD8:Treg ratio. We have also shown that changes in the CTL and Treg fraction have a significant effect OS, with the low CTL, high Treg group, which would equate to a low CD8:Treg ratio. This group had the shortest median survival compared to all other combinations and a 4-fold increased risk compared to the low CD8, low Treg group which had the best probability of survival. Here we have shown that the estimated immune fractions of all of these T cell types, which were found to be significantly altered compared to normal kidney, have significant effects on patent survival and may hold prognostic value in ccRCC. This presents exciting opportunities for potential therapeutic interventions to alter levels of these immune cells to promote an appropriate anti-tumour response.

This data is interesting as even though the estimated immune fraction of Tregs was also found to be significantly higher in ccRCC compared to normal kidney, the fact that levels of other T cell types were also very high suggests that these effector T cells are dysfunctional and unable out their defined roles, potentially due to an altered immune landscape and tumour-mediated immune evasion.

The ccRCC CIBERSORTx data was next split into groups based on patient characteristics of sex, age or primary tumour laterality, however no significant differences in estimated immune fraction of resting or activated NK cells, Tfh cells, CTLs or Tregs were observed. This result is interesting as we have previously shown that both age and tumour laterality have a significant effect on patient overall survival, however we have now shown that these patients characteristics do not appear to be related to the levels of these key immune cells. This data therefore implies that the significant differences we have observed in the levels of these key immune cells between the ccRCC and normal kidney groups are more likely to be due to the presence of the tumour rather than any other general patient characteristic.

Overall, using this data set we have found that the changes in key immune cell level in ccRCC compared to normal kidney have an impact on OS, with low levels of activated NK cells and high levels of effector T cells found to significantly reduce the probability of survival and resulting in a poor prognosis. Based on this data, we can characterise a characteristic ccRCC immune signature associated with poor prognosis comprising of high levels of Tfh cells, CTLs, Tregs and resting NK cells, with low levels of activated NK cells. As we have also shown that levels of these cells increase with advanced ccRCC stage, this signature may also have some prognostic value.

As this analysis was completed using RNAseq data of whole ccRCC tumour samples, which may include non-tumour areas such as stroma and peritumoral normal tissue, our next aim was to investigate this key immune signature using IF staining of patient-derived ccRCC tumour tissue samples, to determine if a similar outcome was observed compared to what was found in the bioinformatic analysis. A limitation of this study was that patient survival data was not available for the TMA samples and so we were unable to calculate the effect of immune cell infiltration on patient survival, however we were still able to determine if the same high effector T

cell signature that we observed in our bioinformatics analysis was present in the tissue samples.

We firstly established that CD45+ cell density and frequency of all cells was significantly higher in all ccRCC stages compared to normal kidney, as was the case for CD3+ T lymphocytes, showing as expected, that overall ccRCC tumour immune infiltrate is significantly higher than normal kidney, and increases as disease progresses. A significant decrease in Th cell density and frequency of CD45+ cells was found with increased ccRCC stage, which was different to the results of our bioinformatic analysis, where a significant increase in estimated immune fraction was found with increased stage, however as CIBERSORTx is only able to calculate the estimated immune fraction of CD4+ T follicular helper (Tfh) cells, a specialised subset of Th cells which are characterised by the presence of CXCR5, which we were not able to stain for, these results are not directly comparable, but imply that the expression of subsets of CD4+ cells are also altered by ccRCC disease state. This issue highlights one of the limitations of IF staining, where only a limited number of markers can be used due to antibody availability and so in this case only 3 markers could be analysed, whereas CIBERSORTx enables a large number of markers to be easily used to specifically characterise cells based on the expression of multiple genes. This is a limitation of the study and may mean that although we have shown bioinformatically that the immune fraction of Tfh cells is estimated to increase with ccRCC stage, our absolute and relative cell numbers of Th cells gained from our IF staining reveals that different subtypes of CD4+ T cells may be altered differently by ccRCC stage. Further study would be required to characterise the levels of all T cell subsets.

A significant increase in cell density and frequency of CTLs was found with increased ccRCC stage, in line with what was observed in our CIBERSORTx bioinformatic analysis. This should imply an activated anti-tumour immune response; however, it is unclear whether these increased numbers of CTLs are functional and therefore able to execute the full cytotoxic response against tumour cells. To determine the overall state of the immune response in our samples, the CD4:CD8 ratio was calculated, where all ccRCC stages were found to have an average ratio of around 1, while the average normal ratio was 1.6. This implies that although the CD4:CD8 ratio does not generally change throughout ccRCC disease progression

and there is no clear correlation between the absolute numbers of CD4+ Th and CD8+ CTL cells in ccRCC, the ratios are clearly different to those observed in normal kidney tissue. This may suggest that the factors in the TME which predispose naïve T cells to differentiate into CTLs are present in higher levels than those required for differentiation into Th cells, resulting in an abnormal ratio in ccRCC, altering the immune infiltrate within the TME compared to normal kidney. Again, these results do not however directly correlate with what we observed in our analysis of the CD4:CD8 cell relationship using our CIBERSORTx estimated immune fraction data, where correlation analysis found a significant positive relationship between CD4 and CD8 cells, however the actual ratio could not be calculated for this data as CIBERSORTx data only provides an estimated immune fraction rather than an absolute number, and as previously discussed CIBERSORTx is only able to provide data for Tfh cells while we are staining for general CD4+ Th cells.

A significant increase in both cell density and frequency of Tregs was observed in ccRCC compared to normal kidney, and between ccRCC stages, which mirrors what we have already found in our bioinformatic analysis. Interestingly, Tregs were also the only cell type to show any significant difference between sex, with male patients having significantly higher density and frequency of Tregs compared to female patients, however the reason for this is unclear. As Tregs are able to suppress T cell responses, these high numbers of Tregs may explain the low numbers of Th cells observed in our TMA samples, however they may also be responsible for dysfunction of the Th and CTL cells creating an ineffective cytotoxic response. The CD8:Treg ratio was next calculated with no change in ratio observed between normal kidney and ccRCC, or between ccRCC stages, which may imply that the high numbers of CD8+ CTL cells found in our samples, which increase with ccRCC disease stage, increase at the same rate as the numbers of Tregs found in most of the samples. However as previously discussed, the CTLs present may be dysfunctional and unable to carry out the cytotoxic response as expected. As the patient survival data was unfortunately unavailable for these samples, we are unable to determine if these high CD8:Treg ratios are helpful to OS or response to chemotherapy, as has been shown in other cancer types, so this would be something to establish in future research.

A significant increase in cell density and frequency of NK cells was found in stage I ccRCC compared to normal kidney, however these levels decreased with increased ccRCC stage. A limitation with IF staining is the limitations due to antibody availability and combinations, meaning that we were not able to determine if these NK cells were resting or activated to correspond with our bioinformatic data, however this would again be an interesting area of future research. The biggest changes in correlation relationships were found between the NK cells with the other cell types, all of which switched from negative or positive relationships in normal kidney to the opposing relationship in ccRCC, implying that NK cells are the most deregulated cell type in ccRCC, and this may be a key factor in ccRCC disease progression.

Overall, this data shows that the complicated relationships between the various types of T cells are altered between normal kidney and ccRCC, and therefore may have an important impact on the overall cytotoxic immune response, with dysfunction and impairment of T cell responses apparent in ccRCC, resulting in disease progression. As patient survival data was unfortunately not available with our TMA samples, we are unable to determine if the alterations in ccRCC immune infiltrate we have observed compared to normal kidney have an impact on patient survival, however this would be an interesting direction for future research.

The common RCC subtypes have histological and genetic differences alongside significantly different clinical characteristics and prognosis. ccRCC is the most common and most aggressive subtype, where common gene mutations including MF12 and APOB result in a predisposition to metastasis, however infiltration of immune cells including T cells and NK cells has been associated with increased aggressiveness and poor prognosis (Puzanov 2022). The immune landscape of ccRCC has been previously described, (Wang et al. 2021b; Saad et al. 2022), however this has been much less widely studied in pRCC and chRCC.

We used the same Firehose Legacy RNAseq data sets for the pRCC and chRCC subtypes to examine their estimated immune fraction, which was found to vary significantly between each RCC subtype, a factor which may contribute to the varying OS and DFS outcomes observed between the subtypes. chRCC had the best OS and DFS, while ccRCC having the worst outcomes, as expected. Variation in immune infiltrate adds to the already complex landscape of RCC and may increase the difficulty of treating RCC with immunotherapy, as each subtype may

require a different, targeted treatment course. While individual samples may differ, group comparisons between RCC subtypes showed more similarities in immune infiltrate between ccRCC and pRCC, with the most significant changes in immune cell levels found between ccRCC and chRCC groups and the pRCC and chRCC groups. The similarity in ccRCC and pRCC could be in line with other similarities found between the two subtypes due to the two reportedly having the same cell of origin, the epithelium of the proximal convoluted tubule, while chRCC originates from the distal renal tubule. The sample size for chRCC was however the smallest out of the three (ccRCC n=512, pRCC n=291, chRCC n=91), so this should be taken into consideration when directly comparing the groups. ccRCC was found to have significantly higher levels of CTLs compared to pRCC and chRCC. ccRCC also had the lowest levels of activated NK cells, with a high level of resting NK cells, as also observed in pRCC. ccRCC was also found to have the highest levels of Tregs out of the three subtypes, resulting in an overall proinflammatory tumour microenvironment with reduced cytotoxic capacity. Naïve B cells and plasma cells were found to be significantly higher in chRCC compared to ccRCC and pRCC. Interestingly, chRCC was found to have the highest levels of activated dendritic cells out of the 3 subtypes, yet the lowest levels of CTL and Tfh cells. This implies that some B cells may not be activated in chRCC and so antigen presentation could be carried out by activated dendritic cells instead. In combination with the low levels of Tfh cells present to assist in B and T cell activation, this may result in a proinflammatory environment with low activation of cytotoxic T cell responses. As we have previously found in our ccRCC analysis, in pRCC and chRCC, no significant differences were found between any of the subtypes for naïve CD4 T cells, activated memory CD4 T cells, activated mast cells, eosinophils or neutrophils, so levels of these cell types may not be changed between the subtypes. Overall, this data implies that ccRCC has a significantly different immune signature to the other common subtypes, pRCC and chRCC. This is interesting as ccRCC has a significantly worse prognosis with the lowest OS statistics out of the three subtypes, so this implies that levels of RCC immune infiltrate are highly important in disease progression and prognosis. Therefore, the characteristic high effector T cell signature comprised of high Tfh cells, CTLs, Tregs and resting NK cells is uniquely found in ccRCC and not the other subtypes.

4.6 Conclusions

In this chapter, we have shown both using bioinformatic analysis of large RNAseq data sets and IF staining of patient derived tissue samples, that the RCC tumour immune infiltrate is significantly altered compared to that of normal kidney, with detrimental effects on patient survival. We have been able to define a characteristic ccRCC immune signature associated with poor prognosis, consisting of high levels of Th cells, CTLs, Tregs and resting NK cells, with low levels of activated NK cells. This signature was found to have significantly poorer prognosis compared to the opposite low levels of each of these cells.

Chapter 5: Characterising RCC Immune Infiltrate by CD200 Expression

5. Characterising RCC Immune Infiltrate by CD200 Expression

5.1 Analysis of ccRCC datasets by CD200 expression

In the previous chapter we established the survival statistics and bioinformatically quantified the immune fraction of both ccRCC and other RCC subtypes. In this chapter, we determine if expression of cell surface immune checkpoints such as CD200 can alter the immune infiltrate of a ccRCC tumour. Earlier in this thesis we showed a significant increase in CD200 expression in ccRCC compared to normal kidney, as well as significant differences in immune infiltrate in ccRCC compared to normal kidney. We next aimed to determine if these altered levels of immune infiltrate could be related to CD200 expression. The interaction of CD200 with its receptor, CD200R is an immune checkpoint which regulates immune responses and has been implicated in the pathogenesis of several cancer types by contributing to tumour cell immune evasion. Increased CD200 expression has been found in many cancer types including multiple myeloma, testicular cancer and chronic lymphocytic carcinoma, with overexpression also reported in RCC (Moreaux et al. 2008). When we examined CD200 expression in normal kidney and RCC subtype tumour tissue, we found significant differences in expression level. As the strongest expression was found in our ccRCC samples, our next aim was to determine whether CD200 expression influenced the composition of the ccRCC immune cell infiltrate using both bioinformatic analysis of RNAseq data and IF staining of patient derived tissue samples.

5.1.1 Patient characteristics by CD200 expression

We firstly split the results of our ccRCC CIBERSORTx analysis into groups of weak (lower quartile), moderate (middle two quartiles) and strong (top quartile) CD200 gene expression, and determined if patient or clinical characteristics correlate with changes in CD200 expression and patient clinical outcome. Patient characteristics by CD200 expression can be found in Table 5.1.

Table 5.1 ccRCC patient characteristics by CD200 expression

	ccRCC		
CD200 Expression	**Weak**	**Moderate**	**Strong**
	n=134	n=269	n=134
Age at Diagnosis			
Median	63	61	58.5
Range	33-88	32-90	26-90
Gender			
Male	87 (65%)	166 (62%)	92 (69%)
Female	46 (35%)	100 (38%)	42 (31%)
Stage			
I	69 (52%)	145 (55%)	53 (40%)
II	16 (12%)	25 (9%)	19 (14%)
III	29 (22%)	62 (23%)	32 (24%)
IV	19 (14%)	34 (13%)	30 (22%)
Tumour			
T1	6 (5%)	10 (3.8%)	5 (3.7%)
T1a	28 (21%)	85 (32.0%)	28 (20.9%)
T1b	38 (29%)	51 (19.2%)	22 (16.4%)
T2	15 (11%)	24 (9.0%)	16 (11.9%)
T2a	0	5 (1.9%)	5 (3.7%)
T2b	1 (1%)	1 (0.4%)	2 (1.5%)
T3	0	4 (1.5%)	1 (0.7%)
T3a	21 (16%)	63 (23.7%)	37 (27.6%)
T3b	15 (11%)	22 (8.3%)	15 (11.2%)
T3c	2 (2%)	0	0
T4	7 (5%)	1 (0.4%)	3 (2.2%)
Node			
NX	62 (47%)	148 (56%)	67 (50%)
N0	64 (48%)	111 (42%)	65 (49%)
N1	7 (5%)	7 (3%)	2 (1%)
N2	0	0	0
Metastasis			
MX	14 (11%)	12 (5%)	6 (4%)
M0	103 (77%)	220 (83%)	99 (74%)
M1	16 (12%)	34 (13%)	29 (22%)
Laterality			
Left	64 (48%)	128 (47%)	59 (44%)
Right	69 (52%)	137 (52%)	75 (56%)
Bilateral	0	1 (1%)	0
Race			
White	101 (76%)	240 (90.2%)	121 (90%)
Black/African American	26 (20%)	21 (7.9%)	9 (7%)
Asian	3 (2%)	3 (1.1%)	2 (1%)
Other	3 (2%)	2 (0.8%)	2 (1%)
Overall Survival (Months)			
Median	33.48	42.84	38.52
Range	0.1-119.28	0.07-133.84	0.43-149.05
Disease Free Survival (Months)			
Median	33.02	37.22	32.62
Range	0.1-119.28	0.1-133.84	0.62-130.98
Vital Status			
Alive	84 (63%)	191 (72%)	83 (62%)
Dead	49 (37%)	75 (28%)	51 (38%)

To firstly check the levels of CD200 expression within the ccRCC dataset, we looked at the CD200 gene expression by ccRCC stage compared to normal kidney and TNM status, as shown in Figure 5.1.

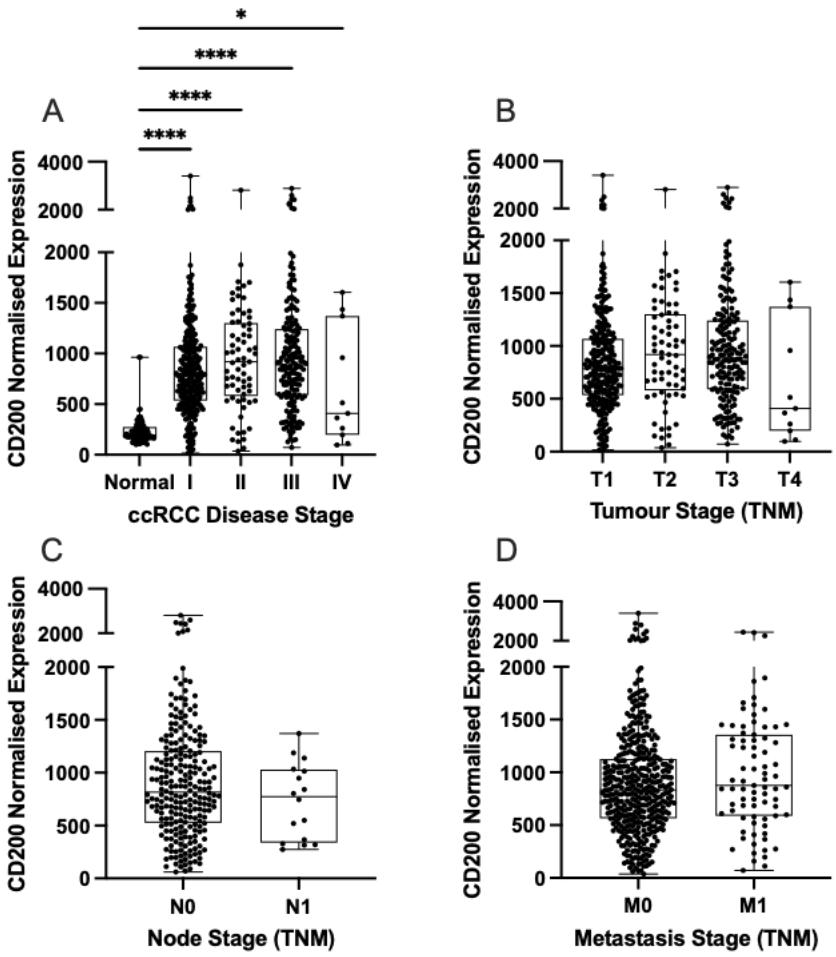

Figure 5.1 CD200 expression by ccRCC stage and TNM status
(A) CD200 expression in normal kidney and ccRCC samples by stage, (B) CD200 expression in TNM tumour stages 1-4, (C) CD200 expression in TNM node stages 0-1, (D) CD200 expression in TNM metastasis status 0-1. Analysis was completed using (A-B) a Kruskal-Wallis with Dunn's multiple corrections tests or (C-D) a Mann-Whitney test, where * represents p <0.05 and **** represents p <0.0001.

All ccRCC stages were found to have significantly higher CD200 expression compared to normal kidney (Figure 5.1a, stage I 841.0 ± 460.5 vs 234.7 ± 133.0, p<0.0001, stage II 942.9 ± 512.6 vs 234.7 ± 133.0, p<0.0001, stage III 960.4 ± 525.9 vs 234.7 ± 133.0, p<0.0001, stage IV 666.1 ± 569.9 vs 234.7 ± 133.0, p=0.0290), with a gradual increase in expression observed from stage I to III, with a decline in expression found at stage IV, however this was not significant compared to the other groups. CD200 levels were consistent between tumour grades T1-3, with a decrease

again observed at T4 (Figure 5.1b), however this group had a much smaller n number compared to the others. A slight decrease in CD200 expression was found in node grade N1 compared to N0 (Figure 5.1c), and a slight increase in expression was found in metastasis grade M1 compared to M1 (Figure 5.1d), however no differences were found to be significant.

CD200 expression was next compared by patient characteristics of sex, age at operation, race and primary tumour laterality, as shown in Figure 5.2.

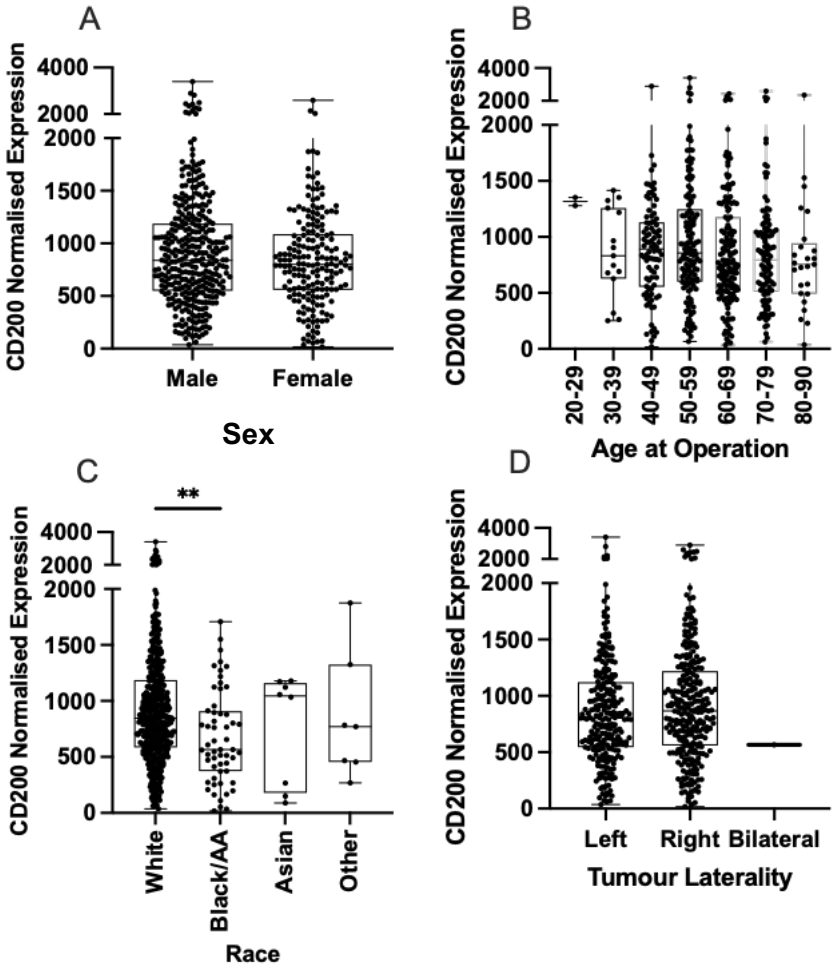

Figure 5.2 CD200 expression by patient characteristics
(A) CD200 expression by sex, (B) CD200 expression by age at operation (C) CD200 expression by race (D) CD200 by primary tumour laterality. Analysis was completed using a Kruskal-Wallis test with Dunn's multiple corrections test, where ** represents $p < 0.01$.

No difference was found in CD200 expression between male and female patients (Figure 5.2a), and a general trend of decreased expression was found with

increased patient age (Figure 5.2b), however there was no significant differences observed between any of the groups. 87% of this cohort were white and this group was found to have the highest CD200 expression, which was significantly higher than the black/African American (AA) group (Figure 5.2c, 920.0± 497.9 vs 674.7 ± 415.8, p=0.0019). No differences were found between right-or left-sided primary tumours (Figure 5.2d), while only 1 patient had bilateral tumours, which interestingly had lower CD200 expression than the average of the other groups.

From this data we can determine that the only clinical characteristic which significantly alters CD200 expression is ccRCC stage, where increased expression was observed in ccRCC compared to normal kidney, and a gradual increase was observed between stages I-III. Interestingly, race was the only patient characteristic which affected CD200 expression, as white patients were found to have higher levels of CD200 compared to other races. It is unclear from this data alone whether CD200 expression is detrimental to survival as its expression increases in ccRCC compared to normal kidney and with ccRCC stage, or protective, as the highest levels were found in the white patients, which had the best overall survival chance of all the races compared.

5.1.2 Survival analysis by CD200 expression

The weak, moderate and strong CD200 expression groups were compared to determine if overall CD200 expression has any impact on overall survival and disease-free survival, as shown in Figure 5.3.

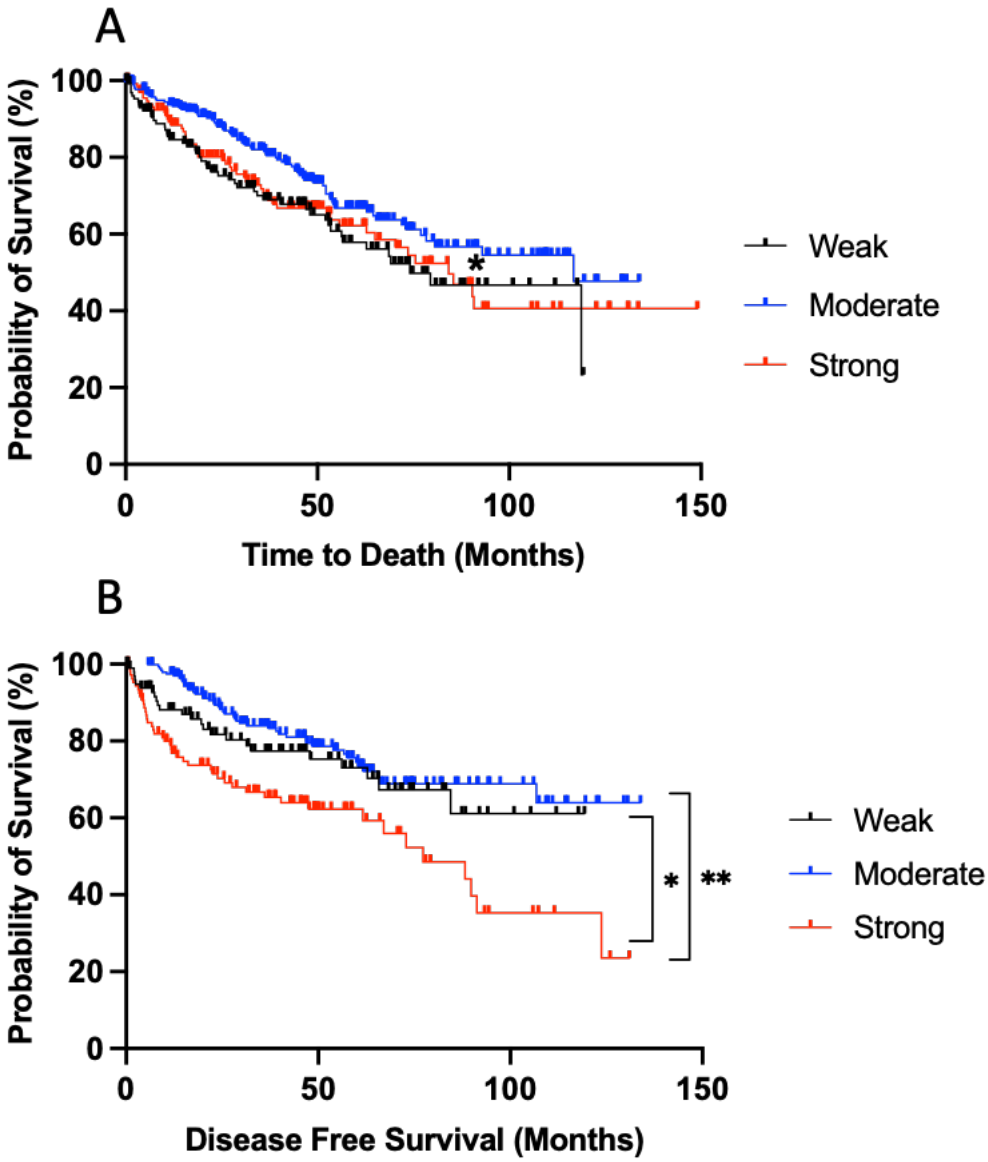

Figure 5.3 Overall survival and disease-free survival by CD200 expression
Logrank analysis was used to compare Kaplan-Meier survival curves in the three CD200 expression groups for (A) overall survival and (B) disease-free survival, where * represents p <0.05 and ** represents p <0.01.

In this data set, the weak CD200 expression group was found to have the shortest median survival (Figure 5.3a, median survival 74.11 months), followed by strong expression (84.23 months). Moderate CD200 expression was found to have the best

median survival (116.75 months) and was significantly better than the weak group (p=0.0277). Disease-free survival was however found to be significantly shorter in the strong CD200 expression group (Figure 5.3b, median survival 77.27 months) compared to both the moderate and weak groups (p=0.0033 and p=0.0258). Median survival could however not be calculated for these groups as over 50% of patients were still alive at the end of the study.

This data suggests that while the level of CD200 expression does have an impact on OS, it is interesting that very high or low levels appear to correlate with a reduced chance of survival compared to a moderate expression level. Interestingly, CD200 expression seems to have a more profound effect on DFS, with the strong group having the lowest chance of survival compared to the weak and moderate groups.

To determine if CD200 influences ccRCC immune cell infiltrate and if so, if this contributes to the changes in survival outcome we have observed, we next studied our previous ccRCC CIBERSORTx estimated immune fraction data calculated earlier in this chapter, split by patient CD200 gene expression.

5.2 Estimation of ccRCC immune infiltrate based on CD200 expression

We next examined the CIBERSORTx results for our key effector immune cell signature of Tfh, CTL, Treg and NK cells and compared them between the weak, moderate and strong CD200 groups, as shown in Figure 5.4.

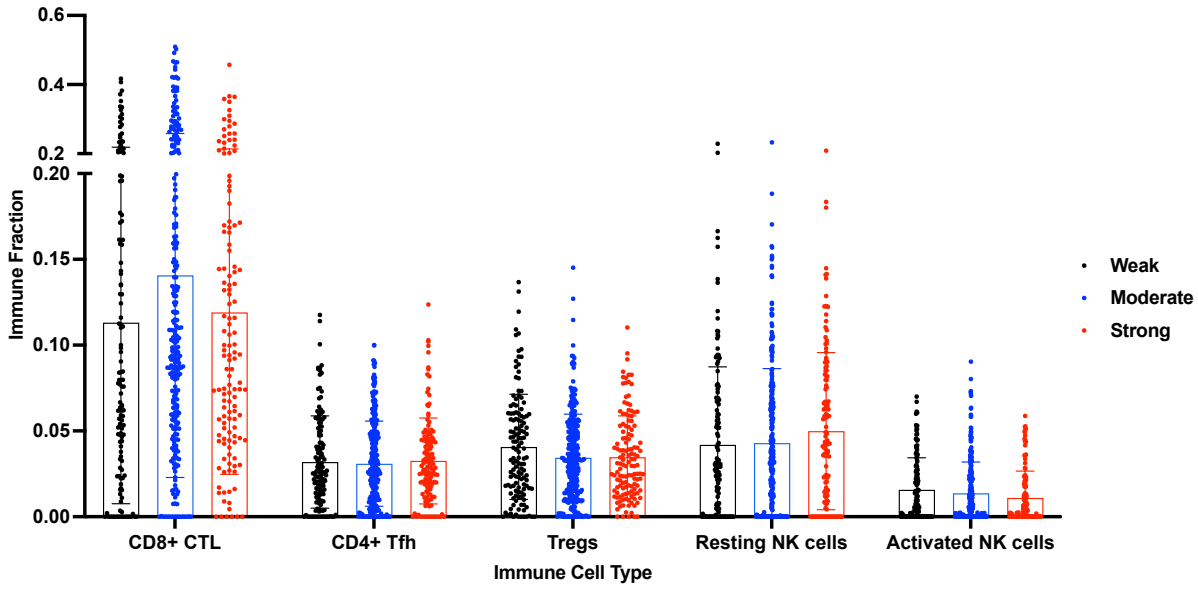

Figure 5.4 Key effector cells by CD200 expression
Estimated immune fraction for our key effector cells was compared between the weak, moderate and strong CD200 expression groups. Analysis was completed using a Kruskal-Wallis test with Dunn's multiple correction tests. No significant differences were observed between any groups.

No significant changes were observed between the levels of any cell types between the three expression groups. A slight increase in resting NK cell level was observed with increased CD200 expression, with the highest numbers found in the strong group compared to moderate and weak groups, while the opposite was found for activated NK cells, which reduced with increased CD200 expression.

5.2.1 CD200 and immune cell correlations

Spearman correlation analysis was next used to determine the relationship between each cell type and CD200 expression, as shown in Figure 5.5.

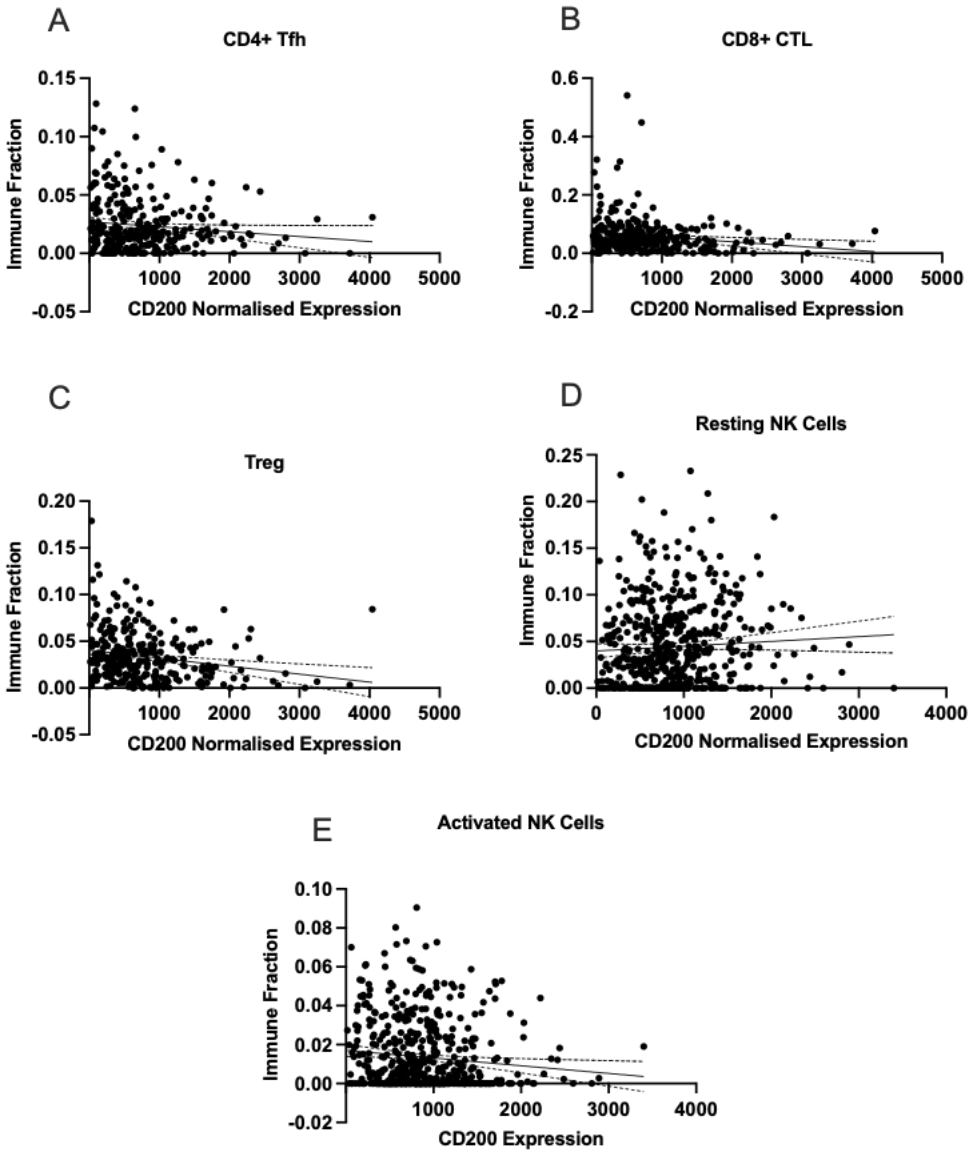

Figure 5.5 Immune cell correlations with CD200
Spearman correlation analysis was used to determine the relationship of ccRCC tumour CD200 with the estimated immune fraction of (A) CD4+ Tfh cells r = -0.0042, (B) CD8+ CTLs, r = 0.0228, (C) Tregs, r = -0.0585, (D) Resting NK cells, r = 0.0756 and (E) Activated NK cells, r = 0.1149, p = 0.0079.

A very weak negative correlation was found between CD200 and Tfh cells (Figure 5.5a, r=-0.0042) and Tregs (Figure 5.5c, r=-0.0585), while a weak positive correlation was found between CD200 and CTLs (Figure 5.5b, r=0.0228) and resting NK cells (Figure 5.**5d**, r=0.0756). The only significant correlation found with CD200

was in activated NK cells, where a weakly negative correlation was observed (Figure 5.5e, r=-0.1149, p=0.0079).

5.2.2 Immune cell correlations by CD200 expression

We next analysed the relationships of our key effector immune cells with each other within the weak, moderate and strong CD200 expression groups, as shown in Figure 5.6.

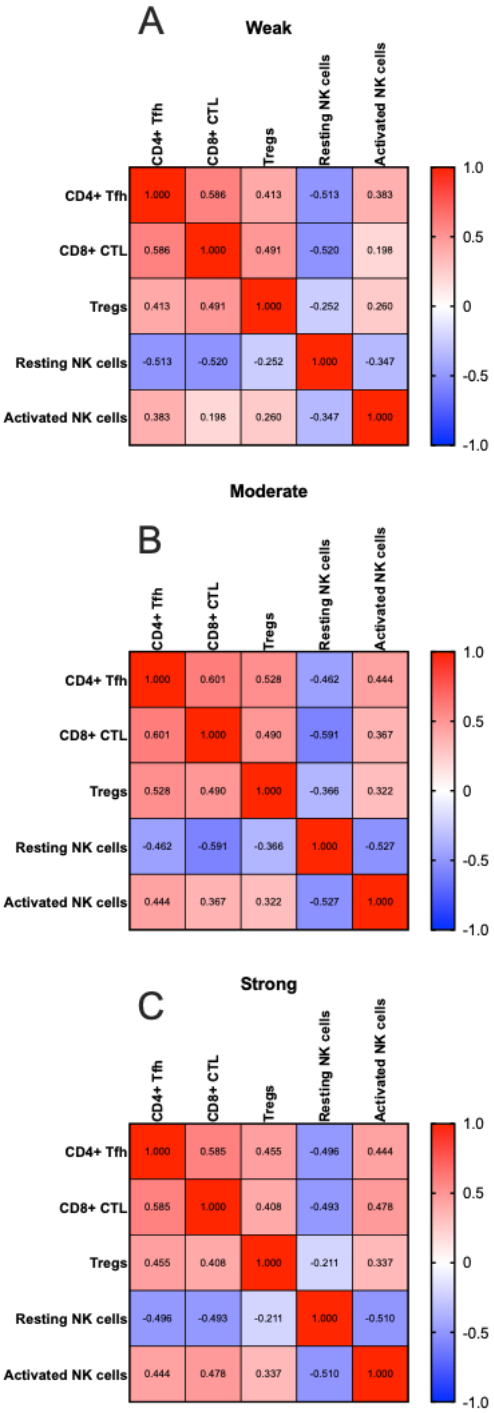

Figure 5.6 Immune cell correlations within CD200 expression groups
Spearman correlation analysis was used to determine the relationships of the estimated immune fractions of key effector cells with each other within the (A) Weak, (B) Moderate and (C) Strong CD200 expression groups. Red represents a positive correlation while blue represents a negative correlation. r numbers are represented within each box.

In the weak CD200 expression group (Figure 5.6a), resting NK cells were found to have significant moderate strength negative relationships with all of the other cell types: Tfh ($r=-0.513$, $p<0.0001$), CTL ($r=-0.520$, $p<0.0001$), Tregs ($r=-0.252$, $p=0.003$) and activated NK cells ($r=-0.346$, $p=0.0001$). All other cell types were found to have positive relationships with each other, with Tfh and CTLs having the strongest positive relationship ($r=-0.585$, $p<0.0001$).

In the moderate correlation group (Figure 5.6b), resting NK cells were again to have moderate strength negative relationships with all other cell types, however the relationships were more negative with CTLs ($r=-0.590$, $p<0.0001$), Tregs ($r=-0.366$, $p<0.0001$) and activated NK cells ($r=-0.527$, $p<0.0001$), however the relationship has become less negative with Tfh cells (($r=-0.462$, $p<0.0001$). Again, Tfh and CTLs were found to have the strongest positive relationship ($r=-0.601$, $p<0.0001$).

In the strong CD200 expression group (Figure 5.6c), the relationship between resting NK cells and Tfh had remained around the same as the moderate group ($r=-0.495$, $p<0.0001$), while the relationships with CTLs ($r=-0.493$, $p<0.0001$), Tregs ($r=-0.211$, $p=0.014$) and activated NK cells (=-0.509, $p<0.0001$) became less negative than the moderate group. The relationship between Tfh and CTLs also became less positive ($r=0.585$, $p<0.0001$).

As the biggest changes in immune cell relationships appear to occur within the moderate group and the weak and strong groups seem to have similar relationship profiles for each cell type, this implies that a moderate level of CD200 expression has the strongest effect on immune infiltrate. As the moderate group was found to have the best chance of overall survival and disease-free survival (Figure 4.56), we can expect that the immune profile found in the moderate group may be the most beneficial level of immune infiltrate to improve patient chance of survival. From Figure 4.58, we can see that the only significant difference in immune composition for any of the cell types was found in CTLs, which had significantly higher levels in the moderate CD200 expression group compared to the weak and strong expression groups.

5.2.3 Overall survival by CD200 expression and immune cell fraction

To determine if CD200 expression and high or low levels of each immune cell type had a significant effect on patient outcome, we next examined each set of patient survival data, as shown in Figure 5.7. A list of p values can be found in supplementary tables S2-S6.

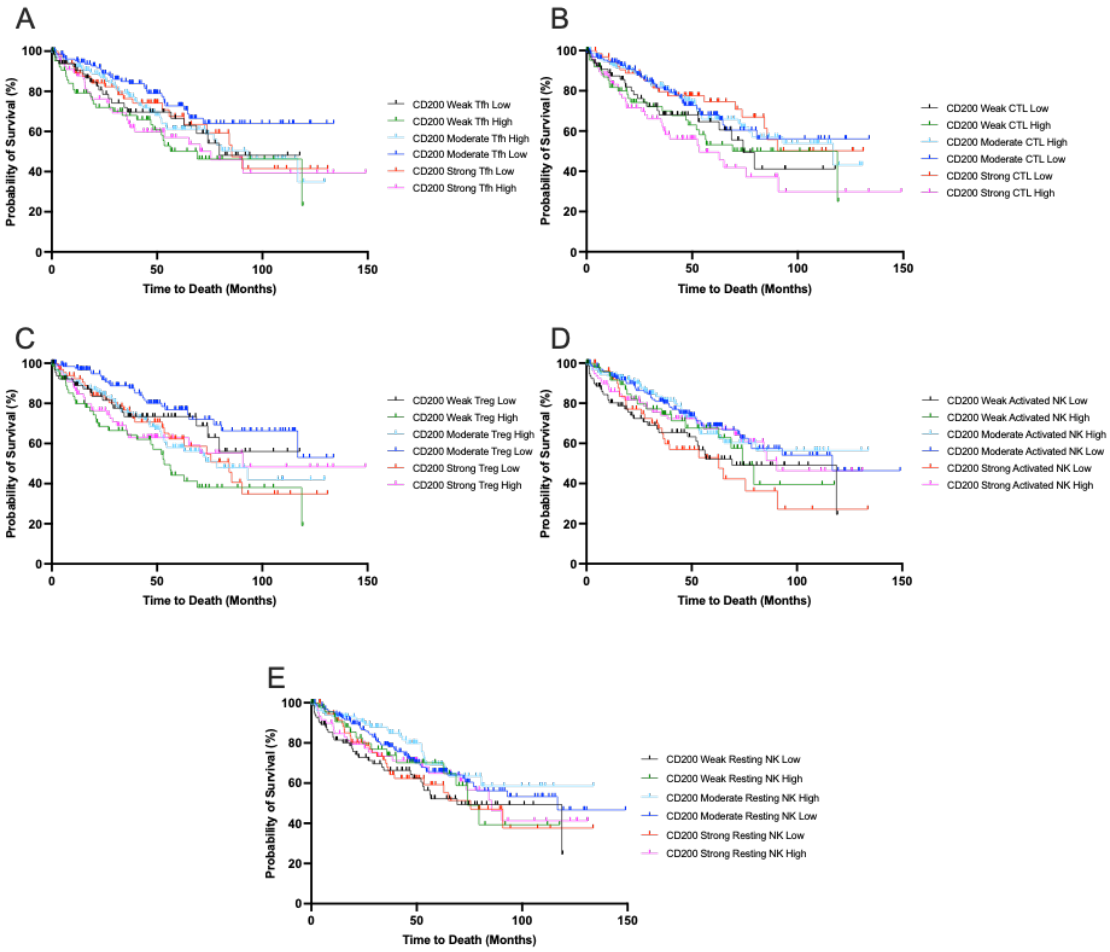

Figure 5.7 Overall survival by CD200 expression and immune cell level
Logrank analysis was used to compare Kaplan-Meier survival curves between the weak, moderate or strong CD200 expression groups and high or low levels of (A) Tfh cells, (B) CTLs, (C) Tregs, (D) Activated NK cells or (E) Resting NK cells. A list of p values for each graph can be found in supplementary tables S2-S6.

The weak CD200 expression, high Tfh group was found to have the shortest median survival (Figure 5.7a, median survival 69.15), while the moderate CD200, high Tfh group was found to have the longest median survival (92.97 months). In the strong CD200 expression group however, the low Tfh group was found to have a longer median survival compared to the high group (85.45 months vs 75.53 months).

In the CTL groups (Figure 5.7b), the strong CD200, high CTL group was found to have the shortest median survival (53.58 months), which was also found to be significantly lower than the strong CD200, low CTL group (p=0.0065). The longest median survival was found in the weak CD200, high CTL group, which was also found to be significantly longer than the weak CD200, low CTL group (118.76 months vs 74.11 months, p=0.0116). The moderate CD200, high CTL group also had a high median survival rate of 116.75 months, however the moderate CD200, low CTL group median survival could not be calculated for comparison as over 50% of the patients were still alive at the end of the study. Comparison of the moderate CD200, high CTL and strong CD200, high CTL group curves revealed that the moderate CD200 group had a significantly better survival outcome than the strong CD200 expression group (p=0.0032).

The weak CD200, high Treg group was found to have the shortest median survival (Figure 5.7c, median survival 53.42 months), which was significantly lower than that of the weak CD200, low Treg group (p=0.0308). The longest median survival was found in the strong CD200, high Treg group (median survival 90.8 months), however this was very similar to that of the strong CD200, low Treg group (median survival 84.23 months).

Comparison of the activated NK cell groups showed the shortest median survival was in the strong CD200, low activated NK cell group (Figure 5.7d, median survival 62.81 months), while the longest median survival was found in the moderate CD200, low activated NK cell group (median survival 116.75 months), and the survival curves were found to be significantly different between these two groups (p=0.0119). Median survival was not able to be calculated for the moderate CD200, high activated NK cell group. The weak CD200, activated NK cell low and high groups both had low median survival outcomes of 69.15 months and 74.11 months respectively.

Conversely, in the resting NK cell analysis (Figure 5.7e), the shortest median survival was found in the weak CD200, low resting NK group (median survival 69.15 months), followed by the weak CD200, high resting NK cell group (median survival 74.11 months). The longest median survival was found in the moderate CD200, low resting NK group (median survival 116.75 months) and again, the median survival was not able to be calculated for the moderate CD200, high resting NK cell group.

The median survival for the strong CD200, high and low resting NK cell groups were similar (85.45 months vs 75.53 months respectively).

Overall, this data implies that CD200 expression strength, in combination with some immune cell types, has an effect on overall patient survival. In some combinations however, CD200 expression strength was the most important factor, as OS stayed the same between some of the low and high immune cell groups.

Moderate CD200 expression most commonly resulted in the best outcomes, which were found in in combination with high Tfh cells, low activated NK cells and low resting NK cells. Weak CD200 expression was found to have the shortest median survival times in combination with low Tfh, high Tregs and low resting NK cells, but the best median survival in combination with high Tfh cells. Strong CD200 expression resulted in poor median survival in combination with high CTL and low activated NK cell levels, however the best median survival was in combination with high Treg levels.

We finally compared the high effector T cell signature to the low signature in relation to weak, moderate and strong CD200 expression to determine the effect on survival, as shown in Figure 5.8.

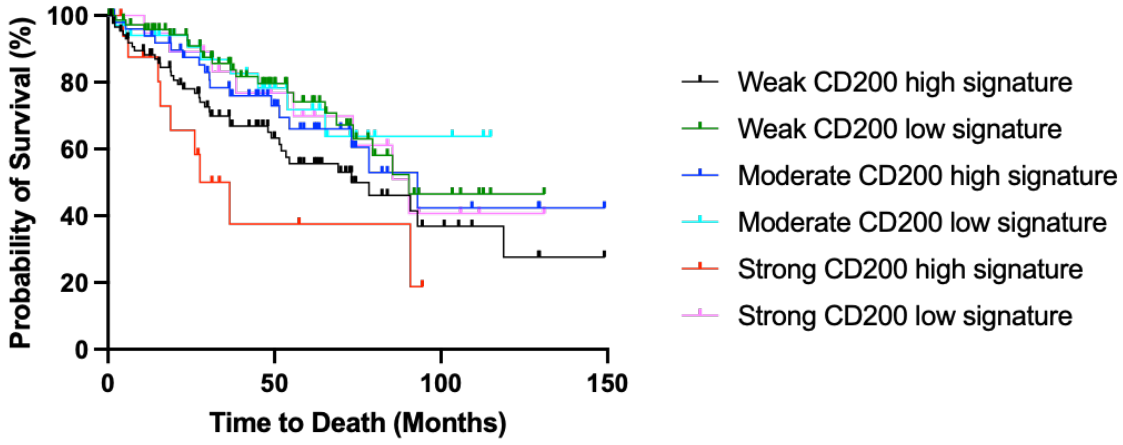

Figure 5.8 Survival analysis comparing the high and low immune signature in combination with CD200 expression.
Logrank analysis was used to compare Kaplan-Meier survival curves between the groups of weak, moderate or strong CD200 expression in combination with the high or low immune signature. The low signature had a significantly better survival chance compared to the high signature in the weak CD200 group ($p = 0.044$) and the strong CD200 group ($p = 0.032$). The high signature moderate CD200 group was also found to have a significantly better chance of survival compared to the high signature strong CD200 expression group ($p = 0.015$).

Survival analysis found significant differences between the high and low signature groups and between the CD200 expression groups. Comparison of the high and low signatures within the weak, moderate and strong CD200 expression groups found that within the weak CD200 expression group, the low effector signature had a significantly better survival chance compared to the high effector signature (90.41 months vs 73.16 months, $p = 0.0444$), and the same effect was also found within the strong CD200 expression group (90.41 months vs 32.06 months, $p = 0.0325$). No significant differences were found between the high and low effector groups in the moderate CD200 expression group. Next, comparison of the survival curves of the high effector signature groups with weak, moderate and strong CD200 expression found that the only significant differences between the groups was between the high signature moderate and strong CD200 expression groups, where the moderate group was found to have a significantly longer median survival compared to the strong group (92.97 months vs 33.06 months, $p = 0.0151$).

This data shows that both the high effector T cell signature of high Tfh cells, CTLs, Tregs and activated NK cells with low resting NK cells compared to the opposite low effector signature, and the level of CD200 expression, have a significant effect on patient overall survival, with the combination of high effector signature and strong CD200 expression found to have the lowest median survival out of all of the groups. The moderate CD200 expression, low effector signature group was found to have the best survival outcome, although this was the only group where median survival could not be calculated as over 50% of patients were still alive at the end of the study.

5.3 Defining ccRCC immune response in patient tissue samples by CD200 expression

5.3.1 TMA core CD200 expression

Having determined the effect of weak, moderate and strong CD200 expression in our CIBERSORTx data, we next determined the effect of CD200 expression on patient tissue using serial sections of the same TMAs we have already used earlier in this chapter. Using IF we stained for CD200 expression in our tissue samples and assigned each sample a H-score which corresponds to the weak (H-score 0-99), moderate (H-score 100-199) and strong (H-score 200-300) expression cut offs we have previously used for our bioinformatic analysis.

CD200 H-scores in the ccRCC and normal kidney samples can be seen in Figure 5.9.

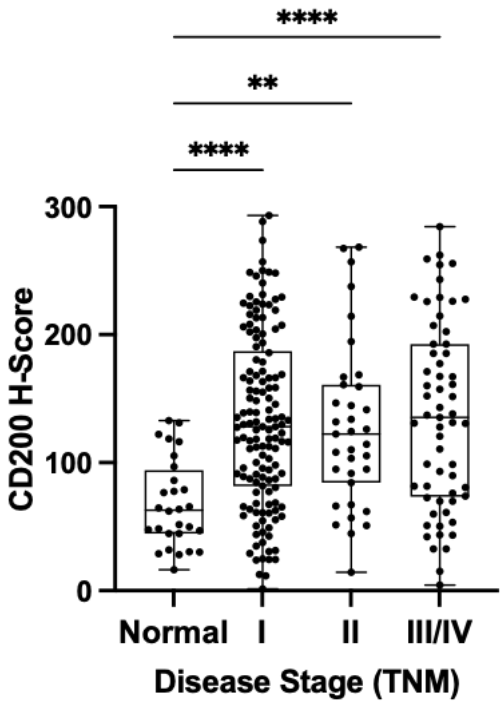

Figure 5.9 CD200 H-score in normal kidney and ccRCC TMA cores
CD200 H-score was examined across normal kidney and ccRCC stages I, II and III/IV. Analysis was completed using a Kruskal-Wallis test with Dunn's multiple comparisons test, where ** represents p <0.01 and **** represents p <0.001.

As expected from our RNAseq data, CD200 expression was significantly higher at all ccRCC stages compared to normal kidney (stage I 133.1 ± 68.31 vs 67.80 ± 34.31

p<0.0001, stage II 128.2 ± 64.60 vs 67.80 ± 34.31, p=0.0012, stage III/IV 136.5 ± 72.80 vs 67.80 ± 34.31, p<0.0001), however no significant changes were observed between the ccRCC disease stages.

5.3.2 TMA immune infiltrate by CD200 expression

We next split the immune cell density/mm^2 and frequency of CD45+ cell data calculated for each TMA sample from earlier in this chapter by CD200 expression.

5.3.2.1 CD45+ tumour infiltrating lymphocytes

The TMA samples were split by weak, moderate and strong CD200 expression to determine if CD200 intensity has any effect on CD45+ cell density/mm^2 and percentage of all cells, as shown in Figure 5.10.

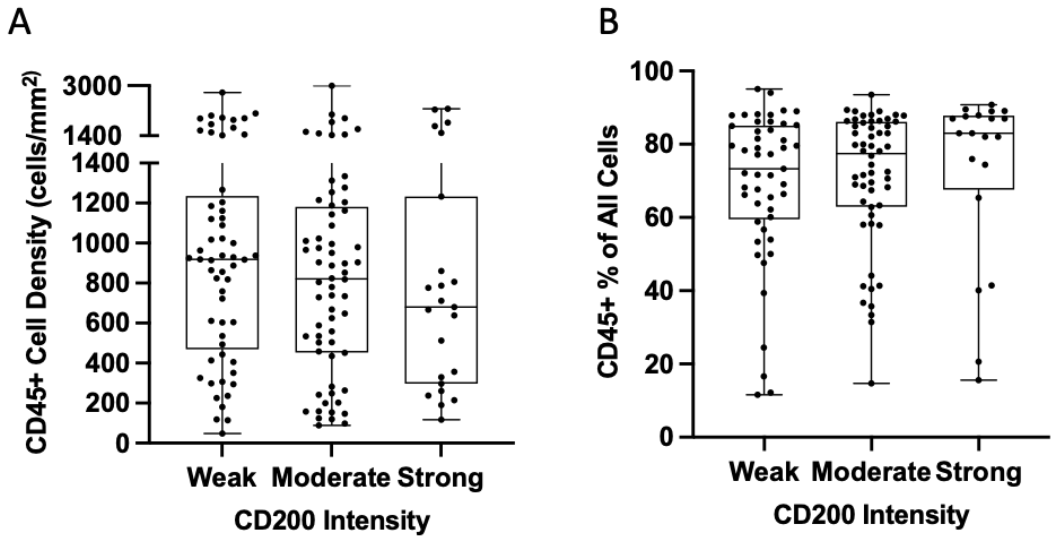

Figure 5.10 CD45+ cell density and frequency of all cells by CD200 expression
(A) CD45+ cell density/mm^2, (B) Frequency of CD45+ of all cells within the TMA core. Analysis was carried out using a Kruskal-Wallis test with Dunn's multiple comparisons test, however no significant differences between groups were observed.

A general decrease in CD45+ cell density/mm^2 was found with increased CD200 expression (Figure 5.10a), however an increase in the percentage of CD45+ cells within the total cell number was observed with increased CD200 expression (Figure 5.10b). This implies that in samples with higher CD200 expression there were generally less CD45+ cells, however with increased CD200 there was less CD45- cells in the sample so there was a higher percentage found. This may be due to the

fact that as ccRCC disease progresses, changes in the tissue structure are observed and a characteristic “nest” structure develops, within which large hollow gaps with no cells are found throughout the sample. These “nests” therefore reduce the total number of cells visible within our samples, so in this case it appears that higher numbers of nests are associated with higher CD200 expression, there are therefore less cells are present within the sample.

5.3.2.2 CD3+ T cell infiltrate

We next calculated the CD3+ T cell density/mm^2 and percentage of CD45+ cells within our weak, moderate and strong CD200 expression groups, as shown in Figure 5.11.

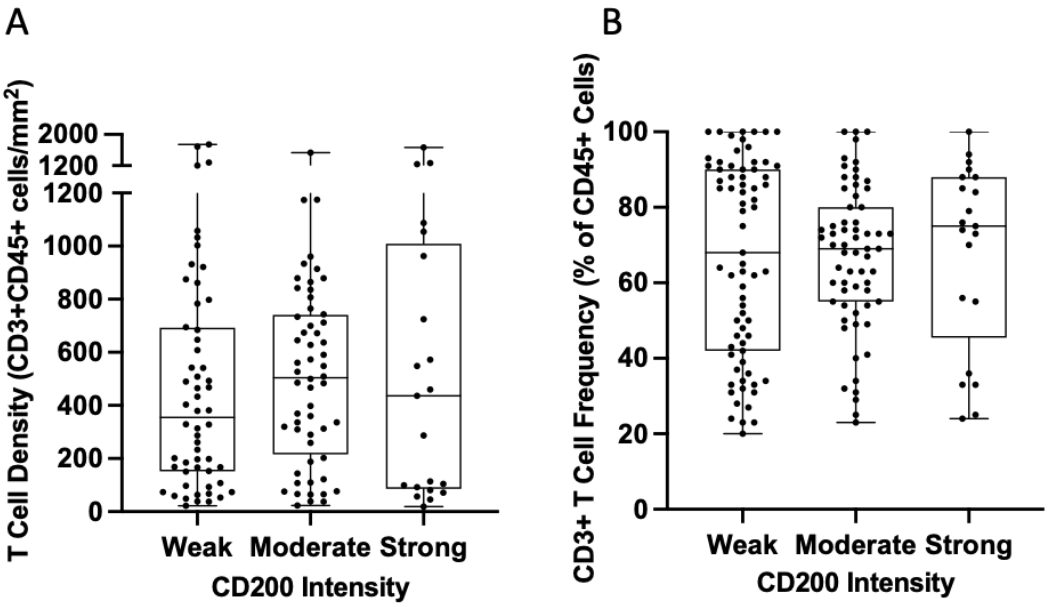

Figure 5.11 CD3+ cell density and frequency of CD45+ cells by CD200 expression
(A) CD3+ T cell density/mm^2, (B) Frequency of CD45+ cells within the TMA core. Analysis was carried out using a Kruskal-Wallis test with Dunn’s multiple comparisons test, however no significant differences between groups were observed.

The highest average number of CD3+ cells/mm^2 was found in the moderate CD200 expression group (Figure 5.11a), however no significant differences were found between the three groups. High frequencies of CD3+ cells were found in all CD200 expression groups, and generally the mean CD3+ percentage of CD45+ cells increased with CD200 expression (Figure 5.11b). The highest mean frequency was

found in the strong CD200 expression group, however again no significant differences were found between the groups.

5.3.2.3 CD4+ T Helper cells (Th)

Having determined the pattern of CD3+ T cell infiltrate in our weak, moderate and strong CD200 expression groups, we next aimed to split the numbers of our key immune cells of interest by their CD200 expression, to determine any effect on density/mm^2 and percentage of CD45+ cells. We firstly examined the numbers of CD4+ T helper (Th) cells within our TMA samples, as shown in Figure 5.12.

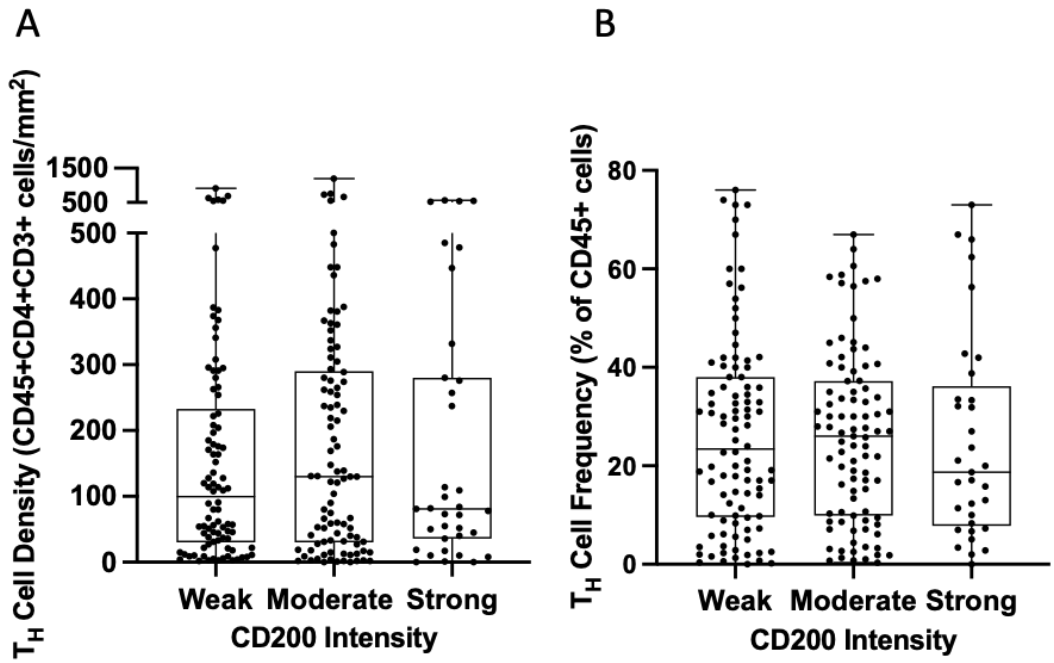

Figure 5.12 Th cell density and frequency of CD45+ cells by CD200 expression
(A) CD4+ Th cell density/mm^2, (B) Th frequency of CD45+ cells within the TMA core. Analysis was carried out using a Kruskal-Wallis test with Dunn's multiple comparisons test, however no significant differences between groups were observed.

The highest average Th cells/mm^2 (Figure 5.12a) and frequency of CD45+ cells (Figure 5.12b) were both observed in the intermediate group, with no significant differences found between any of the groups.

5.3.2.4 CD8+ Cytotoxic T cells (CTLs)

We next split our CTL results of density/mm^2 and percentage of CD45+ cells by CD200 expression, as shown in Figure 5.13.

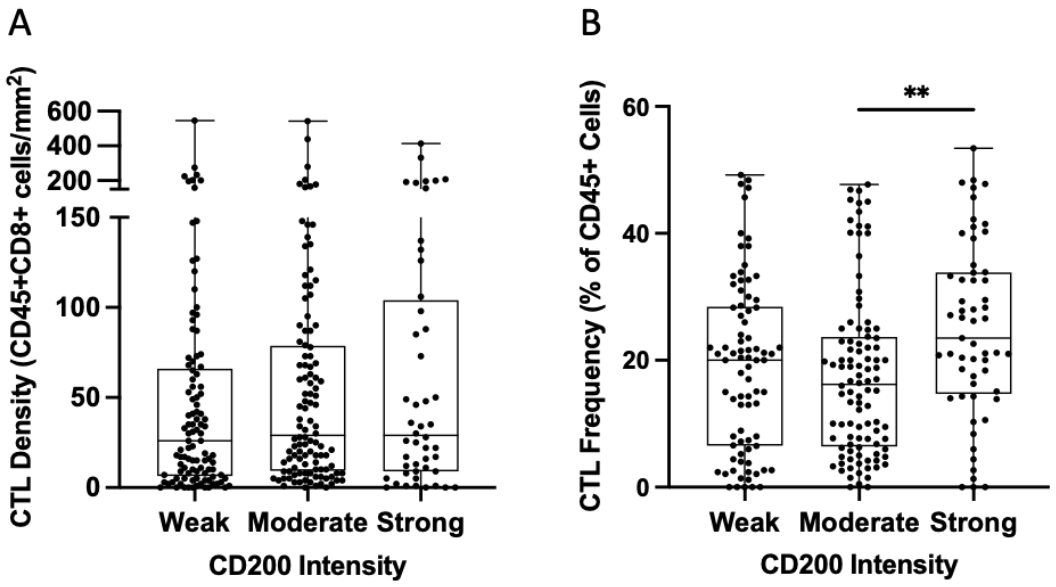

Figure 5.13 CTL cell density and frequency of CD45+ cells by CD200 expression
(A) CD8+ CTL density/mm^2, (B) CTL frequency of CD45+ cells within the TMA core. Analysis was carried out using a Kruskal-Wallis test with Dunn's multiple comparisons test, where ** represents $p < 0.01$.

A general increase in CTL density/mm^2 was observed with increased CD200 expression (Figure 5.13a), however no significant differences were found between the groups. The frequency of CD45+ cells was however ground to be significantly higher in the strong group compared to the moderate group (Figure 5.13b, 24.84 ± 13.85 vs 17.57 ± 13.03, p=0.0038).

5.3.2.5 CD4:CD8 ratio

We next calculated the CD4:CD8 ratio for our samples to determine if CD200 expression has any effect on the ratio, as shown in Figure 5.14.

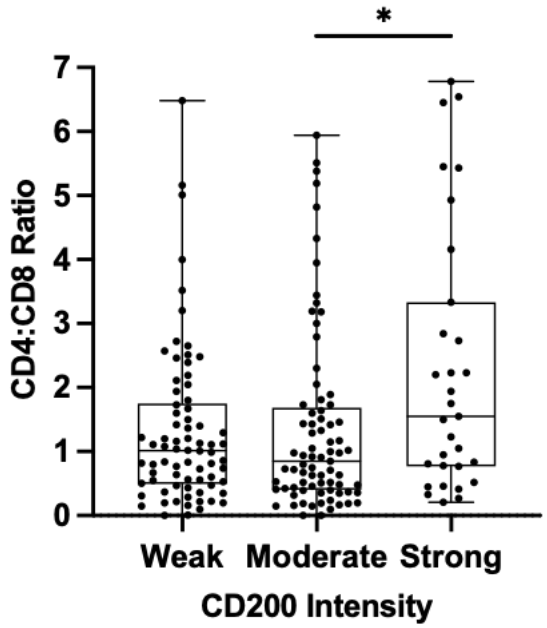

Figure 5.14 CD4:CD8 ratio by CD200 expression
The CD4:CD8 ratio was examined within the weak, moderate and strong CD200 expression groups. Analysis was completed using a Kruskal-Wallis test with Dunn's multiple comparisons test, where * represents $p < 0.05$.

The CD4:CD8 ratio was found to be very similar in the weak and moderate CD200 expression groups, however the strong group was found to have significantly higher ratios than the moderate group (2.294 ± 2.066 vs 1.363 ± 1.435, $p=0.0328$), which is as expected as the numbers of CTLs in Figure 4.67a remain similarly low in all groups while the Th cells observed in Figure 4.66a are found to be at higher numbers which would increase this ratio within the same sample.

5.3.2.6 Tregs

We next investigated the Treg density/mm^2 and frequency of CD45+ cells in our TMA samples as shown in Figure 5.15.

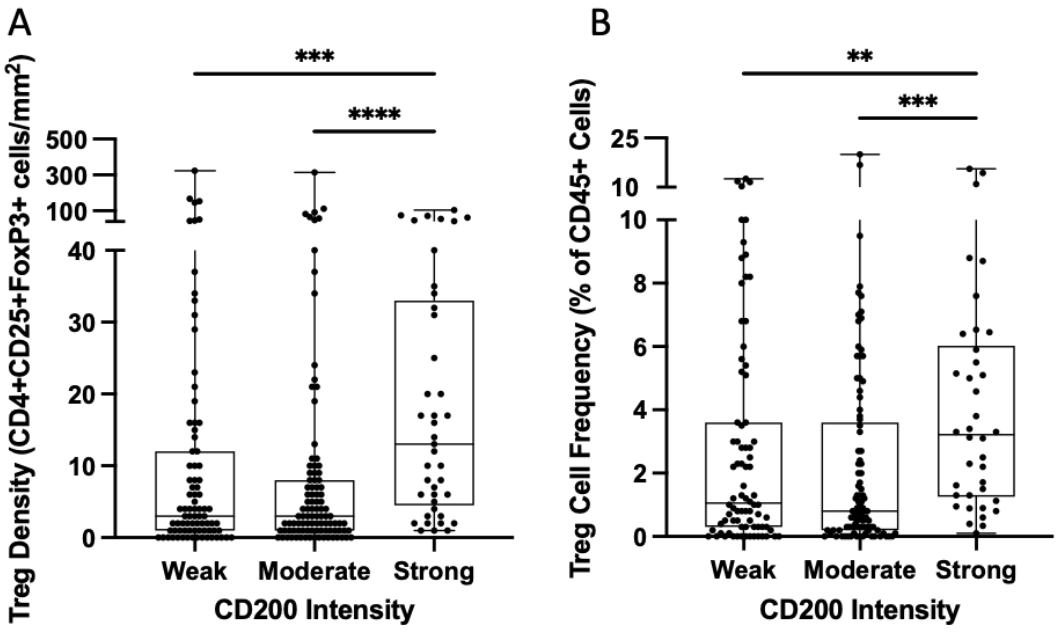

Figure 5.15 Treg cell density and frequency of CD45+ cells by CD200 expression
(A) Treg density/mm^2, (B) Treg frequency of CD45+ cells within the TMA cores. Analysis was carried out using a Kruskal-Wallis test with Dunn's multiple comparisons test, where ** represents p <0.01, *** represents p <0.001 and **** represents p <0.0001.

Tregs appear to be the cell type most influenced by CD200 expression, with significantly higher cell density/mm^2 found in the strong CD200 group compared to both the moderate (15.50 ± 14.35 vs 6.61 ± 9.30, p=0.0001) and weak groups (15.50 ± 14.35 vs 8.09 ± 10.67, p=0.0013, Figure 5.15a). Treg frequency of CD45+ cells also showed a similar pattern, with the strong group again showing significantly higher percentage of CD45+ cells compared to the moderate (Figure 5.15b, 2.64 ± 1.85 vs 1.83 ± 2.11, p=0.0057) and weak (2.64 ± 1.85 vs 1.60 ± 1.76, p=0.0034) groups.

5.3.2.7 CD8:Treg ratio

We next calculated the CD8:Treg ratio to determine if CD200 expression has an overall effect on this ratio in our samples, as shown in Figure 5.16.

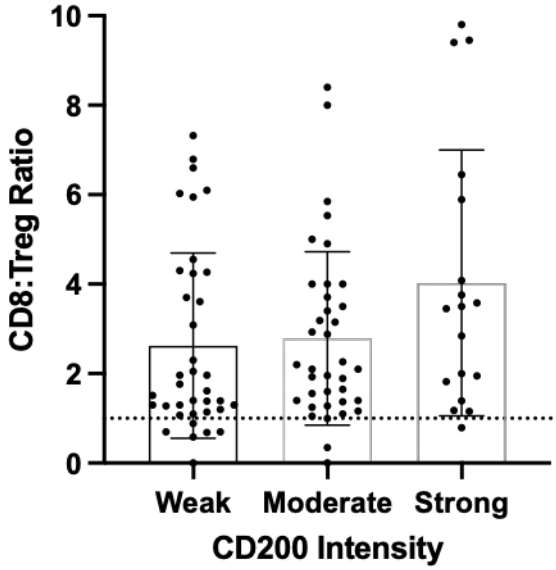

Figure 5.16 CD8:Treg ratio by CD200 expression
The CD8:Treg ratio was examined within each ccRCC core by weak, moderate and strong expression of CD200. Analysis was completed using a Kruskal-Wallis test with Dunn's multiple comparisons test; however, no significant differences were found between the groups.

As expected, due to the low Treg/mm^2 numbers observed, the CD8:Treg ratio was found to increase with CD200 expression (Figure 5.16), with the highest ratios found in the strong CD200 expression group, however no significant differences were found between the three groups. An increased CD8:Treg ratio is generally associated with better prognosis, so as we found an increase in CD200 expression with advanced ccRCC stage, this this ratio alone may not be a complete indicator of prognosis and this data may need to be taken into consideration alongside the activity of other immune cells.

5.3.2.8 NK cells

We next split the NK cells/mm^2 and frequency of CD45+ cells in our TMAs by their CD200 expression, as shown in Figure 5.17.

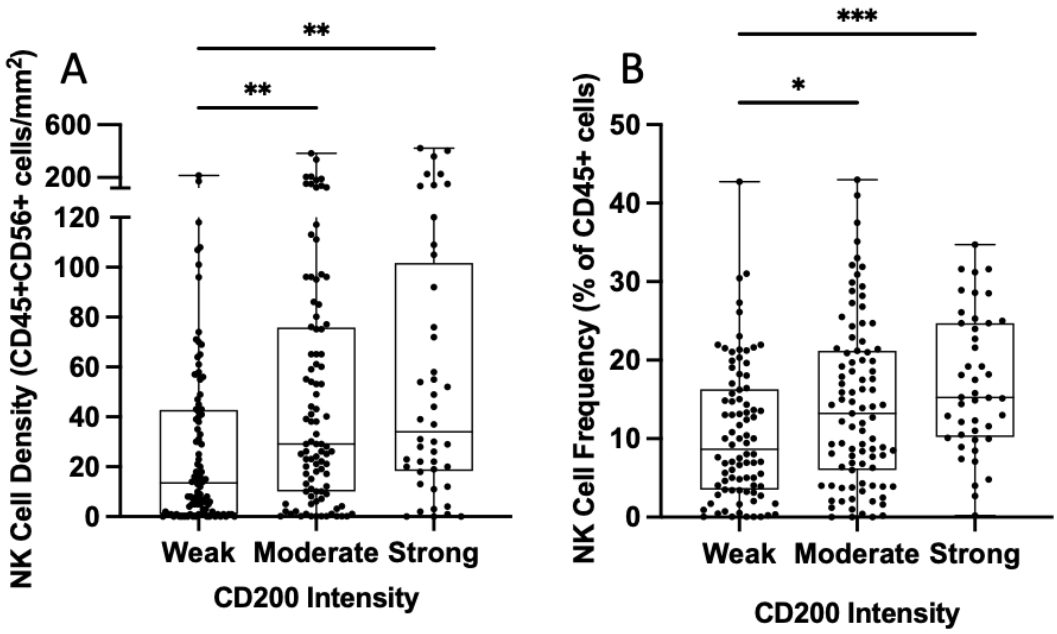

Figure 5.17 NK cell density and frequency of CD45+ cells by CD200 expression
NK cell density and frequency were examined in the weak, moderate and strong CD200 expression groups. (A) NK density/mm^2, (B) NK frequency of CD45+ cells within the TMA cores. Analysis was carried out using a Kruskal-Wallis test with Dunn's multiple comparisons test, where * represents p <0.05, ** represents p <0.01 and *** represents p <0.001.

NK cell density/mm^2 was found to significantly increase with CD200 expression (Figure 5.17a), with the strong group found to have significantly higher numbers of NK cells than the weak group (76.45 ± 103.5 vs 27.91 ± 37.67, p=0.0013), as was also found to be the case for the moderate group compared to the weak group (53.49 ± 66.37 vs 27.91 ± 37.67, p=0.0030).

A similar pattern was found in the frequency of CD45+ cells (Figure 5.17b), with the strong group again having the highest percentage of CD45+ cells and was significantly higher than the weak group (17.03 ± 8.74 vs 10.63 ± 8.78, p=0.0002). The moderate group was also found to have significantly higher percentages of CD45+ cells compared to the weak group (14.39 ± 10.53 vs 10.63 ± 8.67, p=0.0310).

5.3.3 Immune cell correlations by CD200 expression

We have now shown that the density and frequency of each of our key immune cell types is either increased or decreased as a result of changes in CD200 expression. To next investigate the relationships of these immune cells with each other within the CD200 expression groups, we next used Spearman correlation analysis in the weak, moderate and strong CD200 expression groups, as shown in Figure 5.18.

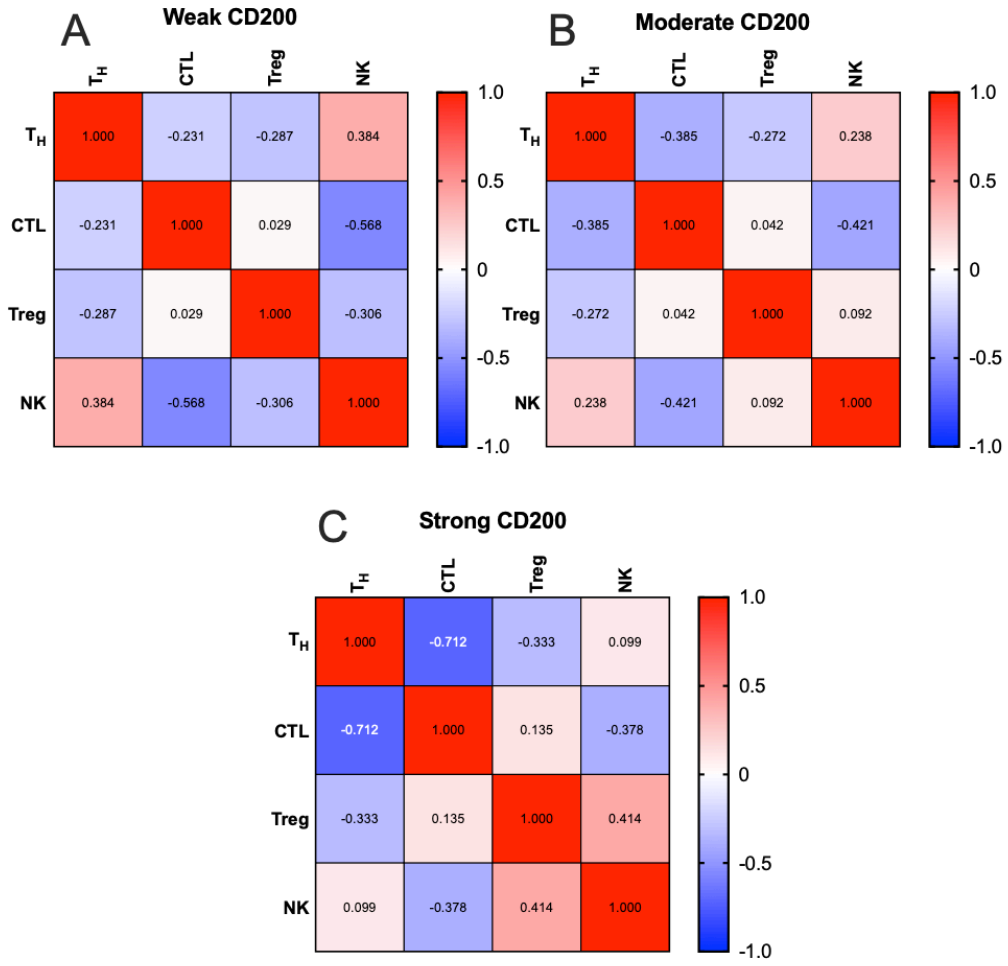

Figure 5.18 Immune cell correlations within the weak, moderate and strong CD200 expression groups
Spearman correlation analysis was used to compare the relationships of estimated immune fractions of key immune cells within the (A) Weak, (B) Moderate and (C) Strong CD200 expression groups. Red represents a positive correlation while blue represents a negative correlation. r values are represented within each box.

Spearman correlation analysis revealed that ccRCC CD200 expression has a significant impact on the relationships of immune cells with each other. In the weak CD200 expression group (Figure 5.18a), we observed that NK cells and CTLs have

a moderately strong negative relationship (r=-0.568, p=0.001) while NK cells and Th cells have a moderate positive relationship (r=0.384, p=0.027) and a moderate negative but not significant relationship with Tregs (r=-0.306). Th and CTL cells were found to have a weak negative relationship which was not found to be significant (r=-0.231).

These relationships were found to alter in the moderate CD200 expression group (Figure 5.18b), where the NK and CTL relationship became less negative (r=-0.421, p=0.020). The relationship between Th and CTLs however became more negative and was now found to be significant (r=-0.385, p=0.036). The relationship of NK cells with Th cells became less positive and no longer significant (r=0.238), while the NK and Treg relationship became weakly positive (r=0.092).

In the strong CD200 expression group (Figure 5.18c), the relationship between CTLs and NK became less negative again (r=-0.378) and the relationship between Th and CTLs was now found to be strongly negative (r=-0.712, p=0.017). The relationship between NK cells and Th cells was now less positive (r=0.099) and with Tregs was now found to be moderately positive but still not significant (r=0.414).

This data shows the most obvious change between the CD200 expression groups is in the relationship between Th and CTL cells, which became much more negative with increased CD200 expression. This data fits with the significant increase in CTL relative frequency we observed in the strong CD200 expression group compared to the moderate and weak group. The relationship between NK cells and Tregs was found to change from a negative relationship in the weak expression group to a moderately positive relationship in the strong CD200 group, which again ties in with our previous data due to the significant increase in cell density and frequency we have already observed in the strong CD200 expression groups for these cell types.

This data shows that CD200 expression may not only affect the number of immune cells present in a sample, but also may have a significant effect on the overall immune infiltrate within a sample and the interactions of each immune cell type, resulting in a strongly altered TME with reduced cytotoxic capacity, potentially resulting in ccRCC disease progression.

To understand this relationship further, we next carried out *in vitro* tumour and NK cell co-culture experiments in the presence of CD200 to determine the effect of CD200 on NK cell cytotoxic ability.

5.4 Determining the effect of CD200 on NK cell cytotoxic ability

5.4.1 Cytotoxic assessment of NK cells

We next aimed to explore how the interaction of membrane-bound CD200 and sCD200 with CD200R-expressing NK cells affects their activity and cytotoxic abilities. For these studies, we used the CD200R+ NK92MI cell line (Rees 2020), an IL-2 independent cell line derived from the NK92 cell line by transfection, which is highly cytotoxic towards a variety of malignant target cells (Tam et al. 1999). Using tumour and NK cell co-culture assays, we aimed to determine the cytotoxicity of NK cells with varying CD200 levels against different tumour cell lines.

5.4.1.1 A498 tumour cell killing by NK92MI cells

We firstly aimed to determine the ability of the NK92MI cells to act on CD200- tumour cells by using the ccRCC cell line, A498. The CD200R+ NK cells and CD200- A498 cells were incubated together for 4 hours at different effector:target ratios, followed by counting of the number of live cells at the end of the time period to determine the percentage of tumour cell death, as shown in Figure 5.19.

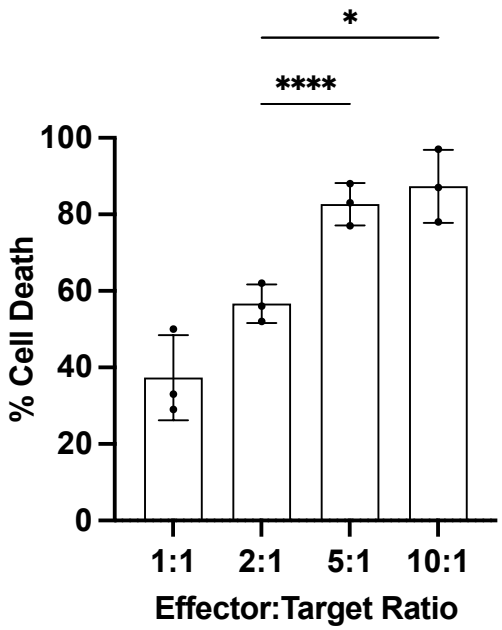

Figure 5.19 Cell death following A498 and NK cell co-culture
A498 and NK cells were incubated together for 4 hours at various effector:target ratios before counting the number of live cells and calculating percentage of cell death. Results are averages of 3 wells, and each experiment was completed a minimum of 3 times. Analysis was completed using Kruskal-Wallis test with Dunn's multiple comparisons test, where * represents $p < 0.05$ and **** represents $p < 0.0001$.

A significantly higher percentage of tumour cell death was observed at effector:target ratios. Cell death was significantly higher compared to the 2:1 ratio at the 5:1 ratio (56.67 ± 5.03 vs 82.67 ± 5.51, $p < 0.0001$) and the 10:1 ratio (87.73 ± 9.50 vs 56.67 ± 5.03, $p=0.018$). This data strongly suggests that increased numbers of NK cells have a greater cytotoxic response, and so NK cells may benefit from 'strength in numbers'. The 10:1 and 5:1 effector:target ratios were found to have very high tumour cell death percentages, however at lower ratios the cell death rate is still substantial compared to the control samples.

5.4.1.2 HeLa CD200+ and CD200- tumour cell killing by NK92MI cells

As we have shown that the NK92MI cell line is able to effectively kill A498 CD200- tumour cells, we next examined this effect using our CD200+ transduced HeLa cell line. Using the same co-culture conditions, we co-cultured CD200+ and CD200- HeLa cells with the NK92MI cells at different effector:target ratios to determine the effect of CD200 on tumour cell killing, as shown in Figure 5.20.

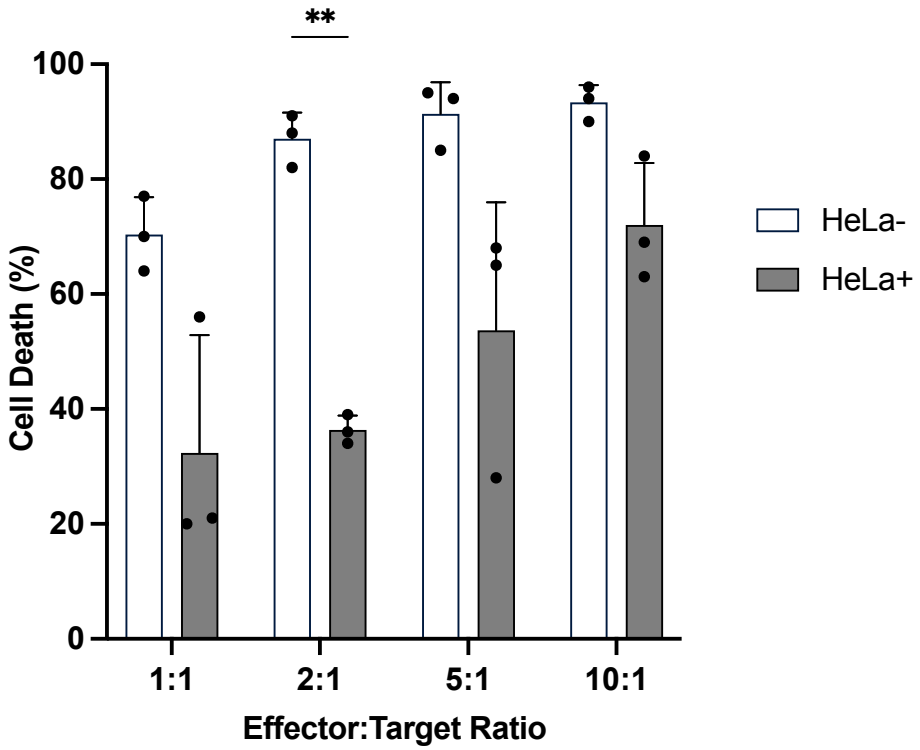

Figure 5.20 Cell death following HeLa CD200+ and CD200- cells with NK cell co-culture
CD200+ and CD200- HeLa cells were co-cultured with NK92MI cells were incubated together for 4 hours at various effector:target ratios before counting the number of live cells and calculating percentage of cell death. Results are averages of 3 wells, and each experiment was completed a minimum of 3 times. Analysis was completed using an unpaired t-test, where ** represents $p < 0.01$.

Tumour cell killing was reduced in the CD200+ HeLa cell line compared to the CD200- HeLa cell lines at all effector target ratios, with a significant difference in percentage of tumour death found at the 2:1 ratio (CD200+ 36.33 ± 2.51 vs CD200- 87.00 ± 4.58, p=0.001). A step wise increase in percentage of tumour cell death was observed with increased NK cell to tumour cell numbers in both the CD200- and CD200+ conditions.

5.4.1.3 Tumour cell killing in the presence of sCD200+ supernatant

We have shown so far that the presence of membrane bound CD200 on the surface of CD200+ HeLa cells is able to protect the cell from killing by NK cells, however we have also shown in the previous chapter that CD200 can be cleaved from the cell surface creating the functionally active soluble form, sCD200. We next aimed to establish if sCD200 is able to protect tumour cells from NK cell killing, as shown in Figure 5.21.

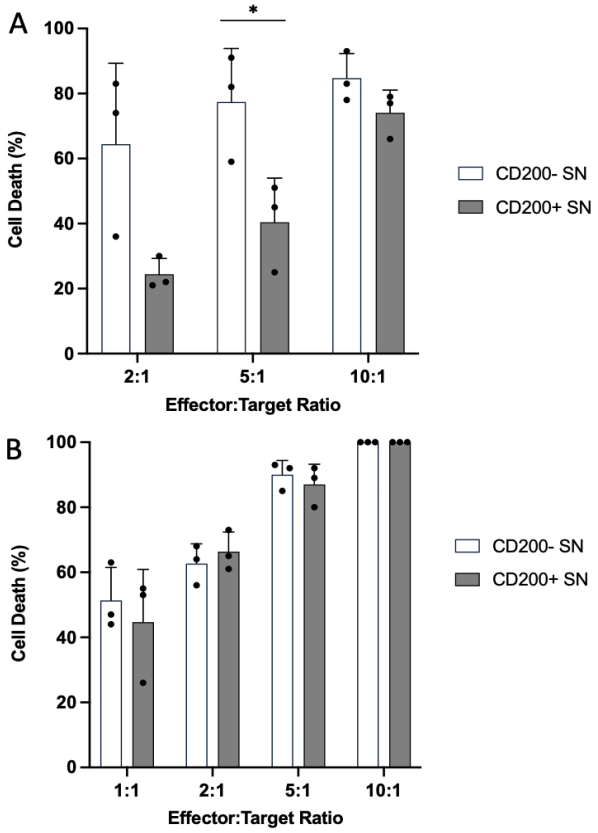

Figure 5.21 Cell death following A498 and HeLa CD200- cell co-culture with NK cells in the presence of CD200+ and CD200- cell line supernatant
(A) CD200- HeLa cells were incubated with NK cells in the presence of supernatant (SN) taken from CD200+ and CD200- HeLa cells at various effector:target ratios. Data was not available for the 1:1 ratio. (B) CD200- A498 cells were incubated with NK cells in the presence of SN taken from CD200+ and CD200- HeLa cells at various effector:target ratios. Results are averages of 3 wells, and each experiment was completed a minimum of 3 times. Analysis was completed using an unpaired t-test, where * represents $p < 0.05$.

HeLa CD200- tumour cell killing was reduced in the presence of sCD200+ supernatant compared to the sCD200- supernatant (Figure 5.21a), with the percentage of tumour killing found to be significantly lower in the sCD200+ condition at the 5:1 ratio compared to the sCD200- condition (40.33 ± 13.61 vs 77.33 ± 16.50, p=0.0401). This data shows that sCD200 is still able to block tumour cell killing by NK cells in comparable levels to membrane bound CD200. A498 cell killing was also reduced in the presence of sCD200+ supernatant (Figure 5.21b), however the effects do not appear to be as strong as those observed in the HeLa cell line, with only small reductions found in tumour cell death in the sCD200+ conditions compared to the sCD200- conditions, while more cell death was actually observed in the sCD200+ condition for the 2:1 effector target ratio.

5.5 Discussion

In this chapter we have investigated the relationship of ccRCC immune infiltrate to tumour CD200 expression by bioinformatic analysis, IF staining and functional co-culture assays.

We found that CD200 was significantly overexpressed at all ccRCC stages compared to normal kidney, however the only patient characteristic which resulted in any significant change in CD200 expression was race, where the white group had significantly higher CD200 expression than the black/African American group, however the reasons and implications of this are unclear. Interestingly, survival analysis of the weak, moderate and strong CD200 expression groups found that the moderate expression group had significantly better OS and DFS compared to the weak and strong groups, implying that prognosis is worse when CD200 expression is low or high. As we found that CD200 expression as significantly increased in all ccRCC stages compared to normal kidney, we can determine that CD200 is associated with ccRCC disease progression and patient survival, however no significant changes in expression level were associated with stage or TNM status.

Analysis of the three CD200 expression groups revealed a general increase in our key effector T cells and a general reduction of activated NK cells with increased CD200 expression. This effect is interesting as this data implies that CD200 can affect ccRCC immune infiltrate and this effect also appears to be related to the expression strength. CTLs were significantly higher in the moderate CD200 group compared to the weak group, and so CTLs may have a role in the protective effect seen in the moderate CD200 group. With increased CD200 expression, the relationships of resting NK cells with Tfh cells, CTLs and Tregs were all found to become less negative, while the relationship of activated NK cells with these cell types also became more positive. Positive relationships were found between all cell types except for resting NK cells which were found to have significant negative correlations with the other cell types, including activated NK cells. This data suggests that estimated immune fraction is not strongly correlated with CD200 expression, however the relationship of the immune cells with each other is changed by the strength of CD200 expression and the strongest relationships are found when CD200 expression is moderate.

Taking all of this data into consideration, we next compared OS statistics for patient groups of weak, moderate or strong CD200 expression in combination with low or high levels of each immune cell. We found significant differences between these groups, implying that CD200 expression has an effect on immune cell infiltration and therefore patient survival. Moderate CD200 expression most commonly resulted in the best outcomes, particularly when found in in combination with high Tfh cells, low activated NK cells and low resting NK cells. Interestingly, weak CD200 expression was found to have the shortest median survival times in combination with low Tfh, high Tregs and low resting NK cells, but the best median survival in combination with high Tfh cells. Strong CD200 expression resulted in poor median survival in combination with high CTL and low activated NK cell levels, however the best median survival was in combination with high Treg levels.

Survival analysis combining our high effector T cell signature with CD200 expression level found that a low effector signature combined with moderate CD200 expression had the best outcome, while a high effector signature combined with strong CD200 expression had the shortest median survival times. This indicates that both immune infiltrate and CD200 expression level have a significant impact on patient survival. As none of the immune cells were found to correlate directly with CD200 expression level, this may imply that additional factors are responsible for the changes found in both the immune infiltrate and CD200 expression level, however the two factors do combine to influence each other with a resulting effect on patient survival. CD200 expression therefore may have a significant effect on the relationships of NK cells with other immune cell types and could be responsible for the unexpected high levels of resting NK cells and low levels of activated NK cells found previously in this chapter. As increased CD200 expression is associated with positive relationships between NK cells and the key effector T cell types, we can determine that ccRCC CD200 expression has an important role of regulation of the NK antitumour response and therefore could be responsible for dysregulation of the ccRCC overall immune response, resulting in disease progression and patient survival.

CD200 IF staining was next completed on serial sections of the same TMAs and the patients were again split into weak, moderate and strong expression groups based on their CD200 H-score. Cell density and frequency of Th cells was not found to alter with CD200 expression; however, CTL cell density was found to generally increase

with increased CD200 expression, and CTL percentage of CD45+ cells was found to significantly increase in the strong CD200 group compared to the weak group. This is interesting as we have already discussed how the ccRCC CTL cytotoxic response is increased at a late disease stage, but may be dysfunctional resulting in a poor anti-tumour immune response. This result is mirrored in our CD4:CD8 ratio analysis, where a significant increase in ratio was again observed between the moderate and strong CD200 expression groups, with a mean ratio in the strong group of 2.29, which would be generally considered a protective ratio with a positive prognosis. Treg cell density and frequency of CD45+ cells were significantly higher in the strong CD200 groups compared to the weak and moderate groups. This result is interesting as Treg tumour infiltrate has positive prognostic effects in some cancer types but negative prognostic outcome in others. As CD200 levels were higher in ccRCC compared to normal kidney, and Tregs are found to increase significantly with CD200 expression, in combination with what we observed in our bioinformatic survival analysis, we can determine that increased Treg infiltration in ccRCC is detrimental to patient survival and may be the cause of T cell dysregulation throughout the ccRCC tumour, resulting in a poor cytotoxic response.

CD8:Treg ratio increased with CD200 expression, which again is generally associated with a positive effect on prognosis, however as we suspect the CD8+ CTLs are dysfunctional, this ratio may not actually be protective. NK cell density and frequency of CD45+ cells were next examined by CD200 expression, where a significant increase in both cell density and frequency was seen with increased CD200 expression. Our group has already shown that CD200 is able to dysregulate NK cytotoxic function and cause apoptosis in other cancer types (Morgan et al. 2022), so it is likely that this increased NK cell expression is dysfunctional and ineffective as the primary anti-tumour response.

To examine this further, we next used cell line co-culture experiments comprising of incubation of CD200- A498 ccRCC cells and transduced CD200+ and CD200- HeLa cells with the functionally active CD200R+ NK92MI cell line at various effector:target ratios. The NK cell line was effectively able to kill a high percentage of the CD200- A498 and HeLa- cell lines, however this killing was significantly reduced in the CD200+ HeLa cell line. We next investigated if functionally active sCD200, created by proteolytic cleavage from the cell membrane, is also able to protect tumour cells

from NK cell cytotoxic activity. In the presence of sCD200+ cell line supernatant, HeLa CD200- cell killing was reduced, implying the protective effect of CD200 is still present in the soluble form, however the effect is less strong. Interestingly, A498 cells were found to be less protected by the presence of sCD200 and this may indicate that some cell lines are more susceptible to NK cell killing than others, even in the protective presence of CD200 and sCD200. This could be due to varying expression of other immune checkpoints and cell surface proteins; however further research would be required to establish this.

This data is highly interesting as it shows a protective effect of CD200 against NK mediated cell killing, which is also carried through into the soluble form after ectodomain shedding, however CD200 expression alone does not appear to be enough to fully stop tumour killing by NK cells. The protective effect of CD200 may also vary according to cancer type, and the strength of expression may depend on disease stage and other patient and clinical characteristics, so this would be an interesting direction for future research. A further direction would be to study this effect in a naturally CD200 positive cell line to confirm the same effect.

5.6 Conclusions

CD200 expression was found to be significantly higher in ccRCC compared to normal kidney, with differences in key immune cell expression levels relating to CD200 expression strength. A further combined signature of strong CD200 expression with high levels of our key immune cells resulted in the worse prognosis compared to both groups with lower CD200 expression and low levels of the key immune cells. This data presents interesting opportunities for both anti-CD200 and anti-immune cell interventions, potentially with scope to improve patient survival.

Chapter 6: General discussion

6. General Discussion

Tumour immune evasion is a well-studied mechanism of cancer progression, which occurs through a variety of mechanisms (Wang et al. 2021a). In recent years, the interaction between tumours and cells of the immune system, combined with the ability of immune checkpoints to supress anti-tumour immune responses and immune evasion, have become of great interest for the development anti-cancer therapeutics (Kim and Cho 2022). Under normal physiological conditions, immune checkpoints protect against autoimmunity and an overactive immune response through the maintenance of immune homeostasis. However, overexpression of immune checkpoints such as PD-1 and CTLA-4 is regularly observed in cancer, enabling immune escape and tumour progression (Jian et al. 2021). CD200, in combination with its receptor, CD200R, is a further example of an immune checkpoint which is overexpressed by several types of cancers, including RCC, to evade anti-tumour immune responses (Moreaux et al. 2008; Love et al. 2017a; El Hanbuli et al. 2021). CD200 overexpression results in modulation of the immune infiltrate within the TME, creating an immunosuppressive environment and an overall dysfunctional anti-tumour immune response (Talebian et al. 2021). This dysfunctional TME has been shown to affect several types of key anti-tumour immune cells in several ways, including the inefficient function and apoptosis of NK cells (Morgan et al. 2022) and reduced cytotoxic capacity of CD3+ T cells (Shah et al. 2022).

The development of immune checkpoint inhibitors (ICIs) targeting the CTLA-4 and PD-1/PD-L1 axis has revolutionised immunotherapy-based cancer treatments in recent years (He and Xu 2020). ICI interruption of immunosuppressive signalling and co-inhibitory T-cell signalling can reinvigorate natural anti-tumour immunity, however in some highly immunogenic cancer types such as RCC, overall results are generally modest with little improvement in OS and DFS (Papathanassiou et al. 2022). Rates of relapse and disease progression are also high due to acquired secondary resistance mechanisms within the TME (Jenkins et al. 2018). Therefore, identification of additional immune checkpoints to be used to generate multi-modality immunological therapies could greatly improve the success of ICI therapies in RCC.

CD200 is subject to ectodomain shedding, creating the functionally active soluble form, sCD200, however the full mechanism and proteases involved in this mechanism have not yet been fully established. Elevated protease activity has been reported in many cancer types including RCC, and overexpression of both active MMP and ADAM protease family members, and inhibitory TIMPs, is generally associated with poor prognosis (Fritzsche et al. 2008; Gao et al. 2022; Shou et al. 2022). ADAM17 and ADAM28 have been shown to have roles in CD200 ectodomain shedding in CLL (Twito et al. 2013a; Wong et al. 2016), while MMP3 and MMP11 were found to contribute to this process in BCC (Morgan et al. 2022). It is however unknown if these proteases alone, or alongside others, carry out this process in other CD200-overexpressing solid tumours such as RCC. From a clinical perspective, CD200 overexpression is interesting as it is feasible that following ectodomain shedding, sCD200 may reside in the urine in elevated levels compared to that of normal kidney. This may present an opportunity to detect sCD200 in RCC patient urine for potential use as a diagnostic biomarker.

In this thesis, RCC CD200 expression was examined, following which key proteases were established and their role in the ectodomain shedding of CD200 was explored. The role of CD200 in RCC immune evasion was then studied to determine if tumour CD200 expression has an effect on immune infiltrate and patient survival.

Using bioinformatics, patient samples and *in vitro* immune cell experiments we have shown that:

(i) CD200 is overexpressed in RCC tumours compared to normal kidney, with the strongest expression found in the ccRCC subtype.

(ii) Numerous proteases are overexpressed in RCC development, however ADAM9 is most strongly overexpressed in ccRCC.

(ii) ADAM9 can cleave CD200 from the cell surface creating the soluble form, sCD200.

(iv) Tumour CD200 expression alters the infiltrating immune cell composition. Strong CD200 expressing tumours demonstrated a characteristic signature of increased numbers of CTLs, Th cells, Tregs and resting NK cells which correlated with poor prognosis.

(v) Membrane-bound CD200 and sCD200 can both protect tumour cells from killing by CD200R+ NK cells.

Taken together, these results suggest that CD200 expression by RCC tumour cells may be a mechanism of immune evasion utilised for disease progression. ADAM9 overexpression may also result in increased CD200 cleavage, so therefore, preventing ADAM9 mediated CD200 ectodomain shedding in combination with blocking CD200 signalling may represent a novel therapeutic opportunity in ccRCC.

6.1 CD200 expression in normal kidney and RCC tumours

There is currently little information in the literature regarding the expression of CD200 in normal kidney and in RCC, with most available information based only on RNAseq or microarray analysis of patient-derived tumours. As CD200 is however expressed on kidney glomeruli (D'Arena et al. 2020), endothelial cells and epithelia of the convoluted tubules (Love et al. 2017a), the cells of origin for the most common RCC subtypes, one aim of this thesis was to characterise CD200 expression throughout the normal kidney and in RCC tumours. Examination of CD200 expression using IF staining revealed significant previously unreported differences in expression location and strength in the main structures of the normal kidney. The strongest expression was found on structures of the renal cortex, namely the glomerulus and proximal and distal convoluted tubules. Significantly lower expression was observed on the structures of the medulla: the loop of Henle and the collecting duct. Interestingly, we found significantly stronger CD200 expression on the cells of the proximal convoluted tubule compared to the distal tubule, alongside a general decrease in CD200 expression strength with increased distance along the nephron. As most previous reports of CD200 expression in normal kidney are from bulk RNAseq samples, this finding is important as CD200 expression is not uniform throughout the kidney, and so depending on the anatomical area of the sample used, the resulting levels of CD200 expression may vary significantly. CD200 staining of RCC tumours found that average overall CD200 expression was found to be similar between ccRCC, pRCC and chRCC, which was an unexpected result as CD200 expression on the proximal convoluted tubule, the cell of origin for ccRCC and pRCC, was significantly higher than the expression on the distal convoluted tubule,

the cell of origin for chRCC. This data indicates that CD200 expression is increased generally in the development of RCC and so may have a beneficial effect on disease progression due to its roles in tumour cell immune evasion, however the strength of the resulting tumour expression does not appear to be related to the expression strength on the originating cell. CD200 expression strength was also not found to be associated with TNM status or patient characteristics such as patient age or sex, suggesting that any differences in CD200 expression strength are related to the tumour only.

To date, CD200 expression has not been reported in the literature in any RCC cell line, however, as CD200 staining was observed throughout ccRCC tumour tissue, we expected that established ccRCC cell lines would express CD200. Surprisingly, no CD200 expression was observed in any ccRCC cell lines at the mRNA or protein level. While this result was unexpected, there are several reasons why this may the case. Increased RCC CD200 has been previously reported in microarray analysis carried out using patient-derived tumours instead of cell lines (Lenburg et al. 2003), so we consider that this difference in expression could be due to differences in the overall gene and protein expression found in cultured cell lines as opposed to that of patient-derived tumour samples. In recent years, the use of cell lines for research and drug development has become less favourable, with unexpected gene and protein expression of long-term cell cultivations just one common issue. Cell culture techniques however still remain the first line methodology for initial experimentation due to the ease, speed and low cost of cell line use (Birgersdotter et al. 2005). Genetic drift and altered gene expression in long term cultures have become well-known issues, with one report showing that 106 protein-coding genes were found in their cell lines but not tissues, while 1787 genes were found in the tissues but never in cell lines, many of which were associated with differentiated cells in specialized tissues or subcompartments of tissues, which are not represented in the cell line panels (Uhlén et al. 2015). Many reports (Edmondson et al. 2014; Kapałczyńska et al. 2018; Jensen and Teng 2020) have also raised further questions around the physiological relevance of 2D culture, where cell lines are allowed to grow in perfect atmospheric conditions with easy access to nutrients, with no competition or interference from other cell types. Cells in 2D culture have been shown to have altered morphology (Breslin and O'Driscoll 2016), resulting in abnormal cell

behaviours and resulting expression of cell surface proteins and receptors. To resolve this issue, 3D culture techniques have been continually developed and are now thought to be significantly more physiologically relevant and representative of conditions within a tumour. Importantly, cells in 3D culture have been shown to retain their correct morphology, and when grown in a sphere, the outer cells are able to easily access nutrients and oxygen, while the layers of the inner core become increasingly hypoxic (Bhattacharya et al. 2020). To determine if the 2D culture conditions used to grow our cell lines could have therefore affected CD200 expression, we grew RCC cell lines in 3D non-adherent culture. Of our 7 cell lines, only A498 (Rausch et al. 2021) and CAKI2 (Maliszewska-Olejniczak et al. 2019) had been previously reported to grow in 3D culture, however we managed to grow spheres in all cell lines to some extent over a 14-day period. qRT-PCR on the resulting sphere mRNA however again found no CD200 expression in any cell line. It is unclear why CD200 was not expressed in these cell lines in either 2D or 3D culture conditions, however as CD200 is an immune checkpoint, as no immune cells or other competing cell types were present to interact with these cells, CD200 expression may not be necessary in these conditions. Furthermore, a lack of cell line CD200 expression has been previously reported in other cancer types, such as in a study by Shah et al. 2022, where 70% of patient-derived MM cells were found to express CD200, but no CD200 expression could be detected in 9 established MM cell lines at the protein or mRNA level. Therefore, this issue may be a widespread issue with cell line experiments in CD200-expressing tumour types, possibly requiring the use of other naturally CD200-expressing cell lines or genetic manipulation of cell lines to force CD200 expression *in vitro.* RNAseq was completed using RNA from the RCC CD200-negative cell lines, however as expected, the read count for CD200 in all cell lines was very low or zero. While this is a limitation of this study, we have already shown using IF that CD200 is expressed throughout RCC tumours and so a transduced HeLa CD200+ cell line was used instead for proof-of-concept experiments, which could be repeated in future work on a CD200+ RCC cell line if one can be made available, or in other naturally CD200-expressing cancer types.

6.2 Protease expression in normal kidney and RCC tumours

Ectodomain shedding is the mechanism of proteolytic cleavage of cell surface molecules leading to the release of an active soluble form of the molecule into the extracellular microenvironment, with roles in both normal and pathological processes (Shirakabe et al. 2017). Protease expression is dysregulated in many diseases, with overexpression frequently observed in cancer, impacting pathophysiology and drug responses (Miller et al. 2017). Many ADAM species including ADAM8, ADAM9, ADAM10, ADAM12, ADAM15, ADAM17, ADAM19 and ADAM28 have been shown to be overexpressed in various cancer types including RCC, ovarian, NSCLC and breast cancer (Mochizuki and Okada 2007; Mullooly et al. 2016; Ueno et al. 2018; Gao et al. 2022), with overexpression leading to increased cell growth and invasion (Mochizuki and Okada 2007). The precise mechanisms in cancer development and full range of substrates have however not yet been fully established.

In RCC, a number of proteases have previously been associated with tumour development and poor outcome including MMP2, ADAM8, ADAM9, ADAM17, ADAM19 and ADAM28 (Roemer et al. 2004a; Mochizuki and Okada 2007; Fritzsche et al. 2008; Lipe et al. 2011; Erin et al. 2017), however their full list of substrates has not been fully elucidated. One of the aims of this thesis was to determine which proteases are involved in RCC development and the ectodomain shedding of CD200. The exact cleavage site of CD200 remains to be elucidated, however ADAM17 and ADAM28 have been reported to have roles in CD200 ectodomain shedding in CLL (Twito et al. 2013a; Wong et al. 2016), while MMP3 and MMP11 contribute to this process in BCC (Morgan et al. 2022). It is however unknown if these proteases alone, or alongside others, carry out this process in other CD200-overexpressing solid tumours such as RCC. Completion of a thorough literature search found 18 proteases with reported roles in RCC, with a range of functions including cell adhesion, growth, migration and metastasis. From this list we extracted ADAM17 and ADAM28 which have been implicated in both RCC development and CD200 ectodomain shedding (Twito et al. 2013a; Wong et al. 2016). In our ccRCC cell line RNAseq data, ADAM9 was found to be the only consistently overexpressed protease in all ccRCC samples. Interestingly, ADAM17 expression was not significantly altered compared to normal kidney and ADAM28 was found to be

upregulated in just 2 of the 6 ccRCC samples. ADAM9 has been strongly implemented in cancer progression and aggressiveness in a wide range of cancer types including breast, lung, ovarian, prostate cancer and RCC (Shintani et al. 2004b; Mochizuki and Okada 2007; Fritzsche et al. 2008; Zhou et al. 2020). CD200 has not yet been examined as a potential substrate for ectodomain cleavage by ADAM9, however as the substrates for many ADAMs overlap, we chose to examine this further.

IF staining was used to examine the cellular expression of ADAM9, ADAM17 and ADAM28 in normal kidney tissue. As was observed for CD200, expression strength and distribution varied between normal kidney structures. Interestingly, ADAM9 expression was strong throughout the proximal and distal convoluted tubules with the strongest mean expression in the proximal tubules, in a similar expression pattern to that previously observed for CD200. ADAM17 expression was similar to that of ADAM9, while ADAM28 expression was weak throughout the normal kidney structures. RCC staining found overall ADAM9 expression was highest in chRCC. This result was unexpected as the strongest expression in normal tissue was found in the proximal convoluted tubules, the cell of origin for ccRCC and pRCC. No previous associations between ADAM9 and chRCC have been reported, as most protease research has focussed on ccRCC, however this data may indicate that strong ADAM9 expression is more advantageous for chRCC development compared to other subtypes. Interestingly, ADAM9 expression was found to significantly decrease with increased ccRCC tumour stage, however node or metastasis status had no effect on expression, which could imply that ADAM9 expression is necessary for initial development of ccRCC. ADAM9 and ADAM17 have been shown to share a number of substrates (Mochizuki and Okada 2007) and are expressed in similar levels and locations, however their biological roles are different and may be related to their unique substrates. Both ADAM9 (Chou et al. 2020a) and ADAM17 (Li et al. 2014b) have been implicated ccRCC, which metastasises early in disease progression (Lieder et al. 2017), and so this could be a reason for this strong expression of both proteases at the early stage, with a decrease in expression observed with increased disease stage. ADAM28 expression was strongest in pRCC, which interestingly was significantly higher than that observed in ccRCC, which shares the same cell of origin. ADAM28 has not been widely studied in RCC,

however it has also been implicated in the development of metastasis (Mochizuki et al. 2012). The low expression observed throughout the TMA samples however implies that ADAM28 is not a key protease in RCC development and may only play a small role in disease progression.

The highest number of ADAM9 and CD200 double positive cells was found in ccRCC and was found to significantly increase with tumour status. This result is interesting as ADAM9 expression to significantly decreased with increased tumour status, implying that although less cells are positive for ADAM9 in the higher ccRCC stages, a high percentage of the ADAM9 positive cells were also positive for CD200. Conversely, high numbers of ADAM17 and CD200 positive cells were observed in all RCC subtypes, however chRCC was found to have a significantly higher mean percentage of double positive cells compared to ccRCC. chRCC had the highest overall ADAM17 expression out of the three subtypes, however it appears that a high percentage of ADAM17 positive cells in all subtypes also express CD200. As expected, the number of ADAM28 and CD200 double positive cells was the lowest of the three proteases, as ADAM28 expression was generally low in all three subtypes. Taken together, this data implies that ADAM9 and ADAM17 are both expressed on a high number of CD200 expressing RCC cells, while ADAM28 is only expressed on a small percentage of CD200 expressing cells. These findings are important as we have shown for the first time that ADAM9, ADAM17 and CD200 appear to be placed in a similar location on the cell membrane in RCC tissue. As ADAM17, which has been shown to have a role in CD200 ectodomain shedding (Twito et al. 2013a), shares a high number of substrates with ADAM9, we hypothesised that ADAM9 could also have a role in CD200 ectodomain shedding.

Addition of active ADAM9 peptide to CD200+ HeLa cells found a dose-dependent increase in sCD200 level in supernatant via ELISA. Furthermore, siRNA knock down of ADAM9 revealed a slight reduction in sCD200 concentration in the supernatant. This data presents a novel role for ADAM9 in CD200 ectodomain shedding, however a limitation of this study is that this was not completed in an RCC cell line. An important future direction would be to repeat this experiment in a CD200+ RCC cell line, and also in other naturally CD200+ cell lines to determine if this cleavage occurs in other cancer types. These experiments could also be repeated using ADAM17 peptide and siRNA to determine if ADAM17 carries out CD200 ectodomain

shedding in RCC. A further interesting future direction to complete would be triple IF staining for ADAM9, ADAM17 and CD200 within RCC tumours to determine if a high percentage of cells are triple positive, or if CD200 positive cells tend to overexpress either ADAM17 or ADAM9 to enable disease progression.

A further exciting further direction for this would be to use this work in a clinical application through study of sCD200 concentration in RCC patient urine, in conjunction with tumour biopsy data of CD200, ADAM9 and ADAM17 expression and patient outcome data. If urine sCD200 levels are found to increase in RCC compared to normal samples, and if the effect is disease stage-dependant, this could present an opportunity for a new, non-invasive urine biomarker with potential prognostic roles.

6.3 CD200 expression alters RCC immune infiltrate

RCC tumours induce a strong immune response and are heavily infiltrated by myeloid cells and CD4+ and CD8+ T cells, which are associated with high tumour grade and shorter OS (Kawashima et al. 2020). High levels of Tregs are also present within the RCC TME (Díaz-Montero et al. 2020), creating an immunosuppressive environment where cytotoxic effector cells are likely to be dysfunctional and unable to carry out their normal anti-tumour functions. The complexity and composition of the RCC immune landscape arises from the interaction of several factors including tumour mutational burden, RCC subtype, tumour histology and acquired mechanisms of immune evasion including the expression of immune checkpoints (Hanna 2019; Díaz-Montero et al. 2020; Wang et al. 2021b). One of the aims of this project was to determine the effect of RCC tumour CD200 expression on tumour immune infiltrate and patient outcomes.

The CIBERSORTx algorithm was used to calculate estimated immune infiltrate in publicly available large RCC tumour data sets compared to normal kidney. Significant differences in the levels of 9 out of the 22 cell types examined were found, with naïve B cells, plasma cells and activated NK cells found to be significantly higher in normal kidney compared to ccRCC, and M0 and M1 macrophages, Tregs, Tfh cells, CTLs and resting NK cells found to be significantly higher in ccRCC compared to normal kidney. This data showed a clear trend of

decreased B cells and increased T cells between the normal and ccRCC samples, indicative of a suppressed effector T cell response. However, the significant increase in resting NK cells and decrease in activated NK cells observed in ccRCC was unexpected, as NK cells are the first line defence against tumour cells in the humoral immune response (Ziblat et al. 2021). Resting NK cells have decreased cytotoxic activities due to lack of target cell interaction with their activating receptors (Bryceson et al. 2006), implying that the usual cytotoxic NK cell response is dysregulated in ccRCC. ccRCC is associated with a high T cell infiltrate, with high levels of CD4+ Tfh cells and CD8+ CTLs previously described (Wang et al. 2021b) and associated with poor prognosis (Su et al. 2021). In our data, both Tfh and CTLs were found to have significantly higher levels in ccRCC compared to normal kidney, and both cell types also significantly increased with disease stage. While generally protective in normal circumstances with key roles in maintenance of immune homeostasis, high levels of Tregs have also been previously observed in ccRCC and are associated with poor prognosis (Wang et al. 2021b), and we also observed a significant increase in Treg level with increased ccRCC stage. The combination of high levels of Tfh cells and CTLs, and high CTLs and Tregs were found to have the worst OS outcomes compared to any other combination. High levels of Tfh cells, CTLs and Tregs have been previously reported to result in disease progression and poor prognosis in ccRCC (Griffiths et al. 2007; Mier 2019; Kawashima et al. 2020), however the high levels of resting NK cells and low levels of activated NK cells observed in our samples is a key finding and implies disruption of normal cytotoxic NK responses in early stage ccRCC. Correlation analysis found a clear set of significant positive relationships was observed within the ccRCC samples between Tfh cells, CTLs, Tregs and activated NK cells, with negative relationships between all cell types and resting NK cells. This result was not found in the normal kidney samples and reinforces the notion that these key effector cells are dysfunctional, but together contribute to disease progression in a manner which is not found in the normal kidney state. From this data, we were able to propose a ccRCC-specific “high effector cell” immune signature comprised of high levels of Tfh cells, CTLs, Tregs and resting NK cells, in combination with low levels of activated NK cells. When compared to the opposite low group in survival analysis, patients with this signature were found to have a significantly lower chance of survival. This data not been

previously reported and is a key finding as this immune signature has clear prognostic significance.

Analysis of RNAseq datasets allows us to study a large number of samples quickly and easily with associated clinical data, however a limitation of the work carried out so far is that the datasets used were obtained from bulk tumour samples, which may contain non-tumour tissue, stroma, tissue artefacts and surrounding normal tissue. Another limitation is that CIBERSORTx is only able to estimate immune fractions within a sample, rather than absolute cell number numbers, meaning absolute ratios such as the CD4:CD8 ratio cannot be calculated, which is widely used as a measure of immune system activity. Therefore, to make our current data more robust, double- or triple-IF staining was used on patient-derived ccRCC TMA samples for key immune cells. This staining allowed quantification of the number of each immune cells/mm^2 and calculation of the relative frequencies of total CD45+ cells. As expected, levels of CD45+ and CD3+ cells were significantly increased in ccRCC compared to normal kidney, indicating an increased immune response. Interestingly however, in these samples, the density and frequency of CD4+ Th cells/mm^2 significantly reduced with tumour stage, which is the opposite to what was observed in our CIBERSORTx data. A further significant limitation of CIBERSORTx is that not all possible immune cell types can be calculated, and the only CD4+ cell type calculated is follicular T helper cells (Tfh), a specialised subset of T helper cells with key roles in B cell differentiation and development of germinal centres. Another limitation of this study is that IF is limited by antibody availability and combinations, meaning that we could only classify CD45+CD3+CD4+ cells as T helper (Th) cells. Therefore, this outcome is different from the bioinformatic result due to the different sets of markers used. As expected from the literature (Wu et al. 2021), a significant increase in CD8+ cell density was observed with increased ccRCC stage. As in this study we calculated Th cells and CTLs/mm^2, we could calculate the CD4:CD8 ratio, which was decreased in ccRCC compared to normal kidney, indicative of an abnormal immune response and associated with poor prognosis (McBride and Striker 2017). Treg density and frequency also significantly increased with ccRCC stage, indicating an increasingly immunosuppressive TME with advanced disease stage. Interestingly, this was the only cell type found to be affected by patient sex, with females found to have significantly less Treg cell density and frequency

compared to males, an observation which has been only previously noted in adolescent studies and may be due to differences in lipoprotein metabolism and hormones (Robinson et al. 2019). Finally, a significant increase in NK cell density and frequency was found compared to normal kidney, however another limitation of this IF study is that we are unable to determine if these NK cells were resting or activated. Unfortunately, patient clinical data was not available with our TMA samples and so survival analysis could not be completed on this data to determine the effect of changed immune infiltrate in ccRCC, however taken in combination with the CIBERSORTx data which does provide full OS and DFS clinical data, we can conclude that there is a significant change in immune infiltrate in these key cell types in ccRCC compared to normal kidney, which is likely to have a significant effect on patient prognosis.

Although the common RCC subtypes differ at both a genetic and histological level (Truong and Shen 2011; Muglia and Prando 2015), differences in immune infiltrate have previously been examined in only a small number of studies (Ricketts et al. 2018; Díaz-Montero et al. 2020). The highest number of tumour-infiltrating T cells in the subtypes has been previously reported in ccRCC (Zhang et al. 2019), and were associated with poor prognosis. Comparison of survival data revealed that ccRCC has significantly shorter OS and DFS compared to the other two subtypes, with chRCC having the best overall outcomes. Examination of the immune infiltrate for the three subtypes found that ccRCC Tfh, CTL, resting NK cells and Treg levels were all higher than the other subtypes, while the level of activated NK cells was the lowest. This data suggests that the characteristic “high effector T cell” immune signature is unique to ccRCC and correlates with poor prognosis. Conversely, chRCC was found to have the best prognosis and showed the opposite immune signature to ccRCC, presenting the lowest levels of Tfh cells, CTL and Tregs with the highest level of activated NK cells. This implies that RCC subtype immune infiltrate is significantly related to patient outcome and that levels of these key immune cells within the TME could be a prognostic marker.

While CD200 is known to generally alter tumour immune infiltrate through creation of an immunosuppressive TME (Kotwica-Mojzych et al. 2021), the effect of CD200 expression on OS and levels of tumour infiltrating immune cells has not been previously reported in RCC. Interestingly, the weak CD200 expressing group had the

shortest median OS, while the moderate expression group had the longest OS. Conversely, the strong CD200 group was found to have the shortest DFS, while the moderate group was again found to have the longest DFS. This data implies that CD200 is implicated in both OS and DFS outcomes, but with opposing roles.

The average immune fractions were found to change between the CD200 expression groups, particularly CTLs, which may imply a protective effect of CTLs in the moderate CD200 expression group, with no other immune cell types significantly altered between any of the expression groups. A general trend of increased resting NK cells and decreased activated NK cells was observed with increased CD200 expression. As CD200 expression generally increases between ccRCC stages I-III, where we would expect to see high levels of activated NK cells to indicate an active cytotoxic response, the increased resting NK cells we observed implies immune dysfunction. Survival analysis of high and low levels of each immune cell in combination with weak, moderate or strong CD200 expression revealed that moderate CD200 expression most commonly resulted in the best outcomes, when found in in combination with high Tfh cells, low activated NK cells and low resting NK cells. Taken together, this data suggests that CD200, in combination with some immune cell types has an important effect on overall patient survival, however in some cases, CD200 expression strength is the most important factor as OS stayed the same between some of the low and high immune cell groups.

Importantly, comparison of survival data for the “high effector T cell” immune signature against the opposite signature, in combination with weak, moderate or strong CD200 expression found that the high effector, strong CD200 group was found to have the shortest OS. The moderate CD200 expression, low effector signature group was found to have the best survival outcome, and this was the only group where median survival could not be calculated as over 50% of patients were still alive at the end of the study. Taken together, this data is notable as it demonstrates the significant impact of CD200 expression on ccRCC immune infiltrate, with significant effects on patient outcomes.

6.4 Tumour CD200 expression causes CD200R+ NK cell dysfunction *in vitro*

NK cells are potent cytotoxic innate immune cells, that unlike cytotoxic CD8+ T cells, can rapidly identify and kill transformed cells without the requirement for prior sensitisation (Kumar 2018). The NK cell anti-tumour response has been reported in many *in vivo* studies, which demonstrate that mice deficient in NK cells or with dysfunctional NK cell cells undergo greater tumour growth and increased metastasis (Vyas et al. 2023). However, despite NK cell infiltration into the RCC TME, tumours are still able to grow and so the role of NK cells in RCC development is not yet fully understood (Terrén et al. 2020). During RCC development, NK cells within the TME become dysfunctional and demonstrate diminished cytotoxicity, decreased responsiveness, and impaired viability, reduced degranulation and lower anti-tumour cytotoxicity (Xia et al. 2017; Ziblat et al. 2021). Interestingly, a similar dysfunctional NK cell phenotype is seen in AML and BCC patients with high tumour CD200 expression (Coles et al. 2011; Morgan et al. 2022). ccRCC tumour CD200 expression was found to be positively associated with the cell density and relative frequencies of NK cells in both our RNAseq and IF patient tissue studies, suggesting that CD200 expression may affect interacting NK cell function and viability. To explore the effects of tumour CD200 expression on interacting CD200R+ NK cells*, in vitro* models of NK cell activity were generated. In co-culture experiments on CD200+ HeLa cells, expression of CD200 demonstrated a protective role against NK92MI cytotoxicity, with CD200+ tumours demonstrating significantly improved viability. This protective effect was also observed when A498 and CD200- HeLa cells were co-cultured in the presence of CD200+ cell line supernatant, however to a lesser extent. This data suggests that evasion of NK cell cytotoxicity is CD200-dependent, and that blocking CD200 signalling may be sufficient to prevent this immunosuppression. Following ectodomain shedding, sCD200 is still functionally active (Wong et al. 2016) and here we show it is still able to prevent NK cell killing, although to a lesser extent than membrane-bound CD200. An interesting future direction for this experiment would be to repeat using higher sCD200 concentrations to determine if this is a dose-dependent effect.

This data shows that CD200 expression by CD200+ cancer cells can cause significant dysfunction in interacting CD200R+ NK cells by reducing their cytotoxic ability. This protects the CD200+ target cell from NK cell killing, resulting in

increased tumour cell viability, suggesting that CD200 signalling is an immune evasion mechanism utilised to prevent tumour cell death. Here we show for the first time that sCD200 is also able to exert these protective effects, potentially in dose-dependent manner, however it is unknown if sCD200 is as effective as the membrane-bound form at activating CD200R (Wong et al. 2016), or if the membrane-bound form competes with sCD200 for CD200R binding. In this thesis we have shown a novel role for ADAM9 in CD200 ectodomain shedding, with the overexpression of ADAM9 observed in RCC potentially resulting in increased levels of sCD200 in the TME. This finding may indicate an indirect link between ADAM9 expression and NK cell dysfunction via creation of sCD200, however this is just one piece of the puzzle and likely involves interactions with numerous other molecules and cell types. An interesting future direction for this work would include studies with longer timepoints, the use of CD200 blocking antibodies and experiments involving ADAM9+ cells or active peptide co-culture to fully determine the effect of CD200 expression on NK cell dysfunction in RCC. To validate this data in RCC, these experiments could be repeated on a CD200+ RCC cell line, and in other naturally CD200+ cancer types. If tumour CD200 expression contributes to NK cell dysfunction, this represents a novel mechanism by which CD200 overexpression by tumour cells can evade NK cell cytotoxic attacks enabling tumour progression.

6.5 Conclusions

To conclude, in this thesis we have examined the protease expression in RCC tumours, their relationship with CD200 expression and potential roles in CD200 ectodomain shedding. We have also studied RCC immune infiltrate and its relationship with CD200 in relation to patient outcomes.

ADAM9 was found to be strongly overexpressed in ccRCC compared to normal kidney and alongside ADAM17, was found to be co-expressed with CD200 on a high percentage of RCC cells. ADAM9 was also found to have a novel role in CD200 ectodomain shedding which has not been previously reported. Secondly, we examined the immune infiltrate in RCC tumours compared to normal kidney, where a characteristic ccRCC “high effector T cell” signature was determined which had a significant prognostic effect. The effect of tumour CD200 expression on immune cell

density and frequency was then determined, where both NK cells and immunosuppressive Tregs were found to positively correlate with CD200 expression, resulting in NK cell dysfunction. Finally, we examined the effect of membrane bound and soluble CD200 on the cytotoxic abilities of CD200R+ NK cells *in vitro*, where we found that both CD200 and sCD200 are able to protect tumour cells from NK cell killing. Taken together, we demonstrate a link between RCC tumour ADAM9 overexpression, an increase in TME CD200 and sCD200 levels, and NK cell dysfunction, leading to a reduction in tumour cell killing and subsequent RCC disease progression.

Chapter 7.
Supplementary Data

7. Supplementary data

Supplementary Table S1. Genes used to identify immune cells by CIBERSORTx

Tfh	CTL	Treg	Resting NK	Activated NK
ATHL1	*BCL11B*	*BARX2*	*AZU1*	*APOBEC3G*
BCL11B	*CCL5*	*BCL11B*	*BPI*	*APOL6*
CA8	*CD2*	*CD2*	*CAMP*	*CCL4*
CD2	*CD247*	*CD247*	*CCL5*	*CCL5*
CD247	*CD27*	*CD27*	*CD160*	*CCND2*
CD27	*CD3D*	*CD28*	*CD2*	*CD244*
CD3D	*CD3E*	*CD3D*	*CD244*	*CD247*
CD3G	*CD3G*	*CD3E*	*CD247*	*CD69*
CD40LG	*CD6*	*CD3G*	*CD7*	*CD7*
CD69	*CD69*	*CD4*	*CD96*	*CD96*
CD7	*CD7*	*CD5*	*CDHR1*	*CDK6*
CHI3L2	*CD8A*	*CD6*	*CEACAM8*	*CSF2*
CTLA4	*CD8B*	*CD70*	*CST7*	*CST7*
CXCL13	*CD96*	*CD96*	*CTSW*	*CTSW*
CXCR5	*CRTAM*	*CEMP1*	*DEFA4*	*DPP4*
DGKA	*CST7*	*CLEC2D*	*ELANE*	*FASLG*
FAIM3	*CTSW*	*CTLA4*	*GFI1*	*GNLY*
FOSB	*DPP4*	*DGKA*	*GNLY*	*GPR171*
FZD3	*DSC1*	*DPP4*	*GZMA*	*GPR18*
GPR19	*DUSP2*	*EFNA5*	*GZMB*	*GRAP2*
GZMM	*FAIM3*	*FOXP3*	*GZMH*	*GZMA*
ICA1	*FLT3LG*	*FRMD8*	*GZMK*	*GZMB*
ICOS	*GNLY*	*GPR1*	*GZMM*	*GZMH*
IL21	*GPR171*	*GPR171*	*IL12RB2*	*GZMM*
ITK	*GRAP2*	*GPR19*	*IL18R1*	*IFNG*
KLRB1	*GZMA*	*GZMM*	*IL18RAP*	*IL12RB2*
LAG3	*GZMB*	*HIC1*	*IL2RB*	*IL18R1*
LAT	*GZMH*	*HMGB3P30*	*KIR2DL1*	*IL18RAP*
LCK	*GZMK*	*ICOS*	*KIR3DL2*	*IL2RB*
LEF1	*GZMM*	*IL2RA*	*KLRB1*	*KIR2DL1*
LTA	*ICOS*	*IL2RB*	*KLRC3*	*KIR2DL4*
MAP4K1	*IGKC*	*ITK*	*KLRC4*	*KIR2DS4*
MAP9	*IL7R*	*KIRREL*	*KLRD1*	*KIR3DL2*
PASK	*ITK*	*LAIR2*	*KLRF1*	*KLRB1*
PDCD1	*KLRB1*	*LCK*	*KLRK1*	*KLRC3*
PTPRCAP	*KLRC3*	*LILRA4*	*LCK*	*KLRD1*
PVRIG	*KLRC4*	*LOC126987*	*MGAM*	*KLRF1*
RGS1	*KLRD1*	*LTB*	*MS4A3*	*KLRK1*
RPL3P7	*KLRF1*	*MAP4K1*	*NAALADL1*	*LCK*
SH2D1A	*KLRK1*	*MBL2*	*NKG7*	*LTA*
SIK1	*LAG3*	*NPAS1*	*NME8*	*LTB*
SIRPG	*LCK*	*NTN3*	*PLEKHF1*	*NAALADL1*
SLC7A10	*LEF1*	*PCDHA5*	*PRF1*	*NCR3*
ST8SIA1	*LIME1*	*PLCH2*	*PRR5L*	*NKG7*
TCF7	*LTB*	*PMCH*	*PTGDR*	*OSM*
TNFRSF4	*LY9*	*PTGIR*	*PTPRCAP*	*PRF1*
TRAC	*MAP4K1*	*PTPRG*	*PVRIG*	*PRR5L*
TRAT1	*MAP9*	*RCAN3*	*S1PR5*	*PTGDR*
TRAV13-1	*NCR3*	*RYR1*	*SH2D1A*	*PTGER2*
TRAV8-6	*NKG7*	*SEC31B*	*TBX21*	*PTPRCAP*
TRAV9-2	*PIK3IP1*	*SEPT5*	*TEP1*	*PVRIG*
TRBC1	*PRF1*	*SH2D1A*	*TRBC1*	*S1PR5*
TRIB2	*PTGDR*	*SIRPG*	*TRDC*	*SH2D1A*
TSHR	*PTPRCAP*	*SIT1*	*TTC38*	*SOCS1*
UBASH3A	*PVRIG*	*SKAP1*	*TXK*	*TBX21*
ZAP70	*RASA3*	*SPOCK2*	*ZAP70*	*TNFSF14*
ZBTB10	*RPL3P7*	*SSX1*	*ZNF135*	*TRDC*
	SH2D1A	*TRAC*		*TXK*
	SIRPG	*TRAT1*		*ZAP70*
	TCF7	*TRAV9-2*		
	TRAC	*TRBC1*		
	TRAT1	*TYR*		
	TRAV12-2	*UBASH3A*		
	TRAV13-1	*ZAP70*		
	TRBC1			
	TRDC			
	UBASH3A			
	ZAP70			

Supplementary Table S2. Survival curve comparison p values for high or low CTL levels by CD200 expression strength.

		CD200 Weak		CD200 Moderate		CD200 Strong	
		CTL Low	CTL High	CTL Low	CTL High	CTL Low	CTL High
CD200 Weak	CTL Low		ns	ns	ns	ns	ns
	CTL High	ns		ns	ns	ns	ns
CD200 Moderate	CTL Low	ns	ns		ns	ns	0.0032
	CTL High	ns	ns	ns		ns	0.0030
CD200 Strong	CTL Low	ns	ns	ns	ns		0.0065
	CTL High	ns	ns	0.0032	0.0030	0.0065	

Supplementary Table S3. Survival curve comparison p values for high or low Tfh levels by CD200 expression strength.

		CD200 Weak		CD200 Moderate		CD200 Strong	
		Tfh Low	Tfh High	Tfh Low	Tfh High	Tfh Low	Tfh High
CD200 Weak	Tfh Low		ns	ns	ns	ns	ns
	Tfh High	ns		0.0029	ns	ns	ns
CD200 Moderate	Tfh Low	ns	0.0029		0.0114	0.0107	0.0036
	Tfh High	ns	ns	0.0114		ns	ns
CD200 Strong	Tfh Low	ns	ns	0.0107	ns		ns
	Tfh High	ns	ns	0.0036	ns	ns	

Supplementary Table S4. Survival curve comparison p values for high or low Treg levels by CD200 expression strength.

		CD200 Weak		CD200 Moderate		CD200 Strong	
		Treg Low	Treg High	Treg Low	Treg High	Treg Low	Treg High
CD200 Weak	Treg Low		0.0308	ns	ns	ns	ns
	Treg High	0.0308		<0.0001	ns	ns	ns
CD200 Moderate	Treg Low	ns	<0.0001		0.0051	ns	0.0110
	Treg High	ns	ns	0.0051		ns	ns
CD200 Strong	Treg Low	ns	ns	ns	ns		ns
	Treg High	ns	ns	0.0110	ns	ns	

Supplementary Table S5. Survival curve comparison p values for high or low activated NK cell levels by CD200 expression strength.

		CD200 Weak		CD200 Moderate		CD200 Strong	
		Resting NK Low	Resting NK High	Resting NK Low	Resting NK High	Resting NK Low	Resting NK High
CD200 Weak	Activated NK Low		ns	0.0307	0.0442	ns	ns
	Activated NK High	ns		ns	ns	ns	ns
CD200 Moderate	Activated NK Low	0.0307	ns		ns	0.0421	ns
	Activated NK High	0.0442	ns	ns		ns	ns
CD200 Strong	Activated NK Low	ns	ns	0.0421	ns		ns
	Activated NK High	ns	ns	ns	ns	ns	

Supplementary Table S6. Survival curve comparison p values for high or low resting NK cell levels by CD200 expression strength.

		CD200 Weak		CD200 Moderate		CD200 Strong	
		Activated NK Low	Activated NK High	Activated NK Low	Activated NK High	Activated NK Low	Activated NK High
CD200 Weak	Resting NK Low		ns	ns	0.023	ns	ns
	Resting NK High	ns		ns	ns	ns	ns
CD200 Moderate	Resting NK Low	ns	ns		ns	ns	ns
	Resting NK High	0.023	ns	ns		0.0391	ns
CD200 Strong	Resting NK Low	ns	ns	ns	0.0391		ns
	Resting NK High	ns	ns	ns	ns	ns	

References

Abel, A.M., Yang, C., Thakar, M.S. and Malarkannan, S. 2018. Natural killer cells: Development, maturation, and clinical utilization. *Frontiers in Immunology*, 9(AUG), p. 1869. doi:10.3389/fimmu.2018.01869

Acharya, N., Acharya, N., Sabatos-Peyton, C., Anderson, A.C. and Anderson, A.C. 2020. Tim-3 finds its place in the cancer immunotherapy landscape. *Journal for ImmunoTherapy of Cancer*, 8(1), p. e000911. doi:10.1136/JITC-2020-000911

Adrain, C., Zettl, M., Christova, Y., Taylor, N. and Freeman, M. 2012. Tumor necrosis factor signaling requires iRhom2 to promote trafficking and activation of TACE. *Science*, 335(6065), p. 225. doi:10.1126/SCIENCE.1214400

Agarwal, S., Piesco, N.P., Johns, L.P. and Riccelli, A.E. 1995. Differential Expression of IL-1β, TNF-α, IL-6, and IL-8 in Human Monocytes in Response to Lipopolysaccharides from Different Microbes. *http://dx.doi.org/10.1177/00220345950740040501*, 74(4), pp. 1057–1065. doi:10.1177/00220345950740040501

Aguirre, L.E., Guzman, M.E., Lopes, G. and Hurley, J. 2019. Immune Checkpoint Inhibitors and the Risk of Allograft Rejection: A Comprehensive Analysis on an Emerging Issue. *The Oncologist*, 24(3), p. 394. doi:10.3389/fimmu.2018.01869

Ai, L., Chen, J., Yan, H., He, Q., Luo, P., Xu, Z. and Yang, X. 2020. Research Status and Outlook of PD-1/PD-L1 Inhibitors for Cancer Therapy. *Drug Design, Development and Therapy*, 14, p. 3625. doi:10.2147/DDDT.S267433

Aifantis, I., Gounari, F., Scorrano, L., Borowski, C. and Von Boehmer, H. 2001. Constitutive pre-TCR signaling promotes differentiation through Ca2+ mobilization and activation of NF-κB and NFAT. *Nature Immunology 2001 2:5*, 2(5), pp. 403–409. doi:10.1038/87704

Aldera, A. Pietro and Govender, D. 2021. Carbonic anhydrase IX: a regulator of pH and participant in carcinogenesis. *Journal of Clinical Pathology*, 74(6), pp. 350–354. doi:10.1136/JCLINPATH-2020-207073

Aldin, A. et al. 2023. First-line therapy for adults with advanced renal cell carcinoma: a systematic review and network meta-analysis. *Cochrane Database of Systematic Reviews*, 2023(5). doi:10.1002/14651858.CD013798.PUB2

Alleman, W.G. et al. 2004. The in vitro and in vivo effects of re-expressing methylated von Hippel-Lindau tumor suppressor gene in clear cell renal carcinoma with 5-aza-2′-deoxycytidine. *Clinical Cancer Research*, 10(20), pp. 7011–7021. doi:10.1158/1078-0432.CCR-04-0516

Amin, A. et al. 2018. Safety and efficacy of nivolumab in combination with sunitinib or pazopanib in advanced or metastatic renal cell carcinoma: the CheckMate 016 study. *Journal for ImmunoTherapy of Cancer*, 6(1), p. 109. doi:10.1186/S40425-018-0420-0

Amin, A. and White, R.L. 2014. Interleukin-2 in Renal Cell Carcinoma: A Has-Been or a Still-Viable Option? *Journal of Kidney Cancer and VHL*, 1(7), p. 74. doi:10.15586/JKCVHL.2014.18

Angori, S., Lobo, J. and Moch, H. 2022. Papillary renal cell carcinoma: current and controversial issues. *Current Opinion in Urology*, 32(4), p. 344. doi:10.1097/MOU.0000000000001000

Anton, D., Burckel, H., Josset, E. and Noel, G. 2015. Three-Dimensional Cell Culture: A Breakthrough in Vivo. *International Journal of Molecular Sciences*, 16(3), p. 5517. doi:10.3390/IJMS16035517

Aref, S., Azmy, E. and El-Gilany, A.H. 2017. Upregulation of CD200 is associated with regulatory T cell expansion and disease progression in multiple myeloma. *Hematological Oncology*, 35(1), pp. 51–57. doi:10.1002/hon.2206

Arpino, V., Brock, M. and Gill, S.E. 2015. The role of TIMPs in regulation of extracellular matrix proteolysis. *Matrix Biology*, 44–46, pp. 247–254. doi:10.1016/J.MATBIO.2015.03.005

Ayerbes, M.V., Gallego, G.A., Prado, S.D., Fonseca, P.J., Campelo, R.G. and Aparicio, L.M.A. 2008. Origin of renal cell carcinomas. *Clinical and Translational Oncology*, 10(11), pp. 697–712. doi:10.1007/s12094-008-0276-8

Baek, J.Y., Morris, S.M., Campbell, J., Fausto, N., Yeh, M.M. and Grady, W.M. 2010. TGF-beta

inactivation and TGF-alpha overexpression cooperate in an in vivo mouse model to induce hepatocellular carcinoma that recapitulates molecular features of human liver cancer. *International journal of cancer*, 127(5), pp. 1060–1071. doi:10.1002/IJC.25127

Baghban, R. et al. 2020. Tumor microenvironment complexity and therapeutic implications at a glance. *Cell Communication and Signaling 2020 18:1*, 18(1), pp. 1–19. doi:10.1186/S12964-020-0530-4

Bagnall, P. 2014. Haematuria: classification, causes and investigations. *British Journal of Nursing*, 23(20), pp. 1074–1078.

Baldewijns, M.M., Van Vlodrop, I.J.H., Vermeulen, P.B., Soetekouw, P.M.M.B., Van Engeland, M. and De Bruïne, A.P. 2010. VHL and HIF signalling in renal cell carcinogenesis. *Journal of Pathology*, 221(2), pp. 125–138. doi:10.1002/path.2689

Bankhead, P. et al. 2017. QuPath: Open source software for digital pathology image analysis. *Scientific Reports*, 7(1), pp. 1–7. doi:10.1038/s41598-017-17204-5

Baras, A.S. et al. 2016. The ratio of CD8 to Treg tumor-infiltrating lymphocytes is associated with response to cisplatin-based neoadjuvant chemotherapy in patients with muscle invasive urothelial carcinoma of the bladder. *Oncoimmunology*, 5(5). doi:10.1080/2162402X.2015.1134412

Bardhan, K., Anagnostou, T. and Boussiotis, V.A. 2016. The PD1: PD-L1/2 pathway from discovery to clinical implementation. *Frontiers in Immunology*, 7(DEC), p. 550. doi:10.3389/FIMMU.2016.00550

Barry, M. and Bleackley, R.C. 2002. Cytotoxic T lymphocytes: all roads lead to death. *Nature Reviews Immunology 2002 2:6*, 2(6), pp. 401–409. doi:10.1038/nri819

Barton Grossman, H., Wedemeyer, G. and Ren, L. 1985. Human renal carcinoma: characterization of five new cell lines. *Journal of surgical oncology*, 28(3), pp. 237–244. doi:10.1002/JSO.2930280320

Basu, A. et al. 2021. Differentiation and Regulation of TH Cells: A Balancing Act for Cancer Immunotherapy. *Frontiers in immunology*, 12, p. 669474. doi:10.3389/FIMMU.2021.669474

Bhattacharya, S., Calar, K. and De La Puente, P. 2020. Mimicking tumor hypoxia and tumor-immune interactions employing three-dimensional in vitro models. *Journal of Experimental & Clinical Cancer Research 2020 39:1*, 39(1), pp. 1–16. doi:10.1186/S13046-020-01583-1

Bi, J. and Tian, Z. 2017. NK cell exhaustion. *Frontiers in Immunology*, 8(JUN). doi:10.3389/fimmu.2017.00760

Birgersdotter, A., Sandberg, R. and Ernberg, I. 2005. Gene expression perturbation in vitro--a growing case for three-dimensional (3D) culture systems. *Seminars in cancer biology*, 15(5), pp. 405–412. doi:10.1016/J.SEMCANCER.2005.06.009

Borriello, F., Iannone, R. and Marone, G. 2017. Histamine Release from Mast Cells and Basophils. *Handbook of experimental pharmacology*, 241, pp. 121–139. doi:10.1007/164_2017_18

Bosch, F.X., Lorincz, A., Muñoz, N., Meijer, C.J.L.M. and Shah, K. V. 2002. The causal relation between human papillomavirus and cervical cancer. *Journal of Clinical Pathology*, 55(4), p. 244. doi:10.1136/JCP.55.4.244

Breslin, S. and O'Driscoll, L. 2016. The relevance of using 3D cell cultures, in addition to 2D monolayer cultures, when evaluating breast cancer drug sensitivity and resistance. *Oncotarget*, 7(29), pp. 45745–45756. doi:10.18632/ONCOTARGET.9935

Brew, K. and Nagase, H. 2010. The tissue inhibitors of metalloproteinases (TIMPs): An ancient family with structural and functional diversity. *Biochimica et biophysica acta*, 1803(1), p. 55. doi:10.1016/J.BBAMCR.2010.01.003

Brodaczewska, K.K., Szczylik, C., Fiedorowicz, M., Porta, C. and Czarnecka, A.M. 2016. Choosing the right cell line for renal cell cancer research. *Molecular Cancer*, 15(1), pp. 1–15. doi:10.1186/s12943-016-0565-8

Brookman-May, S. et al. 2013. Role of carbonic anhydrase IX (CAIX) in patients with renal cell carcinoma: can we currently assess its definitive value in prognosis, prediction to treatment response and diagnosis, and as a therapeutic approach? *BJU International*, 111(7), pp. 1015–1017. doi:10.1111/BJU.12188

Brugarolas, J. 2013. PBRM1 and BAP1 as Novel Targets for Renal Cell Carcinoma. *Cancer J*, 19(4), pp. 324–332. doi:10.1097/PPO.0b013e3182a102d1.PBRM1

Bryceson, Y.T., March, M.E., Ljunggren, H.G. and Long, E.O. 2006. Activation, co–activation, and co–stimulation of resting human NK cells. *Immunological reviews*, 214(1), pp. 73–91. doi:10.1111/J.1600-065X.2006.00457.X

Caescu, C.I., Jeschke, G.R. and Turk, B.E. 2009. Active site determinants of substrate recognition by the metalloproteinases TACE and ADAM10. *The Biochemical journal*, 424(1), p. 79. doi:10.1042/BJ20090549

Calligaris, M., Cuffaro, D., Bonelli, S., Spanò, D.P., Rossello, A., Nuti, E. and Scilabra, S.D. 2021. Strategies to Target ADAM17 in Disease: From Its Discovery to the iRhom Revolution. *Molecules*, 26(4). doi:10.3390/MOLECULES26040944

Campbell, K.S. and Purdy, A.K. 2011. Structure/function of human killer cell immunoglobulin-like receptors: lessons from polymorphisms, evolution, crystal structures and mutations. *Immunology*, 132(3), p. 315. doi:10.1111/J.1365-2567.2010.03398.X

Cancer Research UK. *Kidney cancer statistics | Cancer Research UK*.

Cancer survival in England - adults diagnosed - Office for National Statistics.

Caoili, E.M. and Davenport, M.S. 2014. Role of Percutaneous Needle Biopsy for Renal Masses. *Seminars in Interventional Radiology*, 31(1), p. 20. doi:10.1055/S-0033-1363839

Di Carlo, A. 2014. Matrix metalloproteinase-2 and -9 and tissue inhibitor of metalloproteinase-1 and -2 in sera and urine of patients with renal carcinoma. *Oncology Letters*, 7(3), pp. 621–626. doi:10.3892/ol.2013.1755

Carril-Ajuria, L., Santos, M., Roldán-Romero, J.M., Rodriguez-Antona, C. and de Velasco, G. 2020. Prognostic and Predictive Value of PBRM1 in Clear Cell Renal Cell Carcinoma. *Cancers*, 12(1). doi:10.3390/CANCERS12010016

Castilho, J.L. et al. 2022. CD4/CD8 Ratio and Cancer Risk Among Adults With HIV. *Journal of the National Cancer Institute*, 114(6), pp. 854–862. doi:10.1093/JNCI/DJAC053

Casuscelli, J. et al. 2019. Chromophobe renal cell carcinoma: results from a large single-institutional series. *Clinical genitourinary cancer*, 17(5), p. 373. doi:10.1016/J.CLGC.2019.06.011

Chaplin, D.D. 2010. Overview of the Immune Response. *The Journal of allergy and clinical immunology*, 125(2 Suppl 2), p. S3. doi:10.1016/J.JACI.2009.12.980

Chapman, J.R., Webster, A.C. and Wong, G. 2013. Cancer in the Transplant Recipient. *Cold Spring Harbor Perspectives in Medicine*, 3(7). doi:10.1101/CSHPERSPECT.A015677

Chen, C.M., Hsieh, Y.H., Hwang, J.M., Jan, H.J., Hsieh, S.C., Lin, S.H. and Lai, C.Y. 2015. Fisetin suppresses ADAM9 expression and inhibits invasion of glioma cancer cells through increased phosphorylation of ERK1/2. *Tumour biology : the journal of the International Society for Oncodevelopmental Biology and Medicine*, 36(5), pp. 3407–3415. doi:10.1007/S13277-014-2975-9

Chen, D.S. and Mellman, I. 2013. Oncology meets immunology: the cancer-immunity cycle. *Immunity*, 39(1), pp. 1–10. doi:10.1016/J.IMMUNI.2013.07.012

Chen, J. et al. 2019. T Helper 9 Cells: A New Player in Immune-Related Diseases. *DNA and Cell Biology*, 38(10), p. 1040. doi:10.1089/DNA.2019.4729

Chen, T. et al. 2020. Th9 Cell Differentiation and Its Dual Effects in Tumor Development. *Frontiers in Immunology*, 11, p. 1026. doi:10.3389/FIMMU.2020.01026

Chiu, S. and Bharat, A. 2016. Role of monocytes and macrophages in regulating immune response following lung transplantation. *Current opinion in organ transplantation*, 21(3), p. 239. doi:10.1097/MOT.0000000000000313

Cho, H. et al. 2016. On-Target Efficacy of a HIF2α Antagonist in Preclinical Kidney Cancer Models. *Nature*, 539(7627), p. 107. doi:10.1038/NATURE19795

Chou, C.W., Huang, Y.K., Kuo, T.T., Liu, J.P. and Sher, Y.P. 2020a. An overview of ADAM9: Structure, activation, and regulation in human diseases. *International Journal of Molecular Sciences*, 21(20), pp. 1–22. doi:10.3390/ijms21207790

Chou, C.W., Huang, Y.K., Kuo, T.T., Liu, J.P. and Sher, Y.P. 2020b. An Overview of ADAM9: Structure, Activation, and Regulation in Human Diseases. *International Journal of Molecular Sciences*, 21(20), pp. 1–22. doi:10.3390/IJMS21207790

Choueiri, T.K. et al. 2021. Adjuvant Pembrolizumab after Nephrectomy in Renal-Cell Carcinoma. *The New England journal of medicine*, 385(8), pp. 683–694. doi:10.1056/NEJMOA2106391

Clark, P. 2014. Protease-mediated ectodomain shedding. *Thorax*, 69(7), pp. 682–684. doi:10.1136/thoraxjnl-2013-204403

Clark, P.E. 2009. The role of VHL in clear-cell renal cell carcinoma and its relation to targeted therapy. *Kidney international*, 76(9), p. 939. doi:10.1038/KI.2009.296

Clifford, G.M., Lise, M., Franceschi, S. and Scherrer, A.U. 2017. CD4/CD8 ratio and lung cancer risk. *The Lancet HIV*, 4(3), p. e103. doi:10.1016/S2352-3018(17)30027-9

Coles, S.J., Hills, R.K., Wang, E.C.Y., Burnett, A.K., Man, S., Darley, R.L. and Tonks, A. 2012. Increased CD200 expression in acute myeloid leukemia is linked with an increased frequency of FoxP3+ regulatory T cells. *Leukemia 2012 26:9*, 26(9), pp. 2146–2148. doi:10.1038/leu.2012.75

Coles, S.J., Wang, E.C.Y., Man, S., Hills, R.K., Burnett, A.K., Tonks, A. and Darley, R.L. 2011. CD200 expression suppresses natural killer cell function and directly inhibits patient anti-tumor response in acute myeloid leukemia. *Leukemia*, 25(5), pp. 792–799. doi:10.1038/leu.2011.1

Colmont, C.S. et al. 2013. CD200-expressing human basal cell carcinoma cells initiate tumor growth. *Proceedings of the National Academy of Sciences of the United States of America*, 110(4), pp. 1434–1439. doi:10.1073/pnas.1211655110

Cornel, A.M., Mimpen, I.L. and Nierkens, S. 2020. MHC Class I Downregulation in Cancer: Underlying Mechanisms and Potential Targets for Cancer Immunotherapy. *Cancers*, 12(7), pp. 1–33. doi:10.3390/CANCERS12071760

Corrò, C. and Moch, H. 2018. Biomarker discovery for renal cancer stem cells. *Journal of Pathology: Clinical Research*, 4(1), pp. 3–18. doi:10.1002/cjp2.91

Cowey, C.L. and Rathmell, W.K. 2009. VHL gene mutations in renal cell carcinoma: Role as a biomarker of disease outcome and drug efficacy. *Current Oncology Reports*, 11(2), pp. 94–101. doi:10.1007/s11912-009-0015-5

Crotty, S. 2019. T follicular helper cell biology: A decade of discovery and diseases. *Immunity*, 50(5), pp. 1132–1148. doi:10.1016/j.immuni.2019.04.011T

Cui, W. and Kaech, S.M. 2010. Generation of effector CD8+ T cells and their conversion to memory T cells. *Immunological reviews*, 236(1), p. 151. doi:10.1111/J.1600-065X.2010.00926.X

Curiel, T.J. et al. 2004. Specific recruitment of regulatory T cells in ovarian carcinoma fosters immune privilege and predicts reduced survival. *Nature medicine*, 10(9), pp. 942–949. doi:10.1038/NM1093

Curry, A., Khatri, I., Kos, O., Zhu, F. and Gorczynski, R. 2017. Importance of CD200 expression by tumor or host cells to regulation of immunotherapy in a mouse breast cancer model. *PLoS ONE*, 12(2), pp. 1–19. doi:10.1371/journal.pone.0171586

D'arena, G. et al. 2021. CD200 Baseline Serum Levels Predict Prognosis of Chronic Lymphocytic Leukemia. *Cancers*, 13(16). doi:10.3390/CANCERS13164239

D'Arena, G. et al. 2020. CD200 and Chronic Lymphocytic Leukemia: Biological and Clinical Relevance. *Frontiers in Oncology*, 10(November). doi:10.3389/fonc.2020.584427

D'Avella, C., Abbosh, P., Pal, S.K. and Geynisman, D.M. 2018. Mutations in renal cell carcinoma. *Urologic Oncology: Seminars and Original Investigations*, 000. doi:10.1016/j.urolonc.2018.10.027

D'Avella, C., Abbosh, P., Pal, S.K. and Geynisman, D.M. 2020. Mutations in renal cell carcinoma. *Urologic Oncology: Seminars and Original Investigations*, 38(10), pp. 763–773. doi:10.1016/J.UROLONC.2018.10.027

Deleuze, A., Saout, J., Peyronnet, B., Laguerre, B. and Rioux-leclercq, N. 2020. Immunotherapy in Renal Cell Carcinoma : The Future Is Now. *International Journal of Molecular Sciences*, 21, p. 2532. doi:10.3390/ijms21072532

Díaz-Montero, C.M., Rini, B.I. and Finke, J.H. 2020. The immunology of renal cell carcinoma. *Nature*

Reviews Nephrology 2020 16:12, 16(12), pp. 721–735. doi:10.1038/s41581-020-0316-3

Doberstein, K. et al. 2013. MicroRNA-145 targets the metalloprotease ADAM17 and is suppressed in renal cell carcinoma patients. *Neoplasia (United States)*, 15(2), pp. 218–230. doi:10.1593/neo.121222

Doulabi, H., Masoumi, E., Rastin, M., Foolady Azarnaminy, A., Esmaeili, S.A. and Mahmoudi, M. 2022. The role of Th22 cells, from tissue repair to cancer progression. *Cytokine*, 149. doi:10.1016/J.CYTO.2021.155749

Drahansky, M., Paridah, M.., Moradbak, A., Mohamed, A.., Owolabi, F. abdulwahab taiwo, Asniza, M. and Abdul Khalid, S.H.. 2016. Overview of MMP Biology and Gene Associations in Human Diseases. *Intech*, i(tourism), p. 13. doi:http://dx.doi.org/10.5772/57353

Duffy, M.J., Mullooly, M., O'Donovan, N., Sukor, S., Crown, J., Pierce, A. and McGowan, P.M. 2011. The ADAMs family of proteases: New biomarkers and therapeutic targets for cancer? *Clinical Proteomics*, 8(1), pp. 1–13. doi:10.1186/1559-0275-8-9/TABLES/2

Dunn, G.P., Old, L.J. and Schreiber, R.D. 2004. The Three Es of Cancer Immunoediting. *Annual Review of Immunology*, 22(1), pp. 329–360. doi:10.1146/annurev.immunol.22.012703.104803

Dyck, L. and Mills, K.H.G. 2017. Immune checkpoints and their inhibition in cancer and infectious diseases. *European Journal of Immunology*, 47(5), pp. 765–779. doi:10.1002/EJI.201646875

Edmondson, R., Broglie, J.J., Adcock, A.F. and Yang, L. 2014. Three-Dimensional Cell Culture Systems and Their Applications in Drug Discovery and Cell-Based Biosensors. *Assay and Drug Development Technologies*, 12(4), p. 207. doi:10.1089/ADT.2014.573

Eggermont, A.M.M. et al. 2016. Prolonged Survival in Stage III Melanoma with Ipilimumab Adjuvant Therapy. *New England Journal of Medicine*, 375(19), pp. 1845–1855. doi:10.1056/NEJMOA1611299/SUPPL_FILE/NEJMOA1611299_DISCLOSURES.PDF

Ellyard, J.I., Simson, L. and Parish, C.R. 2007. Th2-mediated anti-tumour immunity: friend or foe? *Tissue antigens*, 70(1), pp. 1–11. doi:10.1111/J.1399-0039.2007.00869.X

Erin, N., İpekçi, T., Akkaya, B., Özbudak, İ.H. and Baykara, M. 2017. Changes in expressions of ADAM9, 10, and 17 as well as α-secretase activity in renal cell carcinoma. *Urologic Oncology: Seminars and Original Investigations*, 35(1), pp. 36.e15-36.e22. doi:10.1016/j.urolonc.2016.08.010

Erin, N., Podnos, A., Tanriover, G., Duymuş, Cote, E., Khatri, I. and Gorczynski, R.M. 2015. Bidirectional effect of CD200 on breast cancer development and metastasis, with ultimate outcome determined by tumor aggressiveness and a cancer-induced inflammatory response. *Oncogene*, 34(29), pp. 3860–3870. doi:10.1038/onc.2014.317

Faes, S., Demartines, N. and Dormond, O. 2021. Mechanistic Target of Rapamycin Inhibitors in Renal Cell Carcinoma: Potential, Limitations, and Perspectives. *Frontiers in Cell and Developmental Biology*, 9, p. 459. doi:10.3389/FCELL.2021.636037

Farber, N.J., Kim, C.J., Modi, P.K., Hon, J.D., Sadimin, E.T. and Singer, E.A. 2017. Renal cell carcinoma: The search for a reliable biomarker. *Translational Cancer Research*, 6(3), pp. 620–632. doi:10.21037/tcr.2017.05.19

Fecher, L.A., Agarwala, S.S., Hodi, F.S. and Weber, J.S. 2013. Ipilimumab and Its Toxicities: A Multidisciplinary Approach. *The Oncologist*, 18(6), p. 733. doi:10.1634/THEONCOLOGIST.2012-0483

Fedele, V. and Melisi, D. 2020. Permissive State of EMT: The Role of Immune Cell Compartment. *Frontiers in Oncology*, 10, p. 587. doi:10.3389/FONC.2020.00587

Fellner, C. 2012. Ipilimumab (Yervoy) Prolongs Survival In Advanced Melanoma: Serious Side Effects and a Hefty Price Tag May Limit Its Use. *Pharmacy and Therapeutics*, 37(9), p. 503.

Fessas, P., Lee, H., Ikemizu, S. and Janowitz, T. 2017. A molecular and preclinical comparison of the PD-1–targeted T-cell checkpoint inhibitors nivolumab and pembrolizumab. *Seminars in Oncology*, 44(2), p. 136. doi:10.1053/J.SEMINONCOL.2017.06.002

Frauwirth, K.A. and Thompson, C.B. 2002. Activation and inhibition of lymphocytes by costimulation. *The Journal of Clinical Investigation*, 109(3), p. 295. doi:10.1172/JCI14941

Fritzsche, F.R. et al. 2008. ADAM9 is highly expressed in renal cell cancer and is associated with tumour progression. *BMC Cancer*, 8, pp. 1–9. doi:10.1186/1471-2407-8-179

Gao, J., Yang, D., Xu, H., Yang, K., Ma, J., Xia, J. and Pan, X. 2022. ADAM metallopeptidase domain 12 overexpression correlates with prognosis and immune cell infiltration in clear cell renal cell carcinoma. *Bioengineered*, 13(2), p. 2412. doi:10.1080/21655979.2021.2010313

Garje, R. et al. 2018. Current landscape and the potential role of hypoxia-inducible factors and selenium in clear cell renal cell carcinoma treatment. *International Journal of Molecular Sciences*, 19(12). doi:10.3390/ijms19123834

Garje, R., Elhag, D., Yasin, H.A., Acharya, L., Vaena, D. and Dahmoush, L. 2021. Comprehensive review of chromophobe renal cell carcinoma. *Critical Reviews in Oncology/Hematology*, 160, p. 103287. doi:10.1016/J.CRITREVONC.2021.103287

Gaudino, S.J. and Kumar, P. 2019. Cross-talk between antigen presenting cells and T cells impacts intestinal homeostasis, bacterial infections, and tumorigenesis. *Frontiers in Immunology*, 10(MAR), p. 360. doi:10.3389/FIMMU.2019.00360

Gay, L., Baker, A.M. and Graham, T.A. 2016. Tumour Cell Heterogeneity. *F1000Research*, 5. doi:10.12688/F1000RESEARCH.7210.1

Gebrael, G., Sahu, K.K., Agarwal, N. and Maughan, B.L. 2023. Update on combined immunotherapy for the treatment of advanced renal cell carcinoma. *Human Vaccines & Immunotherapeutics*, 19(1), p. 2193528. doi:10.1080/21645515.2023.2193528

Geindreau, M., Ghiringhelli, F. and Bruchard, M. 2021. Vascular Endothelial Growth Factor, a Key Modulator of the Anti-Tumor Immune Response. *International Journal of Molecular Sciences*, 22(9). doi:10.3390/IJMS22094871

Gersh, I. and Catchpole, H.R. 1949. The organization of ground substance and basement membrane and its significance in tissue injury disease and growth. *The American journal of anatomy*, 85(3). doi:10.1002/AJA.1000850304

Giese, A.A., Babendreyer, A., Krappen, P., Gross, A., Strnad, P., Düsterhöft, S. and Ludwig, A. 2021. Inflammatory activation of surface molecule shedding by upregulation of the pseudoprotease iRhom2 in colon epithelial cells. *Scientific Reports 2021 11:1*, 11(1), pp. 1–15. doi:10.1038/s41598-021-03522-2

Ginhoux, F. and Jung, S. 2014. Monocytes and macrophages: developmental pathways and tissue homeostasis. *Nature Reviews Immunology 2014 14:6*, 14(6), pp. 392–404. doi:10.1038/nri3671

Goda, N. et al. 2022. The ratio of CD8 + lymphocytes to tumor-infiltrating suppressive FOXP3 + effector regulatory T cells is associated with treatment response in invasive breast cancer. *Discover Oncology*, 13(1), pp. 1–12. doi:10.1007/S12672-022-00482-5/FIGURES/2

Golubovskaya, V. and Wu, L. 2016. Different subsets of T cells, memory, effector functions, and CAR-T immunotherapy. *Cancers*, 8(3). doi:10.3390/cancers8030036

González-Rodríguez, P., Engskog-Vlachos, P., Zhang, H., Murgoci, A.N., Zerdes, I. and Joseph, B. 2020. SETD2 mutation in renal clear cell carcinoma suppress autophagy via regulation of ATG12. *Cell Death & Disease 2020 11:1*, 11(1), pp. 1–15. doi:10.1038/s41419-020-2266-x

Gonzalez, H., Hagerling, C. and Werb, Z. 2018. Roles of the immune system in cancer: from tumor initiation to metastatic progression. *Genes & Development*, 32(19–20), p. 1267. doi:10.1101/GAD.314617.118

Gorczynski, R., Chen, Z., Khatri, I. and Yu, K. 2013. SCD200 present in mice receiving cardiac and skin allografts causes immunosuppression in vitro and induces tregs. *Transplantation*, 95(3), pp. 442–447. doi:10.1097/TP.0b013e3182754c30

Gorczynski, R.M. 2001. Transplant tolerance modifying antibody to CD200 receptor, but not CD200, alters cytokine production profile from stimulated macrophages. *European Journal of Immunology*, 31(8), pp. 2331–2337. doi:10.1002/1521-4141(200108)31:8<2331::aid-immu2331>3.0.co;2-#

Gorczynski, R.M. 2012. CD200:CD200R-Mediated Regulation of Immunity. *ISRN Immunology*, 2012, pp. 1–18. doi:10.5402/2012/682168

Gorczynski, R.M., Chen, Z., Diao, J., Khatri, I., Wong, K., Yu, K. and Behnke, J. 2010. Breast cancer cell CD200 expression regulates immune response to EMT6 tumor cells in mice. *Breast cancer research and treatment*, 123(2), pp. 405–415. doi:10.1007/S10549-009-0667-8

Griffiths, R.W., Elkord, E., Gilham, D.E., Ramani, V., Clarke, N., Stern, P.L. and Hawkins, R.E. 2007. Frequency of regulatory T cells in renal cell carcinoma patients and investigation of correlation with survival. *Cancer Immunology, Immunotherapy*, 56(11), pp. 1743–1753. doi:10.1007/s00262-007-0318-z

Gross, J. and Lapiere, C.M. 1962. Collagenolytic activity in amphibian tissues: a tissue culture assay. *Proceedings of the National Academy of Sciences of the United States of America*, 48(6), pp. 1014–1022. doi:10.1073/PNAS.48.6.1014

Gulati, S., Previtera, M. and Lara, P.N. 2022. BRCA1-Associated Protein 1 (BAP-1) as a Prognostic and Predictive Biomarker in Clear Cell Renal Cell Carcinoma: A Systematic Review. *Kidney Cancer*, 6(1), pp. 23–35. doi:10.3233/KCA-210006

Guo, S., Yao, K., He, X., Wu, S., Ye, Y., Chen, J. and Wu, C.L. 2019. Prognostic significance of laterality in renal cell carcinoma: A population-based study from the surveillance, epidemiology, and end results (SEER) database. *Cancer Medicine*, 8(12), p. 5629. doi:10.1002/CAM4.2484

Gurski, L.A., Petrelli, N.J., Jia, X. and Farach-Carson, M.C. 2017. 3D Matrices for Anti-Cancer Drug Testing and Development. *Oncology Issues*, 25(1), pp. 20–25. doi:10.1080/10463356.2010.11883480

Gutiérrez-Melo, N. and Baumjohann, D. 2023. T follicular helper cells in cancer. *Trends in Cancer*, 9(4), pp. 309–325. doi:10.1016/J.TRECAN.2022.12.007

Ha, D. et al. 2019. Differential control of human Treg and effector T cells in tumor immunity by Fc-engineered anti–CTLA-4 antibody. *Proceedings of the National Academy of Sciences of the United States of America*, 116(2), pp. 609–618. doi:10.1073/PNAS.1812186116/SUPPL_FILE/PNAS.1812186116.SAPP.PDF

Hadler-Olsen, E., Fadnes, B., Sylte, I., Uhlin-Hansen, L. and Winberg, J.O. 2011. Regulation of matrix metalloproteinase activity in health and disease. *FEBS Journal*, 278(1), pp. 28–45. doi:10.1111/j.1742-4658.2010.07920.x

Hanahan, D. and Weinberg, R.A. 2011. Hallmarks of cancer: The next generation. *Cell*, 144(5), pp. 646–674. doi:10.1016/j.cell.2011.02.013

El Hanbuli, H.M., Ibrahim, H.A. and Soliman, S.A.M. 2021. Immunohistochemical expression of CD200 in renal cell carcinoma. *Journal of Microscopy and Ultrastructure*, 9(3), pp. 136–140. doi:10.4103/JMAU.JMAU_29_20

Hanna, K.S. 2019. A review of checkpoint inhibitors in the management of renal cell carcinoma. *J Oncol Pharm Pract.*,. doi:10.1177/1078155219881178

Hannani, D. et al. 2015. Anticancer immunotherapy by CTLA-4 blockade: obligatory contribution of IL-2 receptors and negative prognostic impact of soluble CD25. *Cell Research*, 25(2), p. 208. doi:10.1038/CR.2015.3

Haoyuan, M.A. and Yanshu, L.I. 2020. Structure, regulatory factors and cancer-related physiological effects of ADAM9. *Cell Adhesion and Migration*, 14(1), pp. 165–181. doi:10.1080/19336918.2020.1817251

Harjunpää, H. and Guillerey, C. 2020. TIGIT as an emerging immune checkpoint. *Clinical and experimental immunology*, 200(2), pp. 108–119. doi:10.1111/CEI.13407

Hatherley, D., Cherwinski, H.M., Moshref, M. and Barclay, A.N. 2005. Recombinant CD200 Protein Does Not Bind Activating Proteins Closely Related to CD200 Receptor. *The Journal of Immunology*, 175(4), pp. 2469–2474. doi:10.4049/jimmunol.175.4.2469

Hatherley, D., Lea, S.M., Johnson, S. and Barclay, A.N. 2013. Structures of CD200 / CD200 Receptor Family and Implications for Topology , Regulation , and Evolution. *Structure/Folding and Design*, 21(5), pp. 820–832. doi:10.1016/j.str.2013.03.008

Hayakawa, K., Wang, X. and Lo, E.H. 2016. CD200 increases alternatively activated macrophages through CREB - C/EBP-beta signaling. *Journal of Neurochemsitry*, 136(5), pp. 900–906. doi:10.1111/jnc.13492

He, X. and Xu, C. 2020. Immune checkpoint signaling and cancer immunotherapy. *Cell Research 2020*, 30(8), pp. 660–669. doi:10.1038/s41422-020-0343-4

Heidegger, I., Pircher, A. and Pichler, R. 2019. Targeting the tumor microenvironment in renal cell

cancer biology and therapy. *Frontiers in Oncology*, 9(JUN), pp. 1–11. doi:10.3389/fonc.2019.00490

Hernberg, M., Muhonen, T. and Pyrhonen, S. 1997. Can the CD4+/CD8+ ratio predict the outcome of interferon-a therapy for renal cell carcinoma? *Annals of Oncology*, 8, pp. 71–77. doi:10.1023/a:1008293117223

Hoek, R.H. et al. 2000. Down-Regulation of the Macrophage Lineage Through Interaction with OX2 (CD200). *Science*, 290(5497), pp. 1768–1771. doi:10.1126/SCIENCE.290.5497.1768

Hoffman, W., Lakkis, F.G. and Chalasani, G. 2016. B Cells, Antibodies, and More. *Clinical Journal of the American Society of Nephrology : CJASN*, 11(1), p. 137. doi:10.2215/CJN.09430915

Hofmann, F., Hwang, E.C., Lam, T.B.L., Bex, A., Yuan, Y., Marconi, L.S.O. and Ljungberg, B. 2020. Targeted therapy for metastatic renal cell carcinoma. *Cochrane Database of Systematic Reviews*, 2020(10). doi:10.1002/14651858.CD012796.PUB2/MEDIA/CDSR/CD012796/IMAGE_N/NCD012796-CMP-014.01.SVG

Holmannová, D. et al. 2008. Immune modulation by melanoma and ovarian tumor cells through expression of the immunosuppressive molecule CD200. *Acta medica (Hradec Králové) / Universitas Carolina, Facultas Medica Hradec Králové*, 55(2), pp. 987–996. doi:10.1007/s00262-007-0429-6

Hsieh, J.J. et al. 2017. Renal cell carcinoma. *Nature Reviews Disease Primers*, 3. doi:10.1038/nrdp.2017.9

Hsieh, J.J., Le, V.H., Oyama, T., Ricketts, C.J., Ho, T.H. and Cheng, E.H. 2018. Chromosome 3p loss–orchestrated VHL, HIF, and epigenetic deregulation in clear cell renal cell carcinoma. *Journal of Clinical Oncology*, 36(36), pp. 3533–3539. doi:10.1200/JCO.2018.79.2549

Hubeau, C., Rocks, N. and Cataldo, D. 2020. ADAM28: Another ambivalent protease in cancer. *Cancer letters*, 494, pp. 18–26. doi:10.1016/J.CANLET.2020.08.031

Huo, J.L., Wang, Y.T., Fu, W.J., Lu, N. and Liu, Z.S. 2022. The promising immune checkpoint LAG-3 in cancer immunotherapy: from basic research to clinical application. *Frontiers in Immunology*, 13, p. 4133. doi:10.3389/FIMMU.2022.956090

Imran, M. et al. 2021. Fisetin: An anticancer perspective. *Food Science & Nutrition*, 9(1), p. 3. doi:10.1002/FSN3.1872

Ishihara, H. et al. 2020. Genetic and epigenetic profiling indicates the proximal tubule origin of renal cancers in end-stage renal disease. *Cancer Science*, 111(11), p. 4276. doi:10.1111/CAS.14633

Jenkins, R.W., Barbie, D.A. and Flaherty, K.T. 2018. Mechanisms of resistance to immune checkpoint inhibitors. *British Journal of Cancer 2018 118:1*, 118(1), pp. 9–16. doi:10.1038/bjc.2017.434

Jenmalm, M.C., Cherwinski, H., Bowman, E.P., Phillips, J.H. and Sedgwick, J.D. 2006. Regulation of Myeloid Cell Function through the CD200 Receptor. *The Journal of Immunology*, 176(1), pp. 191–199. doi:10.4049/JIMMUNOL.176.1.191

Jensen, C. and Teng, Y. 2020. Is It Time to Start Transitioning From 2D to 3D Cell Culture? *Frontiers in Molecular Biosciences*, 7, p. 33. doi:10.3389/FMOLB.2020.00033

Jian, Y. et al. 2021. Current Advance of Immune Evasion Mechanisms and Emerging Immunotherapies in Renal Cell Carcinoma. *Frontiers in Immunology*, 12, p. 502. doi:10.3389/FIMMU.2021.639636

Jung, Y.S., Vermeer, P.D., Vermeer, D.W., Lee, S.J., Goh, A.R., Ahn, H.J. and Lee, J.H. 2015. CD200 is related to cancer-stem-cell features and modulates response to chemoradiation in head and neck squamous cell carcinoma. *Head & neck*, 37(3), p. 327. doi:10.1002/HED.23608

Kabaria, R., Klaassen, Z. and Terris, M.K. 2016. Renal cell carcinoma: links and risks. *International Journal of Nephrology and Renovascular Disease*, 9, p. 45. doi:10.2147/IJNRD.S75916

Kahlmeyer, A. et al. 2019. Expression of PD-1 and CTLA-4 Are Negative Prognostic Markers in Renal Cell Carcinoma. *Journal of Clinical Medicine*, 8(5). doi:10.3390/JCM8050743

Kapałczyńska, M. et al. 2018. 2D and 3D cell cultures – a comparison of different types of cancer cell cultures. *Archives of Medical Science : AMS*, 14(4), p. 910. doi:10.5114/AOMS.2016.63743

Kappelmann-Fenzl, M. et al. 2021. Molecular changes induced in melanoma by cell culturing in 3D alginate hydrogels. *Cancers*, 13(16). doi:10.3390/CANCERS13164111/S1

Kasatskaya, S.A. et al. 2020. Functionally specialized human cd4+ t-cell subsets express physicochemically distinct tcrs. *eLife*, 9, pp. 1–22. doi:10.7554/ELIFE.57063

Kato, T., Hagiyama, M. and Ito, A. 2018. Renal ADAM10 and 17: Their physiological and medical meanings. *Frontiers in Cell and Developmental Biology*, 6(NOV), pp. 1–8. doi:10.3389/fcell.2018.00153

Katoh, M. and Katoh, M. 2019. CD157 and CD200 at the crossroads of endothelial remodeling and immune regulation. *Stem Cell Investigation*, 6(4), pp. 1–7. doi:10.21037/sci.2019.04.01

Kawasaki, B.T. and Farrar, W.L. 2008. Cancer stem cells, CD200 and immunoevasion. *Trends in Immunology*, 29(10), pp. 464–468. doi:10.1016/j.it.2008.07.005

Kawasaki, B.T., Mistree, T., Hurt, E.M., Kalathur, M. and Farrar, W.L. 2007. CO-EXPRESSION OF THE TOLERAGENIC GLYCOPROTEIN, CD200, WITH MARKERS FOR CANCER STEM CELLS. *Biochemical and biophysical research communications*, 364(4), p. 778. doi:10.1016/J.BBRC.2007.10.067

Kawashima, A. et al. 2020. Tumour grade significantly correlates with total dysfunction of tumour tissue-infiltrating lymphocytes in renal cell carcinoma. *Scientific Reports*, 10(1), pp. 1–13. doi:10.1038/s41598-020-63060-1

Kelso, A., Costelloe, E.O., Johnson, B.J., Groves, P., Buttigieg, K. and Fitzpatrick, D.R. 2002. The genes for perforin, granzymes A–C and IFN-γ are differentially expressed in single CD8+ T cells during primary activation. *International Immunology*, 14(6), pp. 605–613. doi:10.1093/INTIMM/DXF028

Khan, M., Arooj, S. and Wang, H. 2020. NK Cell-Based Immune Checkpoint Inhibition. *Frontiers in immunology*, 11(February), p. 167. doi:10.3389/fimmu.2020.00167

Kidney Cancer UK. *Kidney Cancer UK Incidence of Kidney Cancer in the UK - Kidney Cancer UK*.

Kim, H., Shim, B.Y., Lee, S.J., Lee, J.Y., Lee, H.J. and Kim, I.H. 2021. Loss of Von Hippel–Lindau (VHL) Tumor Suppressor Gene Function: VHL–HIF Pathway and Advances in Treatments for Metastatic Renal Cell Carcinoma (RCC). *International Journal of Molecular Sciences 2021, Vol. 22, Page 9795*, 22(18), p. 9795. doi:10.3390/IJMS22189795

Kim, S.K. and Cho, S.W. 2022. The Evasion Mechanisms of Cancer Immunity and Drug Intervention in the Tumor Microenvironment. *Frontiers in Pharmacology*, 13. doi:10.3389/FPHAR.2022.868695

Knutson, K.L. and Disis, M.L. 2005. Tumor antigen-specific T helper cells in cancer immunity and immunotherapy. *Cancer immunology, immunotherapy : CII*, 54(8), pp. 721–728. doi:10.1007/S00262-004-0653-2

Kojima, T., Tsuchiya, K., Ikemizu, S., Yoshikawa, S., Yamanishi, Y., Watanabe, M. and Karasuyama, H. 2016. Novel CD200 homologues iSEC1 and iSEC2 are gastrointestinal secretory cell-specific ligands of inhibitory receptor CD200R. *Scientific Reports*, 6(November), pp. 1–5. doi:10.1038/srep36457

Korniluk, A., Koper, O., Kemona, H. and Dymicka-Piekarska, V. 2017. From inflammation to cancer. *Irish Journal of Medical Science*, 186(1), p. 57. doi:10.1007/S11845-016-1464-0

Kotwica-Mojzych, K., Jodłowska-Jędrych, B. and Mojzych, M. 2021. CD200:CD200R Interactions and Their Importance in Immunoregulation. *International Journal of Molecular Sciences*, 22(4), pp. 1–21. doi:10.3390/IJMS22041602

Koyasu, S. and Moro, K. 2011. Type 2 innate immune responses and the natural helper cell. *Immunology*, 132(4), p. 475. doi:10.1111/J.1365-2567.2011.03413.X

Krabbe, L.M., Bagrodia, A., Margulis, V. and Wood, C.G. 2014. Surgical Management of Renal Cell Carcinoma. *Seminars in Interventional Radiology*, 31(1), p. 27. doi:10.1055/S-0033-1363840

Krämer, A., Green, J., Pollard, J. and Tugendreich, S. 2014. Causal analysis approaches in Ingenuity Pathway Analysis. *Bioinformatics (Oxford, England)*, 30(4), pp. 523–530. doi:10.1093/BIOINFORMATICS/BTT703

Kraus, R.F. and Gruber, M.A. 2021. Neutrophils—From Bone Marrow to First-Line Defense of the Innate Immune System. *Frontiers in Immunology*, 12, p. 5503. doi:10.3389/FIMMU.2021.767175

Kretz-Rommel, A. et al. 2007. CD200 expression on tumor cells suppresses antitumor immunity: new approaches to cancer immunotherapy. *Journal of immunology (Baltimore, Md. : 1950)*, 178(9), pp. 5595–5605. doi:10.4049/JIMMUNOL.178.9.5595

Krystel-Whittemore, M., Dileepan, K.N. and Wood, J.G. 2016. Mast cell: A multi-functional master cell. *Frontiers in Immunology*, 6(JAN), p. 620. doi:10.3389/FIMMU.2015.00620

Kubelkova, K. and Macela, A. 2019. Innate Immune Recognition: An Issue More Complex Than Expected. *Frontiers in Cellular and Infection Microbiology*, 9, p. 241. doi:10.3389/FCIMB.2019.00241

Kubiczkova, L., Sedlarikova, L., Hajek, R. and Sevcikova, S. 2012. TGF-β - an excellent servant but a bad master. *Journal of Translational Medicine*, 10(1), pp. 1–24. doi:10.1186/1479-5876-10-183/FIGURES/4

Kumar, S. 2018. Natural killer cell cytotoxicity and its regulation by inhibitory receptors. *Immunology*, 154(3), p. 383. doi:10.1111/IMM.12921

Kushwah, R. and Hu, J. 2011. Complexity of dendritic cell subsets and their function in the host immune system. *Immunology*, 133(4), p. 409. doi:10.1111/J.1365-2567.2011.03457.X

Kuzmin, I., Geil, L., Ge, H., Bengtsson, U., Duh, F.M., Stanbridge, E.J. and Lerman, M.I. 1999. Analysis of aberrant methylation of the VHL gene by transgenes, monochromosome transfer, and cell fusion. *Oncogene*, 18(41), pp. 5672–5679. doi:10.1038/sj.onc.1202959

Labani-Motlagh, A., Ashja-Mahdavi, M. and Loskog, A. 2020. The Tumor Microenvironment: A Milieu Hindering and Obstructing Antitumor Immune Responses. *Frontiers in Immunology*, 11, p. 940. doi:10.3389/FIMMU.2020.00940

Lanier, L.L. 2008. Up on the tightrope: natural killer cell activation and inhibition. *Nature immunology*, 9(5), p. 495. doi:10.1038/NI1581

Lao, Y., Shen, D., Zhang, W., He, R. and Jiang, M. 2022. Immune Checkpoint Inhibitors in Cancer Therapy—How to Overcome Drug Resistance? *Cancers*, 14(15). doi:10.3390/CANCERS14153575

Laronha, H. and Caldeira, J. 2020. Structure and Function of Human Matrix Metalloproteinases. *Cells*, 9(5). doi:10.3390/CELLS9051076

Laurent, C., Fazilleau, N. and Brousset, P. 2010. A novel subset of T-helper cells: follicular T-helper cells and their markers. *Haematologica*, 95(3), p. 356. doi:10.3324/HAEMATOL.2009.019133

Leite, K.R.M., Reis, S.T., Junior, J.P., Zerati, M., Gomes, D. de O., Camara-Lopes, L.H. and Srougi, M. 2015. PD-L1 expression in renal cell carcinoma clear cell type is related to unfavorable prognosis. *Diagnostic Pathology*, 10(1), pp. 1–6. doi:10.1186/S13000-015-0414-X/FIGURES/2

Lenburg, M.E., Liou, L.S., Gerry, N.P., Frampton, G.M., Cohen, H.T. and Christman, M.F. 2003. Previously unidentified changes in renal cell carcinoma gene expression identified by parametric analysis of microarray data. *BMC Cancer*, 3, pp. 1–19. doi:10.1186/1471-2407-3-31

Leroy, B., Girard, L., Hollestelle, A., Minna, J.D., Gazdar, A.F. and Soussi, T. 2014. Analysis of TP53 Mutation Status in Human Cancer Cell Lines: A Reassessment. *Human mutation*, 35(6), p. 756. doi:10.1002/HUMU.22556

Li, G., Forest, F., Feng, G., Gentil-Perret, A., Péoc'h, M., Cottier, M. and Mottet, N. 2014a. A novel marker ADAM17 for clear cell renal cell carcinomas: implication for patients' prognosis. *Urologic oncology*, 32(8), pp. 1272–1276. doi:10.1016/J.UROLONC.2014.05.011

Li, Y., Wang, W., Yang, F., Xu, Y., Feng, C. and Zhao, Y. 2019. The regulatory roles of neutrophils in adaptive immunity. *Cell Communication and Signaling*, 17(1), pp. 1–11. doi:10.1186/S12964-019-0471-Y/FIGURES/1

Lieder, A., Guenzel, T., Lebentrau, S., Schneider, C. and Franzen, A. 2017. Diagnostic relevance of metastatic renal cell carcinoma in the head and neck: An evaluation of 22 cases in 671 patients. *International Brazilian Journal of Urology : official journal of the Brazilian Society of Urology*, 43(2), p. 202. doi:10.1590/S1677-5538.IBJU.2015.0665

Lipe, B., Ernstoff, M.S., Gui, J., Seigne, J.D., Schned, A. and Petrella, B. 2011. Extracellular proteases in renal cell carcinoma. *https://doi.org/10.1200/jco.2011.29.7_suppl.363*, 29(7_suppl), pp. 363–363. doi:10.1200/JCO.2011.29.7_SUPPL.363

Liu, J.-Q. et al. 2016. A Critical Role for CD200R Signaling in Limiting the Growth and Metastasis of CD200 + Melanoma . *The Journal of Immunology*, 197(4), pp. 1489–1497. doi:10.4049/jimmunol.1600052

Liu, J., Chen, Z., Li, Y., Zhao, W., Wu, J.B. and Zhang, Z. 2021a. PD-1/PD-L1 Checkpoint Inhibitors in Tumor Immunotherapy. *Frontiers in Pharmacology*, 12, p. 2339. doi:10.3389/FPHAR.2021.731798

Liu, M., Liang, S. and Zhang, C. 2021b. NK Cells in Autoimmune Diseases: Protective or Pathogenic? *Frontiers in Immunology*, 12, p. 624687. doi:10.3389/FIMMU.2021.624687

Liu, X. De et al. 2020. PBRM1 loss defines a nonimmunogenic tumor phenotype associated with checkpoint inhibitor resistance in renal carcinoma. *Nature Communications 2020 11:1*, 11(1), pp. 1–14. doi:10.1038/s41467-020-15959-6

Löffek, S., Schilling, O. and Franzke, C.W. 2011. Biological role of matrix metalloproteinases: a critical balance. *European Respiratory Journal*, 38(1), pp. 191–208. doi:10.1183/09031936.00146510

Long, H., Liao, W., Wang, L. and Lu, Q. 2016. A Player and Coordinator: The Versatile Roles of Eosinophils in the Immune System. *Transfusion Medicine and Hemotherapy*, 43(2), pp. 96–108. doi:10.1159/000445215

Lopez-Beltran, A. et al. 2018. The identification of immunological biomarkers in kidney cancers. *Frontiers in Oncology*, 8(NOV), pp. 1–13. doi:10.3389/fonc.2018.00456

López-Otín, C. and Bond, J.S. 2008. Proteases: Multifunctional Enzymes in Life and Disease. *The Journal of Biological Chemistry*, 283(45), p. 30433. doi:10.1074/JBC.R800035200

Love, J.E. et al. 2017. CD200 Expression in Neuroendocrine Neoplasms. *American journal of clinical pathology*, 148(3), pp. 236–242. doi:10.1093/ajcp/aqx071

Luckheeram, R.V., Zhou, R., Verma, A.D. and Xia, B. 2012. CD4+T Cells: Differentiation and Functions. *Clinical and Developmental Immunology*, 2012, p. 12. doi:10.1155/2012/925135

Magg, T., Mannert, J., Ellwart, J.W., Schmid, I. and Albert, M.H. 2012. Subcellular localization of FOXP3 in human regulatory and nonregulatory T cells. *European Journal of Immunology*, 42(6), pp. 1627–1638. doi:10.1002/EJI.201141838

Mahadevan, D. et al. 2019. Phase I study of samalizumab in chronic lymphocytic leukemia and multiple myeloma: blockade of the immune checkpoint CD200. *Journal for ImmunoTherapy of Cancer*, 7(1), pp. 1–13. doi:10.1186/s40425-019-0710-1

Makhov, P., Joshi, S., Ghatalia, P., Kutikov, A., Uzzo, R.G. and Kolenko, V.M. 2018. Resistance to systemic therapies in clear cell renal cell carcinoma: Mechanisms and management strategies. *Molecular Cancer Therapeutics*, 17(7), pp. 1355–1364. doi:10.1158/1535-7163.MCT-17-1299

Maleki Vareki, S. 2018. High and low mutational burden tumors versus immunologically hot and cold tumors and response to immune checkpoint inhibitors. *Journal for Immunotherapy of Cancer*, 6(1). doi:10.1186/S40425-018-0479-7

Maliszewska-Olejniczak, K. et al. 2019. Development of extracellular matrix supported 3D culture of renal cancer cells and renal cancer stem cells. *Cytotechnology*, 71(1), p. 149. doi:10.1007/S10616-018-0273-X

Mallikarjuna, P., Sitaram, R.T., Landström, M. and Ljungberg, B. 2018. VHL status regulates transforming growth factor-β signaling pathways in renal cell carcinoma. *Oncotarget*, 9(23), p. 16297. doi:10.18632/ONCOTARGET.24631

Mantegazza, A.R., Magalhaes, J.G., Amigorena, S. and Marks, M.S. 2013. Presentation of phagocytosed antigens by MHC class I and II. *Traffic (Copenhagen, Denmark)*, 14(2), p. 135. doi:10.1111/TRA.12026

Marchioni, M. et al. 2021. Biomarkers for Renal Cell Carcinoma Recurrence: State of the Art. *Current Urology Reports*, 22(6). doi:10.1007/S11934-021-01050-0

De Maria, A., Bozzano, F., Cantoni, C. and Moretta, L. 2011. Revisiting human natural killer cell subset function revealed cytolytic CD56dimCD16+ NK cells as rapid producers of abundant IFN-γ on activation. *Proceedings of the National Academy of Sciences of the United States of America*, 108(2), pp. 728–732. doi:10.1073/PNAS.1012356108/-/DCSUPPLEMENTAL

Marin-Acevedo, J.A., Dholaria, B., Soyano, A.E., Knutson, K.L., Chumsri, S. and Lou, Y. 2018. Next generation of immune checkpoint therapy in cancer: New developments and challenges. *Journal of Hematology and Oncology*, 11(1), pp. 1–20. doi:10.1186/S13045-018-0582-8/METRICS

Marshall, J.S., Warrington, R., Watson, W. and Kim, H.L. 2018. An introduction to immunology and immunopathology. *Allergy, Asthma and Clinical Immunology*, 14(2), pp. 1–10. doi:10.1186/S13223-018-0278-1/TABLES/4

Martinez, F.O. and Gordon, S. 2014. The M1 and M2 paradigm of macrophage activation: time for reassessment. *F1000Prime Reports*, 6. doi:10.12703/P6-13

McBride, J.A. and Striker, R. 2017. Imbalance in the game of T cells: What can the CD4/CD8 T-cell ratio tell us about HIV and health? *PLoS Pathogens*, 13(11). doi:10.1371/JOURNAL.PPAT.1006624

McCaughan, G.W., Clark, M.J. and Neil Barclay, A. 1987. Characterization of the human homolog of the rat MRC OX-2 membrane glycoprotein. *Immunogenetics*, 25(5), pp. 329–335. doi:10.1007/BF00404426

McCoach, C.E. and Bivona, T.G. 2018. The evolving understanding of immunoediting and the clinical impact of immune escape. *Journal of Thoracic Disease*, 10(3), pp. 1248–1252. doi:10.21037/JTD.2018.03.60

Medjouel Khlifi, H., Guia, S., Vivier, E. and Narni-Mancinelli, E. 2022. Role of the ITAM-Bearing Receptors Expressed by Natural Killer Cells in Cancer. *Frontiers in Immunology*, 13, p. 2256. doi:10.3389/FIMMU.2022.898745

Mellman, I. 2013. Dendritic cells: master regulators of the immune response. *Cancer immunology research*, 1(3), pp. 145–149. doi:10.1158/2326-6066.CIR-13-0102

Meuth, S.G. et al. 2008. CNS inflammation and neuronal degeneration is aggravated by impaired CD200–CD200R-mediated macrophage silencing. *Journal of Neuroimmunology*, 194(1–2), pp. 62–69. doi:10.1016/J.JNEUROIM.2007.11.013

Mier, J.W. 2019. The tumor microenvironment in renal cell cancer. *Current Opinion in Oncology*, 31(3), pp. 194–199. doi:10.1097/CCO.0000000000000512

Mihrshahi, R., Barclay, A.N. and Brown, M.H. 2009. Essential roles for Dok2 and RasGAP in CD200 receptor-mediated regulation of human myeloid cells. *Journal of immunology (Baltimore, Md. : 1950)*, 183(8), p. 4879. doi:10.4049/JIMMUNOL.0901531

Mihrshahi, R. and Brown, M.H. 2010. Dok1 and Dok2 play opposing roles in CD200R signaling. *Journal of immunology (Baltimore, Md. : 1950)*, 185(12), p. 7216. doi:10.4049/JIMMUNOL.1002858

Miller, M.A., Sullivan, R.J. and Lauffenburger, D.A. 2017. Molecular Pathways: Receptor Ectodomain Shedding in Treatment, Resistance, and Monitoring of Cancer. *Clinical cancer research : an official journal of the American Association for Cancer Research*, 23(3), p. 623. doi:10.1158/1078-0432.CCR-16-0869

Mills, C.D. 2012. M1 and M2 Macrophages: Oracles of Health and Disease. *Critical reviews in immunology*, 32(6), pp. 463–488. doi:10.1615/CRITREVIMMUNOL.V32.I6.10

Min, B., Le Gros, G. and Paul, W.E. 2006. Basophils: a potential liaison between innate and adaptive immunity. *Allergology international : official journal of the Japanese Society of Allergology*, 55(2), pp. 99–104. doi:10.2332/ALLERGOLINT.55.99

Minas, K. and Liversidge, J. 2006. Is the CD200/CD200 receptor interaction more than just a myeloid cell inhibitory signal? *Critical Reviews in Immunology*, 26(3), pp. 213–230. doi:10.1615/critrevimmunol.v26.i3.20

Miossec, P. and Kolls, J.K. 2012. Targeting IL-17 and TH17 cells in chronic inflammation. *Nature Reviews Drug Discovery 2012 11:10*, 11(10), pp. 763–776. doi:10.1038/nrd3794

Miricescu, D. et al. 2021. PI3K/AKT/mTOR signalling pathway involvement in renal cell carcinoma pathogenesis (Review). *Experimental and Therapeutic Medicine*, 21(5), pp. 1–7. doi:10.3892/ETM.2021.9972

Mishra, H.K., Ma, J. and Walcheck, B. 2017. Ectodomain shedding by ADAM17: Its ole in neutrophil recruitment and the Impairment of this process during sepsis. *Frontiers in Cellular and Infection Microbiology*, 7(APR), p. 138. doi:10.3389/FCIMB.2017.00138

Mitsui, Y. et al. 2006. ADAM28 is overexpressed in human breast carcinomas: Implications for carcinoma cell proliferation through cleavage of insulin-like growth factor binding protein-3. *Cancer Research*, 66(20), pp. 9913–9920. doi:10.1158/0008-5472.CAN-06-0377

Mittal, D., Gubin, M.M., Schreiber, R.D. and Smyth, M.J. 2014. New insights into cancer immunoediting and its three component phases — elimination, equilibrium and escape. *Current opinion in immunology*, 27(1), p. 16. doi:10.1016/J.COI.2014.01.004

Miyamae, Y. et al. 2016. ADAM28 is expressed by epithelial cells in human normal tissues and protects from C1q-induced cell death. *The FEBS Journal*, 283(9), pp. 1574–1594. doi:10.1111/FEBS.13693

Mizuno, R., Sugiura, D., Shimizu, K., Maruhashi, T., Watada, M., Okazaki, I. mi and Okazaki, T. 2019. PD-1 primarily targets TCR signal in the inhibition of functional T cell activation. *Frontiers in Immunology*, 10(MAR), p. 630. doi:10.3389/FIMMU.2019.00630

Mochizuki, S. et al. 2012. Effect of ADAM28 on carcinoma cell metastasis by cleavage of von willebrand factor. *Journal of the National Cancer Institute*, 104(12), pp. 906–922. doi:10.1093/jnci/djs232

Mochizuki, S. and Okada, Y. 2007. ADAMs in cancer cell proliferation and progression. *Cancer Science*, 98(5), pp. 621–628. doi:10.1111/j.1349-7006.2007.00434.x

Monteiro, F.S.M., Soares, A., Rizzo, A., Santoni, M., Mollica, V., Grande, E. and Massari, F. 2023. The role of immune checkpoint inhibitors (ICI) as adjuvant treatment in renal cell carcinoma (RCC): A Systematic Review and Meta-Analysis. *Clinical Genitourinary Cancer*, 0(0). doi:10.1016/j.clgc.2023.01.005

Mootha, V.K. et al. 2003. PGC-1α-responsive genes involved in oxidative phosphorylation are coordinately downregulated in human diabetes. *Nature Genetics 2003 34:3*, 34(3), pp. 267–273. doi:10.1038/ng1180

Mora, A. et al. 2019. CD200 is a useful marker in the diagnosis of chronic lymphocytic leukemia. *Cytometry Part B - Clinical Cytometry*, 96(2), pp. 143–148. doi:10.1002/cyto.b.21722

Moreaux, J., Veyrune, J.L., Reme, T., De Vos, J. and Klein, B. 2008. CD200: A putative therapeutic target in cancer. *Biochemical and Biophysical Research Communications*, 366(1), pp. 117–122. doi:10.1016/j.bbrc.2007.11.103

Moretta, L. 2010. Dissecting CD56dim human NK cells. *Blood*, 116(19), pp. 3689–3691. doi:10.1182/BLOOD-2010-09-303057

Morgan, H.J. et al. 2022. CD200 ectodomain shedding into the tumor microenvironment leads to NK cell dysfunction and apoptosis. *The Journal of clinical investigation*, 132(21). doi:10.1172/JCI150750

Morris, R.M., Mortimer, T.O. and O'Neill, K.L. 2022. Cytokines: Can Cancer Get the Message? *Cancers*, 14(9). doi:10.3390/CANCERS14092178

Morrissey, J.J. and Kharasch, E.D. 2013. The specificity of urinary aquaporin 1 and perilipin 2 to screen for renal cell carcinoma. *Journal of Urology*, 189(5), pp. 1913–1920. doi:10.1016/j.juro.2012.11.034

Motz, G.T. and Coukos, G. 2013. Deciphering and Reversing Tumor Immune Suppression. *Immunity*, 39(1), pp. 61–73. doi:10.1016/J.IMMUNI.2013.07.005

Motzer, R.J. et al. 2018. Nivolumab plus Ipilimumab versus Sunitinib in advanced renal-cell carcinoma. *New England Journal of Medicine*, 378(14), pp. 1277–1290. doi:10.1056/NEJMoa1712126

Motzer, R.J. et al. 2023. Adjuvant nivolumab plus ipilimumab versus placebo for localised renal cell carcinoma after nephrectomy (CheckMate 914): a double-blind, randomised, phase 3 trial. *The Lancet*, 401(10379), pp. 821–832. doi:10.1016/S0140-6736(22)02574-0

Muglia, V.F. and Prando, A. 2015. Renal cell carcinoma: histological classification and correlation withimaging findings. *Radiologia Brasileira*, 48(3), p. 166. doi:10.1590/0100-3984.2013.1927

Mullooly, M., McGowan, P.M., Crown, J. and Duffy, M.J. 2016. The ADAMs family of proteases as targets for the treatment of cancer. *Cancer Biology & Therapy*, 17(8), p. 870. doi:10.1080/15384047.2016.1177684

Nabi, S., Kessler, E.R., Bernard, B., Flaig, T.W. and Lam, E.T. 2018. Renal cell carcinoma: a review of biology and pathophysiology. *F1000Research*, 7, p. 307. doi:10.12688/F1000RESEARCH.13179.1

Da Nagaprashantha, L. et al. 2013. Proteomic Analysis of Signaling Network Regulation in Renal Cell Carcinomas with Differential Hypoxia-Inducible Factor-2α Expression. *PLoS ONE*, 8(8). doi:10.1371/JOURNAL.PONE.0071654

Nagase, H., Visse, R. and Murphy, G. 2006. Structure and function of matrix metalloproteinases and TIMPs. *Cardiovascular Research*, 69(3), pp. 562–573. doi:10.1016/J.CARDIORES.2005.12.002/2/69-3-562-FIG3.GIF

Nakanishi, K. 2010. Basophils are potent antigen-presenting cells that selectively induce Th2 cells. *European Journal of Immunology*, 40(7), pp. 1836–1842. doi:10.1002/EJI.201040588

Nakano, O. et al. 2001. Proliferative activity of intratumoral CD8+ T-lymphocytes as a prognostic factor in human renal cell carcinoma: Clinicopathologic demonstration of antitumor immunity. *Cancer Research*, 61(13), pp. 5132–5136.

Ndiaye, P.D. et al. 2019. VEGFC acts as a double-edged sword in renal cell carcinoma aggressiveness. *Theranostics*, 9(3), p. 661. doi:10.7150/THNO.27794

Newman, A.M. et al. 2019. Determining cell type abundance and expression from bulk tissues with digital cytometry. *Nature Biotechnology*, 37(7), pp. 773–782. doi:10.1038/s41587-019-0114-2

Newton, K. and Dixit, V.M. 2012. Signaling in Innate Immunity and Inflammation. *Cold Spring Harbor Perspectives in Biology*, 4(3). doi:10.1101/CSHPERSPECT.A006049

Ngwa, C. and Liu, F. 2019. CD200-CD200R signaling and diseases: a potential therapeutic target? *International Journal of Physiology, Pathophysiology and Pharmacology*, 11(6), p. 297.

NICE. *Recommendations organised by site of cancer | Suspected cancer: recognition and referral | Guidance | NICE*.

Nicholson, L.B. 2016. The immune system. *Essays in Biochemistry*, 60(3), p. 275. doi:10.1042/EBC20160017

Niogret, J. et al. 2021. Follicular helper-T cells restore CD8+-dependent antitumor immunity and anti-PD-L1/PD-1 efficacy. *Journal for ImmunoTherapy of Cancer*, 9(6), p. e002157. doi:10.1136/JITC-2020-002157

North, J. et al. 2007. Tumor-Primed Human Natural Killer Cells Lyse NK-Resistant Tumor Targets: Evidence of a Two-Stage Process in Resting NK Cell Activation. *The Journal of Immunology*, 178(1), pp. 85–94. doi:10.4049/JIMMUNOL.178.1.85

O'Donnell, J.S., Teng, M.W.L. and Smyth, M.J. 2018. Cancer immunoediting and resistance to T cell-based immunotherapy. *Nature Reviews Clinical Oncology 2018 16:3*, 16(3), pp. 151–167. doi:10.1038/s41571-018-0142-8

Ohyama, M. et al. 2006. Characterization and isolation of stem cell–enriched human hair follicle bulge cells. *Journal of Clinical Investigation*, 116(1), p. 249. doi:10.1172/JCI26043

Olive, C., Cheung, C., Nicol, D. and Falk, M.C. 1999. Expression of apoptotic regulatory molecules in renal cell carcinoma: elevated expression of Fas ligand. *Immunology and cell biology*, 77(1), pp. 11–18. doi:10.1046/J.1440-1711.1999.00791.X

Omilusik, K.D. and Goldrath, A.W. 2017. The origins of memory T cells. *Nature 2021 552:7685*, 552(7685), pp. 337–339. doi:10.1038/d41586-017-08280-8

Orange, J.S. 2008. Formation and function of the lytic NK-cell immunological synapse. *Nature Reviews Immunology 2008 8:9*, 8(9), pp. 713–725. doi:10.1038/nri2381

Oweira, H. et al. 2019. Pre-transplant CD200 and CD200R1 concentrations are associated with post-transplant events in kidney transplant recipients. *Medicine (United States)*, 98(37). doi:10.1097/MD.0000000000017006

Ozcan, A., Krishnan, B. and Truong, L. 2014. Renal Tumors. *Pathobiology of Human Disease: A Dynamic Encyclopedia of Disease Mechanisms*, pp. 2869–2899. doi:10.1016/B978-0-12-386456-7.05415-0

Padala, S.A. and Kallam, A. 2022. Clear Cell Renal Carcinoma. *StatPearls*,.

Pan, Y., Du, D., Wang, L., Wang, X., He, G. and Jiang, X. 2022. The Role of T Helper 22 Cells in Dermatological Disorders. *Frontiers in Immunology*, 13. doi:10.3389/FIMMU.2022.911546/FULL

Pantuck, A.J. et al. 2007. Use of carbonic anhydrase IX (CAIX) expression and Von Hippel Lindau (VHL) gene mutation status to predict survival in renal cell carcinoma. *https://doi.org/10.1200/jco.2007.25.18_suppl.5042*, 25(18_suppl), pp. 5042–5042. doi:10.1200/JCO.2007.25.18_SUPPL.5042

Papathanassiou, M. et al. 2022. Immune-based treatment re-challenge in renal cell carcinoma: A systematic review and meta-analysis. *Frontiers in Oncology*, 12, p. 6469. doi:10.3389/FONC.2022.996553

Pasha, M., Sivaraman, S.K., Frantz, R., Agouni, A. and Munusamy, S. 2019. Metformin induces different responses in clear cell renal cell carcinoma caki cell lines. *Biomolecules*, 9(3). doi:10.3390/biom9030113

Pastore, A.L. et al. 2015. Serum and urine biomarkers for human renal cell carcinoma. *Disease Markers*, 2015. doi:10.1155/2015/251403

Patente, T.A., Pinho, M.P., Oliveira, A.A., Evangelista, G.C.M., Bergami-Santos, P.C. and Barbuto, J.A.M. 2019. Human dendritic cells: Their heterogeneity and clinical application potential in cancer immunotherapy. *Frontiers in Immunology*, 10(JAN), p. 3176. doi:10.3389/FIMMU.2018.03176

Paul, S. and Lal, G. 2017. The molecular mechanism of natural killer cells function and its importance in cancer immunotherapy. *Frontiers in Immunology*, 8(SEP), p. 1124. doi:10.3389/FIMMU.2017.01124

Peduto, L. 2009. ADAM9 as a Potential Target Molecule in Cancer. *Current Pharmaceutical Design*, 15(20), pp. 2282–2287. doi:10.2174/138161209788682415

Peng, X. et al. 2018. ADAM17 overexpression is associated with poorer clinical outcomes in cancer patients: a systematic review and meta-analysis. *Oncotarget*, 5(0). doi:10.18632/ONCOTARGET.23999

Petejova, N. and Martinek, A. 2016. Renal cell carcinoma: Review of etiology, pathophysiology and risk factors. *Biomedical Papers*, 160(2), pp. 183–194. doi:10.5507/bp.2015.050

Philips, E.A. et al. 2020. The structural features that distinguish PD-L2 from PD-L1 emerged in placental mammals. *The Journal of Biological Chemistry*, 295(14), p. 4372. doi:10.1074/JBC.AC119.011747

Piersma, S.J. and Brizić, I. 2022. Natural killer cell effector functions in antiviral defense. *The FEBS Journal*, 289(14), pp. 3982–3999. doi:10.1111/FEBS.16073

Pillai, S. and Cariappa, A. 2009. The follicular versus marginal zone B lymphocyte cell fate decision. *Nature Reviews Immunology 2009 9:11*, 9(11), pp. 767–777. doi:10.1038/nri2656

Poli, A., Michel, T., Thérésine, M., Andrès, E., Hentges, F. and Zimmer, J. 2009. CD56bright natural killer (NK) cells: an important NK cell subset. *Immunology*, 126(4), pp. 458–465. doi:10.1111/J.1365-2567.2008.03027.X

Pontikoglou, C. et al. 2016. CD200 expression in human cultured bone marrow mesenchymal stem cells is induced by pro-osteogenic and pro-inflammatory cues. *Journal of Cellular and Molecular Medicine*, 20(4), pp. 655–665. doi:10.1111/jcmm.12752

Puzanov, G.A. 2022. Identification of key genes of the ccRCC subtype with poor prognosis. *Scientific Reports 2022 12:1*, 12(1), pp. 1–10. doi:10.1038/s41598-022-18620-y

Qi, X., Li, Q., Che, X., Wang, Q. and Wu, G. 2021. The Uniqueness of Clear Cell Renal Cell Carcinoma: Summary of the Process and Abnormality of Glucose Metabolism and Lipid Metabolism in ccRCC. *Frontiers in Oncology*, 11. doi:10.3389/FONC.2021.727778

Qu, X., Tang, Y. and Hua, S. 2018. Immunological approaches towards cancer and inflammation: A cross talk. *Frontiers in Immunology*, 9(MAR), p. 563. doi:10.3389/FIMMU.2018.00563

Rafty, L.A. and Khachigian, L.M. 2002. von Hippel-Lindau tumor suppressor protein represses platelet-derived growth factor B-chain gene expression via the Sp1 binding element in the proximal PDGF-B promoter. *Journal of Cellular Biochemistry*, 85(3), pp. 490–495. doi:10.1002/JCB.10152

Rassy, E., Flippot, R. and Albiges, L. 2020. Tyrosine kinase inhibitors and immunotherapy

combinations in renal cell carcinoma. *Therapeutic Advances in Medical Oncology*, 12. doi:10.1177/1758835920907504

Rausch, M., Blanc, L., De Souza Silva, O., Dormond, O., Griffioen, A.W. and Nowak-Sliwinska, P. 2021. Characterization of renal cell carcinoma heterotypic 3d co-cultures with immune cell subsets. *Cancers*, 13(11). doi:10.3390/CANCERS13112551/S1

Rawlings, N.D. and Barrett, A.J. 1993. Evolutionary families of peptidases. *Biochemical Journal*, 290(Pt 1), p. 205. doi:10.1042/BJ2900205

Rees, E. 2020. Evaluating the role of CD200 signalling in renal cell carcinoma immune evasion.

Reigle, J. et al. 2021. Tobacco smoking induces metabolic reprogramming of renal cell carcinoma. *The Journal of Clinical Investigation*, 131(1). doi:10.1172/JCI140522

Ribatti, D. 2022. Immunosuppressive effects of vascular endothelial growth factor. *Oncology Letters*, 24(4). doi:10.3892/OL.2022.13489

Ricketts, C.J. et al. 2018. The Cancer Genome Atlas Comprehensive Molecular Characterization of Renal Cell Carcinoma. *Cell Reports*, 23(1), pp. 313-326.e5. doi:10.1016/j.celrep.2018.03.075

Rijkers, E.S.K., de Ruiter, T., Baridi, A., Veninga, H., Hoek, R.M. and Meyaard, L. 2008. The inhibitory CD200R is differentially expressed on human and mouse T and B lymphocytes. *Molecular immunology*, 45(4), pp. 1126–1135. doi:10.1016/J.MOLIMM.2007.07.013

Rini, B.I. et al. 2008. Bevacizumab plus interferon alfa compared with interferon alfa monotherapy in patients with metastatic renal cell carcinoma: CALGB 90206. *Journal of clinical oncology : official journal of the American Society of Clinical Oncology*, 26(33), pp. 5422–5428. doi:10.1200/JCO.2008.16.9847

Robert, C. 2020. A decade of immune-checkpoint inhibitors in cancer therapy. *Nature Communications 2020 11:1*, 11(1), pp. 1–3. doi:10.1038/s41467-020-17670-y

Robinson, G.A. et al. 2019. Sex differences in autoimmunity could be associated with altered regulatory T cell phenotype and lipoprotein metabolism. *bioRxiv*, p. 760975. doi:10.1101/760975

Roche, P.A. and Furuta, K. 2015. The ins and outs of MHC class II-mediated antigen processing and presentation. *Nature Reviews Immunology 2015 15:4*, 15(4), pp. 203–216. doi:10.1038/nri3818

Rodriguez-Zhurbenko, N., Quach, T.D., Hopkins, T.J., Rothstein, T.L. and Hernandez, A.M. 2019. Human B-1 cells and B-1 cell antibodies change with advancing age. *Frontiers in Immunology*, 10(MAR), p. 483. doi:10.3389/FIMMU.2019.00483

Roemer, A. et al. 2004a. THE MEMBRANE PROTEASES ADAMS AND HEPSIN ARE DIFFERENTIALLY EXPRESSED IN RENAL CELL CARCINOMA. ARE THEY POTENTIAL TUMOR MARKERS? *The Journal of Urology*, 172(6 I), pp. 2162–2166. doi:10.1097/01.JU.0000144602.01322.49

Roemer, A.P. et al. 2004b. Increased MRNA Expression of ADAMs (A Disintegrin and Metalloproteinase) in Renal Cell Carcinoma and their Association with Clinical Outcome. *Journal of Urology*, 171(4S), pp. 263–263. doi:10.1016/s0022-5347(18)38231-4

Rojas-Domínguez, A., Arroyo-Duarte, R., Rincón-Vieyra, F. and Alvarado-Mentado, M. 2022. Modeling cancer immunoediting in tumor microenvironment with system characterization through the ising-model Hamiltonian. *BMC Bioinformatics*, 23(1), pp. 1–25. doi:10.1186/S12859-022-04731

Rosenblum, M.D. et al. 2004. CD200 is a novel p53-target gene involved in apoptosis-associated immune tolerance. *Blood*, 103(7), pp. 2691–2698. doi:10.1182/BLOOD-2003-09-3184

Rossi, S.H., Klatte, T., Usher-Smith, J. and Stewart, G.D. 2018. Epidemiology and screening for renal cancer. *World Journal of Urology*, 36(9), pp. 1341–1353. doi:10.1007/s00345-018-2286-7

Ryan, M.J., Johnson, G., Kirk, J., Fuerstenberg, S.M., Zager, R.A. and Torok-Storb, B. 1994. HK-2: an immortalized proximal tubule epithelial cell line from normal adult human kidney. *Kidney international*, 45(1), pp. 48–57. doi:10.1038/KI.1994.6

Saad, M.I., Rose-John, S. and Jenkins, B.J. 2019. ADAM17: An Emerging Therapeutic Target for Lung Cancer. *Cancers*, 11(9). doi:10.3390/CANCERS11091218

Saad, O.A. et al. 2022. The renal clear cell carcinoma immune landscape. *Neoplasia (United States)*,

24(2), pp. 145–154. doi:10.1016/j.neo.2021.12.007

Sahni, V.A. and Silverman, S.G. 2009. Biopsy of renal masses: when and why. *Cancer Imaging*, 9(1), p. 44. doi:10.1102/1470-7330.2009.0005

Samji, T. and Khanna, K.M. 2017. Understanding Memory CD8+ T cells. *Immunology letters*, 185, p. 32. doi:10.1016/J.IMLET.2017.02.012

Sánchez-Gastaldo, A., Kempf, E., González del Alba, A. and Duran, I. 2017. Systemic treatment of renal cell cancer: A comprehensive review. *Cancer Treatment Reviews*, 60, pp. 77–89. doi:10.1016/j.ctrv.2017.08.010

Sanif, R. and Nurwany, R. 2019. Prognostic significance of CD4/CD8 ratio in patients with advanced cervical cancer. *Journal of Physics: Conference Series*, 1246(1), p. 012053. doi:10.1088/1742-6596/1246/1/012053

Sansom, D.M. 2000. CD28, CTLA-4 and their ligands: who does what and to whom? *Immunology*, 101(2), p. 169. doi:10.1046/J.1365-2567.2000.00121.X

Schleinitz, N., Vély, F., Harlé, J.R. and Vivier, E. 2010. Natural killer cells in human autoimmune diseases. *Immunology*, 131(4), p. 451. doi:10.1111/J.1365-2567.2010.03360.X

Schmetterer, K.G., Neunkirchner, A. and Pickl, W.F. 2012. Naturally occurring regulatory T cells: markers, mechanisms, and manipulation. *The FASEB Journal*, 26(6), pp. 2253–2276. doi:10.1096/FJ.11-193672

Schmidt, A., Oberle, N. and Krammer, P.H. 2012. Molecular Mechanisms of Treg-Mediated T Cell Suppression. *Frontiers in Immunology*, 3(MAR). doi:10.3389/FIMMU.2012.00051

Schmitt, E.G. and Williams, C.B. 2013. Generation and function of induced regulatory T cells. *Frontiers in Immunology*, 4(JUN), p. 152. doi:10.3389/FIMMU.2013.00152

Schreiber, S., Hammers, C.M., Kaasch, A.J., Schraven, B., Dudeck, A. and Kahlfuss, S. 2021. Metabolic Interdependency of Th2 Cell-Mediated Type 2 Immunity and the Tumor Microenvironment. *Frontiers in Immunology*, 12, p. 632581. doi:10.3389/FIMMU.2021.632581

Seals, D.F. and Courtneidge, S.A. 2003. The ADAMs family of metalloproteases: multidomain proteins with multiple functions. doi:10.1101/gad.1039703

Serra, R. 2020. Matrix Metalloproteinases in Health and Disease. *Biomolecules*, 10(8), pp. 1–3. doi:10.3390/BIOM10081138

Shah, P. et al. 2022. Immune Checkpoint CD200/CD200R Decreases T Cell-Mediated Cytotoxicity Via Dok2 and Is Regulated By P53 in Multiple Myeloma. *Blood*, 140(Supplement 1), pp. 7076–7077. doi:10.1182/BLOOD-2022-166283

Shahaf, G., Zisman-Rozen, S., Benhamou, D., Melamed, D. and Mehr, R. 2016. B cell development in the bone marrow is regulated by homeostatic feedback exerted by mature B cells. *Frontiers in Immunology*, 7(MAR), p. 77. doi:10.3389/FIMMU.2016.00077

Shevach, E.M. and Thornton, A.M. 2014. tTregs, pTregs, and iTregs: Similarities and Differences. *Immunological reviews*, 259(1), p. 88. doi:10.1111/IMR.12160

Shintani, Y. et al. 2004a. Overexpression of ADAM9 in non-small cell lung cancer correlates with brain metastasis. *Cancer research*, 64(12), pp. 4190–4196. doi:10.1158/0008-5472.CAN-03-3235

Shirakabe, K. et al. 2017. Mechanistic insights into ectodomain shedding: Susceptibility of CADM1 adhesion molecule is determined by alternative splicing and O-glycosylation. *Scientific Reports*, 7(March), pp. 1–12. doi:10.1038/srep46174

Shiravand, Y. et al. 2022. Immune Checkpoint Inhibitors in Cancer Therapy. *Current oncology (Toronto, Ont.)*, 29(5), pp. 3044–3060. doi:10.3390/CURRONCOL29050247

Shoemaker, R.H. 2006. The NCI60 human tumour cell line anticancer drug screen. *Nature Reviews Cancer*, 6(10), pp. 813–823. doi:10.1038/nrc1951

Shou, Y. et al. 2022. TIMP1 Indicates Poor Prognosis of Renal Cell Carcinoma and Accelerates Tumorigenesis via EMT Signaling Pathway. *Frontiers in Genetics*, 13. doi:10.3389/FGENE.2022.648134/FULL

Silva, D.D.O., Noronha, J.A.P., da Costa, B.E.P., Zandona, P.C.E. and Carvalhal, G.F. 2018. Serum tissue factor as a biomarker for renal clear cell carcinoma. *International Braz J Urol*, 44(1), pp. 38–44. doi:10.1590/S1677-5538.IBJU.2017.0007

Singh, N., Baby, D., Rajguru, J., Patil, P., Thakkannavar, S. and Pujari, V. 2019. Inflammation and Cancer. *Annals of African Medicine*, 18(3), p. 121. doi:10.4103/AAM.AAM_56_18

Sitaram, R.T., Mallikarjuna, P., Landström, M. and Ljungberg, B. 2016. Transforming growth factor-β promotes aggressiveness and invasion of clear cell renal cell carcinoma. *Oncotarget*, 7(24), p. 35917. doi:10.18632/ONCOTARGET.9177

Siva, A., Xin, H., Qin, F., Oltean, D., Bowdish, K.S. and Kretz-Rommel, A. 2008. Immune modulation by melanoma and ovarian tumor cells through expression of the immunosuppressive molecule CD200. *Cancer Immunology, Immunotherapy*, 57(7), pp. 987–996. doi:10.1007/s00262-007-0429-6

Sivori, S., Vacca, P., Del Zotto, G., Munari, E., Mingari, M.C. and Moretta, L. 2019. Human NK cells: surface receptors, inhibitory checkpoints, and translational applications. *Cellular & Molecular Immunology 2019 16:5*, 16(5), pp. 430–441. doi:10.1038/s41423-019-0206-4

Solis-Castillo, L.A. et al. 2020. Tumor-infiltrating regulatory T cells, CD8/Treg ratio, and cancer stem cells are correlated with lymph node metastasis in patients with early breast cancer. *Breast Cancer*, 27(5), pp. 837–849. doi:10.1007/S12282-020-01079-Y/FIGURES/6

Somekawa, K. et al. 2022. Adverse events induced by nivolumab and ipilimumab combination regimens. *Therapeutic Advances in Medical Oncology*, 14. doi:10.1177/17588359211058393

Song, J.B. et al. 2019. Urinary aquaporin 1 and perilipin 2: Can these novel markers accurately characterize small renal masses and help guide patient management? *International Journal of Urology*, 26(2), pp. 260–265. doi:10.1111/iju.13854

Sordo-Bahamonde, C., Lorenzo-Herrero, S., Payer, Á.R., Gonzalez, S. and López-Soto, A. 2020. Mechanisms of Apoptosis Resistance to NK Cell-Mediated Cytotoxicity in Cancer. *International Journal of Molecular Sciences*, 21(10). doi:10.3390/IJMS21103726

Sourbier, C. et al. 2012. Targeting HIF2α Translation with Tempol in VHL-Deficient Clear Cell Renal Cell Carcinoma. *Oncotarget*, 3(11), p. 1472. doi:10.18632/ONCOTARGET.561

Spellberg, B. and Edwards, J.E. 2001. Type 1/Type 2 Immunity in Infectious Diseases. *Clinical Infectious Diseases*, 32(1), pp. 76–102. doi:10.1086/317537

Stebegg, M., Kumar, S.D., Silva-Cayetano, A., Fonseca, V.R., Linterman, M.A. and Graca, L. 2018. Regulation of the germinal center response. *Frontiers in Immunology*, 9(OCT), p. 2469. doi:10.3389/FIMMU.2018.02469

Su, S., Akbarinejad, S. and Shahriyari, L. 2021. Immune classification of clear cell renal cell carcinoma. *Scientific Reports*, 11(1), pp. 1–10. doi:10.1038/s41598-021-83767-z

Subramanian, A. et al. 2005. Gene set enrichment analysis: A knowledge-based approach for interpreting genome-wide expression profiles. *Proceedings of the National Academy of Sciences of the United States of America*, 102(43), pp. 15545–15550. doi:10.1073/PNAS.0506580102/SUPPL_FILE/06580FIG7.JPG

Sugimura, K., Ikemoto, S.I., Kawashima, H., Nishisaka, N. and Kishimoto, T. 2001. Microscopic hematuria as a screening marker for urinary tract malignancies. *International Journal of Urology*, 8(1), pp. 1–5. doi:10.1046/j.1442-2042.2001.00235.x

Sun, C. et al. 2017. High NKG2A expression contributes to NK cell exhaustion and predicts a poor prognosis of patients with liver cancer. *OncoImmunology*, 6(1), pp. 1–12. doi:10.1080/2162402X.2016.1264562

Swami, U., Nussenzveig, R.H., Haaland, B. and Agarwal, N. 2019. Revisiting AJCC TNM staging for renal cell carcinoma: quest for improvement. *Annals of Translational Medicine*, 7(Suppl 1), pp. S18–S18. doi:10.21037/ATM.2019.01.50

Swiatek, M. et al. 2020. Various forms of HIF-1α protein characterize the clear cell renal cell carcinoma cell lines. *IUBMB Life*, 72(6), pp. 1220–1232. doi:10.1002/IUB.2281

Syler, L.B., Gooden, C. and Riddle, N. 2021. Plasma Cell Myeloma Within a Renal Cell Carcinoma, an Intimate Histologic Relationship: A Case Report and Literature Review. *Cureus*, 13(1), pp. 1–6.

doi:10.7759/cureus.12898

Takahashi, Y., Hori, Y., Yamamoto, T., Urashima, T., Ohara, Y. and Tanaka, H. 2015. 3D spheroid cultures improve the metabolic gene expression profiles of HepaRG cells. *Bioscience Reports*, 35(3), pp. 1–7. doi:10.1042/BSR20150034/56877

Talebian, F., Liu, J.Q., Liu, Z., Khattabi, M., He, Y., Ganju, R. and Bai, X.F. 2012. Melanoma Cell Expression of CD200 Inhibits Tumor Formation and Lung Metastasis via Inhibition of Myeloid Cell Functions. *PLoS ONE*, 7(2). doi:10.1371/JOURNAL.PONE.0031442

Talebian, F., Yu, J., Lynch, K., Liu, J.Q., Carson, W.E. and Bai, X.F. 2021. CD200 Blockade Modulates Tumor Immune Microenvironment but Fails to Show Efficacy in Inhibiting Tumor Growth in a Murine Model of Melanoma. *Frontiers in Cell and Developmental Biology*, 9, p. 2844. doi:10.3389/FCELL.2021.739816

Tam, Y.K., Maki, G., Miyagawa, B., Hennemann, B., Tonn, T. and Klingemann, H.G. 1999. Characterization of genetically altered, interleukin 2-independent natural killer cell lines suitable for adoptive cellular immunotherapy. *Human gene therapy*, 10(8), pp. 1359–1373. doi:10.1089/10430349950018030

Taylor, B.C. and Balko, J.M. 2022. Mechanisms of MHC-I Downregulation and Role in Immunotherapy Response. *Frontiers in Immunology*, 13, p. 771. doi:10.3389/FIMMU.2022.844866

Terrén, I., Orrantia, A., Mikelez-Alonso, I., Vitallé, J., Zenarruzabeitia, O. and Borrego, F. 2020. NK cell-based immunotherapy in renal cell carcinoma. *Cancers*, 12(2), pp. 1–24. doi:10.3390/cancers12020316

Tesmer, L.A., Lundy, S.K., Sarkar, S. and Fox, D.A. 2008. Th17 cells in human disease. *Immunological Reviews*, 223(1), p. 87. doi:10.1111/J.1600-065X.2008.00628.X

Tokumaru, Y. et al. 2020. Association of Th2 high tumors with aggressive features of breast cancer. *https://doi.org/10.1200/JCO.2020.38.15_suppl.e12584*, 38(15_suppl), pp. e12584–e12584. doi:10.1200/JCO.2020.38.15_SUPPL.E12584

Tonks, A., Tonks, A.J., Pearn, L., Mohamad, Z., Burnett, A.K. and Darley, R.L. 2005. Optimized retroviral transduction protocol which preserves the primitive subpopulation of human hematopoietic cells. *Biotechnology progress*, 21(3), pp. 953–958. doi:10.1021/BP0500314

Tremblay-Mclean, A., Coenraads, S., Kiani, Z., Dupuy, F.P. and Bernard, N.F. 2019. Expression of ligands for activating natural killer cell receptors on cell lines commonly used to assess natural killer cell function. *BMC Immunology*, 20(1), pp. 1–13. doi:10.1186/S12865-018-0272-X/FIGURES/3

Trotta, A.M. et al. 2018. Mutated von Hippel-Lindau-renal cell carcinoma (RCC) promotes patients specific natural killer (NK) cytotoxicity. *Journal of Experimental and Clinical Cancer Research*, 37(1), pp. 1–12. doi:10.1186/s13046-018-0952-7

Truong, L.D. and Shen, S.S. 2011. Immunohistochemical diagnosis of renal neoplasms. *Archives of Pathology and Laboratory Medicine*, 135(1), pp. 92–109. doi:10.1043/2010-0478-RAR.1

Turtle, C.J., Swanson, H.M., Fujii, N., Estey, E.H. and Riddell, S.R. 2009. A distinct subset of self-renewing human memory CD8+ T cells survives cytotoxic chemotherapy. *Immunity*, 31(5), p. 834. doi:10.1016/J.IMMUNI.2009.09.015

Twito, T., Chen, Z., Khatri, I., Wong, K., Spaner, D. and Gorczynski, R. 2013a. Ectodomain shedding of CD200 from the B-CLL cell surface is regulated by ADAM28 expression. *Leukemia Research*, 37(7), pp. 816–821. doi:10.1016/j.leukres.2013.04.014

Ueno, M. et al. 2018. ADAM9 is over-expressed in human ovarian clear cell carcinomas and suppresses cisplatin-induced cell death. *Cancer Science*, 109(2), pp. 471–482. doi:10.1111/cas.13469

Uhlén, M. et al. 2015. Tissue-based map of the human proteome. *Science (New York, N.Y.)*, 347(6220). doi:10.1126/SCIENCE.1260419

Upshaw, J.L., Arneson, L.N., Schoon, R.A., Dick, C.J., Billadeau, D.D. and Leibson, P.J. 2006. NKG2D-mediated signaling requires a DAP10-bound Grb2-Vav1 intermediate and phosphatidylinositol-3-kinase in human natural killer cells. *Nature Immunology 2006 7:5*, 7(5), pp. 524–532. doi:10.1038/ni1325

Urb, M. and Sheppard, D.C. 2012. The Role of Mast Cells in the Defence against Pathogens. *PLoS Pathogens*, 8(4). doi:10.1371/JOURNAL.PPAT.1002619

Vafaei, S., Zekiy, A.O., Khanamir, R.A., Zaman, B.A., Ghayourvahdat, A., Azimizonuzi, H. and Zamani, M. 2022. Combination therapy with immune checkpoint inhibitors (ICIs); a new frontier. *Cancer Cell International 2021 22:1*, 22(1), pp. 1–27. doi:10.1186/S12935-021-02407-8

Valente, T., Serratosa, J., Perpiñá, U., Saura, J. and Solà, C. 2017. Alterations in CD200-CD200R1 system during EAE already manifest at presymptomatic stages. *Frontiers in Cellular Neuroscience*, 11, p. 129. doi:10.3389/FNCEL.2017.00129

Vasudev, N.S. et al. 2020. Challenges of early renal cancer detection: symptom patterns and incidental diagnosis rate in a multicentre prospective UK cohort of patients presenting with suspected renal cancer. *BMJ Open*, 10(5), p. e035938. doi:10.1136/BMJOPEN-2019-035938

Vaughan, J.W., Shi, M., Horna, P. and Olteanu, H. 2020. Increased CD200 expression in post-transplant lymphoproliferative disorders correlates with an increased frequency of FoxP3(+) regulatory T cells. *Annals of diagnostic pathology*, 48. doi:10.1016/J.ANNDIAGPATH.2020.151585

Verhagen, J., Sabatos, C.A. and Wraith, D.C. 2008. The role of CTLA-4 in immune regulation. *Immunology Letters*, 115(1–4), p. 73. doi:10.1016/J.IMLET.2007.10.010

Verma, S.K. and Molitoris, B.A. 2015. Renal Endothelial Injury and Microvascular Dysfunction in Acute Kidney Injury. *Seminars in nephrology*, 35(1), p. 96. doi:10.1016/J.SEMNEPHROL.2015.01.010

Vesely, M.D., Kershaw, M.H., Schreiber, R.D. and Smyth, M.J. 2011. Natural Innate and Adaptive Immunity to Cancer. *https://doi.org/10.1146/annurev-immunol-031210-101324*, 29, pp. 235–271. doi:10.1146/ANNUREV-IMMUNOL-031210-101324

Vyas, M., Requesens, M., Nguyen, T.H., Peigney, D., Azin, M. and Demehri, S. 2023. Natural killer cells suppress cancer metastasis by eliminating circulating cancer cells. *Frontiers in Immunology*, 13. doi:10.3389/FIMMU.2022.1098445/FULL

Wagner, J.A. et al. 2017. CD56bright NK cells exhibit potent antitumor responses following IL-15 priming. *The Journal of Clinical Investigation*, 127(11), pp. 4042–4058. doi:10.1172/JCI90387

Walker, D.G. and Lue, L.F. 2013. Understanding the neurobiology of CD200 and the CD200 receptor: A therapeutic target for controlling inflammation in human brains? *Future Neurology*, 8(3), pp. 321–332. doi:10.2217/fnl.13.14

Walser, T. et al. 2008. Smoking and Lung Cancer: The Role of Inflammation. *Proceedings of the American Thoracic Society*, 5(8), p. 811. doi:10.1513/PATS.200809-100TH

Wang, B., Liu, L., Wu, J., Mao, X., Fang, Z., Chen, Y. and Li, W. 2022. Construction and Verification of a Combined Hypoxia and Immune Index for Clear Cell Renal Cell Carcinoma. *Frontiers in Genetics*, 13, p. 192. doi:10.3389/FGENE.2022.711142

Wang, K., Shen, T., Siegal, G.P. and Wei, S. 2017. The CD4/CD8 ratio of tumor-infiltrating lymphocytes at the tumor-host interface has prognostic value in triple-negative breast cancer. *Human Pathology*, 69, pp. 110–117. doi:10.1016/J.HUMPATH.2017.09.012

Wang, W., Qi, L., Tan, M., Zhang, Z., Du, J., Wei, X. and Yao, X. 2015. Effect of platelet-derived growth factor-B on renal cell carcinoma growth and progression. *Urologic oncology*, 33(4), pp. 168.e17-168.e27. doi:10.1016/J.UROLONC.2014.12.015

Wang, X., Lopez, R., Luchtel, R.A., Hafizi, S., Gartrell, B. and Shenoy, N. 2021a. Immune evasion in renal cell carcinoma: biology, clinical translation, future directions. *Kidney International*, 99(1), pp. 75–85. doi:10.1016/j.kint.2020.08.028

Wang, Y., Yin, C., Geng, L. and Cai, W. 2021b. Immune Infiltration Landscape in Clear Cell Renal Cell Carcinoma Implications. *Frontiers in Oncology*, 10(February), pp. 1–15. doi:10.3389/fonc.2020.491621

Warburton, H.E., Brady, M., Vlatkovic´, Vlatkovic´, N., Linehan, W.M., Parsons, K. and Boyd, M.T. 2005. p53 Regulation and Function in Renal Cell Carcinoma. *Cancer Research*, 65(15), pp. 6498–6503. doi:0.1158/0008-5472.CAN-05-0017

Warren, A.Y. and Harrison, D. 2018. WHO/ISUP classification, grading and pathological staging of renal cell carcinoma: standards and controversies. *World Journal of Urology*, 36(12), pp. 1913–1926.

doi:10.1007/s00345-018-2447-8

Wei, L., Wen, J.Y., Chen, J., Ma, X.K., Wu, D.H., Chen, Z.H. and Huang, J.L. 2019. Oncogenic ADAM28 induces gemcitabine resistance and predicts a poor prognosis in pancreatic cancer. *World Journal of Gastroenterology*, *25*(37), p. 5590. doi:10.3748/WJG.V25.I37.5590

Wierzbicki, P.M. et al. 2019. Prognostic significance of VHL, HIF1A, HIF2A, VEGFA and p53 expression in patients with clear-cell renal cell carcinoma treated with sunitinib as first-line treatment. *International Journal of Oncology*, 55(2), pp. 371–390. doi:10.3892/IJO.2019.4830/HTML

Willerslev-Olsen, A. et al. 2013. Bacterial Toxins Fuel Disease Progression in Cutaneous T-Cell Lymphoma. *Toxins*, 5(8), p. 1402. doi:10.3390/TOXINS5081402

Winandy, S., Wu, L., Wang, J.H. and Georgopoulos, K. 1999. Pre–T Cell Receptor (Tcr) and Tcr-Controlled Checkpoints in T Cell Differentiation Are Set by Ikaros. *The Journal of Experimental Medicine*, 190(8), p. 1039. doi:10.1084/JEM.190.8.1039

Wong, K.K., Zhu, F., Khatri, I., Huo, Q., Spaner, D.E. and Gorczynski, R.M. 2016. Characterization of CD200 ectodomain shedding. *PLoS ONE*, 11(4), pp. 1–19. doi:10.1371/journal.pone.0152073

Wright, G.J. et al. 2003. Characterization of the CD200 Receptor Family in Mice and Humans and Their Interactions with CD200. *The Journal of Immunology*, 171(6), pp. 3034–3046. doi:10.4049/jimmunol.171.6.3034

Wu, X., Jiang, D., Liu, H., Lu, X., Lv, D. and Liang, L. 2021. CD8+ T Cell-Based Molecular Classification With Heterogeneous Immunogenomic Landscapes and Clinical Significance of Clear Cell Renal Cell Carcinoma. *Frontiers in Immunology*, 12, p. 5390. doi:10.3389/FIMMU.2021.745945

Wu, Y., Guo, Y., Huang, A., Zheng, P. and Liu, Y. 1997. CTLA-4–B7 Interaction Is Sufficient to Costimulate T Cell Clonal Expansion. *The Journal of Experimental Medicine*, 185(7), p. 1327. doi:10.1084/JEM.185.7.1327

Wykoff, C.C., Sotiriou, C., Cockman, M.E., Ratcliffe, P.J., Maxwell, P., Liu, E. and Harris, A.L. 2004. Gene array of VHL mutation and hypoxia shows novel hypoxia-induced genes and that cyclin D1 is a VHL target gene. *British Journal of Cancer 2004 90:6*, 90(6), pp. 1235–1243. doi:10.1038/sj.bjc.6601657

Xia, Y. et al. 2017. Negatively regulation of tumor-infiltrating NK cell in clear cell renal cell carcinoma patients through the exosomal pathway. *Oncotarget*, 8(23), pp. 37783–37795. doi:10.18632/oncotarget.16354

Xu, J., Gu, Y., Sun, J., Zhu, H., Lewis, D.F. and Wang, Y. 2018. Reduced CD200 expression is associated with altered Th1/Th2 cytokine production in placental trophoblasts from preeclampsia. *American Journal of Reproductive Immunology*, 79(1), pp. 0–2. doi:10.1111/aji.12763

Xu, Y., Cheng, Q., Yang, B., Yu, S., Xu, F., Lu, L. and Liang, X. 2015. Increased sCD200 Levels in Vitreous of Patients With Proliferative Diabetic Retinopathy and Its Correlation With VEGF and Proinflammatory Cytokines. *Investigative Ophthalmology & Visual Science*, 56(11), pp. 6565–6572. doi:10.1167/IOVS.15-16854

Yang, J.C. et al. 2007. Ipilimumab (Anti-CTLA4 Antibody) Causes Regression of Metastatic Renal Cell Cancer Associated With Enteritis and Hypophysitis. *Journal of immunotherapy (Hagerstown, Md. : 1997)*, 30(8), p. 825. doi:10.1097/CJI.0B013E318156E47E

Yang, X. et al. 2015. VEGF-B promotes cancer metastasis through a VEGF-A-independent mechanism and serves as a marker of poor prognosis for cancer patients. *Proceedings of the National Academy of Sciences of the United States of America*, 112(22), pp. E2900–E2909. doi:10.1073/PNAS.1503500112

Yao, Y. and Dai, W. 2014. Genomic Instability and Cancer. *Journal of carcinogenesis & mutagenesis*, 5(02). doi:10.4172/2157-2518.1000165

Yaohai, W. et al. 2020. Low Level of Macrophages M0 in Primary Tumors is a Favorable Factor for Metastasis in Renal Clear Cell Carcinoma. *Research Square*, pp. 1–17. doi:https://doi.org/10.21203/rs.3.rs-120214/v1

Yeap, W.H. et al. 2016. CD16 is indispensable for antibody-dependent cellular cytotoxicity by human monocytes. *Scientific Reports 2016 6:1*, 6(1), pp. 1–22. doi:10.1038/srep34310

Zamora, A.E., Grossenbacher, S.K., Aguilar, E.G. and Murphy, W.J. 2015. Models to study NK cell biology and possible clinical application. *Current protocols in immunology*, 110, p. 14.37.1. doi:10.1002/0471142735.IM1437S110

Zeng, Q., Sun, S., Li, Y., Li, X., Li, Z. and Liang, H. 2020. Identification of Therapeutic Targets and Prognostic Biomarkers Among CXC Chemokines in the Renal Cell Carcinoma Microenvironment. *Frontiers in Oncology*, 9(February), pp. 1–14. doi:10.3389/fonc.2019.01555

Zhang, C., Yang, M. and Ericsson, A.C. 2021. Function of Macrophages in Disease: Current Understanding on Molecular Mechanisms. *Frontiers in Immunology*, 12, p. 635. doi:10.3389/FIMMU.2021.620510

Zhang, S. et al. 2019. Immune infiltration in renal cell carcinoma. *Cancer Science*, 110(5), pp. 1564–1572. doi:10.1111/cas.13996

Zhang, Y., Zou, J. and Chen, R. 2022. An M0 macrophage-related prognostic model for hepatocellular carcinoma. *BMC Cancer*, 22(1), pp. 1–13. doi:10.1186/S12885-022-09872-Y

Zhao, X., Li, J. and Sun, H. 2019. CD200-CD200R Interaction: An Important Regulator After Stroke. *Frontiers in Neuroscience*, 13(August), pp. 1–6. doi:10.3389/fnins.2019.00840

Zhou, R. et al. 2020. ADAM9 Mediates Triple-Negative Breast Cancer Progression via AKT/NF-κB Pathway. *Frontiers in Medicine*, 7(June). doi:10.3389/fmed.2020.00214

Zhu, J., Yamane, H. and Paul, W.E. 2010. Differentiation of Effector CD4 T Cell Populations. *Annual review of immunology*, 28, p. 445. doi:10.1146/ANNUREV-IMMUNOL-030409-101212

Ziblat, A. et al. 2021. Circulating and Tumor-Infiltrating NK Cells From Clear Cell Renal Cell Carcinoma Patients Exhibit a Predominantly Inhibitory Phenotype Characterized by Overexpression of CD85j, CD45, CD48 and PD-1. *Frontiers in Immunology*, 12. doi:10.3389/FIMMU.2021.681615/FULL

Zwirner, N.W. and Ziblat, A. 2017. Regulation of NK cell activation and effector functions by the IL-12 family of cytokines: The case of IL-27. *Frontiers in Immunology*, 8(JAN), p. 25. doi:10.3389/FIMMU.2017.00025